A Thesis Entitled

SYNTHESIS AND CHARACTERIZATION OF NON-HEME LIGAND BASED TRANSITION METAL COMPLEXES AND THEIR ROLE IN BIOMIMETIC OXIDATIONS

THESIS

Submitted to

GOA UNIVERSITY

For the award of the degree of

DOCTOR OF PHILOSOPHY

In

CHEMISTRY

By

Mr. DATTAPRASAD D. NARULKAR

M. Sc.

Under the guidance of

Dr. S. N. DHURI

Department of Chemistry

Goa University

Taleigao Plateau, Goa 403206

INDIA

MAY 2018

A Thesis Entitled

SYNTHESIS AND CHARACTERIZATION OF NON-HEME LIGAND BASED TRANSITION METAL COMPLEXES AND THEIR ROLE IN BIOMIMETIC OXIDATIONS

THESIS

Submitted to

GOA UNIVERSITY

For the award of the degree of

DOCTOR OF PHILOSOPHY

In

CHEMISTRY

By

Mr. DATTAPRASAD D. NARULKAR

M. Sc.

Under the guidance of

Dr. S. N. DHURI

Department of Chemistry

Goa University

Taleigao Plateau, Goa 403206

INDIA

MAY 2018

DECLARATION

I hereby declare that the work embodied in the thesis entitled "**SYNTHESIS AND CHARACTERIZATION OF NON-HEME LIGAND BASED TRANSITION METAL COMPLEXES AND THEIR ROLE IN BIOMIMETIC OXIDATIONS**" is the result of investigations carried out by me under the guidance of **Dr. S. N. Dhuri** at Department of Chemistry, Goa University and that it has not previously formed the basis for the award of any degree or diploma or other similar titles.

In keeping with the general practice of reporting scientific observations, due acknowledgement has been made wherever the work described is based on the findings of other investigators.

Goa University
May 2018

Mr. Dattaprasad D. Narulkar
Research Student
Department of Chemistry
Goa University, Goa

DEPARTMENT OF CHEMISTRY

CERTIFICATE

This is to certify that the thesis entitled, "**SYNTHESIS AND CHARACTERIZATION OF NON-HEME LIGAND BASED TRANSITION METAL COMPLEXES AND THEIR ROLE IN BIOMIMETIC OXIDATIONS**" submitted by **Mr. Dattaprasad D. Narulkar**, is a record of research work carried out by the candidate during the period of study under my supervision and that it has not previously formed the basis for the award of any degree or diploma or other similar titles.

Goa University
May 2018

Dr. S. N. Dhuri
Research Guide
Department of Chemistry
Goa University, Goa

Dedicated to

my uncle and aunty

late Shri Sitaram S. Gawas

and

late Smt. Suvarnlaxmi S. Gawas

for their motivation, support and encouragement for my Ph.D.

TABLE OF CONTENTS

List of Abreviation

General abreviations

AR	Analytical reagent
CV	Cyclic voltametry
DPV	Differntial pulse voltametry
DEPT	Distortionless enhancement by polarization
ESR	Electron Spin Resonance
GC	Gas cgromatography
IR	Infrared
NMR	Nuclear Magnetic Resonanace
UV-Vis	UV-Visible
XRD	X-ray diffractometry
nm	Nanometer, 10^{-9} m
Å	Angström unit, 10^{-10} m
V	Volt
υ	Frequency
cm^{-1}	Unit of Wavenumber
λ	Wavelength
h	Hours
ε	Molar absorptivity
S. D.	Standard deviation
e.s.d.	Estimated standard deviation
CAN	Ceric ammonium nitrate
H_2O_2	Hydrogen peroxide
m-CPBA	metachloroperbenzoic acid
PhIO	Iodosylbenzene
t-BuOOH	tert- butyl hydroperoxide
THF	Tetrahydrofuran
TEA	Ttriethylamine
NADH	Nicotinamide adenine dinucleotide

Abreviations of ligands

TAPM = 1,4,8,12-tetramethyl-1,4,8,121-tetraazacyclopentadecane

BPMEN = *N*,*N*-dimethyl-*N'*,*N'*-bis(pyridin-2-ylmethyl)ethane-1,2-diamine

TPA = tris-(2-pyridylmethyl)-amine

TATM= 1,4,7,10-tetramethyl-1,4,7,10-tetraazacyclotridecane

BPMCN = *N*,*N*-bis(2-pyridylmethyl)-*N*,*N*-dimethyl-trans-1,2-diaminocyclohexane

BQCN = *N,N'*-dimethyl-*N,N'*-bis(8-quinolyl)cyclohexanediamine

QBPA (2-quinolylmethyl)bis(2-pyridylmethyl)amine

14-TMC = 1,4,8,11-tetramethyl-1,4,7,10-tetraazacyclotridecane

13-TMC = 1,4,7,10-tetramethyl-1,4,8,11-tetraazacyclotetradecane

12- TMC = 1,4,7,10-tetramethyl-1,4,8,11-tetraazacyclododecane

Bn-TPEN = *N*-benzyl-*N,N',N'*-tris(2-pyridylmethyl)ethane-1,2- diamine

N4Py = *N*,*N*-bis(2-pyridylmethyl)-*N*-bis(2-pyridyl)methylamine.

phen = phenanthroline

en = ethylenediamine

bpy = bipyridine

bqenH_2 = *N*,*N'*-bis(8-quinolyl)ethane-1,2-diamine

bqenMe_2 = *N,N'*-dimethyl-*N,N'*-bis(8-quinolyl)ethane-1,2-diamine

TPA = [tris(2-pyridylmethyl)amine

TEPA = tris[2-(2-pyridyl)ethyl]amine

^{Bz}Pym2 = *N*-benzyl-bis(2-pyridylmethyl)amine

^{Bz}Pye2 = *N*-benzyl-bis[2-(2-pyridyl)ethyl]amine

^{Dtbp}Pym2H = 6-[*N*,*N*-bis(2-pyridylmethyl)aminomethyl]-2,4-di-*tert*-butylphenol

Pye2H = 6-[*N*,*N*-bis[2-(2-pyridyl)ethyl]aminomethyl]-2,4-di-*tert*-butylphenol

L2H_2 = [*N*-(2-pyridylmethyl)-*N*,*N*-bis(2-hydroxy-3,5-di-*tert*-butylbenzyl)amine]

L3H_3 = [tris(2-hydroxy-3,5-di-*tert*-butylbenzyl)amine]

L6 = tris(benzimidazol-2-ylmethyl)amine

L5 = *N*,*N*-dimethyl- *N'*,*N'*bis(quinolin-2-ylmethyl)ethane-1,2-diamine

L1 = *N*,*N*-dimethyl-*N'*,*N'*-bis(pyrid-2-ylmethyl)ethane-1,2-diamine

L2 = *N*,*N*-diethyl- *N'*,*N'*-bis(pyrid-2-ylmethyl)ethane-1,2-diamine

L3 = *N*,*N*-dimethyl-*N*-(1-methyl-*1H*-imidazol-2-ylmethyl)-*N'*-(pyrid-2-ylmethyl)ethane-1,2- diamine

L4 = *N*,*N*-dimethyl- *N'*,*N'*bis(1-methyl-*1H*-imidazol-2-ylmethyl)ethane-1,2-diamine

L-1= *N,N'*-bis(2-pyrid-2-ylmethyl)-1,4-diazepane

L-2 = *N*-(6-methylpyrid-2-ylmethyl)-*N'*-(pyrid-2-ylmethyl)-1,4-diazepane

L-3 = *N,N'*-bis(6-methyl-2-pyridylmethyl)-1,4-diazepane

L-4 = *N,N'*-bis((1-methyl-1H-imidazole-2-yl)methyl)-1,4-diazepane,

L-5 = *N,N'*-dimethyl-*N,N'*-bis(2-pyridylmethyl)ethylenediamine

^{Me,H}PyTACN = 1-(2-pyridylmethyl)-4,7-dimethyl-1,4,7-triazacyclononane

L'1 = *N*-methyl-*N,N',N'*-tris(pyrid-2-ylmethyl)-ethylenediamine

L’2 = *N*-benzyl-*N,N’,N’*-tris(pyrid-2-yl-methyl)-ethylenediamine

L’3 = *N*-methyl-*N,N’*-bis(pyrid-2-ylmethyl)-*N’*-(6-methyl-pyrid-2-yl-methyl)-ethylenediamine

L’4 = *N*-methyl-*N,N’*-bis(pyrid-2-ylmethyl)-*N’*-(quinolin-2-ylmethyl)-ethylenediamine

L’5 = *N*-methyl-*N,N’*-bis(pyrid-2-ylmethyl)-*N’*-imidazole-2-ylmethyl)-ethylenediamine

Tp^{ipr} = hydrotris(3,5-di-2-propylpyrazolyl)borate

H_{2L} = 2,6-pyridinedicarboxamidate ligand

TMG_3tren = (*tris*[2-(*N*-tetramethylguanidyl)ethyl]amine)

L = *N*,*N′*-(2,6-dimethylphenyl)-2,6-pyridinedicarboxamidate

H_2TPP = *meso*-tetraphenylporphyrin

pz ^{iPr2}H = 3,5-isopropylpyrazole

$L^7py_2^H$ = 1,4-bis[(2-pyridylmethyl]-1,4-diazepane

$L^7py_2^{6\text{-}Me}$ = 1,4-bis[(6-methyl-2-pyridylmethyl]-1,4-diazepane

$L^7py_2^{Br}$ = 1,4-bis[(5-bromo-2-pyridylmethyl]-1,4-diazepane

$L^7py_2^{6\text{-}MeO}$ = 1,4-bis[(6-methoxy-2-pyridylmethyl]-1,4-diazepane

$L^7py_2^{4\text{-}Me}$ = 1,4-bis[(4-methyl-2-pyridylmethyl]-1,4-diazepane

L^7q_2 = 1,4-bis[(2-quinolinyl)methyl]-1,4-diazepane

$L^8py_2^H$ = 1,5-bis(2-pyridylmethyl)-1,5-diazacyclooctane

$L^7py_2^{4\text{-}Cl}$ = 1,4-bis[(4-chloro-2-pyridyl)-methyl]-1,4-diazepane

$L^7iso\text{-}q_2$ = 1,4-bis[(2-isoquinolinyl)methyl]-1,4-diazepane

mL_5^2 = (*N*-methyl-*N,N’,N’*-tris(2-pyridylmethyl)ethane-1,2-diamine),

imL_5^2 = (*N*-methyl-*N,N,N’*-tris((1-methyl-4-imidazolyl)methyl)ethane-1,2-diamine),

H_2bupa = Bis[(*N′*-tert-butylurealy)-*N*-ethyl]-(6-pivalamido-2-pyridylmethyl)amine

H_2bpaa = *N*-[Bis(6-pivalamido-2-pyridylmethyl)](*N’*-4-fluorophenylcarbamoylmethyl-amine

pz ^{iPr2}H = 3,5-isopropylpyrazole

Tp^{Ph2} = tris(3,5-diphenylpyrazol)hydroborate

$im^{Me}H$ = 2-methylimidazole

Me_3TPADP^+ = 3,6,9-trimethyl-3,6,9-triaza-1(2,6)-pyridinacyclodecaphane

$H_4[^{Br}HBA\text{-}Et]$ = *N,N’*-(ethane-1,2-diylbis(5-bromo-2-hydroxybenzamide)

bbpc = *N,N’*- dibenzyl- *N,N’*- bis(2-pyridylmethyl)-1,2-cyclohexanediamineTAML = tetra amido macrocyclic ligand

TMG_3tren = tris[2-(*N*-tetramethylguanidyl)ethyl]amine

H_2bpc = 4,5-dichloro-1,2-bis(2-pyridine-2-carboxamido)benzeneHB(3,5-*i*-Prpz)$_3$ = hydrotris(pyrazolyl)-borate

CHDAP = *N*,*N'*-dicyclohexyl-2,11-diaza[3,3](2,6)pyridinophane; R = $C(CH_3)_2Ph$ and ^tBu)

bpc = *N*,*N'*- dibenzyl- *N*,*N'*- bis(2-pyridylmethyl)-1,2-cyclohexanediamine

L^{N3} = (1-[2-(2-pyridyl)ethyl]-1,5-diazacyclooctane

L^{N2S} = N-(2-(Pyridin-2-yl)ethyl)-1-thia-5-azacyclooctane

DIEN-pyr = (2-pyridylmethyl)(2-((2-pyridylmethyl)amino)ethyl)amine

Tet-Me_6 = *N*,*N*,*N'*,*N'*,3,6-Hexamethyl-3,6-diazaoctane-1,8-diamine

terpy = 2,2':6',2''-terpyridine

Me_3tacn = *N,N',N''*-Trimethyl-l,4,7-triazacyclononane

PHAB = 1,2-(bis-2,20diphenyl-2-hydroxyethanamido)benzene

SYNOPSIS

SYNTHESIS AND CHARACTERIZATION OF NON-HEME LIGAND BASED TRANSITION METAL COMPLEXES AND THEIR ROLE IN BIOMIMETIC OXIDATIONS

General Introduction

The thesis entitled *"Synthesis and Characterization of Non-heme Ligand based Transition Metal Complexes and their role in Biomimetic Oxidations"* deals with the study on several new transition metal complexes stabilized by non-heme ligands. The study involves an understanding of biomimetic roles of newly synthesized compounds in the oxidation reactions such as C-H activation, epoxidation and aldehyde deformylation besides the primary focus on the characterization of the compounds. As Ronald Breslow said, the biomimetic chemistry is the branch of the science which mirrors the activity that humans have pursued for a long time: inventing new things inspired by what Nature does.[1] The metalloenzymes occurring in nature catalyze a variety of reactions under mild reaction conditions with high selectivity[2] and therefore mimicking of a metal active site of an enzyme often help to understand the mechanistic pathways occurring in enzymatic reactions. The oxidative transformations catalyzed by metals and their complexes are an important class of reactions in synthetic organic chemistry as well as in industrial catalysis.[3,4] Cytochrome P450, a heme enzyme as well as non-heme taurine/α-ketoglutarate dioxygenase (TauD), ribonucleotide reductase and methane monooxygenase (MMO) enzymes are largely studied[5-8]. In the last three decades, various bioinorganic chemistry groups are actively involved in modelling of metalloenzymes and thus this area is extensively explored in recent past.[9,10,11] Inspired by the work carried out by various groups in this field, herein we have placed our attention in developing the new non-heme ligands as well as their transition metal complexes as efficient catalysts in oxidative

organic transformations. The metalloenzymes make use of dioxygen (O_2) to carry out biological oxidation reactions.[12] In the present work, we have used artificial oxidants; *m*-CPBA, H_2O_2 and PhIO. We have synthesized and fully characterized several of the transition metal complexes containing non-heme ligands (**Scheme 1**). The non-heme ligands which were employed in this study were either prepared by following the reported procedure or by employing the newly designed synthetic method. The non heme ligands *N*,*N*′-Bis(8-quinoline)ethane-1,2-diamine ($bqenH_2$), *N*,*N*′-dimethyl-*N*,*N*′-bis(8-quinolin)ethane-1,2-diamine ($bqenMe_2$), *N*,*N*'-dimethyl-*N*-(2-(methyl(pyridin-2-ylmethyl)amino)ethyl)-*N*'-(pyridin-2-ylmethyl)ethane-1,2-diamine (N3Py2) and 1,4,8,11-tetramethyl-1,4,8,11-tetraazacyclotetradecane (TMC) employed in this work are shown in **Scheme 1**.

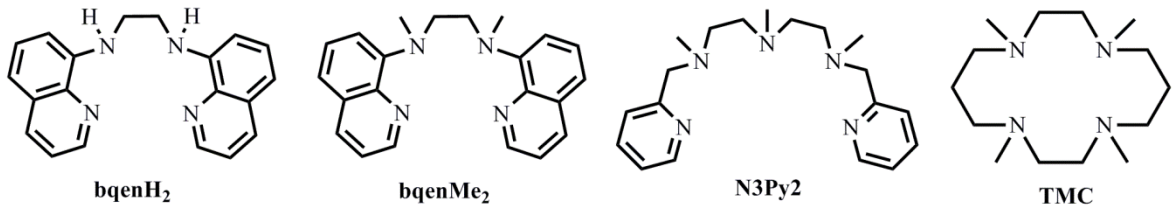

Scheme 1. Chemical structure of non-heme ligands employed in the current study.

In addition to the synthesis and characterization of several M(II) complexes, we have also spectroscopically trapped and characterized new Mn(III)-peroxo species of N3Py2 and investigated its reactivity in the aldehyde deformylation reactions. We have also achieved the characterization and C-H activation reactions by high valent *trans*-dioxoruthenium(VI)(TMC).[13]

The thesis has been divided into the following six chapters.

Chapter I: Introduction

This chapter covers the brief introduction on the research topic focusing the aims and objectives of the research and the literature review in general.

Chapter II: Materials and methods

Chapter-II includes details of all the materials, general procedures for synthesis, purification, recrystallization, technical aspects of instruments used in the characterization of the compounds. The generalized overview of methods used in this work is depicted in **Scheme 2** and while the chemical structures of all the compounds synthesised and characterized are shown in **Scheme 3**.

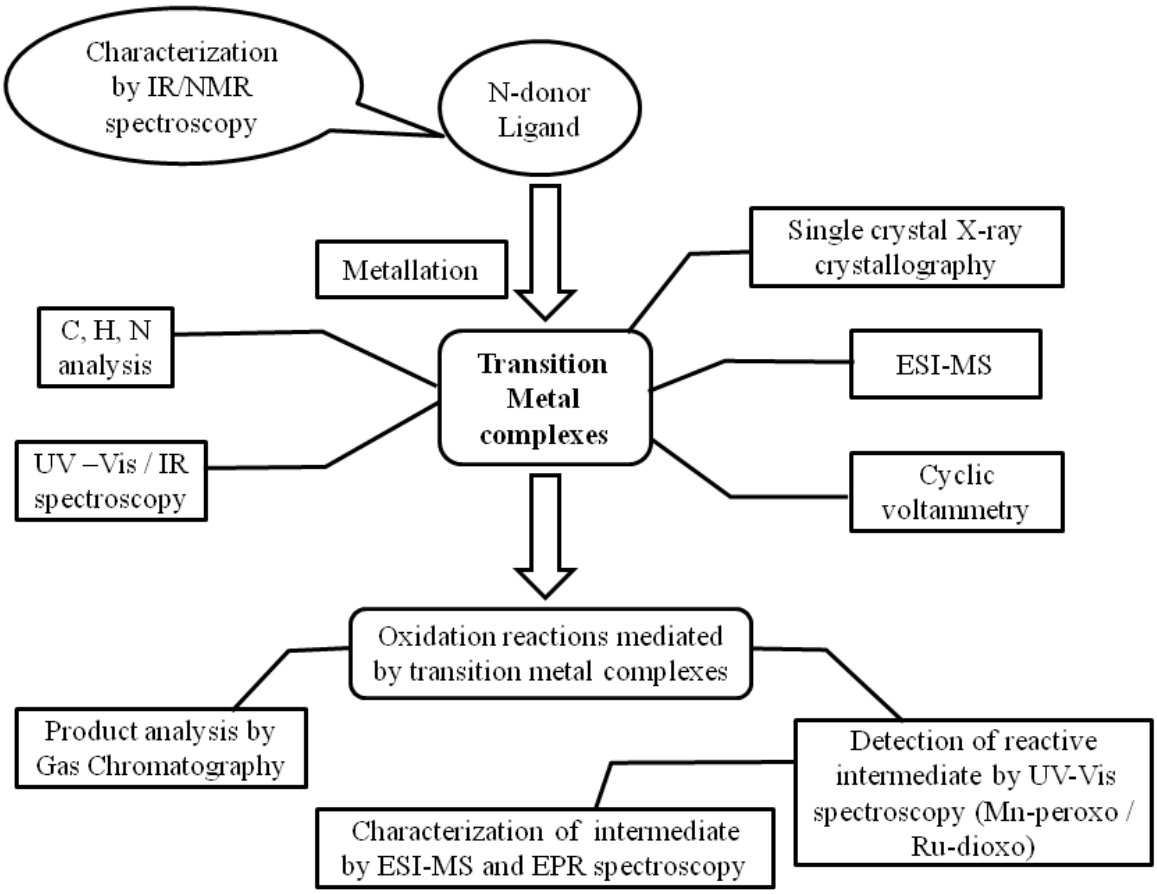

Scheme 2. General Techniques utilised for characterization of new compounds.

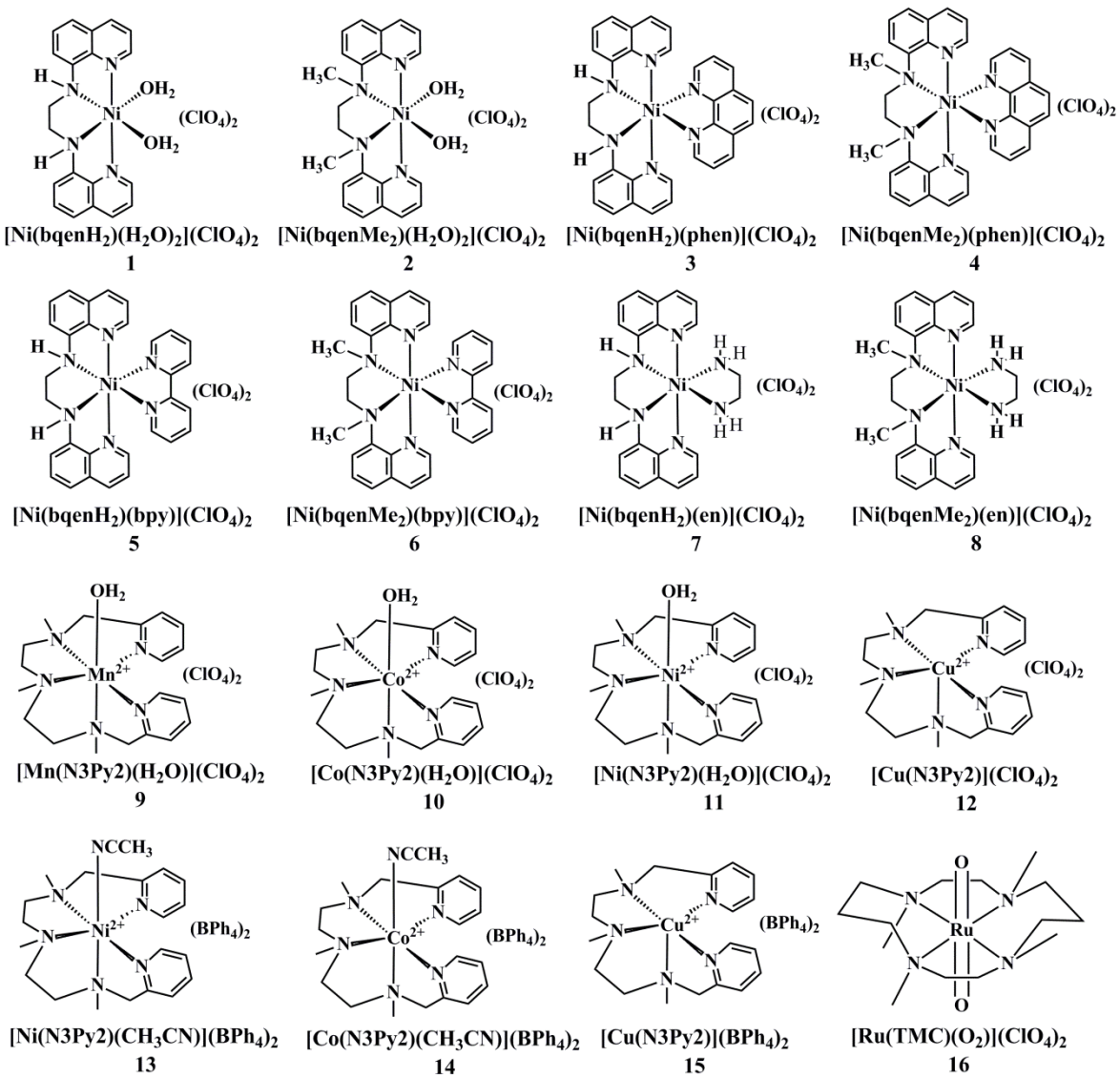

Scheme 3: Chemical structures of the new compounds **1-16** discussed in the subsequent chapters in the thesis.

CHAPTER III: Synthesis and characterization of mononuclear nickel(II) complexes and their role in catalytic alkane hydroxylation

The selective oxidation of alkanes is one of the objectives of the synthetic as well as the industrial chemist. The iron containing enzymes occurring in nature such as methane monooxygenase catalyzes the selective oxidation of methane to methanol using dioxygen in a unique manner. [14] Although the iron complexes are considered as potential catalysts in alkane hydroxylation reactions, the efficacy of other transition metal complexes such as

nickel(II) in these reactions is also investigated by several groups. [15-17]

This chapter includes the synthesis and characterization of Ni(II) complexes containing the tetradentate quinolyl based ligands *N,N′*-Bis(8-quinolin)ethane-1,2-diamine ($bqenH_2$) and *N,N′*-dimethyl-*N,N′*-bis(8-quinolin)ethane-1,2-diamine ($bqenMe_2$). The $bqenMe_2$ ligand has been prepared by a simple modification to the Britovsek procedure[18, 19]. The $bqenH_2$ and $bqenMe_2$ were metallated with $Ni(ClO_4)_2.6H_2O$ to obtain $[Ni(bqenH_2)(H_2O)_2](ClO_4)_2$ **1** and $[Ni(bqenMe_2)(H_2O)_2](ClO_4)_2$ **2** and characterized by various techniques. Both compounds were tested as catalysts in alkane hydroxylation reactions using *m*-CPBA as an oxidant at room temperature (**Scheme 4**). The high yields of alcohol over ketone were obtained for **2** unlike **1**, details of which have been described in the thesis. When two *cis* sites occupied by water molecules in **1** and **2** were replaced by auxiliary ligands such as phenanthroline (phen), bipyridine (bpy) or ethylenediamine (en) thus giving compounds $[Ni(bqenH_2)(phen)](ClO_4)_2$ **3**, $[Ni(bqenMe_2)(phen)](ClO_4)_2.CH_3CN$ **4**, $[Ni(bqenH_2)(bpy)](ClO_4)_2.0.125H_2O$ **5**, $[Ni(bqenMe_2)(bpy)](ClO_4)_2$ **6** $[Ni(bqenH_2)(en)](ClO_4)_2$ **7** and $[Ni(bqenMe_2)(en)](ClO_4)_2$ **8**. The four compounds **3-5** and **7** were structurally characterized that showed blocking of *cis* sites by the auxiliary ligands (**Fig.1**).

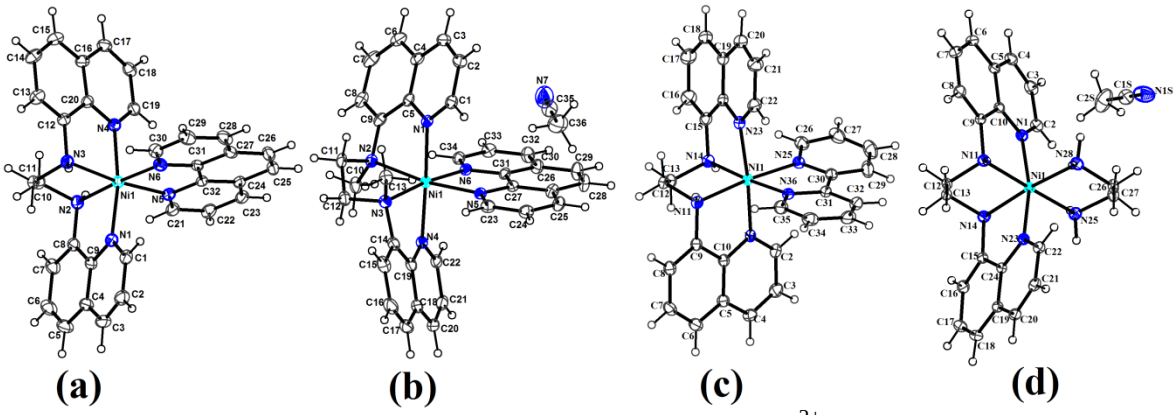

Fig. 1 Crystal structures of compounds a) $[Ni(bqenH_2)(phen)]^{2+}$ **3**, b) $[Ni(bqenMe_2)(phen)]$ **4**, c) **5** $[Ni(bqenH_2)(bpy)]^{2+}$ and d) **7** $[Ni(bqenH_2)(en)]^{2+}$with atom labelling scheme. Displacement ellipsoids are drawn at 50 % probability except for the H atoms, which are shown as circles of arbitary radius.

The catalytic utility of compounds **3**-**8** in hydroxylation of alkanes was achieved and compared with compounds **1** and **2**. We have also proposed the mechanism involving $[Ni^{II}\text{-}O^{\bullet}(bqen)(CH_3CN)]^+$ on the same lines as reported by others.[16,17,20]

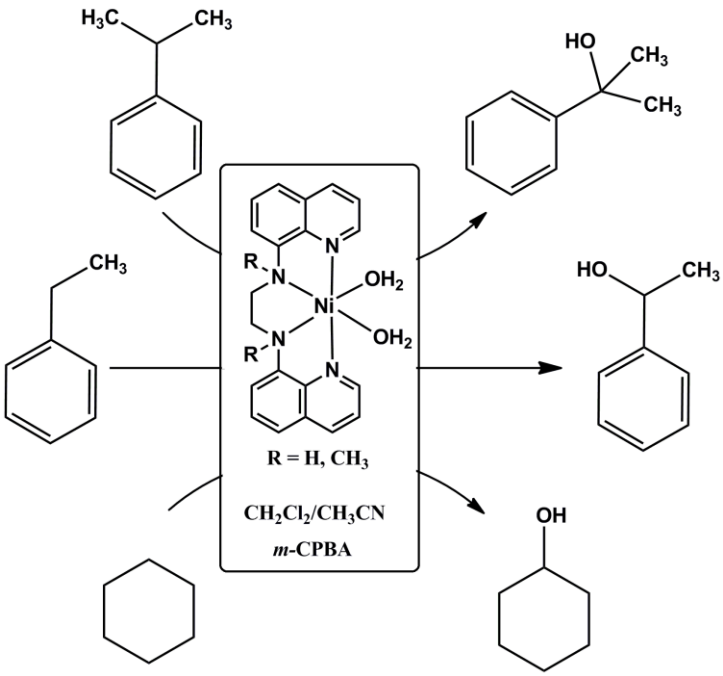

Scheme 4. The C-H activation reactions catalyzed by **1** and **2**

CHAPTER IV: Mn(II) complex and Mn(III) peroxo intermediate bearing novel non-heme N3Py2 ligand : Reactivity study in oxidation reactions

Manganese is another transition metal which is an active component of several metalloenzymes, for example, Mn-SOD, manganese ribonucleotide reductase, manganese homoprotocatechuate 2,3-dioxygenase (Mn-HPCD), oxygen evolving complexes of photosystem II.[21-25] Manganese(III)-peroxo species have been invoked as an active species in these enzymes and its participation is backed by spectroscopic and computational studies. Inspired by such studies we have investigated Mn(II) and Mn(III)-peroxy complex as discussed below.

The chapter IV focuses on the synthesis of a new non-heme ligand *N*,*N*'-dimethyl-*N*-(2-(methyl(pyridin-2-ylmethyl)amino)ethyl)-*N*'-(pyridin-2-ylmethyl)ethane-1,2-diamine (N3Py2), the synthesis and structural characterization of manganese(II) complex $[Mn(N3Py2)(H_2O)](ClO_4)_2$ (**9**) and generation, stability and spectroscopic characterization of intermediate Mn(III)-peroxy species, $[Mn(N3Py2)(O_2)]^+$ (**9a**). The pentadentate N3Py2 have been reported for the first time by our group and have been characterized by NMR spectroscopy.[26] The crystal structure of compound **9** possesses a distorted octahedral coordination geometry with the manganese(II) ion at the centre surrounded by five nitrogen atoms of ligand N3py2 and the sixth coordination site is occupied by a water molecule (**Fig 2a**).

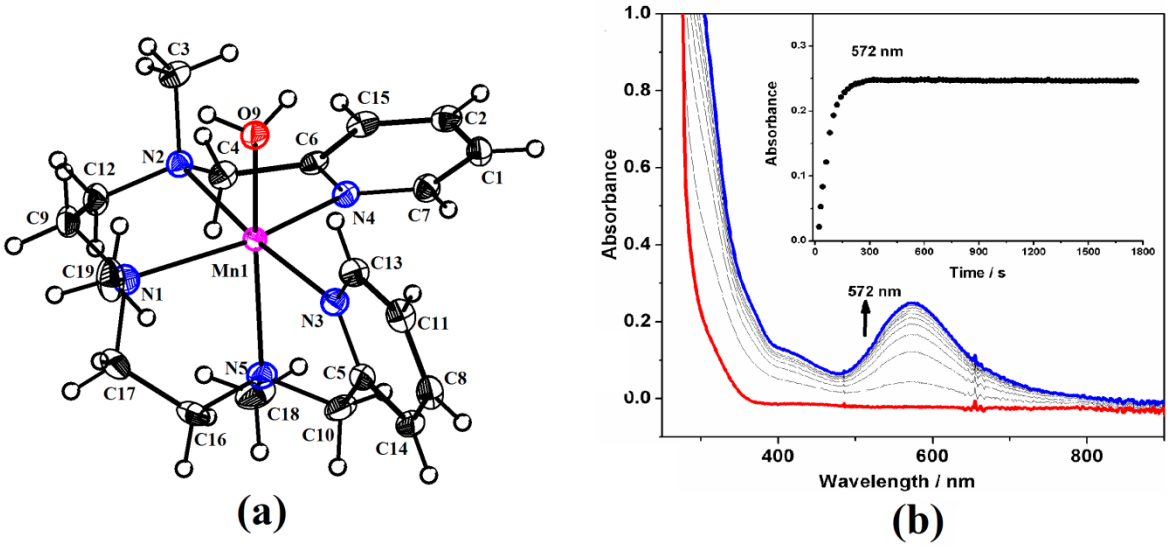

Fig. 2: (a) The crystal structure of $[Mn(N3Py2)(H_2O)]^{2+}$ **9** with atom labelling scheme. Displacement ellipsoids are drawn at 50% probability except for the H atoms, which are shown as circles of arbitrary radius.(**b**) UV-Visible spectral changes after addition of H_2O_2 in the presence of TEA (triethylamine) at 15 °C. Inset shows time trace monitored at 572 nm for the formation of the peak.

Compound **9** on reacting with H_2O_2 in the presence of triethylamine in CH_3CN at 15 °C results in the formation of a new species (**9a**) as evidenced by the appearance of the new band at 572 nm in its UV-Vis spectrum (**Fig. 2b**). Since species **9a** was quite stable, we characterized **9a** by ESI-MS and EPR spectroscopy and based on this analysis we have formulated **9a** as $[Mn(N3Py2)(O_2)]^+$. We have also done the DFT calculations to

understand the exact structure of **9a** and which has been presented in the thesis. As the half life for **9a** was quite high, we were able to investigate its reactivity with organic substrates such as aldehydes. Upon addition of 2-PPA (2-phenyl propionaldehyde) at 25 °C, a band at 572 nm corresponding to **9a** decayed slowly giving us a pseudo-first order kinetic time trace. Pseudo-first order rate constants increased with increase in the concentration of 2-PPA thus affording us second-order rate constants. We also investigated the temperature dependence of reaction rates and obtained activation parameter of $\Delta H^{\ddagger}$ and $\Delta S^{\ddagger}$. Product analysis by GC revealed acetophenone as the product. The nucleophilicity of Mn(III)-peroxy species was also evidenced by plotting Hammett constants (σ_p) of *para*-substituted benzaldehyde *para*-X−Ph−CHO (X = Cl, F, H, Me) versus log k_{obs}. The role of compound was **9** also investigated in the oxidation reactions. The compound **16** in presence of PhIO (iodosyl benzene) shows the conversion of alkenes to their corresponding epoxide at room temperature.

CHAPTER V: Synthesis and characterization of N3Py2 ligand-based cobalt(II), nickel(II) and copper(II) catalysts for efficient conversion of hydrocarbons to alcohols

The study carried out in chapter IV inspired us to explore more model compounds of other metals in the same series that are obtained from N3Py2 ligand. The peroxo complexes of cobalt(III), nickel(III) and copper(II) are well known in the literature.[27-29] Apart from their peroxy species, proficiency of metal complexes of Co(II), Ni(II) and Cu(II) have also been exploited in the C-H activation reactions which proceeds by formation of alkyl peroxo species.[20,30-32.] Here, we have studied the hydrocarbon oxidation reactions by three new compounds $[Co(N3Py2)(H_2O)]^{2+}$ **10**, $[Ni(N3Py2)(H_2O)]^{2+}$ **11**, and $[Cu(N3Py2)]^{2+}$ **12**. In this chapter, we have discussed the synthesis and characterization of

complexes **10-12** of cobalt (II), nickel (II) and copper (II) respectively and their roles in the C-H activation oxidations.

The three new complexes $[Co(N3Py2)(H_2O)](ClO_4)_2$ **10**, $[Ni(N3Py2)(H_2O)](ClO_4)_2$ **11** and $[Cu(N3Py2)](ClO_4)_2$ **12** have been prepared by the reaction of $M(ClO_4).6H_2O$ salt and N3Py2. Compounds **10-12** were characterised by C, H, N analysis, ESI-MS, IR and UV-Vis Spectroscopy and cyclic voltammetry. Compounds **10** and **11** as indicated by single crystal X-ray diffractometry are isostructural and crystallize in a centrosymmetric space group $P2_1/c$. The octahedral structures of **10** and **11** are shown in **Fig. 3**.

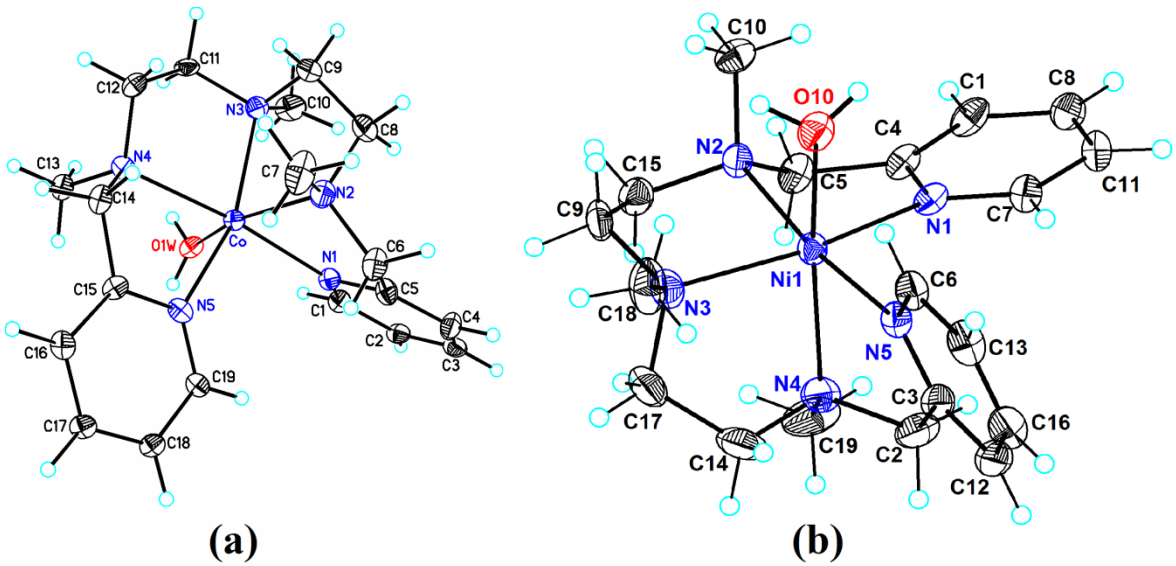

Fig. 3. Crystal structure of a) $[Co(N3Py2)(H_2O)]^{2+}$ **10** and b) $[Ni(N3Py2)(H_2O)]^{2+}$ **11** showing atom labelling scheme. Displacement ellipsoids are drawn at 50% probability except for H atoms which are shown as circles of arbitrary radius. The perchlorate anions are not shown for the clarity.

Further, powder X-ray diffractograms of **10-12** suggest that the compound **12** has ultimately a different structure than **10** and **11**. The catalytic activity of these three compounds was studied in the C-H activation of cumene and adamantane in presence of *m*-CPBA. The cumene gave 2-phenyl-2-propanol as the major product while adamantane afforded 1-adamantanol as the major product (**Scheme 5**). The effect of the counter anion on the product yields was investigated for all three complexes by replacing perchlorates of **10-12** with tetraphenylborates to obtain $[Co(N3Py2)(CH_3CN)](BPh_4)_2$ **13**,

$[Ni(N3Py2)(CH_3CN)](BPh_4)_2$ **14** and $[Cu(N3Py2)](BPh_4)_2$ **15**. The details of this investigation and the structural aspects of compounds **10-14** are discussed in this chapter.

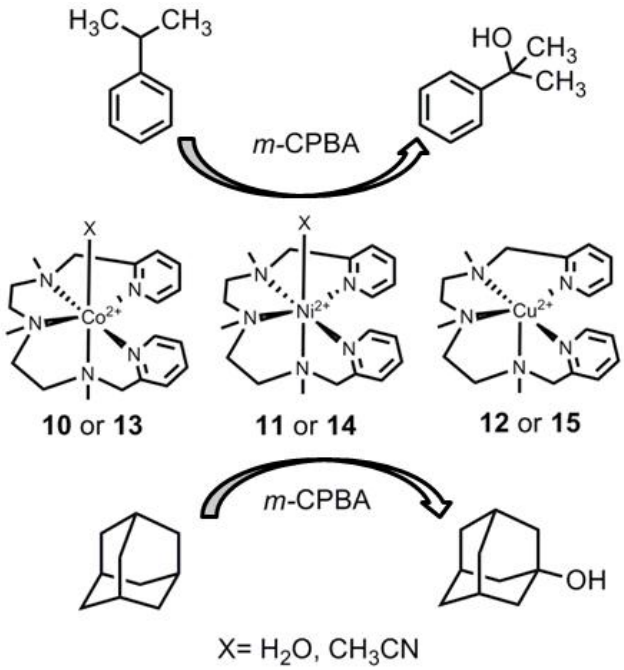

Scheme 5. The reaction scheme showing the conversion of cumene and adamantane to 2-phenyl-2-propanol and 1-adamantanol respectively by catalysts **10**–**12** and **13**–**15**.

Chapter VI: Mechanistic insights into the reactions of hydride transfer versus hydrogen atom transfer by a *trans*-dioxoruthenium(VI) complex

A wide range of chemical oxidations, as well as biological reactions, proceeds by formation of high valent ruthenium complexes.[33,34] This chapter discusses about the synthesis, characterisation and C-H activation reactions of a mononuclear high-valent *trans*-dioxoruthenium(VI) complex, *trans*-$[Ru^{VI}(TMC)(O)_2]^{2+}$ **16** (TMC = 1,4,8,11-tetramethyl-1,4,8,11-tetraazacyclotetra-decane)[35] and its reactivity study in hydride transfer and hydrogen atom transfer reactions.

Compound **16** has been characterized by UV-Vis, ESI-MS, 2D ^{1}H-NMR, EPR and CV techniques along with single crystal X-ray crystallography. The structure of **16** displays octahedral geometry with two oxo ligands located *trans* to each other (**Fig. 4**). In

this structure, one oxo ligand is located *trans* to the other oxo ligand, and two N-methyl groups of the TMC ligand point toward one oxo ligand and the other two N-methyl groups of the TMC ligand point toward the other oxo ligand symmetrically.

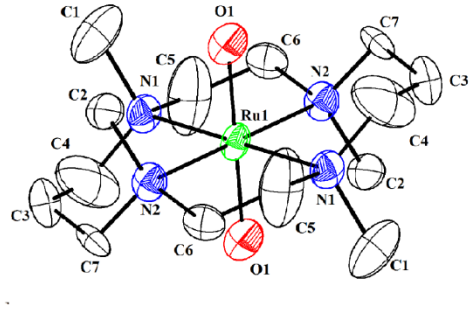

Fig. 4

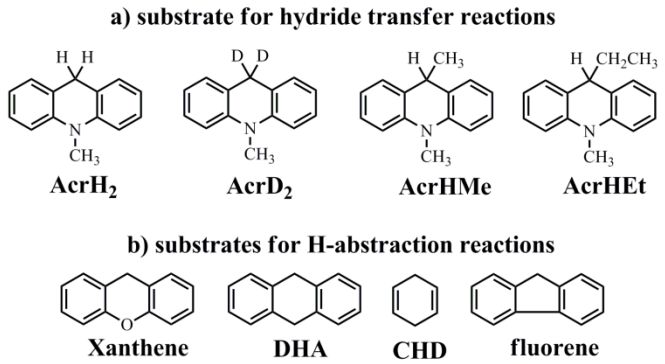

Scheme 6

Fig. 4. Crystal structure of *trans*-$[Ru^{VI}(TMC)(O)_2]^{2+}$ **16**. Displacement ellipsoids are drawn at 50% probability except for H atoms, are not shown for clarity. **Scheme 6** Substrate used for C-H activation reaction for the reactivity with compound **16**.

The reactivity of **16** was investigated in hydride transfer (HT) and hydrogen atom abstraction reactions with biologically relevant NADH (dihydronicotinamide adenine dinucleotide) analogues, 10-methyl-9,10-dihydroacridine ($AcrH_2$) and its derivatives and alkyl hydrocarbons in CH_3CN at 0 °C. For NADH analogues, the reactions were monitored by UV-Vis spectroscopy and reveals the formation of 10-methylacridinium ion ($AcrH^+$) quantitatively based on the full formation band at 358 nm with a concordant formation of $[Ru^{IV}(TMC)(O)]^{2+}$.[36] The second order rate constants determined by fitting of pseudo-first order kinetic data for the formation of $AcrH^+$ monitored at 358 nm which increased linearly with an increase in the concentration of AcH_2. With dideurated substrate ($AcrD_2$), a large kinetic isotope effect (KIE) was obtained. The HT reactions were investigated with other $AcrH_2$ derivatives such as AcrHMe (methyl acridine), AcrHEt (ethyl acridine) showed lesser reactivity than $AcrH_2$. A good linear correlation between the log rate constants of *trans*-$[Ru^{VI}(TMC)(O)_2]^{2+}$ and *p*-chloranil (Cl_4Q) was obtained.[37,38]

Based on these observations, a proton-coupled electron transfer (PCET), followed by a rapid electron transfer (ET) mechanism was proposed.

The reactivity of **16** was investigated in the oxidation of alkyl hydrocarbons having weak C-H bond dissociation energies (BDE) such as xanthene, dihydroanthracene, 1,4-cyclohexadiene and fluorene in CH_3CN at 35 °C. A large KIE value was obtained for the reaction of xanthene *versus* xanthenes-d_2 with complex **16**. Also the second order rate constants (k_{HAT}) decreased with increase in the C-H BDE of alkyl hydrocarbons and show a linear correlation between the second order rate constant and the C-H BDE values of the substrates. This observation along with large KIE indicates that the C–H bond activation of alkyl hydrocarbons proceeds via H-atom abstraction.

References

1. a) Breslow, R. *J. Biological. Chem*. **2009**, *284*, 1337. b) Breslow, R. *Acc. Chem. Res*. **1995**, *28*, 146.
2. Valdez, C. E.; Smith, Q. A.; Nechay, M. R.; Alexandrova, A. N.; *Acc. Chem. Res*. **2014**, *47*, 3110.
3. Punniyamurthy, T.; Velusamy S.; Iqbal J. *Chem. Rev.* **2005**, *105*, 2329.
4. Shilov, A. E.; Shul'pin, G. B. *Chem. Rev.* **1997**, *97*, 2879.
5. Woggon, W. -D. *Acc. Chem. Res.* **2005**, *38*,127.
6. Price, J. C.; Barr, E. W.; Glass, T. E.; Krebs, C.; Bollinger, J. M. Jr.; *J. Am. Chem. Soc.* **2003**, *125*,13008.
7. Proshlyakov, D. A.; Henshaw, T. F.; Monterosso, G. R.; Ryle, M. J.; Hausinger, R. P. *J. Am. Chem. Soc.* **2004**, *126*,1022.
8. Lee D., Lippard S. J., *J. Am. Chem. Soc.* **1998**, *120*, 12153.
9. Nam, W.; *Acc. Chem. Res*. **2007**, *40*, 522.
10. Nam, W. *Acc. Chem. Res.* **2015**, *48*, 2415.
11. Dhuri, S. N.; Lee Y. –M.; Seo, M. S.; Cho J.; Narulkar, D. D.; Fukuzumi, S.; Nam, W. *Dalton Trans.* **2015**, *44*, 7634.
12. Chiang, C.-W.; Kleespies, S. T.; Stout, H. D.;Meier K. K.; Li, P. Y.; Bominaar, E. L.; Que, L.,Jr.; Münck, E.; Lee W.-Z. J. *Am. Chem. Soc.* **2014**, *136*, 10846.
13. Leto, D. F.; Jackson, T. A. J. Biol. Inorg. Chem. **2014**, *19*, 1.
14. Baik, M. –H.; Newcomb M.; Friesner, R. A.; Lippard, S. J.; *Chem. Rev.* **2003**, *103*, 2385.
15. Nagataki, T.; Tachi Y.; Itoh S.; *Chem. Commun.*, **2006**, 4016.
16. Sankaralingam, M.; Balamurugan, M.; Palaniandavar M.; Vadivelu, P.; Suresh C. H. *Chem. Eur. J*. **2014**, *20*, 11346.
17. Hikichi, S.; Hanaue K.; Fujimura T.; Okuda, H.; Nakazawa, J.; Ohzu, Y.; Kobayashi, C.; Akita, M.; *Dalton Trans.* **2013**, *42*, 3346.

18. England J.; Britovsek, G. J. P.; Rabadia, N; White, A. J. P. *Inorg. Chem.* **2007**, *46*, 3752.
19. Narulkar, D. D.; Patil, A. R.; Naik, C. C.; Dhuri S. N. *Inorg. Chim. Acta*, **2015**, *427*, 248.
20. Nagataki, T.; Ishii, K.; Tachi, Y.; Itoh, S.; *Dalton Trans.* **2007,** 1120.
21. Bull, C.; Niederboffer, E. C.; Yoshida, T.; Fee, J. A. *J. Am. Chem. Soc*., **1991**, *113*, 4069.
22. Hearn, A. S.; Tu, C.; Nick, H. S.; Silverman, D. N. *J. Biol. Chem*, **1999**, *274*, 24457.
23. Cotruvo, J. A., Jr.; Stich, T. A; Britt, R. D.; Stubbe, J; *J. Am. Chem. So*c., **2013,** *135*, 4027.
24. Gunderson, W. A.; Zatsman, A. I.; Emerson, J. P.; Farquhar E. R., Que, L. Jr.; Lipscomb, J. D.; Hendrich, M. P.; *J. Am. Chem. Soc.*, **2008**, *130*, 14465.
25. McEvoy, J. P.; Brudvig G. W., **2006**, *106*, 4455.
26. Narulkar, D. D.; Srivastava, A. K.; Butcher, R. J.; Ansy, K. M.;. Dhuri, S. N; *Inorg. Chim. Acta.* **2017**, *467*, 405–414.
27. Cho, J.; Sarangi, R.; Kang, H. Y.; Lee, J. Y.; Kubo, M.; Ogura, T.; Solomon, E. I.; Nam, W.; *J. Am. Chem. Soc.*, **2010**, *132*, 16977.
28. Cho, J.; Sarangi, R.; Kang, H. Y.; Lee, J.Y.; Kubo, M.; Ogura, T.; Solomon, E. I.; Nam, W. *Nat. Chem.* **2009**, *1*, 568.
29. Keown, W.; Gary, J. B.; Stack, T. D. P. *J. Biol. Inorg. Chem.* **2017**, *22*, 289.
30. Chavez, F. A.; Mascharak, P. K. *Acc. Chem. Res*. **2000**, *33*, 539.
31. Hikichi, S.; Okuda, H.; Ohzu, Y.; Akita, M. *Angew. Chem. Int. Ed*. **2009**, *48*, 188.
32. Tano, T.; Ertem, M. Z.; Yamaguchi, S.; Kunishita, A.; Sugimoto, H.; Fujieda, N.; Ogura, T.; Cramer, C. J.; Itoh, S. *Dalton Trans*.**2011**, *40*, 10326.
33. Ohzu, S.; Ishizuka,T.; Hirai, Y.; Jiang, H.;Sakaguchi, M.;Ogura, T.;Fukuzumi, S.;Kojima, T. *Chem sci*, **2012**, *3*, 3421.
34. Lam,W. W. Y.; Man, W. L.; Lau, T.-C. *Coordination Chemistry Reviews* **2007**, 251, 2238.
35. Che, C.-M.; Wong, K.-Y.; Poon, C. -K.; *Inorg. Chem.*, **1985**, *24*, 1797.
36. Dhuri, S. N.; Seo, M. S.; Lee, Y.-M.; Hirao, H.; Wang, Y.; Nam, W.; Shaik, S. *Angew. Chem., Int. Ed.* **2008**, *47*, 3356.
37. Fukuzumi, S.; Kotani H.; Lee, Y.-M.; Nam W., *J. Am.Chem. Soc.,***2008**, *130*, 15134.
38. Jeong, Y. J.; Kang, Y.; Han, A.-R.; Lee, Y.-M.; Kotani, H.; Fukuzumi, S.; Nam, W.; *Angew. Chem., Int. Ed*. **2008**, *47*, 7321.

CHAPTER –I

Introduction

General Introduction

The transition metal and their compounds play vital roles in biology and are indispensable for a living system. Understanding the importance of metals in biological systems needs a multi-disciplinary approach which focuses on research at the interface of chemical science and biology.[1] The bioinorganic chemistry is an interdisciplinary science that has its main focus on the roles of the metals in biological systems.[2,3] Metals forms an integral part of enzymes and it is anticipated that nearly one-third of all enzymes known so far are metalloenzymes.[4] These metalloenzymes carry out biological transformations like water to oxygen, methane to methanol etc. that are extremely unfeasible to occur spontaneously.[4,5] The metal cofactors in the metalloenzymes are fixed by the amino acid residues in the protein framework which indirectly affects its functions.[6] The variety of reactions catalyzed by metalloenzymes operates at mild reaction conditions with high selectivity.[7] Understanding the reactions occurring in nature catalyzed by enzymes in detail is a complex phenomenon and therefore approach of biomimetic chemistry is useful.

The term biomimetic chemistry is coined by Ronald Breslow as the branch of science which mirrors the activity that humans have pursued for a long time: inventing new things inspired by what nature does.[8,9] The term biomimetics originates from the Greek words, ‘‘bios’’ (life, nature) and ‘‘mimesis’’ (imitation, copy) that has emerged in the 1960s.[10] The study in biomimetic chemistry involves the applications of the principles based on observations from nature for the invention of novel synthetic compounds for producing same functional goal rather than exact duplication of the structures. One of the major goals in the biomimetic chemistry is to understand the reactions catalyzed by the metalloenzymes so that their functional aspects can be understood to synthesize artificial catalysts. The oxidation is the most elementary processes that occur in nature that is catalysed by diverse metalloenzymes. For example, desaturation of fatty acids in plants,

biosynthesis of a *β*-lactam antibiotic, hydroxylation of methane etc. are some of the complex metabolic functions that need controlled oxidation of organic substrates and are mediated by metal at the active site.[11–15] The process of oxidation is also of great significance in industries and organic synthesis especially the C-H activation reactions. However, due to the inertness of chemical bonds, their functionalization is often not an easy task. The noble and late transition metals especially of the second-row transition metals have been effectively used in oxidative synthesis of organic compounds. However, the high cost, less abundance and toxicity puts up a restriction for their use in industries.[16] Hence first-row transition metals that are abundant and inexpensive are suitable alternative.[16]

The reactivity study of metalloenzymes can be understood by synthesising the model complexes which are structurally and functionally similar to the active site of the enzymes.[17] Besides this, such study also helps in determining the structural properties of the active centre which is often not feasible in case of the native systems. The metalloenzymes that are involved in dioxygen activation and oxygenation reactions are highly evolved at their active sites. These metalloenzymes are structurally diverse and contains heme, non-heme iron, mono- and dinuclear copper sites, a heteronuclear heme iron–copper site, and other metal sites.[18] Due to the easy accessibility of iron in nature and also its ability to exhibit multiple oxidation states, the iron-containing enzymes constitute a large number O_2-activating enzyme.[19] Besides iron, manganese and copper also constitute a large number of metalloenzymes. The study of other transition metals that can furnish supplementary chemical base for the understanding of mechanism of the reactions of metalloenzymes also lead to the development of artificial oxidation catalysis.[20]

As, the literature pertaining to the study under investigation is very exhaustive, the introductory Chapter only covers a background of the research carried out in recent years

by bioinorganic chemists. The literature survey is included Chapterwise in Chapter III-VI, which is relevant to the topic under investigation. The thesis deals with the investigations of several new transition metal complexes (Mn, Co, Ni, Cu and Ru) stabilized by non-heme ligands. The synthesized compounds have been thoroughly characterized and used in the oxidation reactions namely C-H activation, epoxidation and aldehyde deformylation. Wherever possible the attempts have been made to propose a mechanism based on the experimental evidences.

The iron enzymes which contain a macrocyclic porphyrin ligand with metal at the centre are known as heme enzymes, whereas non-heme enzymes constitute iron coordinated by non-porphyrinoid ligands.[19] The terminology "heme ligand" and "non-heme ligands" have also been often referred to the porphyrinoid and non-porphyrinoid ligands respectively. The cytochrome P450 and taurine/α-ketoglutarate dioxygenase (TauD) represent heme and non-heme iron oxygenase enzymes respectively wherein iron(IV/V)-oxo species proposed as the reactive intermediates in the catalytic cycle of C-H activation of alkanes.[21] Several heme-based complexes are extensively studied and paradigm is shifted to non-heme metal complexes in recent years. The four important high valent metal-oxygen intermediates namely metal-superoxo, metal-peroxo, metal-hydroperoxo and metal-oxo are identified and spectroscopic evidences have been provided in the enzymatic reactions. To give few representative examples, diiron^{III}-superoxo was characterized by EPR spectroscopy in the mammalian enzyme *myo*-inositol oxygenase (MIOX) that converts *myo*-inositol to D-glucuronate that proceeds by activation of dioxygen at a mixed valent diiron$^{II/III}$.[22] The manganese^{III}-superoxo (S = 5/2) species in manganese-substituted HPCD (Mn-HPCD) (homoprotocatechuate 2,3-dioxygenase) was also characterized by EPR spectroscopy.[23] The several Mn^{III}-peroxo intermediates successfully investigated and characterized in enzymes are accumulated in **Table 4.4** in

Chapter IV. The metal-hydroperoxo species have also been detected as a key intermediate in the enzymatic reactions. For example, the EPR and Mössbauer studies provide an evidence for the high spin (S = 5/2) iron^{III}-hydroperoxo species in benzoate 1,2-dioxygenase.[24] The end-on binding mode of the iron^{III}-hydroperoxo ligand is also evident from the crystal structure in dioxygen-bound carbazole 1,9a-dioxygenase that belongs to the member of the Rieske dioxygenase family.[25] The manganese^{IV}–oxo complexes that catalyze the four-electron oxidation of H_2O to O_2 are key intermediates in the oxygen-evolving complex (OEC) in photosystem II.[26–28] The mononuclear non-heme Fe^{IV}=O intermediate have been identified in the catalytic cycles of pterin-dependent hydroxylases like phenylalanine hydroxylases[29] and tyrosine[30], α-KG-dependent oxygenase such as propyl-4-hydroxylase[31] and taurine dioxygenase[32], halogenases enzymes like cytochrome c_3 halogenases[33,34] and SyrB2 halogenase.[35,36]

Based on the literature survey on these intermediates general synthetic route for generation of metal-oxygen intermediates through dioxygen activation is shown in shown in **Scheme 1.1**[37]. The mechanism proceeds by the binding of a kinetically inert ground state dioxygen with the metal at the active site to form a metal-superoxo intermediate, thus converting oxygen into reactive doublet state $O_2^{\bullet-}$. When the metal−superoxo species does not play a part directly in substrate oxidation reactions, they may reduce by an electron source can be converted to metal-peroxo. The metal-peroxo then can abstract a proton from the substrate to form metal-hydroperoxo species. The metal-hydroperoxo species can also be directly formed in one step by abstraction of a hydrogen atom. Subsequently the cleavage of O-O bond in metal-hydroperoxo species, homolytically or heterolytically results in the formation of high valent metal-oxo species. The dinuclear superoxo-bridged, peroxo-bridged and oxo-bridged high valent intermediates can also be generated by following the same sequential steps as shown in **Scheme 1.1**.

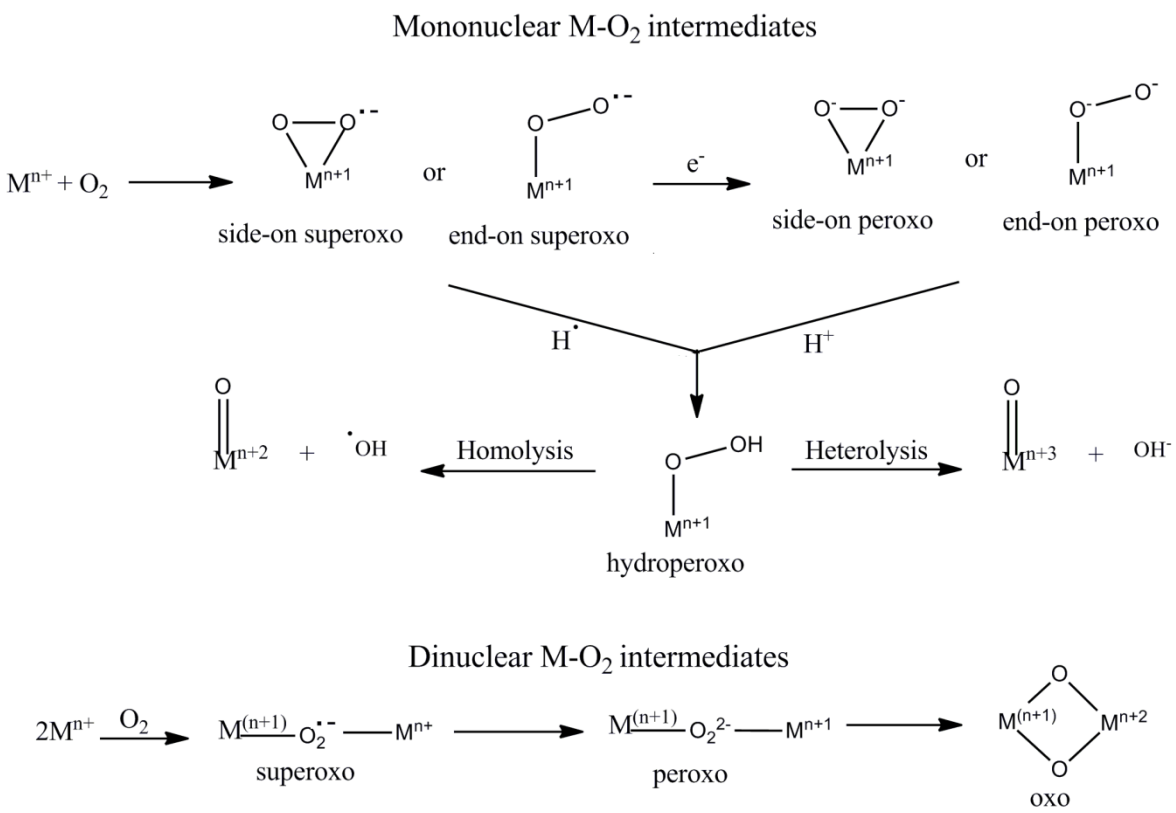

Scheme1.1 *The synthetic routes showing formation of reactive intermediates in the enzymatic reactions by the reaction of the dioxygen with mononuclear and dinuclear metal centre at the active sites.*

The systematic study of enzymatic reactions thus provides an appropriate skeleton to the general chemists to design and prepare transition metal based small-molecules based on their choice. Owing to the transient nature of these reactive species and sensitivity towards air, handling them is a skilful task. The active site of metalloenzymes constitutes primary and secondary coordination environment that facilitates activation of dioxygen and the reaction to proceed in a controlled manner. The secondary coordination spheres in enzymes constitute amino acids which do not participate in metal coordination however are involved in non-covalent interactions such as Van der Waals forces, hydrogen bonding, hydrophobic effect and electrostatic interactions that influence the activity of the active site. Therefore designing a small molecules model complexes would be a useful strategy.

Considering this, the number of biomimetic complexes of transition metals have been synthesised as model complexes which mimic the metal active sites of enzymes. The choice of the appropriate metal, coordination environment around the metal provided by the ligand and the selection of suitable oxidants and desirable reaction condition such as choice of solvent, temperature etc. are of fundamentally important in order to mimic a chemistry occurring in nature. The late first-row transition metals (Co, Ni and Cu) are considered as powerful oxidants in selective functionalization of C-H bonds.[38] The strong repulsion between the electronically rich late transition metal and the electron-rich oxo ligand provides hindrance for modelling metal-oxo (M = Co, Ni, Cu) cores in coordination complexes.[39] However, number model complexes of these metals have been prepared by employing a suitable synthetic strategy has been discussed in Section 3.1 and 5.1 of Chapter III and V respectively.

The metalloenzymes occurring in nature are structurally diverse, which basically composed of metal ion that is coordinated by various donor group of high molecular weight protein chain along with small exogenous ligand.[40] In an artificial system such coordination environment around the metal ion is mimicked by designing small ligand molecules containing hetero donor atoms such as N, O, S. The coordinated ligand after complexation with metal affects its activity by exerting the changes in electronic, steric and redox properties of metals. The wide range of ligand structures that exhibit flexibility in their coordination around different metals results in different oxidation state and spin state (no. of an unpaired electron) in the metal complex. This subsequently leads to the different structural properties that in turn results in different reactivity pattern depending on the ligand.[41] Hence the appropriate choice of ligands that is achieved by the proper synthetic skill becomes an important part in the synthesis of model complexes. From this viewpoint, there exists a considerable interest in employing smaller size non-heme ligands that can

mirror the vital features of the coordination environment without the inclusion of secondary coordination sphere provided by protein framework. In order to achieve an efficient oxidative catalytic reaction, a ligand should possess an oxidative resistant property and in addition they should be capable of stabilizing metals in their higher oxidation states which is a necessary factor in oxidative reaction. The **Scheme 1.2** shows the chemical structures of few reported non-heme ligands which have been frequently used by the several research groups. The tetramethylated macrocyclic cyclam ligands with a varying ring size (12-TMC, 13-TMC, 14-TMC, 15 -TMC)[42] have been employed to stabilize metal-oxo, metal-peroxo, metal superoxo and metal-hydroperoxo of first-row transition metals. The pentadentate ligand Bn-tpen[43] and N4Py[44] have often been employed to stabilize the metal-oxo complexes at even room temperature. The thermal stability of these high valent meta-oxygen complexes is governed by the topology of ligand and type of metal. For example, the high valent metal oxo complexes of Fe and Mn, supported by ligand TPA and BQCN are ($[Fe^{IV}(TPA)(O)]^{2+}$ and $[Mn^{IV}(BQCN)(O)]^{2+}$) are stable only at low temperatures,[45] while those supported by ligand N4Py and Bn-tpen ($[Fe^{IV}(N4Py)(O)]^{2+}$, $[Fe^{IV}(Bn\text{-}tpen)(O)]^{2+}$, $[Mn^{IV}(N4Py)(O)]^{2+}$ and $[Mn^{IV}(Bn\text{-}tpen)(O)]^{2+}$)[46,47] are very stable even at room temperature. In case of the macrocyclic ligand, size of the ring is a significant factor which influences the reactivity. For example in a comparative study of iron^{IV}-oxo complexes bearing macrocyclic ligands 13-TMC and 14-TMC showed more reactivity in case of $[Fe^{IV}(13\text{-}TMC)(O)]^{2+}$ due to the smaller size of the ring (13-TMC) in the oxidation reaction.[48] The similar observation has been observed for Co^{III}-peroxo species, in which $[Co^{III}(12\text{-}TMC)(O)_2]^{+}$ showed greater reactivity that possesses smaller ring size compared to $[Co^{III}(13\text{-}TMC)(O)_2]^{+}$ in nucleophilic aldehyde deformylation reaction.[49] Apart from these multidentate ligands, the small exogenous ligands are also found to affect the reactivity. For example axial ligand *trans* to the metal-

oxo showed the tremendous effect on the reactions such as OAT (oxygen atom transfer) and HAT (hydrogen atom abstraction) as observed incase of $[Fe^{IV}(O)(TMC)(X)]^{n+}$ and $[Ru^{IV}(O)(TMC)(X)]^{n+}$.[50–52,53,54] The axial ligand effect is al so observed in case of Mn-peroxo species.[55] The axial ligands found to influence the electrochemical property of the metal ions and thereby affecting its reactivity

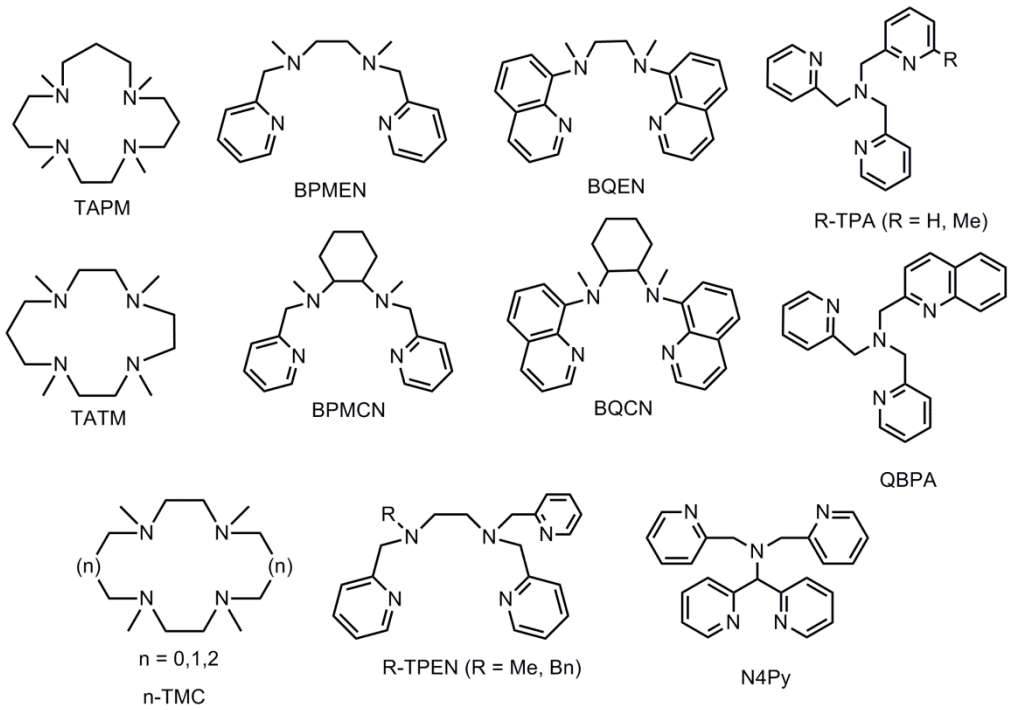

Scheme 1.2 *The structure of non-heme ligands that are frequently employed for stabilizing high valent metal-O_2 species.*

The presence of redox-inactive metal ions which functions as lewis acids was found to influence the reactivity of metal-oxo species in different oxidation reactions.[56–59] It is proposed that in the PS II, the redox-inactive Ca^{2+} ion promotes the formation of O-O bond to evolve dioxygen in the oxidation of water at the manganese-calcium active site.[60–63] The non-heme Fe^{IV}-oxo complex binding with Sc^{3+} ion was characterized by X-ray crystallography.[61] The binding of such ions to Mn^{IV}-oxo and Fe^{IV}-oxo showed enhanced reactivity in the oxidation reaction.[65,66]

The metal at the active site in the enzymes reacts with dioxygen and its reduced species (water, O_2^{2-}, O_2^{-}) to form a high valent metal-oxygen adduct. Inorder to mimic such activity different oxidants are employed like H_2O_2, peroxy acids like peracetic acid, *m*-CPBA, PhIO, KO_2, CAN in presence of water.[67] Hydrogen peroxide a greener oxidant have been employed to generate diverse reactive intermediate like end-on superoxo, side-on superoxo or peroxo,etc. Though ozone not been used must frequently, the first report of iron(IV)-oxo was generated by ozonolysis of iron cyclam-acetate[68]. PhIO acts as two electron terminal oxidants which have been utilized to generate a number of metal oxo-intermediate. The first spectroscopically characterized synthetic mononuclear iron^{III}-superoxo was generated by bubbling dioxygen into a THF solution of Fe^{II} complex i.e. Fe^{II}(BDPP) at -80 °C [BDPP is a deprotonated 2,6-bis(((S)-2-(diphenylhydroxymethyl)-1-pyrrolidinyl)methyl)pyridine ligand][69]. The manganese^{III}-linear end-on superoxo species was also generated by dioxygen generation.[70] There are few examples wherein metal-oxo reactive intermediates have also been generated using water as the oxygen source.[71–73] The reaction conditions and type of oxidants are important in determining the stability of the metal-oxo intermediates. $[Fe^{IV}(O)(N4Py)]^{2+}$, $[Fe^{IV}(O)(Bn\text{-}tpen)]^{2+}$ and $[Mn^{IV}(O)(BQEN)]^{2+}$ can be generated by reaction of their corresponding Fe(II) complexes with ceric ammonium nitrate (CAN) in presence of water as well as using PhIO but showed better thermal stability when generated from CAN. Here water serves as oxygen source and Ce^{IV} as one electron oxidant. It is one of the important findings as the source of the oxygen is derived from water.[45,46] The number of Mn^{III}-peroxo intermediates have been reported using different oxidants that are details are discussed in Chapter IV. The *m*-CPBA in presence of Ni(II) complexes have been used to carry out C-H activation reactions and are discussed in Chapter III.

The objectives of the present investigation are as follows

1. Designing new oxidative resistant ligands by using appropriate synthetic methodology followed by their purification.
2. The characterization of the ligands using IR and NMR spectroscopy.
3. Synthesis of the new transition metal complexes from the ligands.
4. The characterization of synthesized complexes by using techniques like CHN analysis, IR, UV-Vis spectroscopic techniques, ESI-MS spectrometry, single crystal X-ray diffractometry and electrochemical characterization by cyclic voltammetry and differential pulse voltammetry.
5. Investigation of the biomimetic role of complexes in the catalytic oxidations using different organic substrates in the presence of artificial oxidants like H_2O_2, PhIO, *m*-CPBA, KO_2,*t*-BuOOH, CAN etc.
6. Analysis of the products of oxidation reactions by chromatographic techniques (GC), thereby determining the efficiency of the catalysts.
7. Detection of the reactive intermediates (metal-oxygen species) in the oxidation reactions by UV-Vis spectroscopy.
8. The characterization of reactive intermediates by spectroscopic techniques

References

(1) Lippard, S. J. *J. Am. Chem. Soc.* **2010**, *132*, 14689–14693.

(2) Barton, J. K.; Karlin, K. D. *Curr. Opin. Chem. Biol.* **2001**, *5*, 165–167.

(3) Que L. Jr.; Banci, L. *Curr. Opin. Chem. Biol.* **2002**, *6*, 169–170.

(4) Rosenzweig, A. C.; Dooley, D. M. *Curr. Opin. Chem. Biol.* **2006**, *10*, 89–90.

(5) Lu, Y.; Yeung, N.; Sieracki, N.; Marshall, N. M. *Nature* **2009**, *460*, 855–862.

(6) Zhao, M.; Wang, H.-B.; Ji, L.-N.; Mao, Z.-W. *Chem. Soc. Rev.* **2013**, *42*, 8360–8375.

(7) Valdez, C. E.; Smith, Q. A.; Nechay, M. R.; Alexandrova, A. N. *Acc. Chem. Res.* **2014**, *47*, 3110–3117.

(8) Breslow, R. *J. Biol. Chem.* **2009**, *284*, 1337–1342.

(9) Breslow, R. *Chem. Biol.* **1998**, *5*, 27–28.

(10) Bar-Cohen, Y. *Biomimetics: Biologically Inspired Technologies*, 1st ed.; Taylor and Francis: California, USA, 2006; Vol. 9

(11) Loenarz, C.; Schofield, C. J. *Nat. Chem. Biol.* **2008**, *4*, 152–156.

(12) Kovaleva, E. G.; Lipscomb, J. D. *Nat. Chem. Biol.* **2008**, *4*, 186–193.

(13) Hausinger, R. P. *Crit. Rev. Biochem. Mol. Biol.* **2004**, *39*, 21–68.

(14) Costas, M.; Mehn, M. P.; Jensen, M. P.; Que, L., Jr., J. *Chem. Rev.* **2004**, *104*, 939–986.

(15) Solomon, E. I.; Brunold, T. C.; Davis, M. I.; Kemsley, J. N.; Lee, S.-K.; Lehnert, N.; Neese, F.; Skulan, A. J.; Yang, Y.-S.; Zhou, J. *Chem. Rev.* **2000**, *100*, 235–349.

(16) Shi, Z.; Zhang, C.; Tang, C.; Jiao, N. *Chem. Soc. Rev.* **2012**, *41*, 3381–3430.

(17) Rebilly, J.-N.; Colasson, B.; Bistri, O.; Over, D.; Reinaud, O. *Chem. Soc. Rev.* **2015**, *44*, 467–489.

(18) Nam, W. *Acc. Chem. Res.* **2007**, *40*, 465.

(19) Sahu, S.; Goldberg, D. P. *J. Am. Chem. Soc.* **2016**, *138*, 11410–11428.

(20) Suzuki, M. *Acc. Chem. Res.* **2007**, *40*, 609–617.

(21) Morimoto, Y.; Park, J.; Suenobu, T.; Lee, Y. M.; Nam, W.; Fukuzumi, S. *Inorg. Chem.* **2012**, *51*, 10025–10036.

(22) Xing, G.; Diao, Y.; Hoffart, L. M.; Barr, E. W.; Prabhu, K. S.; Arner, R. J.; Reddy,

C. C.; Krebs, C.; Bollinger, J. M. *Proc. Natl. Acad. Sci.* **2006**, *103*, 6130–6135.

(23) Gunderson, W. A.; Zatsman, A. I.; Emerson, J. P.; Farquhar, E. R.; Que, L., Jr.; Lipscomb, J. D.; Hendrich, M. P. *J. Am. Chem. Soc.* **2008**, *130*, 14465–14467.

(24) Wolfe, M. D.; Altier, D. J.; Stubna, A.; Popescu, C. V.; Münck, E.; Lipscomb, J. D. *Biochemistry* **2002**, *41*, 9611–9626.

(25) Ashikawa, Y.; Fujimoto, Z.; Usami, Y.; Inoue, K.; Noguchi, H.; Yamane, H.; Nojiri, H. *BMC Struct. Biol.* **2012**, *12*, 1–14.

(26) McEvoy, J. P.; Brudvig, G. W. *Chem. Rev.* **2006**, *106*, 4455–4483.

(27) Meyer, T. J.; Huynh, M. H. V.; Thorp, H. H. *Angew. Chem. - Int. Ed.* **2007**, *46*, 5284–5304.

(28) Pecoraro, V. L.; Hsieh, W.-Y. *Inorg. Chem.* **2008**, *47*, 1765–1778.

(29) Panay, A. J.; Lee, M.; Krebs, C.; Bollinger, J. M., Jr.; Fitzpatrick, P. F. *Biochemistry* **2011**, *50*, 1928–1933.

(30) Eser, B. E.; Barr, E. W.; Frantom, P. A.; Saleh, L.; Bollinger, J. M.; Krebs, C.; Fitzpatrick, P. F. *J. Am. Chem. Soc.* **2007**, *129*, 11334–11335.

(31) Hoffart, L. M.; Barr, E. W.; Guyer, R. B.; Bollinger, J. M., Jr.; Krebs, C. *Proc. Natl. Acad. Sci.* **2006**, *103*, 14738–14743.

(32) Riggs-Gelasco, P. J.; Price, J. C.; Guyer, R. B.; Brehm, J. H.; Barr, E. W.; Bollinger, J. M., Jr.; Krebs, C. *J. Am. Chem. Soc.* **2004**, *126*, 8108–8109.

(33) Galonić, D. P.; Barr, E. W.; Walsh, C. T.; Bollinger, J. M., Jr.; Krebs, C. *Nat. Chem. Biol.* **2007**, *3*, 113–116.

(34) Fujimori, D. G.; Barr, E. W.; Matthews, M. L.; Koch, G. M.; Yonce, J. R.; Walsh, C. T.; Bollinger, J. M., Jr.; Krebs, C.; Riggs-Gelasco, P. J. *J. Am. Chem. Soc.* **2007**, *129*, 13408–13409.

(35) Wong, S. D.; Srnec, M.; Matthews, M. L.; Liu, L. V.; Kwak, Y.; Park, K.; Bell, C. B.; Alp, E. E.; Zhao, J.; Yoda, Y.; Kitao, S.; Seto, M.;, Krebs, C; Bollinger, J.M., Jr., Solomon, E. I. Nature 2013, 499, 320–323.

(36) Matthews, M. L.; Krest, C. M.; Barr, E. W.; Vaillancourt, F. H.; Walsh, C. T.; Green, M. T.; Krebs, C.; Bollinger, J. M., Jr.; *Biochemistry* **2009**, *48*, 4331–4343.

(37) Ray, K.; Pfaff, F. F.; Wang, B.; Nam, W. *J. Am. Chem. Soc.* **2014**, *136*, 13942–13958.

(38) Ray, K.; Heims, F.; Pfaff, F. F. *Eur. J. Inorg. Chem.* **2013**, 3784–3807.

(39) Limberg, C. *Angew. Chem. Int. Ed.* **2009**, *48*, 2270–2273.

(40) Joshi, T.; Graham, B.; Spiccia, L. *Acc. Chem. Res.* **2015**, *48*, 2366–2379.

(41) Swart, M.; Gruden, M. *Acc. Chem. Res.* **2016**, *49*, 2690–2697.

(42) Cho, J.; Sarangi, R.; Nam, W. *Acc. Chem. Res.* **2012**, *45*, 1321–1330.

(43) Yoon, H.; Morimoto, Y.; Lee, Y.-M.; Nam, W.; Fukuzumi, S. *Chem. Commun.* **2012**, *48*, 11187–11189.

(44) Lee, Y. M.; Dhuri, S. N.; Sawant, S. C.; Cho, J.; Kubo, M.; Ogura, T.; Fukuzumi, S.; Nam, W. *Angew. Chemie - Int. Ed.* **2009**, *48*, 1803–1806.

(45) Sawant, S. C.; Wu, X.; Cho, J.; Cho, K.-B.; Kim, S. H.; Seo, M. S.; Lee, Y.-M.; Kubo, M.; Ogura, T.; Shaik, S.; Nam, W.; *Angew. Chem. Int. Ed.* **2010**, *49*, 8190–8194.

(46) Kaizer, J.; Klinker, E. J.; Oh, N. Y.; Rohde, J. U.; Song, W. J.; Stubna, A.; Kim, J.; Münck, E.; Nam, W.; Que, L., Jr.; *J. Am. Chem. Soc.* **2004**, *126*, 472–473.

(47) Wu, X.; Seo, M. S.; Davis, K. M.; Lee, Y.-M.; Chen, J.; Cho, K.-B.; Pushkar, Y. N.; Nam, W. *J. Am. Chem. Soc.* **2011**, *133*, 20088–20091.

(48) Hong, S.; So, H.; Yoon, H.; Cho, K.-B.; Lee, Y.-M.; Fukuzumi, S.; Nam, W. *Dalt. Trans.* **2013**, *42*, 7842–7845.

(49) Cho, J.; Sarangi, R.; Kang, H. Y.; Lee, J. Y.; Kubo, M.; Ogura, T.; Solomon, E. I.; Nam, W. *J. Am. Chem. Soc.* **2010**, 132, 16977–16986.

(50) Sastri, C. V.; Park, M. J.; Ohta, T.; Jackson, T. A.; Stubna, A.; Seo, M. S.; Lee, J.; Kim, J.; Kitagawa, T.; Münck, E.; Que, L., Jr.; Nam W. *J. Am. Chem. Soc.* **2005**, *127*, 12494–12495.

(51) Bukowski, M. R.; Koehntop, K. D.; Stubna, A.; Bominaar, E. L.; Halfen, J. A.; Münck, E.; Nam, W.; Que, L., Jr., *Science* **2005**, *310*, 1000–1002.

(52) Decker, A.; Solomon, E. I. *Angew. Chemie - Int. Ed.* **2005**, *44*, 2252–2255.

(53) Sastri, C. V.; Lee, J.; Oh, K.; Lee, Y. J.; Lee, J.; Jackson, T. A.; Ray, K.; Hirao, H.; Shin, W.; Halfen, J. A.; Kim, J.; Que, L., Jr; Shaik, S.; Nam, W. *Proc. Natl. Acad. Sci. U. S. A.* **2007**, *104*, 19181–19186.

(54) Dhuri, S. N.; Mi, S. S.; Lee, Y. M.; Hirao, H.; Wang, Y.; Nam, W.; Shaik, S. *Angew. Chem. - Int. Ed.* **2008**, *47*, 3356–3359.

(55) Annaraj, J.; Cho, J.; Lee, Y.-M.; Kim, S. Y.; Latifi, R.; de Visser, S. P.; Nam, W. *Angew. Chem.* **2009**, *121*, 4214 –4217.

(56) Pfaff, F. F.; Kundu, S.; Risch, M.; Pandian, S.; Heims, F.; Pryjomska-Ray, I.; Haack, P.; Metzinger, R.; Bill, E.; Dau, H.; Comba, P.; Ray, K. *Angew. Chemie - Int. Ed.* **2011**, *50*, 1711–1715.

(57) Lam, W. W. Y.; Yiu, S.-M.; Lee, J. M. N.; Yau, S. K. Y.; Kwong, H.-K.; Lau, T.-C.; Liu, D.; Lin, Z. *J. Am. Chem. Soc.* **2006**, *128*, 2851–2858.

(58) Yiu, S.-M.; Wu, Z.-B.; Mak, C.-K.; Lau, T.-C. *J. Am. Chem. Soc.* **2004**, *126*, 14921–14929.

(59) Miller, C. G.; Gordon-Wylie, S. W.; Horwitz, C. P.; Strazisar, S. A.; Peraino, D. K.; Clark, G. R.; Weintraub, S. T.; Collins, T. J. *J. Am. Chem. Soc.* **1998**, *120*, 11540–11541.

(60) Gatt, P.; Petrie, S.; Stranger, R.; Pace, R. J. *Angew. Chemie - Int. Ed.* **2012**, *51*, 12025–12028.

(61) Umena, Y.; Kawakami, K.; Shen, J.-R.; Kamiya, N. *Nature* **2011**, *473*, 55–60.

(62) Kanady, J. S.; Tsui, E. Y.; Day, M. W.; Agapie, T. *Science* **2011**, *333*, 733–736.

(63) Park, Y. J.; Ziller, J. W.; Borovik, A. S. *J. Am. Chem. Soc.* **2011**, *133*, 9258–9261.

(64) Fukuzumi, S.; Morimoto, Y.; Kotani, H.; Naumov, P.; Lee, Y.-M.; Nam, W. *Nat. Chem.* **2010**, *2*, 756–759.

(65) Park, J.; Morimoto, Y.; Lee, Y.-M.; Nam, W.; Fukuzumi, S. *J. Am. Chem. Soc.* **2011**, *133*, 5236–5239.

(66) Chen, J.; Lee, Y.-M.; Davis, K. M.; Wu, X.; Seo, M. S.; Cho, K.-Bin; Yoon, H.; Park, Y. J.; Fukuzumi, S.; Pushkar, Y. N.; Nam W. *J. Am. Chem. Soc.* **2013**, *135*, 6388–6391.

(67) Fukuzumi, S.; Kojima, T.; Lee, Y. M.; Nam, W. *Coord. Chem. Rev.* **2017**, *333*, 44-56.

(68) Grapperhaus C. A., Mienert B., Bill E., Weyhermüller T., Wieghardt K. *Inorg. Chem.* **2000**, *39*, 5306-5317.

(69) Chiang, C. W.; Kleespies, S. T.; Stout, H. D.; Meier, K. K.; Li, P. Y.; Bominaar, E. L.; Que, L., Jr.; Münck, E.; Lee, W. Z. *J. Am. Chem. Soc.* **2014**, *136*, 10846–10849.

(70) Liu, L.-L.; Li, H.-X.; Wan, L.-M.; Ren, Z.-G.; Wang, H.-F.; Lang, J.-P. *Chem. Commun.* **2011**, *47*, 11146–11148.

(71) Kotani, H.; Suenobu, T.; Lee, Y. M.; Nam, W.; Fukuzumi, S. *J. Am. Chem. Soc.* **2011**, *133*, 3249–3251.

(72) Wang, D.; Ray, K.; Collins, M. J.; Farquhar, E. R.; Frisch, J. R.; Gómez, L.; Jackson, T. A.; Kerscher, M.; Waleska, A.; Comba, P.; Costas M.; Que L., Jr;. *Chem. Sci.* **2013**, *4*, 282–291.

(73) Collins, M. J.; Ray, K.; Que, L., Jr. *Inorg. Chem.* **2006**, *45*, 8009–8011.

CHAPTER –II

Materials and methods

The Chapter II deals with the description of synthetic procedures, adopted for the preparations of starting precursors and the technical aspects of instruments used in the characterization of the compounds. The overview picture of the synthetic and characterization methods used in this work is depicted in **Scheme 2.1**.

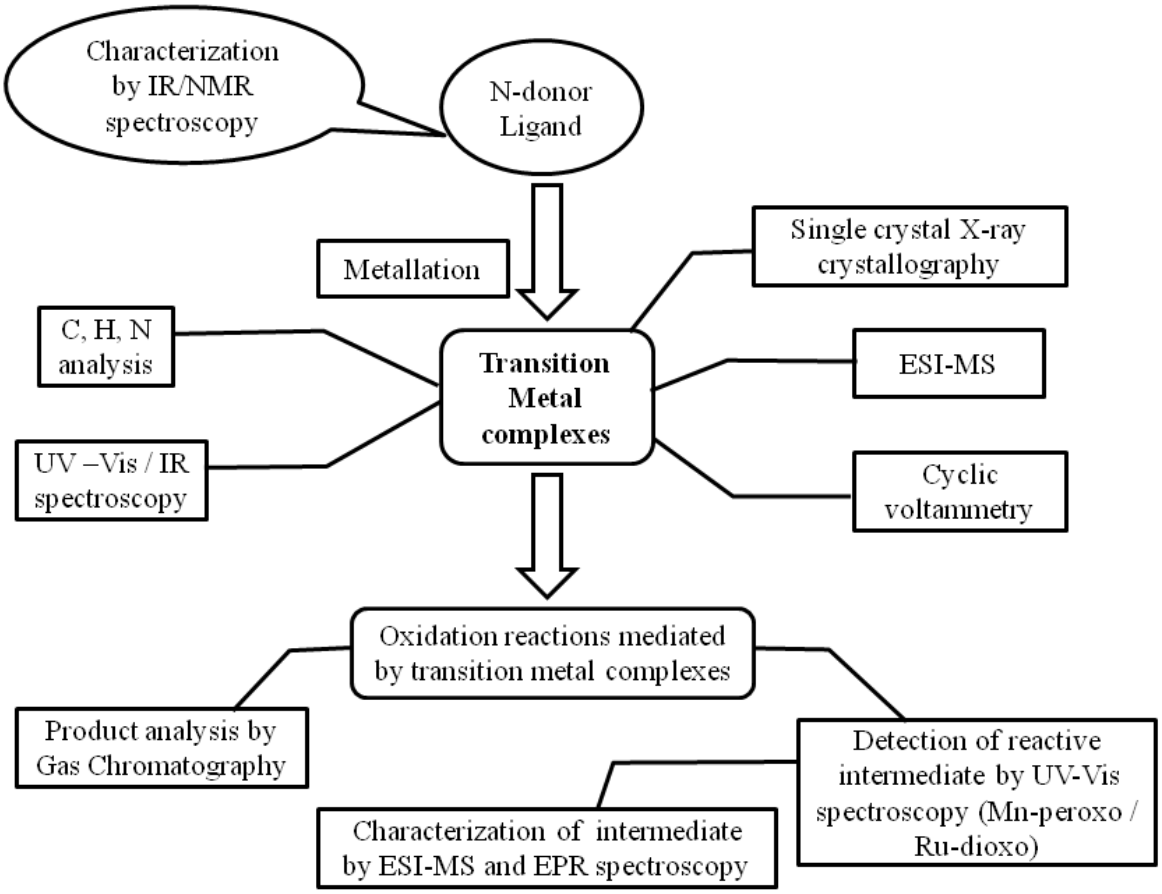

Scheme 2.1 *General overview of the methodology and different techniques utilised for characterization of new compounds.*

All the chemicals employed were of analytical reagent grade and was used without further purification unless specified. The exact amount of peroxide in commercially available 30 % H_2O_2 and *m*-CPBA was estimated from iodometric titrations.[1] The solvents were dried and distilled prior to use under the N_2 atmosphere.

2.1 Preparation of metal perchlorate hexahydrate $M(ClO_4)_2.6H_2O$

The transition metal complexes prepared in this study were obtained by reacting corresponding metal perchlorate salts with non-heme ligands. The metal $M(ClO_4)_2.6H_2O$ salts were prepared by following the previously reported procedure as given below[1]. To the suspension of metal carbonates in water, 70 % aq. perchloric acid was added slowly with stirring till the evolution of CO_2 ceases off. The mixture was filtered to remove unreacted carbonates and the clear solution was slowly evaporated to obtain crystalline product of corresponding metal perchlorate. The $Mn(ClO_4)_2.6H_2O$, $Ni(ClO_4)_2.6H_2O$, $Co(ClO_4)_2.6H_2O$, $Cu(ClO_4)_2.6H_2O$ was obtained as pale pink, green, reddish pink and dark blue coloured crystalline solid respectively.

Caution: *Perchlorates salts are potential explosive and should be handled in small quantity with care.*

2.2 Preparation iodosylbenzene (PhIO)

Iodosylbenzene was prepared by following a literature procedure.[3] A 15 mL of 3 N sodium hydroxide solution was added over five minutes to the vigorous stirring finely ground iodosobenzene diacetate (3.2 g, 0.010 moles) in a 100 mL. The lumps of solid which were forming in the beginning were broken down with a spatula for 15 minutes. The reaction mixture was allowed to stand for an additional 45 minutes to complete the reaction. After 45 minutes 10 mL of water was added and the mixture was allowed to stir vigorously for some more time and the crude iodosobenzene was separated by vacuum filtration. The collected solid was again triturated with 20 mL of water, filtered washed thoroughly using 20 mL water. The yellow solid was dried on the vacuum. The PhIO was purified by triturating with 10 mL of chloroform, filtered and dried in air.

2.3 Preparation of dideuterated xanthene-d_2

The dideuterated substrate xanthene-d_2, was prepared by a literature method.[4] Xanthene (0.50 g, 2.7 mmol) was reacted with NaH (0.20 g, 8.1 mmol) in DMSO-d_6 (3.0 mL) under an inert atmosphere. The deep red solution was stirred at room temperature for 8 h and then quenched with D_2O (5.0 mL). The formation of xanthene-d_2 was confirmed by recording NMR spectra which shows the absence of peak due to aliphatic CH_2 at δ 4.05 (s, 2H, 9-CH_2).

2.2 Reaction setup for the synthesis of metal complexes

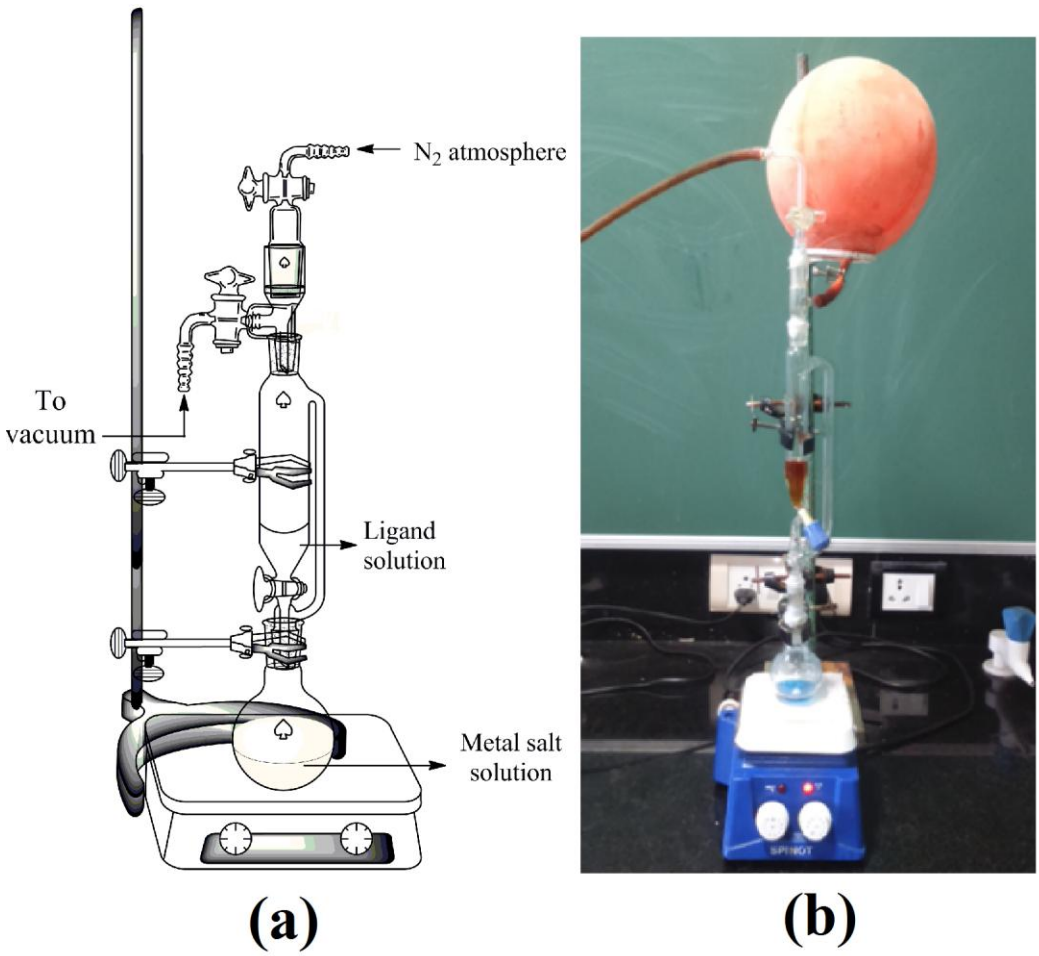

Figure 2.1 *Reaction setup for the synthesis of metal complexes from ligands under an N_2 atmosphere*

The reaction setup for the synthesis of metal complexes is as shown in **Figure 2.1** which is based on the similar principle of schlenk line. The ligand solution and the metal salt solution were placed in the pressure equalizing funnel and the round bottom flask respectively. The vacuum was applied to the reaction assembly by keeping the valve connected to the nitrogen bladder closed. The vacuum inside the reaction was maintained by closing the valve connected to the vacuum pump and the N_2 valve was opened to fill the reaction assembly with N_2 gas. This was repeated five times till the reaction assembly gets saturated with N_2 atmosphere. The ligand solution was then added to the metal salt solution with constant stirring in a suitable solvent.

2.3 Instrumentation techniques

2.3.1 Infrared spectroscopy (IR)

The infrared spectroscopy was used primarily for the characterization of ligands and the complexes. The synthesis of ligand is often a multi-step process which involves the change of functional group while proceeding from one step to another that can be traced out from IR spectra. The IR spectroscopy has been used to extract the information on the ligation behaviour of ligands in the metal complexes. When ligand coordinates, the original bands due to ligand often shift slightly to the lower wavenumbers.[5] The IR spectra of the ligands and the complexes were recorded by diluting the samples in finely ground KBr powder in the region of 4000-400 cm^{-1} using Shimadzu (IR Prestige-21) FT-IR spectrometer with a resolution of 4 cm^{-1}.

2.3.2 Nuclear magnetic resonance (NMR) spectroscopy

The NMR spectroscopy was employed for the characterization of the ligands synthesized in this work. The ^{1}H, ^{13}C NMR and DEPT spectra were obtained by dissolving

the ligand samples in $CDCl_3$ and recorded using Bruker Avance III 400 MHz NMR spectrometer.

2.3.3 Elemental analysis (CHN)

The percentage purity of the ligands as well as metal complexes synthesized in this investigation were determined by CHN analysis on Elementar Variomicro Cube CHNS Analyser using sulphanilamide as standard.

2.3.4 UV-Visible spectroscopy

The UV-Vis spectroscopy was used as the characterization method as it gives information about the electronic structure of metal complexes. All the reactions were performed in a 1 cm quartz cuvette. The formation of metal-based reactive intermediate (Mn- peroxo in Chapter IV and Ru- dioxo in Chapter VI) was monitored by using UV-Vis spectroscopy. The UV-Vis spectral features of this metal-oxygen species are distinctly different from parent metal complex upon reacting with H_2O_2 as the oxidant. The stability of these reactive intermediate was expressed in terms of t½ which is determined by monitoring the decay of the peak at λ_{max}. A further kinetic parameter such as rate constants were obtained in the reactivity of intermediate with the substrate by following decay of peak at highest intensity bands. The rate constants were determined under pseudo-first-order conditions (e.g., [substrate]/[intermediate] > 10), by fitting the changes in absorbance of λ_{max} at appropriate temperature. The pseudo first-order rate constants were obtained by fitting of the kinetic data at λ_{max}. The rate constants of the reactions were correlated with bond dissociations energies of the substrate.[6]

2.3.5 Electron spray ionization mass spectroscopy (ESI-MS)

The ESI-MS is used to characterize the metal complexes as well as the reactive intermediate (Mn-peroxo species discussed in Chapter IV and Ru-dioxo species in Chapter VI) in the solution. The ESI-MS of samples were recorded in CH_3CN using Applied Biosystem Matrix-assisted Laser Desorption Ionization Time-of-flight (MALDI-TOF) spectrometer and Thermo Finnigan (San Jose, CA, USA) LCQ^{TM} Advantage MAX quadrupole ion trap instrument, by infusing samples directly into the source at 20 μL/min using a syringe pump. The spray voltage was set at 4.7 kV and the capillary temperature was set depending on the type and stability of the sample.

2.3.6 Electron paramagnetic resonance (EPR) spectroscopy

The EPR spectra were recorded using an X-band Bruker EMX-plus spectrometer equipped with a dual mode cavity (ER 4116DM). Oxford Instruments ESR900 liquid He quartz cryostat with an Oxford Instruments ITC503 temperature and gas flow controller was used to lower down the temperatures. The experimental parameters for EPR spectra were as follows: microwave frequency = 9.648 GHz, modulation amplitude = 10 G, microwave power = 1.0 mW, modulation frequency 100 kHz, gain = 1 × 104, conversion time = 85.00 ms, measuring temperature = 5 K and time constant = 40.96 ms.

2.3.7 Single crystal X-ray diffractometry

The single crystals suitable for structure determination were obtained by vapour diffusion of diethyl ether into the acetonitrile solution of metal complexes. The single crystals suitable for X-ray studies were picked up using the glycerol loop and mounted directly on a Bruker SMART AXS and Bruker SMART APEX-II Duo diffractometer with Mo-K_α = 0.71073Å radiation. The CCD data were integrated and scaled using Bruker-

SAINT software package while SHEXTL V 6.12 was used for solving and refining the structures.[7] The non-hydrogen atoms were refined with the anisotropic displacement parameters while the hydrogen atoms were located at the calculated positions. In the crystal structure of **10**, the disordered atom positions (in perchlorate anions) were freely refined isotropically over two positions using similar distances and U-restraints. Although the H atoms were not geometrically positioned due to the relatively high degree of disorders in **16**, the structure shows a perfect octahedral geometry. The CIF file containing complete information on the structures have been deposited at The Cambridge Crystallographic Data Centre (CCDC) with CCDC numbers 948509, 1019725, 1517007, 1486163, 1532120, 1532118, 1532119 and 1049483 for compound **3**, **4**, **5**, **7**, **9**, **10**, **11** and **16** respectively and is available free of cost upon request (www.ccdc.cam.ac.uk/data_request/cif). The check CIF/PLATON reports of all the compounds characterized by single crystal X-ray crystallography are given in Appendix.

The XRD powder patterns of the compound were recorded on Rigaku Miniflex Diffractometer with Cu-Kα radiation.

2.3.8 The cyclic voltammograms (CV) and differential pulse voltammograms (DPV)

The CV and DPV were recorded using Electrochemical Workstation-CH Instrument, Inc. CHI6107 electrochemical analyzer. A glass vessel containing sample solution was equipped with a conventional three-electrode cell with a platinum working electrode (surface area of 0.3 mm^2), non-aqueous $Ag/AgNO_3$ (0.01 M) reference electrode and a platinum wire as a counter electrode. The platinum working electrode (BAS) was routinely polished with a BAS polishing alumina suspension and rinsed with CH_3CN before use. The sample solution was prepared in an organic solvent containing 0.1 M tetrabutylammonium hexafluorophosphate ($TBAPF_6$) as a supporting electrolyte. The

solutions were purged with N_2 gas for around ~30 min prior to each measurement. All potentials (vs. Ag/Ag^+) were reported to values vs. SCE (standard calomel electrode) by adding 0.29 V.[8]

2.3.9 Gas chromatography (GC)

In the catalytic oxidation reactions, the organic product analyses were carried out quantified using Agilent Technologies 6890N gas chromatograph and Shimadzu GC 2014 equipped with HP capillary column (30 m x 0.25 mm x 2.5 μM) and FID detector. The retention time and peak areas of the products were compared with the standard curves obtained using authentic samples and decane as an internal standard.

The detail synthetic procedures along with the characterization of the ligands and the new metal complexes employed in this study have been discussed in the subsequent Chapters. The chemical structure of the ligands and the metal complexes **1-16** is depicted in **scheme 2.2** and **2.3** respectively.

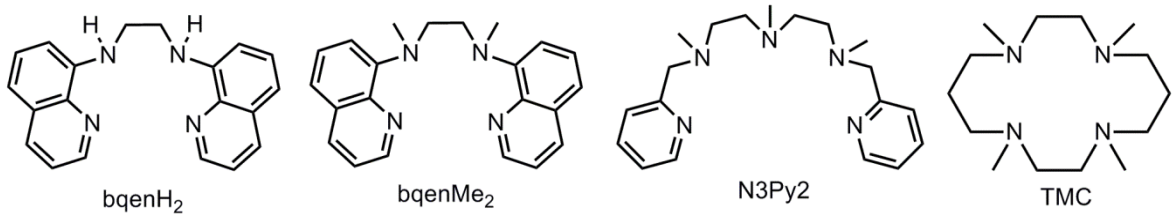

Scheme 2.2 *The chemical structures of all the ligands in this study.*

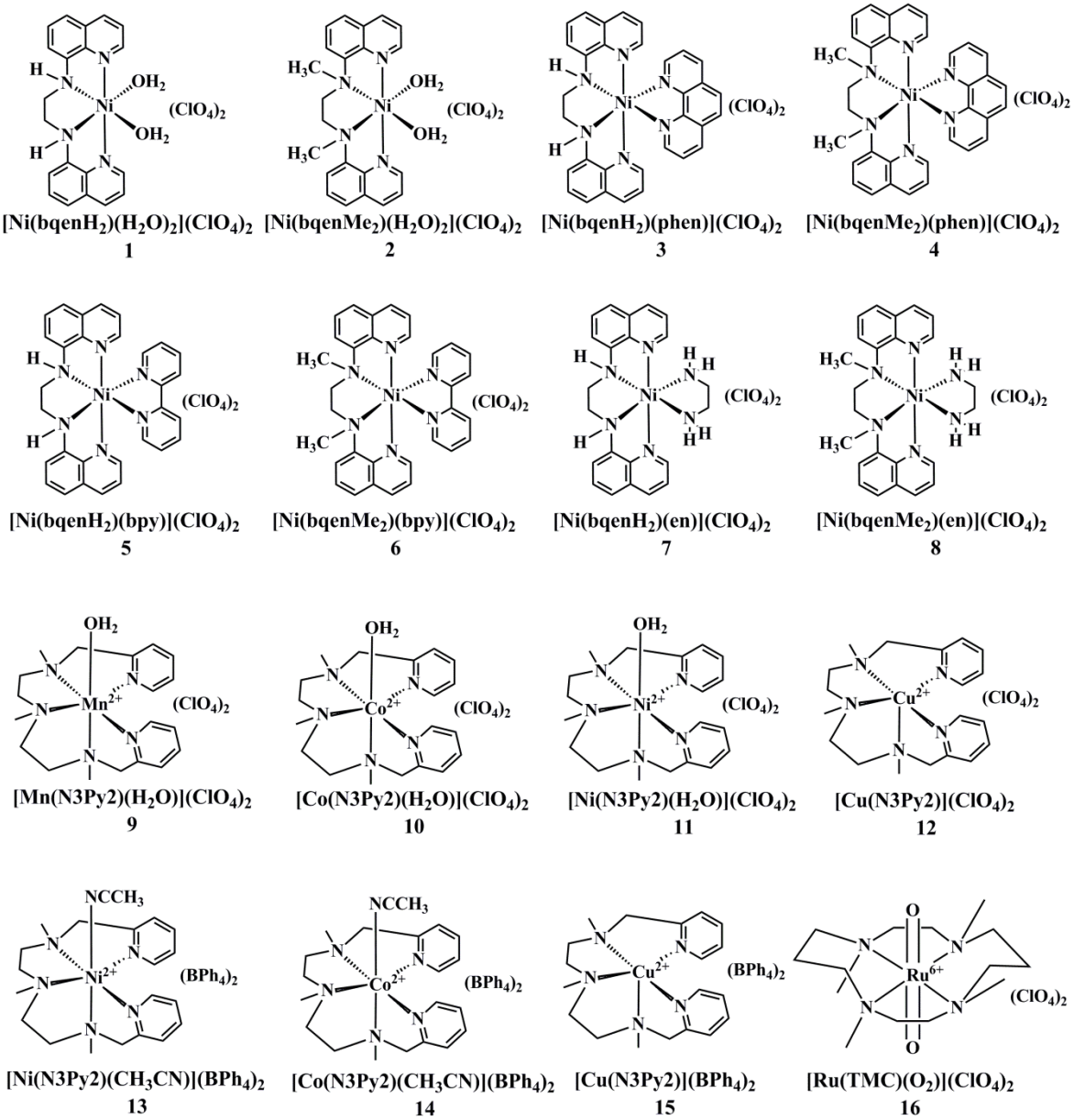

Scheme 2.3: *Chemical structures of the new compounds* ***1-16*** *discussed in the subsequent Chapters of the thesis.*

References

(1) Mendham, J; Denney, R. C.; Barnes, J. D.; Thomas, M.; Sivasankar, B. *Vogel' S Textbook of Quantitative Chemical Analysis,* sixth ed.; (Pearson Education, New Delhi) **2002**.

(2) Rahaman, S. H.; Ghosh, R.; Sarkar, S.K.; Ghosh, B.K. *Indian J. Chem.* **2005**, *44A*, 2474 -2479.

(3) Saltzman H., in *Organic Syntheses*, Vol. V (Eds: J. G. Sharefkin); Wiley, New York, 1973, 658.

(4) Sastri, C. V.; Lee, J.; Oh, K.; Lee, Y. J.; Lee, J.; Jackson, T. A.; Ray, K.; Hirao, H.; Shin, W.; Halfen, J. A.; Kim, J.; Que, L, Jr.; Shaik, S.; Nam, W. *Proc. Natl. Acad. Sci. U. S. A.* **2007**, *104*, 19181–19186.

(5) Nakamoto, K.: *Infrared and Raman Spectra of Inorganic and Coordination Compounds, Part B: Applications in coordination, organometallic, and bioinorganic chemistry,* 6th ed.; John Wiley, Hoboken, NJ) (2009).

(6) Luo, Y.-R., *Handbook of Bond Dissociation Energies in Organic Compounds*, CRC Press, New York, 2003.

(7) Sheldrick, G. M.; *SHELXTL/PC*. Version 6.12 for Windows XP, Bruker AXS Inc., Madison, WI, USA, 2001.

(8) Mann, C. K.; Barnes, K. K.; *Electrochemical Reactions in Non-aqueous Systems,* Marcel Dekker, New York, 1970.

CHAPTER –III

Synthesis and characterization of mononuclear nickel(II) complexes and their role in catalytic alkane hydroxylation

3.1 Introduction and literature

The selective oxidation of hydrocarbons under mild conditions is one of the difficult task for synthetic as well as the industrial chemists. In nature variety of enzymes containing iron active site like methane monooxygenases, cytochrome P450, bleomycin are known to catalyze several essential biological transformation.[1-7] For example, the oxidation of methane to methanol is catalyzed by soluble methane monooxygenase (sMMO) using molecular oxygen at ambient temperature.[4] Inspired by the roles of these enzymes, many bioinorganic chemists have focused the attention in isolation and characterization of the model complexes which could reproduce the functional aspects of the enzymes. The iron complexes have shown high promising catalytic activity in the oxidation of organic substrates. The iron complexes although popular in catalytic alkane hydroxylation reactions, the efficacy of other transition metal complexes like nickel(II) complexes have also investigated by few researchers. The, two enzymes containing nickel namely nickel superoxide dismutase (Ni-SOD) that catalyze the disproportion of superoxide to hydrogen peroxide and dioxygen.[20–24] and nickel dioxygenase that catalyzes oxidative C-C bond ruptures of acireductone, generating formic acid, CO and methylpropionate[25] are reported.

The several dinuclear-oxygen complexes like bis(μ-oxo)dinickel^{III}[26-30] bis(μ-superoxo)dinickel^{II}[30], bis(μ-alkylperoxo)dinickel^{II}[31], (peroxo)dinickel^{II}(μ-O_2)[32] and mononuclearnickel^{II}-superoxo[33] complex have been prepared and well characterised using different techniques. However their role in the oxidation reactions is not been investigated in detail except the oxidation of phenols and the C-H activation of 1,4 cyclohexadiene.[26] Some of these compounds undergo ligand degradation on oxidation and no good yields of oxidized products are reported.[26,29,31-33] The investigation of the gas phase reaction of the first-row metal-oxo species MO^+ with methane by Shröder, Schwarz and coworkers have demonstrated that the NiO^+ was the most ideal oxidant with respect to efficiency and the

alcohol product selectivity.[34] Itoh *et al*., for the first time showed that the mononuclear Ni(II) complex, [Ni(TPA)(OAc)(H_2O)](BPh_4) (TPA is tris(2-pyridylmethyl)amine), (OAc is acetate, BPh_4 is tetraphenylborate) is an efficient and robust catalyst selective for hydroxylation of alkanes using of *m*-chloroperbenzoic acid (*m*-CPBA) as an oxidant.[35] Their experiments also showed the high TON (turnover numbers) of products over related TPA complexes of iron(II), manganese(II), and cobalt(II) in the presence of *m*-CPBA as an oxidant. Later, a handful of nickel(II) compounds bearing tripodal N4, N3O, N3 ligands were isolated by the same group and used as the catalysts emphasizing on the different factors responsible for alkane hydroxylations.[36] The Ni(II) complexes with phenolate ligands, showed higher enhanced reactivity compared to corresponding pyridine donor ligands. Further the TON of products by catalysts containing tetradentate ligands was higher than that of tridentate ligands, and the catalytic efficiency of the nickel(II) complexes involving longer ethylene linker chain was lower than that of Ni(II) complexes with shorter methylene chains. The catalytic yields were also dependent on the counter anions. Based on their study they have proposed nickel-oxo type reactive intermediae although there is no direct evidence for the existence of such an intermediate. They also showed that the Ni(II) complexes obtained from tripodal bis and tris(phenolate) ligands, are capable of catalyzing the oxidation of cyclohexane to cyclohexanol up to 100 % conversion based on *m*-CPBA used as oxidant under solvent-free condition.[37] In recent studies Ni(II) complexes supported by pyridylalkylamine exhibits direct hydroxylation of benzene using hydrogen peroxide.[38] Hikichi and coworkers have structurally characterized nickel(II) alkyl-peroxo complex {$Ni^{II}(Tp^{ipr})$(OOtBu)], (Tp^{ipr} = hydrotris(3,5-di-2-propylpyrazolyl)borate and *t*-Bu is tert-butyl) which is responsible for the catalytic activity of the alkanes.[39] Later they have found out nickel(II) acyl-peroxo species responsible for the catalytic hydroxylation using *m*-CPBA as the oxidant.[40,41] K. Ray *et al*. trapped Ni^{III}=O,

Ni^{III}-OH intermediate and characterised by UV-Vis and ESR spectroscopic techniques in the reaction of Ni(II) complexes with *m*-CPBA.[42] Palaniandavar group isolated several Ni(II) complexes with tripodal and cyclic diamine tetradentate N4, pentadentate N5 and number of the mixed ligand and investigated their use in alkane hydroxylation reaction with *m*-CPBA oxidant.[43–46] Their study showed the importance of ligand denticity, lewis acidity of the Ni(II) centre and π back bonding and metal-ligand covalency parameter influencing the catalytic activity of Ni(II) complexes for the alkane hydroxylation reactions and the proposed existence of $[Ni^{II}\text{-}O^{\bullet}]^{+}$ as an intermediate in their study. In one of the recent studies, the chlorination of alkanes catalyzed by the $[Ni^{II}(Pytacn)(CF_3SO_3)_2]$ (Pytacn = 1-(2ppyridylmethyl)-4,7-dimethyl-1,4,7-triazanonane) in presence of NaOCl oxidant was studied.[47] The reaction of nickel(II) precursor i.e. $[Ni^{II}(L)]$ (L = 2,6-pyridinedicarboxamidate) with *m*-CPBA at low temperature revealed the formation of metastable oxyl-nickel(III) species [Ni(O•)(L)] which showed reactivity in the activation of C-H bonds, C=C and sulfide oxidation.[48,49] A recent study has reported terminal nickel (III)-oxygen adduct that performs hydrogen atom abstraction and oxygen atom transfer.[50,51] The studies in last decade has substantially enhanced the knowledge and understanding the roles pertaining nickel(II) complexes in alkane hydroxylation reactions.

Apart from this, superoxo and peroxo complexes of nickel are also identified and their reactivity in oxidation reactions has been investigated. The mononuclear Ni^{II}-superoxo and Ni^{III}-peroxo complexes have been synthesized from the Ni(II) complexes bearing common ligand (13-TMC) by the reaction with H_2O_2 in presence of base tetramethylammoniumhydroxide (TMAH) and triethylamine (TEA) respectively.[52] Here peroxo ligand is bound in a side-on fashion to the nickel(III) centre while superoxo ligand is bound to Ni(II) centre in an end-on fashion. The reactivity studies have shown that Ni^{II}-peroxo is an active oxidizing species in nucleophilic reactions and Ni^{II}-superoxo in

electrophilic reactions. The effect of ring size (TMC) is also studied in the formation of kind metal oxygen adducts. In one of the finding it was observed that nickel metal supported by 12-TMC ligand and 14-TMC affords side-on Ni^{III}-peroxo and end on Ni^{II}-superoxo complex respectively under an identical conditions.[53,54]

The above literature survey suggests that the nickel complexes supported by different ligand architecture are varied in terms of their structure, kind of donor atoms (N and O), denticity etc. Inspired by the chemistry of *N*-donor non-heme ligand stabilized transition metal complexes, we focused preparing the complexes of Ni(II) stabilized by $bqenH_2$ and $bqenMe_2$ which have previously been not reported. In this study we have chosen ligand $bqenH_2$ (*N,N′*-bis(8-quinolyl)ethane-1,2-diamine) and ligand $bqenMe_2$ (*N,N′*-dimethyl-*N,N′*-bis(8-quinolyl)ethane-1,2-diamine). The ligand $bqenH_2$ and $bqenMe_2$ are quinolyl based tetradentate non heme ligands synthesised for the first time by George J. P. Britovsek, with the objective of understanding the roles of their iron(II) in alkane oxidation reactions.[55] Thus the complexes of ligand $bqenMe_2$ with Fe(II) and Mn(II) have been later proved to the efficient catalyst in several organic oxidative transformations.[55–57] The first iron(II) complex $[Fe(bqenMe_2)(CF_3SO_3)_2]$ containing $bqenMe_2$ was reported to be an excellent catalyst for the oxidation of cyclohexane to cyclohexanol using H_2O_2 oxidant.[55] Nam and co-workers then demonstrated that $bqenMe_2$ complexes of manganese and iron such as $[Mn(bqenMe_2)(CF_3SO_3)_2]$ and $[Fe(bqenMe_2)(CF_3SO_3)_2]$ produce highly reactive intermediates that can oxidize alkanes and alcohols using peracetic acid.[56,57] Unlike $bqenMe_2$, the parent ligand $bqenH_2$ have less explored due to the fact that ligands with secondary nitrogen (-NH group) are prone to oxidative decomposition as reported for Ni(cyclam).[58] The several N donors as well as O donor ligands which have produce redox active environment for the metal and shown profound influence in the catalytic activity are shown in **Scheme 3.1**.

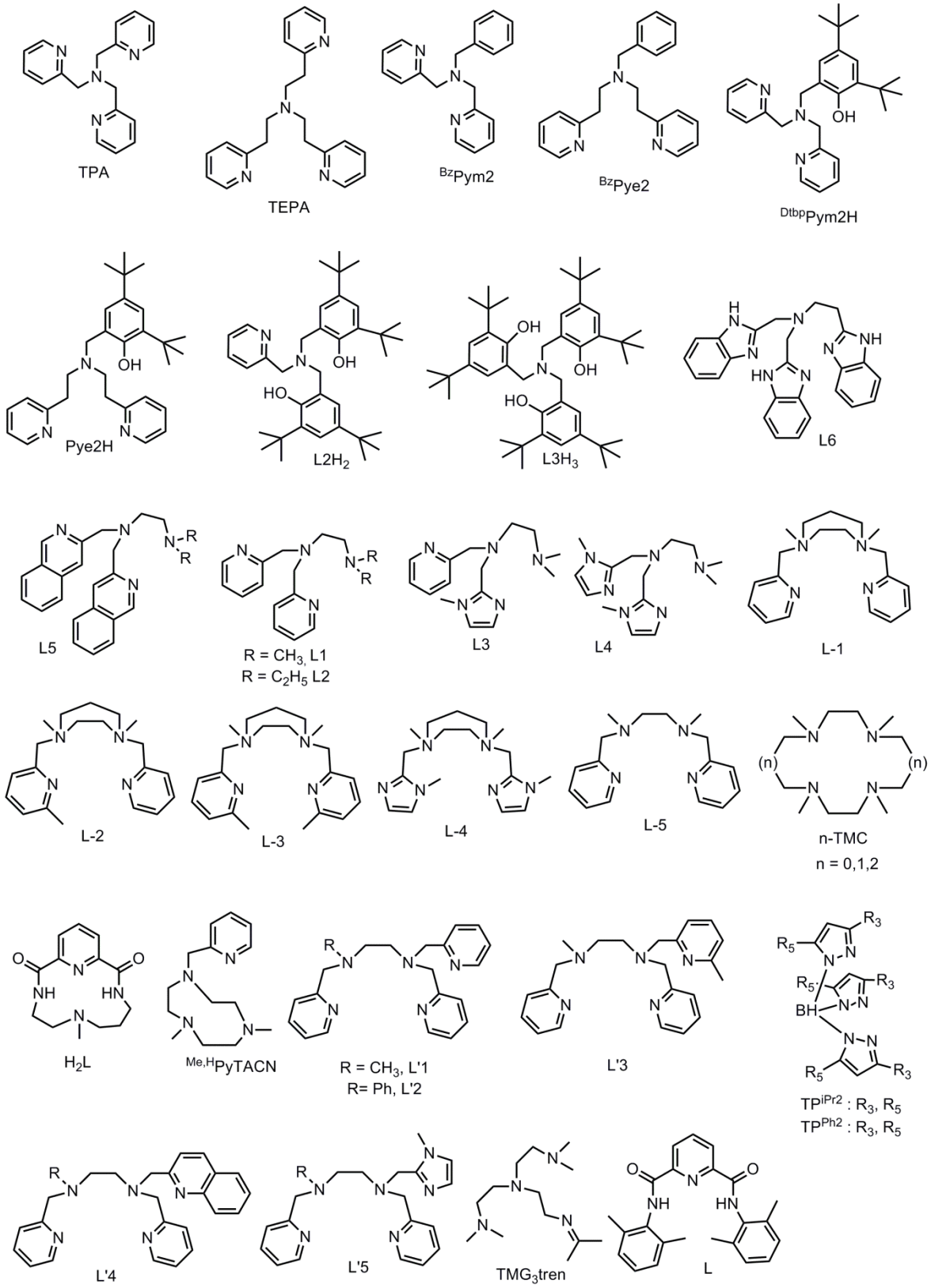

Scheme 3.1: *Diverse set of non-heme ligands supporting nickel complexes which catalyzes alkane hydroxylation reaction.*

3.2 Experimental details

The details of procedures which are employed for the synthesis of two ligands $bqenH_2$, $bqenMe_2$ and eight new complexes (**1-8**) of Ni(II) along with their characterization have been described in this section. The **Scheme 3.2** shows structures of ligands and the Ni(II) complexes that are synthesized in this study.

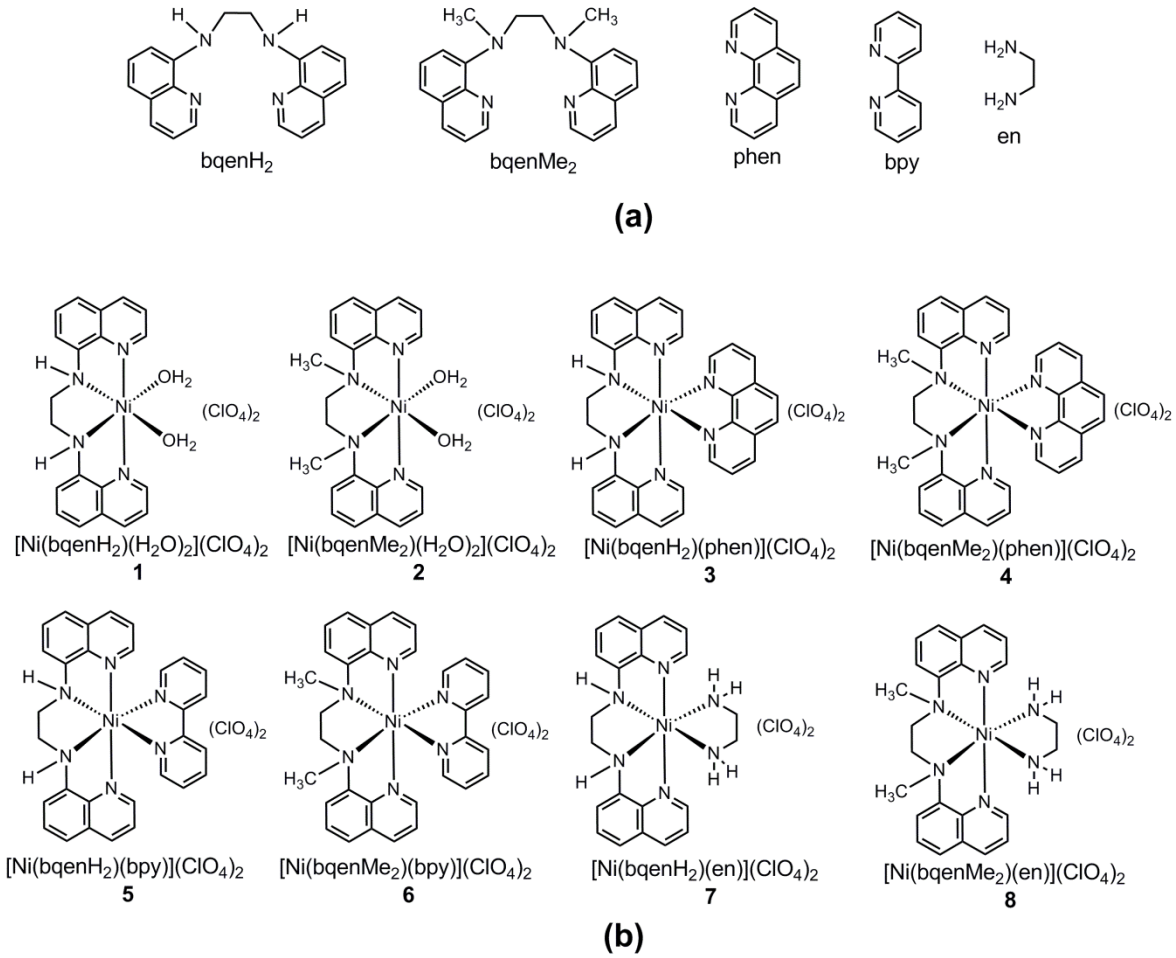

Scheme 3.2 *Structure of the (**a**)ligands employed in this work and (**b**) the corresponding Ni(II) complexes*

3.2.1 Synthesis of ligands $bqenH_2$, $bqenMe_2$ and Ni(II)complexes 1-8

3.2.1a Synthesis of N,N'-Bis(8-quinolin)ethane-1,2-diamine ($bqenH_2$)

The ligand $bqenH_2$ was prepared by following the literature procedure.[55] A mixture of 8-hydroxyquinoline (15.0 g, 103.3 mmol), ethylenediamine (3.1 g, 51.7 mmol), sodium metabisulphite (19.6 g, 103.3 mmol) and water (100 mL) was refluxed for about ~8 days at

110 ^{o}C. The reaction mixture was cooled at room temperature, then basified with aqueous sodium hydroxide solution (pH ~ 12) followed by extraction using dichloromethane (50 mL x 2). The solid formed after removal of dichloromethane was triturated with hot ethanol, filtered and then air dried. Yield of bqenH_2 (7.2 g, 44.0%). *Calc. for* $C_{20}H_{18}N_4$: C, 76.41; H, 5.77; N, 17.82. *Found*: C, 76.22; H, 5.62; N, 17.46 %. *IR-data* (KBr, cm^{-1}): 3383 ν(NH); 1526 ν(C=N); ^{1}*H NMR* ($CDCl_3$, ppm): δ 8.69 (d, 2H, *J* = 2.2 Hz, 2-QnH), δ 8.06 (d, 2H, *J* = 2.2, 4-QnH), δ 7.37 (m, 4H, 3-QnH and 6-QnH), δ 7.07 (d, 2H, *J* = 8Hz, 5-QnH), 6.77 (d, 2H, *J* = 4Hz, 7-QnH), 6.42 (s, 2H, NH), 3.75 (s, 4H, NCH_2).

3.2.1b Synthesis of N,N'-dimethyl-N,N'-bis(8-quinolin)ethane-1,2-diamine (bqenMe$_2$)

The ligand bqenMe_2 was prepared by following a procedure reported by our group[59] by a modification of the earlier procedure.[55] To a stirring yellow coloured THF solution (40 mL) of bqenH_2 (4.0 g, 12.7 mmol), about 21 mL of 37 % aqueous formaldehyde (7.6 g, 254.5 mmol) was added. The solution slowly turned red after ~5 min. To this mixture an aqueous sodium cyanoborohydride (1.6 g, 25.4 mmol) (10 mL) was added upon which the solution slowly turned to the original yellow colour. The reaction mixture was then stirred for 24 h. The THF solvent was removed on a rotary evaporator and the yellow solid was filtered from the remaining aqueous solution. The compound was washed with cold ethanol for several times and dried under vacuum. The yellow solid was recrystallized from hot ethanol. Yield of bqenMe_2 (3.2 g, 74.0 %). *Calc. for* $C_{22}H_{22}N_4$: C, 77.16; H, 6.48; N, 16.36. *Found*: C, 77.21; H, 6.64; N, 16.68 %. *IR-data* (KBr, cm^{-1})1526 ν(C=N). ^{1}*H NMR* ($CDCl_3$, ppm): δ 8.76 (d, 2H, *J* = 6 Hz, 2-QnH,), δ 8.07(d, 2H, *J* = 6 Hz, 4-QnH), δ 7.36 (m, 6H, 3-, 5- and 6-QnH), δ 7.05(d, 2H, *J* = 6 Hz, 7-QnH), δ 3.96 (s, 4H, N-CH_2), δ 3.06 (s, 6H, NMe). ^{13}C NMR ($CDCl_3$, ppm): δ 149.3 (*ipso*), 147.3, 142.6 (*ipso*), 136.2, 129.6, 126.6, 120.73, 119.8, 115.5, 54.1 (N-CH_2), 41.3 (N-Me).

3.2.1c Synthesis of $[Ni(bqenH_2)(H_2O)_2](ClO_4)_2$ (1)

Compound **1** was prepared by adding 5 mL CH_2Cl_2 solution of $bqenH_2$ (1.9 g, 6.0 mmol) to the 5 mL acetonitrile solution of $Ni(ClO_4)_2.6H_2O$ (2.2 g, 6.0 mmol). The mixture was stirred for 2 h at room temperature. The violet coloured crystalline powder obtained by slow diffusion of diethyl ether (10 mL) was isolated by filtration, washed with diethyl ether (10 mL) and finally air dried. Yield of **1** (3.0 g, 83 %). *Calc. for* $C_{20}H_{22}N_4Cl_2O_{10}Ni$: C, 39.51; H, 3.65; N, 9.21 %. *Found* C, 39.46; H, 3.33; N, 9.29 %. *IR-data* (KBr, cm^{-1}): 3265 ν(NH); 1518 ν(C=N); 1093,621 $\nu(ClO_4^{-1})$. *UV-Vis data*, λ_{max}, CH_3CN / nm ($\varepsilon/dm^3\ mol^{-1}cm^{-1}$): 229 (58500), 302 (10216), 314 (8725), 528 (13), 872 (12) *ESI-MS*: *m/z* = 227.0 (*calc*. 227.1) for $[Ni(bqenH_2)(CH_3CN)_2]^{2+}$ and *m/z* = 471.0 (*calc*. 471.0) for $[Ni(bqenH_2)(ClO_4)]^+$.

3.2.1d Synthesis of $[Ni(bqenMe_2)(H_2O)_2](ClO_4)_2$ (2)

Compound **2** was prepared following the similar procedure as in compound **1**. The ligand $bqenMe_2$ (2.1 g, 6.0 mmol) (2 mL CH_2Cl_2) was added to the CH_3CN solution (5 mL) of $Ni(ClO_4)_2.6H_2O$ (2.2 g, 6.0 mmol). The yield of light pink coloured compound **2** was (3.1 g, 81 %). *Calc. for* $C_{22}H_{26}N_4Cl_2O_{10}$ Ni: C, 41.54; H, 4.12; N, 8.81%. *Found* C, 41.16; H, 4.32; N, 8.65%. *IR-data* (KBr, cm^{-1}): 1518 ν(C=N); 1093, 621 $\nu(ClO_4^{-1})$. *UV-Vis data*, λ_{max}, CH_3CN / nm ($\varepsilon/dm^3\ mol^{-1}cm^{-1}$) 228 (57172), 302 (11249), 314 (9195), 528 (9), 872 (8). *ESI-MS*: *m/z* = 220.5 (*calc*. 220.6) for $[Ni(bqenMe_2)(CH_3CN)]^{2+}$ *m/z* = 241.0 (*calc*. 241.1) for $[Ni(bqenMe_2)(CH_3CN)_2]^{2+}$ and *m/z* = 499.1 (*calc*. 499.1) for $[Ni(bqenMe_2)(ClO_4)]^{2+}$

3.2.1e Synthesis of $[Ni(bqenH_2)(phen)](ClO_4)_2$ (3)

Compound **3** was prepared by adding 2 mL CH_3CN solution of 1,10-phenanthroline monohydrate (0.20 g, 1.0 mmol) to the 3 mL acetonitrile solution of **1** (0.61 g, 1.0 mmol).

The red coloured crystals were obtained after 4 days on slow diffusion of diethyl ether. Yield of **3** (0.6 g, 79 %). *Calc. for* $C_{32}H_{26}N_6Cl_2O_8Ni$: C, 51.10; H, 3.48; N, 11.17 %. *Found* C, 51.40; H, 3.71; N, 11.27 %). *IR-data* (KBr, cm^{-1}): 3269 ν(NH); 1518 ν(C=N); 1093,621 ν(ClO_4^{-1}). *UV-Vis data*, λ_{max}, CH_3CN / nm (ε/dm^3 $mol^{-1}cm^{-1}$) 227 (65207), 272 (30099), 294 (15734), 314 (7089), 589 (12), 793 (14) (ε/dm^3 mol^{-1} cm^{-1}). *ESI-MS*: *m/z* = 276.0 (*calc*. 276.1) for $[Ni(bqenH_2)(phen)]^{2+}$

3.2.1f Synthesis of $[Ni(bqenMe_2)(phen)](ClO_4)_2$ (4)

Compound **4** was prepared similarly as **3** by adding 1,10-phenanthroline monohydrate (0.20 g, 1.0 mmol) dissolved in 2 mL CH_3CN to the 2 mL CH_3CN solution of **2** (0.64 g, 1.0 mmol). The whitish pink crystals were obtained after slow diffusion of diethyl ether after two days. Yield of **4** (0.62 g, 76 %.) *Calc. for* $C_{36}H_{33}N_7Cl_2O_8Ni$: C, 55.66; H, 4.05; N, 11.94 %. *Found* C, 55.41; H, 4.17; N, 11.74 %. *IR-data* (KBr, cm^{-1}): 1518 ν(C=N); 1093,621 ν(ClO_4^{-1}). *UV-Vis data*, λ_{max}, CH_3CN / nm (ε/dm^3 $mol^{-1}cm^{-1}$) 225 (67439), 272 (23913), 296 (31074), 315 (6609), 501 (11), 795 (15). *ESI-MS*: *m/z* = 290.0 (*calc*. 290.1) for $[Ni(bqenMe_2)(phen)]^{2+}$

3.3.1g Synthesis of $[Ni(bqenH_2)(bpy)](ClO_4)_2$ (5)

Compound **5** was prepared by adding 2 mL CH_3CN solution of 2,2′-bipyridine (0.16 g, 1.0 mmol) to the 3 mL CH_3CN solution of **1** (0.61 g, 1.0 mmol**)**. The reddish-brown crystalline powder was obtained by the slow diffusion of diethyl ether after 5 days. Yield of **5** (0.7 g, 84 %). *Calc. for* $C_{30}H_{26}N_6Cl_2O_8Ni$: C, 49.48; H, 3.60; N, 11.54 %. *Found* C, 49.76; H, 3.35; N, 11.26 %. *IR-data* (KBr, cm^{-1}): 3228 ν(NH); 1518 ν(C=N); 1093, 621 ν$(ClO_4)^{-1}$. *UV-Vis data*, λ_{max}, CH_3CN / nm (ε/dm^3 $mol^{-1}cm^{-1}$): 230 (57596), 297 (24834), 308 (22673), 489 (12), 793 (9). *ESI-MS*: *m/z* = 264.1 (*calc*. 264.0) for $[Ni(bqenH_2)(bpy)]^{2+}$

3.2.1h Synthesis of [Ni(bqenMe$_2$)(bpy)](ClO$_4$)$_2$ (6)

Compound **6** was prepared by adding 2,2′-bipyridine (0.16 g, 1.0 mmol) in CH_3CN (2 mL) to the CH_3CN solution (2 mL) of **2** (0.64 g, 1.0 mmol) to obtain reddish coloured crystalline compound. Yield of **6** (0.6 g, 82 %). *Calc. for* $C_{32}H_{30}N_6Cl_2O_8Ni$: C, 50.83; H, 4.00; N, 11.11 %. *Found* C, 50.74; H, 4.14; N, 11.38%. *IR-data* (KBr, cm^{-1}): 1518 ν(C=N); 1093, 621 ν$(ClO_4)^{-1}$. *UV-Vis data*, λ_{max}, CH_3CN / nm (ε/dm^3 $mol^{-1}cm^{-1}$): 229 (56136), 283 (19013), 315 (7631), 528 (10), 872 (9) and *ESI-MS*: *m/z* = 264.1 (*calc*. 264.0) for $[Ni(bqenMe_2)(bpy)]^{2+}$

3.2.1i Synthesis of [Ni(bqenH$_2$)(en)](ClO$_4$)$_2$ (7)

Ethylenediamine, en (0.06 g, 1mmol) was added to the light violet CH_3CN solution of **1** (0.61 g, 1mmol) at room temperature. On addition of en, the colour of solution immediately changed to red. The solution was then stirred for ~ 30 min. On addition of diethyl ether into the reaction afforded us pale red coloured precipitate which was collected by filtration. The single crystals were obtained by dissolving the precipitate of the compound in CH_3CN followed by vapour diffusion of diethyl ether into the solution. After two days, the crystals isolated by decanting mother liquor, washed with diethyl ether and air dried. Yield of **7** (0.52 g, 82 %). *Calc. For* $C_{22}H_{26}N_6Cl_2O_8Ni$: C, 41.80; H, 4.15; N, 13.30 % *Found* C, 41.31; H, 3.87; N, 12.96%. *IR-data* (KBr, cm^{-1}): 3354, 3300 ν(NH); 3030-2825 ν(CH); 1093, 621 ν(ClO_4^{-1}). *UV-Vis data*, λ_{max}, CH_3CN / nm (ε/dm^3 $mol^{-1}cm^{-1}$): 227 (57263), 297 (11759), 315 (10169), 530 (12), 862 (9).

3.2.1j Synthesis of [Ni(bqenMe$_2$)(en)](ClO$_4$)$_2$ (8)

Compound **8** was prepared by following a similar procedure as mentioned for **7** by taking compound **2** in place of **1** to obtain a reddish colored powder. No single crystals

were obtained by further recrystallization. Yield of **8** (0.56 g, 85 %) *Calc. for* $C_{24}H_{30}N_6Cl_2O_8Ni$: C, 43.67; H, 4.58; N,12.73% *Found* C, 43.39; H, 4.36; N, 12.86%.). *IR-data* (KBr, cm^{-1}): 3354, 3300 ν(NH); 3030-2825 ν(CH); 1093, 621 ν(ClO_4^{-1}). *UV-Vis data*, λ_{max}, CH_3CN / nm (ε/dm^3 $mol^{-1}cm^{-1}$): 227 (56316), 297 (11798), 530 (12), 862 (9).

3.3 Results and discussion

3.3.1 Description for the synthesis of ligands

The ligand bqenH_2 was prepared by following a known procedure reported by *Britosvek*[55] as described in detail in S*ection 3.2.1a*. For the synthesis of ligands with the amine nitrogen donor groups, the alkylation of R_2N-H is an important step. However in certain cases such reactions are often tedious which is normally carried out using an alkylating agent and strong bases such as sodium hydride or *n*-butyllithium. These reactions need special conditions such as dry solvents, inert atmospheres and low temperature. The ligand bqenMe_2 was earlier reported from the reaction of parent secondary amine bqenH_2, *n*-butyllithium and methyl iodide at -78 ^oC[55] (**Scheme 3.3**).

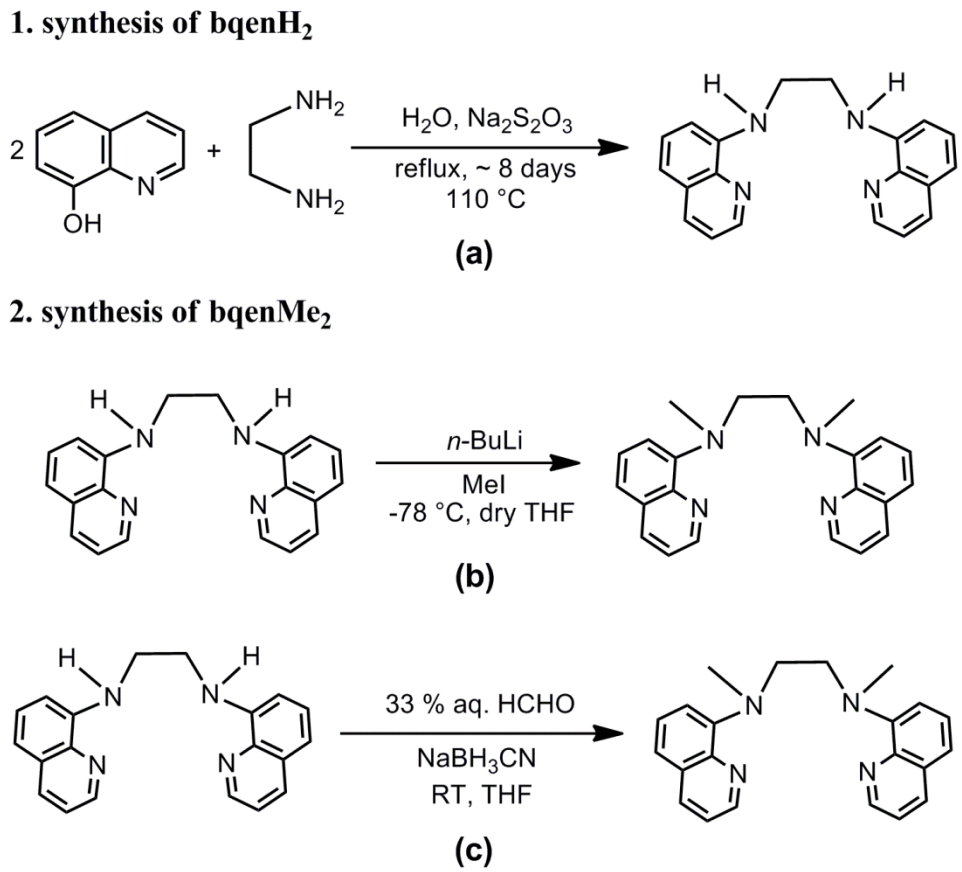

***Scheme 3.3**. The synthetic route for the preparation of (a) bqenH_2 and (b) bqenMe_2 by reported method (c) bqenMe_2 reported by current method.*

The alternative method of reductive methylation is Clarke-Eschweiler reaction using formaldehyde and formic acid.[60] However this reaction did not afford us desired product ($bqenMe_2$) probably due to the occurrence of the multiple side reactions as reported earlier.[61] In the present work, we have synthesized $bqenMe_2$ by a simple method that involves the reductive methylation of $bqenH_2$ using aqueous formaldehyde and sodium cyanoborohydride at room temperature in THF (**Scheme 3.3**) (Section 3.2.1b). This method has been earlier employed for the methylation of unreactive amines.[62] Both the ligands $bqenH_2$ and $bqenMe_2$ were characterized by C, H, N analysis; infrared and NMR spectroscopic techniques (^{1}H and ^{13}C NMR spectroscopy).

3.3.2 Characterization of $bqenH_2$ and $bqenMe_2$ by IR and NMR spectroscopy

The infrared spectroscopy is the most readily available techniques to predict the conversion of the secondary amine to a tertiary amine group. The secondary amine group shows the presence bands in the region 3000-3500 cm^{-1} whereas tertiary amines do not show any bands in this region. The infrared (IR) spectrum of $bqenMe_2$ shows the absence of N-H vibration that is observed at ~3385 cm^{-1} for $bqenH_2$ due to N-H group (**Figure 3.1**). This observation indicates that, the H atoms on two N atoms in $bqenH_2$ are replaced by the $–CH_3$ groups. The presence $–CH_3$ groups on the nitrogen atoms were further confirmed by ^{1}H and ^{13}C NMR spectroscopy and the corresponding peaks are assigned (**Figure 3.2-3.5**). The N-H peak observed at δ 6.415 in the ^{1}H NMR spectrum of $bqenH_2$ is not observed in NMR spectrum of $bqenMe_2$. At the same time there is the appearance of a peak at δ 3.06 corresponding to *N-CH₃* in the ^{1}H NMR spectrum $bqenMe_2$.

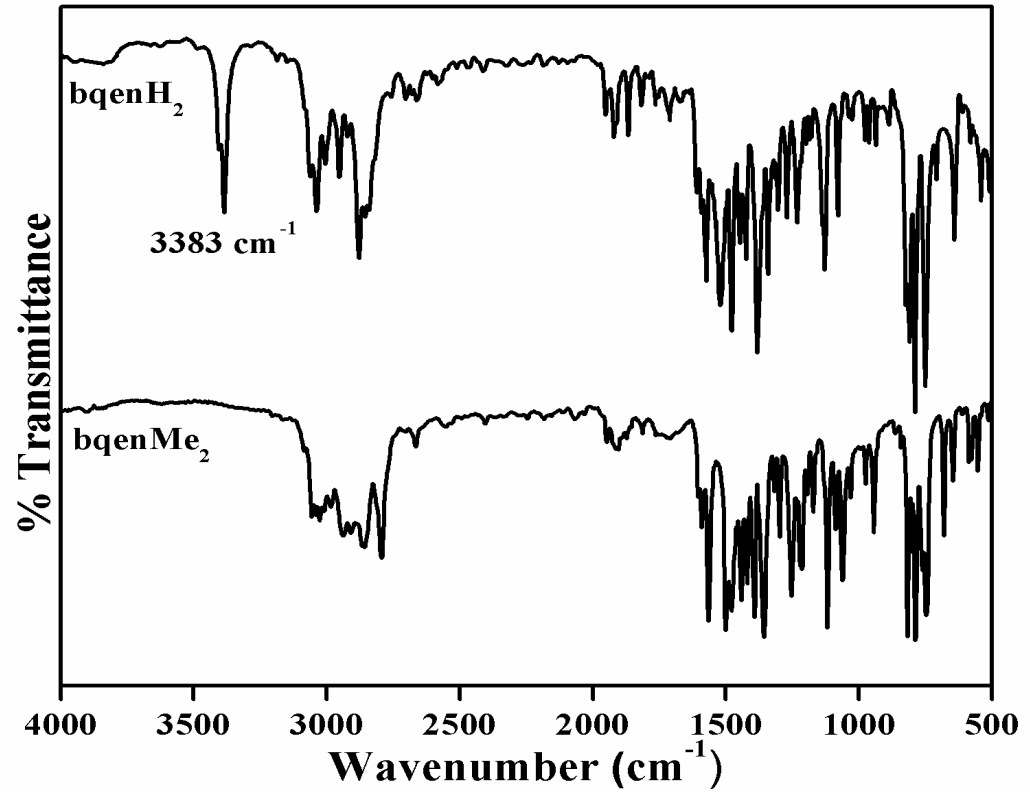

Figure 3.1 *Infrared spectra of ligand bqenH$_2$ and bqenMe$_2$*

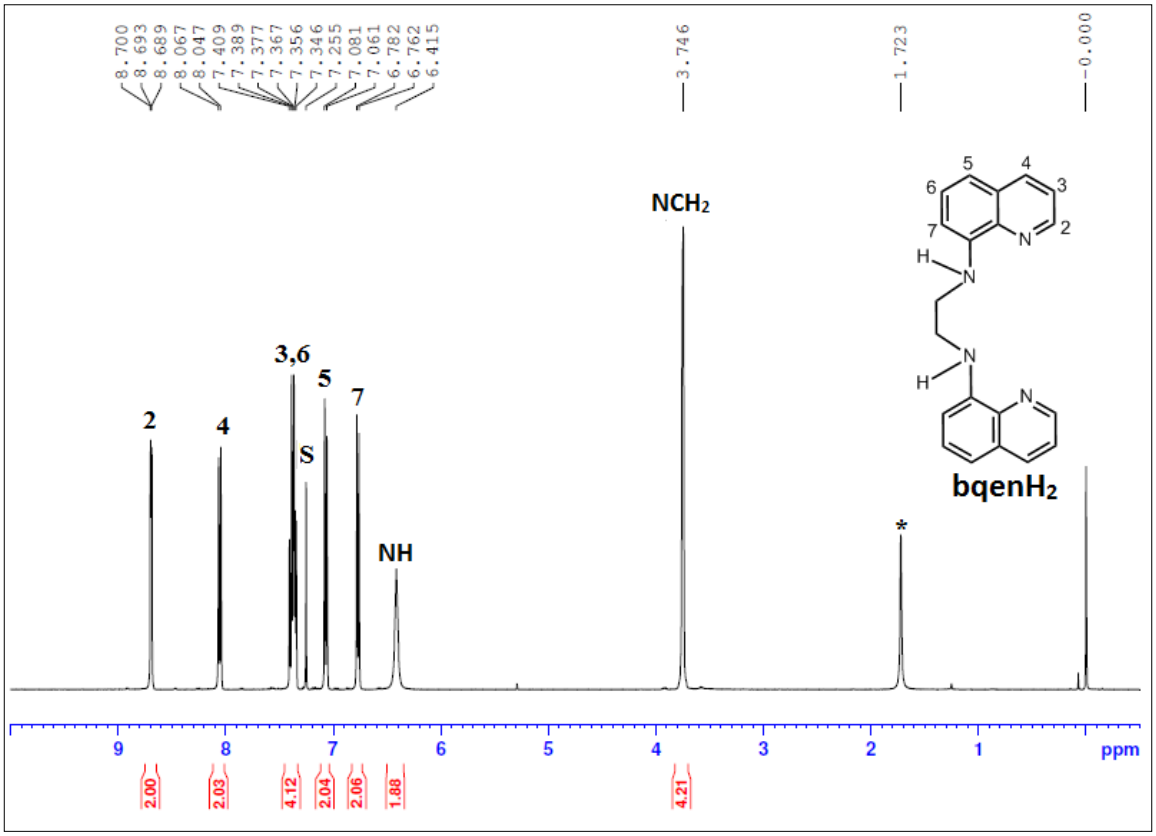

Figure 3.2 *The ^{1}H NMR of bqenH$_2$ in CDCl$_3$ (S stands for solvent peak and asterisk (*) stand for moisture peak).*

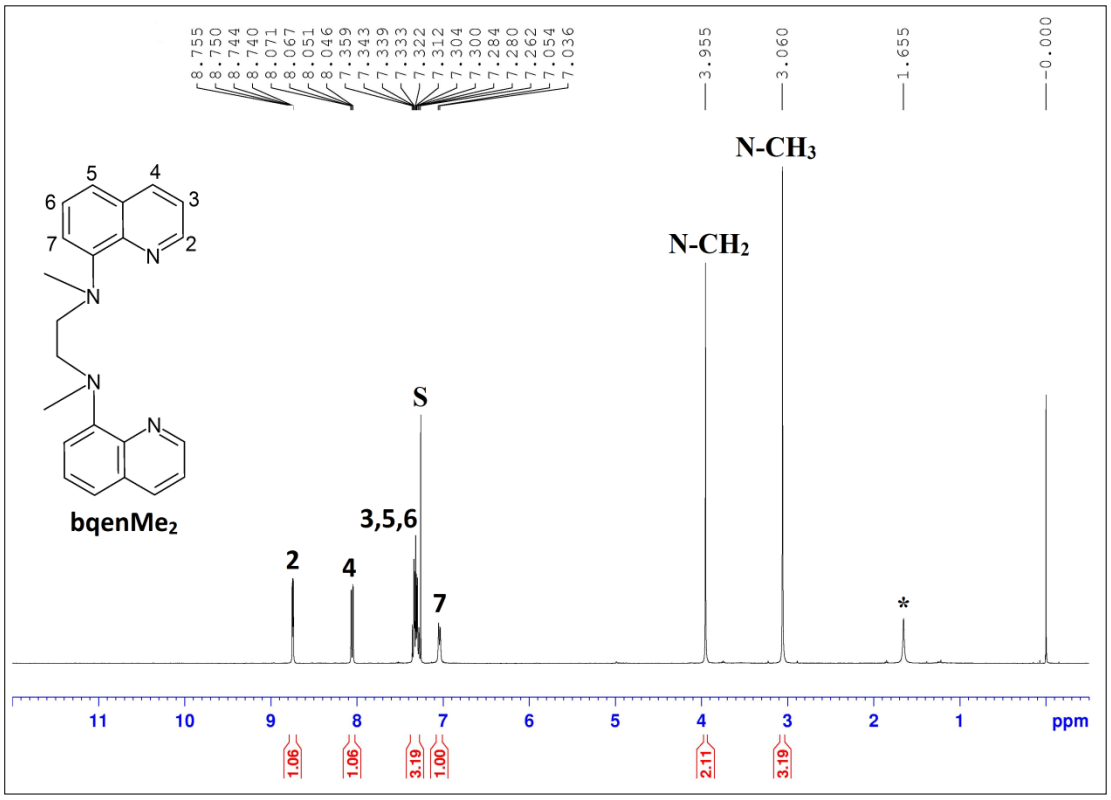

Figure 3.3 *The ^{1}H NMR spectrum of bqenMe$_2$ in CDCl$_3$ (S stands for solvent peak and asterisk (*) stand for moisture peak).*

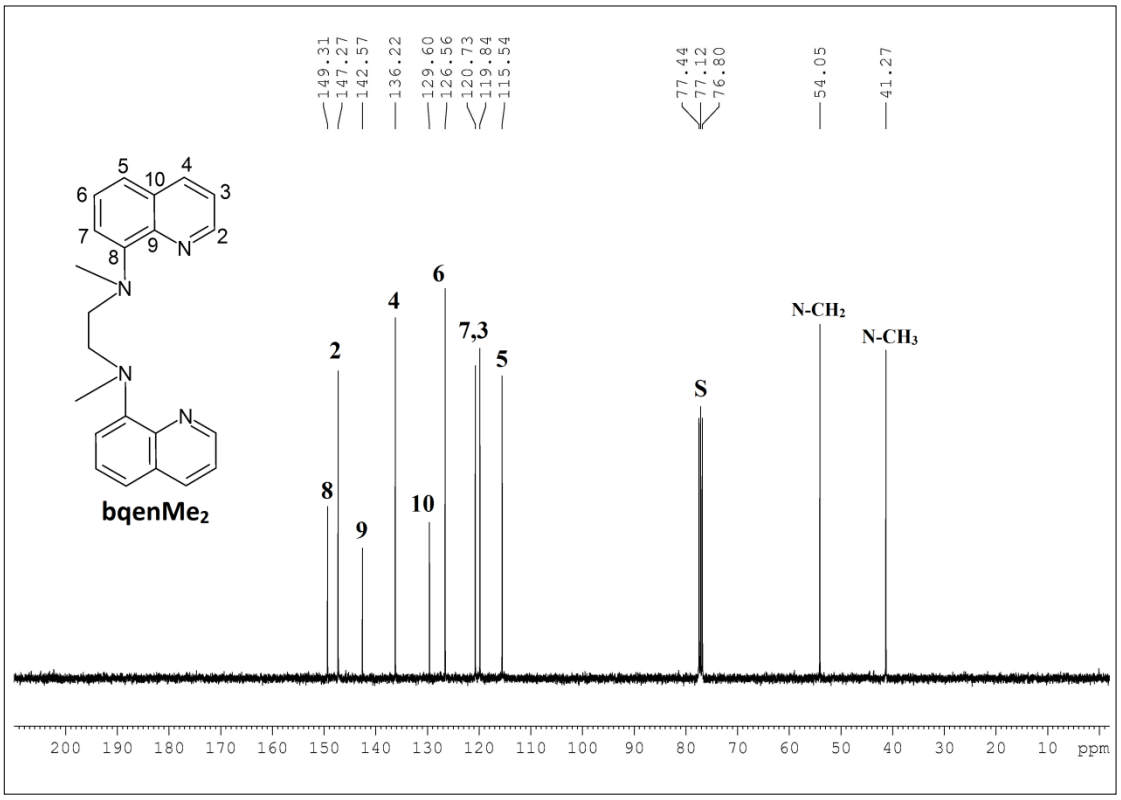

Figure 3.4 *The ^{13}C NMR of bqenMe$_2$ in CDCl$_3$ (S stands for solvent peak).*

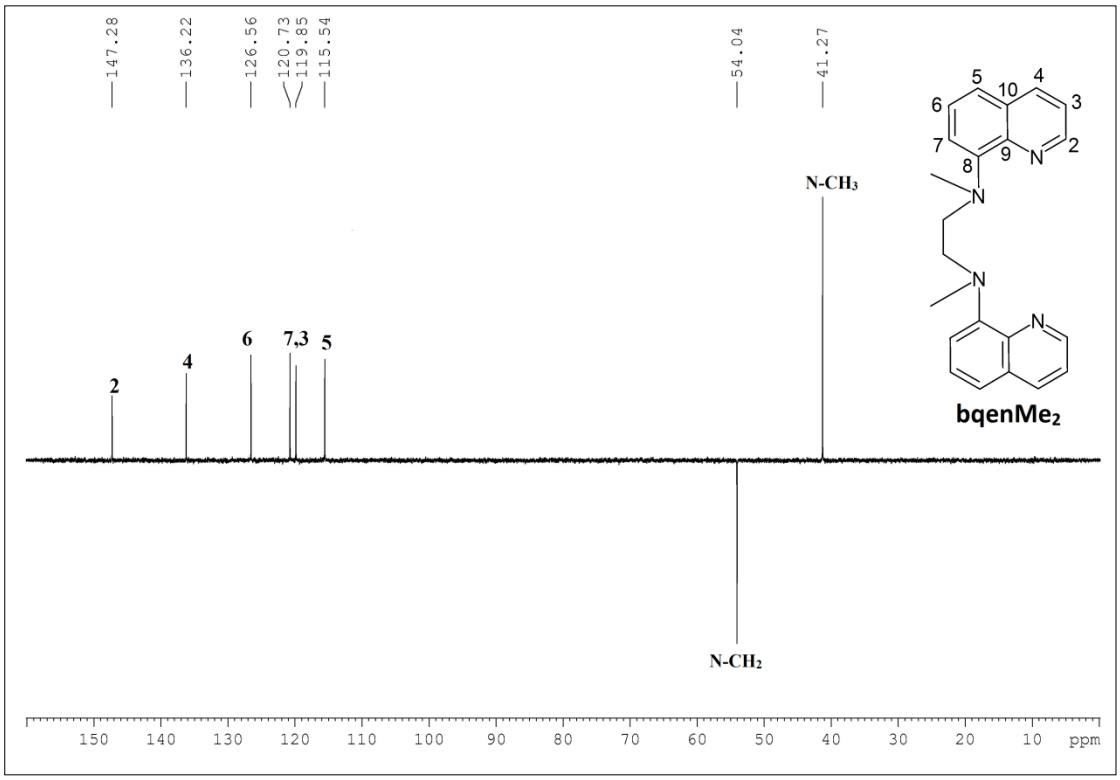

Figure 3.5 *The DEPT spectrum of bqenMe$_2$ in CDCl$_3$.*

3.3.3 Synthesis and characterisation of complexes 1 and 2

The reaction of bqenH$_2$ and bqenMe$_2$ with $Ni(ClO_4)_2 \cdot 6H_2O$ in CH_3CN/CH_2Cl_2 (1:1) at room temperature afforded compounds **1** and **2** respectively in good yields by following the procedure as discussed in section 3.2.1 (**Scheme 3.4**). The complexes have been characterized by C, H, N analysis, IR and UV-Vis spectroscopy, ESI-MS and cyclic voltammetry. Our efforts to obtain the single crystals of compound **1** and **2** suitable for X-ray diffraction studies were not fruitful.

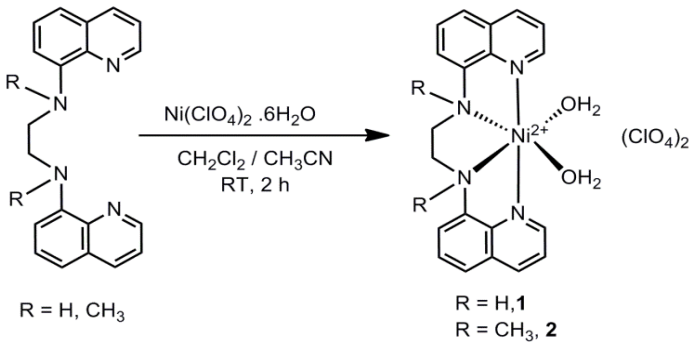

Scheme 3.4 *Synthesis of [Ni(bqenH$_2$)(H$_2$O)$_2$](ClO$_4$)$_2$* ***1*** *and [Ni(bqenMe$_2$)(H$_2$O)$_2$](ClO$_4$)$_2$* ***2***

3.3.3a Characterisation of compounds by infrared spectroscopy

The infrared spectra of **1** and **2** were compared with the ligand $bqenH_2$ and $bqenMe_2$ (**Figure 3.6**). The compounds **1** and **2** exhibit broad peaks at ~3547 cm^{-1} and ~3405 cm^{-1} respectively which are assigned to the O-H stretching vibrations of water. For compounds **1**, the N-H stretching vibrations occur at lower frequency ~3265 respectively compared to that of free ligand. This observation reveals that the ligand $bqenH_2$ is coordinated to the Ni(II). Further, no bands due to N-H stretching were observed for compounds **2** which contain $bqenMe_2$ ligand core. The presence of perchlorate anions in **1**-**2** was revealed from the appearance of strong and medium absorption peaks at ~1093 cm^{-1} and 621 cm^{-1} respectively.[63]

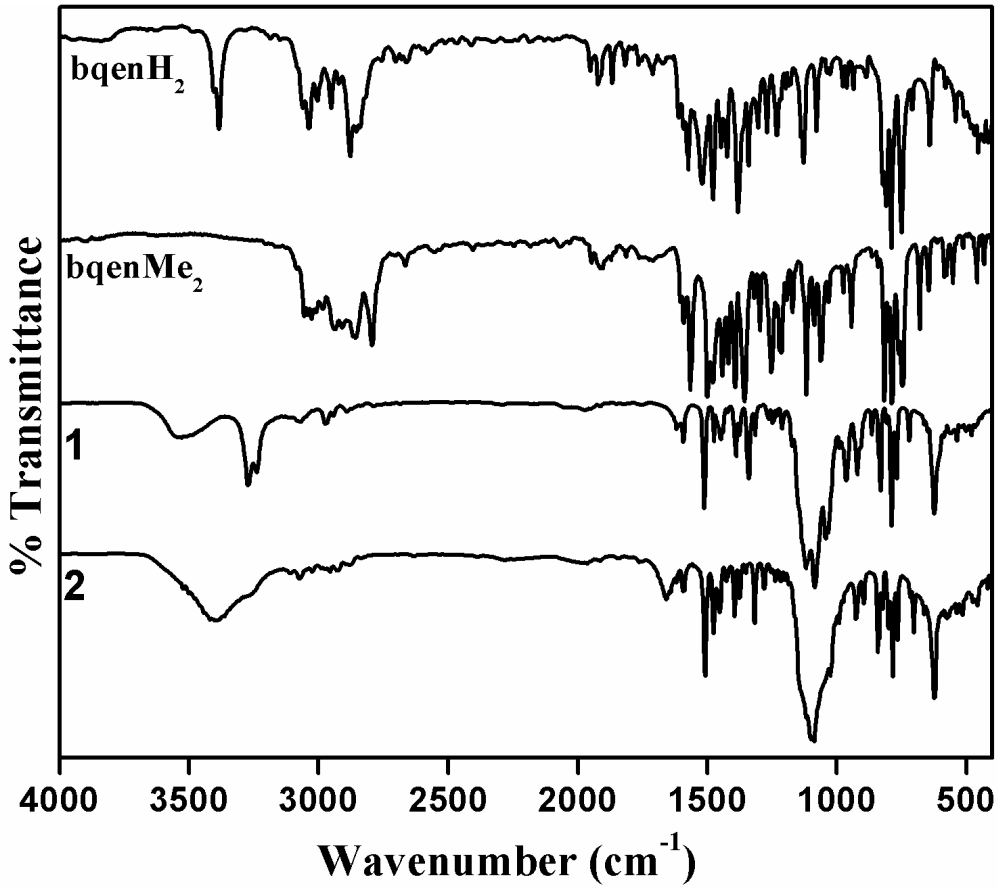

Figure 3.6 *Overlaid infrared spectra of **1** and **2** with ligands $bqenH_2$ and $bqenMe_2$.*

3.3.3b UV-Vis spectroscopy

The electronic spectra of nickel(II) ion in an octahedral environment is expected to show three *d-d* bands assignable for the $^3A_{2g}\rightarrow{}^3T_{2g}$, $^3A_{2g}\rightarrow{}^3T_{1g}(F)$ and $^3A_{2g}\rightarrow{}^3T_{1g}(P)$ transitions.[64] The *d-d* band assigned to $^3A_{2g}\rightarrow{}^3T_{1g}(F)$ transition is observed in the region of 489-553 nm on the other hand the peak due to $^3A_{2g}\rightarrow{}^3T_{2g}$ transition is observed in the wavelength range 793- 872 nm. Both the bands are very weak in intensity and are observed only at higher concentrations of the compounds in CH_3CN. The tailing of a charge transfer band hinders the observation of third *d-d* band assigned to the $^3A_{2g}\rightarrow{}^3T_{1g}(P)$ in both the complexes as observed for some Ni(II) complexes.[65] The high-intensity bands observed in the UV region of 200-320 nm are assigned to the intra-ligand transitions as shown in **Figure 3.7**.

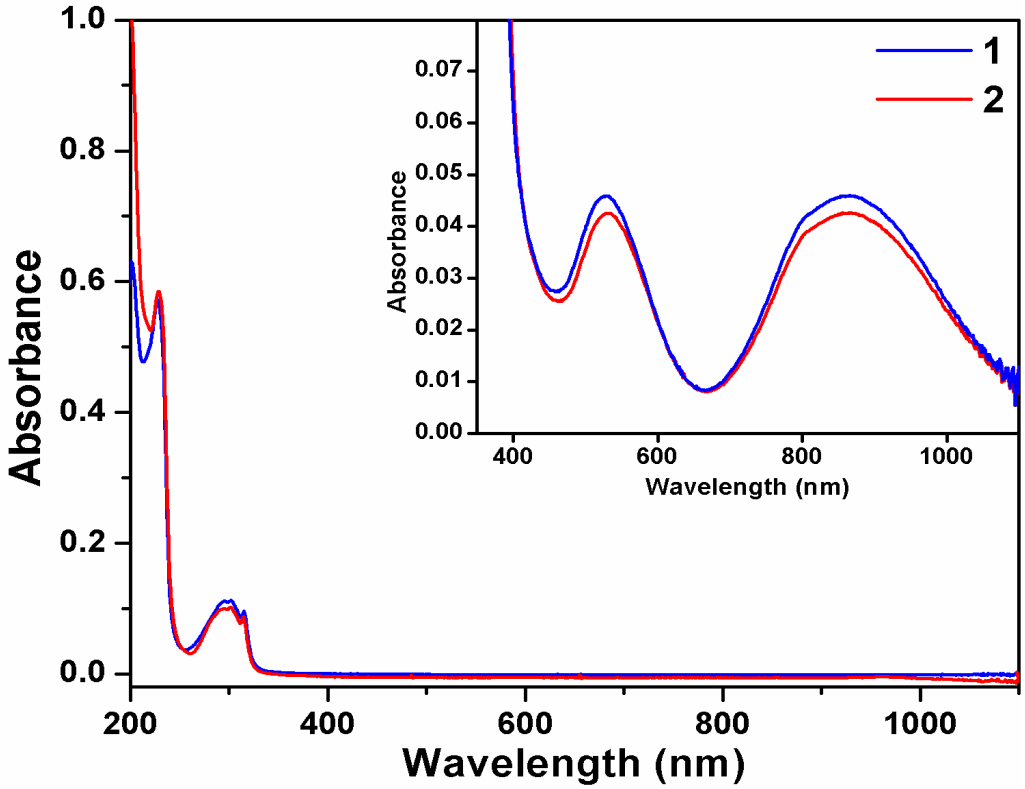

Figure 3.7 *Overlaid UV-Vis spectra of* ***1*** *and* ***2*** *(10^{-5}M) in CH_3CN. The inset shows an expanded view of the region 350 to 1100 nm for d-d bands* ***1*** *and* ***2*** *(5 mM).*

3.3.3c ESI-Mass spectrometry

The compounds **1** and **2** were characterized by using ESI-Mass spectrometry in CH_3CN (**Figure 3.8**). The ESI-MS spectrum of **1**, shows prominent mass peaks at *m/z* 227.0 (calc. *m/z* 227.1) and 471.0 (calc. *m/z* 471.1) which are assigned to the $[Ni(bqenH_2)(CH_3CN)_2]^{2+}$ and $[Ni(bqenH_2)(ClO_4)]^{+}$ species respectively while the mass peak observed at *m/z* 371.1 (calc. *m/z* 371.0) is attributed to the $[Ni(bqenH_2)]^{+}$ species. On other hand, the ESI-MS spectrum of **2** exhibits prominent mass peaks at *m/z* 220.5 (calc. *m/z* 220.6), 241.0 (calc. *m/z* 241.1) and 499.1 (*calc. m/z* 499.1) which are assigned to the $[Ni(bqenMe_2)(CH_3CN)]^{2+}$, $[Ni(bqenMe_2)(CH_3CN)_2]^{2+}$ and $[Ni(bqenMe_2)(ClO_4)]^{+}$ species respectively.

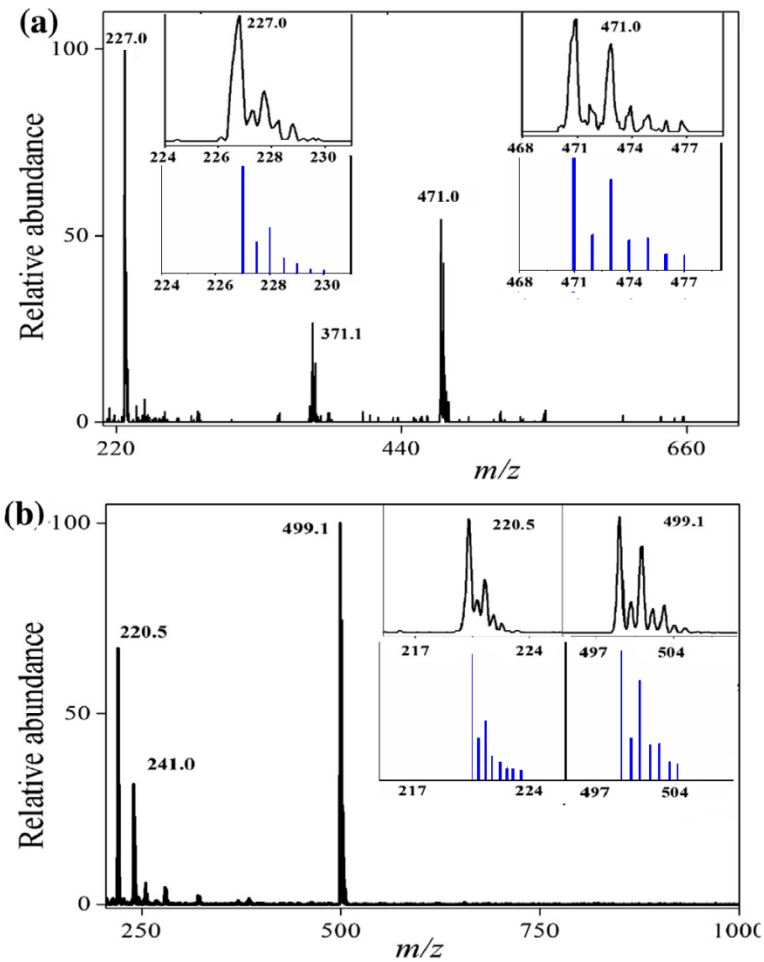

Figure 3.8 *ESI-MS spectrum of* ***1*** *(top) and* ***2*** *(bottom) recorded in acetonitrile solvent. The inset shows the isotope distribution patterns for the prominent peaks in black with simulated pattern in blue colour.*

3.3.3d Cyclic and differential pulse voltammetry

The compounds **1-2** were characterized by using cyclic voltammetry (CV) and differential pulse voltammetry (DPV) to explore their electrochemical properties. Compounds **1** and **2** exhibit a quasi-reversible cathodic and anodic waves which can be attributed to of Ni(II)/Ni(I) redox couples, for which the $E_{1/2}$ value is centred at ~ -1.3 V volts[66–70] (cyclic voltammogram of **1** is shown in **Figure 3.9,** compound **2** exhibits similar pattern**)**. The anodic wave for both the compounds are poorly resolved in CV plots but same is distinctly visible in the DPV plots. The cyclic voltammograms recorded at different scan rates were identical and the peak currents increased proportionally with the increase in scan rates (**Figure 3.10** for **2**). The CV and DPV plots of bqenH_2 as well as bqenMe_2 do not show oxidation-reduction peaks in the measured potential range and thus suggest that both ligands are electrochemically inactive under the experimental conditions (**Figure 3.11**). Hence, the observed peaks in the cyclic voltammograms of **1** and **2** are solely assigned to the quasi-reversible redox process of Ni(II)/Ni(I) couple.

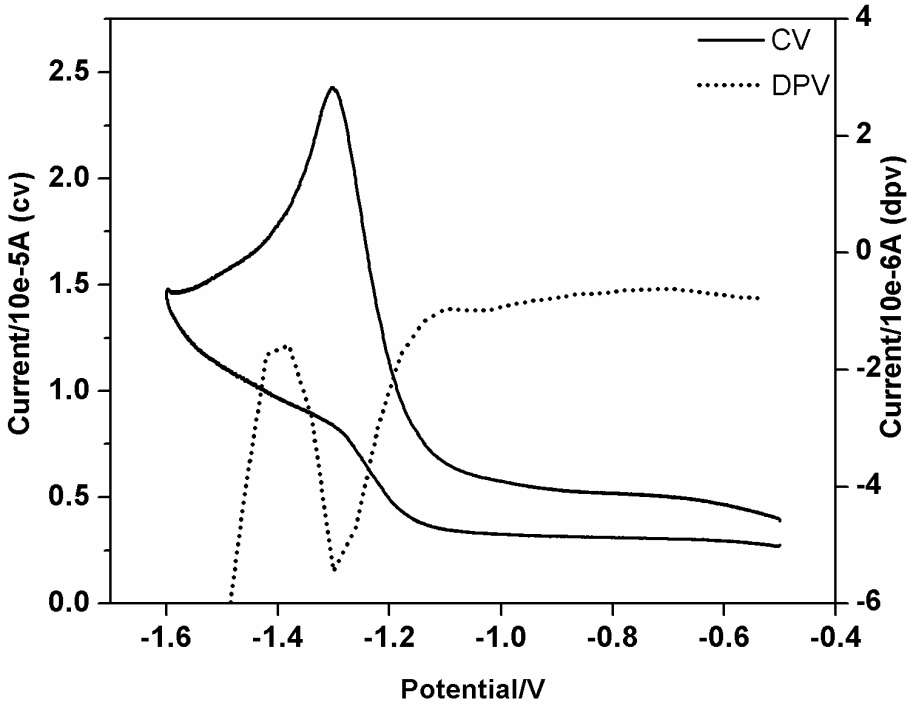

Figure 3.9 *CV (solid line) and DPV (dotted line) of* ***1*** *recorded at a scan rate of 100 mV* s^{-1} *in* CH_3CN *containing 0.1 M of* $TBAPF_6$ *as supporting electrolyte.*

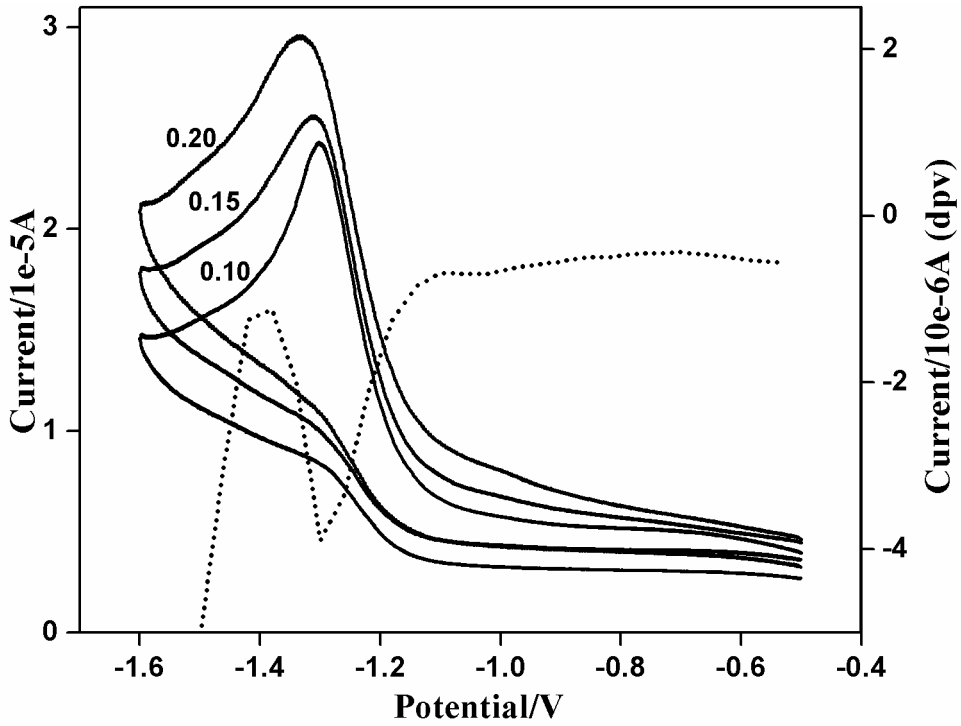

Figure 3.10 *CV of* ***2*** *at scan rates of 0.20, 0.15 and 0.10 V* s^{-1} *and DPV (dotted line) of* ***2*** *recorded in* CH_3CN *containing 0.1 M of* $TBAPF_6$

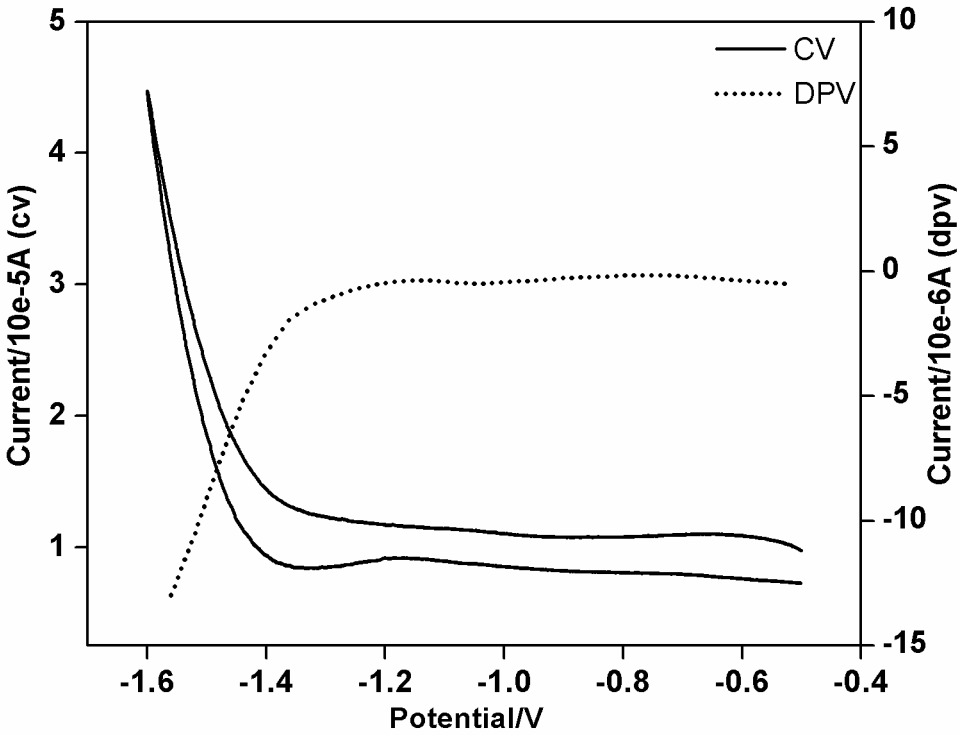

Figure 3.11 *CV (solid line) and DPV (dotted line)* $bqenMe_2$ *in* CH_3CN *containing 0.1 M of* $TBAPF_6$ *at scan rate 0.1 V* s^{-1}.

3.3.4 Catalytic hydroxylation of alkanes by 1 and 2

Compounds **1** and **2** were tested for the efficacy of catalytic oxidations of hydrocarbons such as cumene, ethylbenzene and cyclohexane using *m*-CPBA as an oxidant in CH_3CN at 25 ^oC under N_2 atmosphere. The hydroxylated products of alkanes were analysed and quantified by gas chromatography (GC) using authentic samples and decane as an internal standard. Compounds **1** and **2** efficiently catalysed the hydroxylation of C-H bonds of alkanes used in this study (**Table 3.1**, **Scheme 3.5**). A comparative reactivity of **1** and **2**, revealed that compound **2** gave a higher yield of hydroxylated products. The high yield of alcohol and ketone using compound **2**, can be attributed to the differing nature of ligand in **1** and **2**. In compound **1**, the bqenH_2 has a secondary amine tail (R_2NH) on the other hand in **2** the bqenMe_2 has all alkylated N atoms making it tertiary amine. In one of the study, the oxidation of cyclam ligand which has four R_2NH groups, is reported in Ni(II)-cyclam complexes using H_2O_2 as the oxidant.[58] It is likely that in **1**, the bqenH_2 which has secondary amine functionality can undergo partial oxidation thus reflecting on the observed low yields of organic products compared to **2** (**Table 3.1**). In the oxidation of cumene, 2-phenylpropane-2-ol was obtained in high yield while acetophenone obtained as minor products. Use of ethylbenzene instead of cumene as a substrate, resulted in a high yield of 1-phenylethanol along with minor products acetophenone. Although we do not have crystal structure we propose that compounds **1** and **2** have octahedral geometries with two H_2O molecules occupying the *cis*-positions. However, in the CH_3CN solution, the two H_2O molecules are exchanged rendering the two CH_3CN molecules at *cis* positions. The *cis*-ligands are thus labile and make nickel(II) centre more susceptible to the oxidation by *m*-CPBA oxidant. Further we extended the study of catalytic oxidation using the Ni(II) complexes in which two *cis* sites containing water in **1** and **2** are occupied by bidentate ligands like phenanthroline (phen), bipyridine (bpy) and ethylenediamine (en).

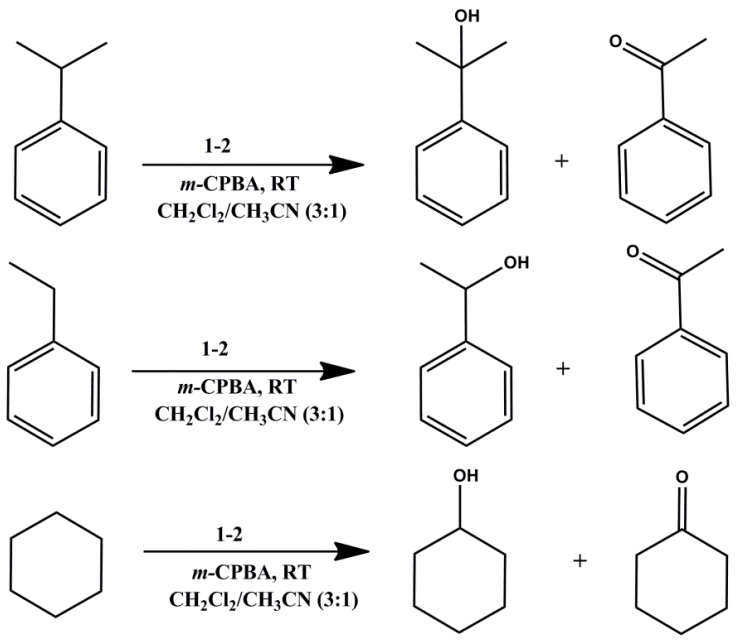

Scheme 3.5 *Alkane hydroxylation reaction catalyzed by compound* ***1*** *and* ***2****.*

Table 3.1 *Organic product analysis using GC in the alkane hydroxylation by* ***1*** *and* ***2***

Catalyst	substrate	alcohol	(TON) (A)	ketone	(TON) (K)	A / K
1	Cumene	2-phenylpropan-2-ol	105	acetophenone	23	4.6
	Ethylbenzene	1-phenylethanol	121	acetophenone	25	4.8
	Cyclohexane	cyclohexanol	116	cyclohexanone	23	5.0
2	Cumene	2-phenylpropan-2-ol	361	acetophenone	42	8.6
	Ethylbenzene	1-phenylethanol	390	acetophenone	38	10.3
	Cyclohexane	cyclohexanol	410	cyclohexanone	50	8.2

Note*: [a]Reaction conditions: [Ni^{2+}] = 0.5 mM; [m-CPBA] = 0.5 M, [substrate] = 1 M in CH_3CN at 25 ^oC for 90 min under N_2; [b]Turnover number [(moles of product)/(moles of catalyst)] determined by GC. [c]Small amounts of desaturated products in the case of cumene and ethylbenzene while the small amount of ε-caprolactone in case of cyclohexanone were observed.*

3.3.5 Synthesis of compound 3-8

The detail synthetic procedure for compound **3-8** is described in section 3.2.1. The reaction of complex **1** with bidentate N-donor ligands such as phen, bpy and en in acetonitrile resulted in the exchange of weakly coordinating solvent molecules (CH_3CN or

H_2O) affording **3, 5** and **7**. Under identical reaction conditions, the compounds **4**, **6** and **8** were prepared using **2** as a starting material (**Scheme 3.6**).

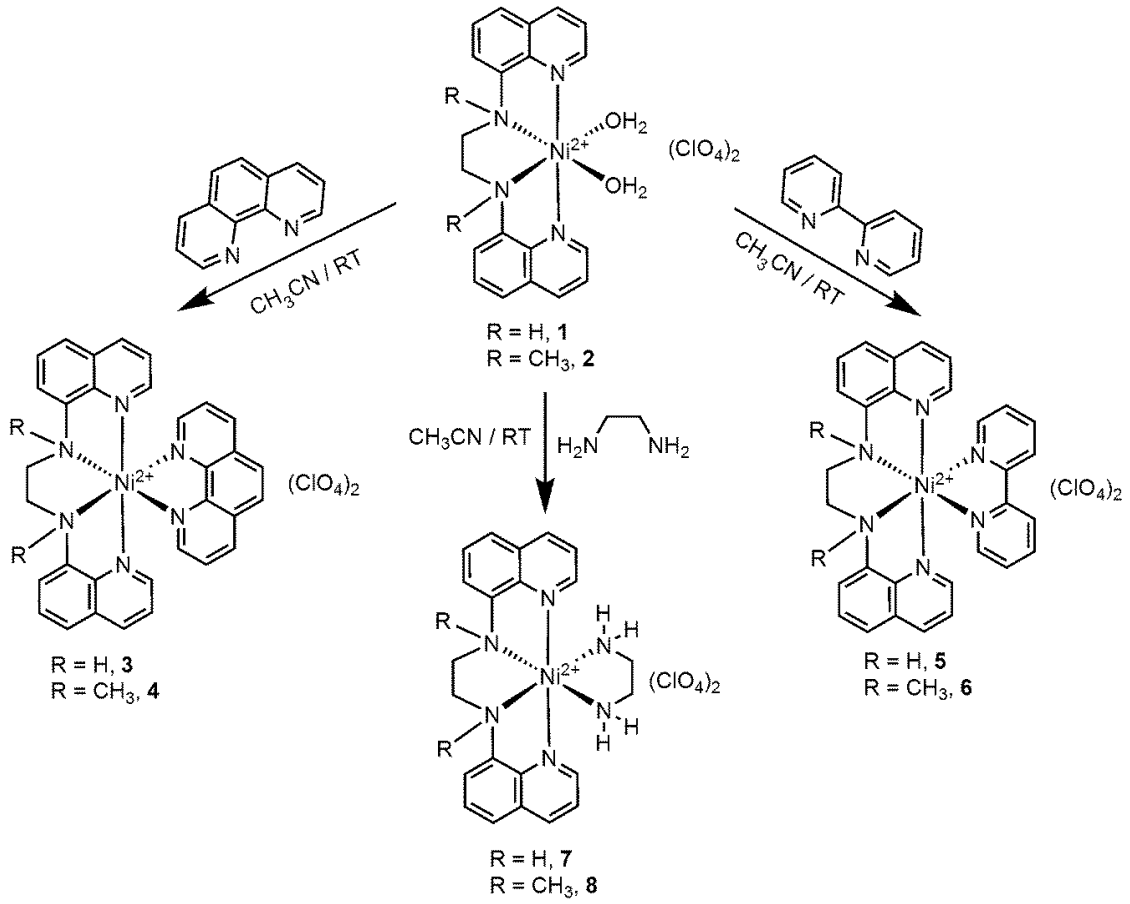

Scheme 3.6 *Synthetic methodology used for the preparation of compounds* ***3-8****.*

3.3.6 Characterization of compound 3-8

The compound **3-8** were characterized by C,H,N analysis, infrared spectroscopy UV-Vis spectroscopy, ESI-MS and cyclic voltammetry. The compounds **3**, **4**, **5** and **7** were also characterized by single crystal X-ray crystallography.

3.3.6a Characterization of compound 3-8 by infrared spectroscopy

The compound **3** and **5** bearing bqenH_2 ligand core shows the N-H stretching vibrations at ~3269 and 3228 respectively. Further, no such bands were observed for compounds **4** and **6** which bear bqenMe_2 core indicating the absence of N-H bonds in these

compounds. The IR spectra of **7** and **8** show the two bands in the region 3380 to 3220 cm^{-1} which are due to the N-H stretching vibrations which are the characteristic absorption pattern of primary amine (ethylenediamine). The complete disappearance of -OH vibrations in **3-8** indicates the substitution of two H_2O molecules from compound **1** and **2** (which may be present as labile ligands) by bidentate phen, bpy and en. As observed for compound **1** and **2**, perchlorate anions show, the strong and medium absorption bands at ~1093 cm^{-1} and 621 cm^{-1} respectively in **3-8**.[63]

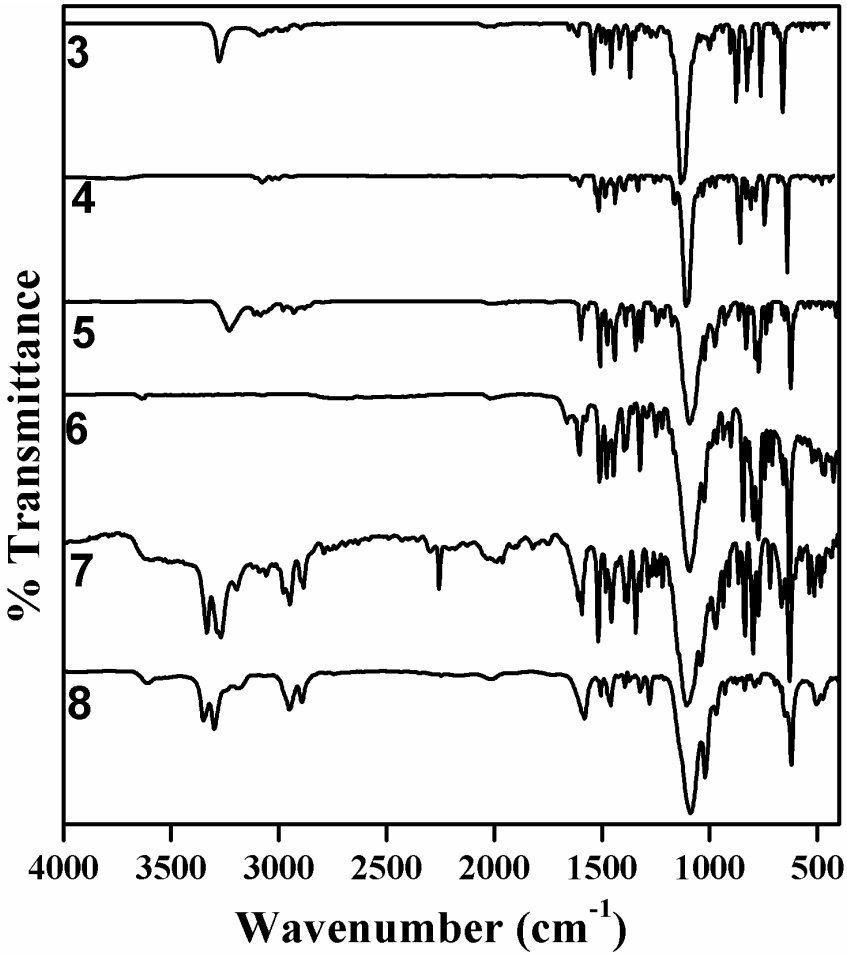

Figure 3.12 *Infrared spectra of compounds **3-8**.*

3.3.6b Characterization of compound 3-8 by UV-Vis spectroscopy

The compound **3-8** shows the strong absorption bands in the UV region of 200-320 nm are assigned due to the intra-ligand transitions. The band at ~ 272 nm in **3** and **4** is

assigned to the π-π* transition that arises from the coordination of the nickel(II) to 1,10-phenanthroline.[71] The π-π* transition due to bipyridine ligand is observed at 284 nm in compound **5** at 296 nm in compound **6**. The *d-d* band assigned to $^3A_{2g} \rightarrow {}^3T_{1g}(F)$ transition is observed in the region of 489-553 nm on the other hand the peak due to $^3A_{2g} \rightarrow {}^3T_{2g}$ transition is observed in the wavelength range 793- 872 nm.[64] Similar to compound **1** and **2,** *d-d* band due to the $^3A_{2g} \rightarrow {}^3T_{1g}(P)$ transition are not observed due to the tailing of a charge transfer band in all six compounds. The UV-Vis spectra of compound **4**, **6** and **8** recorded in acetonitrile are shown in **Figure 3.13**. The UV-Vis spectra of **3**, **5** and **7** show similar absorption features.

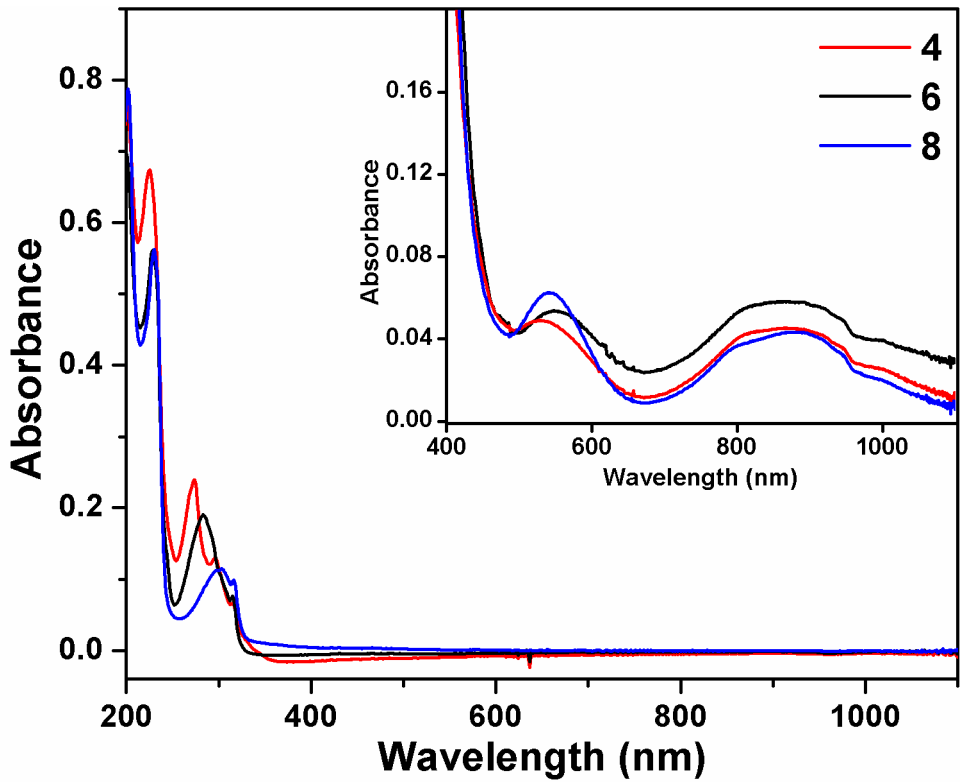

Figure 3.13 *Overlaid UV-vis spectra of **4**, **6** and **8** (10^{-5} M) in CH_3CN. The inset shows an expanded view of the region 400 to 1100 nm for d-d bands.*

3.3.6c ESI-MS spectroscopy

The ESI-MS of the compounds **3-6** is shown in **Figure 3.14** (see **Figure A1** in appendix for simulated pattern). The ESI-MS mass spectra of **3** and **4** show prominent

mass peaks at m/z 276.0 (*calc. m/z* 276.1) and 290.0 (*calc. m/z* 290.1) which are assigned to the $[Ni(bqenH_2)(phen)]^{2+}$ and $[Ni(bqenMe_2)(phen)]^{2+}$ species respectively. For **5** and **6**, the mass peaks at 264.1 (*calc. m/z* 264.0) and 278.1 (*calc. m/z* 278.0) in the ESI-MS spectra are observed for $[Ni(bqenH_2)(bpy)]^{2+}$ and $[Ni(bqenMe_2)(bpy)]^{2+}$ species.

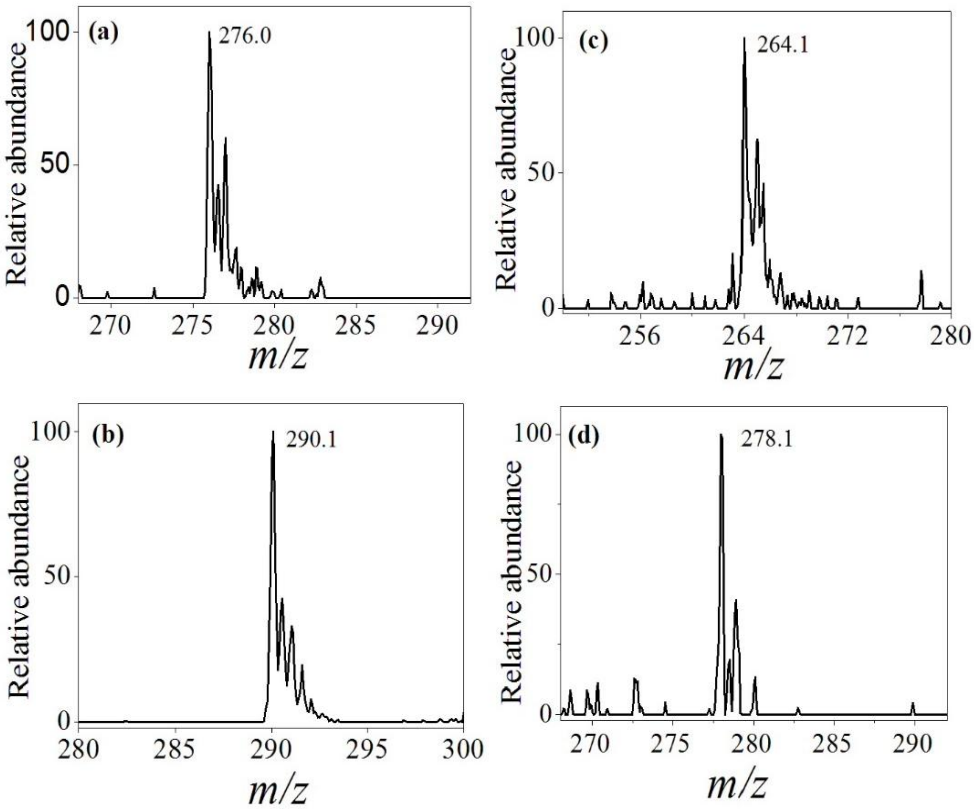

Figure 3.14 *ESI-MS spectra of compounds (a)* ***3****, (b)* ***4****, (c)* ***5*** *and (d)* ***6*** *in acetonitrile solvent showing observed isotopic distribution patten.*

3.3.6d Description of the crystal structures of compounds 3-5 and 7

All six compounds **3-8** were obtained as crystalline solids; however we were able to grow the single crystals of compounds **3**, **4**, **5** and **7** which were characterized by single X-ray crystallography. Single crystals suitable for structure determination were obtained by slow diffusion of diethyl ether into their CH_3CN solutions. The technical details of data acquisition and selected refinement results for **3-4** are given in **Table 3.2** and for **5-6** are given in **Table 3.3**. The compound **3** crystallizes in the non-centrosymmetric orthorhombic

space group $P2_12_12_1$, **4** crystallizes in the centrosymmetric monoclinic space group $P2_1/c$, **5** crystallizes in monoclinic $P2_1/n$ and compound **7** crystallizes in triclinic $P\bar{1}$. In all four compounds, all atoms are located in their general positions. The common feature that has observed in all four compounds is that the quinolyl nitrogen atoms of ligand $bqenH_2$ or $bqenMe_2$ are disposed *trans* to each other while the amine nitrogen atoms of the ligands occupy the adjacent positions. The remaining two *cis* sites are occupied by phen in compound **3** and **4**, bpy in **5** and en in **7**. The compounds **4** and **7** has an additional uncoordinated CH_3CN molecule in its crystal lattice (**Figure 3.15**). The two methyl groups, on the amine nitrogen one on N2 and the other on N3 atoms of $bqenMe_2$ in **4** are located *anti* to each other unlike the *syn* H atoms on $bqenH_2$ in **3**, **5** and **7**. The crystal structure of **5** reveals that its asymmetric unit consists of crystallographically two independent molecules. Both the molecule possesses same octahedral geometry. One of the molecules is shown in **Figure 3.17**. The perchlorate ions in all four compounds remain uncoordinated behave as charge balancing counter anions. All the Ni-N bond distances and N-Ni-N bond angles are in normal range (**Table 3.4** for **3, Table 3.5** for **4, Table 3.6** for **5 and Table 3.7** for **7**) and are in good agreement with literature reports.[72-76] In all the four complexes the N-Ni-N *trans* and *cis* angles deviate from 180° and 90° respectively suggesting the distortion of octahedral geometry. The *trans* angles range from 169.89(5) to 176.76(5)° in **3**, 171.47(6) to 177.84(6)° in **4**, 169.48(9) to 176.03(8)° in **5** and 167.48(5) to 178.56(5)° in **7**. Whereas the *cis* angles vary between 80.10(5) to 98.30(5)° in **3** and 79.42(6) to 100.11(6)° in **4**. Further, the electronegative atoms (N and O as well as C) in these compounds are involved in the intermolecular hydrogen forming a supramolecular three-dimensional networks as shown in **Figure 3.19-3.22**. The N⋯O and C⋯O hydrogen bonds are shorter than the sum of their Van der Waals radii revealing the strength of these H-bonds in stabilizing overall crystal structures of **3** and **4** (**Table 3.8 - 3.10**).

Table 3.2**. Technical details of data acquisition and selected refinement results for **3** and **4

	3	**4**
Empirical formula	$C_{32}H_{26}Cl_2N_6$ NiO_8	C_{36} $H_{33}Cl_2N_7NiO_8$
Formula weight	752.2	821.3
Crystal colour	Red	Violet
Crystal system	Orthorhombic	Monoclinic
Space group	$P2_12_12_1$	$P2_1/c$
Temperature (K)	100(2)	100(2)
Unit cell dimensions	a = 11.304(2) Å	a =18.0780(4) Å
	b = 15.972(3) Å	b =11.3105(2) Å
	c = 17.680(3) Å	c = 17.2253(3) Å
	α = 90.00°	α = 90.00°
	β = 90.00°	β= 100.37°
	γ = 90.00°	γ = 90.00°
volume (Å^3)	3192.3(10)	3464.58(12)
Z	4	4
Radiation type (Mo-Kα)/Å	0.71073	0.71073
Crystal size (mm^3)	0.30 x 0.20 x 0.10	0.20 x 0.20 x 0.10
Diffractometer	Bruker APEX-II CCD	Bruker APEX-II CCD
Absorption correction	None	None
No. measured reflections	9790	9803
Calculated density (g/cm^3)	1.565	1.575
Absorption coefficient (mm^{-1})	0.838	0.780
F(000)	1544	1696
θ range for data collection	2.14 to 28.37	2.40 to 28.31
Flack parameter	0.00	-
Limiting indices	$-15 \leq h \leq 15$	$-22 \leq h \leq 22$
	$-21 \leq k \leq 21$	$-13 \leq k \leq 13$
	$-23 \leq l \leq 23$	$-21 \leq l \leq 21$
Refinement method	SHELXS-97	SHELXS-97
Data / restraints / parameter	7919 / 0 / 442	6817 / 0 / 490
Final R Indices[I>2σ(I)]	R_1 = 0.0233, wR_2 = 0.0592	R_1 =0.0299, wR_2 = 0.1182
R indices (all data)	R_1 = 0.0250, wR_2 = 0.0604	R_1 = 0.0341, wR_2 =0.1239
Goodness of fit on F^2	0.966	1.071

Table 3.3 *Technical details of data acquisition and selected refinement results for* ***5*** *and* ***7***

	5	**7**
Empirical formula	$C_{60}H_{52}Cl_4N_{12}Ni_2O_{16}.0.25H_2O$	$C_{24}H_{29}Cl_2N_7NiO_8$
Formula weight	1460.86	673.15
Crystal colour	Dark red	dark red
Crystal system	Monoclinic	Triclinic
Space group	$P2_1/n$	$P\bar{1}$
Temperature (K)	100(2)	100(2)
Unit cell dimensions	a = 17.3255(11) Å	a = 10.9192(11) Å
	b = 10.6110(7) Å	b = 12.3327(12)Å
	c = 34.328(2) Å	c = 12.6497(13)Å
	α = 90.00°	α = 60.9370(14) °
	β = 93.9480(13)°	β = 70.0320(16)°
	γ = 90.00°	γ = 75.4400(14)°
volume (Å^3)	6295.8(7)	1391.9(2)
Z	4	2
Radiation type (Mo-Kα)/Å	0.71073	0.71073
Crystal size (mm^3)	0.15 x 0.13 x 0.07	0.16 x 0.12 x 0.09
Diffractometer	Bruker Smart APEX-II Duo	Bruker Smart APEX-II Duo
Absorption correction	Semi-empirical from equivalents	Multi scan
No. measured reflections	9787	9872
Calculated density (g/cm^3)	1.541	1.606
Absorption coefficient (mm^{-1})	0.847	0.951
F(000)	3002	696
θ range for data collection	2.009 to 28.308°.	1.90 to 28.44
Flack parameter	0.00	-
Limiting indices	-23<=h<=20	$-14 \leq h \leq 11$
	-10<=k<=14	$-16 \leq k \leq 16$
	-45<=l<=45	$-16 \leq l \leq 16$
Refinement method	Full-matrix least-squares on F^2	Full-matrix least-squares on F^2
Data / restraints / parameter	15530 / 1545 / 983	7007 / 122 / 388
Final R Indices[I>2σ(I)]	$R1$ = 0.0402, $wR2$ = 0.0868	R_1 = 0.0269, wR_2 = 0.0704
R indices (all data)	R1 = 0.0635, wR2 = 0.0966	R_1 = 0.0300, wR_2 = 0.0721
Goodness of fit on F^2	1.013	1.045

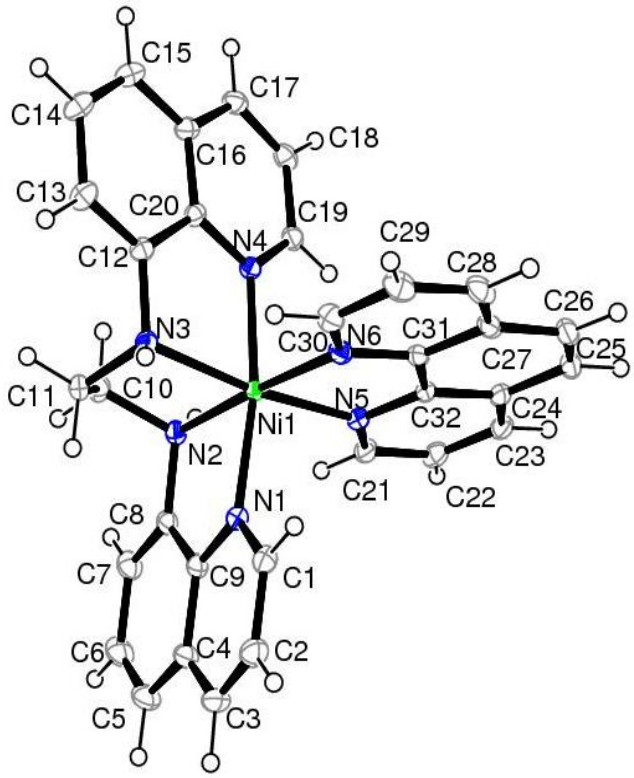

Figure 3.15 *The crystal structure of* $[Ni(bqenH_2)]^{2+}$ *cation in* ***3*** *showing the atom-labelling scheme. Displacement ellipsoids are drawn at 50% probability level except for the H atoms, which are shown as circles of arbitrary radius (top). The perchlorate anions are omitted for clarity.*

Table 3.4 *Selected bond lengths (Å) and angles (°) for* ***3****.*

Bond length (Å)			
Ni1—N5	2.085(1)	Ni1—N4	2.097(1)
Ni1—N6	2.086(1)	Ni1—N2	2.104(1)
Ni1—N1	2.092(1)	Ni1—N3	2.126(1)
Bond angle (°)			
N5—Ni1—N6	80.10(5)	N1—Ni1—N2	80.69(5)
N5—Ni1—N1	93.50(5)	N4—Ni1—N2	90.41(5)
N6—Ni1—N1	97.34(5)	N5—Ni1—N3	172.67(5)
N5—Ni1—N4	97.34(5)	N6—Ni1—N3	98.30(5)
N6—Ni1—N4	91.76(5)	N1—Ni1—N3	93.80(5)
N1—Ni1—N4	169.89(5)	N4—Ni1—N3	80.48(5)
N5—Ni1—N2	97.41(5)	N2—Ni1—N3	84.43(5)
N6—Ni1—N2	176.76(5)		

Note: The values in the parentheses indicate estimated standard deviations.

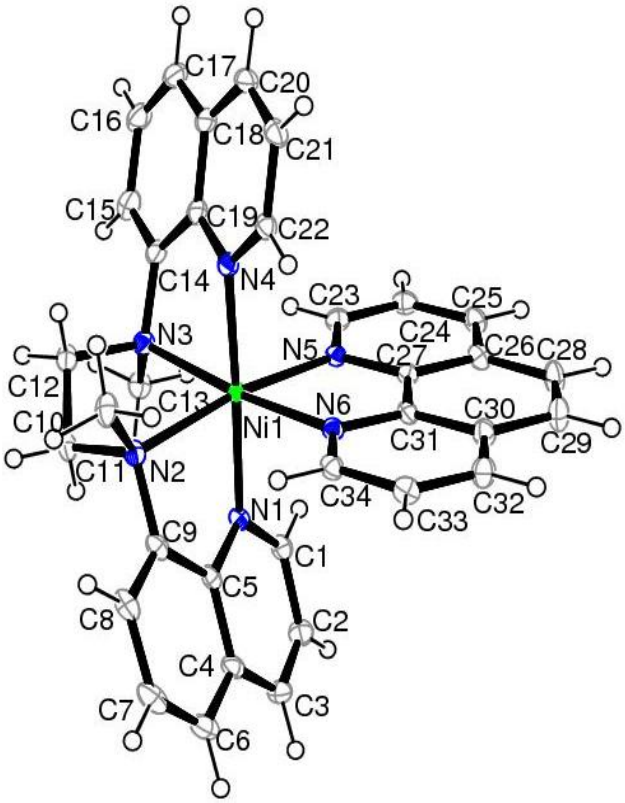

Figure 3.16 *The crystal structure of [Ni(bqenMe$_2$)]$^{2+}$ cation in* ***4*** *showing the atom-labelling scheme. Displacement ellipsoids are drawn at 50% probability level except for the H atoms, which are shown as circles of arbitrary radius. The perchlorate anions are omitted for clarity.*

Table 3.5 *Selected bond lengths (Å) and angles (°) for* ***4****.*

Bond length (Å)			
Ni1—N4	2.067(1)	Ni1—N5	2.116(2)
Ni1—N1	2.079(1)	Ni1—N3	2.162(2)
Ni1—N6	2.111(2)	Ni1—N2	2.182(2)
Bond angle (°)			
N4—Ni1—N1	177.84(6)	N6—Ni1—N3	173.76(6)
N4—Ni1—N6	94.98(6)	N5—Ni1—N3	99.22(6)
N1—Ni1—N6	86.41(6)	N4—Ni1—N2	100.11(6)
N4—Ni1—N5	88.14(6)	N1—Ni1—N2	78.06(6)
N1—Ni1—N5	93.74(6)	N6—Ni1—N2	97.54(6)
N6—Ni1—N5	79.42(6)	N5—Ni1—N2	171.47(6)
N4—Ni1—N3	78.85(6)	N3—Ni1—N2	84.63(6)
N1—Ni1—N3	99.78(6)		

Note: The values in the parentheses indicate estimated standard deviations.

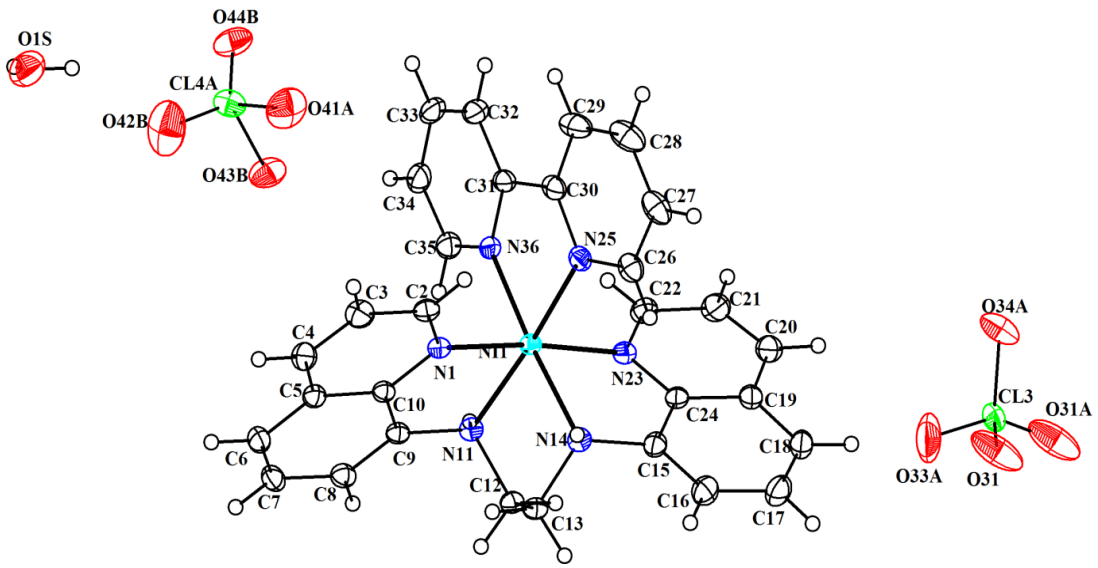

Figure 3.17 *- The crystal structure of [Ni(bqenH$_2$)(bpy)](ClO$_4$)$_2$* ***5*** *with atom-labelling scheme. Displacement ellipsoids are drawn at 50% probability except for the H atoms, which are shown as circles of arbitrary radius. The distortion in perchlorate molecules is not shown for clarity.*

Table 3.6. *Selected bond lengths (Å) and angles (°) for* ***5****.*

Bond length (Å)			
Ni1—N36	2.072(2)	Ni2—N61	2.073(2)
Ni1—N23	2.074(3)	Ni2—N72	2.077(2)
Ni1—N1	2.075(3)	Ni2—N37	2.086(3)
Ni1—N25	2.078(2)	Ni2—N59	2.099(3)
Ni1—N11	2.115(2)	Ni2—N47	2.116(2)
Ni1—N14	2.119(2)	Ni2—N50	2.130(3)
Bond angle (°)			
N36—Ni1—N23	96.40(9)	N61—Ni2—N72	78.78(8)
N36—Ni1—N1	89.74(9)	N61—Ni2—N37	97.11(8)
N23—Ni1—N1	173.67(9)	N72—Ni2—N37	96.99(9)
N36—Ni1—N25	79.11(8)	N61—Ni2—N59	88.56(8)
N23—Ni1—N25	89.11(9)	N72—Ni2—N59	92.80(8)
N1—Ni1—N25	93.56(9)	N37—Ni2—N59	169.48(9)
N36—Ni1—N11	99.34(8)	N61—Ni2—N47	174.83(9)
N23—Ni1—N11	96.24(9)	N72—Ni2—N47	96.65(9)
N1—Ni1—N11	81.21(9)	N37—Ni2—N47	80.96(9)
N25—Ni1—N11	174.58(9)	N59—Ni2—N47	94.11(9)
N36—Ni1—N14	176.03(8)	N61—Ni2—N50	100.59(8)
N23—Ni1—N14	80.70(8)	N72—Ni2—N50	172.93(9)
N1—Ni1—N14	93.24(8)	N37—Ni2—N50	90.07(9)
N25—Ni1—N14	98.06(8)	N59—Ni2—N50	80.14(9)
N11—Ni1—N14	83.73(8)	N47—Ni2—N50	84.25(9)

Note: The values in the parentheses indicate estimated standard deviations.

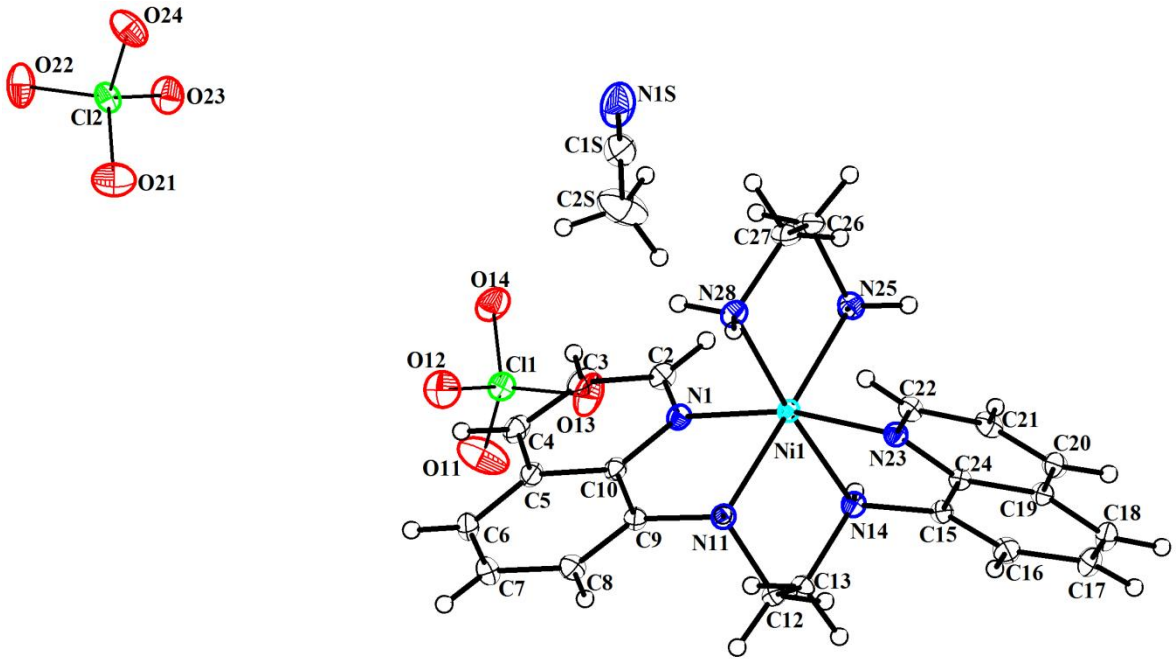

Figure 3.18 *- The crystal structure of [Ni(bqenH$_2$)(en)](ClO$_4$)$_2$* ***7*** *with atom-labelling scheme. Displacement ellipsoids are drawn at 50% probability except for the H atoms, which are shown as circles of arbitrary radius (top).*

Table 3.7 *Selected bond lengths (Å) and angles (°) for* ***7****.*

		7	
Bond length (Å)			
Ni(1)-N(28)	2.0928(12)	Ni(1)-N(23)	2.1084(11)
Ni(1)-N(25)	2.0991(12)	Ni(1)-N(11)	2.1107(12)
Ni(1)-N(14)	2.1038(11)	Ni(1)-N(1)	2.1190(11)
Bond angle (°)			
N(28)-Ni(1)-N(25)	82.74(5)	N(14)-Ni(1)-N(11)	85.77(5)
N(28)-Ni(1)-N(14)	175.35(5)	N(23)-Ni(1)-N(11)	89.51(5)
N(25)-Ni(1)-N(14)	94.42(5)	N(28)-Ni(1)-N(1)	92.61(5)
N(28)-Ni(1)-N(23)	95.80(5)	N(25)-Ni(1)-N(1)	98.34(5)
N(25)-Ni(1)-N(23)	91.92(5)	N(14)-Ni(1)-N(1)	91.45(5)
N(14)-Ni(1)-N(23)	80.57(4)	N(23)-Ni(1)-N(1)	167.48(5)
N(28)-Ni(1)-N(11)	97.16(5)	N(11)-Ni(1)-N(11	80.23(5)
N(25)-Ni(1)-N(11)	178.56(5)		

Note: The values in the parentheses indicate estimated standard deviations.

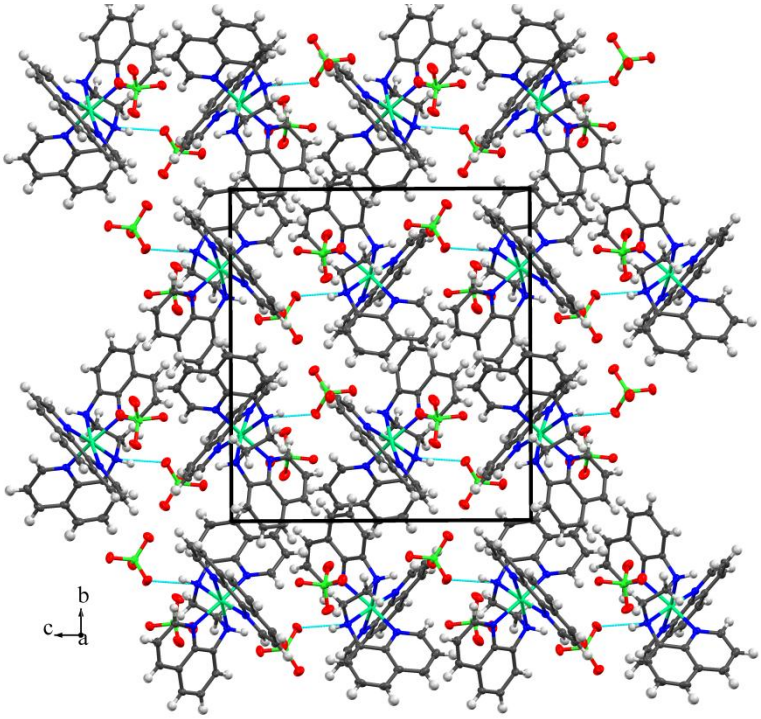

Figure 3.19 *A view of the packing diagram of* ***3*** *along the a-axis showing hydrogen bonding interaction. Color code: C, black; H, medium grey; N, blue; O, red; Cl, green and Ni, sky blue.*

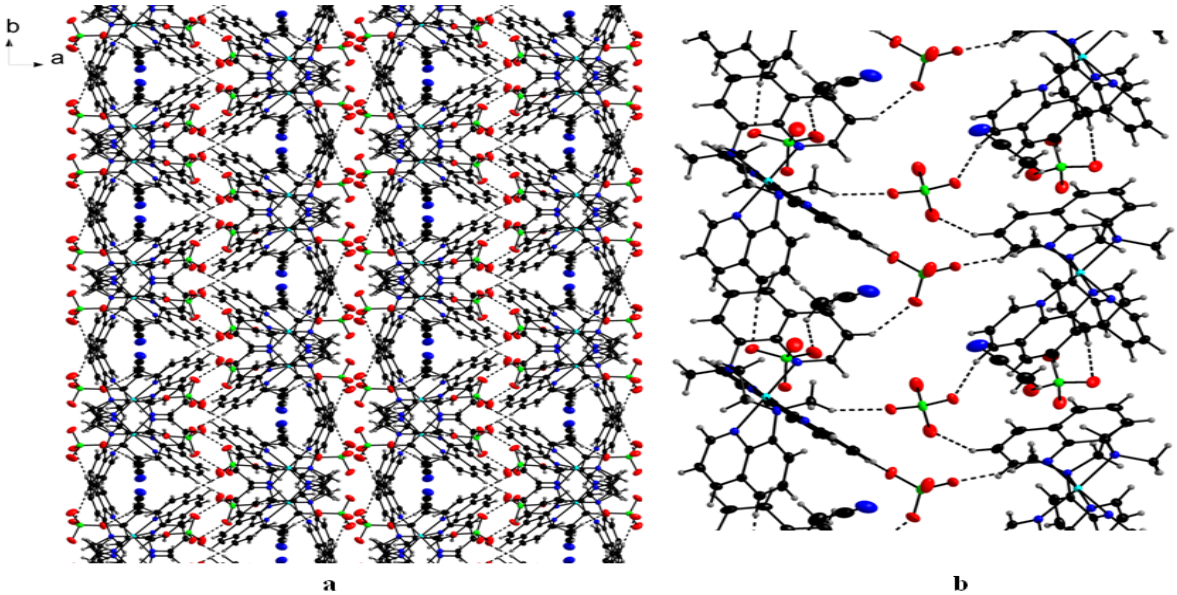

Figure 3.20 *(a) Helical style symmetric organization of* $[Ni(bqen)(phen)]^{2+}$ *cations and* ClO_4^- *anions with the pockets occupied by* CH_3CN *molecules in* ***4*** *along the c-axis. (b) Hydrogen bonding diagram showing C-H···O interactions between cation* $[Ni(bqen)(phen)]^{2+}$ *and* ClO_4^- *anion in* ***4****. Color code: C, black; H, medium grey; N, blue; O, red; Cl, green and Ni, sky blue.*

Table 3.8 *Hydrogen bonding parameters (Å, °) for* ***3*** *and* ***4.***

D-H···A	D-H/Å	H···A/Å	D···A/Å	D-H···A/°
3				
C(15)-H(15) ···O7[a]	0.95(2)	2.397(1)	3.203(2)	142.45(11)
C(6)-H(6) ···O3[b]	0.951(2)	2.418(1)	3.255(2)	146.72(13)
C(10)-H(10A) ···O6	0.99(2)	2.307(1)	3.197(2)	148.94(10)
N(2)-H(31) ···O4	0.93(1)	2.087(1)	2.990(2)	163.57(9)
N(3)-H(32) ···O1[c]	0.93(1)	2.201(1)	3.126(2)	172.90(9)
4				
C(10)-H(10C) ···O8[a]	0.981(2)	2.418(2)	3.321(3)	152.97(12)
C(32)-H(32) ···O5[b]	0.951(2)	2.422(2)	3.288(2)	151.39(12)
C(6)-H(6) ···O3[c]	0.950(2)	2.486(2)	3.432(3)	173.99(13)
C(36)-H(36B) ···O2	0.979(3)	2.439(2)	3.198(3)	134.08(16)
C21(3)-H(21) ···O7[d]	0.950(2)	2.306(2)	3.082(3)	138.41(13)

[a]-0.5+x,0.5-y,1-z. [b] -0.5+x,0.5-y,2-z [c]1-x,0.5+y,1.5-z for ***3***

[a]x,y,1+z. [b]–x,-0.5+y,0.5-z. [c]x,0.5-y,0.5+z [d]-x,0.5+y,0.5-z for ***4***

Note: The values in the parentheses indicate estimated standard deviations.

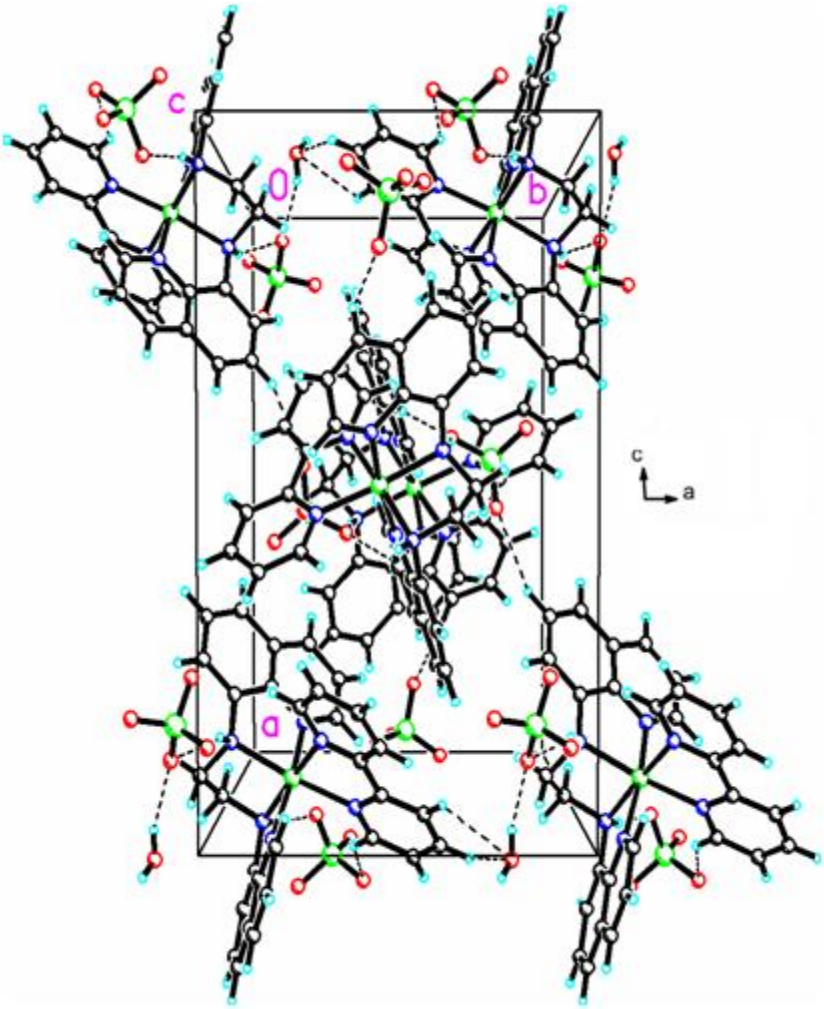

Figure 3.21 *The unit cell of* ***5*** *showing the network of hydrogen bonding.(see figure A3 in appendix for hydrogen bonding interaction in detail)*

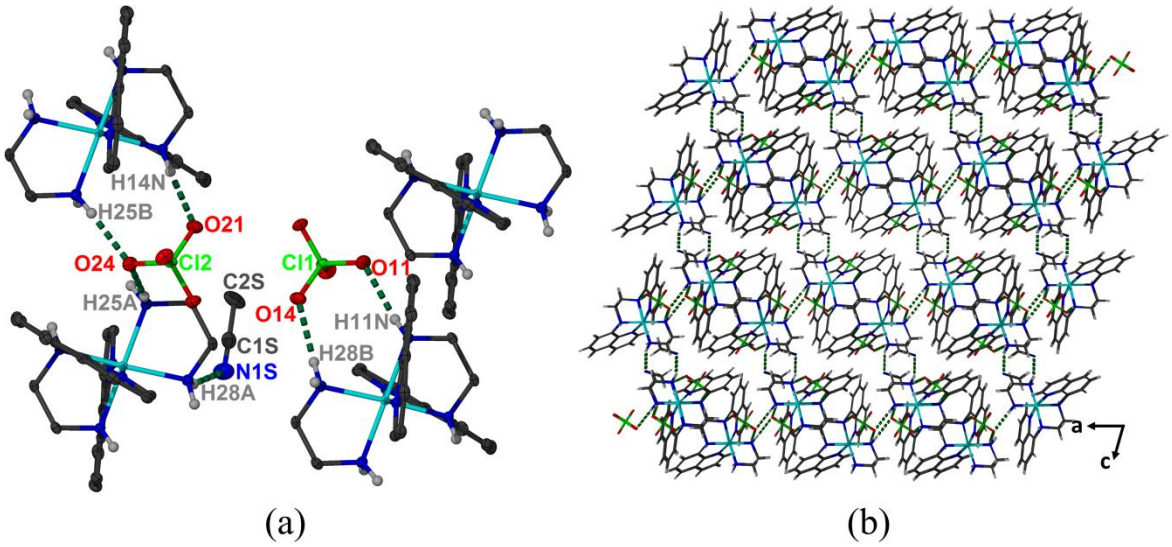

Figure 3.22 *(**a**) Hydrogen bonding interaction in **7** with atom labelling scheme of atoms involved in hydrogen bonding. Hydrogen atoms which are not involved in hydrogen bonding are omitted for clarity (**b**) Enlarged view of a network of hydrogen bonding in **7** showing the symmetric organization of cations $[Ni(bqenH_2)(en)]^{2+}$ and anion ClO_4^- in crystallographic 'ac' plane.*

Table 3.9 *Hydrogen bonding Parameters (Å, °) for **5**.*

D-H⋯A	D-H/Å	H⋯A/Å	D⋯A/Å	D-H⋯A/°
N(11)-H(11) ⋯O(11)[a]	0.848(22)	2.157(20)	2.992(3)	168.24(211)
N(14)-H(14) ⋯O(21)[b]	0.875(22)	2.140(22)	3.013(2)	176.48(213)
N(25)-H(25A) ⋯O(24)[c]	0.920(2)	2.201(2)	3.101(3)	165.70(9)
N(25)-H(25B) ⋯O(24)[b]	0.920(1)	2.099(2)	2.995(3)	164.34(10)
N(28)-H(28B) ⋯O(14)[a]	0.920(1)	2.157(2)	3.063(3)	168.22(10)
N(28)-H(28A) ⋯N(1S)[c]	0.920(2)	2.278(2)	3.148(3)	157.51(9)
[a] x, y+1, z [b] x, y, z+1 [c] -x+2,-y+1,-z+1				

Note: The values in the parentheses indicate estimated standard deviations.

Table 3.10 *Hydrogen bonding Parameters (Å, °) for **7**.*

D-H⋯A	D-H/Å	H…A/Å	D…A/Å	D-H…A/°
O(1S)-H(1S2) ⋯O(31)[a]	0.818(0)	2.651(0)	3.170()	122.86(1)
O(1S)-H(1S1) ⋯O(42A)	0.826(0)	1.890(1)	2.634(0)	149.42(1)
N(50)-H(50) ⋯O(13)	0.821(0)	2.127(0)	2.939(0)	169.47(1)
N(14)-H(14) ⋯O(21B)	0.789(0)	2.301(0)	3.040(1)	156.15(1)
N(14)-H(14) ⋯.O(23A)	0.789(0)	2.188(1)	2.962(1)	166.62(1)
N(11)-H(11) ⋯O(43A)[b]	0.844(0)	2.097(0)	2.889(1)	156.04(1)
N(47)-H(47) ⋯O(42A)	0.827 (0)	2.254 (0)	3.003(0)	150.82(1)
N(14)-H(14) ⋯Cl(2A)	0.789(0)	2.948(0)	3.688(0)	157.15(1)
O(1S)-H(1S1) ⋯.Cl(4A)	0.826(0)	2.958(1)	3.763(1)	165.53(1
[a]1+x, 1+y, z; [b]0.5-x, -0.5+y, 0.5-z.				

Note: The values in the parentheses indicate estimated standard deviations.

Although we could not able to get crystal structure of compound **1** and **2**, the crystal structures of **3-5** and **7** were useful in predicting the structure of **1** and **2**. As the structurally characterized compounds **3-5** and **7** are obtained from the parent compound **1** or **2** further it is be rationalised that the compound **1** and **2** can exist in two isomeric topologies (*cis*-α or *cis*-β) wherein the two H_2O molecules occupies the *cis* positions (**Scheme 3.7**).

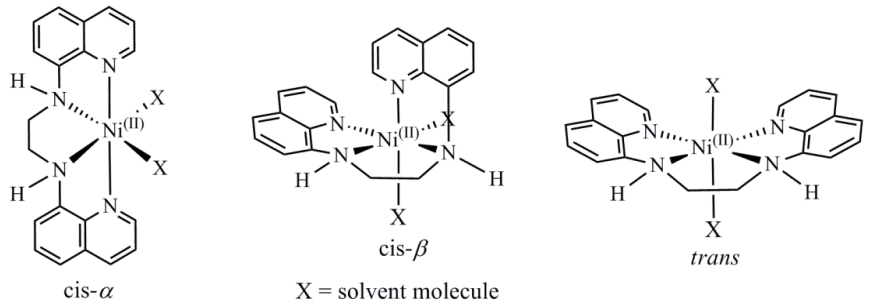

Scheme 3.7 *Proposed isomeric forms of **1** and **2***

3.3.6e Cyclic and differential pulse voltammetry

Compounds **3-8** were also characterized by using cyclic voltammetry (CV) and differential pulse voltammetry (DPV) to explore their electrochemical properties. The CV and DPV plots of compounds **3** and **4** are similar to those of compounds **1** and **2** with $E_{1/2}$ value centred at ~ -1.4 volts (V). Further, the $E_{1/2}$ value for Ni(II)/Ni(I) couple in compounds **5-6** is nearly the same as that observed in **1** and **2**. The cyclic voltammograms recorded at different scan rates were identical and the peak currents increased proportionally with the increase in scan rate.

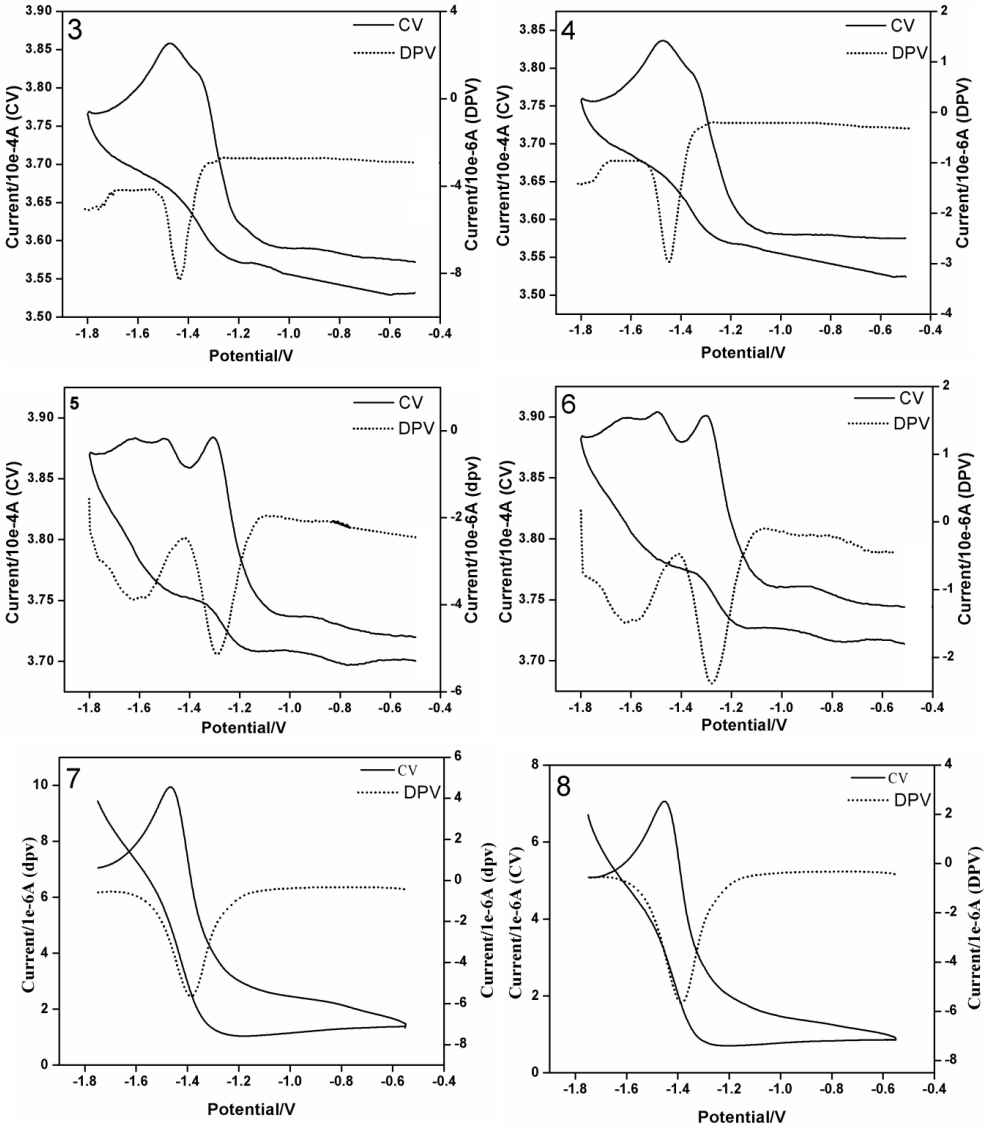

Figure 3.23 *CV(dark solid line) and DPV (dotte line) of* ***3-8*** *recorded in* CH_3CN *containing 0.1 M of* $TBAPF_6$ *as supporting electrolyte with a scan rate of 0.10 V* s^{-1}.

3.3.7 Catalytic hydroxylation of alkanes by 3-8

Compounds **3-8** were tested for the efficacy of catalytic oxidations of hydrocarbons such as cumene, ethylbenzene, and cyclohexane under identical condition as that of **1** and **2**. The hydroxylated products of alkanes were analysed and quantified by gas chromatography (GC) using authentic samples and decane as an internal standard. However no organic products were obtained in the catalytic reactions when compounds **3-8**

were used. There is no surprise in this observation as in the compounds **3-8**, the Ni(II) centre is coordinatively saturated with the strongly bonded six donor N atoms (four of quinoline moiety and two each of phen or bpy) which has resulted in the poor oxidizing power of **3-8**. A mechanism for the C-H activation of alkanes to hydroxylated products is proposed under the similar lines as reported by others.[36,39-42] As shown in **scheme 3.8**, the $[Ni(II)(bqen)(CH_3CN)(m\text{-}CPBA)]^+$ adduct results in the generation of reactive intermediates $[Ni^{II}\text{-}O\cdot(bqen)(CH_3CN)]^+$ and *m*-chlorobenzoic acid radical via homolytic cleavage of O-O bond. We propose that an intermediate $[Ni^{II}\text{-}O\cdot(bqen)(CH_3CN)]^+$ is responsible for the hydroxylation of alkanes giving us alcohols as the major products.

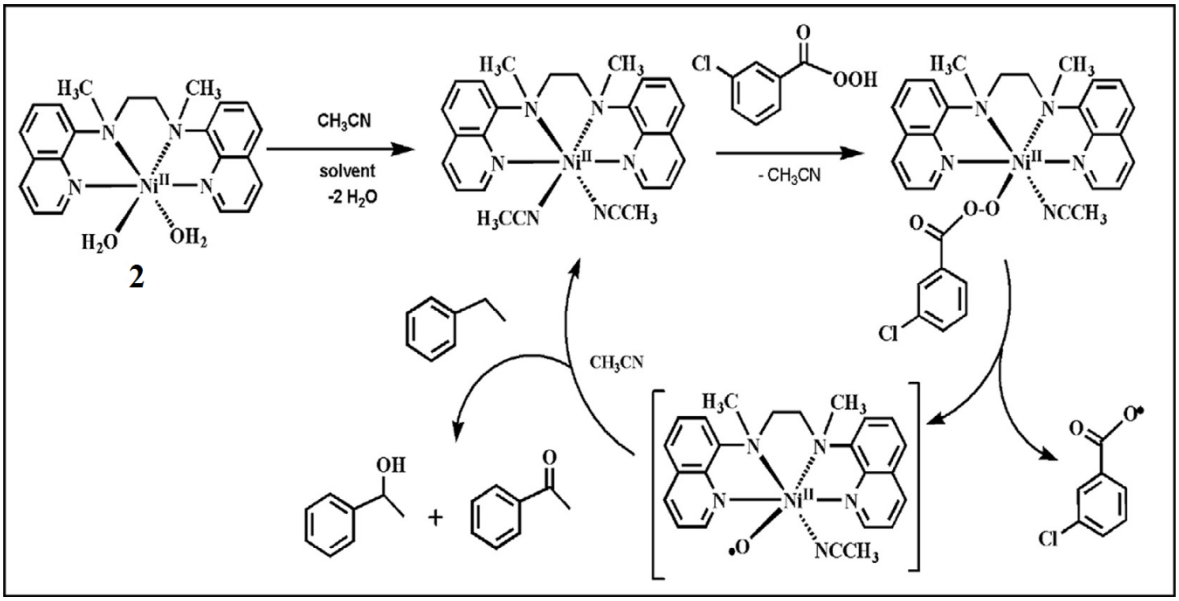

Scheme 3.8 *Proposed mechanism for the alkane hydroxylation by* $[Ni(bqenMe_2)(H_2O)_2]^{2+}$ *using m-CPBA oxidant.*

3.4 Summary and conclusion

In this Chapter, we have reported the synthesis and characterization of eight new Ni(II) octahedral complexes **1-8** containing the tetradentate tripodal ligands bqenH_2 and bqenMe_2. The synthesis of bqenMe_2 was carried out by following the simple alternative route of the reductive methylation of bqenH_2 using $NaCNBH_3$ and formaldehyde at room temperature instead of using n-*B*uLi and CH_3I as reported earlier[55] that require low temperature and dry condition. Both the ligands bqenH_2 and bqenMe_2 were characterized by IR and NMR spectroscopy. The reaction of bqenH_2 and bqenMe_2 with $Ni(ClO_4)_2.6H_2O$ afforded compounds **1** and **2** which were characterized by spectroscopic techniques like IR, UV, ESI-MS, CV and DPV techniques. The efficacy of the compound **1** and **2** were tested in the alkane hydroxylation reaction using cumene, ethyl benzene and cyclohexane to give corresponding alcohol as a major product with the formation of keto product in minor yield. Further, when **1** and **2** were reacted with the auxiliary ligands such as phen, bpy and en we obtained compounds **3-8** by a simple replacement of labile CH_3CN molecules. The compound **3-8** were characterized by spectroscopic and electrochemical techniques and the compounds **3-5** and **7** were structurally characterized by X-ray crystallography. The CV and DPV experiments revealed that compound **1-8** exhibits Ni(II)/Ni(I) quasi-reversible redox couple against SCE in CH_3CN. The compounds **3-8** when tested in the hydroxylation of alkanes using *m*-CPBA oxidant under catalytic conditions did not afford any hydroxylated product. Only **1** and **2** were found to be highly selective in hydroxylating the C-H bonds of alkanes giving alcohols as major products. Interestingly, compound **2** afforded high TON (turn over number) of alcohol and ketone compared to **1**. The observation of high A/K (alcohol/ketone) ratio in the alkane hydroxylation by **1** and **2** thus make these compounds as highly efficient catalysts for alcohol production. The four compounds **3-8** are coordinatively saturated with six donor N making them poor catalysts.

References

(1) Vincent, J. B.; Olivier-Lilley , G. L.; Averill, B. A. *Chem. Rev.* 1990, *90*, 1447–1467.

(2) Feig, A. L.; Lippard, S. J. *Chem. Rev.* 1994, *94*, 759–805.

(3) Wallar, B. J.; Lipscomb, J. D. *Chem. Rev.* 1996, *96*, 2625–2657.

(4) Baik, M. -H.; Newcomb, M.; Friesner , A. R.; Lippard, S. J. *Chem. Rev.* 2003, *103*, 2385–2419.

(5) Costas, M.; Mehn, M. P.; Jensen, M. P.; Jr., L. Q. *Chem. Rev.* 2004, *104*, 939–986.

(6) Tshuva, E. Y.; Lippard, S. J. *Chem. Rev.* 2004, *104*, 987–1012.

(7) Kryatov, S. V.; Rybak-Akimova, E. V.; Schindler, S. *Chem. Rev.* 2005, *105*, 2175–2226.

(8) Kodera, M.; Shimakoshi, H.; Kano, K. *Chem. Commun.* 1996, 1737–1738.

(9) Kitajima, N.; Ito, M.; Fukui, H.; Moro-oka, Y.; *J. Chem. Soc., Chem. Commun.* 1991, 102-104.

(10) Higuchi, T.; Shimada, K.; Maruyama, N.; Hirobe, M. *J. Am. Chem. Soc.* 1993, *115*, 7551–7552.

(11) Nam, W.; Lim, M. H.; Moon, S. K.; Kim, C. *J. Am. Chem. Soc.* 2000, *122*, 10805–10809.

(12) Fish, R. H.; Konings, M. S.; Oberhausen, K. J.; Fong, R. H.; Yu, W. M.; Christou, G.; Vincent, J. B.; Coggin, D. K.; Buchanan, R. M. *Inorg. Chem.* 1991, *30*, 3002-3006.

(13) Tung, H. -C.; Kang, C.; Sawyer, D. T. *J. Am. Chem. Soc.* 1992, *114*, 3445–3455.

(14) Ménage, S.; Vincent, J. M.; Lambeaux, C.; Chottard, G.; Grand, A.; Fontecave ,M. *Inorg. Chem.* 1993, *32*, 4766–4773.

(15) Ménage, S.; Vincent, J. M.; Lambeaux, C.; Fontecave, M. *J. Chem. Soc. Dalton Trans.* 1994, 2081-2084.

(16) Leising, R. A.; Kim, J.; Pérez, M. A.; Jr., L. Q. *J. Am. Chem. Soc.* 1993, *115*, 9524–9530.

(17) Roelfes, G.; Lubben, M.; Hage, R.; Jr., L. Q.; Feringa, B. L. *Chem. Eur. J.* 2000, *6*, 2152-2159.

(18) Chen, K.; Jr., L. Q. *J. Am. Chem. Soc.* 2001, *123*, 6327–6337.

(19) Kaizer, J.; Klinker, E. J.; Oh, N. Y.; Rohde, J. -U.; Song, W. J.; Stubna, A.; Kim, J.; Münck, E.; Nam, W.; Jr., L. Q. *J. Am. Chem. Soc.* 2004, *126*, 472–473.

(20) Leclere, V.; Boiron, P.; Blondeau, R. *Curr. Microbiol.* 1999, *39*, 365–368.

(21) Youn, H. -D.; Youn, H.; Lee, J. -W.; Yim, Y. -I.; Lee, J. K.; Hah, Y. C.; Kang, S.-O. *Arch. Biochem. Biophys.* 1996, *334*, 341–348.

(22) Choudhury, S. B.; Lee, J. -W.; Davidson, G.; Yim, Y. -I.; Bose, K.; Sharma, M. L.; Kang, S. -O.; Cabelli, D. E.; Maroney, M. J. *Biochemistry* 1999, *38*, 3744–3752.

(23) Fiedler, A. T.; Bryngelson, P. A.; Maroney, M. J.; Brunold, T. C. *J. Am. Chem. Soc.* 2005, *127*, 5449–5462.

(24) Pelmenschikov, V.; Siegbahn, P. E. M. *J. Am. Chem. Soc.* 2006, *128*, 7466–7475.

(25) Dai, Y.; Pochapsky, T. C.; Abeles, R. H. *Biochemistry* 2001, *40*, 6379–6387.

(26) Itoh, S.; Bandoh, H.; Nakagawa, M.; Nagatomo, S.; Kitagawa, T.; Karlin, K. D.; Fukuzumi, S. *J. Am. Chem. Soc.* 2001, *123*, 11168–11178

(27) Hikichi, S.; Yoshizawa, M.; Sasakura, Y.; Akita, M.; Moro-oka, Y. *J. Am. Chem. Soc.* 1998, *120*, 10567–10568.

(28) Mandimutsira, B. S.; Yamarik, J. L.; Brunold, T. C.; Gu, W.; Cramer, S. P.; Riordan, C. G. *J. Am. Chem. Soc.* 2001, *123*, 9194-9195.

(29) Hikichi, S.; Yoshizawa, M.; Sasakura, Y.; Komatsuzaki, H.; Moro-oka, Y.; Akita, M. *Chem. Eur. J.* 2001, *7*, 5011-5028.

(30) Shiren, K.; Ogo, S.; Fujinami, S.; Hayashi, H.; Suzuki, M.; Uehara, A.; Watanabe, Y.; Moro-oka, Y. *J. Am. Chem. Soc.* 2000, *122*, 254–262.

(31) Cho, J.; Furutachi, H.; Fujinami, S.; Suzuki, M. Angew. Chem. Int. Ed. 2004, 43 3300–3303.

(32) Kieber-Emmons, M. T.; Schenker, R.; Yap, G. P. A.; Brunold, T. C.; Riordan,C. G. *Angew. Chem. Int. Ed.* 2004, 43, 6716–6718.

(33) Fujita, K.; Schenker, R.; Gu, W.; Brunold, T. C.; Cramer, S. P.; Riordan, C. G. *Inorg. Chem.* 2004, *43*, 3324–3326.

(34) Schröder, D.; Schwarz, H. *Angew. Chem. Int. Ed. Engl.* 1995, *34*,1973-1995.

(35) Nagataki, T.; Tachi, Y.; Itoh, S. *Chem Commun*. 2006, 4016–4018.

(36) Nagataki, T.; Ishii, K.; Tachi, Y.; Itoh, S. *Dalton Trans.* 2007, 1120–1128.

(37) Nagataki, T.; Itoh, S. *Chem. Lett.* 2007, *36*, 748–749.

(38) Morimoto, Y.; Bunno, S.; Fujieda, N.; Sugimoto, H.; Itoh, S. *J. Am. Chem. Soc.* 2015, *137*, 5867–5870.

(39) Hikichi, S.; Okuda, H.; Ohzu, Y.; Akita, M. *Angew. Chem. Int. Ed.* 2009, *48*, 188–191.

(40) Hikichi, S.; Hanaue, K.; Fujimura, T.; Okuda, H.; Nakazawa, J.; Ohzu, Y.; Kobayashi, C.; Akita, M.; *Dalton Trans.* 2013, *42*, 3346–3356.

(41) Nakazawa, J.; Terada, S.; Yamada, M.; Hikichi, S. *J. Am. Chem. Soc.* 2013, *135*, 6010–6013.

(42) Pfaff, F. F.; Heims, F.; Kundu, S.; Mebs, S.; Ray, K. *Chem. Commun.* 2012, *48*, 3730-3732.

(43) Balamurugan, M.; Mayilmurugan, R.; Suresh, E.; Palaniandavar, M. *Dalton Trans.* 2011, *40*, 9413–9424.

(44) Sankaralingam, M.; Vadivelu, P.; Suresh, E.; Palaniandavar, M. *Inorg. Chim. Acta* 2013, *407*, 98–107.

(45) Sankaralingam, M.; Balamurugan, M.; Palaniandavar, M.; Vadivelu, P.; Suresh, C. H. *Chem. Eur. J.* 2014, *20*, 11346–11361.

(46) Sankaralingam, M.; Vadivelu, P.; Palaniandavar, M. *Dalton Trans.* 2017, *46*, 7181–7193.

(47) Draksharapu, A.; Codolà, Z.; Gómez, L.; Lloret-Fillol, J.; Browne, W. R.; Costas, M. *Inorg. Chem.* 2015, *54*, 10656–10666.

(48) Corona, T.; Pfaff ,F. F.; Acuña-Parés, F.; Draksharapu, A.; Whiteoak, C. J.; Martin-Diaconescu, V.; Lloret-Fillol, J.; Browne, W. R.; Ray, K.; Company, A. *Chem. Eur. J.* 2015, *21*, 15029–15038.

(49) Corona, T.; Draksharapu, A.; Padamati, S. K.; Gamba, I.; Martin-Diaconescu, V.; Acuna-Parés, F.; Browne, W. R.; Company, A. *J. Am. Chem. Soc.* 2016, *138*, 12987–12996.

(50) Pirovano, P.; Farquhar, E. R.; Swart, M.; Fitzpatrick, A. J.; Morgan, G. G.; McDonald, A. R. *Chem. Eur. J.* 2015, *21*, 3785–3790.

(51) Pirovano, P.; Farquhar, E. R.; Swart, M.; McDonald, A. R. *J. Am. Chem. Soc.* 2016, *138*, 14362–14370.

(52) Cho, J.; Kang, H. Y.; Liu, L. V; Sarangi, R.; Solomon, E. I.; Nam, W. *Chem. Sci.* 2013, *4*, 1502–1508.

(53) Kieber-Emmons, M. T.; Annaraj, J.; Seo, M. S.; Van Heuvelen, K. M.; Tosha, T.; Kitagawa, T.; Brunold, T. C.; Nam, W.; Riordan, C. G. *J. Am. Chem. Soc.* 2006, *128*, 14230–14231.

(54) Bravo, A.; Bjorsvik, H. R.; Fontana, F.; Minisci, F.; Serri, A. *J. Org. Chem.* 1996, *61*, 9409–9416.

(55) England, J.; Britovsek, G. J. P.; Rabadia, N.; White, A. J. P. *Inorg. Chem.* 2007, *46*, 3752-3767.

(56) Nehru, K.; Kim, S. J.; Kim, I. Y.; Seo, M. S.; Kim, Y.; Kim, S. -J.; Kim, J.; Nam, W. *Chem. Commun.* 2007, 4623-4625.

(57) Yoon, J.; Wilson, S. A; Jang, Y. K.; Seo, M. S.; Nehru, K.; Hedman, B.; Hodgson, K. O.; Bill, E., Solomon, E. I.; Nam, W. *Angew. Chem. Int. Ed.* 2009, 48, 1257–1260.

(58) McAuley, A.; Xu, C. *Inorg. Chem.* 1992, 31, 5549.

(59) Narulkar, D. D.; Patil, A. R.; Naik, C. C.; Dhuri, S. N. *Inorg. Chim. Acta* 2015, *427*, 248–258

(60) Moore, M. L. *Org. React.* 1949, *6*, 301.

(61) Pine, S. H.; Sanchez, B. L. *J* . Org. *Chem.* 1971, *36*, 829.

(62) Borch, R. F.; Hassid, A. I. *J. Org. Chem.* 1971, *37*, 1971–1972.

(63) Nakamoto, K.: *Infrared and Raman Spectra of Inorganic and Coordination Compounds, Part B: Applications in coordination, organometallic, and bioinorganic chemistry,* 6th ed.; John Wiley, Hoboken, NJ) (2009).

(64) Huheey, J. E.; Keiter, E. A.; Keiter, R. L.; Medhi, O. K. *Inorganic Chemistry, Principles of Structure and Reactivity*, 4th ed., *(Pearson)* (1993) 466.

(65) Ali, M. A.; Mirza, A. H.; Hj, F.; Haniti, M.; Hamid, S. A.; Bernhardt, P. V.; *Polyhedron* 2006, *25*, 3245–3252.

(66) Choi, K.-Y.; Choi, S.N.; Suh, I.-H. *Polyhedron* 1998, *17*, 1415.

(67) Temel, H.; Ilhan, S.; Aslanogˇlu, M.; Kılıcl, A.; Tas, E. *J. Chin. Chem. Soc.* 2006, *53*, 1027.

(68) Chandra, S.; Kumar, R. *Spectrochim. Acta, Part. A 2005*, *62*, 518.

(69) Manjunathan, S.; Krishnan, C.N. *Asian J. Chem.* 2007, *19*, 861.

(70) Huh, D.N.; Gibbons, J.B.; Haywood, R.S.; Moore, C.E.; Rheingold, A. L.; Ferguson, M.J. *Inorg. Chim. Acta* 2014, *423*, 290.

(71) El-Said, A.I.; Zidan, A.S.A.; El-Meligy, M.S.; Aly, A.A.M.; Mohammed, O.F. *Trans. Met. Chem*. 2001, *26*, 13.

(72) Frenz, B.A.; IBers, J. A. *Inorg. Chem.* 1972, *11*, 1109.

(73) Sharma, A.K.; Biswas, S.; Barman, S.K.; Mukherjee, R. *Inorg. Chim. Acta* 2010, *363*, 2720.

(74) Garcia-Santos, I.; Sanmartin, J.; Garcia-Deibe, A.M.; Fondo, M.; Gomez, E. *Inorg. Chim. Acta* 2010, *363*, 193.

(75) Sertphon, D.; Harding, D.J.; Harding, P.; Adams, H. *Polyhedron* 2011, *30*, 2740.

(76) Wagner, F.; Mocella, M.T.; D'Aniello, Jr.; M. J., Wang, A .H. J.; Kent, E. *J. Am. Chem.Soc.* 1974, *96*, 2625.

CHAPTER –IV

Mn(II) complex and Mn(III)-peroxo intermediate bearing novel non-heme N3Py2 ligand : Reactivity study in oxidation reactions

4.1 Introduction and literature

Among the biological relevant transition metals, manganese is the metal of the essence as it is the component of an active site of many redox metalloenzymes. The involvement of manganese in biological redox system was recognized after the discovery of manganese superoxide dismutase (Mn-SOD) in 1970.[1] The significance of manganese in the bioinorganic field was further fueled by the finding that manganese constitutes an active site of oxygen-evolving complex (OEC) in photosystem II.[2] Apart from the biological role of manganese in dismutazation and oxygen-evolving in photosynthesis, several other enzymes are known to perform various roles in biology (**Table 4.1**).

Table 4.1 *List of the Mn-enzymes catalyzing specific reaction in the biological system*

Mn-Enzymes	Biological Reactions
Manganese (II) superoxide dismutase (Mn-SOD)	Catalyzes disproportionation of $O_2^{\bullet-}$ to H_2O_2 and O_2[3–6]
(Oxygen-evolving complex (OEC)) in Photosystem II	Water splitting (converts H_2O to O_2)[7,8]
Manganese ribonucleotides reductase	Generates cysteine radical that facilitates the conversion of deoxyribonucleotide from ribonucleotides[9–11]
Manganese catalase	Disproportionation of the reactive H_2O_2[12]
Oxalate oxidase	Oxidation of oxalate using molecular oxygen to H_2O_2 and CO_2[13,14]
Oxalate decarboxylase	Decarboxylation of oxalate by cleavage of C-C to CO_2 and formate using molecular oxygen[15–17]
Manganese-dependent homoprptocatechuate 2,3-dioxygenase (MndD)	Catalyzes the ring opening of homoprotocatechuate (HPCA)[18]

The interaction of manganese present at the active site in these enzymes with O_2^{n-} (n = 0, 1, 2) results in the formation of Mn-dioxygen intermediates which are the key

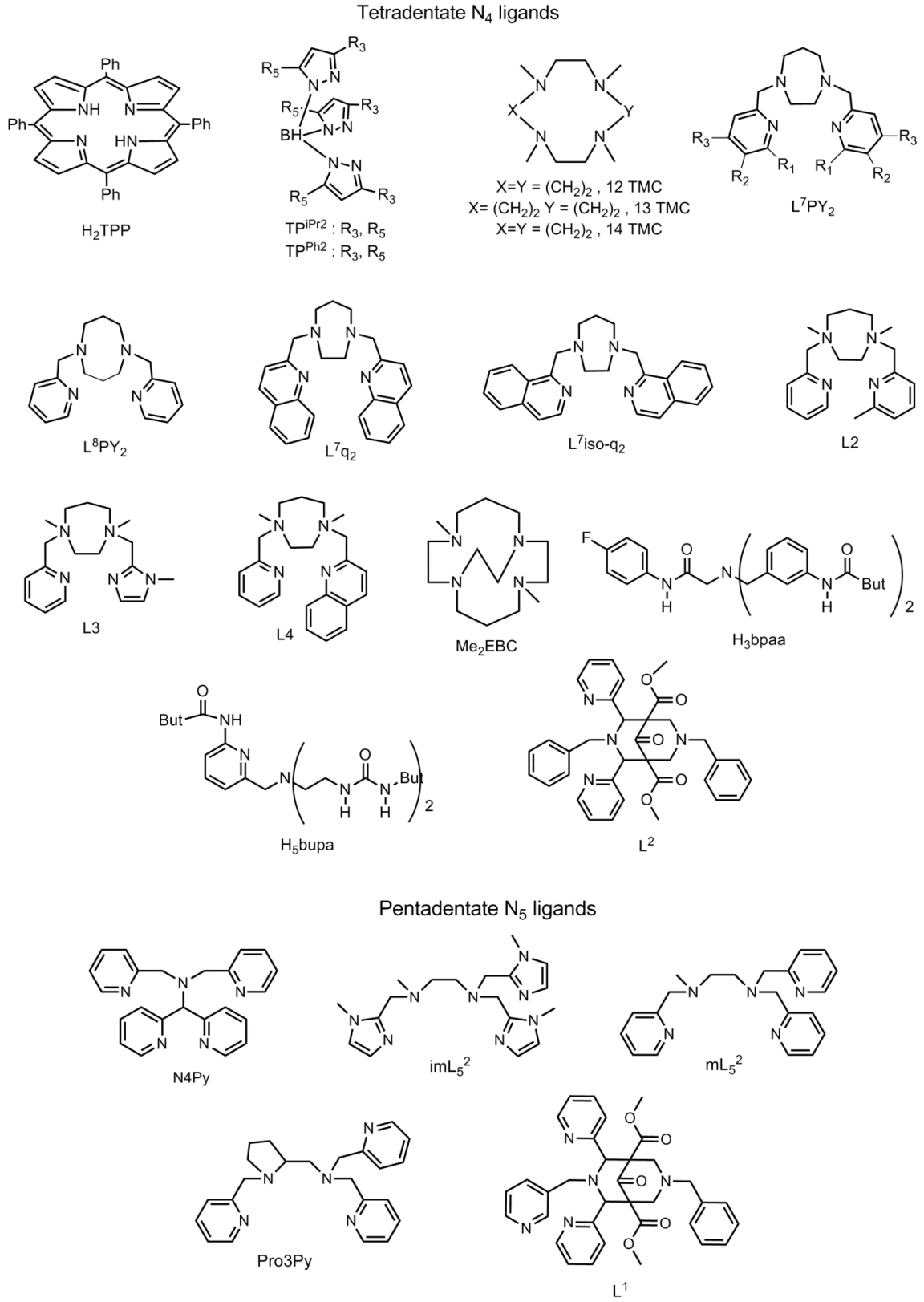

Scheme 4.1 *A reported set of ligands stabilizing manganese^{III}-peroxo intermediates.*

reactive intermediate responsible for the several specific reactions.[19] These intermediates are short-lived owing to their inherent reactivity and hence the chemistry of such species in

enzymatic reactions is difficult to explore.[20] Therefore, the study of structural and functional model complexes of enzymes has provided the aided advantage in understanding the chemistry relevant to enzymes in biological science. In this Chapter we are mainly emphasizing on the Mn^{III}-peroxo intermediate. The Mn^{III}-peroxo species have often been detected as a reactive intermediate in the enzymes such as Mn-SOD[3,4] MndD[18], manganese ribonucleotide reductase[11], OEC in photosystem[7] and they have been well characterized by spectroscopic techniques and supported by computational studies. In biomimetic chemistry a number of such Mn^{III}-peroxo intermediate have been synthesized and characterized by multi spectroscopic techniques like EPR, ESI-MS, Raman and few are even characterized by X-ray crystallography as well as by computational studies. A diverse set of ligands architecture ranging from porphyrin ligand, neutral tetraazamacrocyclic ligand, facially coordinating tris(pyrazolyl)borates, aminopyridyl and aminoquinolyl based ligand have been employed inorder to stabilize the Mn-peroxo intermediate (**Scheme 4.1**).

4.1.1 Synthetic Mn-peroxo complex

The first Mn-dioxygen intermediate was observed by Basolo and coworkers in 1975 in the reaction of synthetic manganese porphyrin Mn^{III}(TPP)(Py) (TPP = meso-tetraphenylporphyrin) with dioxygen at -78 °C.[21] Based on the spectroscopic characterization techniques this compound was formulated as manganese^{IV}-peroxo $Mn^{IV}(TPP)(O_2)$. However in 1989, the first heme-based side-on peroxide manganese(III) porphyrin complex $[Mn^{III}(O_2)(TPP)]^-$ (tpp = *meso*-tetraphenylporphyrin) was characterized crystallographically as a model compound of manganese peroxo intermediate[22] (**Scheme 4.2**). The initial studies in this field were mainly focused on the oxygenation of Mn-porphyrin complex. When it was recognized that the manganese sites in Mn-SOD and the

OEC were non-heme sites, there was a simultaneous shift of focus on synthesizing and modelling non-heme manganese complexes.[19] The Mn-peroxo intermediate in Mn-SOD is the only structurally characterized intermediate in biology so far.[23] The Mn-SOD at its resting state consists of four tetramers, each of which consists of Mn(II) at its active site possessing trigonal bipyramidal geometry contributed by three histidines, an aspartate and a solvent molecule.[24] The crystal structure of Mn-SOD was determined by the treatment of peroxide to the cryo-trapped *Escherichia coli* Mn-SOD which revealed side-on binding of peroxide to manganese, occupying a site of an axial solvent on three out of four tetramers.[23] So far there are only seven manganese peroxo intermediates known which are characterized structurally due to their sufficient thermal stability as shown in **Scheme 4.2**. These intermediates are supported by ligands which include monoanionic facially coordinating trispyrazolyl ligands[25–27] and that of macrocyclic *N*-tetramethylated cyclam (TMC) ligands[28–30] (**Scheme 4.2**). It was observed that the Mn-peroxo complex $[Mn^{III}(O_2)(Tp^{iPr2})(pz^{iPr2})]$ (brown) obtained from tridentate Tp^{ipr2} (hydrotris(3,5-diisopropylpyrazol-1-yl)borate) and monodentate pz^{iPr2} (3,5-isopropylpyrazole) is stable for a few hours at room temperature. This compound upon cooling from 253 K to 193 K results in the formation of intramolecular hydrogen bonding between an O atom of the peroxo group with N-H functional group of pyrazole ligand $pz^{ipr2}H$ to give its isomer $[Mn^{III}(O_2)(Tp^{iPr2})(pz^{iPr2})]$ (blue). These changes reflect in its absorption pattern which shows shifts in λ_{max} from 561 nm to 583 nm.[25] Similar to that, the intermolecular hydrogen bonding is also observed in $[Mn^{III}(O_2)(Tp^{iPr2})(Me\text{-}^{Im}H)]$ complex ($Me^{Im}H$ = 2-methyl imidazole). When Mn-peroxo complexes were tried to obtain by replacing $Me^{Im}H$ by $Im^{Me}Me$ (2,3-dimethylimidazole) and pyridine, the formation of corresponding Mn-peroxo was not observed. This shows that hydrogen bonding is necessary for the stabilization of the peroxo intermediate. The peroxo intermediate $[Mn^{III}(O_2)(Tp^{Ph2})(THF)]$ (Tp^{Ph2} =

tris(3,5-diphenylpyrazol)hydroborate) THF = tetrahydrofuran) which do not show hydrogen bonding are stabilized due to the shielding of peroxo group by phenyl groups of the Tp^{Ph2} ligand. The other three complexes $[Mn^{III}(O_2)(12\text{-}TMC)]^+$, $[Mn^{III}(O_2)(13\text{-}TMC)]^+$, $[Mn^{III}(O_2)(14\text{-}TMC)]^+$ containing four nitrogen of the TMC ligand coordinated to the manganese centre with a peroxo ligand bound to the manganese symmetrically. The *N*-methyl group of the TMC ligand point towards the peroxo group as a result peroxido ligand is well protected from the external environment in the pocket of the four methyl groups giving high thermal stability. All the structurally characterized intermediate revealed side-on peroxo (η^2-O_2) with an O-O bond length ranging from 1.40-1.43 Å and Mn-O ranging from 1.841 to 1.901 Å.

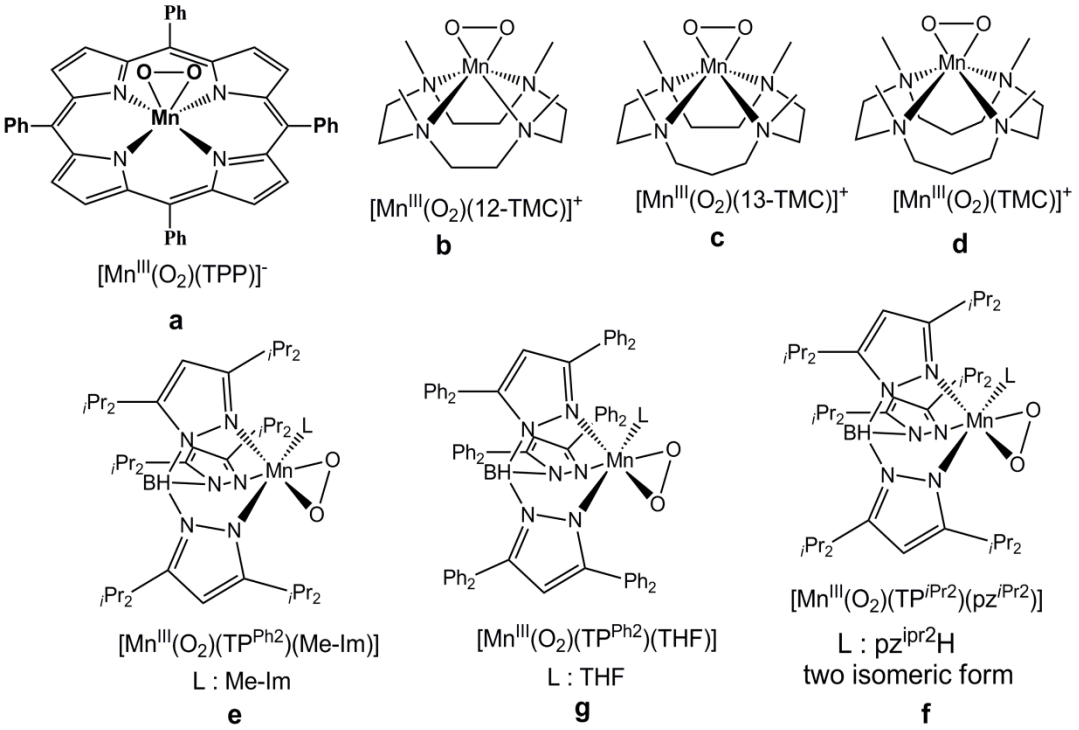

Scheme4.2 *Structurally characterized Mn-peroxo species of heme and non-heme ligands.*

Apart from these structurally characterized Mn-peroxo intermediates, many Mn-peroxo compounds have been prepared by using different oxidants. The reaction of manganese complex with oxidants such as aqueous H_2O_2, potassium superoxide (KO_2), dioxygen under suitable conditions leads to the formation Mn^{III}-peroxo species. The

stability of these is mainly governed by the supporting ligands. **Table 4.2** lists synthetic Mn^{III}-peroxo intermediates with their UV-Vis spectral features and stability, that are obtained from corresponding Mn(II) complex using different oxidants. The formation of these Mn-peroxo species was primarily characterized by UV-Vis spectroscopy which shows distinct absorption features after the reaction of manganese complexes with an oxidant. The stability of these species was monitored by following decay of the peak due to Mn-Peroxo species at its λ_{max} and is represented by their t½ value. A number of Mn-peroxo have been obtained by the reaction of Mn(II) complex with H_2O_2. In some cases a large excess of H_2O_2 is required[25,26,31,32] while in some cases the addition of triethylamine (basic condition) is required.[20,28–38] It is observed that the peroxide occupies the position *trans* to the weakly coordinating solvent molecule. The potassium superoxide (KO_2) which acts as a one-electron oxidant have often been employed and reacts with Mn(II) complex to give Mn^{III}-peroxo complex.[22,27,31,33,39-43] Few of the peroxo complexes $[Mn^{III}(O_2)(H_2bupa)]^-$ and $[Mn^{III}(O_2)(H_2bppa)]$ were obtained by the reaction with dioxygen.[32,44] $[Mn^{II}(O_2)(H_2bupa)]^-$ reacts with O_2 to give $[Mn^{III}(O_2)(H_2bupa)]^-$ in 50 % yield which increases in the presence of diphenylhydrazine (DPH).[44] The complex $[Mn^{II}(H_2bpaa)]$ reacts with O_2 only in the presence of hydrogen atom donors like DPH, indene and fluorene to yield $[Mn^{III}(O_2)(H_2bppa)]$.[32] Recently it is also shown that three Mn^{III}-peroxo intermediates viz. $[Mn^{III}(O_2)(N4py)]^+$, $[Mn^{III}(O_2)(mL_5{}^2)]^+$, $[Mn^{III}(O_2)(imL_5{}^2)]$ can also be obtained in high yield by the reaction of Mn(II) complexes with electrochemically generated superoxide.[40] It is observed that when complex $[Mn^{II}(N4py)(OTf)](OTf)$ was treated with KO_2 and H_2O_2, the product obtained was distinctly different from the one obtained using electrochemically generated superoxide. The transfer of peroxo group from $[Ni^{III}(12\text{-}TMC)(O_2)]^+$ and $[Co^{III}(12\text{-}TMC)(O_2)]^+$ to $[Mn^{II}(14\text{-}TMC)]^{2+}$ have also resulted in the formation of $[Mn^{III}(12\text{-}TMC)(O_2)]^+$.[45]

***Table 4.2**: List of the Mn^{III}-peroxo prepared by a different synthetic approach with their UV-Vis spectral features and stability*

Sr. No.	Mn-Peroxo complex	UV-Vis features (t½)
(I)	Reaction of Mn^{II} complex with H_2O_2	
1[25]	$[Mn^{III}(O_2)(Tp^{iPr2})\ pz^{iPr2}]$	561 (50), (stable at RT for few h)
2[25]	$[Mn^{III}(O_2)(Tp^{iPr2})\ pz^{iPr2}]$	583 (60), (stable at RT for few h)
3[26]	$[Mn^{III}(O_2)(Tp^{iPr2})(Me\text{-}Im)]$	381 (314), 478 (173)
(II)	Reaction of Mn^{II} complex with H_2O_2 in presence of TEA	
4[33]	$[Mn^{III}(O_2)(L^7py_2^{H})]^+$	445(280), 590(120) (15 min at 0°C)
[a]5[33]	$[Mn^{III}(O_2)(L^7py_2^{6\text{-}Me})]^+$	415 (280), 620 (80) (6 min at 0°C)
[a]6[33]	$[Mn^{III}(O_2)(L^7py_2^{6\text{-}MeO})]^+$	416 (250), 560(80) (~ seconds at 0°C)
[a]7[33]	$[Mn^{III}(O_2)(L^7py_2^{5\text{-}Br})]^+$	445 (220), 589 (90) (3 min at 0 °C)
8[34]	$[Mn^{III}(O_2)(L^7q_2)]^+$	415 (305), 606 (70) (4 min at 0°C)
9[34]	$[Mn^{III}(O_2)(L^7py_2^{4\text{-}Me})]^+$	445(260), 588(100) (6 min at 0°C)
10[34]	$[Mn^{III}(O_2)(L^8py_2^{H})]^+$	465 (280), 599 (120) (12 min at 0°C)
11[35]	$[Mn^{III}(O_2)(L^7py_2^{4\text{-}Cl})]^+$	442 (262), 568(102) (10 min at 0°C)
12[35]	$[Mn^{III}(O_2)(L^7iso\text{-}q_2)]^+$	446 (291), 587 (112) (30 min at 0°C)
13[28]	$[Mn^{III}(O_2)(14\text{-}TMC)]^+$	453 (490), 630 (120) (5 h at 25 °C)
14[29]	$[Mn^{III}(O_2)(13\text{-}TMC)]^+$	452 (390), 615 (190) (several days at 25 °C)
15[30]	$[Mn^{III}(O_2)(12\text{-}TMC)]^+$	455 (250), 620 (200) (Stability ND)
16[36]	$[Mn^{III}(O_2)(L2)]^+$	440 (175), 597 (41) (4 min at 0°C)
17[36]	$[Mn^{III}(O_2)(L3)]^+$	434 (214) , 592 (42) (22 min at 0°C)
18[36]	$[Mn^{III}(O_2)(L4)]^+$	435 (149) , 558 (39) (6 min at 0°C)
19[20]	$[Mn^{III}(O_2)(Pro3Py)]^+$	580 (200) (2 h at 0°C)
20[37]	$[Mn^{III}(O_2)(L^1)]^+$	605 (270) (60 min. at 15 °C)
21[38]	$[Mn^{III}(O_2)(L^2)]^+$	450 (160) (100 sec. at 15°C)
(III)	Reaction of Mn^{II} complex with KO_2	
22[22]	$[Mn^{III}(O_2)(TPP)]^-$	983 (50)
23[27]	$[Mn^{III}(O_2)(Tp^{Ph2})(THF)]$	379 (324), 436(73) (4.5 days stability)
24[43]	$[Mn^{III}(O_2)(Me_2EBC)]^+$	650 (530), 400 (185) (decays within 40 min at -60
(IV)	Reaction of Mn^{II} complex with electrochemically generated $O_2^{\bullet-}$	
[a,b]25[40]	$[Mn^{III}(O_2)(imL_5^2)]^+$	542 (484)
[a,b]26[40]	$[Mn^{III}(O_2)(mL_5^2)]^+$	585 (335)
[a,b]27[40]	$[Mn^{III}(O_2)(N4py)]^+$	617 (280)
(V)	Reaction of Mn^{II} complex with dioxygen	
28[44]	$[Mn^{III}(O_2)(H_2bupa)]^-$	660 (300), 490 (ND)
[a]29[32]	$[Mn^{III}(O_2)(H_2bpaa)]$	590 (58),460 (ND)

[a] Mn-peroxo can also be prepared using KO_2, [b]Mn-peroxo intermediate can also be prepared with H_2O_2.

4.1.2 Reactivity studies of Mn^{III}-peroxo species

The reactivity study of know Mn^{III}-peroxo have been investigated in aldehyde deformylation reactions and the reactivity is dependent on several factors. It is reported that the reactivity of Mn^{III}-peroxo supported by tetradentate aminopyridyl ligands($L^7py_2^R$) is influenced by changing the substituents on the pyridine ring due to the steric hindrance of aldehyde-peroxo interaction.[34] Nam and coworkers have studied the Mn^{III}-peroxo complex bearing *N*-methylated cyclam ligands. The nature of the ligand *trans* to the peroxo group was found to have a remarkable effect on the aldehyde deformylation reactions. The incorporation of the anionic ligand to $[Mn^{III}(O_2)(13\text{-TMC})]^+$ resulted in the formation of neutral Mn^{III}-peroxo intermediate $[Mn^{III}(O_2)(13\text{-TMC})(X)]$ (X= CN^-, NCS^-, $CF_3CO_2^-$ and N_3^-) which demonstrated the accelerated rate in deformylation reaction of CCA (cyclohexane carboxaldehyde).[29] It was proposed that the introduction of anionic axial ligand makes the Mn^{III}-peroxo more electron rich as revealed from the shift of the redox potential negatively thus making Mn^{III}-peroxo more nucleophilic. The conversion of side-on peroxo into the end-on peroxo which is more nucleophilic upon binding on the anionic axial ligands).[29] The reactivity study of Mn^{III}-peroxo and bis(μ-oxo)Mn^{III}_2 species both constituting TMC ligand core, showed that the latter do not undergo aldehyde deformylation reaction.[30] So far, the reactivity study carried out in aldehyde deformylation reaction showed that the Mn-peroxo species possesses nucleophilic character. However in one of the recent study by C.V. Sastri on the reactivity of Mn^{III}-peroxo supported by tetradentate N_4 as well as a pentadentate N_5 bispidine ligand, it is observed that the deformylation reaction by Mn^{III}-peroxo complex proceeds by initial hydrogen atom abstraction instead of a nucleophilic attack of peroxo group on the carbonyl carbon of aldehyde.[37,38] The study shown that the aldehyde deformylation proceeds by hydrogen atom abstraction from the α position as evident from a large kinetic isotope effect by using

α-[D_1]-PPA.

In another study it is showed that the formation of kind of Mn-peroxo intermediate depends upon the choice of the oxidant. The [Mn^{II}(N4py)(OTf)](OTf) reacts with one equivalent of KO_2 to give [$Mn^{III}(O_2)$(N4py)]$^+$ (yield =30 %) initially, which further decomposes to give bis(μ-oxo) complex, [$Mn^{II}Mn^{III}(\mu\text{-}O)_2(N4py)_2]^{3+}$. When an excess of KO_2 is used, the formation of [$Mn^{III}(O_2)$(N4py)]$^+$ is observed which thermally decayed to Mn^{II} species with the formation of [$Mn^{II}Mn^{III}(\mu\text{-}O)_2(N4py)_2]^{3+}$ in lesser yield. When [$Mn^{III}(O_2)$(N4py)]$^+$ was reacted with [Mn^{II}(N4py)(OTf)](OTf), [$Mn^{II}Mn^{III}(\mu\text{-}O)_2(N4py)_2]^{3+}$ was formed. The complex [$Mn^{II}Mn^{III}(\mu\text{-}O)_2(N4py)_2]^{3+}$ can be independently prepared by its reaction with H_2O_2 in the presence of TEA.[42]

Since the manganese complexes supported by pentadentate ligands are well stabilized in their high valent oxidation state at room temperature[46–48] we thought of generating the Mn^{III}-peroxo species bearing pentadentate N3Py2 (*N,N'*-dimethyl-N-(2-(methyl(pyridine-2-ylmethyl)amino)ethyl)-N'-(pyridine-2-ylmethyl)ethane-1,2-diamine) ligand In all the Mn^{III}-peroxo intermediates bearing tetradentate ligand, it is observed that the peroxo group is bound to the Mn(III) ion in a side-on (η^2) manner, few of which are evident by X-ray crystallography.[11] However, the peroxo group can bind either in a side-on (η^2) or end-on (η^2) fashion to the metal centre that is supported by pentadentate ligand. Nam and coworker, proposed the probability of conversion of more nucleophilic end-on peroxo with the addition of the anionic axial ligand to the side-on Mn-peroxo supported by tetradentate TMC ligand.[29] Contrary to this, the computational study demonstrated that the Mn-peroxo exists as a side-on isomer by dissociation of one of the coordinated *N*-donor group of pentadentate ligands (mL_5^2 and imL_5^2, N4Py, Pro3Py, bispidine ligand (**Scheme 4.1**) to the Mn(III) center.[20,37,39] In the current work we report the generation and characterization of the Mn^{III}-peroxo intermediate from the corresponding Mn(II) complex

supported by pentadentate N3Py2 ligand and its reactivity in aldehyde deformylation reaction.

4.1.3 Mn(II) complexes in the catalytic epoxidation reaction

The epoxides are excellent building blocks for the subsequent transformation in organic synthesis and are significantly important in the production of fine chemicals and pharmaceuticals.[49,50] Though, numerous procedures are known for such transformation,[49,51,52] demand of highly efficient catalyst with good selectivity is still in demand. Hence, the chemist working in the field of bioinorganic focuses on the synthesis of new as well as known metal complexes to achieve the catalytic transformation of alkenes to epoxides. The manganese, being non-toxic and an inexpensive metal is a choice of chemist's in order to carry out such reactions. The manganese complex containing nitrogen-based ligands along with a suitable oxidant in one of the useful strategy that results in enhanced activity. Several oxidants that are often been employed in combination with manganese catalyst includes H_2O_2[50,53-56] peracetic acid[53,57] *m*-CPBA[66–68] iodoarenes.[57,69–74] Though most of this manganese catalyst are mononuclear, few polynuclear epoxidation catalysts are also known.[53,62,68,70–72,75–77]

4.2 Experimental details

The detail synthetic procedure that has been employed for the synthesis of ligand N3Py2, complex $[Mn(N3Py2)(H_2O)](ClO_4)_2$ **9** and reactive intermediate $[Mn(N3Py2)(O_2)](ClO_4)_2$ **9a** (**Scheme 4.3**) have been described in this section.

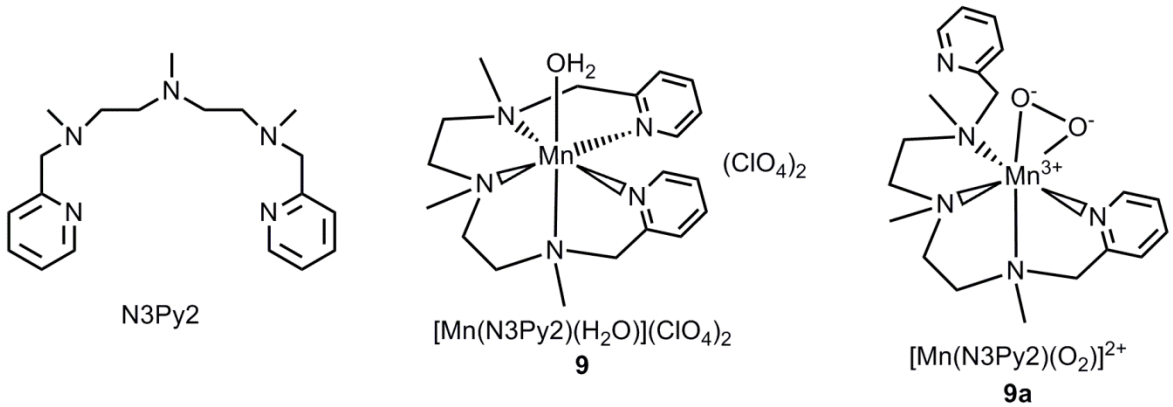

Scheme 4.3 *Chemical structure of the ligand N3Py2, complex* ***9*** *and the Mn-peroxo intermediate* ***9a***

4.2.1 Synthesis of ligand N3Py2 and $[Mn(N3Py2)(H_2O)](ClO_4)_2$ 9 and generation of $[Mn^{III}(N3Py2)(O_2)]^+$ 9a species.

4.2.1a Synthesis of N,N'-dimethyl-N-(2-(methyl(pyridin-2-ylmethyl)amino)ethyl)-N'-(pyridin-2-ylmethyl)ethane-1,2-diamine) (N3Py2)

The ligand N3Py2 was prepared by following a three-step procedure. ***Step-I***: To the ethanolic solution of 2-pyridine-carboxaldehyde (3.0 g, 28.0 mmol) was added 1.52 mL of diethylenetriamine (1.44 g, 14.0 mmol). The mixture was refluxed for ~ 5 h, cooled to room temperature and the solvent was removed to give red semi-solid imine product. The yield of product was 3.1 g (79 %). *IR-data* (KBr, cm^{-1}): 3295 ν(N-H), 3200-2700 ν(C-H), 1648 ν(C=N). ***Step-II***: To the ice-cold methanolic solution of imine product (3.0 g, 10.7 mmol), the sodium borohydride (0.48 g, 12.8 mmol) was added slowly and the mixture on stirring for 6h became brownish-orange in colour (~6 h). The solvent was removed and water (20 mL) was added to the flask containing the crude product. The yellow viscous oil

was then extracted using ethyl acetate (30 mL x 3). The yield of product was 2.8 g (92 %). *IR-data* (KBr, cm^{-1}): 3295 ν(N-H), 3200-2700 ν(C-H), 1670 ν(C=N). ***Step-III***: The product (2.6 g, 9.1 mmol) of the second step was taken in water (3.0 mL) and cooled in ice-bath. To this mixture, formaldehyde (37 %, 22.0 mL) and formic acid (85 %, 15.0 mL) were added and refluxed for ~24 h. The mixture was then cooled and basified (pH = 12) using 2 M NaOH solution. The crude reddish-brown oil obtained after extraction with chloroform (20 mL x 4) was dissolved in HCl solution (pH = ~ 1). The acidic mixture then was basified using NaOH solution (pH = 12) and the product was then extracted using diethyl ether (20 mL x 6). N3Py2 was formed as a yellow oil. Yield of N3Py2 (2.5 g, 72 %). *IR-data* (KBr, cm^{-1}): 3200-2700 ν(C-H), 1670 ν(C=N).^{1}*H NMR* ($CDCl_3$, ppm): δ 8.47 (d, 2H, *J* = 3.2 Hz, 2-PyH), δ 7.57 (t, 2H, *J* = 8.2 Hz, 4-PyH), δ 7.34 (d, 2H, *J* = 3.8 Hz, 5-PyH), δ 7.08 (t, 2H, *J* = 6.16 Hz, 3-PyH), δ 3.63 (s, 4H, Ar-CH_2), δ 2.57 (s, 8H, N-CH_2), δ 2.25 (s, 3H, NMe), δ 2.25 (s, 3H, NMe) δ 2.21 (s, 6H, NMe). ^{13}*C NMR* ($CDCl_3$, ppm): δ 159.1 (C6), 148.1 (C2), 136.2 (C4), 122.9(C5), 121.7(C3), 64.04 (Ar-CH_2), 55.3 (N-CH_2), 42.7 (N-CH_3).

4.2.1b Synthesis of [Mn(N3Py2)(H_2O)](ClO_4)$_2$ (9)

Ligand N3Py2 (0.452g, 1.38 mmol) is dissolved in acetonitrile (2 mL) and added in drops to the constantly stirring acetonitrile solution (2 mL) of $Mn(ClO_4)_2.6H_2O$ (0.5g, 1.38 mmol) under the N_2 atmosphere at room temperature. The mixture was allowed to stir for 12 h to obtain a brownish coloured solution. The addition of diethyl ether to this solution gave a white coloured powder which was separated by filtration, washed with diethyl ether and then dried in vacuo. The single crystal of **9** was obtained by diffusion of diethyl ether into the acetonitrile solution. Yield of **9** (0.68 g, 82 %) *Calc. for* $C_{19}H_{31}N_5Cl_2O_9Mn$: C, 38.08; H, 4.91; N, 11.69 %. *Found* C, 38.19; H, 4.91; N, 11.59%. *IR-data* (KBr, cm^{-1}):

3412 cm^{-1} ν(O-H); 1093, 621 ν(ClO_4^{-1}). *ESI-MS*: *m/z* = 191.18 (*calc*. 191.21) for $[Mn(N3Py2)]^{2+}$ and *m/z* = 481.08 (*calc*. 481.86) for $[Mn(N3Py2)(ClO_4)]^{+}$

4.2.1c Generation and reactivity of Mn(III)-peroxo intermediate (9a) from 9

The Manganese (III)-peroxo complex $[Mn(N3Py2)(O_2)]^{+}$ **(9a)** was prepared by reacting **9** (1 mM solution in 2 mL of CH_3CN) with 10 equiv. of H_2O_2 and 5 equiv. of triethylamine at 15 °C. The generation of Mn(III)-peroxo (**9a**) intermediate was studied with a UV-Vis spectrophotometer by monitoring spectral changes at 572 nm of the reaction solution. *ESI-MS*: *m/z* = 414.17 (*calc*. 414.17) for $[Mn(N3Py2)]^{2+}$

4.2.2 General procedure for catalytic epoxidation reactions of alkenes by 9

In a typical reaction condition, solid PhIO (50 mM) was added to the solution containing substrate (250 mM) and catalyst **9** (0.5 mM) in 2 mL of acetonitrile at 25 ° C. The reaction was stirred for 30 minutes and filtered over silica column and directly analyzed by GC by comparing the retention time and peak area with the authentic sample using decane as internal standard.

4.3 Result and discussion

4.3.1 Synthesis and characterization of ligand N3Py2

In heme and non-heme bioinspired chemistry, the ligands have been known to provide an environment to central metal ions such that the resulting structure behaves as a functional model for the enzymatic reactions. The oxidation reactions catalyzed by transition metal complexes proceeds by the formation of a high valent metal-oxygen intermediate which is stabilized by the highly basic ligands. The pentadentate N_5 donor ligands like BnTPEN (*N*-benzyl-*N*,*N'*,*N'*-tris(2-pyridylmethyl)-1,2-diaminoethane) and N4Py (*N*,*N*-bis(2-pyridylmethyl)-*N*-bis(2-pyridyl)-methylamine) (**Scheme 4.4**) employed in early studies showed that metal complexes were well stabilized in their high valent oxidation state.[46–48] The structure of the ligand should be robust enough to sustain the catalytic oxidative condition. Therefore the methylation of N-H bonds is an important step and ensures the protection of the ligand from decomposition.

Here, the pentadentate ligand N3Py2 was prepared in three steps. In the first step, the diethylenetriamine and pyridine-2-carboxaldehyde were condensed to give Schiff base imine, which was then reduced by sodium borohydride in step *II*.[78–80] The structure of ligand should be robust enough to sustain the oxidative stress generated in the reaction condition. Therefore the methylation of N-H bonds is an important step and ensures the protection of ligand from decomposition. In the final step, the amine was *N*-methylated following Eschweiler-Clarke reaction (**Scheme 4.5**). N3Py2 was characterized using IR, ^{1}H and ^{13}C NMR spectroscopic techniques (**Figure 4.1-4.4**)

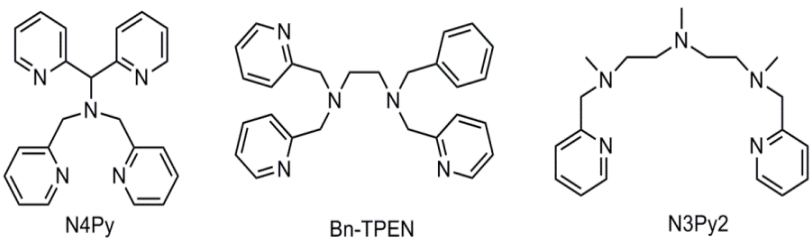

Scheme 4.4 *Chemical structures of non-heme pentadentate nitrogen donor ligands.*

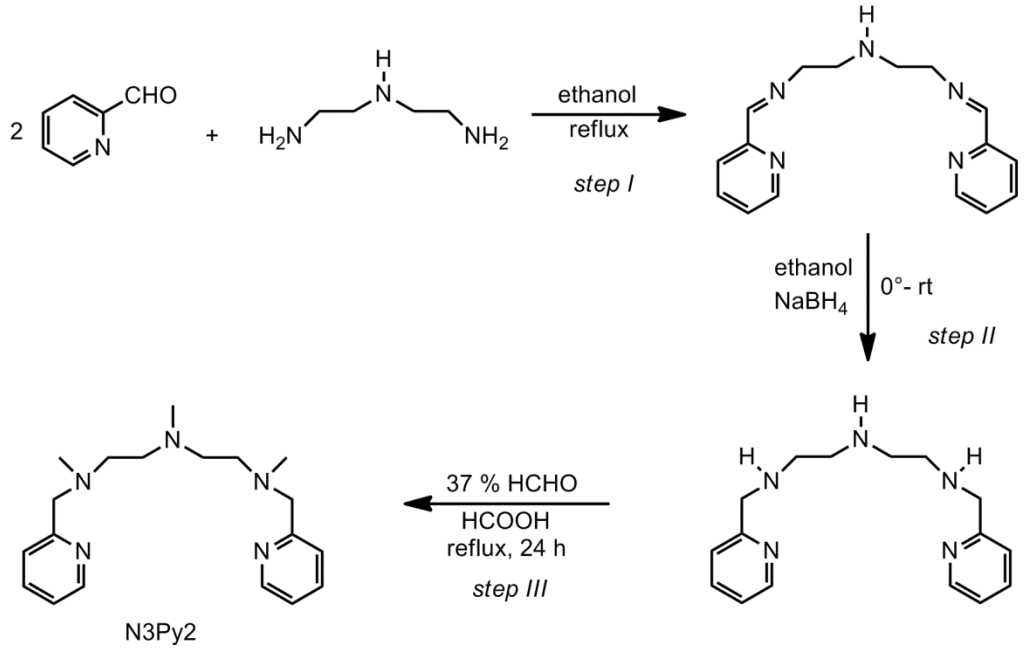

Scheme 4.5 *Three synthetic steps used in the preparation of N3Py2*

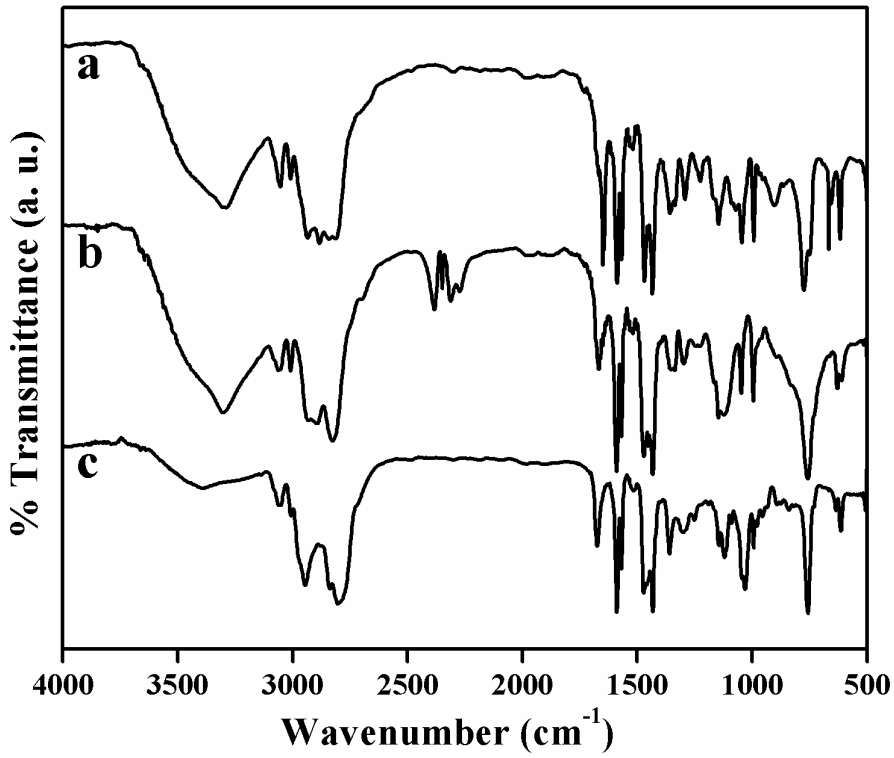

Figure 4.1 *IR spectra of the products formed in (a) step-I, (b) step-II and (c) step-III.*

The products obtained in all the three steps were analyzed by infrared spectroscopy. The product obtained in *step I* shows a sharp strong peak at ~1648 cm^{-1} due to imine (C=N)

formation with the absence of the peak in the region ~1700 cm^{-1} due to the carbonyl of aldehyde indicating the formation of imine ligand by condensation of 2-pyridine carboxaldehyde and diethylenetriamine. In *step II* the peak at ~1648 cm^{-1} disappears due to the reduction of imine group and the peak at ~1670 cm^{-1} could be assigned to C=N group of the pyridine ring. The N-H vibrations are seen at the same position as in *step 1*. In the third step all N-H groups are methylated which could be clearly seen from the disappearance of N-H vibrations at ~3295 cm^{-1}.

The structure of the compound was confirmed by NMR spectroscopy and the corresponding peaks are assigned in ^{1}H and ^{13}C NMR spectra as shown in **Figure 4.2** to **4.5**.

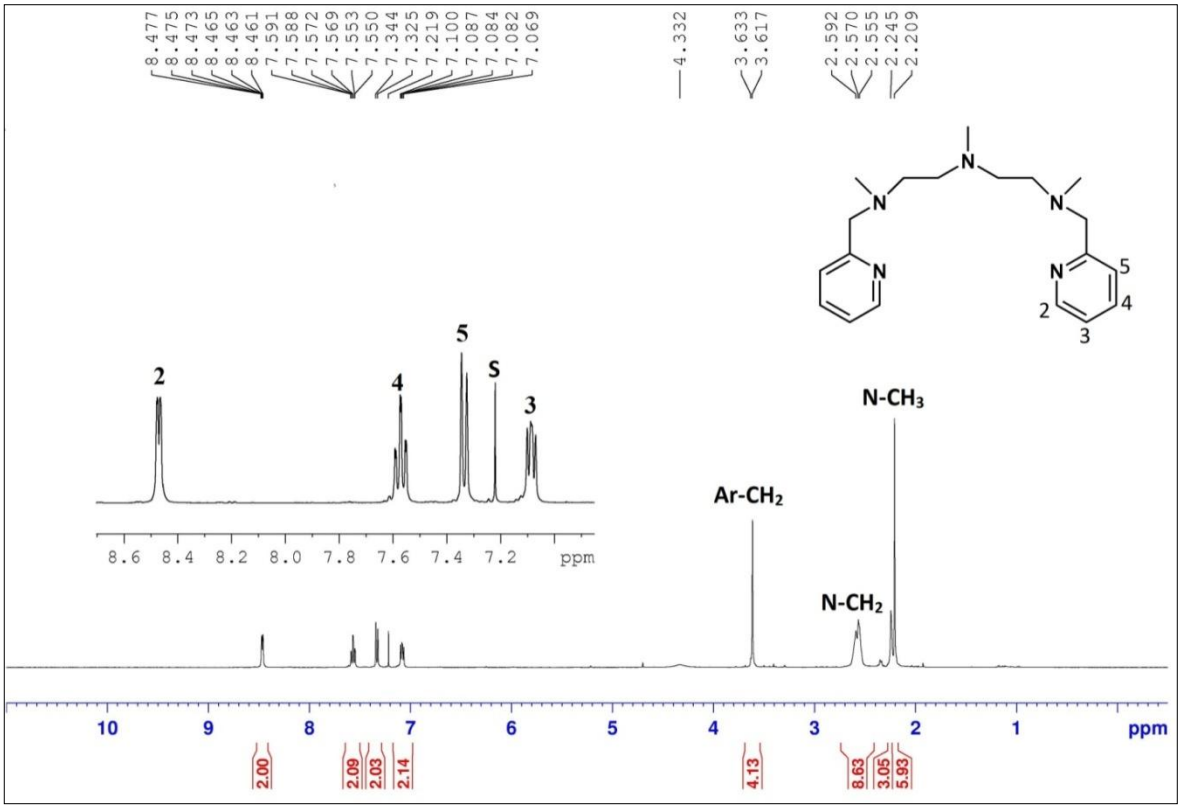

***Figure 4.2**. The ^{1}H-NMR spectrum of N3Py2 recorded in $CDCl_3$.*

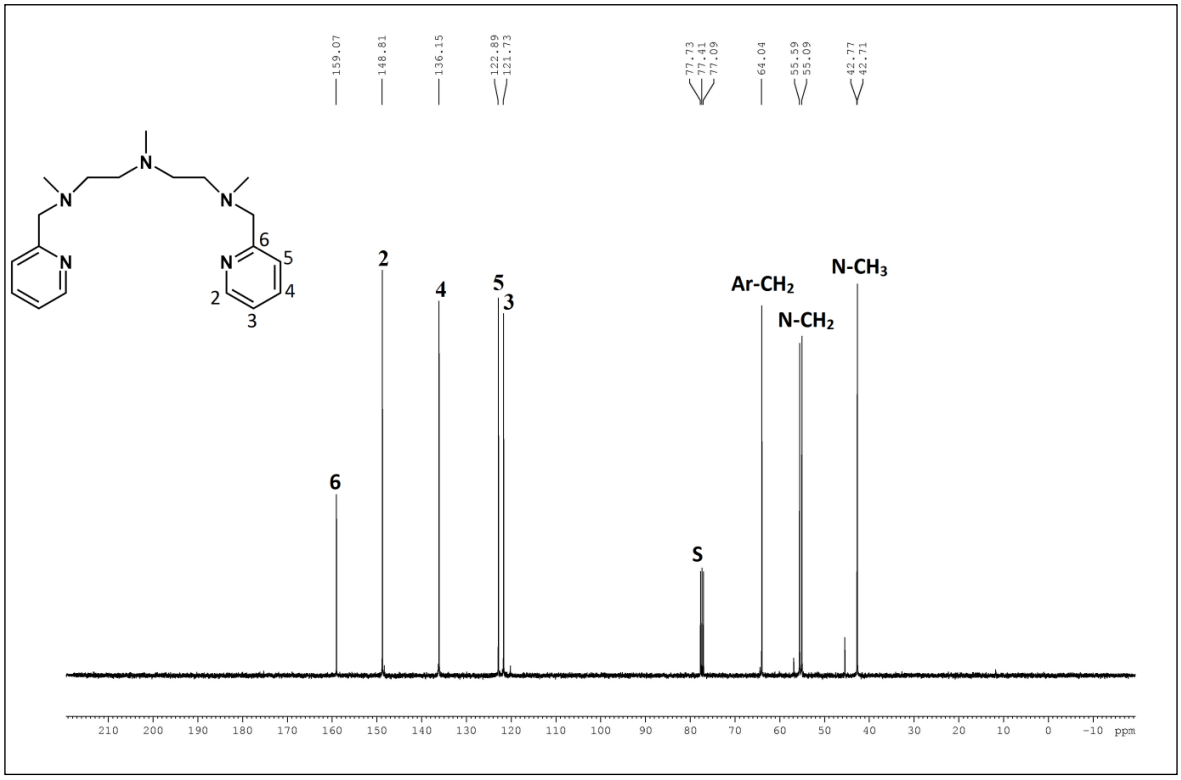

Figure 4.3 *^{13}C NMR spectrum of ligand N3Py2 recorded in $CDCl_3$ (S stands for solvent peak).*

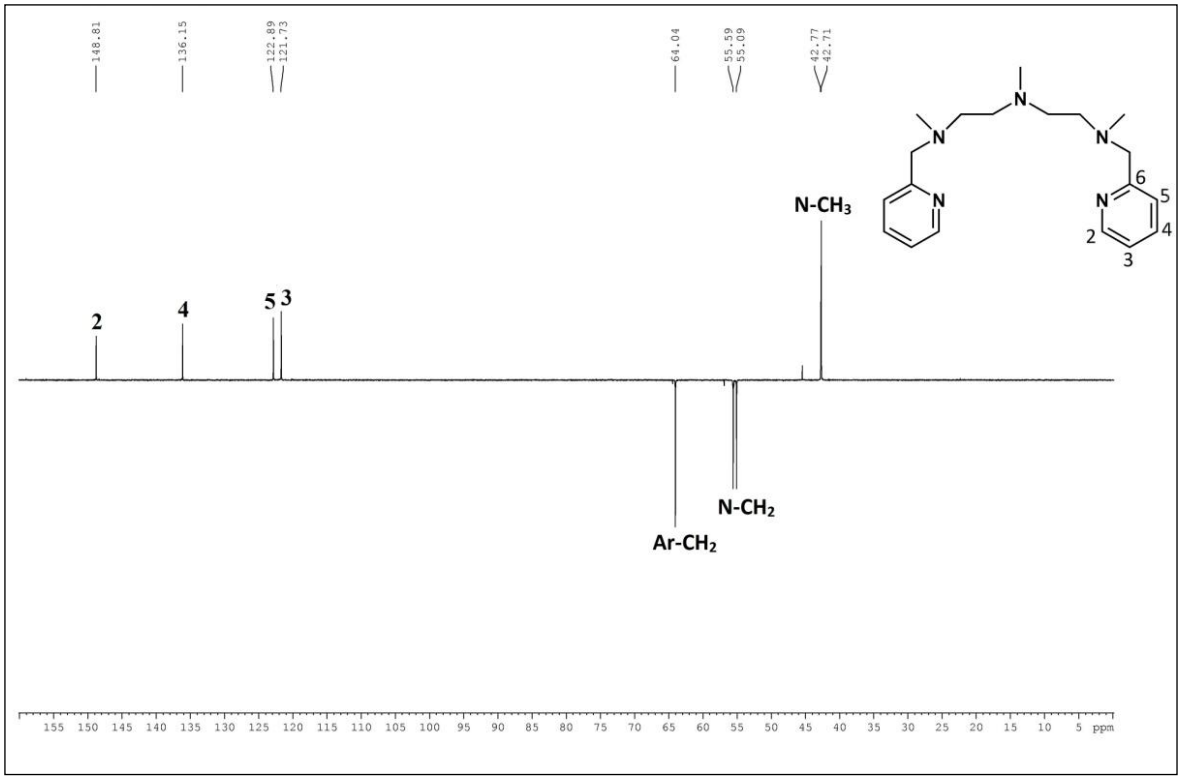

Figure 4.4 *DEPT NMR spectrum of ligand N3Py2 recorded in $CDCl_3$*

4.3.2 Synthesis and characterization of [Mn(N3Py2)(H_2O)](ClO_4)$_2$ (9)

The compound **9** was prepared by reacting ($MnClO_4$).6H_2O with ligand N3Py2 in acetonitrile under the N_2 atmosphere (**Scheme 4.6**). The crystals of compound **9** were obtained by vapour diffusion of diethyl ether into the acetonitrile solution of **9**. The compound **9** was primarily formulated based on C, H, N analysis, infrared spectroscopy and ESI-MS techniques. The compound was further characterized by single crystal X-ray crystallography, EPR spectroscopy and electrochemical techniques as discussed below.

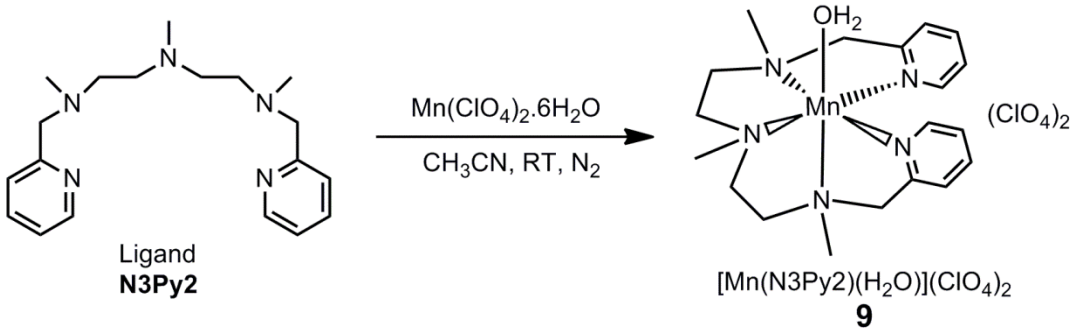

Scheme 4.6 *Synthesis of [Mn(N3Py2)(H_2O)](ClO_4)$_2$ (**9**)*

4.3.2a Characterization of [Mn(N3Py2)(H_2O)](ClO_4)$_2$ (9) by spectroscopic techniques

The infrared spectrum of complexes shows the presence of a peak at around 3412 cm^{-1} due to O-H stretching of H_2O and peaks at ~1091 cm^{-1} and ~615 cm^{-1} due to perchlorate anions[81] which are absent in the infrared spectrum of N3Py2 (**Figure 4.5**). The ESI-MS of **9** recorded in CH_3CN shows prominent mass peak at m/z = 191.18 (calc. m/z 191.21) due to the $[Mn(N3Py2)]^{2+}$ species peak at m/z = 481.08 (calc. m/z 481.86) which is attributed to $[Mn(N3Py2)(ClO_4)]^+$ species (**Figure 4.6**). This shows that in CH_3CN solvent, the coordinated H_2O molecule is replaced by ClO_4^{-1} anion. Based on the C, H, N analysis, infrared spectroscopy and ESI-MS data, the compound is formulated as [Mn(N3Py2)(H_2O)](ClO_4)$_2$. The X-band EPR spectrum of **9** recorded at 298 K depicts an intense six-line hyperfine signal at g = 2.0, which reveals **9** is high-spin (S=5/2) Mn(II)

species (**Figure 4.7**). The compound **9** was also characterized by single crystal X-ray crystallography.

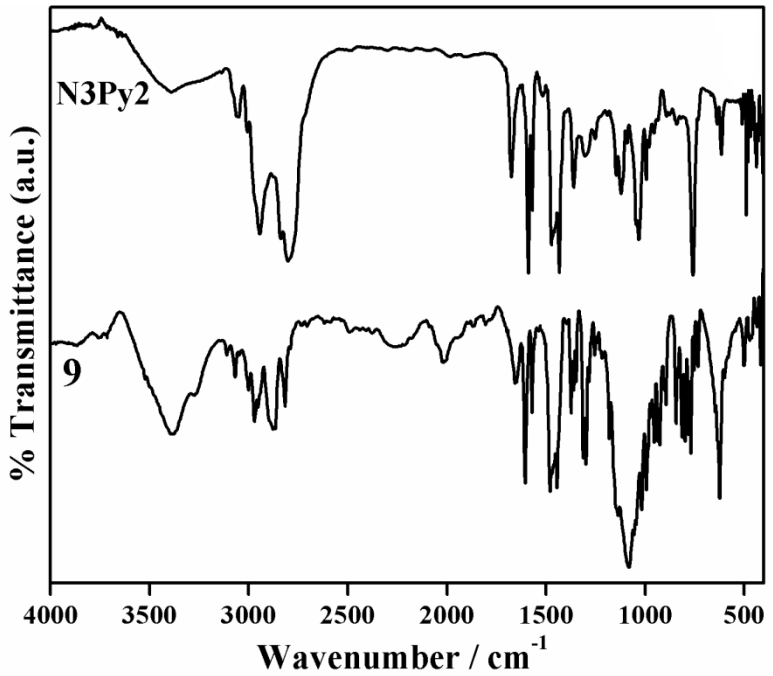

Figure 4.5. *Overlaid infrared spectra of ligand N3Py2 and [Mn(N3Py2)(H$_2$O)]*$(ClO_4)_2$ (**9**)

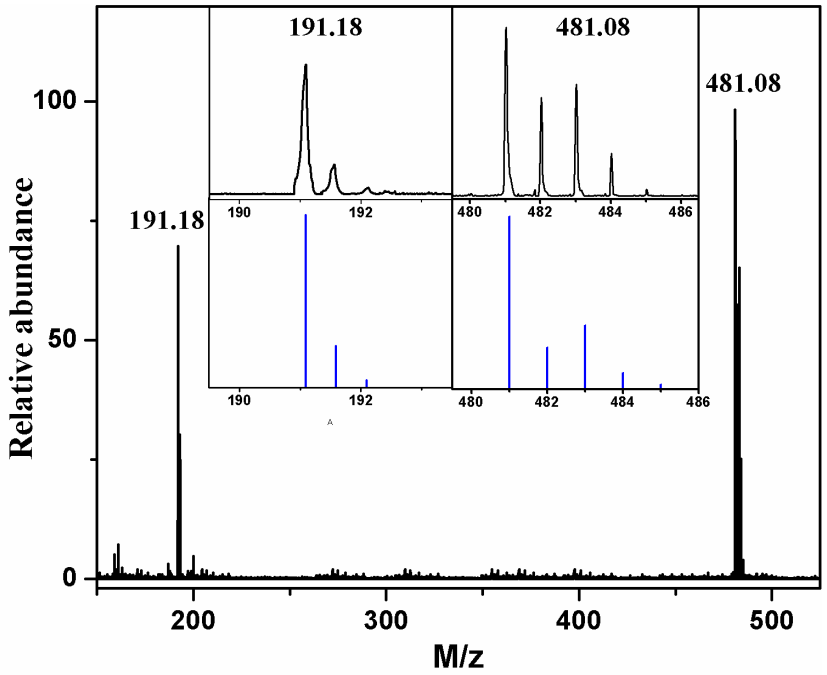

Figure 4.6 *ESI-MS of [Mn(N3Py2)(H$_2$O)]$(ClO_4)_2$ (**9**) recorded in CH_3CN showing a mass peak m/z = 191.18 due to the $[Mn(N3Py2)]^{2+}$ species and peak at m/z = 481.08 due to $[Mn(N3Py2)(ClO_4)]^{+}$ species. The inset shows the isotope distribution patterns for the prominent peaks in black with simulated peaks in blue colour.*

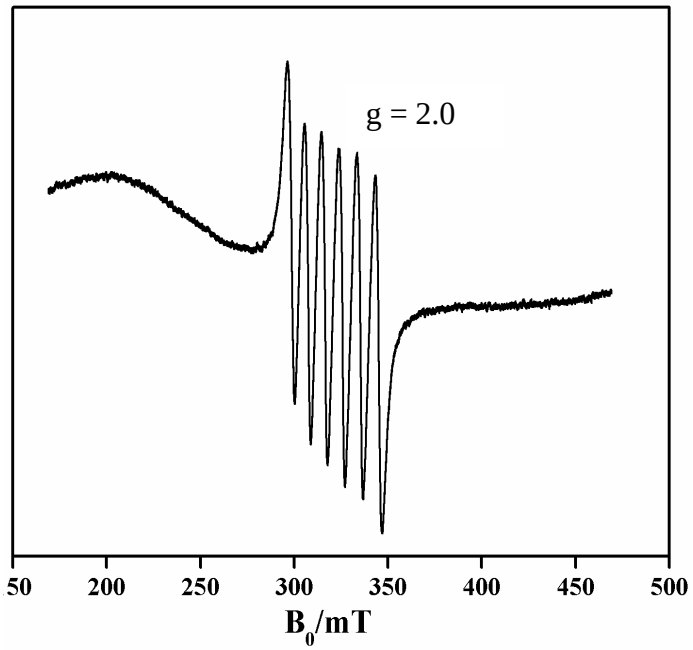

Figure 4.7 *X-band EPR spectrum of* ***9*** *Recording condition 298 K; 9.02 GHz microwave frequency at 1 mW microwave power; modulation 100 kHz modulation frequency.*

4.3.2b Description of the crystal structures of 9

The single crystal suitable for structure determination by X-ray crystallography was obtained by slow diffusion of diethyl ether into the CH_3CN solutions of **9**. The technical details of data acquisition and selected refinement results for **9** are given in **Table 4.3** and the selected bond lengths and bond angles are given in **Table 4.4**. Compound **9** crystallizes in the centrosymmetric monoclinic space group $P2_1/c$. In compound **9** all atoms are located in their general positions. The crystal structure of **9** consists of manganese(II) ions, a pentadentate N5 ligand (N3Py2), a H_2O molecule and two crystallographically independent perchlorate ions. The five nitrogen atoms of ligand N3Py2 can orient around the Mn ion in different ways to form an octahedral complex giving rise to four possible coordination isomers as shown by similar pentadentate ligand[82] (**Scheme 4.7**). The structural characterization by X-ray crystallography reveals that **9** exists in one of the isomeric form II as shown in **Scheme 4.6**. The crystal structure of **9** with atom labelling is shown in **Figure 4.8**. The compound **9** possesses a distorted octahedral coordination geometry with

the manganese(II) ion at the centre surrounded by two pyridine nitrogens (N3 and N5) and three tertiary amine nitrogens (N1, N2 and N5) of the pentadentate ligand (N3Py2). The

Table 4.3 *Technical details of data acquisition and selected refinement results for* ***9***

	Compound **9**
Empirical formula	$C_{19}H_{31}Cl_2MnN_5O_9$
Formula weight	599.33
Crystal description	Block
Crystal colour	White
Crystal system	Monoclinic
Space group	$P2_1/c$(no. 14)
Temperature (K)	100(2)
Unit cell dimensions	a = 8.983(3)Å
	b = 33.268(11)Å
	c = 8.791(3)) Å
	α = 90.00°
	b = 105.287(4)°
	γ = 90.00°
volume (Å^3)	2534.4(15)
Z	4
Radiation type (Mo-Kα)/Å	0.71073
Crystal size (mm^3)	0.40x 0.20 x0.20
Diffractometer	Bruker APEX-II CCD
Absorption correction	Multi scan
No. measured reflections	9794
Calculated density (mg/m^3)	1.571
Absorption coefficient (mm^{-1})	0.790
F(000)	1247
θ range for data collection	2.35 to 24.99
Limiting indices	$-10 \leq h \leq 10$
	$-38 \leq k \leq 39$
	$-10 \leq l \leq 10$
Refinement method	Full-matrix least-squares on F^2
Data / restraints / parameter	4470 / 0 / 344
Final R Indices[I>2σ(I)]	R_1 = 0.0401, wR_2 = 0.0953
R indices (all data)	R_1 = 0.0440, wR_2 = 0.0977
Goodness of fit on F^2	1.042
Largest diff. peak and hole(eÅ^{-3})	1.0754 and -0.7223
Reflections collected / unique	30133 /4470 [R(int) = 0.0571]

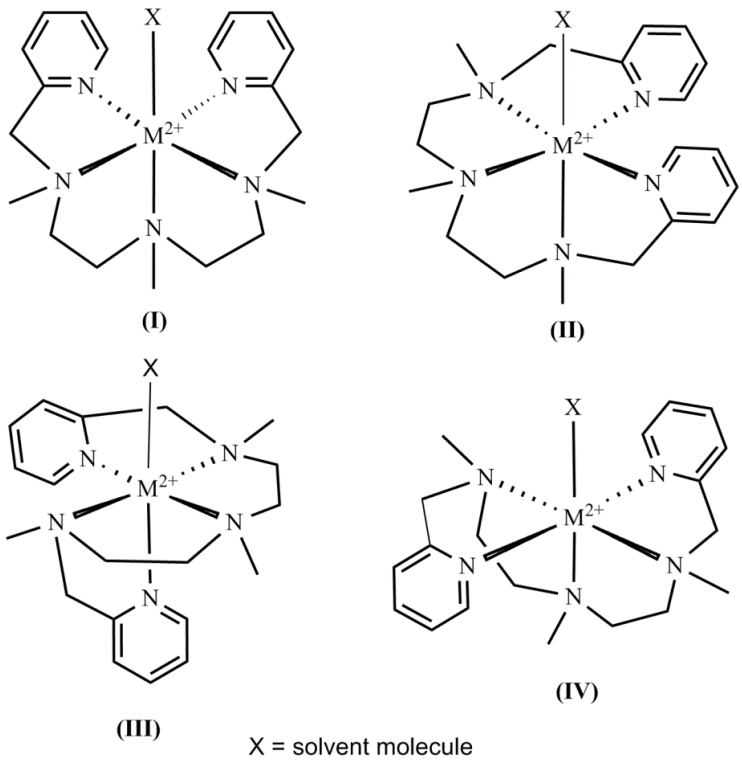

Scheme 4.7 *The probable isomeric structures of* $[Mn(N3Py2)(X)]^{2+}$ *complexes (X =* H_2O*).*

MnN_5O octahedron. The two pyridine nitrogen atoms are oriented in a *cis* manner with respect to each other with a bond angle of 102.50(8) (N4-Mn1-N3). The three amine nitrogen atoms occupy the three facial sites with a bond angle of 109.63(8), 9.79(9), 78.57(7) ° for N2-Mn1-N5, N1-Mn1-N5, N1-Mn1-N2 respectively. The sixth coordination site is occupied by a water molecule (O9), thereby completing the octahedron. The structure of **9** is significantly different from manganese complexes containing an analogous tetradentate ligand with two pyridyl and two amine nitrogen donor atoms in which *trans* orientation of two pyridyl nitrogen atoms are observed.[74,83] The perchlorate ions remain uncoordinated to the Mn(II) ion and behave as charge balancing counter anions. All the Mn-N and Mn-O bond distances and N-Mn-N and N-Mn-O bond angles are in normal range (**Table 4.3**) and are in good agreement with literature reports.[36,46,60,54,74,83] The N-Mn-N *trans* and *cis* angles in complex **9** deviates from 180° and 90° respectively resulting in the distortion of octahedral geometry. The *trans* angles in **9** ranges from 148.98(8) to

175.23(7)° whereas the *cis* angles vary from 74.10 (8) to 105.30(7)° in **9.** The hydrogen atoms of the water molecules are involved in the hydrogen bonding with the oxygen of the perchlorate anion (**Figure 4.9, Table 4.5**).

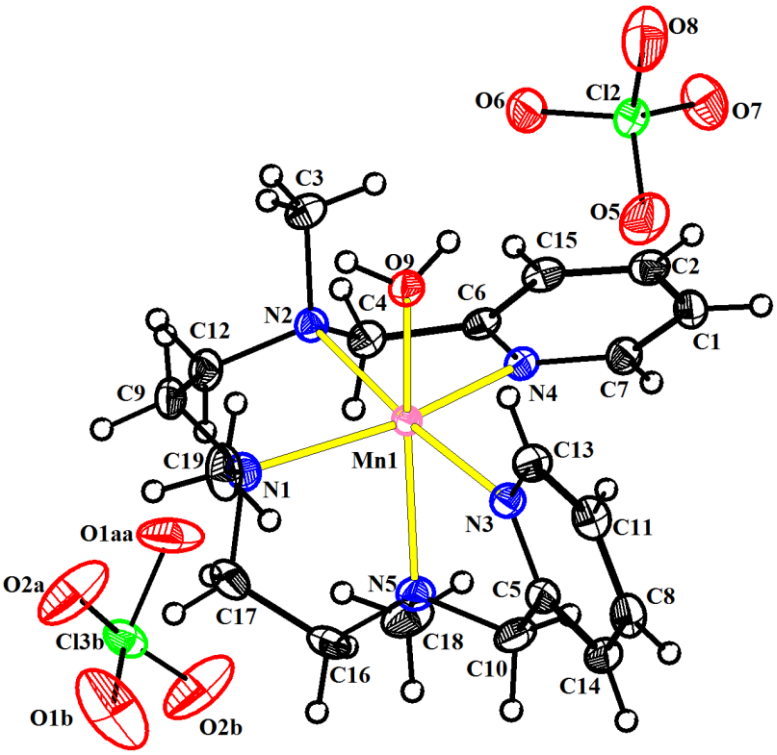

Figure 4.8 *The crystal structure of [Mn(N3Py2)(H₂O)](ClO₄)₂ with atom-labelling scheme. Displacement ellipsoids are drawn at 50% probability except for the H atoms, which are shown as circles of arbitrary radius.*

Table 4.4 *Selected bond lengths (Å) and angles (°) for* ***9***

	9		
Bond length (Å)			
Mn1—N3	2.257(4)	Mn1—N4	2.233(5)
Mn1—N5	2.330(2))	Mn1—N1	2.259(4)
Mn1—N2	2.333(3)	Mn1—O9	2.201(2)
Bond angle (°)			
N5—Mn1—N3	74.10(8)	N1—Mn1—N2	78.57(7)
N2—Mn1—N3	175.23(7)	N1—Mn1—N4	148.98(8)
N2—Mn1—N5	109.63(8)	O9—Mn1—N3	85.58(7)
N4—Mn1—N3	102.50(8)	O9—Mn1—N5	156.84(8)
N4—Mn1—N5	95.00(8)	O9—Mn1—N2	91.31(7)
N4—Mn1—N2	74.47(7)	O9—Mn1—N4	100.24(7)
N1—Mn1—N3	105.30(7)	O9—Mn1—N1	95.38(8)
N1—Mn1—N5	79.79(9)		

Note: The values in the parentheses indicate estimated standard deviations.

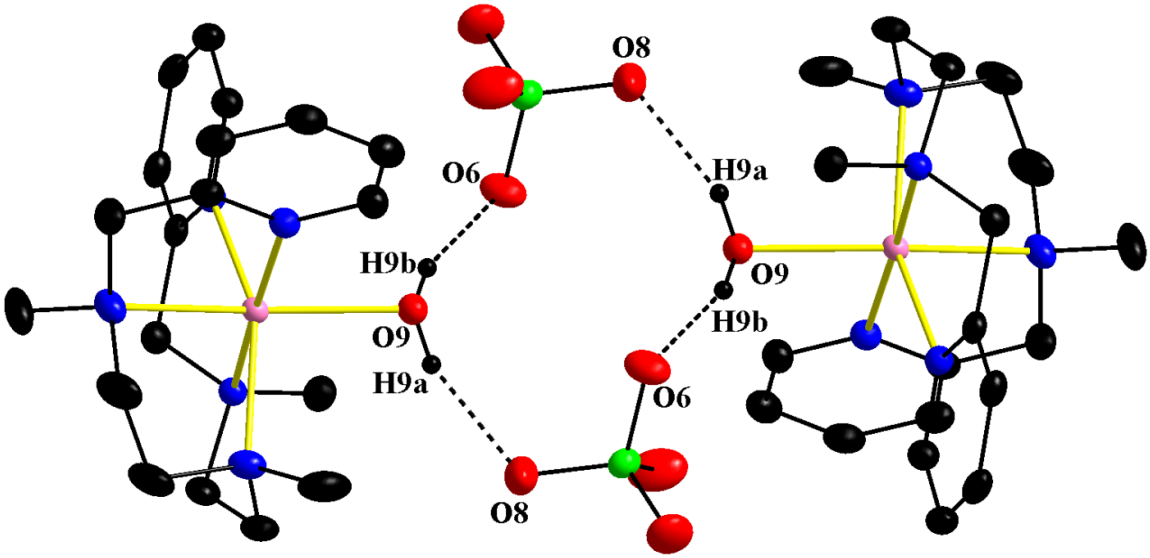

Figure 4.9 *Hydrogen bonding interactions in* ***9*** *with atom labelling scheme of atoms involved hydrogen bonding.*

Table 4.5 *Hydrogen bonding parameters (Å, °) for* ***9.***

D-H···A	D-H/Å	H···A/Å	D···A/Å	D-H···A/°
Compound **9**				
O9-H9a···O8[a]	0.850(08)	1.996(12)	2.802 (6)	157.75(91)
O9-H9b···O6[b]	0.850(12)	1.971(12)	2.788(3)	160.94(102)
[a] 1-x, -y, 1-z, [b] x, y, z				

Note: The values in the parentheses indicate estimated standard deviations.

4.3.2c Electrochemical characterization of 9

An electrochemical property of **9** was explored by employing cyclic voltammetry (CV) and differential pulse voltammetry (DPV). Compound 9 exhibits a quasi-reversible cathodic and anodic waves at 0.57 V v/s (0.86 V v/s SCE) due to Mn(II)/Mn(III) redox couple (**Figure 4.10**) which is slightly positive than similar Mn(II) complexes.[36,74,83,84] The cyclic voltammograms recorded at different scan rates were identical and shows an increase in peak current with increasing scan rate constant (**Figure 4.11, Table 4.6**). $E_{½}$ value remains constant while ΔEp value increases with increase in scan rate which is characteristic of the quasi-reversible process.

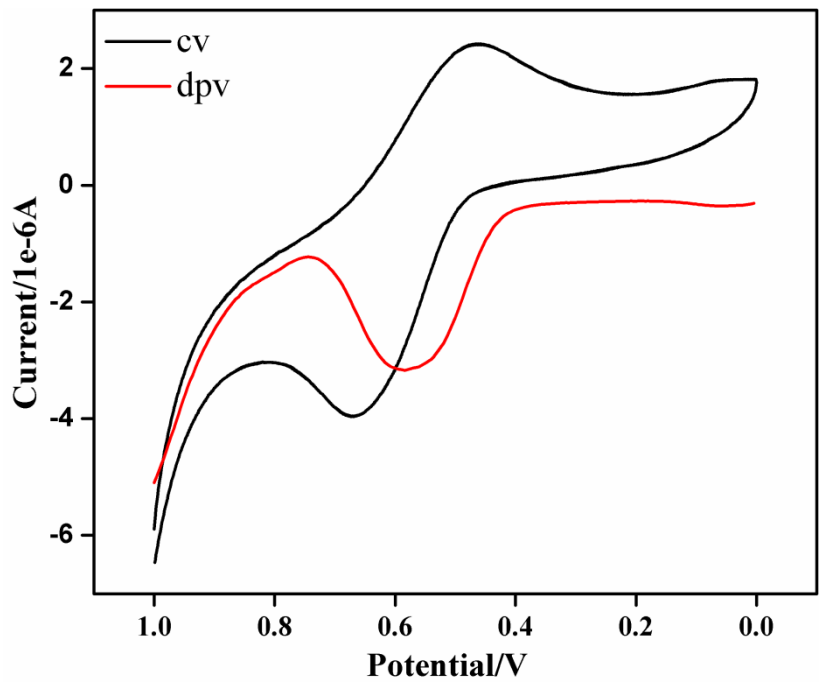

Figure 4.10. *CV (black line) and DPV (red line) of* ***9*** *recorded at a scan rate of 50 mV* s^{-1} *in an acetonitrile solution containing 0.1 M of* $TBAPF_6$ *as supporting electrolyte.*

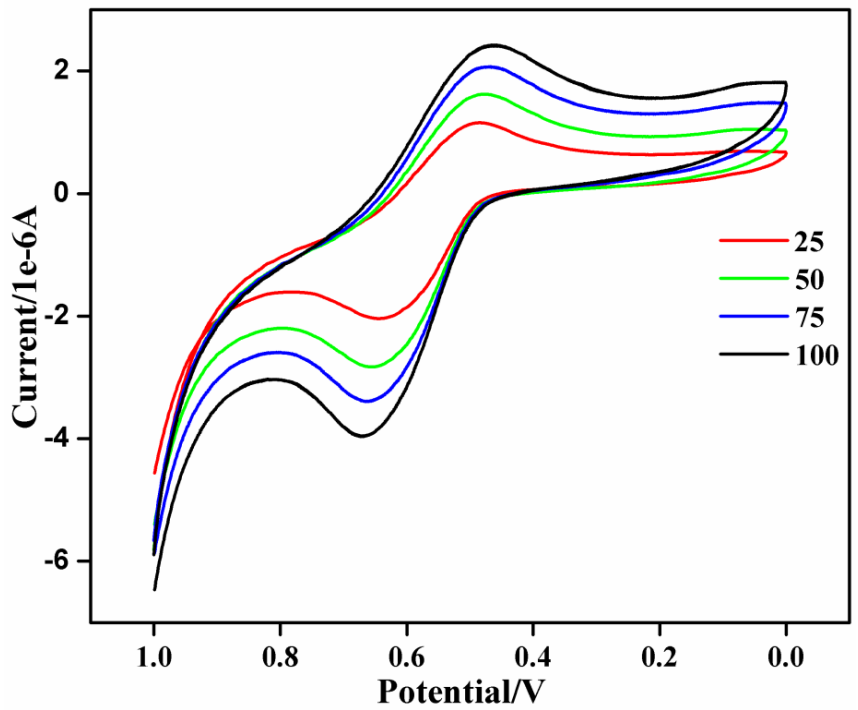

Figure 4.11 *Cyclic voltammogram of* ***9*** *recorded at different scan rate in an acetonitrile solution containing 0.1 M of* $TBAHPF_6$ *supporting electrolyte.*

Table 4.6 *Electrochemical data for complex* ***9***

Scan rate (mVs^{-1})	Epa (V)	Epc (V)	ΔEp (V)	$E_{½}$ (V)
100	0.670	0.461	0.209	0.567
75	0.663	0.470	0.193	0.567
50	0.657	0.478	0.179	0.568
25	0.645	0.484	0.161	0.565

4.3.3 Generation, characterization and the reactivity of manganese(III)-peroxo intermediate (9a)

The formation of manganese(III)-peroxo intermediate (**9a**) was monitored by following UV-Vis spectral changes. The UV-Vis spectrum of **9** in acetonitrile solution shows peaks only in the UV region which is due to the intraligand transition. The absorption spectrum is featureless in the visible region, as the *d-d* transitions are spin forbidden which is the characteristic of high spin Mn(II) centres as observed in the case of similar Mn(II) complexes.[32,36] When 10 eq. of H_2O_2 was added to 1 mM solution of **9** in the presence of 5 eq. of TEA (triethylamine) in acetonitrile at 15 °C, the formation of purple colored intermediate (**9a**) is observed with absorption at 572 nm (254 $M^{-1}cm^{-1}$) and shoulder peak at 412 nm (120 $M^{-1}cm^{-1}$) (**Figure 4.12**). The intermediate (**9a**) was quite stable for at room temperature. This reactive intermediate was further characterized by ESI-MS and EPR.

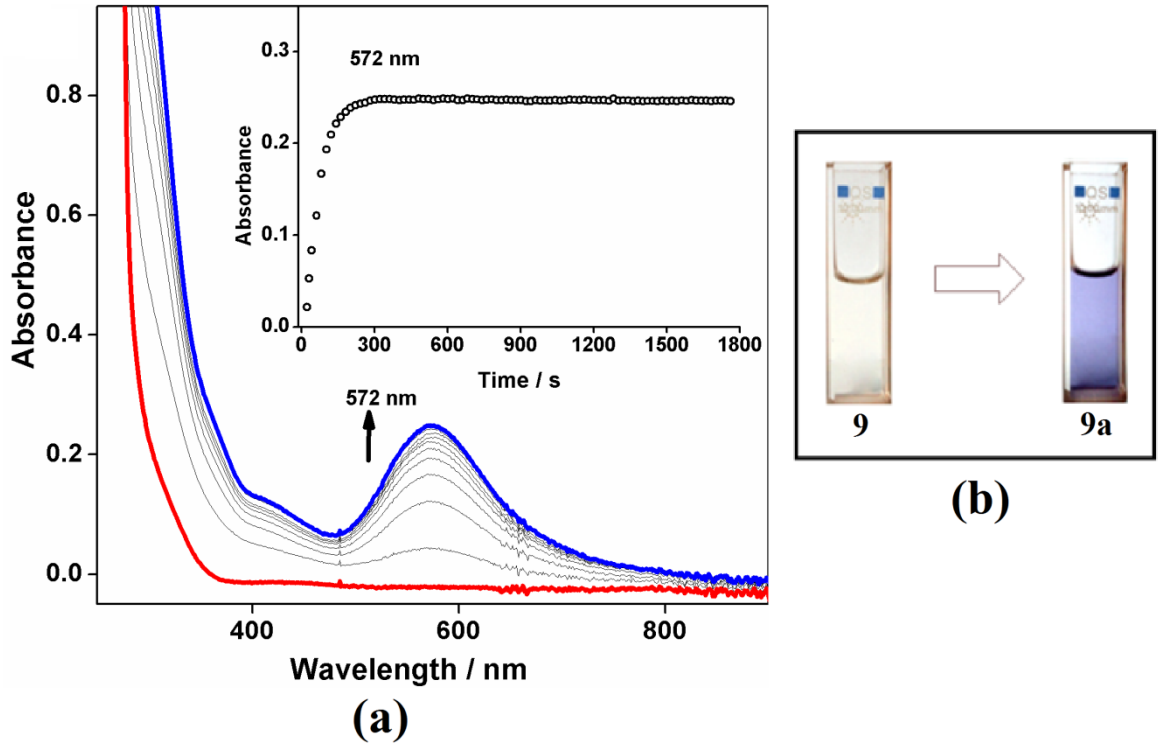

Figure 4.12 (a) *UV-Visible spectral changes after addition of 10 eq. of H_2O_2 in presence of 5 eq. of TEA (triethylamine) at 15 °C. Inset shows time trace monitored at 572 nm for the formation of the peak.* ***(b)*** *colour change observed after formation of* ***9a*** *from* ***9****.*

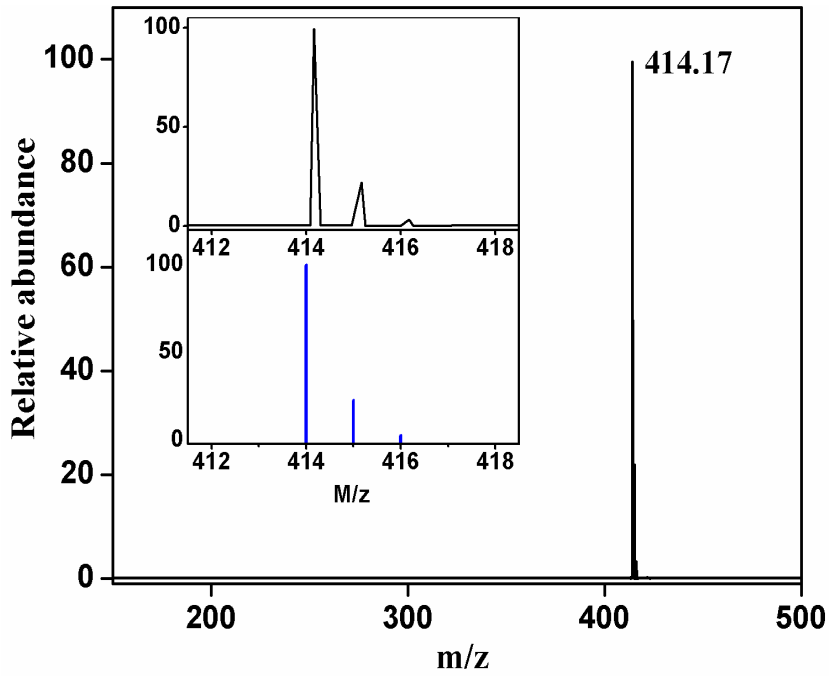

Figure 4.13 *ESI-MS spectrum of* ***9a*** *recorded in CH_3CN showing a mass peak at 414.17 corresponding to $[Mn(N3Py2)(O_2)]^+$ species. Insets show the observed distribution patterns which correspond to the $[Mn(N3Py2)(O_2)]^+$* ***9a*** *in black with simulated patterns in blue colour.*

The ESI-MS of **9a** in acetonitrile shows a peak at m/z = 414.17 whose mass and isotopic distribution pattern corresponds to $[Mn(N3Py2)(O_2)]^+$ (calc. m/z at 414.17) (**Figure 4.13**). The EPR spectrum of **9** when recorded in presence 10 equivalent H_2O_2 in presence of 5 equivalent triethylamine in a perpendicular-mode do not show any signal. This suggests that the **9a** is EPR-silent (**Figure 4.14**) suggesting that manganese in **9a** exists as Mn(III) (d^4 species) as observed for earlier Mn(III)-peroxo species.[28] The ESI-MS and EPR study of species **9a**, both supports the formation Mn(III)-peroxo intermediate. The intermediate **9a** can exist as side-on (η^2) peroxo or end-on (η^1) peroxo as shown in **Scheme 4.8**.

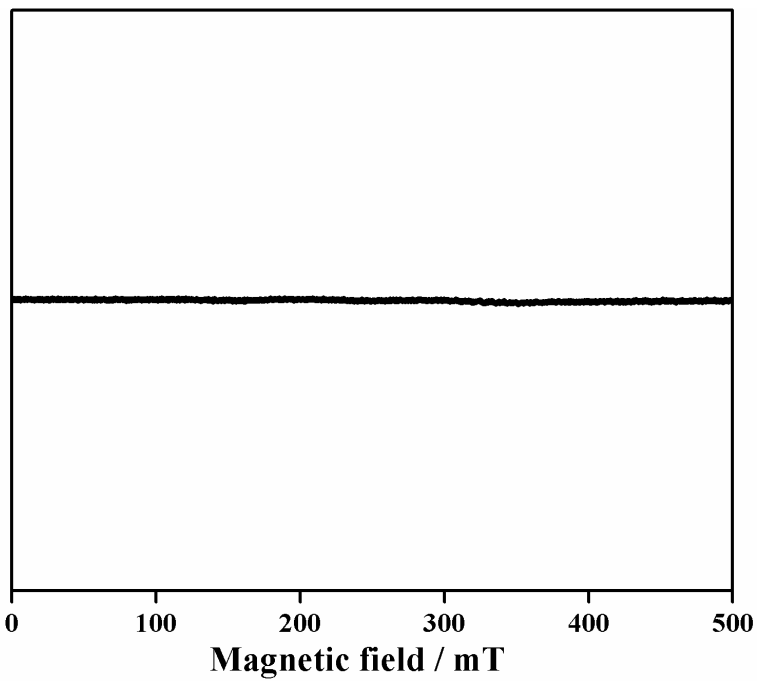

Figure 4.14 *The perpendicular-mode X-band EPR spectrum of* ***9*** *Recording condition 77 K; 9.02 GHz microwave frequency at 1 mW microwave power; modulation 100 kHz modulation frequency.*

.

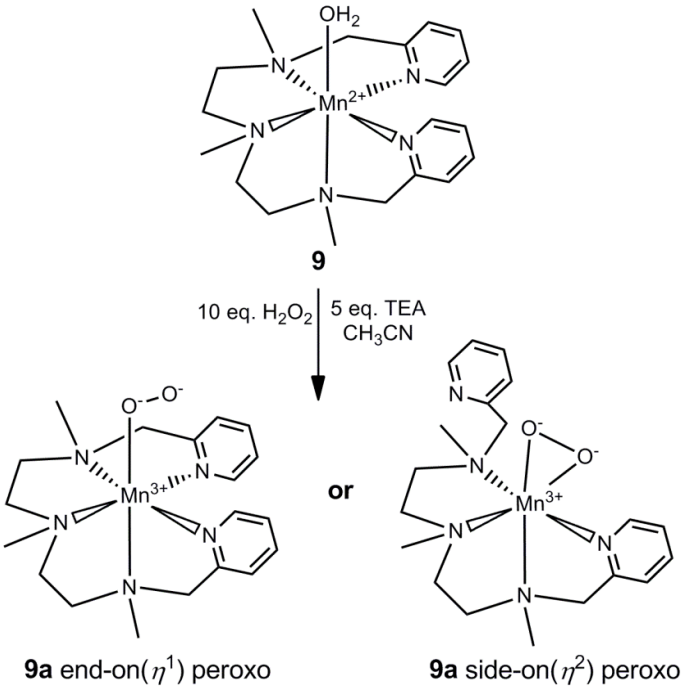

Scheme 4.8 *The probable structure of reactive Mn(III)-peroxo intermediate* ***9a****.*

4.3.4 Computational study

All the geometry optimization was performed using the Gaussian 09, suite of program.[85] In the similar work, several functionals such as B3LYP, B3LYP-D, wB97XD, B97D, M06-2X, OLYP, TPPSh and MP2 were employed and found that B3LYP, B3LYP-D2 and wB97XD were advocated to predict the correct spin ground state of the reactant and intermediates compared to experimental data.[86] Here the calculations are restricted only to two functionals, one is a plain B3LYP and the other is B3LYP-D2 functional. The dispersion corrected B3LYP functional (B3LYP-D2), level of theory was employed for the geometry optimization of the **9a**.[87] Here two different basis sets; LanL2DZ for Mn[88–91] and a 6–31G basis set for the C, H, N and O atoms.[92] Optimized geometries were then used to perform single-point energy calculations using a TZVP [93,94] basis set on all atoms. The quoted DFT energies are B3LYP-D2 solvation including free-energy corrections with TZVP basis set at the temperature of 298.15 K. The optimized geometries were verified by animating frequency by using Chemcraft software. The solvation energies were computed

at the B3LYP-D level by using polarizable continuum model (PCM) with acetonitrile as a solvent.

The experimental study proposed two possible Mn(III)-peroxo intermediate **9a,** end-on $[Mn(N_3Py_2)(\eta^1\text{-}O_2)]^+$ (**9a$_1$**) and side-on $[Mn(N_3Py_2)(\eta^2\text{-}O_2)]^+$ (**9a$_2$**) intermediates. Here computational study is employed to understand the stability of **9a** intermediate.

End-on *$[Mn(N_3Py_2)(\eta^1\text{-}O_2)]^+$ (**9a$_1$**):* The possible spin state of the end-on *$[Mn(N_3Py_2)(\eta^1\text{-}O_2)]^+$* (**9a$_1$**) species is optimized and DFT calculations reveal that quintet state (high spin) is computed as the ground state. The triplet state lies at 107.6 kJ/mol higher in energy while a low-spin singlet lies at 164.4 kJ/mol higher in energy. Optimized structure of the high spin of the end-on $[Mn(N_3Py_2)(\eta^1\text{-}O_2)]^+$ (**9a$_1$**) species is shown in **Figure 4.15a.** The Mn-O1, O1-O2 bond lengths of the ground state of the Mn(III) peroxo species are computed to be 2.004 Å and 1.392 Å. The Mn-N(aq) bond length is found to be 2.401 Å. The O1-Mn-N3 bond angle is computed to be 157.3˚. The computed structural parameters of the quintet, triplet and singlet spin states of the **9a** are shown in **Table 4.6**. The spin density plot of the ground state is shown in **Figure 4.15b** and suggests the presence of four unpaired electrons in the *d*-orbital of **9a**.

*Side-on $[Mn(N_3Py_2)(\eta^1\text{-}O_2)]^+$ (**9a$_2$**):* The optimized possible spin state of the side-on $[Mn(N_3Py_2)(\eta^2\text{-}O_2)]^+$ (**9a$_2$**) species is optimized. The DFT calculations reveal that the high spin state is found to be the ground state with the triplet and the singlet lying at 99.6 and 152.6 kJ/mol, respectively. Optimized structure of the high spin of the side-on $[Mn(N_3Py_2)(\eta^2\text{-}O_2)]^+$ (**9a$_2$**) species is shown in **Figure 4.15c**. The computed bond lengths of Mn-O1, Mn-O2, O1-O2 bond lengths of the ground state are 2.037 Å, 2.044 Å and 1.443 Å. The axial Mn-N bond length is computed to be

2.458 Å. The O1-Mn-N3 and O2-Mn-N3 bond angles are found to be 154.0˚ and 150.3˚. The computed structural parameters of side-on $[Mn(N_3Py_2)(\eta^2\text{-}O_2)]^+$ (**9a$_2$**) species is shown in **Table 4.6**. The spin density plot of the ground state is shown in **Figure 4.15d** and also suggests the presence of four unpaired electrons in the *d*-orbital of **9a**.

DFT calculations predicted that the side-on $[Mn(N_3Py_2)(\eta^2\text{-}O_2)]^+$ (**9a$_2$**) species is found to be the lowest in energy by 14.6 kJ/mol than the end-on $[Mn(N_3Py_2)(\eta^1\text{-}O_2)]^+$ (**9a$_1$**) species. We have also employed B3LYP functional for the optimization and found that high spin is the ground state in both the **9a** species (**Table 4.8**) also suggested that side-on $[Mn(N_3Py_2)(\eta^2\text{-}O_2)]^+$ (**9a$_2$**) is more stable intermediate than the end-on $[Mn(N_3Py_2)(\eta^1\text{-}O_2)]^+$ (**9a$_1$**) species. This is in accordance with similar Mn^{III}-peroxo species with pentadentate ligands[20,37,39]. The axial Mn-N bond length of the side-on $[Mn(N_3Py_2)(\eta^2\text{-}O_2)]^+$ (**9a$_2$**) species is slightly longer than the end-on $[Mn(N_3Py_2)(\eta^1\text{-}O_2)]^+$ (**9a$_1$**) species (**Table 4.6**) and this is due to the presence of two ligated oxygen molecule. A significant spin density on proximal oxygen **(Figure 4.15d)** can facilitate the reactivity of the substrates by **9a**.

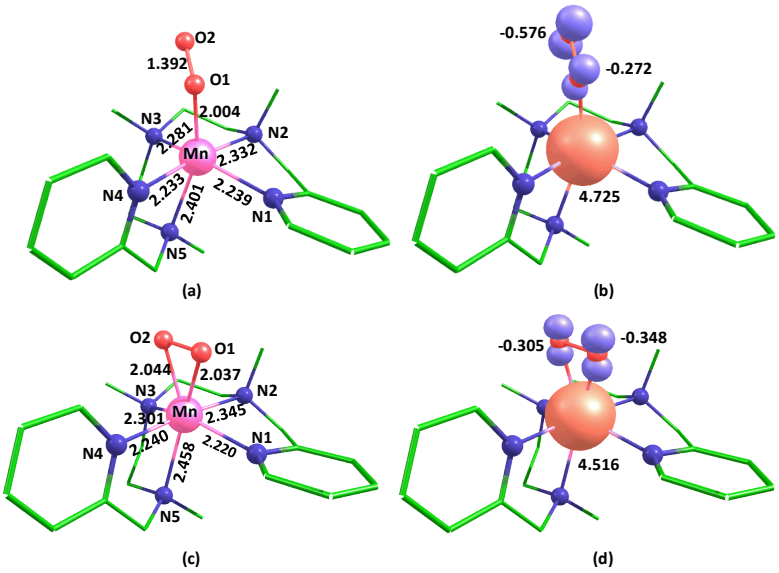

Figure 4.15 *B3LYP-D2 optimized structures and spin density plots of the ground state of end-on* ***9a$_1$*** *and* ***9a$_2$*** *(c and d) species.*

Table 4.6 *Computed structural parameters for* ***9a*** *intermediate.*

*end-on [Mn(N$_3$Py$_2$)(η^1-O$_2$)]$^+$ (**9a$_1$**)*													
B3LYP-D2													
	Mn-O1	Mn-O2	O1-O2	Mn-N1	Mn-N2	Mn-N3	Mn-N4	Mn-N5	Mn-O1-O2	Mn-O2-O1	O1-Mn-N5	N1-Mn-N3	N2-Mn-N4
HS	2.004		1.392	2.239	2.332	2.281	2.233	2.401	122.6		157.3	146.7	172.5
IS	1.882		1.402	2.032	2.143	2.136	2.045	2.240	119.6		164.5	158.0	174.9
LS	1.746		1.412	2.043	2.123	2.120	2.098	2.264	128.9		156.7	157.4	172.2
B3LYP													
HS	2.040		1.391	2.281	2.357	2.323	2.271	2.475	121.3		153.4	142.2	173.2
IS	1.892		1.400	2.061	2.157	2.172	2.065	2.304	118.8		163.8	144.2	174.3
LS	1.913		1.385	2.063	2.150	2.163	2.081	2.292	123.5		160.0	151.5	172.5
*side-on [Mn(N$_3$Py$_2$)(η^2-O$_2$)]$^+$ (**9a$_2$**)*													
B3LYP-D2													
HS	2.037	2.044	1.443	2.220	2.345	2.301	2.240	2.458	69.5	69.0	154.0	141.9	174.9
IS	1.843	2.013	1.497	2.075	2.119	2.270	2.043	2.620	73.3	61.3	155.2	143.0	174.1
LS	1.946	1.942	1.470	2.038	2.161	2.158	2.039	2.231	67.6	67.9	150.9	151.3	176.2
B3LYP													
HS	2.068	2.063	1.439	2.259	2.376	2.338	2.275	2.540	69.4	69.8	154.6	142.2	175.9
IS	1.839	2.023	1.495	2.101	2.130	2.340	2.061	2.669	73.9	60.9	156.8	144.2	175.6
LS	1.946	1.939	1.471	2.060	2.176	2.181	2.051	2.275	67.5	68.0	151.1	151.5	175.3

Note: HS=High spin, IS=Intermediate spin and LS=Low spin

Table 4.7 *Computed Mulliken spin densities for* ***9a***

*end-on [Mn(N_3Py_2)(η^1-O_2)]$^+$ (**9a$_1$**)*			
B3LYP-D2			
Side-on	Mn	O1	O2
HS	4.726	-0.272	-0.576
IS	1.232	0.377	0.465
Ls	0.000	0.000	0.000
B3LYP			
HS	4.769	-0.288	-0.600
IS	1.207	0.3753	0.487
Ls	-1.046	0.602	0.361
*side-on [Mn(N_3Py_2)(η^2-O_2)]$^+$ (**9a$_2$**)*			
B3LYP-D2			
HS	4.516	-0.348	-0.305
IS	2.138	-0.035	-0.087
Ls	0.000	0.000	0.000
B3LYP			
HS	4.576	-0.371	-0.329
IS	2.157	-0.039	-0.096
Ls	0.000	0.000	0.000

.

Table 4.8 *B3LYP-D2 computed potential energy surface (ΔG in kJ mol^{-1})* ***9a****.*

B3LYP-D2	
*side-on [Mn(N_3Py_2)(η^2-O_2)]$^+$ (**9a$_2$**)*	
HS	0
IS	99.6
Ls	152.6
*end-on [Mn(N_3Py_2)(η^1-O_2)]$^+$ (**9a$_1$**)*	
HS	14.6
IS	122.2
Ls	179.1
B3LYP	
*side-on [Mn(N_3Py_2)(η^2-O_2)]$^+$ (**9a$_2$**)*	
HS	0
IS	116.8
Ls	182.5
*end-on [Mn(N_3Py_2)(η^1-O_2)]$^+$ (**9a$_1$**)*	
HS	10.7
IS	145.5
Ls	223.5

4.3.5 Reactivity study of 9a in aldehyde deformylation reaction and 9 in catalytic alkene epoxidation reaction

4.3.5a Reactivity study of 9a in aldehyde deformylation reaction

The reactivity of **9a** was investigated using different substrates and monitored by UV-Vis spectroscopy. Upon addition of substrates like triphenylphosphine (PPh_3), thioanisole (HSC_6H_5), xanthene, cyclohexene, benzyl alcohol and cyclohexane, no spectral changes were observed and the peak at 572 nm remains intact. The product analysis of the reaction revealed that no oxygenated product formation.

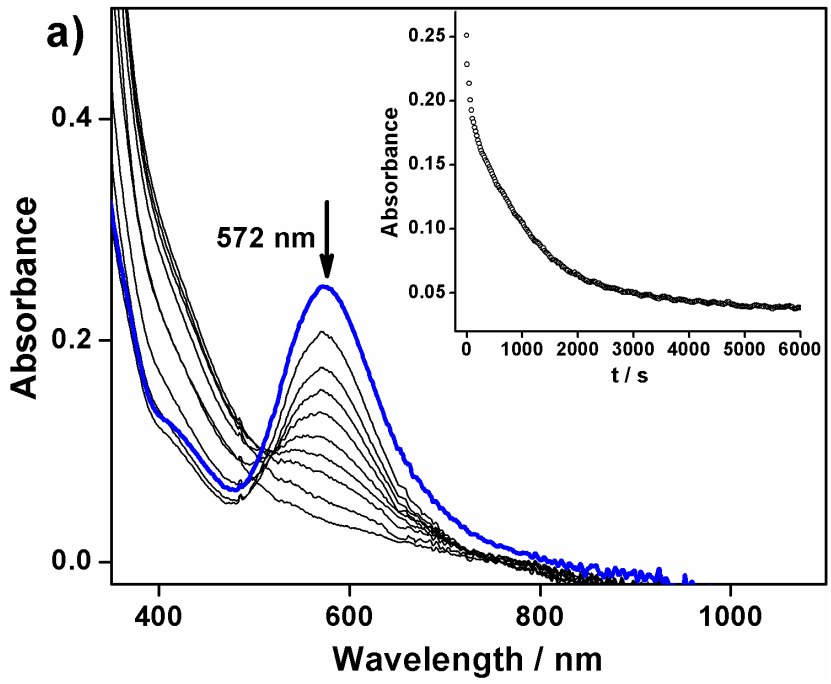

Figure 4.16 *UV-Visible spectral changes of* ***9a*** *(1mM) upon addition of 10 eq. of 2-PPA in acetonitrile. The inset shows the time course of the reaction monitored at 572 nm.*

Upon addition of 2-PPA (2-phenylpropinaldehyde) a characteristic UV-Vis band at 572 nm disappeared with pseudo-first order decay with a clear isobestic point at 501 nm and 778 nm (**Figure 4.16**). The k_{obs} value to be 1.62 x 10^{-3} s^{-1} was obtained by Pseudo-first order fitting of the kinetic data (**Figure 4.16**, **inset**). Upon increasing the concentration of 2-PPA, the pseudo-first-order rate constants increased proportionally giving a second-order rate constant (k_2) of 1.59 x 10^{-1} $M^{-1}S^{-1}$ at 25 °C (**Figure 4.17**).

Product analysis of the reaction mixture by GC revealed acetophenone as a predominant product (**Scheme 4.9**).

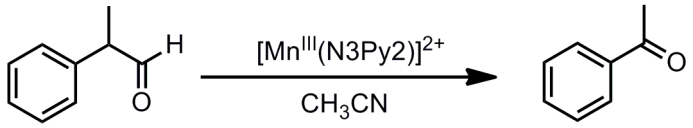

Scheme 4.9 *Upon deformylation of 2-PPA, acetophenone is obtained as the product*

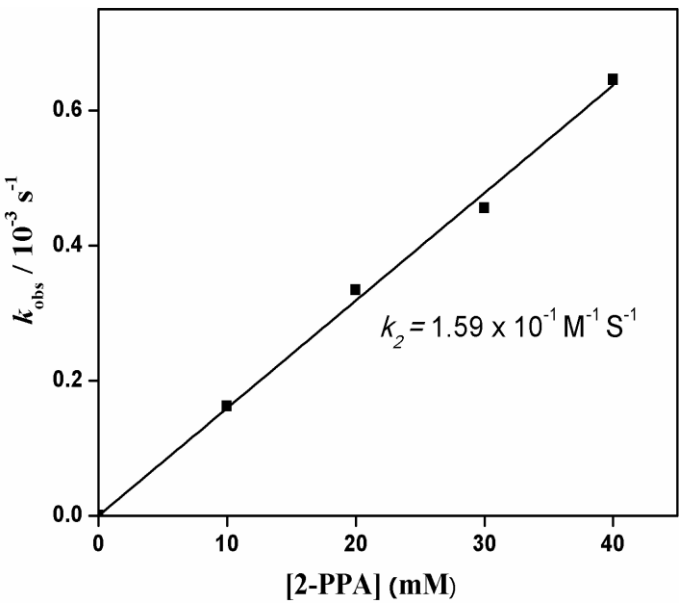

Figure 4.17 *Plot of k_{obs} against the concentration of 2-PPA to determine the second-order rate constant*

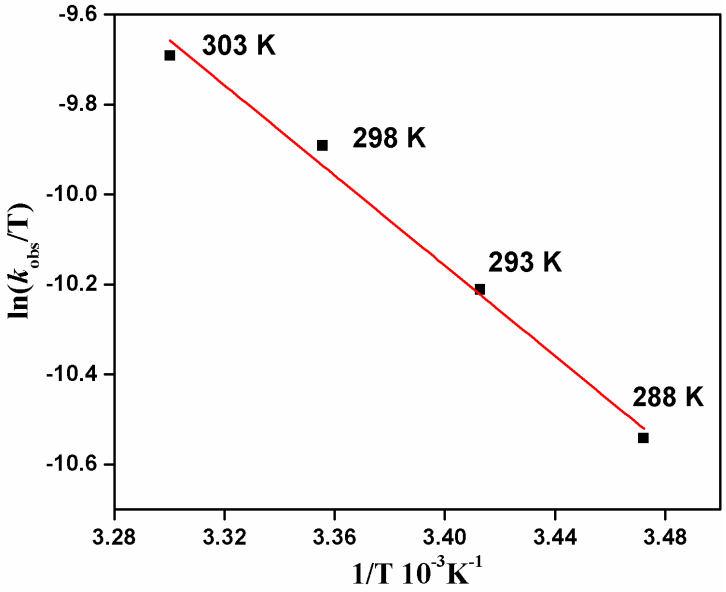

Figure 4.18 *Plot of first-order rate constants against 1/T to determine activation parameters for the reaction of* ***9a*** *(1mM) and 60 eq. of 2-PPA.*

The activation parameters for the aldehyde deformylation reaction were obtained from erying plot to give $\Delta H^{\ddagger}$ and $\Delta S^{\ddagger}$ by determining pseudo-first-order rate constants from 288 K to 303 K (**Figure 4.18**). The reaction rate was dependent on temperature and a linear erying plot was obtained to give activation parameter of $\Delta H^{\ddagger}$ = 42 kJ mol^{-1} and $\Delta S^{\ddagger}$ = -139 J $mol^{-1}K^{-1}$ for the aldehyde deformylation reaction.

The nucleophilic character of the intermediate was further verified by studying the reactivity of intermediate with different *para*-substituted benzaldehyde *para*-X−Ph−CHO (X = Cl, F, H, Me) (**Figure 4.19**). The deformylation of an aldehyde suppose to proceeds by the nucleophilic attack on the carbonyl carbon by the peroxo group bound the manganese complex. It is observed that electron withdrawing *para*-substituents on the benzaldehyde reacts with intermediate at a faster rate compared with electron donating *para*-substituents following the trend Cl >F > H > Me. Plot of log k_{obs} versus Hammett constants (σ_p) was found linear with a ρ value of 3.32. Such large positive value shows that the intermediate **9a** posseses nucleophillic character.

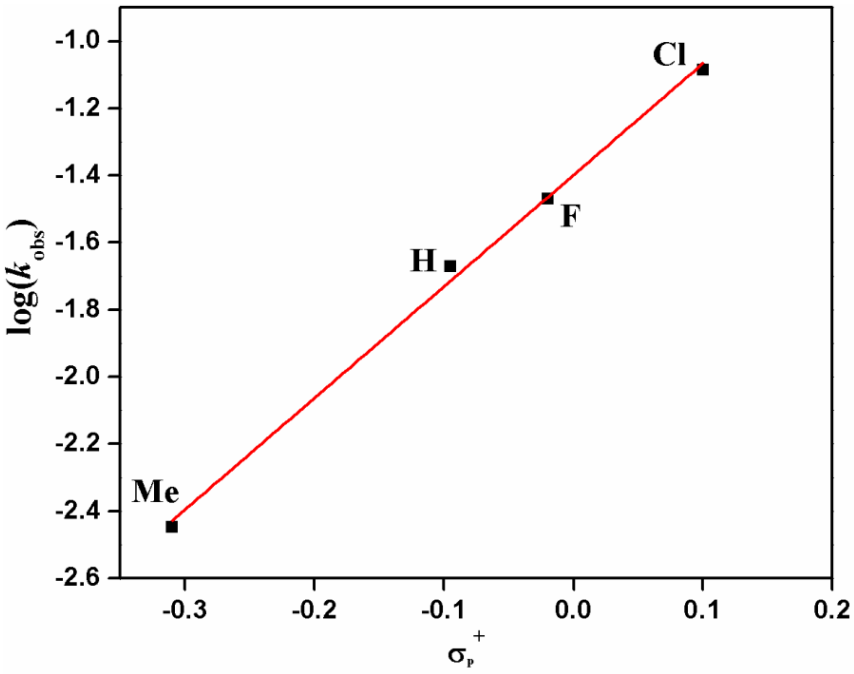

Figure 4.19 *Hammet plot for the oxidation of para-substituted benzaldehydes, para-X-Ph-CHO (X = Cl, F, H, Me) by* $[Mn(N3Py2)(O_2)]^+$ ***9a*** *in* CH_3CN *at 25 °C.*

From the above study we propose a mechanism which is under the similar lines as reported by others.[95] Here the peroxo group possessing nucleophilic character attacks the carbonyl carbon of aldehyde forming peroxyhemiacetal kind of intermediate. O-O bond homolysis in this intermediate yields the deformylated products. It is proposed that ferric peroxo porphyrin intermediate in cytochrome P450 progesterone 17α-hydroxylase-17,20-lyase (CYP $450_{17\alpha}$) attacks the carbonyl carbon of progesterone leading to the formation of androstenedione and acetate[96] (S**cheme 4.10**)

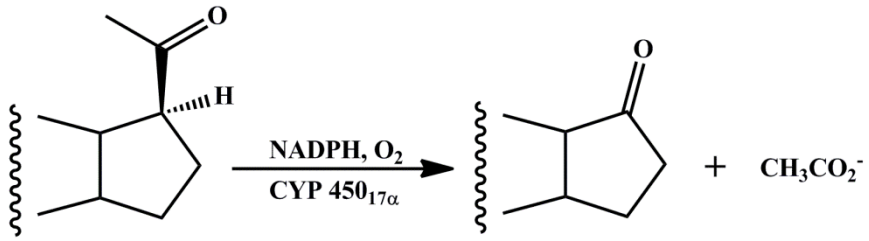

Scheme 4.10 *The reaction catalysed by ferric peroxo porphyrin intermediate in cytochrome P450 progesterone 17α-hydroxylase-17,20-lyase (CYP $450_{17\alpha}$) of progesterone leading to the formation of androstenedione and acetate.*

4.3.5b Catalytic epoxidation of alkenes by 9

The catalytic activity of **9** was investigated in alkene epoxidation reactions in presence of PhIO oxidants as per the procedure described in section 4.2.2. The GC analysis shows the formation of products as shown in **Scheme 4.11**.

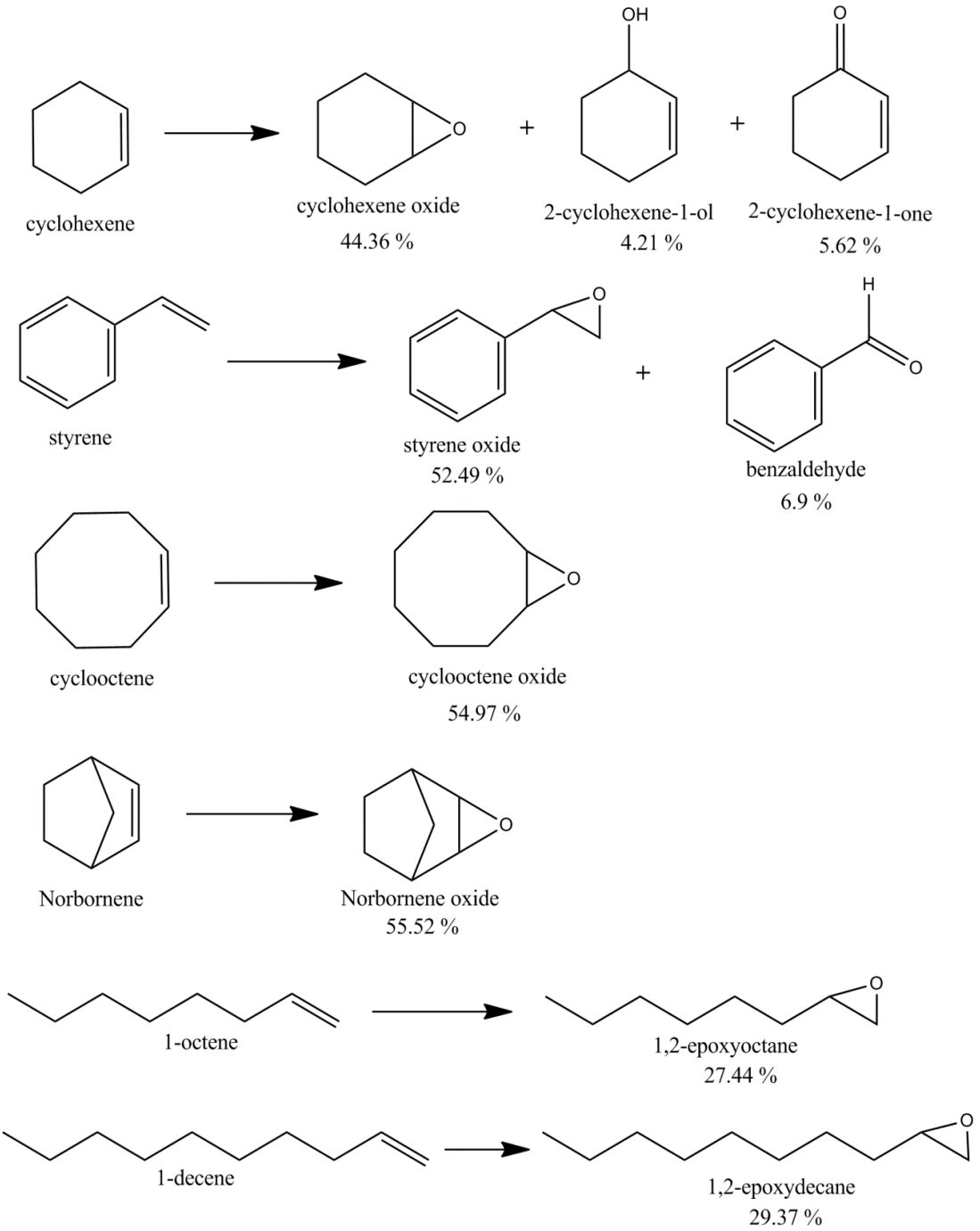

Scheme 4.11 *Oxidation of alkenes to an epoxide by* ***9****. Reaction condition: substrate 250 mM, catalyst 0.5mM, PhIO, 50 mM in 2 mL, 25 °C, Reaction time 30 min. Yield is based on the oxidant.*

The oxidation of cyclohexene resulted in the formation of cyclohexene epoxide as a major product with a formation of 2-cyclohexene-1-ol and 2-cyclohexe-1-none as a minor product as a result of allylic oxidation as observed earlier under identical condition.[97] The epoxidation of styrene resulted in the formation of styrene oxide as major product and benzaldehyde as a minor product. The epoxidation by cyclooctene, norbornene, 1-octene and 1-decene resulted in the formation of the corresponding epoxide with 100 % selectivity without any formation side products. The catalytic epoxidation reactions by Mn(II) complexes show the formation of similar products.[59,73,84,97] Terminal alkene (1-octene and 1-decene) shows a low yield of formation of products due to its electron deficient nature.[59,60,63] At end of the reaction PhIO gets converts into iodobenzene as evident from GC analysis.

Although Mn(IV)=O species is well characterized in presence of PhIO,[46,46,98] we have not observed the formation of such intermediates as monitored by UV-Vis spectroscopy. Therefore we propose a mechanism on similar lines reported by others which predicts the formation of [Mn(II)-O-I^+-Ph] responsible for catalytic epoxidation (**Scheme 4.12**).[73,74] Theoretical study predicts the existence of multiple reactive intermediates in the reaction between Mn(III) complex and PhIO.[99]

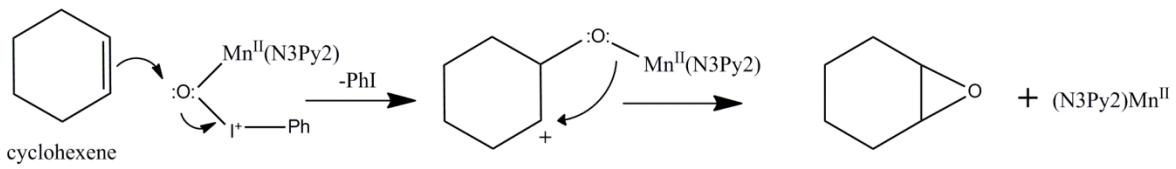

Scheme 4.12 *Proposed mechanism for the epoxidation of an alkene by* ***9*** *in presence of PhIO*

4.4 Summary and conclusion

This chapter deals with synthesis and characterization Mn(III)-peroxo (**9a**) species from Mn(II) complex (**9)** and its reactivity study in the aldehyde deformylation reaction. The complex $[Mn(N3Py2)(H_2O)](ClO_4)_2$ **9** was prepared by the reaction of ligand N3Py2 with $(MnClO_4)_2.6H_2O$ in CH_3CN. The ligand N3Py2 was synthesized, characterized by IR and NMR spectroscopy and reported for the first time. The compound **9** was characterized by CHN analysis, spectroscopic techniques like UV-Vis, IR and EPR, ESI-MS and electrochemical techniques (cyclic voltammetry and differential pulse voltammetry). The compound **9** was structurally characterized by single crystal X-ray crystallography. A mononuclear Mn(III)-peroxo complex $[Mn^{III}(N3Py2)(O_2)]^{2+}$ (**9a**) was generated *in-situ* by the reaction of $[Mn^{II}(N3Py2)(H_2O)](ClO_4)_2$ (**9**) with H_2O_2 in presence of triethylamine in CH_3CN. The formation of Mn(III)-peroxo species $[Mn(III)(N3Py2)(O_2)]^{2+}$ (**9a**) was evident from EPR spectroscopy and ESI-MS techniques. The computational study supports the formation of side-on peroxo species. The reactivity of **9a** was investigated in aldehyde deformylation reaction using 2-PPA (2-phenyl propionaldehyde) as substrate at 25 °C. The kinetics of the reactions was monitored by following the decay of the peak corresponding to **9a**. The activation parameters ΔH‡ and ΔS‡ for the aldehyde deformylation reaction were obtained from erying plot by performing the reactions at different temperature ranging from 288 to 303 K. The reactivity of **9a** with *para*-substituted benzaldehyde yields positive hammet ρ value of 3.32 which suggests the nucleophilic character of **9a** in aldehyde deformylation reaction.The reactivity of **9** was also investigated in catalytic epoxidation reaction of alkene that shows the formation of epoxides in good yields.

References

(1) Keele, B. B.; McCord, J. M.; Fridovich, I. *J. Biol. Chem.* **1970**, *245*, 6176–6181.

(2) Debus, R. J. *Biochim. Biophys. Acta*, **1992**, *1102*, 269-352

(3) Bull, C.; Niederboffer, E. C.; Tatsuro Yoshida, L.; Fee, J. A. *J. Am. Chem. Soc.* **1991**, *113*, 4069–4076.

(4) Hearn, A. S.; Tu, C.; Nick, H. S.; Silverman, D. N. *J. Biol. Chem.* **1999**, *274*, 24457–24460.

(5) Grove, L. E.; Brunold, T. C. *Comments Inorg. Chem.* **2008**, *29*, 134–168.

(6) Miller, A.-F. *Curr. Opin. Chem. Biol.* **2004**, *8*, 162–168.

(7) McEvoy, J. P.; Brudvig, G. W. *Chem. Rev.* **2006**, *106*, 4455–4483.

(8) Cox, N.; Pantazis, D. A.; Neese, F.; Lubitz, W. *Acc. Chem. Res.* **2013**, *46*, 1588–1596.

(9) Cotruvo, J. A.; Stubbe, J. *Biochemistry* **2010**, *49*, 1297–1309.

(10) Zhang, Y.; Stubbe, J. *Biochemistry* **2011**, *50*, 5615–5623.

(11) Cotruvo, J. A.; Stich, T. A.; Britt, R. D.; Stubbe, J. *J. Am. Chem. Soc.* **2013**, *135*, 4027–4039.

(12) Wu, A. J.; Penner-Hahn E, J.; Pecararo, V. L. *Chem. Rev.* **2004**, *104*, 903–938.

(13) Opaleye, O.; Sarah, R.-R.; Whittaker, M. M.; Woo, E.-J.; Whittaker, J. W.; Pickersgill, R. W. *J. Biol. Chem.* **2006**, *281*, 6428–6433.

(14) Borowski, T.; Bassan, A.; Richards, N. G. J.; Siegbahn, P. E. M. *J. Chem. Theory Comput.* **2005**, *1*, 686–693.

(15) Reinhardt, L. A.; Svedruzic, D.; Chang, C. H.; Cleland, W. W.; Richards, N. G. J. *J. Am. Chem. Soc.* **2003**, *125*, 1244–1252.

(16) Svedružić, D.; Jónsson, S.; Toyota, C. G.; Reinhardt, L. A.; Ricagno, S.; Lindqvist, Y.; Richards, N. G. J. *Arch. Biochem. Biophys.* **2005**, *433*, 176–192.

(17) Tanner, A.; Bowater, L.; Fairhurst, S. A.; Bornemann, S. *J. Biol. Chem.* **2001**, *276*, 43627–43634.

(18) Gunderson, W. A.; Zatsman, A. I.; Emerson, J. P.; Farquhar, E. R.; Que, L.; Lipscomb, J. D.; Hendrich, M. P. *J. Am. Chem. Soc.* **2008**, *130*, 14465–14467.

(19) Pecoraro, V. L.; Baldwin, M. J.; Gelasco, A. *Chem. Rev.* **1994**, *94*, 807–826.

(20) Du, J.; Xu, D.; Zhang, C.; Xia, C.; Wang, Y.; Sun, W. *Dalt. Trans.* **2016**, *45*, 10131–10135.

(21) Weschler, C. J.; Hoffman, B. M.; Basolo, F. *J. Am. Chem. Soc.* **1975**, *97*, 5278–5280.

(22) Vanatta, R. B.; Strouse, C. E.; Hanson, L. K.; Valentine, J. S. *J. Am. Chem. Soc.* **1987**, *109*, 1425–1434.

(23) Porta, J.; Vahedi-Faridi, A.; Borgstahl, G. E. O. *J. Mol. Biol.* **2010**, *399*, 377–384.

(24) Edwards, R. a; Baker, H. M.; Whittaker, M. M.; Whittaker, J. W.; Jameson, G. B.; Baker, E. N. **1998**, 97291.

(25) Kitajima, N.; Komatsuzaki, H.; Hikichi, S.; Osawa, M.; Moro-oka, Y. *J. Am. Chem. Soc.* **1994**, *116*, 11596–11597.

(26) Singh, U. P.; Sharma, A. K.; Hikichi, S.; Komatsuzaki, H.; Moro-oka, Y.; Akita, M. *Inorg. Chim. Acta* **2006**, *359*, 4407–4411.

(27) Colmer, H. E.; Geiger, R. A.; Leto, D. F.; Wijeratne, G. B.; Day, V. W.; Jackson, T. A. *Dalt. Trans.* **2014**, *43*, 17949–17963.

(28) Seo, M. S.; Kim, J. Y.; Annaraj, J.; Kim, Y.; Lee, Y. M.; Kim, S. J.; Kim, J.; Nam, W. *Angew. Chemie - Int. Ed.* **2007**, *46*, 377–380.

(29) Annaraj, J.; Cho, J.; Lee, Y.-M.; Kim, S. Y.; Latifi, R.; de Visser, S. P.; Nam, W. *Angew. Chem.* **2009**, *121*, 4214 –4217.

(30) Kang, H.; Cho, J.; Cho, K.-B.; Nomura, T.; Ogura, T.; Nam, W. *Chem. - A Eur. J.* **2013**, *19*, 14119–14125.

(31) Groni, S.; Blain, G.; Policar, C.; Anxolabe´he`re-Mallart, E. *Inorg. Chem.* **2007**, *46*, 1951–1953.

(32) Shook, R. L.; Borovik, A. S. *Inorg. Chem.* **2010**, *49*, 3646–3660.

(33) Geiger, R. A.; Chattopadhyay, S.; Day, V. W.; Jackson, T. A. *J. Am. Chem. Soc.* **2011**, *132*, 1707–1715.

(34) Geiger, R. A.; Chattopadhyay, S.; Day, V. W.; Jackson, T. A. **2011**, 1707–1715.

(35) Geiger, R. A.; Wijeratne, G. B.; Day, V. W.; Jackson, T. A. *Eur. J. Inorg. Chem.* **2012**, 1598–1608.

(36) Saravanan, N.; Sankaralingam, M.; Palaniandavar, M. *RSC Adv.* **2014**, *4*, 12000–12011.

(37) Barman, P.; Upadhyay, P.; Faponle, A. S.; Kumar, J.; Nag, S. S.; Kumar, D.; Sastri, C. V.; de Visser, S. P. *Angew. Chemie - Int. Ed.* **2016**, *55*, 11091–11095.

(38) Cantú Reinhard, F. G.; Barman, P.; Mukherjee, G.; Kumar, J.; Kumar, D.; Kumar, D.; Sastri, C. V.; De Visser, S. P. *J. Am. Chem. Soc.* **2017**, *139*, 18328–18338.

(39) Geiger, R. A.; Leto, D. F.; Chattopadhyay, S.; Dorlet, P.; Jackson, T. A. *Inorg. Chem.* **2011**, *50*, 10190–10203.

(40) El Ghachtouli, S.; Vincent Ching, H. Y.; Lassalle-Kaiser, B.; Guillot, R.; Leto, D. F.; Chattopadhyay, S.; Jackson, T. A.; Dorlet, P.; Anxolabéhère-Mallart, E. *Chem. Commun.* **2013**, *49*, 5696.

(41) Groni, S.; Dorlet, P.; Blain, G.; Bourcier, S.; Guillot, R.; Anxolabéhère-Mallart, E.

Inorg. Chem. **2008**, *47*, 3166–3172.

(42) Leto, D. F.; Chattopadhyay, S.; Day, V. W.; Jackson, T. A. *Dalt. Trans.* **2013**, *42*, 13014–13025.

(43) Colmer, H. E.; Howcroft, A. W.; Jackson, T. A. *Inorg. Chem.* **2016**, *55*, 2055–2069.

(44) Shook, R. L.; Gunderson, W. A.; Greaves, J.; Ziller, J. W.; Hendrich, M. P.; Borovik, A. S. *J. Am. Chem. Soc.* **2008**, *130*, 8888–8889.

(45) Cho, J.; Sarangi, R.; Kang, H. Y.; Lee, J. Y.; Kubo, M.; Ogura, T.; Solomon, E. I.; Nam, W. *J. Am. Chem. Soc.* **2010**, *132*, 16977–16986.

(46) Wu, X.; Seo, M. S.; Davis, K. M.; Lee, Y. M.; Chen, J.; Cho, K. Bin; Pushkar, Y. N.; Nam, W. *J. Am. Chem. Soc.* **2011**, *133*, 20088–20091.

(47) Kaizer, J.; Klinker, E. J.; Oh, N. Y.; Rohde, J. U.; Song, W. J.; Stubna, A.; Kim, J.; Münck, E.; Nam, W.; Que, L. *J. Am. Chem. Soc.* **2004**, *126*, 472–473.

(48) Leto, D. F.; Ingram, R.; Day, V. W.; Jackson, T. A. *Chem. Commun.* **2013**, *49*, 5378–5380.

(49) Jørgensen, K. A. *Chem. Rev.* **1989**, *89*, 431–458.

(50) Lane, B. S.; Burgess, K. *Chem. Rev.* **2003**, *103*, 2457–2473.

(51) Katsuki, T. *Adv. Synth. Catal.* **2002**, *344*, 131–147.

(52) De Vos, D. E.; Sels, B. F.; Jacobs, P. A. *Adv. Synth. Catal.* **2003**, *345*, 457–473.

(53) Brinksma, J.; Hage, R.; Kerschner, J.; Feringa, B. L. *Chem. Commun.* **2000**, *2*, 537–538.

(54) Yu, S.; Miao, C. X.; Wang, D.; Wang, S.; Xia, C.; Sun, W. *J. Mol. Catal. A Chem.* **2012**, *353–354*, 185–191.

(55) Saisaha, P.; de Boer, J. W.; Browne, W. R. *Chem. Soc. Rev.* **2013**, *42*, 2059–2074.

(56) Lyakin, O. Y.; Ottenbacher, R. V.; Bryliakov, K. P.; Talsi, E. P. *ACS Catal.* **2012**, *2*, 1196–1202.

(57) Nehru, K.; Kim, S. J.; Kim, I. Y.; Seo, M. S.; Kim, Y.; Kim, S.-J.; Kim, J.; Nam, W. *Chem. Commun.* **2007**, *1*, 4623.

(58) Garcia-Bosch, I.; Company, A.; Fontrodona, X.; Ribas, X.; Costas, M. *Org. Lett.* **2008**, *10*, 2095–2098.

(59) Murphy, A.; Stack, T. D. P. *J. Mol. Catal. A Chem.* **2006**, *251*, 78–88.

(60) Murphy, A.; Dubois, G.; Stack, T. D. P. *J. Am. Chem. Soc.* **2003**, *125*, 5250–5251.

(61) Hao, E.; Wang, Z.; Jiao, L.; Wang, S. *Dalton Trans.* **2010**, *39*, 2660–2666.

(62) Rich, J.; Rodríguez, M.; Romero, I.; Vaquer, L.; Sala, X.; Llobet, A.; Corbella, M.; Collomb, M.-N.; Fontrodona, X. *Dalt. Trans.* **2009**, 8117.

(63) Murphy, A.; Pace, A.; Stack, T. D. P. *Org. Lett.* **2004**, *6*, 3119–3122.

(64) Gómez, L.; Garcia-Bosch, I.; Company, A.; Sala, X.; Fontrodona, X.; Ribas, X.; Costas, M. *Dalt. Trans.* **2007**, 5539–5545.

(65) Mandelli, D.; Kozlov, Y. N.; Golfeto, C. C.; Shul'pin, G. B. *Catal. Letters* **2007**, *118*, 22–29.

(66) Palucki, M.; McCormick, G. J.; Jacobsen, E. N. *Tetrahedron Lett.* **1995**, *36*, 5457–5460.

(67) Ottenbacher, R. V.; Bryliakov, K. P.; Talsi, E. P. *Inorg. Chem.* **2010**, *49*, 8620–8628.

(68) Lee, S. H.; Xu, L.; Park, B. K.; Mironov, Y. V.; Kim, S. H.; Song, Y. J.; Kim, C.; Kim, Y.; Kim, S. J. *Chem. - A Eur. J.* **2010**, *16*, 4678–4685.

(69) Collman, J. P.; Zeng, L.; Brauman, J. I. *Inorg. Chem.* **2004**, *43*, 2672–2679.

(70) Berben, L. A.; Peters, J. C. *Inorg. Chem.* **2008**, *47*, 11669–11679.

(71) Fraser, C.; Johnston, L.; Rheingold, A. L.; Haggerty, B. S.; Williams, G. K.; Whelan, J.; Bosnich, B. *Inorg. Chem.* **1992**, *31*, 1835–1844.

(72) Oki, A. R.; Glerup, J.; Hodgson, D. J. *Inorg. Chem.* **1990**, *29*, 2435–2441.

(73) Sankaralingam, M.; Palaniandavar, M. *Dalt. Trans.* **2014**, *43*, 538–550.

(74) Saravanan, N.; Palaniandavar, M. *Inorg. Chim. Acta* **2012**, *385*, 100–111.

(75) De Boer, J. W.; Browne, W. R.; Brinksma, J.; Alsters, P. L.; Hage, R.; Feringa, B. L. *Inorg. Chem.* **2007**, *46*, 6353–6372.

(76) De Boer, J. W.; Brinksma, J.; Browne, W. R.; Meetsma, A.; Alsters, P. L.; Hage, R.; Feringa, B. L. *J. Am. Chem. Soc.* **2005**, *127*, 7990–7991.

(77) Sham, K.-C.; Yeung, H.-L.; Yiu, S.-M.; Lau, T.-C.; Kwong, H.-L. *Dalt. Trans.* **2010**, *39*, 9469–9471.

(78) Harris, W. R.; Murase, I.; Timmons, J. H.; Martell, A. E. *Inorg. Chem.* **1978**, *17*, 889–894.

(79) Singha, S.; Parida, K. M. *Catal. Sci. Technol. Catal. Sci. Technol* **1496**, *1*, 1496–1505.

(80) Sánchez-Sandoval, A.; Álvarez-Toledano, C.; Gutiérrez-Pérez, R.; Reyes-Ortega, Y. *Synth. Commun.* **2003**, *33*, 481–492.

(81) Nakamoto, K.: *Infrared and Raman Spectra of Inorganic and Coordination Compounds, Part B: Applications in coordination, organometallic, and bioinorganic chemistry*, 6th ed.; John Wiley, Hoboken, NJ) (2009).

(82) Panja, A.; Kanti, T. *Indian J. Chem.* **2016**, *55*, 137–144.

(83) Hureau, C.; Blondin, G.; Charlot, M.-F.; Philouze, C.; Nierlich, M.; Césario, M.; Anxolabéhère-Mallart, E. *Inorg. Chem.* **2005**, *44*, 3669–3683.

(84) Choe, C.; Yang, L.; Lv, Z.; Mo, W.; Chen, Z.; Li, G.; Yin, G. *Dalt. Trans.* **2015**, *44*, 9182–9192.

(85) Frisch, M. J. et al, *Gaussian 09, revision 02; Gaussian, Inc.: Wallingford, CT*, 2009.

(86) Azaz, A.; Kaushik, A.; Rajaraman, G. *J. Am. Chem. Soc*. **2013**, *135*, 4235–4249.

(87) Grimme, S.; *Comput. Chem.* **2006**, *27*, 1787-1799.

(88) Dunning, T. H., Jr; Hay, P. J. *In Modern Theoretical Chemistry, Vol. 3 (Ed.: Schaefer, H. F. III), Plenum, New York,*, 1976.

(89) Hay, P. J.; Wadt, W. R.; *J. Chem. Phys.* **1985**, *82*, 270-283.

(90) Wadt, W. R.; Hay, P. J.; *J. Chem. Phys.* **1985**, *82*, 284-298.

(91) Hay, P. J.; Wadt, W. R.; *J. Chem. Phys.* **1985**, *82*, 299-310.

(93) Ditchfield, R.; Hehre, W. J.; Pople, J. A.; **1971**, *54*, 724-728.

(94) Schaefer, A.; Horn, H.; Ahlrichs, R.; *J. Chem. Phys.*, **1992**, *97*, 2571-2577.

(95) Schaefer, C.; Huber, C.; Ahlrichs, R.; *Chem. Phys.*, **1994**, *100*, 5829-2835.

(95) Jo, Y.; Annaraj, J.; Seo, M. S.; Lee, Y. M.; Kim, S. Y.; Cho, J.; Nam, W. *J. Inorg. Biochem.* **2008**, *102*, 2155–2159.

(96) Akhtar, M.; Corina, D.; Miller, S.; Shyadehi, A. Z.; Wright, J. N. *Biochemistry* **1994**, *33*, 4410–4418.

(97) Saravanan, N.; Palaniandavar, M. *Inorg. Chim. Acta* **2012**, *385*, 100–111.

(98) Sawant, S. C.; Wu, X.; Cho, J.; Cho, K. Bin; Kim, S. H.; Seo, M. S.; Lee, Y. M.; Kubo, M.; Ogura, T.; Shaik, S.; et al. *Angew. Chemie - Int. Ed.* **2010**, *49*, 8190–8194.

(99) Kang, Y.; Wang, F.; Reinhurd, F. G. K.; Xia, C.; de Visser, S. P.; Wang, Y. *ChemistrySelect* **2018**, *3*, 3208–3213.

CHAPTER –V

Synthesis and characterization of N3Py2 ligand-based cobalt(II), nickel(II) and copper(II) catalysts for efficient conversion of hydrocarbons to alcohols

5.1 Introduction and literature

In Chapter III we have studied the synthesis, characterization and catalytic alkane hydroxylation reactions by nickel(II) complexes containing tetradentate ligands bqenH_2 and bqenMe_2. In this Chapter, we have investigated transition metal complexes of the first row, i.e. Co(II) and Cu(II) along with Ni(II) complexes. Here we have synthesized and well characterized the Co(II), Ni(II) and Cu(II) complexes that are obtained from the pentadentate ligand N3Py2 and their role have been investigated in alkane hydroxylation reactions. The literature survey on Ni(II) complexes has been already discussed in section 3.1 of Chapter III and hence it is not discussed in this Chapter. Here the literature on the Co(II) and Cu(II) have been discussed.

The late transition metal complexes of the first row are now known to be equally proficient catalysts for hydrocarbon oxidations. The reactive intermediates like high valent metal-oxo reactive intermediates of the late transition metals like cobalt, nickel and copper are very rare compared to such reactive intermediates of an early transition metal of the first row. However, they have often been invoked as reactive transient intermediates in different oxidation reactions catalyzed by metal complexes.[1–6] Theoretical studies predict that such intermediates are highly reactive and potent oxidants than even iron-oxo intermediate.[7–9]

5.1.1 Literature on Cobalt complexes

The interaction of cobalt complexes with dioxygen, has widely been investigated and the number of Co-O_2 species has been synthesized as a chemical model of dioxygen carrier proteins, such as haemoglobin and myoglobin.[10-12] The cobalt schiff base complexes in the presence of dioxygen were investigated extensively for the oxidation of organic substrates like phenols and olefins under catalytic conditions.[13-15] In these oxidation

reactions, the end-on cobalt^{III}-superoxo complexes, Co^{III}-(O^{-}) have been proposed as an active oxidant for hydrogen atom abstraction from the weak O-H or C-H bonds of substrates.[14,15] The proposed intermediate end-on(η^1) binding mode in cobalt^{III}-superoxo complex was supported by X-ray crystallography studies.[10,16,17] At present a large number of Co^{III}-O_2 species stabilized by non-heme ligands have been characterized by spectroscopic techniques and few by X-ray crystallography and their reactivity have been investigated in the number of oxidation reactions.

A large number of cobalt(II) complexes in the presence of alkyl peroxides as oxidants proceed via formation of an alkylperoxo complex and perform the oxidation of hydrocarbons.[18] The number of Co(III)-peroxo species with a side-on (η^2) binding, bearing ligands that are varied in their structure have been reported,[11,19–25] some of which showed nucleophilic reactivity in the aldehyde deformylation reaction.[22-25] Compared to the Co^{III}-peroxo species, the reports on cobalt^{III}-hydroperoxo species are very few.[26–29] The end-on Co(III)-hydroperoxo species have reported to form by the protonation of Co^{III}-peroxo species in the presence of acid.[29] The homolytic cleavage of these Co^{III}-hydroperoxo species leads to the formation of reactive Co^{IV}-oxo or Co^{III}-oxyl species that results in hydroxylation of the ligand. In another recent study, it is reported that the Co^{III}-hydroperoxo species is highly reactive in sulfoxidation reaction which possesses the electrophilic character that was confirmed from the hammett plot. However unlike Fe^{III}-hydroperoxo species Co^{III}-hydroperoxo do not show reactivity in hydrogen abstraction reactions.[26]

Yet another powerful oxidant is terminal Co^{IV-}oxo that has been proposed as a reactive intermediate in the alkane hydroxylation reactions mediated by cobalt complexes.[2,20,30] However unlike Fe^{IV}-oxo or Mn^{IV}-oxo species there was no direct spectroscopic characterization of such intermediates and evidence were restricted to mass

spectrometric studies in the gas phase.[31,32] In one of the recent study, it is reported that cobalt(II) complex possessing dianionic ligand capable of activating stronger C-H bonds in the presence of O_2 and other terminal oxidants like PhIO and *p*-tosyl azide in which putative Co^{IV}-oxo intermediate has been proposed as an active oxidant.[4] Another study showed that reactive intermediate $cobalt^{IV}$-oxo supported by two different tetradentate ligands i.e. macrocyclic tetraamido TAML ligand and tripodal TMG_3tren (tris[2-(N-tetramethylguanidyl)ethyl]amine) that can be stabilized in the presence of redox-inactive metal ions such as Sc^{3+}, Ce^{3+} Y^{3+} and Zn^{2+}.[33,34] The reactivity of such intermediates have been further investigated in the C-H activation reactions. Borovik has assigned Co^{IV}-Sc^{3+} as Co^{III}-OH-Sc^{3+} species.[35] The existence of Co^{IV}-oxo species was further evident from the recent study wherein an intermediate $[Co^{IV}(O)(13\text{-}TMC)]^{2+}$ was generated by a photocatalytic method in the presence of $[Ru^{II}(bpy)_3]Cl_2$ as a photosensitizer and $Na_2S_2O_8$ as a sacrificial electron acceptor and H_2O as an oxygen source.[36] The species $[Co^{IV}(O)(13\text{-}TMC)]^{2+}$ showed higher stability when prepared independently using PhIO oxidant in acetone.[36]

The cobalt(II) complex that is obtained from bpc (*N,N'*- dibenzyl- *N,N'*- bis(2-pyridylmethyl)-1,2-cyclohexanediamine) ligand is capable of nucleophilic aldehyde deformylation in the presence of H_2O_2 and TEA via formation of Cobalt(III)-peroxo that has been characterized structurally while the same complex undergoes electrophilic C-H activation reactions in the presence of *m*-CPBA or PhIO.[25] The Cheal kim have proposed the existence of multiple active oxidants Co^{V}=O, Co^{IV}=O and Co^{III}-OO(O)CR that have been supported by amide based non-heme ligand in olefin epoxidation reaction.[37,38] The chemical structures of the non-heme ligand stabilizing different Co-O_2 reactive intermediates are shown in **Scheme 5.1**

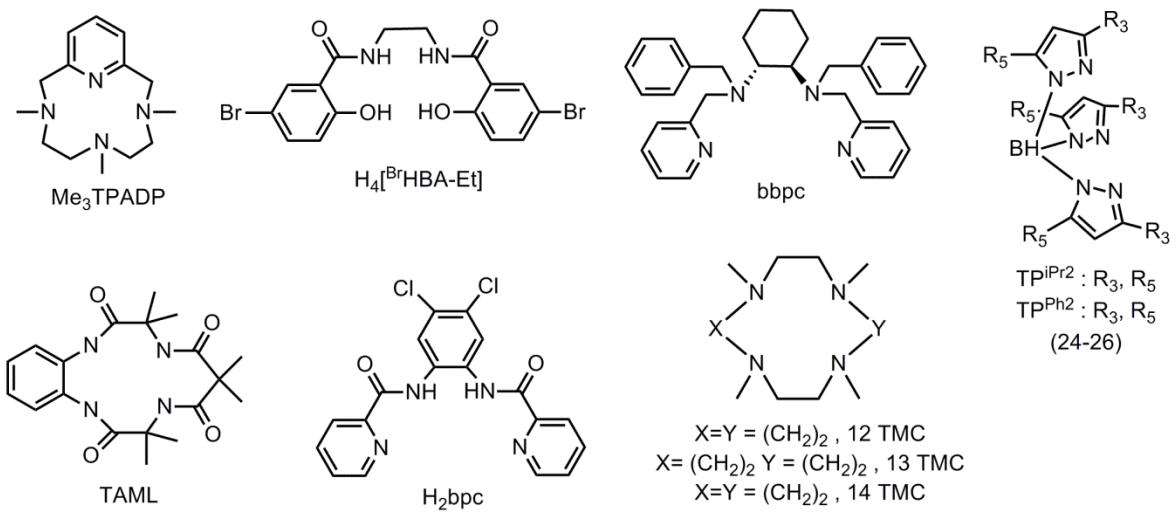

Scheme 5.1 *Ligand stabilizing the high valent Co-O_2 reactive intermediate*

5.1.2 Literature review on copper complexes

The copper(II) complexes have also been investigated in enzymatic, biomimetic and chemical oxidation reactions to a large extent. The number of copper(II)-dioxygen (Cu-O_2) species have been frequently invoked as the reactive intermediates in C-H bond activation reactions catalyzed by copper(II) complexes.[39–40] A study of the number of small molecules containing Cu-O_2 core has significantly contributed in understanding the metal site of enzymes like particulate methane monooxygenase (pMMO), peptidylglycine α-amidating monooxygenase and dopamine *β*-monooxygenase (D*β*M) that are involved in dioxygen-activation and hydrocarbon oxidation chemistry[46,51]. This copper dioxygen core (Cu_n-O_2) is structurally diverse depending upon the ligand coordination that subsequently shows the effect on the reactivity in the oxidation reactions.[52] A mononuclear copper(II) superoxide complexes supported by tridentate N3 and N2S (L^{N3} and L^{N2S}) as well as TMG_3tren ligand was studied as a model complexes of copper enzymes that have found to be similar in their structure and reactivity in the C-H activation reactions of monooxygenase enzymes like peptidylglycine α-hydroxylating monooxygenase (PHM) and dopamine β-monooxygenase (DβM).[53–56] A 1:1 copper-dioxygen adduct that is bound

in the end-on superoxo mode to the copper(II) complex has shown to undergoes oxygenation reactions with Phenols.[57] The copper(II)-alkyl peroxide bearing different geometry based on ligand coordination are reflected in their reactivity patterns towards the hydrogen abstraction from the substrate cyclohexadiene (CHD).[45,58] The first crystal structure of Cu(II)-alkylperoxo complex supported by hydrotris(pyrazolyl)-borate ligand have been reported by Kitajima.[59] Further, a number of alkyl peroxo have been synthesized and their reactivity has been investigated in different reactions exhibiting electrophilic reactivity in the oxidation reaction that proceeds by homolytic cleavage of Cu-O and O-O bond formation.[49,59–61] In one of the study it is reported that, Cu-alkyl peroxo exhibits nucleophilic reactivity at low temperature whereas electrophilic reactivity at high temperature.[62] The chemical structures of the non-heme ligand stabilizing different Cu-O_2 reactive intermediates are shown in **Scheme 5.2**

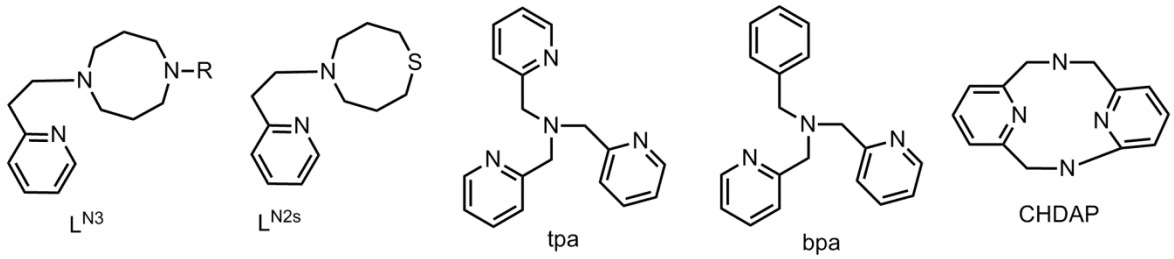

Scheme 5.2 *Ligand stabilizing the high valent Cu-O_2 reactive intermediate*

5.2 Experimental details

5.2.1 Synthesis of N3Py2 and compounds 10-15

The detail synthetic procedure that has been employed for the synthesis of the complexes of Co(II), Ni(II) and Cu(II) from the ligand N3Py2 have been described in this section. The **Scheme 5.3** depicts the structure of the ligand N3Py2 and the complexes **10-15** that have been synthesized, characterized utilized in the catalytic alkane hydroxylation reaction study.

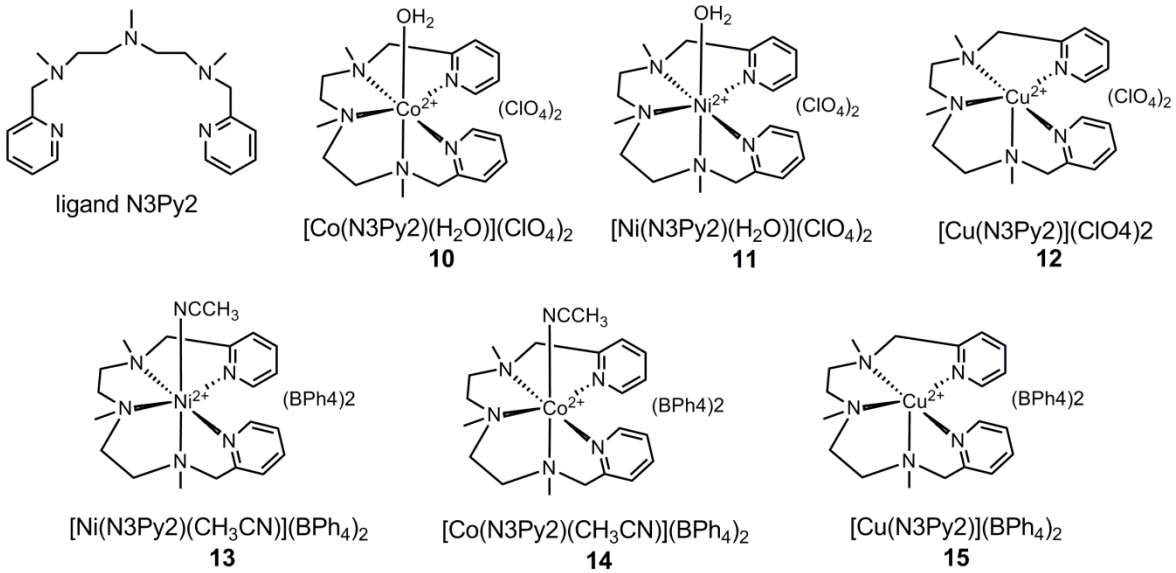

Scheme 5.3 *Chemical structures of the N3Py2 and the complexes synthesized in this study*

5.2.1a Synthesis of ligand N,N'-dimethyl-N-(2-(methyl(pyridin-2-ylmethyl)amino)ethyl)-N'-(pyridin-2-ylmethyl)ethane-1,2-diamine (N3Py2)

The synthesis of ligand N3Py2 is described in section 4.2.1 of Chapter IV

5.2.1b Synthesis of [Co(N3Py2)(H_2O)](ClO_4)$_2$ 10

N3Py2 (0.452 g, 1.37 mmol) was dissolved in CH_3CN (2 mL) and added to the stirring CH_3CN solution of $Co(ClO_4)_2.6H_2O$ (0.5 g, 1.37 mmol) under the N_2 atmosphere at room temperature. The mixture was stirred for ~12 h and filtered. To the resulting dark reddish-pink solution, diethyl ether (10 mL) was added and the mixture was kept undisturbed for

crystallization. The crystals formed after two days were isolated by filtration and dried in air. The yield of **10** (0.7 g, 80 %). *calc*., $C_{19}H_{31}N_5Cl_2O_9Co$: C, 37.82; H, 5.18; N, 11.61 %. *Found*, C, 37.78; H, 4.98; N, 11.62 %. *IR-data* (KBr, cm^{-1}): 3420 ν(OH); 3137-2752 ν(CH); 1090, 621 ν(ClO_4^{-1}). *UV-Vis data*, λ_{max}, CH_3CN / nm (ε/dm^3 $mol^{-1}cm^{-1}$): 262 (81642), 494 (42), 1028 (8). *ESI-MS*: *m/z* = 193.2 (*calc*. 193.2) for $[Co(N3Py2)]^{2+}$ and *m/z* = 485.9 (*calc*. 485.9) for $[Co(N3Py2)(ClO_4)]^+$.

5.3.1c Synthesis of [Ni(N3Py2)(H_2O)](ClO_4)$_2$ 11

Compound **11** was prepared in a similar way as **10** by reacting N3Py2 (0.452 g, 1.37 mmol) and $Ni(ClO_4)_2.6H_2O$ (0.5 g, 1.37 mmol) in CH_3CN. Yield of **11** (0.7 g, 84 %). *calc. for* $C_{19}H_{31}N_5Cl_2O_9Ni$:. C, 37.84; H, 5.18; N, 11.61 %. *Found*, C, 37.78; H, 5.26; N, 11.90 %. *IR-data* (KBr, cm^{-1}): 3420 ν(OH); 3137-2752 ν(CH); 1090, 621 ν(ClO_4^{-1}). *UV-Vis data*, λ_{max}, CH_3CN / nm (ε/dm^3 $mol^{-1}cm^{-1}$): 262(85439), 554(38), 920(27). *ESI-MS*: *m/z* = 193.1 (*calc*. 193.1) for $[Ni(N3Py2)]^{2+}$ and *m/z* = 485.5 (*calc*. 485.6) for $[Ni(N3Py2)(ClO_4)]^+$.

5.2.1d Synthesis of [Cu(N3Py2)](ClO_4)$_2$ 12

Compound **12** was prepared using similar methodology as in **10** and **11** wherein N3Py2 (0.452 g, 1.37 mmol) was reacted with $Cu(ClO_4)_2.6H_2O$ (0.5 g, 1.349 mmol) in CH_3CN. The dark blue crystalline powder of **12** was obtained with a yield (0.64 g, 78 %). *Calc. for* $C_{19}H_{29}N_5Cl_2O_8Cu$: C, 38.68; H, 4.96; N, 11.87 %. *Found*, C, 38.70; H, 5.06; N, 11.89%. *IR-data* (KBr, cm^{-1}): 3030-2825 ν(CH); 1093, 621 ν(ClO_4^{-1}). *UV-Vis data*, λ_{max}, CH_3CN / nm (ε/dm^3 $mol^{-1}cm^{-1}$): 256 (10804), 592 (216). *ESI-MS data*: m/z = 194.6 (*calc*. 194.6) for $[Cu(N3Py2)]^{2+}$ and *m/z* = 489.1 (*calc*. 489.1) for $[Cu(N3Py2)(ClO_4)]^+$.

5.2.1e Synthesis of compounds 13-15

Three other compounds, $[Co(N3Py2)(CH_3CN)](BPh_4)_2$ **13**, $[Ni(N3Py2)(CH_3CN)](BPh_4)_2$ **14** and $[Cu(N3Py2)](BPh_4)_2$ **15** were prepared by the reaction of **10**, **11** and **12** with two equivalents of $Na(BPh_4)$ (0.45 g, 1.3 mmol) in CH_3CN at room temperature. Analytical data for compounds **13**, **14** and **15** is as follows. Yield of **13** was 86 %. *calc. for* $C_{69}H_{72}N_6B_2Co$: C, 77.57; H, 6.81; N, 7.88 %. *Found*, C, 77.90; H, 6.72; N, 7.95 %. *IR-data* (KBr, cm^{-1}): 3137-2752 ν(CH); 2280 $\nu(NCCH_3)$; 734, 705 (BPh_4). Yield of **14** was 85 %. *calc. for* $C_{69}H_{72}N_6B_2Ni$: C, 77.77; H, 6.81; N, 7.89 %. *Found,* C, 77.60; H, 6.88; N, 7.61%. *IR-data* (KBr, cm^{-1}): 3137-2752 ν(CH); 2275 ν(NCCH3); 734, 705 (BPh_4). Yield of **15** was 83 %. *calc. for* $C_{67}H_{69}N_5B_2Cu$: calc., C, 78.17; H, 6.76; N, 6.80%. *Found*, C, 77.84; H, 6.90; N, 7.51%. *IR-data* (KBr, cm^{-1}): 3137-2752 ν(CH); 734, 705 (BPh_4).

5.2.2 Catalytic oxidations of cumene and adamantane

Compounds **10-15** were tested in the oxidation of alkyl hydrocarbons namely cumene and adamantane using *m*-CPBA as an oxidant in CH_2Cl_2:CH_3CN (3:1) mixture at room temperature under N_2 atmosphere. In a typical catalytic reaction, the complex dissolved in CH_3CN (80 μL, 2.5 mM) was added to the stirring solution of cumene (350 mM) or adamantane (250 mM) in 3:1 CH_2Cl_2-CH_3CN (4 mL) in the presence of *m*-CPBA (50 mM). At every fixed interval of time, a fraction of the reaction mixture was quenched using triphenylphosphine and eluted over a silica column using diethyl ether. The eluted sample was then directly infused into the GC column using *n*-decane internal standard.

5.3 Results and discussion

5.3.1 Synthesis and characterization of 10-12

The reaction of N3Py2 with metal salts, $Co(ClO_4)_2.6H_2O$ or $Ni(ClO_4)_2.6H_2O$ or $Cu(ClO_4)_2.6H_2O$ in CH_3CN in equal molar concentration afforded us three new compounds $[Co(N3Py2)(H_2O)](ClO_4)_2$ **10**, $[Ni(N3Py2)(H_2O)](ClO_4)_2$ **11,** $[Cu(N3Py2)](ClO_4)_2$ **12** respectively **(Scheme 5.4)**.

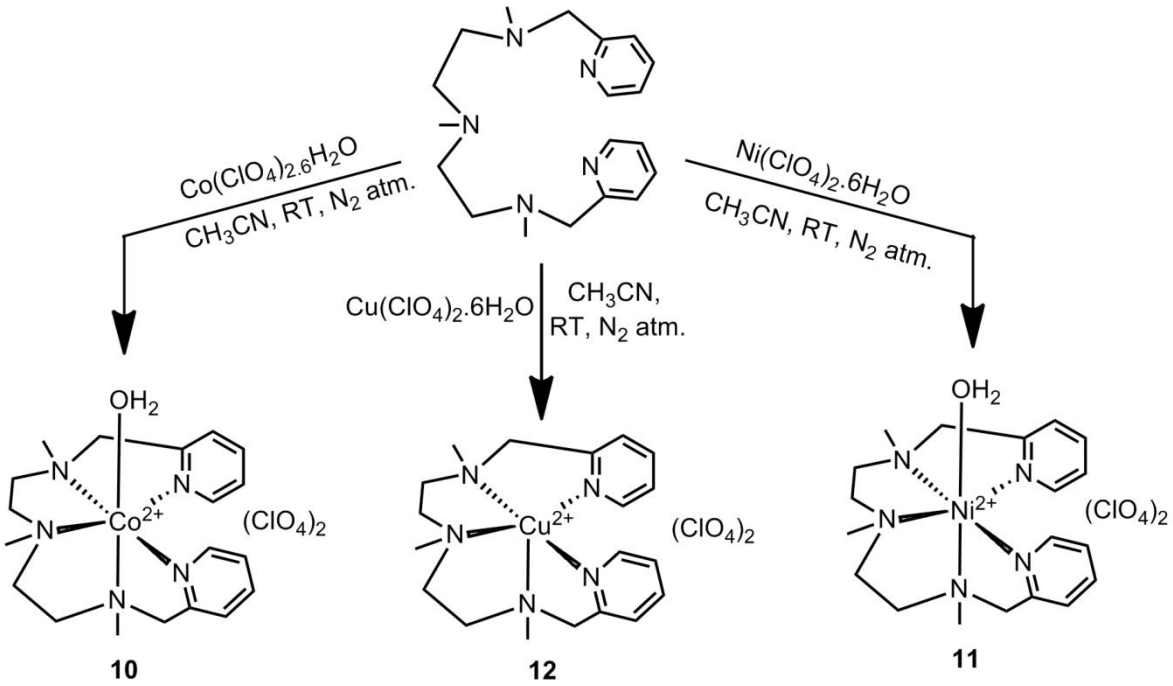

Scheme 5.4 *Synthetic method for the metal complexes of ligand N3Py2.*

The characteristic spectroscopic features of N3Py2 in all the compounds were traced from their IR and UV-Vis spectra. The cyclic and differential pulse voltammetric techniques (CV/DPV) were used to obtain redox potentials of **10**-**12**. Based on the IR and UV-Vis spectroscopy, C,H,N analysis, ESI-MS and CV/DPV data, the compounds **10**-**12** were unambiguously formulated as $[Co(N3Py2)(H_2O)](ClO_4)_2$, $[Ni(N3Py2)(H_2O)](ClO_4)_2$ and $[Cu(N3Py2)](ClO_4)_2$. Compounds **10** and **11** were then characterized by single-crystal X-ray structure analysis. Compounds **10**-**12** were tested as catalysts in the oxidation of two alkyl hydrocarbons, cumene and adamantane using *m*-CPBA as an oxidant. We also

investigated the counter anion effect on the product yields formed in the oxidation of cumene and adamantane. The perchlorates of **10-12** were replaced by tetraphenylborates in acetonitrile to afford us compounds $[Co(N3Py2)(CH_3CN)](BPh_4)_2$ **13**, $[Ni(N3Py2)(CH_3CN)](BPh_4)_2$ **14** and $[Cu(N3Py2)](BPh_4)_2$ **15**.

5.3.1a *Infrared spectroscopy*

The overlaid IR spectra of N3Py2 and compounds **10-12** are shown in **Figure 5.1**. The IR spectra of **10** and **11** show a broad band centred at ~3420 cm^{-1} which have been assigned to the O-H vibration of a water molecule. Interestingly, no O-H vibration was observed for compound **12** which suggests the absence of water molecule as observed in $[Cu(bpmen)(ClO_4)]^+$ (bpmen is tetradentate,N′-dimethyl-N,N′-bis(2-pyridylmethyl)ethane-1,2-diamine) possessing square pyramidal geometry.[63] The lack of water or solvent molecule in some nickel(II) and copper(II) complexes have been reported.[63,64] Further, the IR spectra of **10-12** shows strong absorption signals at ~1090 cm^{-1} and ~621 cm^{-1} due to uncoordinated perchlorates.[65] When we replaced two perchlorates by two tetraphenylborate anions in **10-12**, the IR spectra of the resulting compounds **13-15** showed the bands at ~734 cm^{-1} and ~705 cm^{-1} corresponding to tetraphenylborates[66] (**Figure 5.2**). In addition to tetraphenylborate bands, we also observed a new band at 2275 cm^{-1} for **13** and 2280 cm^{-1} for **14** due to the incorporation of CH_3CN molecule.[65,67] Thus, from IR spectra, we infer that H_2O and CH_3CN molecules are essential components to stabilize the structures of **10-11** and **13-14**. The IR spectrum of **15** showed no vibration attributed to CH_3CN indicating that complex **15** adopts same geometry as in **12**.[68,69]

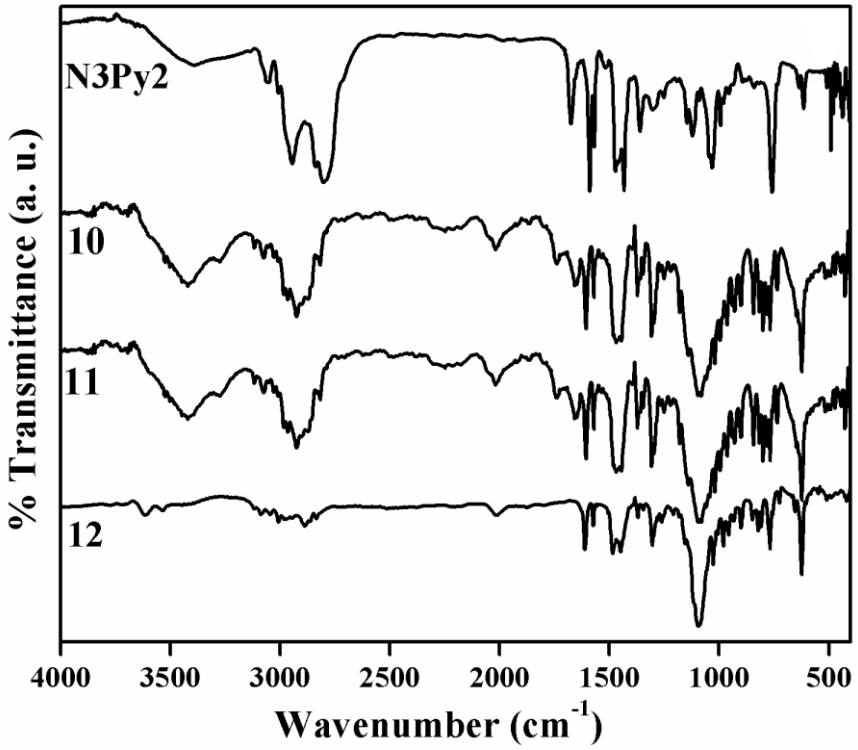

Figure 5.1. *The overlaid IR spectrum of ligand N3Py2 with* ***10-12*** *with perchlorate counters anion.*

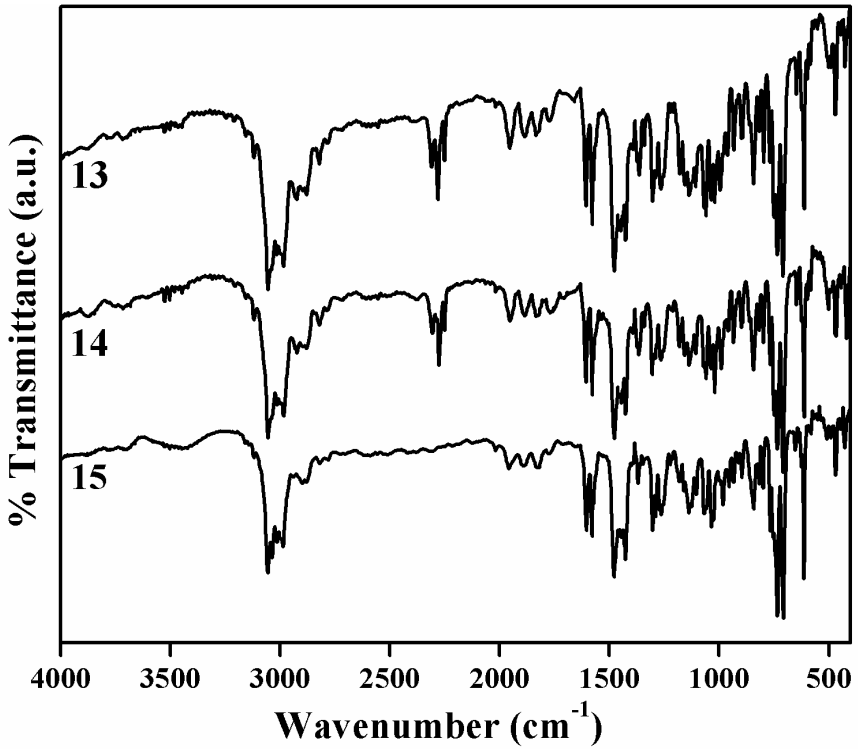

Figure 5.2 *The overlaid infrared spectra of compounds* ***13-15*** *with tetraphenylborate anions.*

5.3.1b UV-Vis spectra of 10-12

The UV-Vis spectra of **10-12** were recorded in CH_3CN showed an intense band at ~262 nm in all compounds and this band has been assigned to the intra-ligand charge transfer transition. The weak bands due to spin allowed *d-d* transitions were observed in the visible region (**Figure 5.3**). In the UV-Vis spectrum of **10**, the bands at ~494 and ~1028 nm were assigned to $^4T_{1g}(F)\rightarrow{}^4A_{2g}(F)$ and $^4T_{1g}(F)\rightarrow{}^4T_{2g}(F)$ transitions respectively.[70] For compound **11,** the bands at 554 and 920 nm were attributed to $^3A_{2g}(F)\rightarrow{}^3T_{1g}(F)$ and $^3A_{2g}(F)\rightarrow{}^3T_{2g}(F)$ transitions respectively.[71–73] The third band due to $^4T_{1g}(F) \rightarrow {}^4T_{1g}(P)$ in **10** and $^3A_{2g}(F)\rightarrow{}^3T_{1g}(P)$ in **11** were tailed in UV region due to overlapping with charge transfer band of N3Py2 and thus not observed in the spectra.[71,74] Unlike low-intensity bands in the UV-Vis spectra of **10** and **11**, the compound **12** exhibited a high-intensity band at ~592 nm. Such bands are often seen in the spectrum when a molecule is non-centrosymmetric[75]. The high absorbance band was also observed in the UV-Vis spectrum of a square pyramidal non-centrosymmetric $[Cu^{II}DIEN\text{-}pyr)]^{2+}$ complex.[68,69]

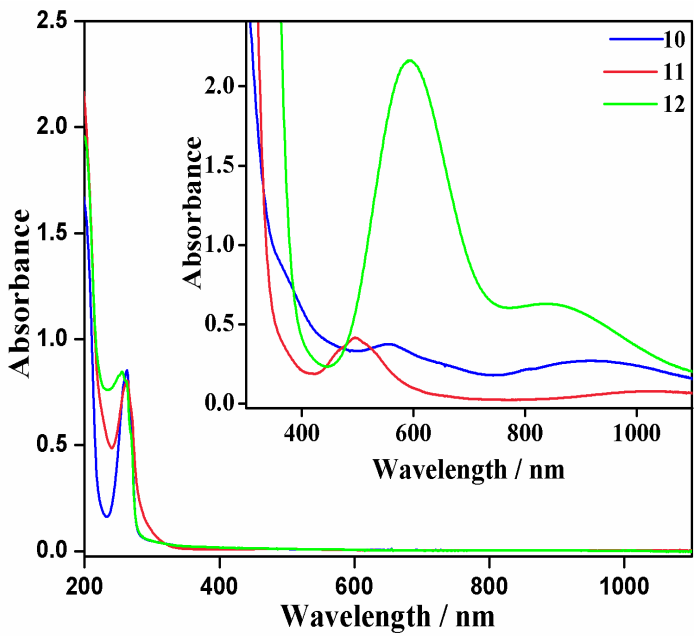

Figure 5.3 *Overlaid UV-Vis spectra of* ***10***, ***11*** and ***12*** *(10^{-2} mM) in CH_3CN. The inset shows an expanded view of the region 300 to 1100 nm for d-d bands of* ***10***, ***11*** *and* ***12*** *(10 mM).*

5.3.1c ESI-Mass spectrometry

The ESI-MS spectra of compounds **10** and **11** are shown in **Figure *5.3***. The ESI-MS spectrum of **10** in CH_3CN showed two prominent mass peaks at *m/z* = 193.2 and 485.9, which were assigned to $[Co(N3Py2)]^{2+}$ and $[Co(N3Py2)(ClO_4)]^{+}$ species respectively (**Figure 5.3a**). Compound **11** showed two peaks at *m/z* = 193.1and 485.5 corresponding to $[Ni(N3Py2)]^{2+}$ and $[Ni(N3Py2)(ClO_4)]^{+}$ species respectively (**Figure 5.3b**). On measuring the ESI-MS spectrum of **12**, two peaks at *m/z* = 194.6 and 489.1 corresponding to $[Cu(N3Py2)]^{2+}$ and $[Cu(N3Py2)(ClO_4)]^{+}$ ions respectively were observed.

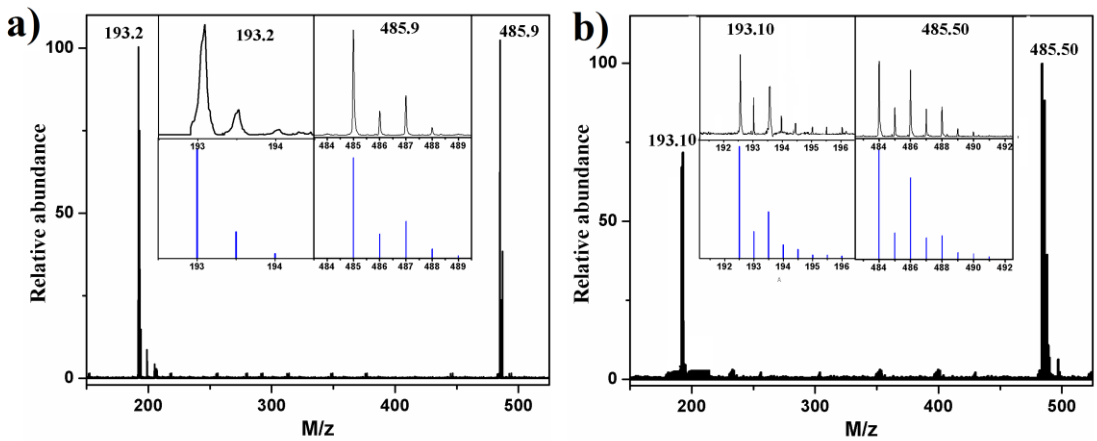

Figure 5.3 *ESI-MS spectra of 2 mM solution of (a)* ***10*** *(b)* ***11*** *recorded in CH_3CN. The inset shows the isotope distribution patterns for the prominent peaks in black with simulated pattern in blue colour.*

5.3.1d Description of crystal structures of 10 and 11

Single crystals of **10** and **11** suitable for X-ray crystallography were obtained by the slow diffusion of diethyl ether into their CH_3CN solutions. The technical details of data acquisition and selected refinement results for **10** and **11** are listed in **Table 5.1**. The selected bond lengths and bond angles for **10** and **11** are shown in **Table 5.2**. It has been reported that the metal complexes with the pentadentate N5 ligands can exist in four isomeric forms[76] as shown in **Scheme 4.7** in Chapter IV. Based on this report and our X-ray structural characterization, we propose the isomeric structure II for compounds **10** and

Table 5.1 *Technical details of data acquisition and selected refinement for* ***10*** *and* ***12****.*

	10	**11**
Empirical formula	$C_{19}H_{31}Cl_2N_5CoO_9$	$C_{19}H_{31}Cl_2N_5NiO_9$
Formula weight	603.32	603.08
Crystal description	Block	Block
Crystal colour	Brick red	Blue
Crystal system	Monoclinic	Monoclinic
Space group	$P2_1/c$(no. 14)	$P2_1/c$(no. 14)
Temperature (K)	100(2)	100(2)
Unit cell dimensions	a = 8.967 (3)Å	a = 9.027 (4)Å
	b = 32.954 (12)Å	b = 33.134 (15)Å
	c = 8.662 (3) Å	c = 8.668 (4) Å
	$\alpha = \gamma = 90$ °	$\alpha = \gamma = 90$ °
	β = 105.509 (8)°	β = 105.805 (6)°
volume (Å^3)	2466.4(16)	2494.6(19)
Z	4	4
Radiation type (Mo-Kα)/Å	0.71073	0.71073
Crystal size (mm)	0.18 x 0.13 x 0.07	0.40 x 0.30 x 0.10
Diffractometer	Bruker Smart APEX-II Duo	Bruker Smart APEX-II Duo
Absorption correction	Semi-empiricalfrom equivalents	Semi-empirical from equivalents
No. measured reflections	3363	6824
Calculated density (mg/m^3)	1.625	1.606
Absorption coefficient (mm^{-1})	0.972	1.051
F(000)	1252	1259
θ range for data collection	0.618 to 25.280	2.34 to 25.04
Limiting indices	$-10 \leq h \leq 8$	$-9 \leq h \leq 10$
	$-39 \leq k \leq 39$	$-37 \leq k \leq 39$
	$-10 \leq l \leq 10$	$-10 \leq l \leq 9$
Refinement method	Full-matrix least-squares on F^2	Full-matrix least-squares on F^2
Data / restraints / parameter	4455 / 23 / 352	4366 / 0 / 328
Final R Indices[I>2σ(I)]	R_1 = 0.0995, wR_2 = 0.2029	R_1 = 0.0572, wR_2 = 0.1100
R indices (all data)	R_1 = 0.1222, wR_2 = 0.2143	R_1 = 0.0718, wR_2 = 0.1160
Goodness of fit on F^2	1.211	1.072
Largest diff. peak and hole (eÅ^{-3})	1.531 and -1.797e.Å^{-3}	1.0110 and -0.8095 e.Å^{-3}
Reflections collected / unique	27156/ 4455 [R(int) = 0.1163]	14244 / 4366 [R(int) = 0.0444]

11 (**Figure 5.4** and **Figure 5.5**). Compounds **10** and **11** are isostructural and crystallize in a centrosymmetric space group $P2_1/c$. The crystal structures of both consist of a centrally located metal(II) ion (Co(II) in **10** and Ni(II) in **11**), a pentadentate N3Py2 and a H_2O molecule besides two crystallographically independent perchlorates (**Figure 5.4 and Figure 5.5**). The octahedral $[MN_5O]^{2+}$ unit (M = Co(II), Ni(II)) is slightly distorted due to the presence of two types of nitrogen-donor atoms (two of pyridyl part and three of tertiary amine backbone) and a water molecule. The octahedral distortion is clearly evident from the (N-Co-N and N-Ni-N) *cis* angles which range from 76.30(2)-108.71(3) Å in **10** and 76.92(14)-109.00(14) Å in **11** and similarly from the *trans* angles which range between 154.63(2)-173.45(2) Å in **10** and 160.04(15)-172.88(14) in **11** (**Table 5.2**). In both the structures, the pyridyl nitrogen atoms are disposed *syn* to one another and the triamine part occupies the facial positions of the octahedron. The similar dispositions of donor atoms were also observed in compounds with pyrrole based pentadentate ligands.[77] The examples of triamine nitrogens occupying meridional positions of the octahedron are also reported.[78] The perchlorates in **10** and **11** only behave as the counter anions for $[Co(N3Py2)]^{2+}$ and $[Ni(N3Py2)]^{2+}$ cations and do not participate in bonding with cobalt(II) or nickel(II) ions (**Figure 5.4** and **Figure 5.5**). However, the perchlorate anions play important role in building the extended network through its oxygen atoms (O12 and O14 in **10** and O6 and O8 in **11**) which are involved in weak hydrogen bonding with a water molecule (**Table 5.3**). The resulting three-dimensional metal-organic framework structures formed by Cl-O···H contacts, $[MN_5O]^{2+}$ motifs, and perchlorates anions are shown in **Figure 5.6** and **Figure 5.7**. The two O-Cl-O and two H-O-H linked through hydrogen bonds forms a twelve membered ring structure in **10** and 1**2** and these rings resemble like a chair form of cyclohexane when viewed along the '*ab'* plane (**Figure 5.7a**, **Figure 5.7a**). The hydrogen bond distances in **10** and **11** are quite shorter than the sum of their Van der Waals radii of

the atoms involved in hydrogen bonding. The hydrogen bond distances range from 2.02 (4) to 1.988 (7) Å in **10** and from 2.037 (21) to 2.070 (21) Å in **11** (**Table 5.3**). Hydrogen bond distances in **10** are relatively shorter than in **11** with an average difference of 0.0495 Å. It is evident from the structural data that the hydrogen bonding basically originates due to the presence of a water molecule and perchlorate ions in **10** and **11**. In spite of using acetonitrile as the solvent, the incorporation of water in the crystal structure of **10** and **11** could be justified based on the use of metal perchlorate hexahydrates in the synthesis. In other related nickel(II) compounds, the incorporation of water molecule was also observed although the reactions were carried out in methanol.[6,66,79] When the perchlorates ions were replaced by tetraphenylborate in acetonitrile, the new compounds **13** and **14** indeed showed the presence of acetonitrile. Our attempts to grow single crystals of $[Cu(N3Py2)](ClO_4)_2$ **12** were not fruitful and hence the compound **12** along with **10** and **11** were also characterized by powder X-ray diffraction (PXRD) technique.

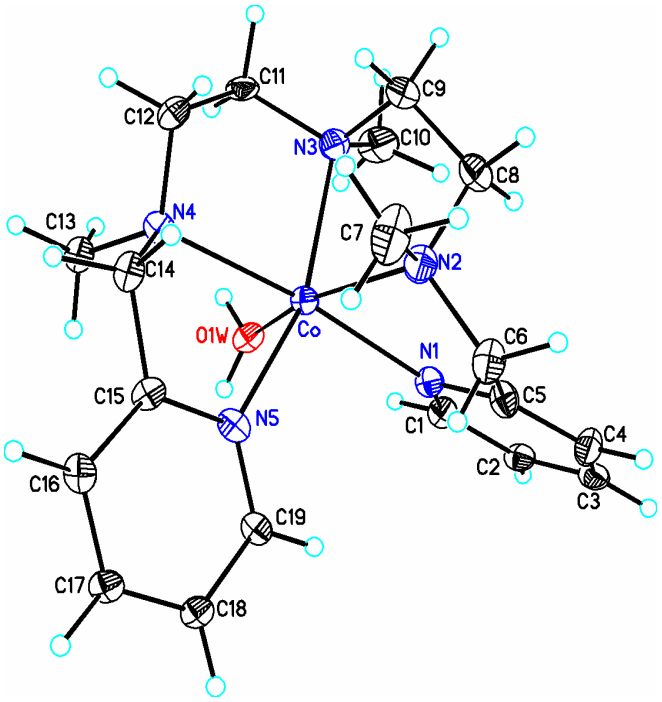

Figure 5.4 *Crystal structure of* $[Co(N3Py2)(H_2O)](ClO_4)_2$ *showing atom-labelling scheme. Displacement ellipsoids are drawn at 50% probability except for H atoms which are shown as circles of arbitrary radius. The perchlorate anions are not shown for clarity.*

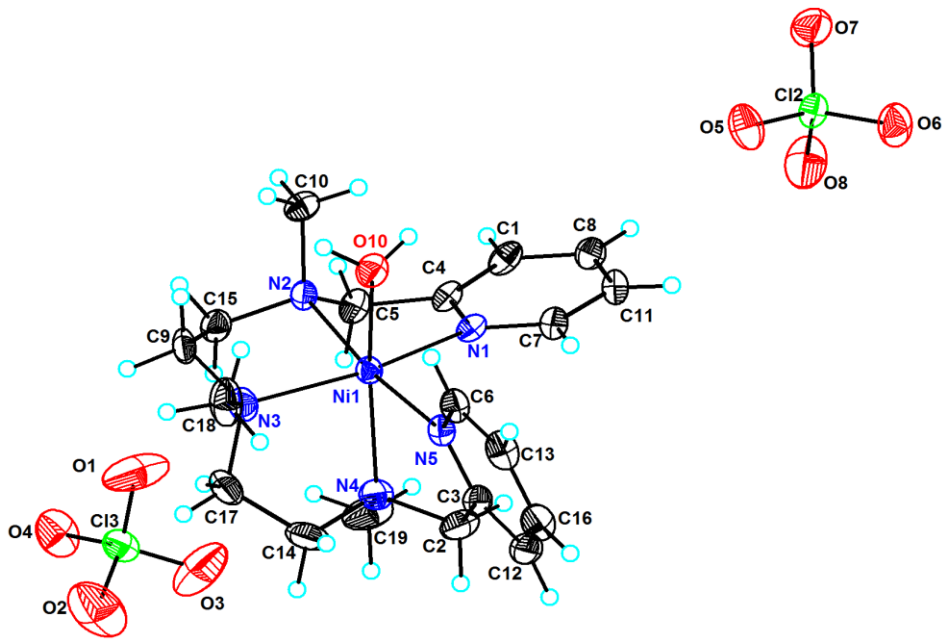

Figure 5.5. *Crystal structure of [Ni(N3Py2)(H_2O)](ClO_4)$_2$ showing atom-labelling scheme. Displacement ellipsoids are drawn at 50% probability except for H atoms, which are shown as circles of arbitrary radius.*

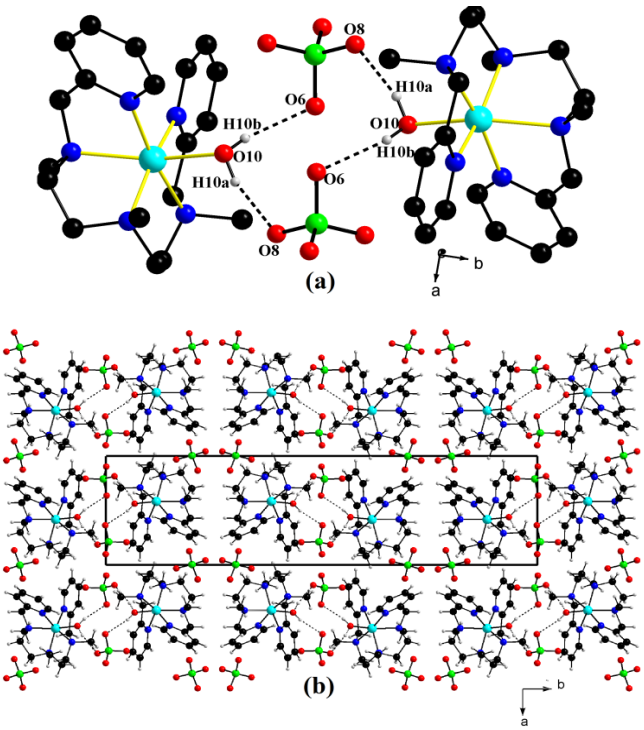

Figure 5.6. *(a) The cyclic structure formed due to hydrogen bonding interactions in **2** with atom labelling scheme of atoms involved in hydrogen bonding. Hydrogen atoms attached to carbon are omitted for clarity (b) Enlarged view of a three-dimensional network in **2** showing the symmetric organisation of [Ni(N3Py2)(H_2O)]$^{2+}$ cations and perchlorate anions in the crystallographic ab plane.*

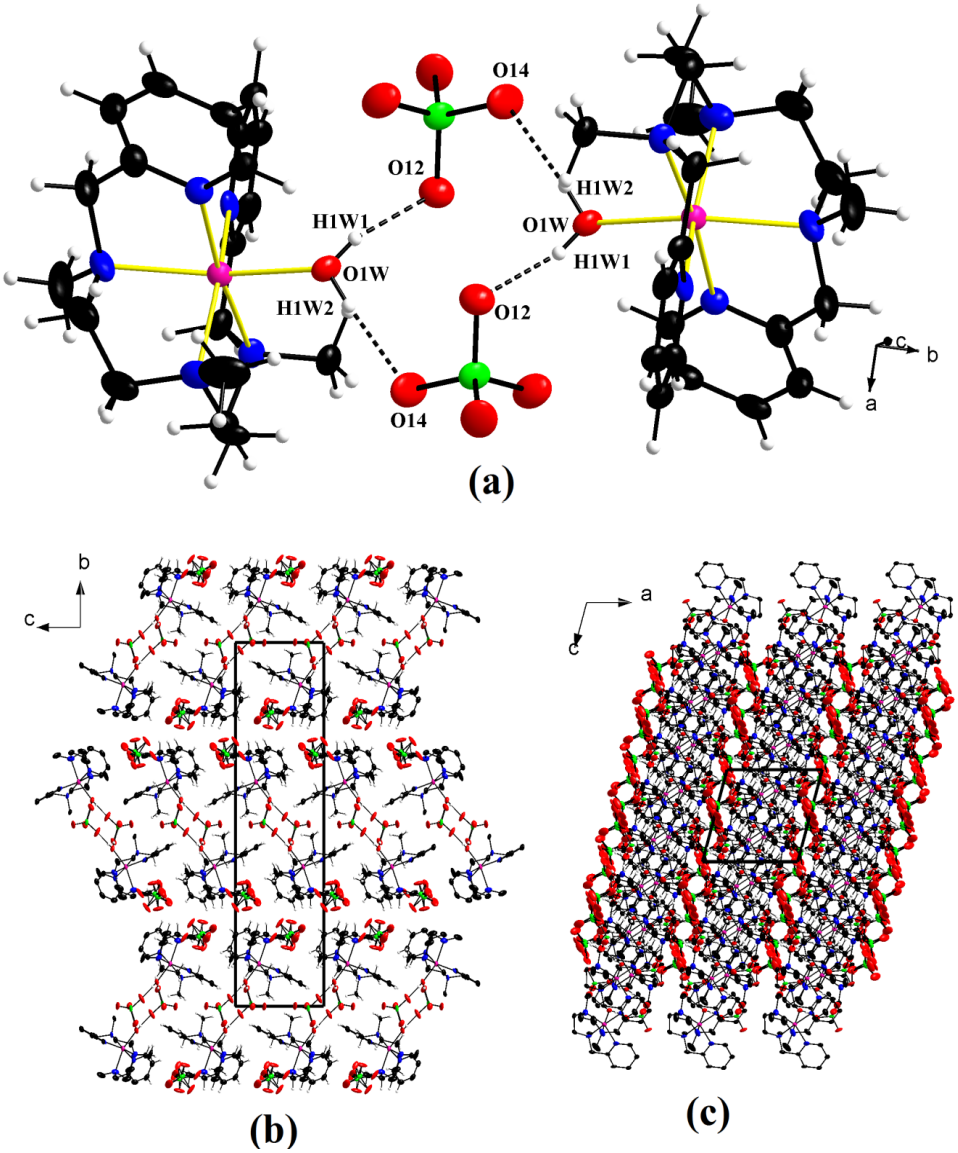

Figure 5.7 *(a) Hydrogen bonding interactions in* ***12*** *with atom labelling scheme of atoms involved in hydrogen bonding. The enlarged view of a network of hydrogen bonding in* ***12*** *showing the symmetric organisation of* $[Co(N3Py2)(H_2O)]^{2+}$ *cations and perchlorate anions in the crystallographic (b) ab plane and (c) ac plane.*

The PXRD patterns of **10** and **11** were identical and support the notion that they have same space groups as obtained from single crystal X-ray structure analysis (**Figure 5.8, Figure A4** and **A5** in appendix). On the contrary, the PXRD pattern of **12** was quite different and did not match with the powder patterns of **10** and **11** (**Figure 5.8**). The single crystal X-ray data and PXRD patterns thus confirm that compounds **10** and **11** are isostructural while **12** crystallizes in a different space group.

Table 5.2 *– Selected bond lengths (Å) and bond angles (°) for* ***10*** *and* ***11****.*

(10)			
Bond lengths (Å)			
Co-N1	2.140(7)	Co-N4	2.219(7)
Co-N2	2.239(7)	Co-N5	2.149(6)
Co-N3	2.153(7)	Co-O1	2.132(6)
Bond angles (°)			
O1-Co-N1	85.93(2)	N5-Co-N4	77.49(1)
O1-Co-N5	98.06(1)	N3-Co-N4	80.76(1)
N1-Co-N5	98.30(1)	O1-Co-N2	160.31(2)
O1-Co-N3	94.71(2)	N1-Co-N2	76.30(2)
N1-Co-N3	104.41(2)	N5-Co-N2	92.90(2)
N5-Co-N3	154.63(2)	N3-Co-N2	81.80(2)
O1-Co-N4	89.68(1)	N4-Co-N2	108.71(3)
N1-Co-N4	173.45(2)		
(11)			
Bond lengths (Å)			
Ni1-N1	2.103(8)	Ni1-N4	2.201(4)
Ni1-N5	2.120(5)	Ni1-N8	2.238(1)
Ni1-N2	2.166(5)	Ni1-O10	2.134(3)
Bond angles (°)			
N1-Ni1-O10	94.29(12)	N4-Ni1-N5	76.92(14)
N5-Ni1-O10	84.79(13)	N4-Ni1-N2	109.00(14)
N5-Ni1-N1	96.96(13)	N3-Ni1-O10	94.05(14)
N2-Ni1-O10	89.74(12)	N3-Ni1-N1	160.04(15)
N2-Ni1-N1	78.87(13)	N3-Ni1-N5	101.83(15)
N2-Ni1-N5	172.88(14)	N3-Ni1-N2	83.07(14)
N4-Ni1-O10	160.53(13)	N3-Ni1-N4	83.35(15)
N4-Ni1-N1	94.50(14)		

Note: The values in the parentheses indicate estimated standard deviations.

Table 5.3 *Hydrogen bonding parameters (Å, °) for* ***10*** *and* ***11****.*

D-H····A	D-H/Å	H····A/Å	D····A/Å	D-H····A/°
Compound **10**				
O1w-H1W1····O12[c]	0.81(2)	2.02(4)	2.810(9)	162.00(9)
O1W-H1W2····O14	0.815(3)	1.988(7)	2.801(9)	174.50(4)
Compound **11**				
O10-H10b····O6[a]	0.847(19)	2.070(21)	2.840(5)	150.85(164)
O10-H10a····O8[b]	0.849(14)	2.037(21)	2.838(9)	156.99(157)

[a] 1-x, 1-y, 1-z [b]2-x, -y, 2-z, z [c] -1+x, y,

Note: The values in parentheses indicate estimated standard deviations.

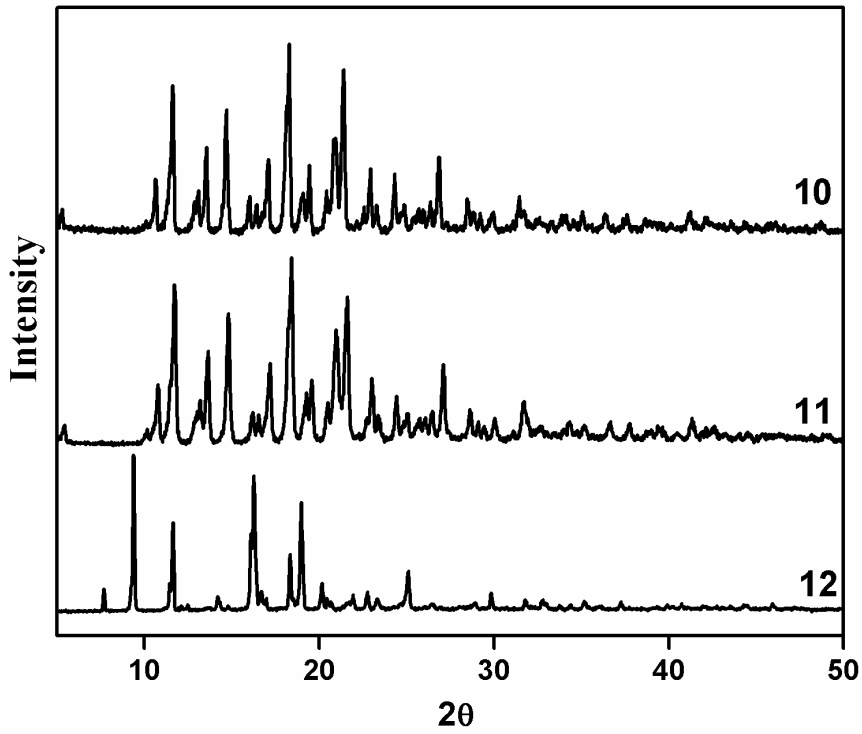

Figure 5.8 *Comparative PXRD patterns of [Co(N3Py2)(H$_2$O)](ClO$_4$)$_2$* ***10*** *[Ni(N3Py2)(H$_2$O)](ClO$_4$)$_2$* ***11*** *and [Cu(N3Py2)](ClO$_4$)$_2$* ***12****.*

5.3.1e Electrochemical properties of 10-12

Cyclic voltammetry (CV) and differential pulse voltammetry (DPV) techniques were applied to understand the redox behaviour of compounds **10**-**12**. CV of compound **10** in CH_3CN showed the anodic and cathodic waves corresponding to the Co(II)/Co(III) couple with a $E_{½}$ = 0.56 V v/s Ag/$AgNO_3$ (0.86 V v/s SCE) (**Figure 5.9**). The $E_{½}$ value was further confirmed from the DPV technique and was in good agreement with those of known cobalt(II) complexes with multidentate nitrogen donor ligands.[83–85] When we measured CV of **11** under identical conditions, we observed the peak attributed to Ni(II)/Ni(III) redox couple centred at quite higher potential of 1.39 V v/s Ag/$AgNO_3$ (1.68 V v/s SCE) (**figure 5.10**).[71,83,84] On the contrary to the positive $E_{½}$ values of **10** and **11**, the complex **12** exhibited a reversible peak at $E_{½}$ = -0.52 V v/s Ag/$AgNO_3$ (-0.22 V v/s SCE) due to

Cu(II)/Cu(I) redox couple (**Figure 5.11**).[45,85,86] This large deviation of $E_{½}$ value for **12** compared to those of **10** and **11** suggests that compound **12** has different structural properties. N3Py2 showed no peaks under the identical conditions indicating the redox peaks in the CV of **10-12** are solely due to the metal ions. The CV plots of **10** as well as **11** and **12** recorded at different scan rates were identical and showed a proportional increase in the peak currents (**Figure 5.12 -5.14**). Δ*Ep* values at scan rates suggest the quasi-reversible redox phenomenon in **10** and **11** while the reversible couple in **12** (**Table 3.4**).

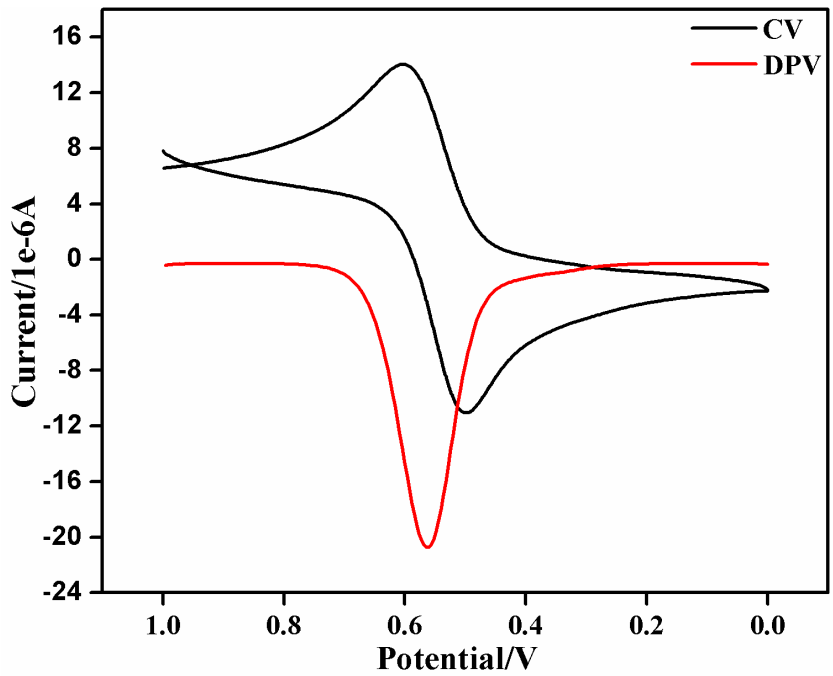

Figure 5.9 *CV and DPV of* ***10*** *recorded at a scan rate of 100 mVs^{-1} in CH_3CN containing 0.1 M of $TBAPF_6$ as supporting electrolyte against $Ag/AgNO_3$ (0.01 M) reference electrode.*

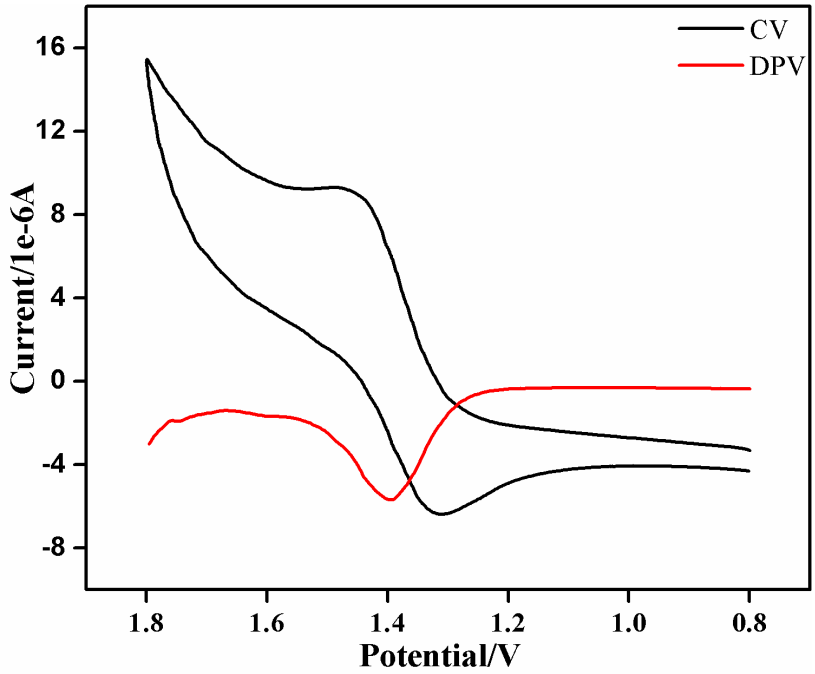

Figure 5.10 *CV and DPV of* ***11*** *recorded at a scan rate of 100 mVs^{-1} in CH_3CN containing 0.1 M of $TBAPF_6$ as supporting electrolyte against $Ag/AgNO_3$ (0.01 M) reference electrode.*

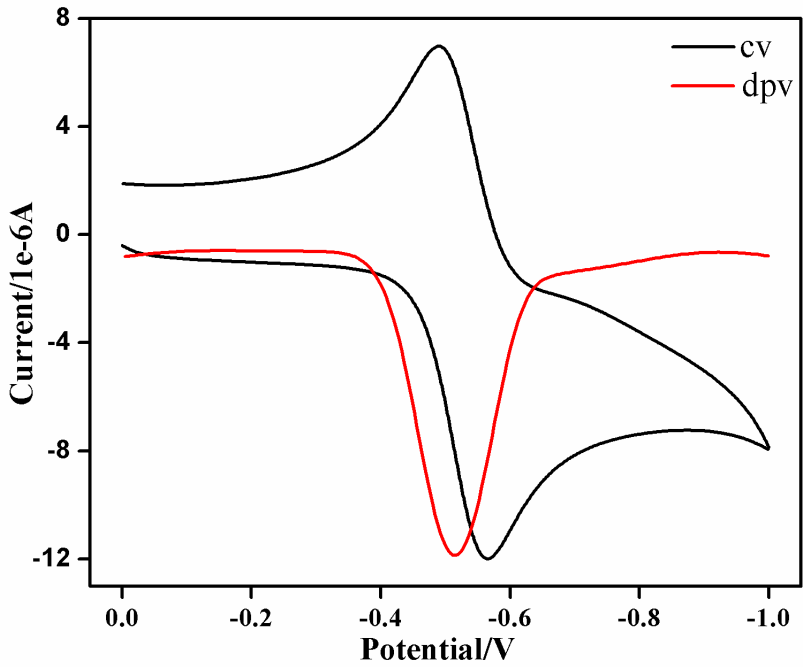

Figure 5.11 *CV and DPV of* ***12*** *recorded at a scan rate of 100 mVs^{-1} in CH_3CN containing 0.1 M of $TBAPF_6$ as supporting electrolyte against $Ag/AgNO_3$ (0.01 M) reference electrode.*

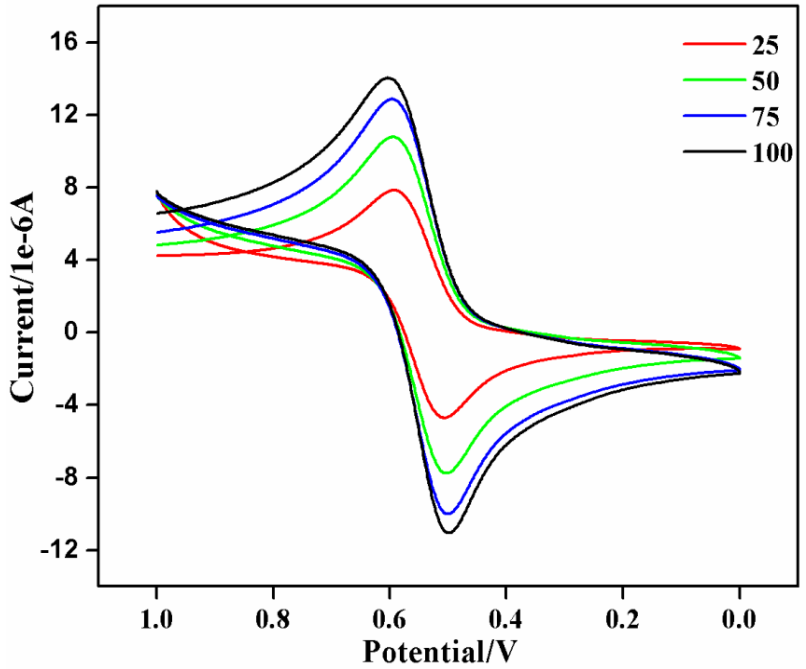

Figure 5.12 *CV and DPV of* ***10*** *recorded at different scan rates in CH_3CN containing 0.1 M of $TBAPF_6$ as supporting electrolyte against $Ag/AgNO_3$ (0.01 M) reference electrode.*

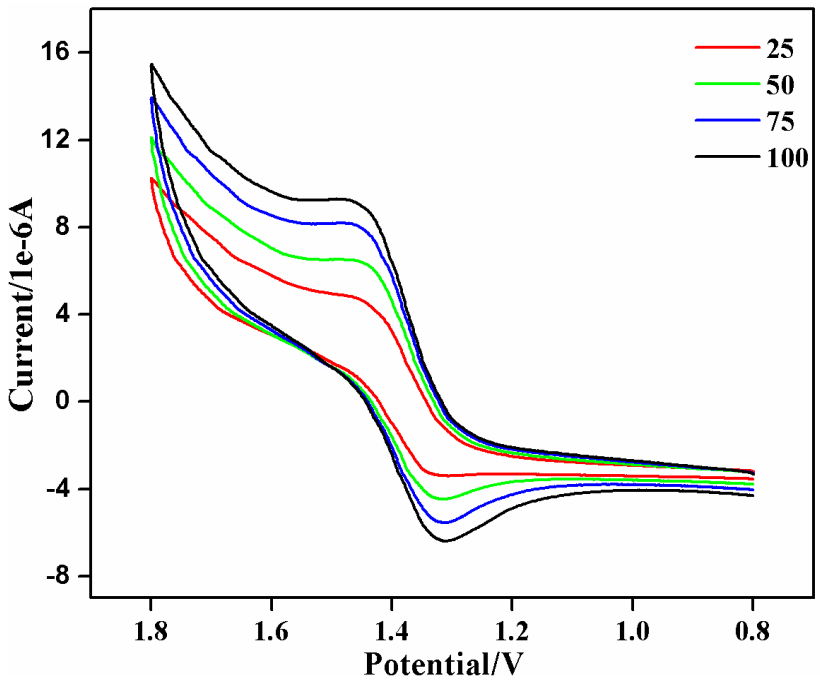

Figure 5.13 *CV and DPV of* ***11*** *recorded at different scan rates in CH_3CN containing 0.1 M of $TBAPF_6$ as supporting electrolyte against $Ag/AgNO_3$ (0.01 M) reference electrode.*

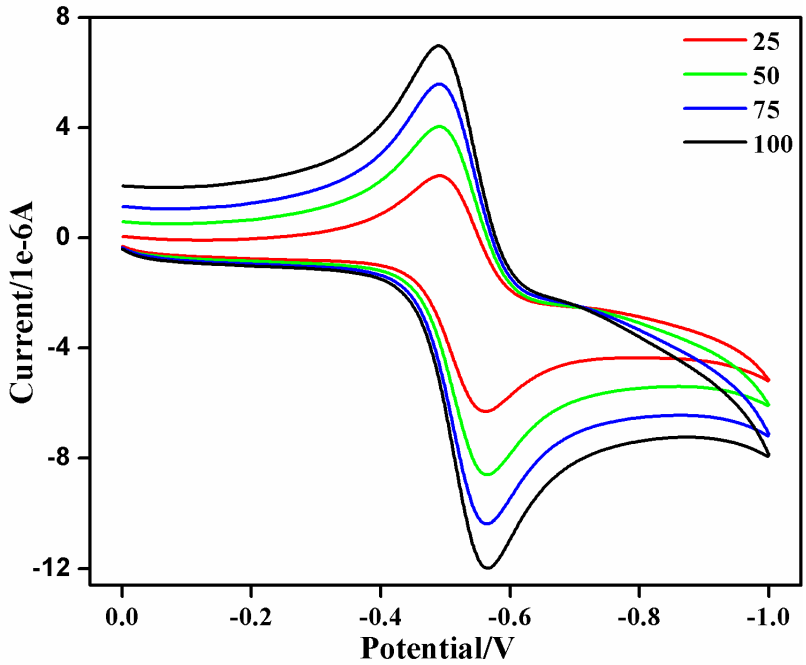

Figure 5.14 *CV and DPV of* ***12*** *recorded at different scan rate in CH_3CN containing 0.1 M of $TBAPF_6$ as supporting electrolyte against $Ag/AgNO_3$ (0.01 M) reference electrode.*

Table 5.4- *Electrochemical data for complex*

Scan rate (mVs^{-1})	E_{pa} (V)	E_{pc} (V)	ΔE_p (V)	$E_{½}$ (V)
		10		
100	0.602	0.498	0.104	0.550
75	0.596	0.502	0.094	0.549
50	0.593	0.504	0.089	0.549
25	0.591	0.508	0.083	0.550
		11		
100	1.477	1.313	0.164	1.395
75	1.469	1.318	0.151	1.394
50	1.460	1.320	0.14	1.390
25	1.458	1.328	0.13	1.393
		13		
100	-0.492	-0.564	0.072	-0.528
75	-0.491	-0.563	0.072	-0.527
50	-0.491	-0.563	0.072	-0.527
25	-0.491	-0.562	0.071	-0.527

5.3.2. Catalytic oxidations of cumene and adamantane by 10-15

Since compounds **10-12** were stabilized by a non-heme ligand N3Py2 and differ from each other in terms of structural and electronic properties, we then decided to test their utility in the catalytic hydroxylation of alkyl hydrocarbons (cumene and adamantane) using *m*-CPBA as an oxidant. The catalytic oxidation of cumene by **10-12** gave 2-phenyl-2-propanol as the major product along with acetophenone (**Table 5.5, Scheme 5.5**). The oxidation of alkanes catalyzed by nickel(II) complexes in the presence of *m*-CPBA with different counter anions such as acetate and nitrate have been previously reported[68]. It was observed that the yields of organic products were highly influenced by the type of counter anions present in the nickel(II) complexes. On similar lines, we investigated the catalytic reactions of three compounds **13-15** which were prepared by a simple metathesis reaction of **10-12** with two equivalents of sodium tetraphenylborate. Interestingly, the TONs of 2-phenyl-2-propanol and acetophenone increased considerably when compounds **13-15** were used as catalysts instead of **10-12** (**Table 5.6**). This observation suggests that the product yields could be fine-tuned using different counter anions keeping the metal ions and N3Py2 unchanged. We also studied the time-dependent oxidation of cumene in the presence of catalysts **10-13** and **11-14**. The yield of 2-phenyl-2-propanol increased with time and the yields were higher for compound **10** than those for **11** (**Figure 5.15 and 5.16**). On reacting adamantane (250 mM) with **10-12** and **13-15** (5×10^{-5} M) in the presence of *m*-CPBA (50 mM), we obtained 1-adamantanol in high yields and 2-admantanol with 2-adamantanone as the minor products (**Table 5.6, Scheme 5.5**). The selectivity of catalysts **10-12** and **13-15** in hydroxylation of cumene and adamantane followed Co > Ni > Cu order and our results were comparable with the reported cases[87]. When the reactions were carried out only in presence of *m*-CPBA and substrates or in the presence of **10-12** or **13-15** and

substrates, no organic products were detected.[88] When H_2O_2 and *t*-BuOOH were used as oxidants instead of *m*-CPBA, only trace amounts of alcohol products were formed.[79,84]

Table 5.5 *Products formed in the reaction of cumene and catalysts* ***10-12*** *and* ***13-15*** *the in presence of m-CPBA*[a].

catalyst	cumene oxidation[a]			
	2-Phenyl-2-propanol (TON)	acetophenone (TON)	Total TON[c]	A/K[d]
10	150	105	255	1.4
13	293	210	503	1.4
11	142	101	243	1.4
14	223	144	367	1.5
12	107	85	192	1.3
15	152	108	260	1.4

[a] Yield based on the oxidant. [b]Reaction conditions: catalyst (0.05 mmol dm^{-3}), cumene (350 mmol dm^{-3}), *m*-CPBA (50 mmol dm^{-3}) in CH_2Cl_2/CH_3CN solvent mixture (3:1 v/v, 4 mL); reaction time 12 h. [c]Total TON = mmol of product/ no. of mmol of catalyst, [d]A/K = TON of 2-Phenyl-2-propanol / TON of acetophenone,

Table 5.6 *Products formed in the reaction of adamantane and catalysts* ***1-3*** *and* ***1a-3a*** *in the presence of m-CPBA*[a].

catalyst	adamantane oxidation[b]				
	1-adamantanol (TON)	2-adamantanol (TON)	2-adamantanone (TON)	total TON[c]	A/K[d]
10	132	30	22	184	2.5
13	281	67	44	392	2.5
11	123	27	20	162	2.6
14	241	59	42	342	2.3
12	100	24	18	142	2.4
15	143	35	22	200	2.5

[a]Yield based on the oxidant.
[b]Reaction condition: catalyst (0.05 mmol dm^{-3}), adamantane (250 mmol dm^{-3}), *m*-CPBA (50 mmol dm^{-3}) in CH_2Cl_2/CH_3CN solvent mixture (3:1 v/v, 4 mL); reaction time = 12 h, [c]Total TON = mmol of product/ no. of mmol of catalyst, [d]A/K = TON of 1-adamantanol/ TON of 2-adamantanol + TON of 2-adamantanone.

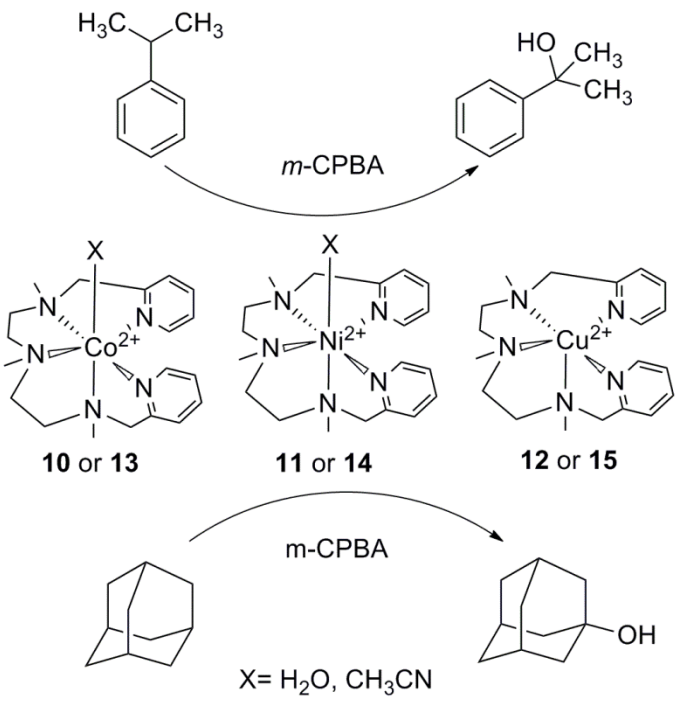

Scheme 5.5: *Oxidized products of 1) cumene 2) adamantane by* ***10-15***

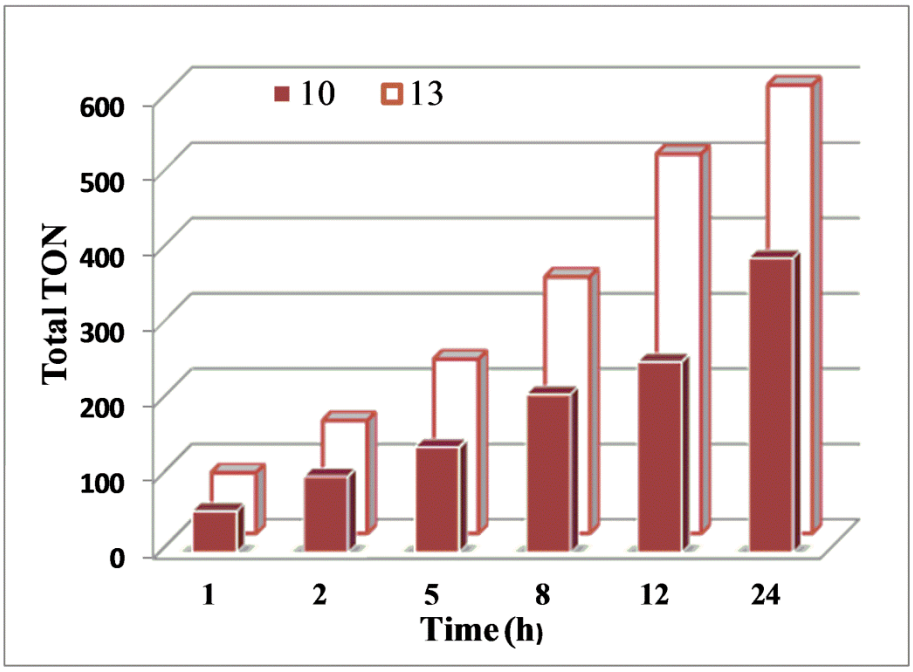

Figure 5.15 *Bar graph representation showing the counter anion effect on the time-dependent oxidation to corresponding oxidized products by [Co(N3Py2)(H_2O)](ClO_4)$_2$* ***10*** *and [Co(N3Py2)(CH_3CN)](BPh_4)$_2$* ***13*** *in CH_2Cl_2/CH_3CN (3:1 v/v) solvent mixture at room temperature.*

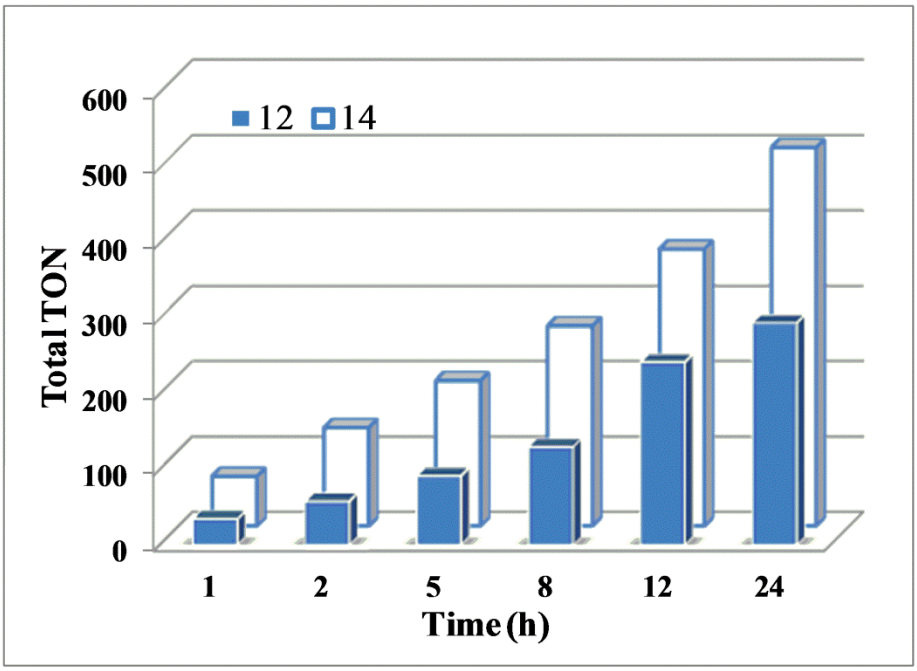

Figure 5.16 *Bar graph representation showing the counter anion effect on the time-dependent oxidation to corresponding oxidized products by [Ni(N3Py2)(H_2O)](ClO_4)$_2$* ***11*** *and [Ni(N3Py2)(CH_3CN)](BPh_4)$_2$* ***14*** *CH_2Cl_2/CH_3CN (3:1 v/v) solvent mixture at room temperature.*

5.4 Summary and conclusion

In this Chapter we have reported the synthesis and characterization of three new complexes, $[Co(N3Py2)(H_2O)](ClO_4)_2$ **10**, $[Ni(N3Py2)(H_2O)](ClO_4)_2$ **11** and $[Cu(N3Py2)](ClO_4)_2$ **12** obtained from non-heme N3Py2 ligand. The compounds **10** and **11** were structurally characterized by single crystal X-ray diffractometry. Both are isostructural and crystallize in centrosymmetric space group $P2_1/c$. The structures of **10** and **11** shows, cobalt(II) and nickel(II) ions coordinating to N3Py2 and H_2O molecule forming a slightly distorted octahedral geometry. The PXRD patterns of **10** and **11** are similar and distinctly different from **12** suggesting that the compound **12** has a different structure. Based on the spectroscopic and elemental analysis, the square pyramidal geometry has been proposed for **12**. The catalytic activity of **10-12** was studied in the C-H activation of cumene and adamantane in the presence the of *m*-CPBA. The cumene gave 2-phenyl-2-propanol as the sole product while adamantane afforded 1-adamantanol as the major product. The counter anion effect on product yields by replacing perchlorates of **10-12** with tetraphenylborates to obtain **13-15** was also investigated.

References

(1) Ray, K.; Heims, F.; Pfaff, F. F. *Eur. J. Inorg. Chem.* **2013**, 3784–3807.

(2) Nam, W.; Kim, I.; Kim, Y.; Kim, C. *Chem. Commun.* **2001**, 1262–1263.

(3) Fukuzumi, S.; Mandal, S.; Mase, K.; Ohkubo, K.; Park, H.; Benet-Buchholz, J.; Nam, W.; Llobet, A. *J. Am. Chem. Soc.* **2012**, *134*, 9906–9909.

(4) Nguyen, A. I.; Hadt, R. G.; Solomon, E. I.; Tilley, T. D. *Chem. Sci.* **2014**, 2874–2878.

(5) Pfaff, F. F.; Heims, F.; Kundu, S.; Mebs, S.; Ray, K. *Chem. Commun.* **2012**, *48*, 3730–3732.

(6) Nagataki, T.; Tachi, Y.; Itoh, S. *Chem. Commun.* **2006**, 4016–4018.

(7) Schröder, D.; Holthausen, M. C.; Schwarz, H. *J. Phys. Chem. B* **2004**, *108*, 14407–14416.

(8) Truhlar, D. G. *J. Comput. Chem.* **2009**, *28*, 73–86.

(9) Pierpont, A. W.; Cundari, T. R. *Inorg. Chem.* **2010**, *49*, 2038–2046.

(10) Smith T. D., P. J. R. *Coord. Chem. Rev.* **1981**, *39*, 295–383.

(11) Hikichi, S.; Akita, M.; Moro-oka, Y. *Organomet. Chem.* **2000**, *198*, 61–87.

(12) Busch, D. H.; Alcock, N. W. *Chem. Rev.* **1994**, *94*, 585–623.

(13) Cynthia L. Bailey, R. L. D. *Coord. Chem. Rev.* **1987**, *79*, 321–332.

(14) Zombeck, A.; Drago, R. S.; Corden, B. B.; Gaul, J. H. *J. Am. Chem. Soc.* **1981**, *103*, 7580–7585.

(15) Hamilton, D. E.; Drago, R. S.; Zombeck, A. *J. Am. Chem. Soc.* **1987**, *109*, 374–379.

(16) Busch, D. H.; Jackson, P. J.; Kojima, M.; Chmielewski, P.; Matsumoto, N.; Stevens, J. C.; Wu, W.; Nosco, D.; Herron, N.; Ye, N.; et al. *Inorg. Chem.* **1994**, *33*, 910–923.

(17) Schaefer, W. P.; Huie, B. T.; Kurilla, M. G.; Ealick, S. E. *Inorg. Chem.* **1980**, *19*, 340–344.

(18) Chavez, F. A.; Mascharak, P. K. *Acc. Chem. Res.* **2000**, *33*, 539–545.

(19) Gleiter, R.; Werthemann, D.; Behringer, H. *J. Am. Chem. Soc.* **1972**, *94*, 653–655.

(20) Egan, J. W.; Haggerty, B. S.; Rheingold, A. L.; Sendlinger, S. C.; Theopold, K. H. *J. Am. Chem. Soc.* **1990**, *112*, 2445–2446.

(21) Rahman, A. F. M. M.; Jackson, W. G.; Willis, A. C. *Inorg. Chem.* **2004**, *43*, 7558–7560.

(22) Cho, J.; Sarangi, R.; Kang, H. Y.; Lee, J. Y.; Kubo, M.; Ogura, T.; Solomon, E. I.; Nam, W. *J. Am. Chem. Soc.* **2010**, *132*, 16977–16986.

(23) Jo, Y.; Annaraj, J.; Seo, M. S.; Lee, Y.; Kim, S. Y.; Cho, J.; Nam, W. *J. Inorg. Biochem.* **2008**, *102*, 2155–2159.

(24) Zhang, Q.; Bell-taylor, A.; Bronston, F. M.; Gorden, J. D.; Goldsmith, C. R. *Inorg. Chem.* **2017**, *56*, 773–782.

(25) Shin, B.; Sutherlin, K. D.; Ohta, T.; Ogura, T.; Solomon, E. I.; Cho, J. *Inorg. Chem.* **2016**, *55*, 12391–12399.

(26) Bayston, J. H.; Winfield, M. E. *J. Catal.* **1964**, *3*, 123–128.

(27) Wang, W. D.; Bakac, A.; Espenson, J. H. *Inorg. Chem.* **1995**, *34*, 4049–4056.

(28) Guzei, I. A.; Bakac, A. *Inorg. Chem.* **2001**, *40*, 2390–2393.

(29) Kim, D.; Cho, J.; Lee, Y. M.; Sarangi, R.; Nam, W. *Chem. - A Eur. J.* **2013**, *19*, 14112–14118.

(30) Reinaud, O. M.; Theopold, K. H. *J. Am. Chem. Soc.* **1994**, *116*, 6979–6980.

(31) Schlangen, M.; Schwarz, H. *Chem. Commun.* **2010**, *46*, 1878–1880.

(32) Jackson, P.; Attalla, M. I. *Rapid Commun. Mass Spectrom.* **2010**, *24*, 1142–1146.

(33) Pfaff, F. F.; Kundu, S.; Risch, M.; Pandian, S.; Heims, F.; Pryjomska-Ray, I.; Haack, P.; Metzinger, R.; Bill, E.; Dau, H.; et al. *Angew. Chemie - Int. Ed.* **2011**, *50*, 1711–1715.

(34) Hong, S.; Pfaff, F. F.; Kwon, E.; Wang, Y.; Seo, M. S.; Bill, E.; Ray, K.; Nam, W. *Angew. Chemie - Int. Ed.* **2014**, *53*, 10403–10407.

(35) Lacy, D. C.; Park, Y. J.; Ziller, J. W.; Yano, J.; Borovik, A. S. *J. Am. Chem. Soc.* **2012**, *134*, 17526–17535.

(36) Wang, B.; Lee, Y. M.; Tcho, W. Y.; Tussupbayev, S.; Kim, S. T.; Kim, Y.; Seo, M. S.; Cho, K. Bin; Dede, Y.; Keegan, B. C.; et al. *Nat. Commun.* **2017**, *8*, 1–10.

(37) Song, Y. J.; Hyun, M. Y.; Lee, J. H.; Lee, H. G.; Kim, J. H.; Jang, S. P.; Noh, J. Y.; Kim, Y.; Kim, S. J.; Lee, S. J.; et al. *Chem. - A Eur. J.* **2012**, *18*, 6094–6101.

(38) Hyun, M. Y.; Kim, S. H.; Song, Y. J.; Lee, H. G.; Jo, Y. D.; Kim, J. H.; Hwang, I. H.; Noh, J. Y.; Kang, J.; Kim, C. *J. Org. Chem.* **2012**, *77*, 7307–7312.

(39) Keown, W.; Gary, J. B.; Stack, T. D. P. *J. Biol. Inorg. Chem.* **2017**, *22*, 289–305.

(40) Itoh, S. *Acc. Chem. Res.* **2015**, *48*, 2066–2074.

(41) Halvagar, M. R.; Solntsev, P. V.; Lim, H.; Hedman, B.; Hodgson, K. O.; Solomon, E. I.; Cramer, C. J.; Tolman, W. B. *J. Am. Chem. Soc.* **2014**, *136*, 7269–7272.

(42) Peterson, R. L.; Himes, R. A.; Kotani, H.; Suenobu, T.; Tian, L.; Siegler, M. A.; Solomon, E. I.; Fukuzumi, S.; Karlin, K. D. *J. Am. Chem. Soc.* **2011**, *133*, 1702–1705.

(43) Kirillov, A. M.; Kirillova, M. V.; Shul'Pina, L. S.; Figiel, P. J.; Gruenwald, K. R.; Guedes Da Silva, M. F. C.; Haukka, M.; Pombeiro, A. J. L.; Shul'Pin, G. B. *J. Mol. Catal. A Chem.* **2011**, *350*, 26–34.

(44) Champness, N. R. *Dalt. Trans.* **2011**, *40*, 10311.

(45) Martins, L. R.; Souza, E. T.; Fernandez, T. L.; Souza, B. De; Pinheiro, C. B.; Faria, R. B.; Casellato, A.; Mangrich, A. S.; Scarpellini, M. *J. Braz. Chem. Soc* **2010**, *21*, 1218–1229.

(46) Himes, R. A.; Karlin, K. D. *Curr. Opin. Chem. Biol.* **2009**, *13*, 119–131.

(47) Kunishita, A.; Ishimaru, H.; Nakashima, S.; Ogura, T.; Itoh, S. *J. Am. Chem. Soc.* **2008**, *130*, 4244–4245.

(48) Hoffman, S. *J. Common Mark. Stud.* **2000**, *38*, 189–198.

(49) Lockwood, M. A.; Blubaugh, T. J.; Collier, A. M.; Lovell, S.; Mayer, J. M. *Angew. Chem. Int. Ed.* **1999**, *38*, 225–227.

(50) Obias, H. V.; Lin, Y.; Murthy, N. N.; Pidcock, E.; Solomon, E. I.; Ralle, M.; Blackburn, N. J.; Neuhold, Y. M.; Zuberbuhler, A. D.; Karlin, K. D. *J. Am. Chem. Soc.* **1998**, *120*, 12960–12961.

(51) Itoh, S. *Curr. Opin. Chem. Biol.* **2006**, *10*, 115–122.

(52) Hatcher, L. Q.; Karlin, K. D. *J. Biol. Inorg. Chem.* **2004**, *9*, 669–683.

(53) Kunishita, A.; Kubo, M.; Sugimoto, H.; Ogura, T.; Sato, K.; Takui, T.; Itoh, S. *J.*

Am. Chem. Soc. **2009**, *131*, 2788–2789.

(54) Kunishita, A.; Ertem, M. Z.; Okubo, Y.; Tano, T.; Sugimoto, H.; Ohkubo, K.; Fujieda, N.; Fukuzumi, S.; Cramer, C. J.; Itoh, S. *Inorg. Chem.* **2012**, *51*, 9465–9480.

(55) Tano, T.; Mieda, K.; Sugimoto, H.; Ogura, T.; Itoh, S. *Dalt. Trans.* **2014**, *43*, 4871–4877.

(56) Maiti, D.; Lee, D. H.; Gaoutchenova, K.; Würtele, C.; Holthausen, M. C.; Narducci Sarjeant, A. A.; Sundermeyer, J.; Schindler, S.; Karlin, K. D. *Angew. Chemie - Int. Ed.* **2008**, *47*, 82–85.

(57) Maiti, D.; Fry, H. C.; Woertink, J. S.; Vance, M. A.; Solomon, E. I.; Karlin, K. D. *J. Am. Chem. Soc.* **2007**, *129*, 264–265.

(58) Abe, T.; Morimoto, Y.; Mieda, K.; Sugimoto, H.; Fujieda, N.; Ogura, T.; Itoh, S. *J. Inorg. Biochem.* **2017**, *177*, 375–383.

(59) Kitajima, N.; Katayama, T.; Fujisawa, K.; Iwata, Y.; Morooka, Y. *J. Am. Chem. Soc.* **1993**, *115*, 7872–7873.

(60) Kunishita, A.; Teraoka, J.; Scanlon, J. D.; Matsumoto, T.; Suzuki, M.; Cramer, C. J.; Itoh, S. *J. Am. Chem. Soc.* **2007**, *129*, 7248–7249.

(61) Chen, P.; Fujisawa, K.; Solomon, E. I. *J. Am. Chem. Soc.* **2000**, *122*, 10177–10193.

(62) Kim, B.; Jeong, D.; Cho, J. *Chem. Commun.* **2017**, *53*, 9328–9331.

(63) Singh, N.; Niklas, J.; Poluektov, O.; Van Heuvelen, K. M.; Mukherjee, A. *Inorg. Chim. Acta* **2017**, *455*, 221–230.

(64) Kryatova, M. S.; Makhlynets, O. V.; Nazarenko, A. Y.; Rybak-Akimova, E. V. *Inorg. Chim. Acta* **2012**, *387*, 74–80.

(65) Nakamoto, K.: *Infrared and Raman Spectra of Inorganic and Coordination Compounds, Part B: Applications in coordination, organometallic, and bioinorganic chemistry*, 6th ed.; John Wiley, Hoboken, NJ) (2009).

(66) Nagataki, T.; Ishii, K.; Tachi, Y.; Itoh, S. *Dalt. Trans.* **2007**, 1120–1128.

(67) Wickenden, A. E.; Krause, R. A. *Inorg. Chem.* **1965**, *4*, 404–407.

(68) Hartman, J. A. R.; Vachet, R. W.; Pearson, W.; Wheat, R. J.; Callahan, J. H. *Inorg.*

Chim. Acta **2003**, *343*, 119–132.

(69) Hartman, J. A. R.; Kammier, A. L.; Spracklin, R. J.; Pearson, W. H.; Combariza, M. Y.; Vachet, R. W. *Inorg. Chim. Acta* **2004**, *357*, 1141–1151.

(70) García-Santos, I.; Sanmartín, J.; García-Deibe, A. M.; Fondo, M.; Gómez, E. *Inorg. Chim. Acta* **2010**, *363*, 193–198.

(71) Hartman, J. R.; Vachet, R. W.; Callahan, J. H. *Inorg. Chim. Acta* **2000**, *297*, 79–87.

(72) Ivaniková, R.; Boča, R.; Dlháň, L.; Fuess, H.; Mašlejová, A.; Mrázová, V.; Svoboda, I.; Titiš, J. *Polyhedron* **2006**, *25*, 3261–3268.

(73) Narulkar, D. D.; Patil, A. R.; Naik, C. C.; Dhuri, S. N. *Inorg. Chim. Acta* **2015**, *427*, 248–258.

(74) Akbar Ali, M.; Mirza, A. H.; Bujang, F. H.; Hamid, M. H. S. A.; Bernhardt, P. V. *Polyhedron* **2006**, *25*, 3245–3252.

(75) Huheey, J. E.; Keiter, E. A.; Keiter, R. L.; Medhi, O. K. *Inorganic Chemistry, Principles of Structure and Reactivity*, 4th ed., *(Pearson)* (1993) 466.

(76) Panja, A.; Kanti, T. *Indian J. Chem.* **2016**, *55 A*, 137–144.

(77) Meghdadi, S.; Amirnasr, M.; Mereiter, K.; Karimi Abdolmaleki, M. *Acta Crystallogr. Sect. E Struct. Reports Online* **2010**, *66*, 332–333.

(78) Panja, A. *Dalt. Trans.* **2014**, *43*, 7760.

(79) Balamurugan, M.; Mayilmurugan, R.; Suresh, E.; Palaniandavar, M. *Dalt. Trans.* **2011**, *40*, 9413.

(80) Wei, Z.; Peng, Y.; Hughes, D. L.; Zhao, J.; Huang, L.; Liu, X. *Polyhedron* **2014**, *69*, 181–187.

(81) Silva, T. F. S.; Martins, L. M. D. R. S.; Guedes da Silva, M. F. C.; Fernandes, A. R.; Silva, A.; Borralho, P. M.; Santos, S.; Rodrigues, C. M. P.; Pombeiro, A. J. L. *Dalt. Trans.* **2012**, *41*, 12888–12897.

(82) Nandi, S.; Bannerjee, D.; Datta, P.; Lu, T. H.; Slawin, A. M. Z.; Sinha, C. *Polyhedron* **2009**, *28*, 3519–3525.

(83) Brodovitch, J. C.; Haines, R.I.; McAuley, A. *Can. J. Chem.* **1981** 59, 1610-1614.

(84) Sankaralingam, M.; Balamurugan, M.; Palaniandavar, M.; Vadivelu, P.; Suresh, C.

H. *Chem. - A Eur. J.* **2014**, *20*, 11346–11361.

(85) Congreve, A.; Kataky, R.; Knell, M.; Parker, D.; Puschmann, H.; Senanayake, K.; Wylie, L. *New J. Chem.* **2003**, *27*, 98–106.

(86) Romanowski, S. M. D. M.; Tormena, F.; Santos, V.; Hermann, M. D. F.; Mangrich, A. S. *J. Braz. Chem. Soc.* **2004**, *15*, 897–903.

(87) Tordin, E.; List, M.; Monkowius, U.; Schindler, S.; Knör, G. *Inorg. Chim. Acta* **2013**, *402*, 90–96.

(88) Bravo, A.; Bjorsvik, H. R.; Fontana, F.; Minisci, F.; Serri, A. *J. Org. Chem.* **1996**, *61*, 9409–9416.

CHAPTER –VI

Mechanistic insights into the reactions of hydride transfer versus hydrogen atom transfer by a *trans*-dioxoruthenium(VI) complex

6.1 Introduction and literature

Mononuclear high-valent metal-oxo complexes of heme and non-heme ligands are active oxidants in a wide range of biological and chemical oxidation reactions.[1-6] The non-heme iron^{IV}-oxo species exhibit reactivities in the activation of C–H bonds of substrates that usually occurs via a hydrogen atom abstraction as the rate-determining step (r.d.s.).[7–14] Analogous to iron(IV)-oxo complexes, high-valent ruthenium^{IV}-oxo species are capable of oxidizing organic substrates with activated C–H bonds by an electron transfer (ET), proton-coupled electron transfer (PCET), hydrogen atom transfer (HAT), hydride transfer (HT) or oxygen atom transfer (OAT) in aqueous and non-aqueous media.[15–23] The present scenario in ruthenium chemistry reveals that ruthenium complexes with different oxidation states play dynamic roles in water oxidation catalysis (WOC), wherein various mononuclear high-valent ruthenium-oxygen intermediates, such as $[Ru^{IV}(O)]^{2+}$, $[Ru^{V}(O)]^{3+}$, $[Ru^{III}(OOH)]^{2+}$, $[Ru^{IV}(O_2)]^{2+}$ and $[Ru^{V}(O_2)]^{3+}$, have been proposed to initiate the O–O formation.[24–29] Unfortunately, many of these intermediates have yet to be captured and characterized due to their instability in nature. Beyond the field of WOC, however, there has been much demand to develop ruthenium catalysts for the oxidation of biologically and industrially relevant organic substrates.[30–35] While a large number of non-heme ruthenium^{IV}-oxo complexes have been explored, the enhanced reactivity of the higher oxidation state of ruthenium such as dioxoruthenium(VI) has merited special attention.[36–46] In ruthenium-oxo chemistry, Groves and co-workers have reported the first example of a Ru-based biomimetic dioxygenase catalyst and reported a dioxo(tetramesitylporphyrinato)ruthenium(VI), which is an efficient catalyst in an aerobic epoxidation of olefins at ambient temperatures.[47] The reaction of Ru(II)-bleomycins with O_2, H_2O_2 or PhIO was subsequently reported by Garnier-Suillerot and coworkers.[48] While Che and co-workers were the pioneers in the chemistry of high-valent dioxoruthenium^{VI}

species, such as trans-$[Ru^{VI}L(O)_2]^{2+}$ where L is the tertiary macrocyclic amine (e.g., 1,4,8,11-tetramethyl-1,4,8,11-tetraaza-cyclotetradecane (TMC), 1,4,8,12-tetramethyl-1,4,8,12-tetraaza-cyclopentadecane (15-TMC), 1,5,9,13-tetramethyl-1,5,9,13-tetraazacyclohexadecane (16-TMC) and 1,12-dimethyl-3,4:9,10-dibenzo-1,12-diaza-5,8-dioxacyclopentadecane (N_2O_2)),[36,44,49] to the best of our knowledge, the reactivity of only two compounds, namely *trans*-$[Ru^{VI}(N_2O_2)(O)_2]^{2+}$ and *trans*-$[Ru^{VI}(TMC)(O)_2]^{2+}$ (**16**; **see Scheme 6.1**), has been explored to a large extent in the oxidative reactions of organic and inorganic substrates.[50,51–56] The oxidation reactions of organic compounds with **16** reported so far are summarized in **Scheme 6.1**.[50]

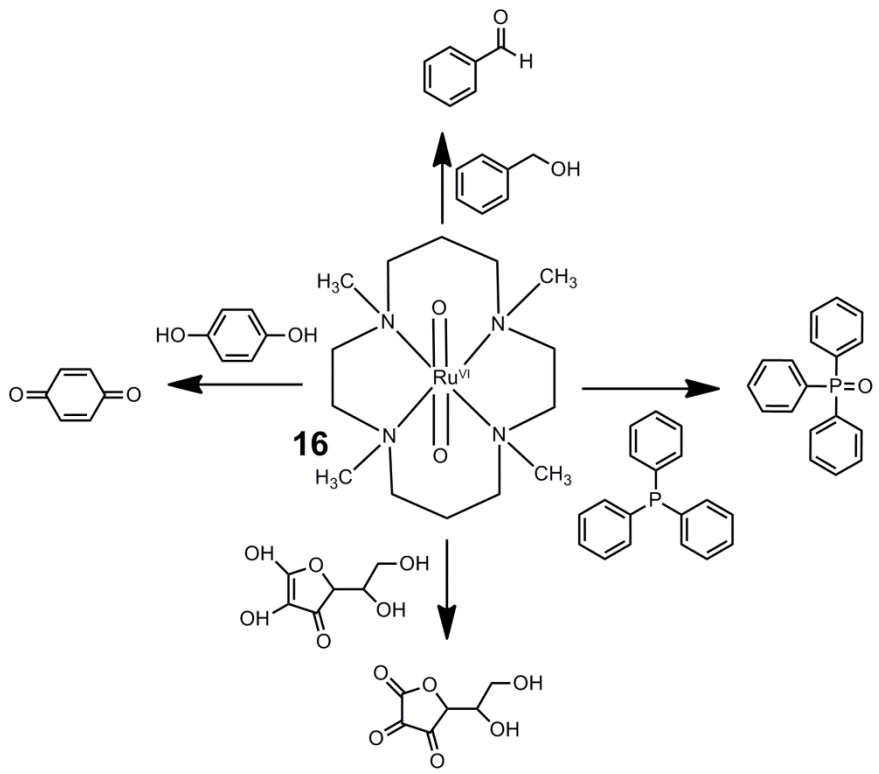

Scheme 6.1 *Chemical structure of* ***16*** *and its reactivity in various oxidation reactions*.

It is noteworthy that the dioxoruthenium^{VI} complexes often react with substrates via different mechanisms unlike the monooxoruthenium^{IV} species. For example, the oxidation of biologically relevant dihydronicotinamide adenine dinucleotide (NADH) analogues by the monooxoruthenium^{IV} species, *cis*-$[Ru^{IV}(bpy)_2(py)(O)]^{2+}$, was proposed to follow

hydrogen atom transfer (HAT) rather than hydride transfer (HT).[57] However, there has been no report on the reactivity of dioxo-ruthenium^{VI} species with the NADH analogues, such as 10-methyl-9,10-dihydroacridine ($AcrH_2$) and its derivatives (**Scheme 6.4**).[58,59]Although oxidation of NADH follows multiple pathways, it is usually converted to the corresponding cationic form, NAD^+, suggesting a preference the two-electron and one-proton transfer mechanism of HT.[60]

In this Chapter we report a detailed characterization of *trans*-$[Ru^{VI}(TMC)(O)_2]^{2+}$ (**16**) by various spectroscopic techniques together with X-ray crystallography and the first example of hydride transfer from NADH analogues to the high-valent dioxo-ruthenium(VI) complex **16**. In addition, C–H bond activation reactions of alkyl hydrocarbons by **16** were investigated to provide insights into the mechanism by which the C–H bond activation reaction proceeds via an H-atom abstraction as the rate-determining step. The chemical structures of the few structurally characterized Ru^{VI}-complexes bearing non-heme ligands are shown in **Scheme 6.2.**[61-68]

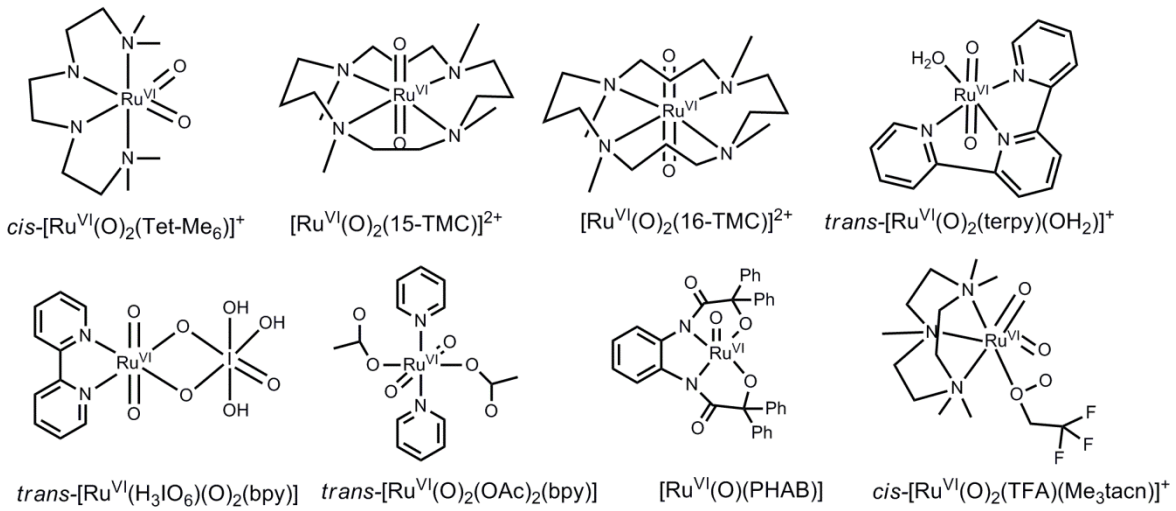

Scheme 6.2 *chemical structures of structurally characterized Ru^{VI}-complexes bearing non-heme ligands*

6.2 Experimental details

6.2.1 Preparation of trans-[$Ru^{VI}(TMC)(O)_2]^{2+}$ (16)

trans-[$Ru^{VI}(TMC)(O)_2]^{2+}$ **(16)** was prepared by a literature procedure[49]. Silver *p*-toluenesulfonate (0.54 g, 1.9 mmol) was added to the aqueous solution of *trans*-[$Ru^{III}(TMC)Cl_2$]Cl (0.30 g, 0.58 mmol) and the mixture was warmed on a water bath for 30 min. The white precipitates of AgCl formed were filtered and H_2O_2 (30%, 3.0 mL) was added to the filtrate. The solution was then heated on a water bath until the full formation of a peak at 388 nm in the UV-Vis spectrum for **16** was observed. The saturated solution (5.0 mL) of $NaClO_4$ was then added to the mixture and kept for cooling in a refrigerator. After 2 days, a yellow solid complex with a yield of 55% was formed.

6.2.2 Kinetic measurements and reactivity study

All the reactions were run in a 1 cm quartz cuvette and followed by monitoring the UV-Vis spectral changes of the reaction solutions. The rate constants were determined under pseudo-first-order conditions (e.g., [substrate]/[16] > 10), by fitting the changes in absorbance for the formation of a 358 nm peak due to $AcrH^+$ ions in the reaction of **16** with NADH analogues at 0 °C. In the oxidation of alkyl hydrocarbons by **16**, the reactions were monitored by UV-Vis spectral changes of the absorption band at 388 nm due to the decay of **16**. First order rate constants were obtained by fitting of the kinetic data at 388 nm. The hydrocarbons with C-H bond dissociation energies (BDE) ranging between 75-80 kcal mol^{-1} were chosen for the reactivity studies.

6.2.3 Product analysis

The organic product $AcrH^+$ formed in the reaction of **16** and $AcrH_2$ was quantitatively detected by the absorption band at 358 nm due to $AcrH^+$ ions by UV-Vis

spectroscopy. The $AcrH^+$ was also detected by an ESI-MS spectrum, which showed a peak at m/z = 194.1 for $AcrH^+$. In the oxidation of xanthene, DHA and CHD by **16**, the complete reaction solutions were analyzed by GC. Product yields were determined by comparing the peak areas with the standard curves obtained using authentic samples and decane as an internal standard. The reaction products for xanthene, DHA and CHD were determined to be xanthone (87 ± 4%), anthracene (90 ± 4%) and benzene (88 ± 5%) as the major organic products, respectively. The ruthenium products formed in the reaction of **16** with $AcrH_2$ as well as alkyl hydrocarbons were analyzed by EPR and ESI-MS techniques. In both reactions, $[Ru^{IV}(TMC)(O)]^{2+}$ species was formed as a final product[36,69]

6.3 Results and discussion

6.3.1 Synthesis of trans-[Ru^{VI}(TMC)(O)$_2$](ClO$_4$)$_2$ (16)

The *trans*-[Ru^{VI}(TMC)(O)$_2$](ClO$_4$)$_2$ (**16**) complex was synthesized according to the literature procedure (**Scheme 6.3**) as mentioned in section 6.2.1[49]. The reaction of [Ru^{III}(H$_2$O)$_5$Cl]Cl$_2$ with TMC ligand in ethanol afforded [Ru^{III}(TMC)(Cl)]Cl$_2$ which on further oxidation with H$_2$O$_2$ gave *trans*-[Ru^{VI}(TMC)(O)$_2$](ClO$_4$)$_2$ **(16)** as per the procedure discussed in section 6.2.1. The compound **16** prepared is relatively stable in CH$_3$CN at 0 °C ($t_{1/2} \approx 6$ h).

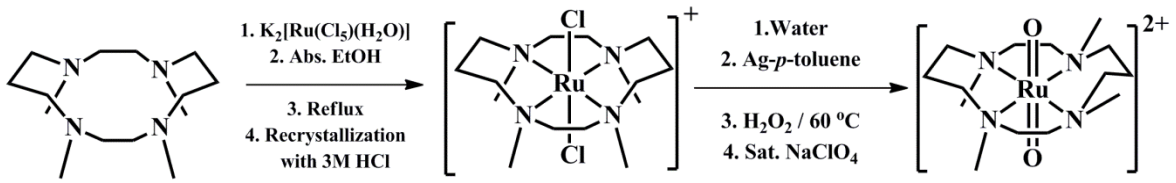

Scheme 6.3 *Synthesis of trans-[Ru^{VI}(TMC)(O)$_2$](ClO$_4$)$_2$ (**16**)*

The compound **16** was further characterized using various spectroscopic methods, such as UV-Vis, ESI-MS, and EPR and X-ray crystallography.

6.3.2 Characterization of trans-[Ru^{VI}(TMC)(O)$_2$](ClO$_4$)$_2$ (16)

6.3.2a Characterization of 16 by spectroscopic techniques (UV-Vis, ESI-Ms, EPR)

Although the UV-Vis spectrum of **16** was reported previously,[49] no other spectroscopic and structural characterization of **16** has been reported. The UV-Vis spectrum of **16** exhibits a vibronic band centred at 388 nm, which is characteristic of dioxo-metal complexes[36] (**Figure 6.1**). The ESI-MS of **16** exhibits prominent ion peaks at m/z = 195.1 and 489.0, whose mass and isotope distribution patterns correspond to [Ru^{VI}(TMC)(O)$_2$]$^{2+}$ (calc. m/z = 195.1) and [Ru^{VI}(TMC)(O)$_2$(ClO$_4$)]$^{+}$ (calc. m/z = 489.1) species, respectively (**Figure 6.2**).

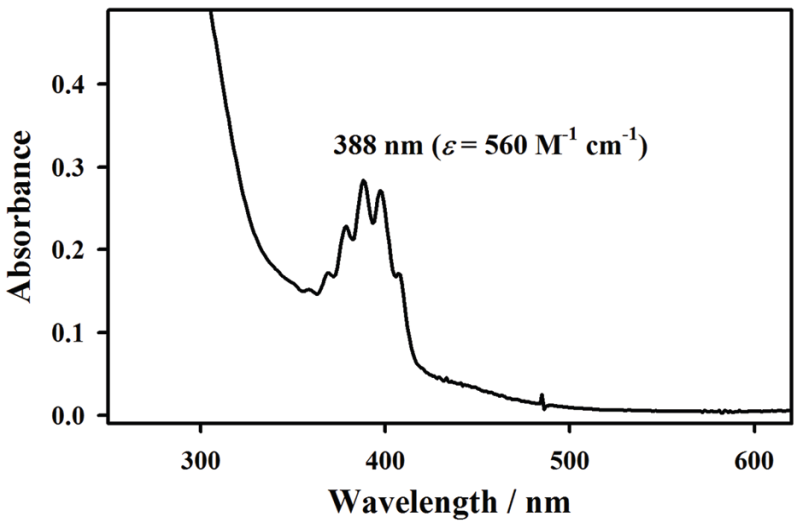

Figure 6.1. *UV-Vis spectrum of trans-[Ru^{VI}(TMC)(O)$_2$]$^{2+}$* ***16*** *in CH_3CN at 0 °C.*

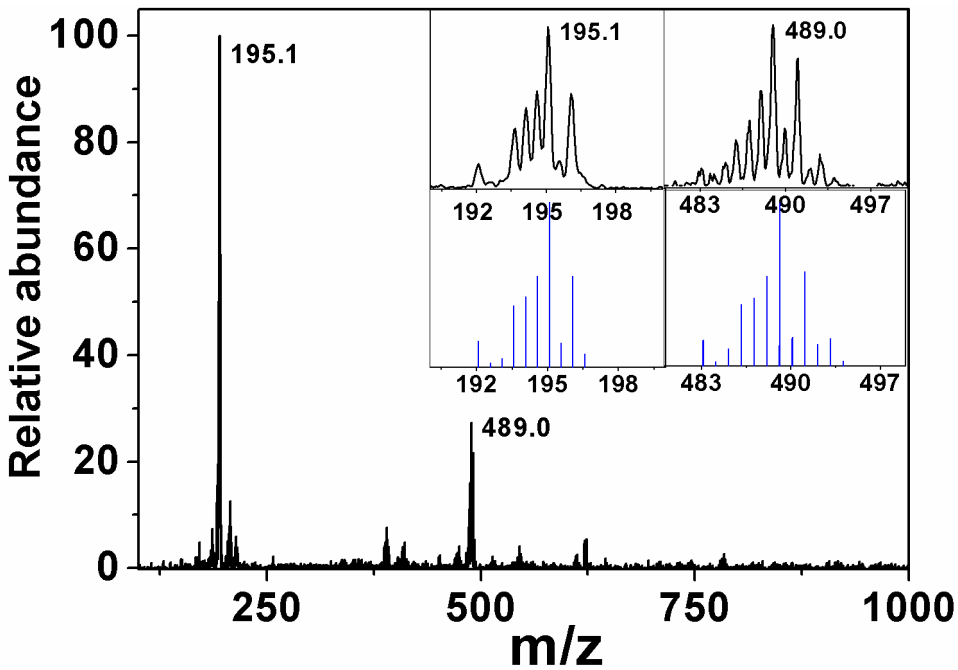

Figure 6.2 *ESI-MS spectrum of* ***16*** *in CH_3CN. The inset shows the isotope distribution patterns for the prominent peaks in black with simulated pattern in blue colour.*

The characterization by EPR spectroscopy reveals that **16** is EPR silent (**Figure 6.3**) and indicate that **16** is a diamagnetic low-spin (S = 0) d^2 Ru^{VI} species. Taken together, all the spectroscopic data demonstrate that **16** is a dioxoruthenium^{VI} species. In addition to the spectroscopic characterization described above, compound **16** was characterized structurally by X-ray crystallography.

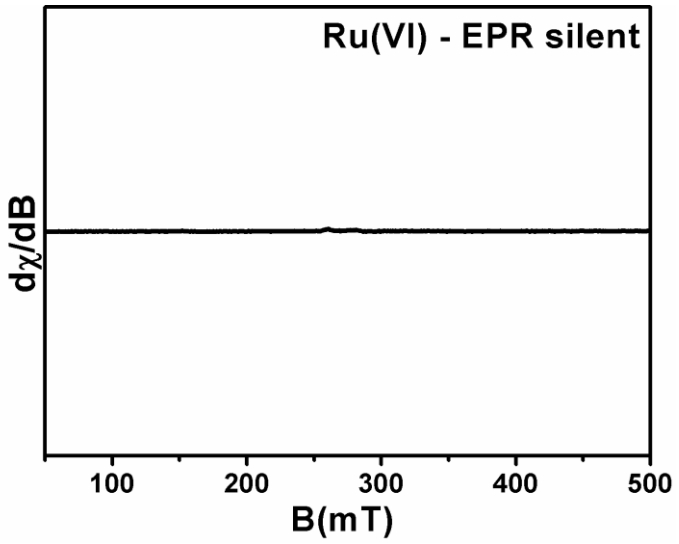

Figure 6.3 *EPR spectra of* ***16*** *recorded in CH_3CN solvent.*

6.3.2b Characterization of single crystal X-ray crystallography

The greater thermal stability of **16** allowed the isolation of single crystals suitable for X-ray crystal structural analyses. Although H atoms were not geometrically positioned due to the relatively high degree of disorders, the structure of **16** shows a perfect octahedral geometry with the space group $P2_1/c$ (**Figure 6.4 and Table 6.1**).

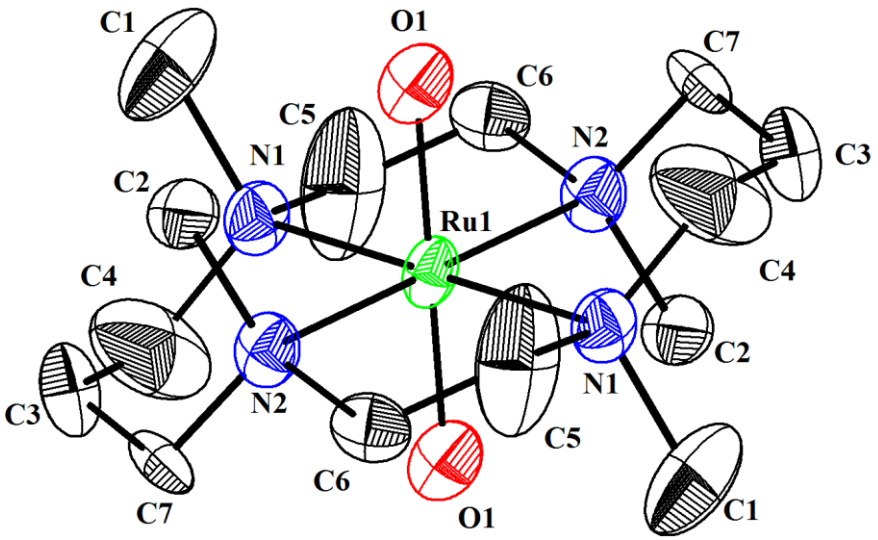

Figure 6.4 *ORTEP diagram of $[Ru^{VI}(TMC)(O)_2]^{2+}$ unit in* ***16*** *showing the atom-numbering scheme and 30 % probability ellipsoids [Symmetry code: (i) 1-x, 1-y, 1-z]. Selected bond distances (Å): Ru-O1 1.712(4), Ru-N1 2.149(4), Ru-N2 2.146(4). H atoms could not be geometrically positioned due to the relatively high degree of disorders.*

Table 6.1**. Technical details of data acquisition and selected refinement results for **16

	16
Empirical formula	$C_{14}Cl_2N_4O_{10}Ru$
Formula weight	556.15
Crystal description	Block
Crystal colour	Brick red
Crystal system	Monoclinic
Space group	$P2_1/c$(no. 14)
Temperature (K)	170(2)
Unit cell dimensions	a = 6.3282 (6) Å
	b = 16.9820 (17)Å
	c = 10.1870 (10) Å
	α = 90 °
	β = 94.132 (8)°
	γ = 90°
volume (Å^3)	1091.91(18)
Z	2
Radiation type (Mo-Kα)/Å	0.71073
Crystal size (mm)	0.4 x 0.2 x 0.1
Diffractometer	Bruker Smart APEX-II Duo
Absorption correction	Semi-empirical from equivalents
No. measured reflections	3363
Calculated density (g/cm^3)	1.692
Absorption coefficient (mm^{-1})	1.018
F(000)	540
θ range for data collection	2.34 to 27.42
Limiting indices	$-10 \leq h \leq 8$
	$-39 \leq k \leq 39$
	$-10 \leq l \leq 10$
Refinement method	Full-matrix least-squares on F^2
Data / restraints / parameter	1679 / 0 / 179
Final R Indices[I>2σ(I)]	R_1 = 0.0547, wR_2 = 0.1534
R indices (all data)	R_1 = 0.0650, wR_2 = 0.1574
Goodness of fit on F^2	1.100
Extinction coefficient	0.0041 (16)
Largest diff. peak and hole(eÅ^{-3})	1.554 and -0.527e.Å^{-3}
Reflections collected / unique	6032 / 2150 [R(int) = 0.0320]

In this structure, one oxo ligand is located *trans* to the other oxo ligand, and two *N*-methyl groups of the TMC ligand point toward one oxo ligand and the other two N-methyl groups of the TMC ligand point toward the other oxo ligand symmetrically. Both the *trans* Ru–O bond distances are 1.712(4) Å, which is quite similar to those reported in the dioxoruthenium(VI) complexes.[68,70-72]

6.3.3 Reactivity study of compound 16 in hydride transfer reaction and H-abstraction reaction

6.3.3a Reactivity of 16 in hydride transfer (HT) from NADH analogues

The reactivity of **16** was investigated in hydride transfer (HT) reactions with NADH analogues, 10-methyl 9,10-dihydroacridine ($AcrH_2$) and its derivatives (**Scheme 6.4**) in CH_3CN at 0 °C.

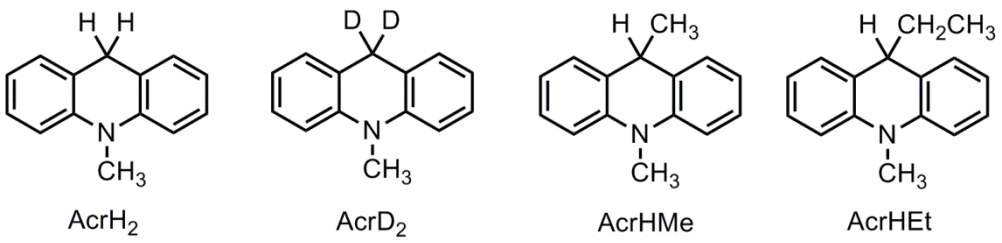

Scheme 6.4 *Substrates for hydride transfer reaction*

Upon addition of $AcrH_2$ to a solution of **16** (5×10^{-5} M), $AcrH_2$ was converted to 10-methylacridinium ion ($AcrH^+$)[73] quantitatively as evidenced from the full formation of a band at 358 nm ($\varepsilon = 1.8 \times 104$ $M^{-1}cm^{-1}$) due to $AcrH^+$ (**Figure 6.4**) and the metal product was $[Ru^{IV}(TMC)(O)]^{2+}$ as evident from ESI-MS(**Figure 6.5**).[69]

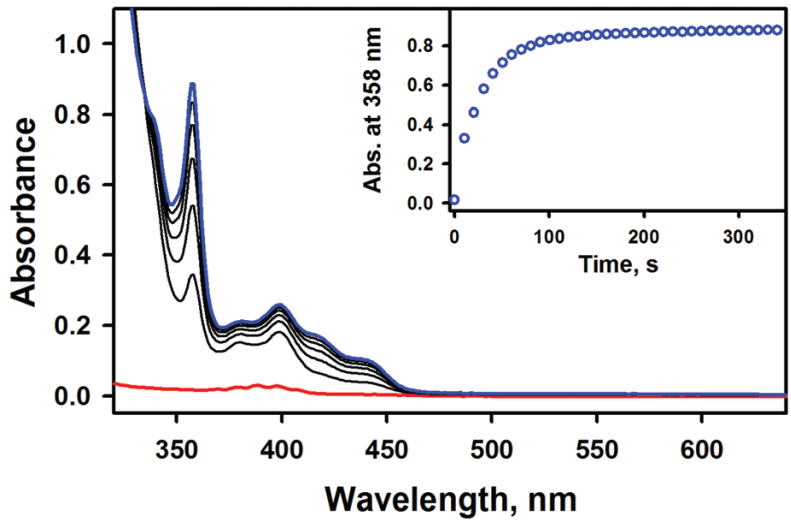

Figure 6.4 *UV-Vis spectral changes of* ***16*** *observed in the reaction of* ***16*** *(0.050 mM) and* $AcrH_2$ *(1.0 mM) in acetonitrile at 0 °C. The inset shows the time course monitored at 358 nm due to the formation of* $AcrH^+$.

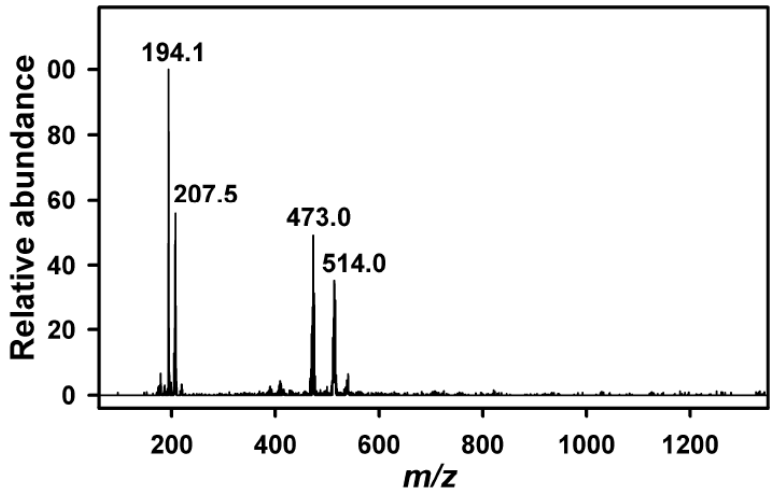

Figure 6.5 *ESI-MS spectrum of the reaction solution obtained in the reaction of* ***16*** *(1.0 mM) with* $AcrH_2$ *(20 mM) in* CH_3CN *at 0* ^{o}C. *The peaks at m/z = 194.1, 207.5, 473.0 and 514.0 correspond to* $AcrH^+$ *(calc. m/z = 194.1),* $[Ru^{IV}(TMC)(O)(CH_3CN)]^{2+}$ *(calc. m/z = 207.6),* $[Ru^{IV}(TMC)(O)(ClO_4)]^+$ *(calc. m/z = 473.1) and* $[Ru^{IV}(TMC)(O)(ClO_4)(CH_3CN)]^+$ *(calc. m/z = 514.1), respectively.*

First-order rate constants (k_{obs}), determined by pseudo-first order fitting of the kinetic data for the formation of $AcrH^+$ monitored at 358 nm, increased linearly with an increase in the concentration of $AcrH_2$, leading us to determine the second-order rate constant. (k_{HT}) of 63(4) M^{-1} s^{-1} (**Figure 6.6**). By using the dideuterated substrate, $AcrD_2$, a

large kinetic isotope effect (KIE) value of 13(1) was obtained in the reactions of $AcrH_2$ *versus* $AcrD_2$ (**Figure 6.6**), indicating that the C–H bond cleavage of NADH analogues is involved in the rate-determining step in the HT reactions by **16**.

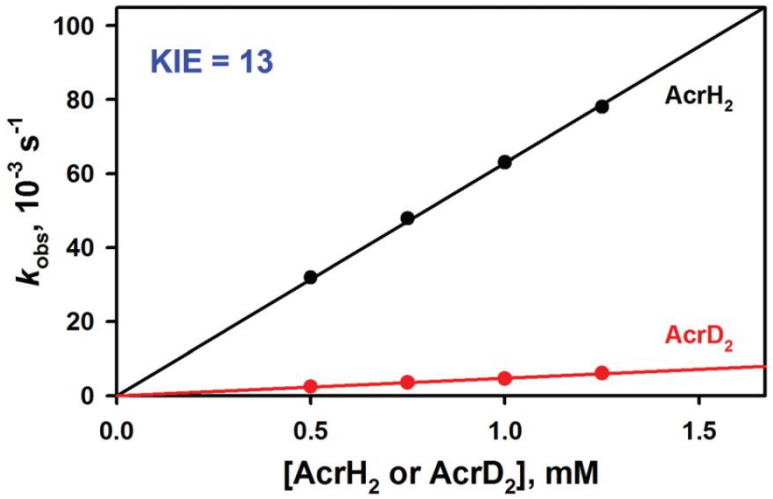

Figure 6.6 *Plots of k_{obs} against the concentrations of $AcrH_2$ and $AcrD_2$.*

The HT reactions were also investigated with other $AcrH_2$ derivatives bearing a substituent R at the C-9 position (i.e., AcrHR), such as AcrHMe and AcrHEt. The reaction rates (k_{HT}), which were determined to be 2.7(2) M^{-1} s^{-1} for AcrHMe and 1.3(1) M^{-1} s^{-1} for AcrHEt (**Figure 6.7**), were significantly affected by the substituent R in the AcrHR. The observation that reactivity of AcrHR bearing an electron-donating R group is lower than that of $AcrH_2$ suggests that the HT reaction occurs via a sequential electron and proton transfer, followed by a rapid ET, rather than a one-step HT mechanism.[74,75] The decrease in the second-order rate constants with the increasing electron-donating ability of R (methyl or ethyl) at the C-9 position rather indicates that the reactivity is determined by the process in which a positive charge is released.[73,74] It should be noted that the reaction of $[Ru^{IV}(TMC)(O)]^{2+}$ with $AcrH_2$, which was performed as a control experiment, does not occur under identical conditions.

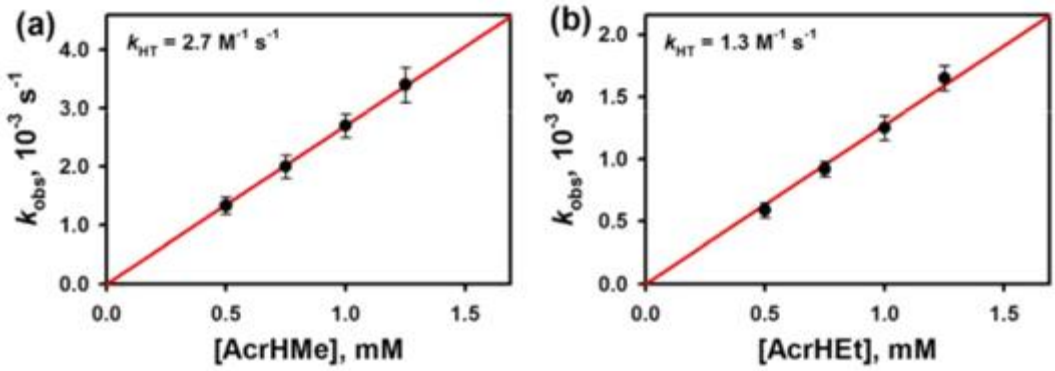

Figure 6.7 *Plots of first-order rate constant (k_{obs}) against the concentration of NADH analogues to determine the second-order rate constants (k_{HT}) in the oxidation of (**a**) AcrHMe and (**b**) AcrHEt by **16** in CH_3CN at 0 °C.*

As reported previously, HT from NADH analogues to hydride acceptors, such as *p*-chloranil (Cl_4Q) and 2,3-dichloro-5,6-dicyano-*p*-benzoquinone, occurs via a proton-coupled electron transfer (PCET), followed by a rapid ET.[76–78] Further, the reactivity comparison between high-valent metal-oxo complexes and Cl_4Q was used as indirect evidence for proposing the PCET mechanism in HT reactions.[78] Thus, the rate constants of HT (k_{HT}) from NADH analogues to **16** were compared with those of HT from the same NADH analogues to Cl_4Q.[73,78–82] As shown in **Figure 6.8**, there is a good linear correlation between the k_{HT} values of **16** and the corresponding values of Cl_4Q with the slope of ∼1, implying that HT from NADH analogues to **16** follows the same HT mechanism of Cl_4Q, which is the PCET, followed by rapid ET.[76,77] In addition, the k_{HT} values of HT from NADH analogues to **16** are also well correlated with the rate constants of deprotonation (k_d) of NADH radical cations (i.e., one-electron oxidized product of AcrHR, $AcrHR^{\bullet+}$) as shown in **Figure 6.9**. As reported previously, the decay of $AcrHR^{\bullet+}$ obeys first-order kinetics and thedecay rate constant of $AcrHR^{\bullet+}$ (k_d) corresponds to the rate constant of deprotonation from $AcrHR^{\bullet+}$ to produce $AcrR^{\bullet}$.[73,74] The k_d value becomes smaller by changing R from H to Me and Et because of an increase in the deprotonation barrier to form the planar $AcrR^{\bullet}$ caused by the increase in the magnitude of nonplanarity of the

acridine ring upon introduction of a substituent R at the C-9 position in $AcrH_2$.[73,74] Therefore, such a linear correlation between the k_{HT} values of HT from NADH analogues to **16** and the k_d values of deprotonation of $AcrHR^{\bullet+}$ (**Figure 6.9**) indicates that the proton transfer (PT) from $AcrHR^{\bullet+}$ to $[Ru^{V}(TMC)(O)_2]^+$, which is the one-electron reduced species of 1, is involved as the rate-determining step.[73,74] Based on the results of the

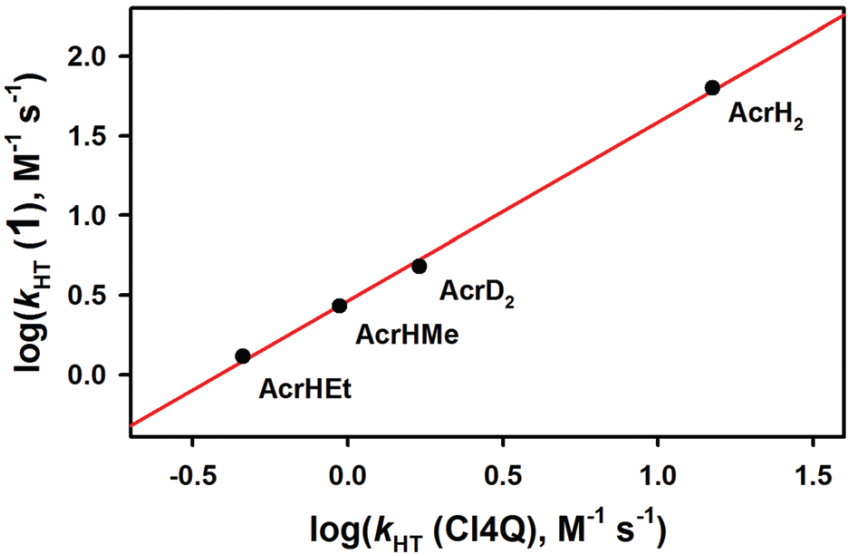

Figure 6.8 *Plot of log k_{HT} for hydride transfer from NADH analogues to* ***16*** *in CH_3CN at 0 °C versus log k_{HT} for hydride transfer from the same series of NADH analogues to Cl_4Q*[22] *in CH_3CN at 25 °C.*

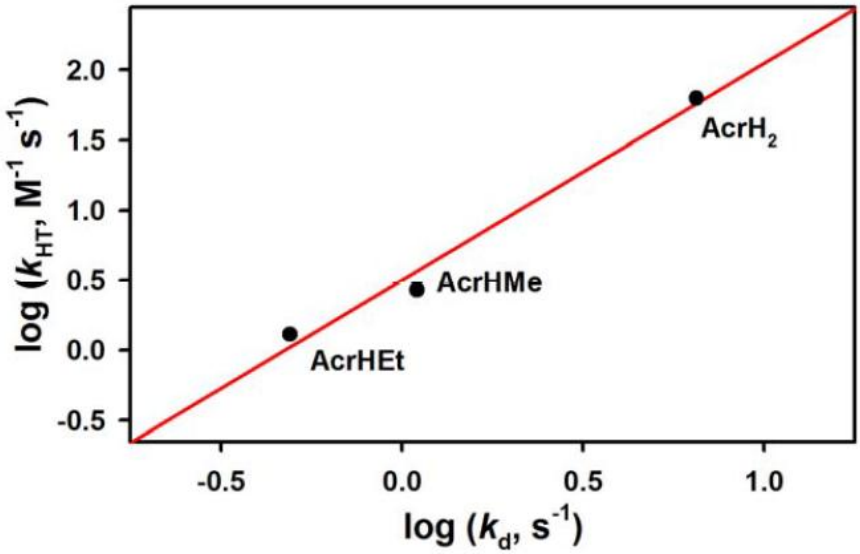

Figure 6.9 *Plot of log k_{HT} for hydride transfer from NADH analogues to* ***16*** *in CH_3CN at 0 ^oC versus log kd for deprotonation of $AcrHR^{\bullet+}$ (R = H, Me and Et) in CH_3CN at 25 ^oC.*

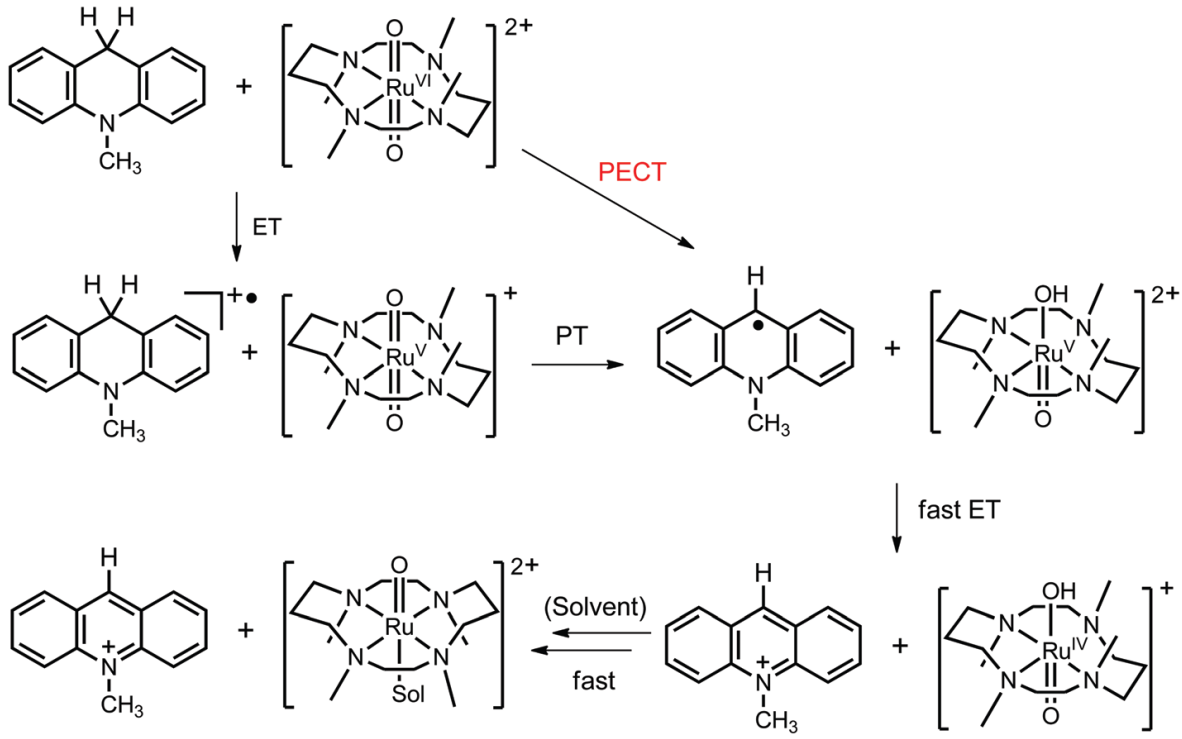

Scheme 6.5 *Proposed mechanism for HT from NADH analogues, AcrHR, to* ***16****.*

mechanistic studies discussed above, we propose the following mechanism in the HT reactions by **16** (**Scheme 6.5**) the HT from NADH analogues, AcrHR, to **16** occurs via an uphill ET from AcrHR to **16**, followed by the rate-limiting PT from $AcrHR^{\bullet+}$ to $[Ru^{V}(TMC)(O)_2]^{+}$ in competition with the back electron transfer, and then a rapid ET from $AcrR^{\bullet}$ to the $[Ru^{V}(TMC)(O)(OH)]^{2+}$ species to produce $AcrR^{+}$, which is an NAD^{+} analogue, and the $[Ru^{IV}(TMC)(O)]^{2+}$ complex.

6.3.3b Reactivity of compound 16 in C-H bond activation of alkyl hydrocarbons by 16

The reactivity of compound **16** in the oxidation of alkyl hydrocarbons was also investigated. The reactions of **16** with alkyl hydrocarbons having weak C–H bond dissociation energies (BDE),[27] such as xanthene (75.5 kcal mol^{-1}), dihydroanthracene (DHA; 77.0 kcal mol^{-1}), 1,4-cyclohexadiene (CHD; 78.0 kcal mol^{-1}) and fluorene (80.0 kcal mol^{-1}) (**Scheme 6.6**), were carried out in CH_3CN at 35 °C. As shown in **Figure 6.10**, addition of xanthene to the CH_3CN solution of **16** (0.50 mM) afforded the disappearance

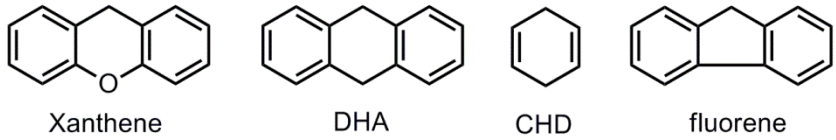

Scheme 6.6 *Substrates for C-H activation reaction*

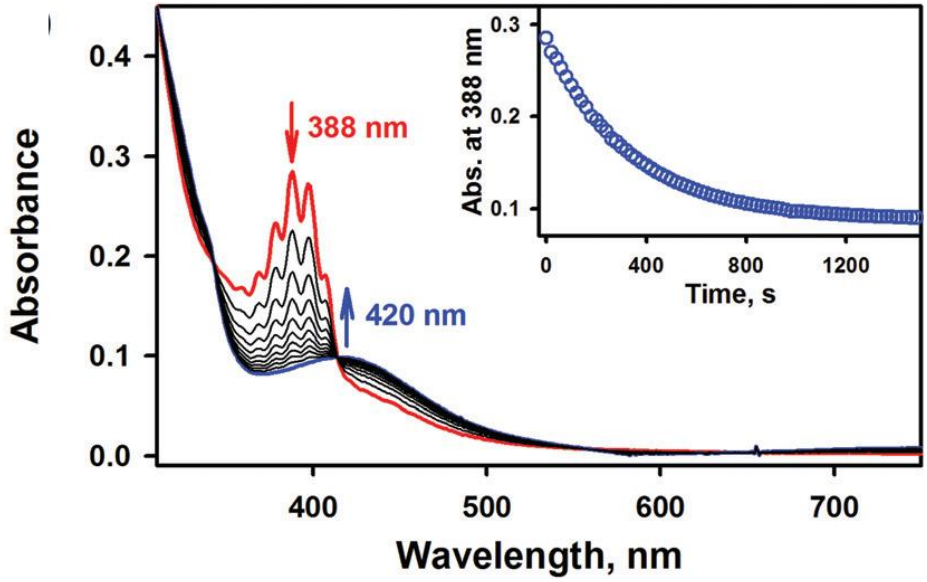

Figure 6.10 *UV-vis spectral changes of* ***16*** *(0.50 mM) upon the addition of xanthene (50 mM) at 35 °C. The inset shows the time course of the decay of* ***16*** *monitored at 388 nm.*

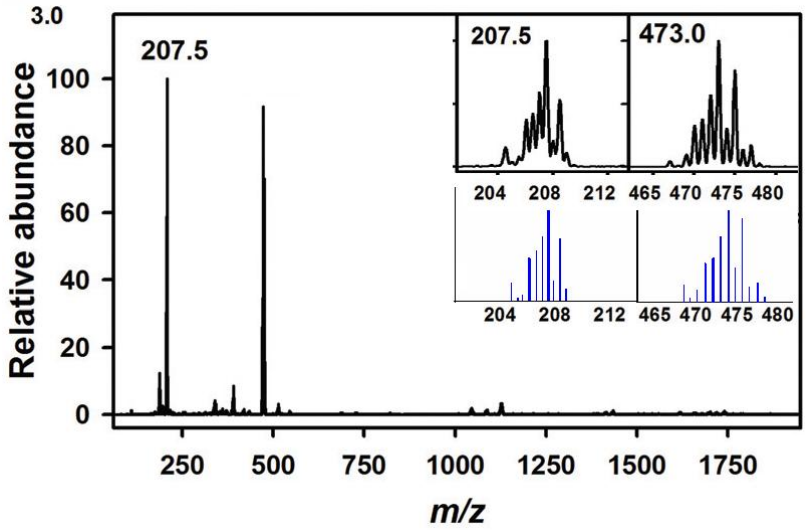

Figure 6.11 *ESI-MS spectrum of the reaction solution obtained in the reaction of* ***16*** *(1.0 mM) with xanthene (50 mM) in CH_3CN at 35 °C. The peaks at m/z = 207.5 and 473.0 correspond to $[Ru^{IV}(TMC)\text{-}(O)(CH_3CN)]^{2+}$ (calc. m/z = 207.6) and $[Ru^{IV}(TMC)(O)(ClO_4)]^{+}$ (calc. m/z 473.1), respectively. Insets show the isotopic distribution patterns of the peaks at m/z = 207.5 and 473.0 with simulated pattern.*

of a vibronic structural absorption peak at 388 nm due to **16**, accompanied by a new absorption band formation at 420 nm, which corresponds to $[Ru^{IV}(TMC)(O)(CH_3CN)]^{2+}$,[69] with clean isosbestic points at 345 and 415 nm (**Figure 6.10**). This was also confirmed by cyclic voltammetry for the reaction of **16** with DHA (**Figure 6.12**).

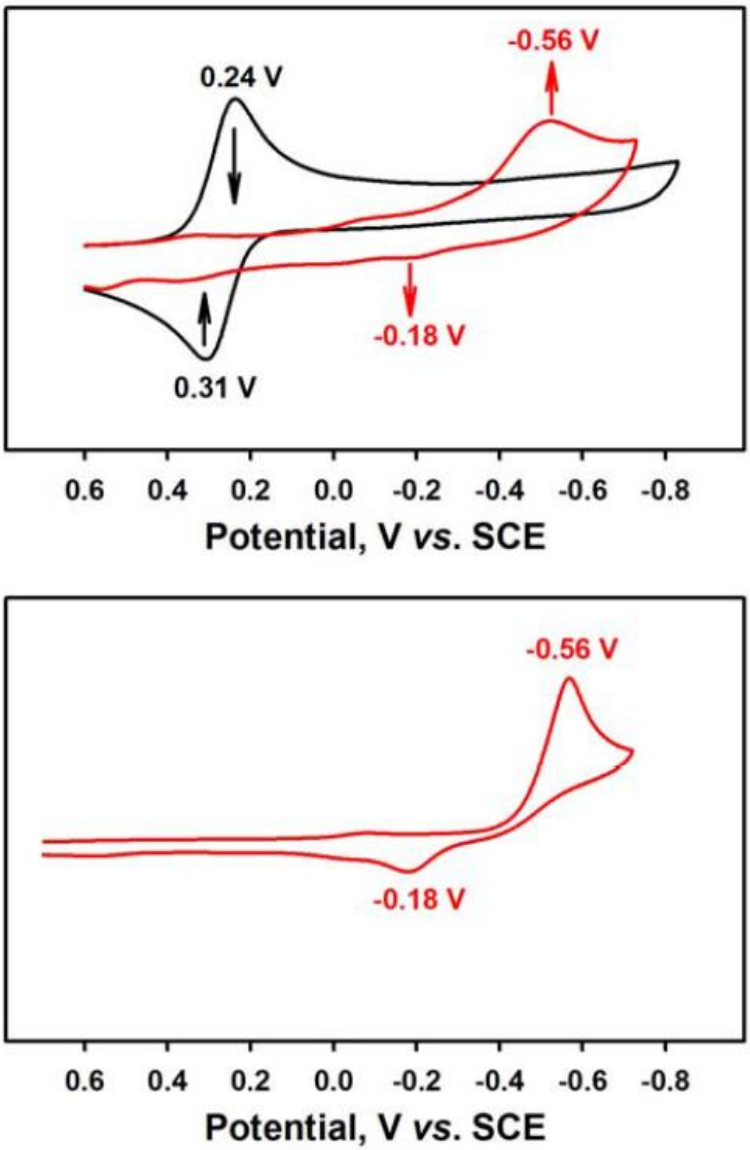

Figure 6.12 *(a) Cyclic voltammograms of* ***16*** *(1.0 mM) and the complete reaction solution obtained in the reaction of* ***16*** *(1.0 mM) and DHA (50 mM) in deaerated CH_3CN containing 0.10 M $TBAPF_6$ at 25 ^oC. (b) Cyclic voltammogram of $[Ru^{IV}(TMC)(O)(CH_3CN)](ClO_4)_2$, which is an authentic reference, in deaerated CH_3CN containing 0.10 M $TBAPF_6$ at 25 ^oC. A Pt working electrode was used with a scan rate of 100 mV s^{-1}.*

The first-order rate constants (k_{obs}) determined by pseudo-first-order fitting of the kinetic data for the decay of **16** at 388 nm increased proportionally with the increase of xanthene concentration, leading us to determine the second-order rate constant (k_{HAT}) of 5.7(4) × 10^{-2} M^{-1} s^{-1} at 35 °C (**Figure 6.13**). It should be noted that, although the reaction product, $[Ru^{IV}(TMC)(O)(CH_3CN)]^{2+}$, reacts further with xanthene,[69] the rate of xanthene oxidation by **16** is 20-fold faster than that of the $[Ru^{IV}(TMC)(O)(CH_3CN)]^{2+}$ reaction with xanthene at the same temperature. In order to determine the KIE value, xanthene-d_2 was used as a substrate and the second-order rate constant of 2.2(2) × 10^{-3} M^{-1} s^{-1} was obtained (**Figure 6.13**), resulting in a large KIE value of 26 (2) for the reactions of xanthene versus xanthene-d_2 (**Figure 6.13**). This result indicates that the H-atom abstraction of alkyl hydrocar-bons by **16** is involved in the rate-determining step. It should be noted that such a large KIE value in HAT reactions as well as in HT reactions is probably attributable to the tunneling effects.[15–17,37,38,57]

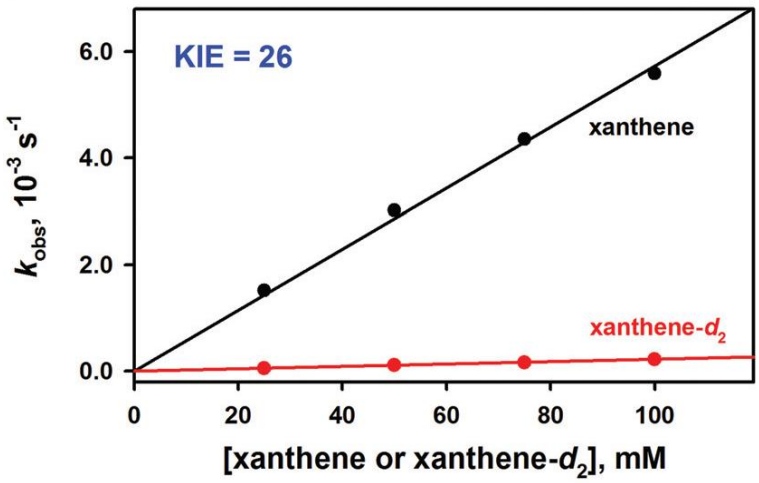

Figure 6.13 *Plots of k_{obs} against the concentrations of xanthene and xanthene-d_2 to determine the KIE value of 26(2).*

The C–H bond activation reactions were also investigated with other alkyl hydrocarbons, such as DHA, CHD and fluorene.The second-order rate constants (k_{HAT}) of 1.5(2) × 10^{-2} M^{-1} s^{-1} and 3.6(4) × 10^{-2} were obtained in the reactions of **16** with CHD and

DHA respectively (**Figure 6.14**). However, **16** did not show a reactivity with fluorene, which has a relatively strong C–H BDE value (80.0 kcal mol^{-1}) compared to other alkyl hydrocarbons used in this study. As expected, the rate constants (k_{HAT}) decreased with an increase in the C–H BDE of alkyl hydrocarbons. **Figure 6.15** shows a linear correlation between the log k'_2 values and the C-H BDE values of the substrates (the 2 k_{HAT} values are

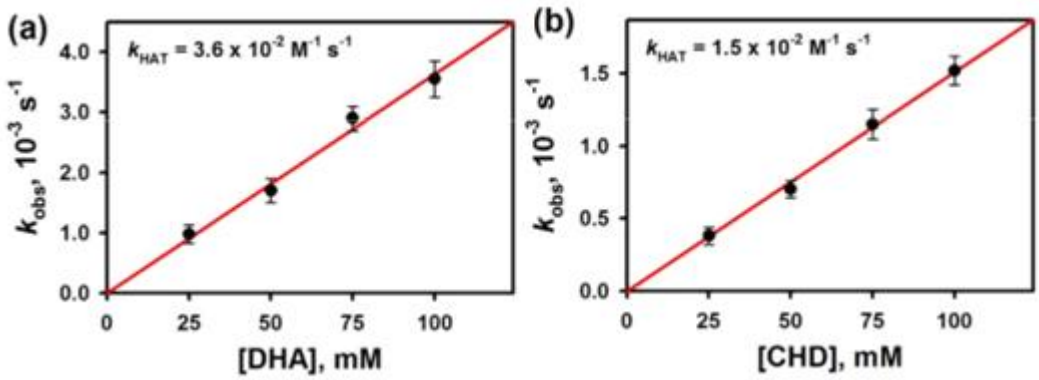

Figure 6.14 *Plots of first-order rate constant (k_{obs}) against the concentration of alkyl hydrocarbons to determine the second-order rate constants (k_{HAT}) in the oxidation of (**a**) DHA and (**b**) CHD by **16** in CH_3CN at 35 °C.*

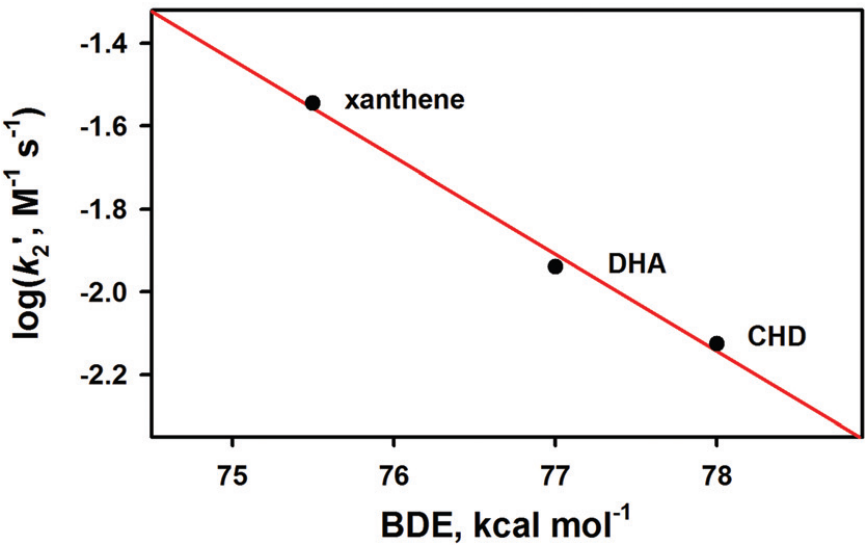

Figure 6.15 *Plot of log k'_2 of **16** against C–H BDE of the substrates. Second-order rate constants (k_{HAT}) were determined at 35 °C and then adjusted for the reaction stoichiometry to yield k'_2 based on the number of equivalent target C–H bonds of the substrates (e.g., 2 for xanthene and 4 for DHA and CHD).*

divided by the number of equivalent target C–H bonds of substrates to obtain the *k′* values).[83–87] The final reaction solutions obtained in the oxidation of alkyl hydrocarbons by **16** were analyzed by gas chromatography (GC). Xanthone (87 ± 4%), anthracene (90 ± 4%) and benzene (88 ± 5%) were formed as the major organic products in the oxidation of xanthene, DHA and CHD by **16**, respectively.

The good correlation between the log k_{HAT} and C–H BDE of alkyl hydrocarbons, and large KIE values, and analyses of the organic/inorganic product allowed us to propose that the C–H bond activation of alkyl hydrocarbons by **16** occurs via an H-atom abstraction mechanism as shown in **Scheme 6.7**.

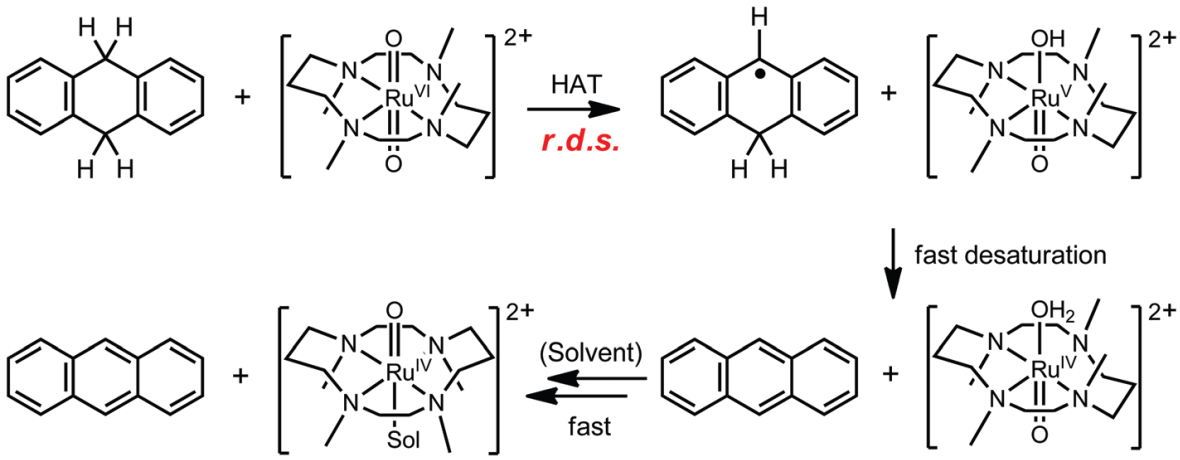

Scheme 6.7 *Proposed mechanism for HAT reactions of DHA by* ***16.***

6.4 Summary and conclusions

In this chapter, we have synthesized and characterized the mono-nuclear high-valent trans-dioxoruthenium^{VI} complex bearing a macrocyclic supporting ligand, *trans*-$[Ru^{VI}(TMC)(O)_2]^{2+}$ (**16**). Reactivities of **16** in HT reactions with NADH analogues and HAT reactions with alkyl hydrocarbons were investigated. On the basis of the reactivity studies, the mechanisms of HT from the NADH analogues to **16** and the HAT of alkyl hydrocarbons by **16** have been proposed; the HT from NADH analogues, AcrHR, to **16** occurs via an uphill ET from AcrHR to **16**, followed by the rate-limiting PT from $AcrHR^{\bullet+}$ to $[Ru^{V}(TMC)(O)_2]^{+}$ species, and then a rapid ET from $AcrR^{\bullet}$ to the $[Ru^{V}(TMC)(O)(OH)]^{2+}$ species. In the case of the HAT reaction by **16**, the C–H bond activation of alkyl hydrocarbons by **16** occurs via an H-atom abstraction mechanism. The mechanistic distinction between NADH analogues and alkyl hydrocarbons may result from the significantly lower one-electron oxidation potentials of NADH analogues than those of alkyl hydrocarbons, which enables the ET pathway. Thus, the present work provides valuable insights into the mechanism of the HT and HAT reactions by high-valent dioxoruthenium^{VI} species.

References

(1) Borovic, A. S. *Chem. Soc. Rev.* **2011**, *40*, 1870-1874.

(2) Kotani, H.; Kaida, S.; Ishizuka, T.; Sakaguchi, M.; Ogura, T.; Shiota, Y.; Yoshizawa, K.; Kojima, T. *Chem. Sci.* **2015**, *6*, 945–955.

(3) Punniyamurthy, T.; Velusamy, S.; Iqbal, J. *Chem. Rev*. **2005**, *105*, 2329-2363.

(4) Che, C.-M.; Lo, V. K.-Y.; Zhou, C. -Y.; Huang, J.-S., Chem Soc. Rev. **2011**, *40*, 1950-1975

(5) Hohenberger, J.; Ray, K.; Meyer, K. *Nat. Commun.* **2012**.

(6) Krebs, C.; Fujimori, D. G.; Jr., J. M. B. *Acc. Chem. Res.* **2007**, *40*, 484–492.

(7) Kaizer, J.; Klinker, E. J.; Oh, N. Y.; Rohde, J. -U.; Song, W. J.; Stubna, A.; Kim, J.; Münck, E.; Nam, W.; Jr., L. Q. *J. Am. Chem. Soc.* **2004**, *126*, 472–473.

(8) Nam, W.; Lee, Y. -M.; Fukuzumi, S. *Acc. Chem. Res.* **2014**, *47*, 1146-1154.

(9) Nam, W. *Acc. Chem. Res.* **2007**, *40*, 522–531.

(10) Visser, S. P. d.; Rohde, J. -U.; Lee, Y. -M.; Cho, J.; Nam, W. *Coord. Chem. Rev.* **2013**, *257*, 381–393.

(11) Shaik, S.; Hirao, H.; Kumar, D. *Acc. Chem. Res.* **2007**, *40*, 532–542.

(12) Green, M. T. *Curr. Opin. Chem. Biol.* **2009**, *13*, 84-88.

(13) Gunay, A.; Theopold, K. H. *Chem. Rev.* **2010**, *110*, 1060–1081.

(14) Ray, K.; Pfaff, F. F.; Wang, B.; Nam, W. *J. Am. Chem. Soc.* **2014**, *136*, 13942-13958.

(15) Roecker, L.; Meyer, T. J. *J. Am. Chem. Soc.* **1987**, *109*, 746–754.

(16) Thompson, M. S.; Meyer, T. J. *J. Am. Chem. Soc.* **1982**, *104*, 4106–4115.

(17) Bryant, J. R.; Mayer, J. M. *J. Am. Chem. Soc.* **2003**, *125*, 10351–10361.

(18) Trammell, S. A.; Wimbish, J. C.; Odobel, F.; Gallagher, L. A.; Narula, P. M.; Meyer, T. J. *J. Am. Chem. Soc.* **1998**, *120*, 13248–13249.

(19) Stultz, L. K.; Huynh, M. H. V.; Binstead, R. A.; Curry, M.; Meyer, T. J. *J. Am. Chem. Soc.* **2000**, 122, 5984–5996.

(20) Seok, W. K.; Meyer, T. J. *J. Am. Chem. Soc.* **1988**, 110, 7358–7367.

(21) Thompson, M. S.; Meyer, T. J. *J. Am. Chem. Soc.* **1982**, *104*, 5070–5076.

(22) Seok, W. K.; Meyer, T. J. *Inorg. Chem.* **2004**, *43*, 5205–5215.

(23) Bryant, J. R.; Mayer, J. M. *J. Am. Chem. Soc.* **2003**, 1*25*, 10351–10361.

(24) Concepcion, J. J.; Jurss, J. W.; Templeton, J. L.; Meyer, T. J. *J. Am. Chem. Soc.* **2008**, *130*, 16462–16463.

(25) Chen, Z.; Concepcion, J. J.; Luo, H.; Hull, J. F.; Paul, A.; Meyer, T. J. *J. Am. Chem. Soc.* **2010**, *132*, 17670–17673.

(26) Che, C. -M.; Yam, V. W. -W.; Mak, T. C. W. *J. Am. Chem. Soc.* **1990**, *112*, 2284–2291.

(27) López, I.; Ertem, M. Z.; Maji, S.; Benet-buchholz, J.; Keidel, A.; Kuhlmann, U.; Hildebrandt, P.; Cramer, C. J.; Batista, V. S.; Llobet, A. *Angew. Chem. Int. Ed.* **2014**, *53*, 205–209.

(28) Liu, X.; Wang, F. *Coord. Chem. Rev.* **2012**, *256*, 1115–1136.

(29) Guan, X.; Chan, S. L. -F.; Che, C. -M. *Chem. Asian J.* **2013**, *8*, 2046–2056.

(30) Vannucci, A. K.; Hull, J. F.; Chen, Z.; Binstead, R. A.; Concepcion, J. J.; Meyer, T. J. *J. Am. Chem. Soc.* **2012**, *134*, 3972-3975.

(31) Naota, T.; Takaya, H.; Murahashi, S.-I. *Chem. Rev*. **1998**, *98*, 2599-2660.

(32) Pagliaro, M.; Campestrini, S.; Ciriminna, R. *Chem. Soc. Rev.* **2005**, 34, 837-845.

(33) Arockiam, P. B.; Bruneau, C.; Dixneuf, P. H. *Chem. Rev*. **2012**, *112*, 5879-5918.

(34) Ishizuka, T.; Ohzu, S.; Kotani, H.; Shiota, Y.; Yoshizawa, K.; Kozima T. *Chem. Sci.* **2014**, *5*, 1429–1436.

(35) Ohzu, S.; Ishizuka, T.; Hiray, Y.; Jiang, H.; Sakaguchi, M.; Ogura, T.; Fukuzumi, S.; Kozima, T. *Chem. Sci.* **2012**.

(36) Che, C. -M.; Lai, T. -F.; Wong, K. -Y. *Inorg. Chem.* **1987**, *26*, 2289–2299.

(37) Lam, W. W. Y.; Yiu, S. -M.; Yiu, D. T. Y.; Lau, T. -C.; Yip, W. -P.; Che, C. M. *Inorg. Chem.* **2003**, *42*, 8011–8018.

(38) Lebeau, E. L.; Meyer, T. J. *Inorg. Chem.* **1999**, *38*, 2174–2181.

(39) Chan, S. L. -F.; Kan, Y. -H.; Yip, K. -L.; Huang, J. -S.; Che, C. -M. *Coord. Chem. Rev.* **2011**, *255*, 899–919.

(40) Kojima, T.; Hirai, Y.; Ishizuka, T.; Shiota, Y.; Yoshizawa, K.; Ikemura, K.; Ogura, T.; Fukuzumi, S. *Angew. Chem. Int. Ed.* **2010**, *49*, 8449–8453.

(41) Rodríguez, M.; Romero, I.; Sens, C.; Llobet, A. *J. Mol. Cat. A: Chem.* **2006**, *251*, 215–220.

(42) Wang, Y. -N.; Lau, K. -C.; Lam, W. W. Y.; Man, W. -L.; Leung, C. -F.; Lau, T. -C. *Inorg. Chem*. **2009**, *48*, 400–406.

(43) Huang, Y.; Vanover, E.; Zhang, R. *Chem. Commun.* **2010**, *46*, 3776–3778.

(44) Che, C. -M.; Tang, W. -T.; Wong, W. -T.; Lai, T. -F. *J. Am. Chem. Soc.* **1989**, *111*, 9048–9056.

(45) Abebrese, C.; Huang, Y.; Pan, A.; Yuan, Z.; Zhang, R. *J. Inorg. Biochem.* **2011**, *105*, 1555–1561.

(46) Che, C. -M.; Tang, W. -T.; Lee, W. -O.; Wong, K. -Y.; Lau, T. -C. *J. Chem. Soc. Dalton Trans.* **1992**, 1551–1556.

(47) Groves, J. T.; Quinn, R. *J. Am. Chem. Soc.* **1985**, *107*, 5790–5792.

(48) Mouzopoulou, B.; Kozlowski, H.; Katsaros, N.; Garnier-suillerot, A. *Inorg. Chem.* **2001**, *49*, 6923–6929.

(49) Che, C. -M.; Wong, K. -Y.; Poon, C. -K. *Inorg. Chem.* **1985**, *24*, 1797–1800.

(50) Lam, W. W. Y.; Man, W. -L.; Lau, T.-C. *Coord. Chem. Rev.* **2007**, *251*, 2238–2252.

(51) Cheng, W. -C.; Yu, W. -Y.; Li, C. -K.; Che, C. -M. *J. Org. Chem*. **1995**, *60* 6840–6846.

(52) Lam, W. W. Y.; Man, W. -L.; Wang, Y. -N.; Lau, T. -C. *Inorg. Chem.* **2008**, *47*, 6771–6778.

(53) Lam, W. W. Y.; Lee, M. F. W.; Lau, T. -C. *Inorg. Chem*. **2006**, *45*, 315-321.

(54) Man, W. -L.; Lam, W. W. Y.; Wong, W. -Y.; Lau, T. -C. *J. Am. Chem. Soc.* **2006**, *128*, 14669–14675.

(55) Che; C. -M.; Wong, K. -Y. *J. Chem. Soc. Dalton Trans*. **1989**, 2065–2067.

(56) Yiu, D. T. Y.; Lee, M. F. W.; Lam, W. W. Y.; Lau, T. -C. *Inorg. Chem.* **2003**, *42*, 1225–1232.

(57) Matsuo, T.; Mayer, J. M. *Inorg. Chem.* **2005**, *44*, 2150–2158.

(58) Mauzerall, D.; Westheimer, F. H. *1- Benzildihydronicotinamide- A Model for reduced DPN*, **1955**, *77*, 2261-2264.

(59) Man, W. -L.; Lam, W. W. Y.; Ng, S. -M.; Tsang, W. Y. K.; Lau, T. -C. *Chem. Eur. J.* **2012**, *18*, 138–144.

(60) Song, N.; Zhang, M. -T.; Binstead, R. A.; Fang, Z.; Meyer, T. J. *Inorg. Chem*. **2014**, *53*, 4100-4105.

(61) Fackler, N. L. P.; Zhang, S.; O'Halloran, T. V.; *J. Am.Chem. Soc.*, **1996**, *118*, 481-482.

(62) Lau, T.-C.; Kochi, J. K.; *J. Chem. Soc., Chem.Commun.*, **1987**, 798-799;

(63) Lau, T.-C.; Kochi, J. K. *Inorg. Chem*., **1990**, *29*, 4190-4195.

(64) Bailey, A. J.; Griffith, W. P.; White A. J. P.; Williams, D. J. ; *J. Chem. Soc., Chem. Commun.*, **1994**, 1833-1834.

(65) Cheung, W.-C.; Yu, W.-Y.; Cheung, K.-K.; Che, C.-M. *J. Chem. Soc., Chem. Commun*., **1994**, 1063-1064.

(66) Dovletoglou, A.; Adeyemi, S. A.; Lynn, M. H.; Hodgson, D. J.; Meyer, T. J. *J. Am. Chem. Soc.*, **1990**, *112*, 8989-8990.

(67) Li, C.-K.; Che, C.-M.; Tong, W.-F.; Tang, W.-T.; Wong K.-Y.; Lai, T.-F. *J. Chem. Soc., Dalton Trans.*, **1992**, 2109-2116.

(68) Mak, T. C. W.; Che, C. -M.; Wong, K. -Y. *J. Chem. Soc., Chem. Commun.* **1985**, 986–988.

(69) Dhuri, S. N.; Mi, S. S.; Lee, Y. M.; Hirao, H.; Wang, Y.; Nam, W.; Shaik, S. *Angew. Chemie - Int. Ed.* **2008**, *47*, 3356–3359.

(70) Che, C. -M.; Zhang, J. -L.; Zhang, R.; Huang, J. -S.; Lai, T. -S.; Tsui, W. -M.; Zhou, X. -G.; Zhou, Z. -Y.; Zhu, N.; Chang, C. K. *Chem. Eur. J.* **2005**, *11*, 7040–7053.

(71) Lai, T. -S.; Zhang, R.; Cheung, K. -K.; Kwong, H. -L.; Che, C. -M. *Chem. Commun.* **1998**, 1583–1584.

(72) Meyer, T. J.; Huynh, M. H. V. *Inorg. Chem.* **2003**, *42*, 8140–8160.

(73) Fukuzumi, S.; Kotani, H.; Lee, Y. -M.; Nam, W. *J. Am. Chem. Soc.* **2008**, *130*, 15134–15142.

(74) Fukuzumi, S.; Tokuda, Y.; Kitano, T.; Okamoto, T.; Otera, J. *J. Am. Chem. Soc.* **1993**, *115*, 8960–8968.

(75) Yoon, H.; Lee, Y. -M.; Nam, W.; Fukuzumi, S. *Chemcomm*. **2012**.

(76) Fukuzumi, S.; Koumitsu, S.; Hironaka, K.; Tanaka, T. *J. Am. Chem. Soc*. **1987**, *109*, 305–316.

(77) Fukuzumi, S.; Ohkubo, K.; Tokuda, Y.; Suenobu, T. *J. Am. Chem. Soc*. **2000**, *122*, 4286–4294.

(78) Jeong, Y. J.; Kang, Y.; Han, A. -R.; Lee, Y. -M.; Kotani, H.; Fukuzumi, S. *Angew. Chem. Int. Ed*. **2008**, *47*, 7321–7324.

(79) Lee, J. Y.; Lee, Y. -M.; Kotani, H.; Nam, W.; Fukuzumi, S. *Chem, Commun*. **2009**, 704–706.

(80) Fukuzumi, S.; Fujioka, N.; Kotani, H.; Ohkubo, K.; Lee, Y. -M.; Nam, W. *J. Am. Chem. Soc.* **2009**, *131*, 17127–17134.

(81) Han, Y.; Lee, Y. -M.; Mariappan, M.; Fukuzumi, S.; Nam, W. *Chem. Commun.* **2010**, *46*, 8160–8162.

(82) Fukuzumi, S.; Kotani, H.; Prokop, K. A.; Goldberg, D. P. *J. Am. Chem. Soc.* **2011**, *133*, 1859–1869.

(83) Mayer, J. M. *Acc. Chem. Res.* **1998**, *31*, 441–450.

(84) Borovik, A. S. *Acc. Chem. Res*. **2005**, *38*, 54–61.

(85) Goldsmith, C. R.; Cole, A. P.; Stack, T. D. P. *J. Am. Chem. Soc*. **2005**, *127*, 9904–9912.

(86) Kojima, T.; Nakayama, K.; Ikemura, K.; Ogura, T.; Fukuzumi, S. *J. Am. Chem. Soc.* **2011**, *133*, 11692–11700.

(87) Cho, K. -B.; Wu, X.; Lee, Y. -M.; Kwon, Y. H.; Shaik, S.; Nam, W. *J. Am. Chem. Soc.* **2012**, *134*, 20222-20225.

Overall Summary and conclusion

The thesis incorporates synthesis and characterization sixteen new compounds and their roles in catalytic oxidative transformations. The non heme ligands employed in this study includes *N*,*N′*-Bis(8-quinoline)ethane-1,2-diamine (bqenH_2), *N*,*N′*-dimethyl-*N*,*N′*-bis(8-quinolin)ethane-1,2-diamine (bqenMe_2), *N*,*N*'-dimethyl-*N*-(2-(methyl(pyridin-2-ylmethyl)amino)ethyl)-*N*'-(pyridin-2-ylmethyl)ethane-1,2-diamine (N3Py2) and 1,4,8,11-tetramethyl-1,4,8,11-tetraazacyclotetradecane (14-TMC). The ligand bqenMe_2 and N3Py2 were prepared reductive methylation. The bqenH_2 and bqenMe_2 along with auxiliary ligands were used for the synthesise of eight new nickel(II) compounds **1**-**8**. All compounds were characterized by spectroscopic (IR, UV-Vis), elemental analysis, ESI-MS and electrochemical techniques. The compound **3-5** and **7** were characterized by single crystal X-ray diffractometry. The efficacy of **1-8** in oxidation of alkanes using *m*-CPBA was investigated and the finding of this study revealed that only two nickel(II) compounds (**1** and **2)** showed high reactivity towards the oxidation of alkanes giving alcohol as the major product. The ligand N3Py2 is reported for the first time and it gave a single aqua site compound **9** which was thoroughly characterized using combination seveal techniques including single crystal X-ray crystallography. The reaction of **9** with H_2O_2 and trimethylamine gave a quite stable stable intermediate in solution proposed as Mn(III)-peroxo species **9a** which showed efficient reactivity towards aldehyde oxidation. The reactivity of intermediate **9a** was investigated in aldehyde deformylation reaction and possesses nucleophilic character. **9** also behaved as efficient catalyst in the epoxidation of alkenes. N3Py2 also gave compounds of Co(II), Ni(II) and Cu(II) (**10-12)** which have well characterized. **10-12** were tested in catalytic alkanes hydroxylation in presence of *m*-CPBA. The effect of counter anions on the yields of organic products was investigated for compounds **10-15**. This work also incorporates a study on the reactivity of high valent

trans-dioxoruthenium(VI) perchlorate **16** containing 14-TMC towards NADH analogues and alkanes. The mechanisms of hydride ion transfer vs hydrogen atom transfer have been proposed with sufficient evidences obtained from spectroscopy.

Appendix

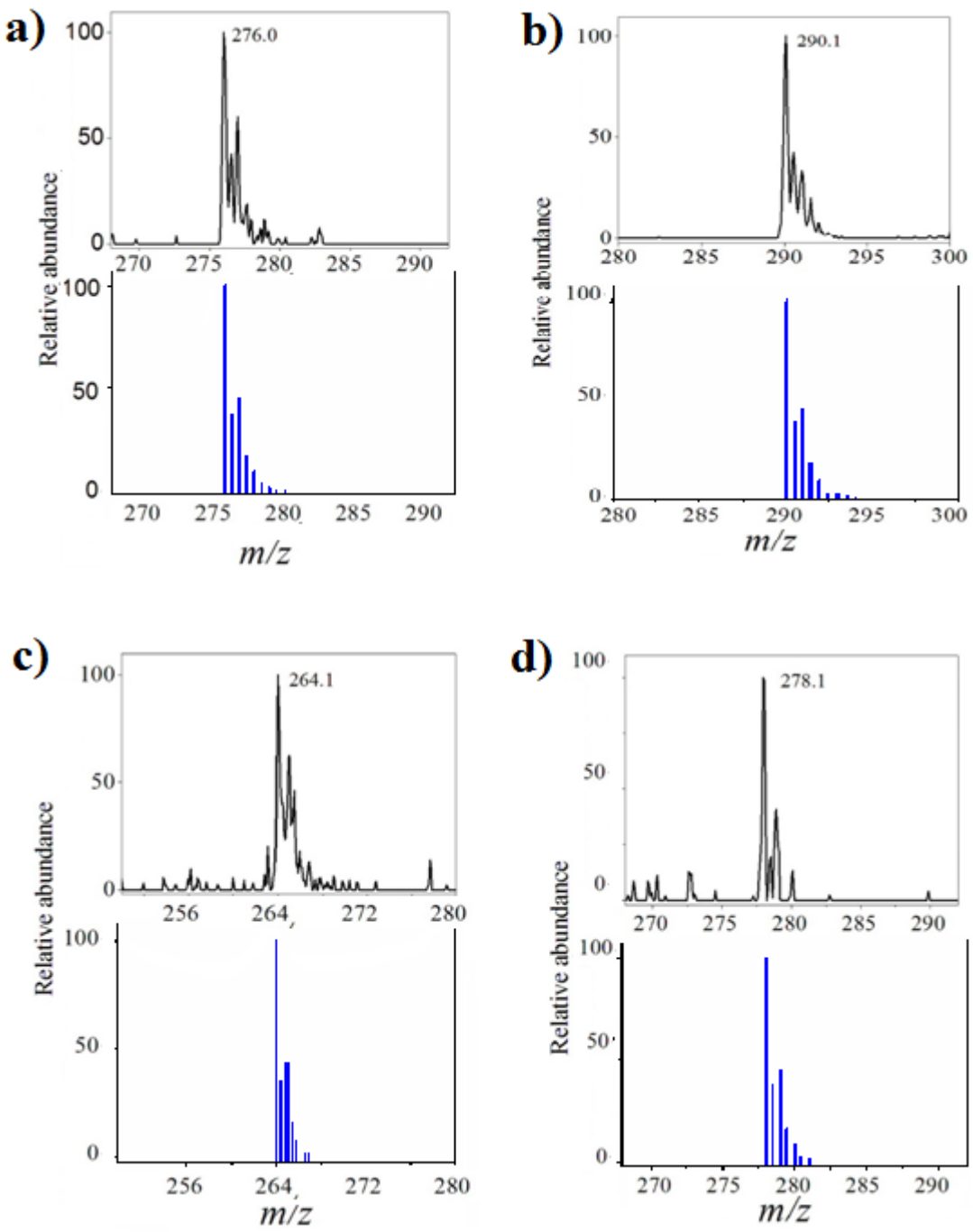

Figure A1 *ESI-MS spectra of compounds (a)* ***3****, (b)* ***4****, (c)* ***5*** *and (d)* ***6*** *in acetonitrile solvent showing observed isotopic distribution pattern (black) with simulation (blue)*

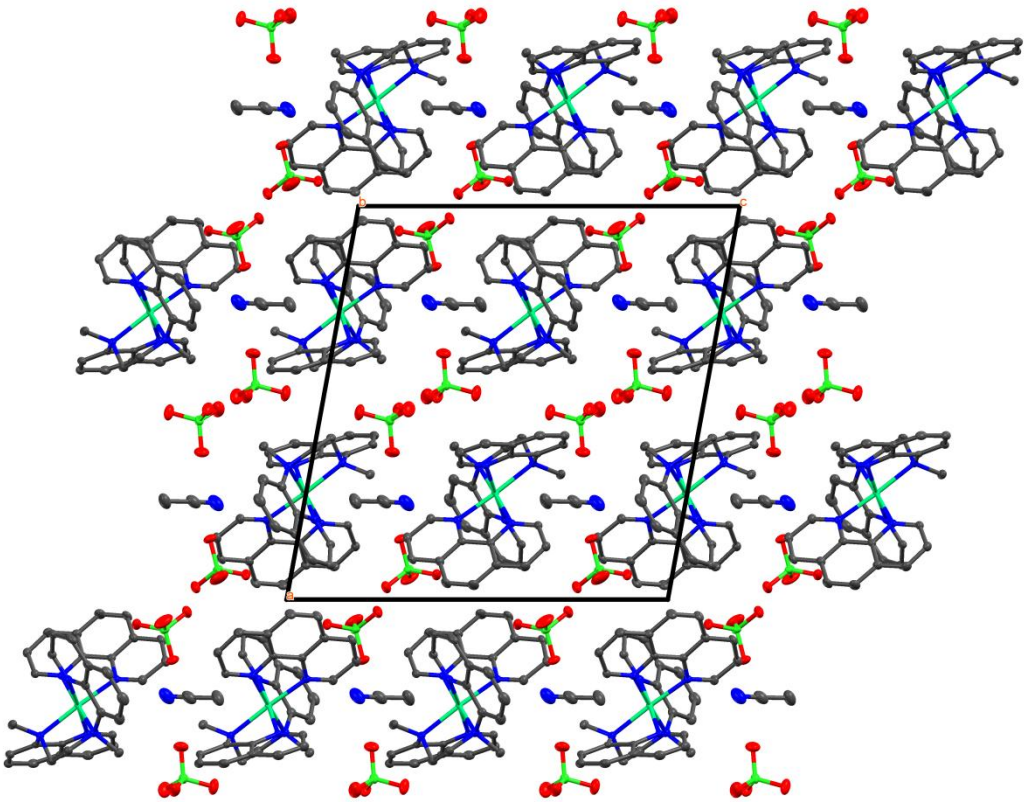

Figure A2 *A view of the packing diagram of* ***3*** *along the a-axis. Color code: C, black; H, medium grey; N, blue; O, red; Cl, green and Ni, sky blue.*

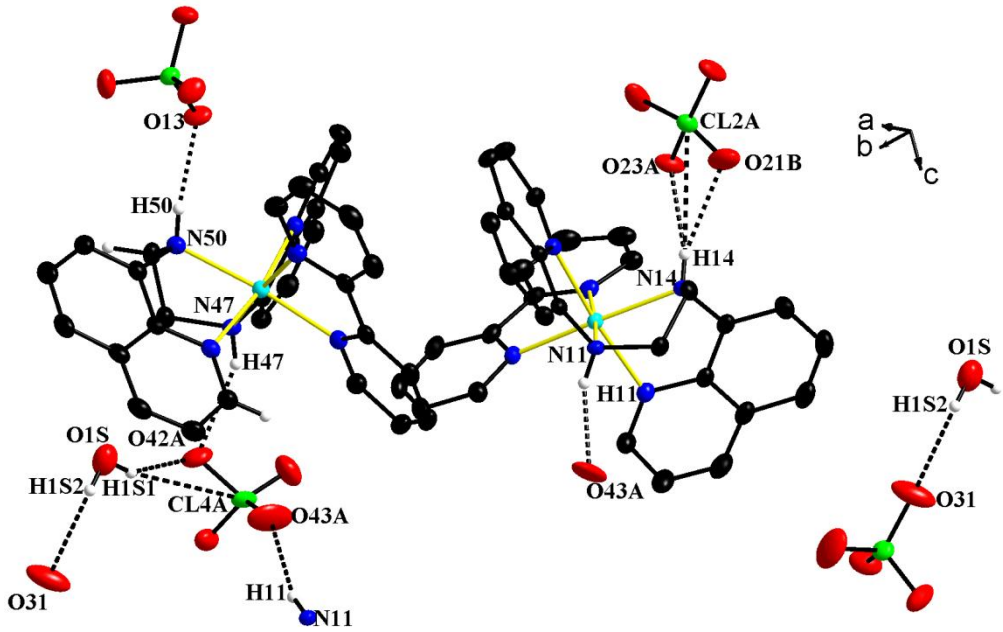

Figure A3 *Hydrogen bonding interactions in* ***5*** *with atom labelling scheme of atoms involved in hydrogen bonding. Hydrogen atoms which are not involved in hydrogen bonding are omitted for clarity.*

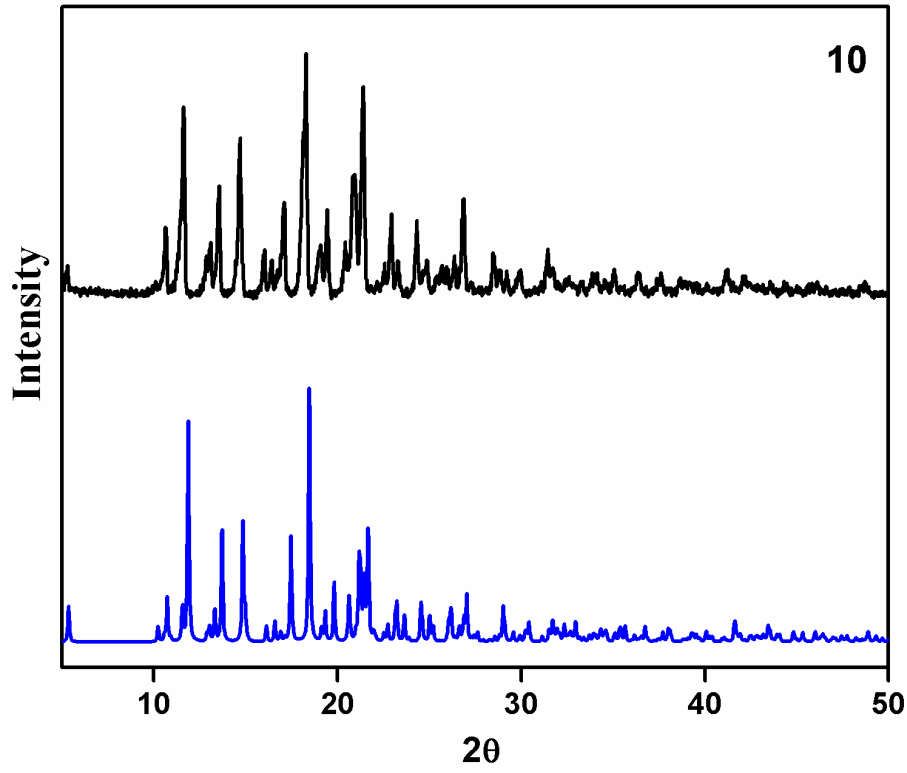

Figure A4 *PXD pattern of the* ***10*** *(black) obtained experimentally compared with the PXD pattern generated from the single crystal data(blue)showing similar pattern*

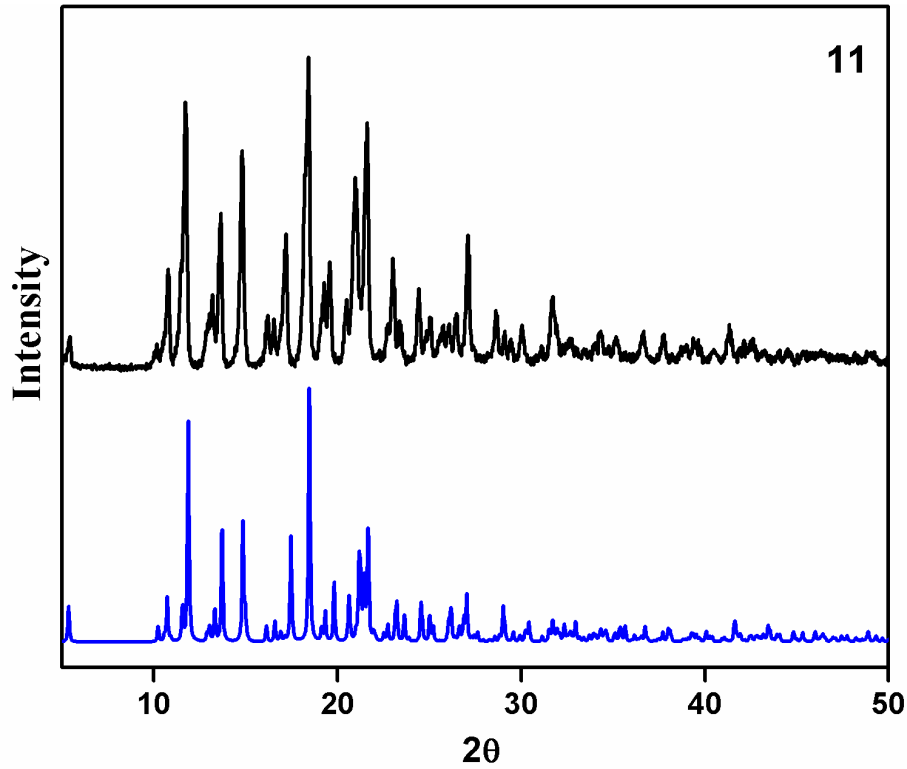

Figure A5 *PXD pattern of the* ***11*** *(black) obtained experimentally compared with the PXD pattern generated from the single crystal data(blue) showing similar pattern*

List of publications and manuscript under preparation

1. **Narulkar, D. D.**; Patil, A. R.; Naik, C. C.; Dhuri, S. N.; "Synthesis, Characterisation, *cis*-Ligand Substitution and Catalytic Alkane Hydroxylation by Mononuclear Nickel(II) Complexes Stabilized with Tetradentate Tripodal Ligands" *Inorganica Chimica Acta* **2015**, *427*, 248–258. DOI:10.1016/j.ica.2015.01.009 (IF: 2.002) (**Chapter III**)

2. **Narulkar, D. D.**; Srivastava, A. K.; Butcher, R. J.; Dhuri, S. N. "Crystal structure of mononuclear non-heme Ni(II) octahedral complex: $[Ni(II)(bqenH_2)(bpy)](ClO_4)_2$" *Journal of structural Chemistry* **2018**, 59, 1207-1214 DOI:10.26902/JSC20180520 (IF: 0.472) (**Chapter III**)

3. Harmalkar S. S., Narulkar D. D., Butcher R. J. Deshmukh M. S., Srivastava A. K., Mariappan M., Lama Prem, Dhuri S. N."Dual-site aqua mononuclear nickel(II) complexes of non-heme trtradentate ligands: Synthesis, characterization and reactivity" " *Inorganica Chimica Acta* **2019**, *486*, 425–434. DOI:10.1016/j.ica.2018.10.069 (IF: 2.002) (**Chapter III**)

4. "Mn(III)-peroxo complex supported by non-heme pentadentate ligand N3Py2: Reactivity in oxidative reactions" (manuscript under preparation) (**Chapter IV**)

5. **Narulkar, D. D.**; Srivastava, A. K.; Butcher, R. J.; Ansy, K. M.; Dhuri, S. N. "Synthesis and characterization of N3Py2 ligand-based cobalt(II), nickel(II) and copper(II) catalysts for efficient conversion of hydrocarbons to alcohols" in *Inorganica Chimica Acta* **2017**, *467*, 405–414. DOI:10.1016/j.ica.2017.08.027. (IF: 2.002) (**Chapter V**)

6. Dhuri, S. N.; Lee, Y. –M.; Seo, M. S.; Cho, J.; **Narulkar D. D.**; Fukuzumi S.; Nam, W. "Mechanistic insights into the reactions of hydride transfer versus hydrogen atom transfer by a trans-dioxoruthenium(VI) complex" *Dalton Trans*., **2015**, *44*, 7634–7642. DOI:10.1039/C5DT00809C. (IF: 4.029) (**Chapter VI**)

7. **Narulkar, D. D**.; Jalmi Gaude, T. A.; Dhuri, S. N. "Phthalate precursor mediated synthesis of cadmium oxide nanoparticles and their photocatalytic application*" Indian Journal of Chemistry*, **2017**, 56A, 1014-1020. (IF: 0.494)

Papers presented at conferences/symposia

1. "Hexacoordinated Nickel(II) complexes derived from Nitrogen donor ligands: synthesis and characterization" at the National Conference on "Current Research in Chemical Sciences (CRCS-2013)" held on January 22nd and 23rd, 2013 organized by Department of Chemistry, Shivaji University, Kolhapur.

2. "*trans*-Ruthenium(VI)-Dioxo Complex in the Hydride Transfer and H-atom Abstraction reactions" at the "CRSI (Chemical Research Society of India) Mid year symposium 2013" held on July 12-13, 2013 organized by Department of Chemistry, National Institute of Technology Karnataka, Mangalore, Karnataka.

3. "Synthesis and characterizations of cadmium oxide nanoparticles and their photocatalytic application" at the National level Symposium on "Materials characterization and Manufacturing (MCM-2016)" held on August 18th and 19th, 2016 jointly organized by Department of Mechanical Engineering, Padre Conceicao College of Engineering and Department of Physics, Goa University at Goa University.

4. "Synthesis, characterization, *cis*-ligand substitution and catalytic alkane hydroxylation by mononuclear nickel(II) complexes stabilized with tetradentate tripodal ligands" at the Symposium on "Recent Advancements in Chemical Sciences and RSC Research Scholar Meet" held on 13th November 2016 at Bits Pilani, K K Birla Goa Campus.

5. "The reactivity study of high valent *trans*-dioxoruthenium(VI) complex in hydride transfer and hydrogen atom transfer reactions at the "National Conference on New Frontiers in Chemistry-from Fundamentals to Applications-II (NFCFA2017)" held on Jan 28th-29th 2017 organized by BITS Pilani KK Birla Goa Campus.

6. "Synthesis and characterization of Mn(III)-peroxo complex: Reactivity in oxidative nucleophilic reactions and epoxidation reactions" at the 21st CRSI (Chemical Research society of India) held on July 14-16, 2017 organized by CSIR-Indian Institute of Chemical Technology, Hyderabad, India.

Conference / Workshop Attended

1. Attended the International Conference on "Green Chemistry: Catalysis, Energy and Environment" held on January 22-24, 2015 organized by Department of chemistry, Goa University.

2. Attended and Participated in the One day State level workshop on "Chromatographic Techniques in Pharmaceutical Analysis" held on 21st March 2017 organized by the Department of Chemistry, Dnyanprassarak Mandal's College and Research Centre, Assagao, Bardez-Goa.

Inorganica Chimica Acta 427 (2015) 248–258

Contents lists available at ScienceDirect

Inorganica Chimica Acta

journal homepage: www.elsevier.com/locate/ica

Synthesis, characterization, *cis*-ligand substitution and catalytic alkane hydroxylation by mononuclear nickel(II) complexes stabilized with tetradentate tripodal ligands

Dattaprasad D. Narulkar, Amit R. Patil, Chandan C. Naik, Sunder N. Dhuri *

Department of Chemistry, Goa University PO, Taleigao Plateau, Panaji 403206, Goa, India

ARTICLE INFO

Article history:
Received 25 October 2014
Received in revised form 23 December 2014
Accepted 5 January 2015
Available online 12 January 2015

Keywords:
Nickel
N,N′-bis(8-quinolyl)ethane-1,2-diamine
N,N′-dimethyl-*N,N′*-bis(8-quinolyl)ethane-1,2-diamine
Crystal structure
ESI-mass spectra
Hydroxylation

ABSTRACT

The synthesis and spectroscopic characterization of the mononuclear complexes $[Ni(bqenH_2)(H_2O)_2](ClO_4)_2$ **1** and $[Ni(bqenMe_2)(H_2O)_2](ClO_4)_2$ **2** (where $bqenH_2$ = *N,N′*-bis(8-quinolyl)ethane-1,2-diamine and $bqenMe_2$ = *N,N′*-dimethyl-*N,N′*-bis(8-quinolyl)ethane-1,2-diamine) is reported. The $bqenMe_2$ ligand was prepared by a simple modification to the earlier procedure. The reaction of **1** and **2** with 1,10-phenanthroline (phen) or 2,2′-bipyridine (bpy) resulted in the formation of $[Ni(bqenH_2)(phen)](ClO_4)_2$ **3**, $[Ni(bqenMe_2)(phen)](ClO_4)_2$ CH_3CN **4**, $[Ni(bqenH_2)(bpy)](ClO_4)_2$ **5**, and $[Ni(bqenMe_2)(bpy)](ClO_4)_2$ **6**. The redox properties of **1**–**6** are reported. The crystal structures of **3** and **4** consist of distorted octahedral $[Ni(bqenH_2)(phen)]^{2+}$ and $[Ni(bqenMe_2)(phen)]^{2+}$ cations which are stabilized by N–H···O and C–H···O interactions. Compounds **1** and **2** afforded hydroxylation of alkanes with high alcohol to ketone ratio in the presence of *m*-CPBA oxidant.

1. Introduction

In biomimetic chemistry, the metal complexes are designed such that they resemble the active parts of metalloenzymes and correlate their structure–function relationship [1]. Several reports on non-heme metal complexes are available, especially of the first-row transition metals such as manganese [2–5], iron [6–11], copper [12–14] and cobalt [15] in their high valent metal-oxo, peroxo, superoxo forms and play crucial roles in the organic oxygenation reactions. The nickel metal is not an exception to this list, as a large number of nickel complexes with tripodal ligands such as tris(2-pyridylmethyl)amine (TPA), *N*-tetramethylated cyclam (*n*-TMC), *N*,*N*-dimethyl-*N′*,*N′*-bis(pyridin-2-ylmethyl)ethane-1,2-diamine (*iso*-BPMEN), *N*,*N*-dimethyl-*N′*,*N′*-bis(quinolin-2-ylmethyl)ethane-1,2-diamine (*iso*-BQMEN) are known (Scheme 1) [16–20]. In high valent nickel chemistry, the reactive nickel-dioxygen species such as nickel-superoxo, peroxo, acyl/alkyl peroxo are all well characterized [16–21]. The putative nickel-oxygen species (Ni^{III}=O or Ni^{II}–O) for the catalytic hydroxylation of alkanes using *m*-CBPA (*m*-chloroperbenzoic acid) has also been proposed in the literature [20–24].

The applications of nickel complexes are not exclusively limited to the chemical science and biomimetic fields, but vitally important in the different branches of biological sciences. A wide range of nickel complexes are known to exhibit an antioxidant and antimicrobial activity against the several microorganisms [25,26]. The nickel complexes of 1,10-phenanthroline (phen) and 2,2′-bipyridine (bpy) derivatives have shown the binding and cleavage of DNA residues [27–31]. Thus tuning the properties of metal complexes using an appropriate nonheme ligand architecture has become an art for the inorganic chemist from the days of Alfred Werner. Inspired by the versatility of nickel complexes and their applications in various fields especially in the organic oxidative transformations, here we focus on the synthesis of new Ni(II) compounds namely $[Ni(bqenH_2)(H_2O)_2](ClO_4)_2$ **1** and $[Ni(bqenMe_2)(H_2O)_2](ClO_4)_2$ **2** containing the tetradentate tripodal N4 ligands *N,N′*-bis(8-quinolyl)ethane-1,2-diamine ($bqenH_2$) and *N,N′*-dimethyl-*N,N′*-bis(8-quinolyl)ethane-1,2-diamine ($bqenMe_2$) respectively (Fig. 1).

The reactivity of **1** and **2** with 1,10-phenanthroline (phen) and 2,2′-bipyridine (bpy) has been investigated for the formation of compounds **3**–**6** (Fig. 1). Spectroscopic characterization, redox properties, crystal structure determination of **3** and **4** have been carried out. To probe the efficacy of synthesized compounds **1**–**6** for alkane hydroxylation, the catalytic oxidation of alkanes using

* Corresponding author. Tel.: +91 832 6519318.
E-mail address: sndhuri@unigoa.ac.in (S.N. Dhuri).

http://dx.doi.org/10.1016/j.ica.2015.01.009
0020-1693/

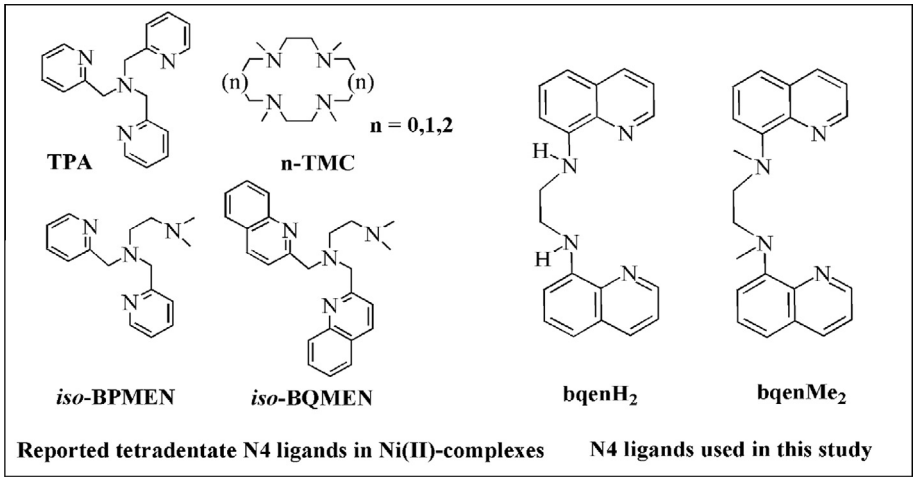

Scheme 1. Chemical structures of tetradendate tripodal ligands.

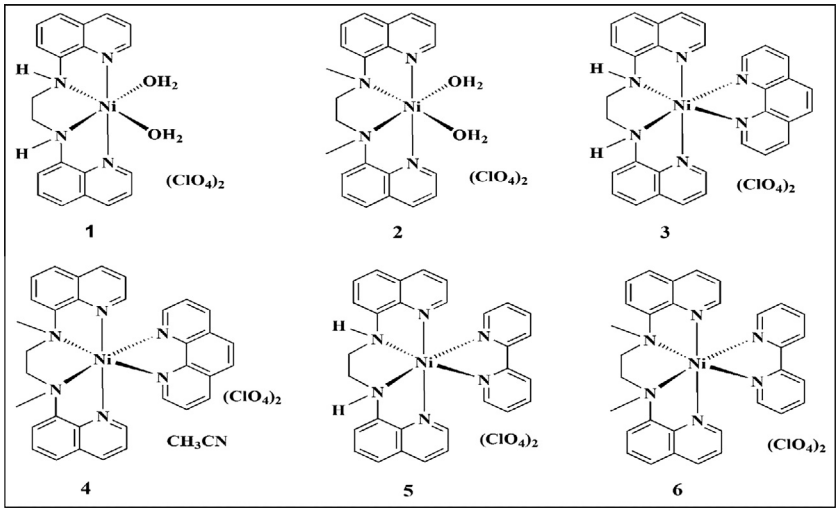

Fig. 1. Chemical structures of compounds **1**–**6**.

m-chloroperbenzoic acid (*m*-CPBA) as an oxidant has been studied. The results of these investigations are described in this paper.

2. Experimental details

2.1. Materials and methods

All the chemicals used in this study were purchased from commercial sources. The solvents were dried and distilled prior to use under the Ar or N_2 atmosphere. Elemental analysis was carried out on Elementar Variomicro Cube CHNS Analyser. Electrospray ionization mass (ESI-MS) spectra were measured on Thermo Finnigan (San Jose, CA, USA) LCQ™ Advantage MAX quadrupole ion trap instrument, by infusing samples directly into the source at 20 μL/min using a syringe pump. The spray voltage was set at 4.7 kV and the capillary temperature at 240 °C. The UV–Vis spectra were recorded in CH_3CN in the range 200–1100 nm using Agilent diode array 8453 UV–Vis spectrophotometer. The compounds were diluted in KBr powder and the infrared (IR) spectra were recorded in the region of 4000–400 cm^{-1} using Shimadzu (IR Prestige-21) FT-IR spectrometer. The ^1H and ^{13}C NMR spectra were recorded in $CDCl_3$ on Bruker Avance III 400 MHz NMR spectrometer. The cyclic voltammograms (CV) and differential pulse voltammograms (DPV) were recorded using Electrochemical Workstation-CH Instrument, Inc. CHI6107. A glass vessel containing sample solution was equipped with three-electrodes namely a platinum working electrode, platinum wire as counter electrode and standard calomel electrode as reference electrode. The experiments were carried in DMSO containing 0.1 M tetrabutylammonium hexafluorophosphate ($TBAPF_6$) as a supporting electrolyte and the solutions were purged with N_2 gas for around ~30 min prior to the each measurement. The single crystals of **3** and **4** suitable for X-ray studies were picked up and mounted directly on a Bruker SMART AXS diffractometer equipped with Mo Kα = 0.71073 Å radiation. The CCD data were integrated and scaled using Bruker-SAINT software package while SHEXTL V 6.12 was used for solving and refining the structures [32]. The non-hydrogen atoms were refined with the anisotropic displacement parameters while the hydrogen atoms were located at the calculated positions. In the catalytic oxidation reactions, the organic product analyses were carried out using Agilent Technologies 6890 N gas chromatograph (GC). The retention time and peak areas of the products were compared with authentic samples using decane as an internal standard.

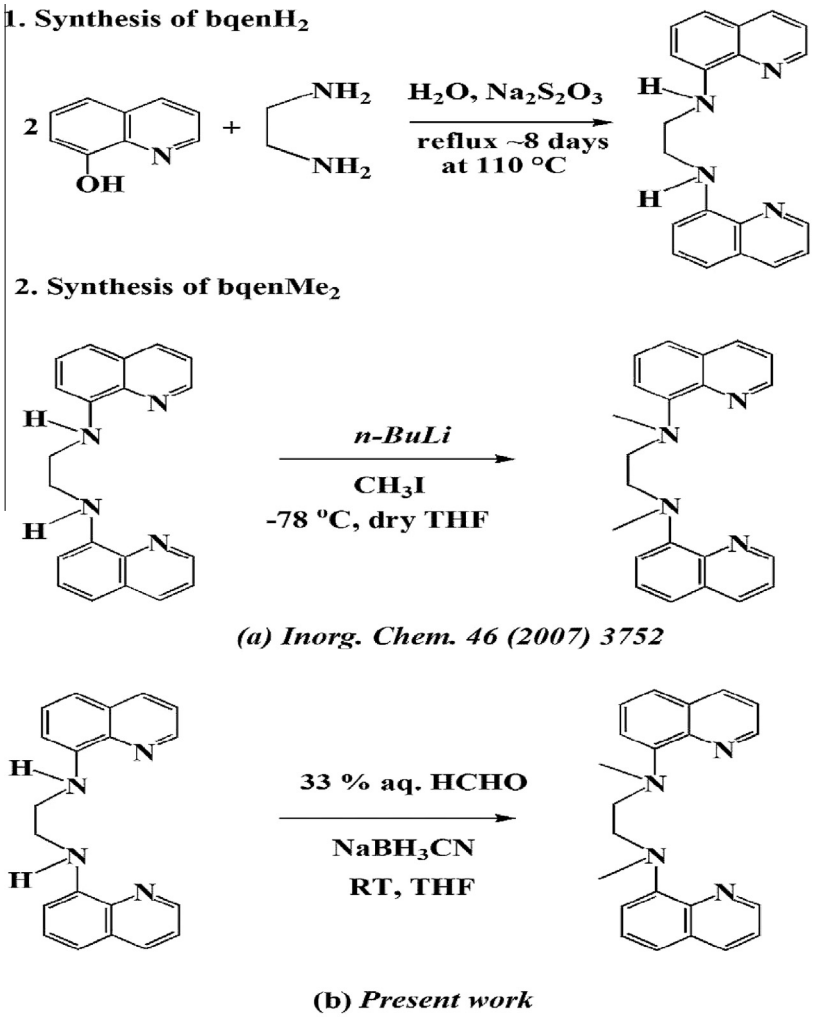

Scheme 2. Synthetic method used for the preparation of $bqenH_2$ and $bqenMe_2$.

2.2. Synthesis of ligands and compounds 1–6

2.2.1. Synthesis of N,N′-bis(8-quinolyl)ethane-1,2-diamine ($bqenH_2$)

The ligand $bqenH_2$ was prepared by following the literature procedure [33]. A mixture of 8-hydroxyquinoline (15.0 g, 103.3 mmol), ethylenediamine (3.1 g, 51.7 mmol), sodium metabisulphite (19.6 g, 103.3 mmol) and water (100 mL) was refluxed for about ~8 days at 110 °C. The reaction mixture was cooled at room temperature, then basified with aqueous sodium hydroxide solution (pH ~12) followed by extraction using dichloromethane (50 mL × 2). The solid formed after removal of dichloromethane was triturated with hot ethanol, filtered and then air dried. Yield of $bqenH_2$ (7.2 g, 44.0%). *Anal.* Calc. for $C_{20}H_{18}N_4$: C, 76.41; H, 5.77; N, 17.82. Found: C, 76.22; H, 5.62; N, 17.46%. IR (KBr, cm^{-1}): 3383 ν(NH); 1526 ν(C=N); ^{1}H NMR ($CDCl_3$, ppm): δ 8.69 (d, 2H, J = 2.2 Hz, 2-QnH), δ 8.06 (d, 2H, J = 2.2, 4-QnH), δ 7.37 (m, 4H, 3-QnH and 6-QnH), δ 7.07 (d, 2H, J = 8 Hz, 5-QnH), 6.77 (d, 2H, J = 4 Hz, 7-QnH), 6.42 (s, 2H, NH), 3.75 (s, 4H, NCH_2).

2.2.2. Synthesis of N,N′-dimethyl-N,N′-bis(8-quinolyl)ethane-1,2-diamine ($bqenMe_2$)

The ligand $bqenMe_2$ was prepared by a modification of the earlier procedure [33]. To a stirred THF solution (40 mL) of $bqenH_2$ (4.0 g, 12.7 mmol), about 21 mL of 37% aqueous formaldehyde (7.6 g, 254.5 mmol) was added. The solution slowly turned red after ~5 min. To this mixture solid sodium cyanoborohydride (1.6 g, 25.4 mmol) was added upon which the solution slowly turned to the original yellow color. The reaction mixture was then stirred for 24 h. The THF solvent was removed on a rotary evaporator and the yellow solid was filtered from the remaining aqueous solution. The compound was washed with cold ethanol for several times and dried under vacuum. The yellow solid was recrystallized from hot ethanol. Yield of $bqenMe_2$ (3.2 g, 74.0%). *Anal.* Calc. for $C_{22}H_{22}N_4$: C, 77.16; H, 6.48; N, 16.36. Found: C, 77.21; H, 6.64; N, 16.68%. IR (KBr, cm^{-1})1526 ν(C=N). ^{1}H NMR ($CDCl_3$, ppm): δ 8.76 (d, 2H, J = 6 Hz, 2-QnH,), δ 8.07(d, 2H, J = 6 Hz, 4-QnH), δ 7.36 (m, 6H, 3-, 5- and 6-QnH), δ 7.05(d, 2H, J = 6 Hz, 7-QnH), δ 3.96 (s, 4H, N-CH_2), δ 3.06 (s, 6H, NMe). ^{13}C NMR ($CDCl_3$, ppm): δ 149.3 (*ipso*), 147.3, 142.6 (*ipso*), 136.2, 129.6, 126.6, 120.73, 119.8, 115.5, 54.1 (N-CH_2), 41.3 (N-Me).

2.2.3. Synthesis of [Ni($bqenH_2$)(H_2O)$_2$](ClO_4)$_2$ (**1**)

Green colored $Ni(ClO_4)_2{\cdot}6H_2O$ (2.2 g, 6.0 mmol) was dissolved in CH_3CN (5 mL). To this, was added a solution of $bqenH_2$ (1.9 g, 6.0 mmol) in CH_2Cl_2 (5 mL) in drop wise manner. Color of the reaction mixture was observed to change slowly from blue to violet. After 2 h diethyl ether (10 mL) was added to the reaction mixture to obtain violet colored crystalline solid which was isolated by filtration, washed with diethyl ether (10 mL) and finally air dried. Yield of **1** (3.0 g, 83.0%). *Anal.* Calc. for $C_{20}H_{22}N_4Cl_2O_{10}Ni$: C, 39.51; H, 3.65; N, 9.21. Found: C, 39.46; H, 3.33; N, 9.29%. IR (KBr, cm^{-1}): 3265 ν(NH); 1518 ν(C=N); 1093, 621 ν(ClO_4^{-1}). λ_{max} (CH_3CN)/nm: 229, 302, 314, 528, 872 (ε/dm^3 mol^{-1} cm^{-1}) 58 500, 10 216, 8725, 8, 8.

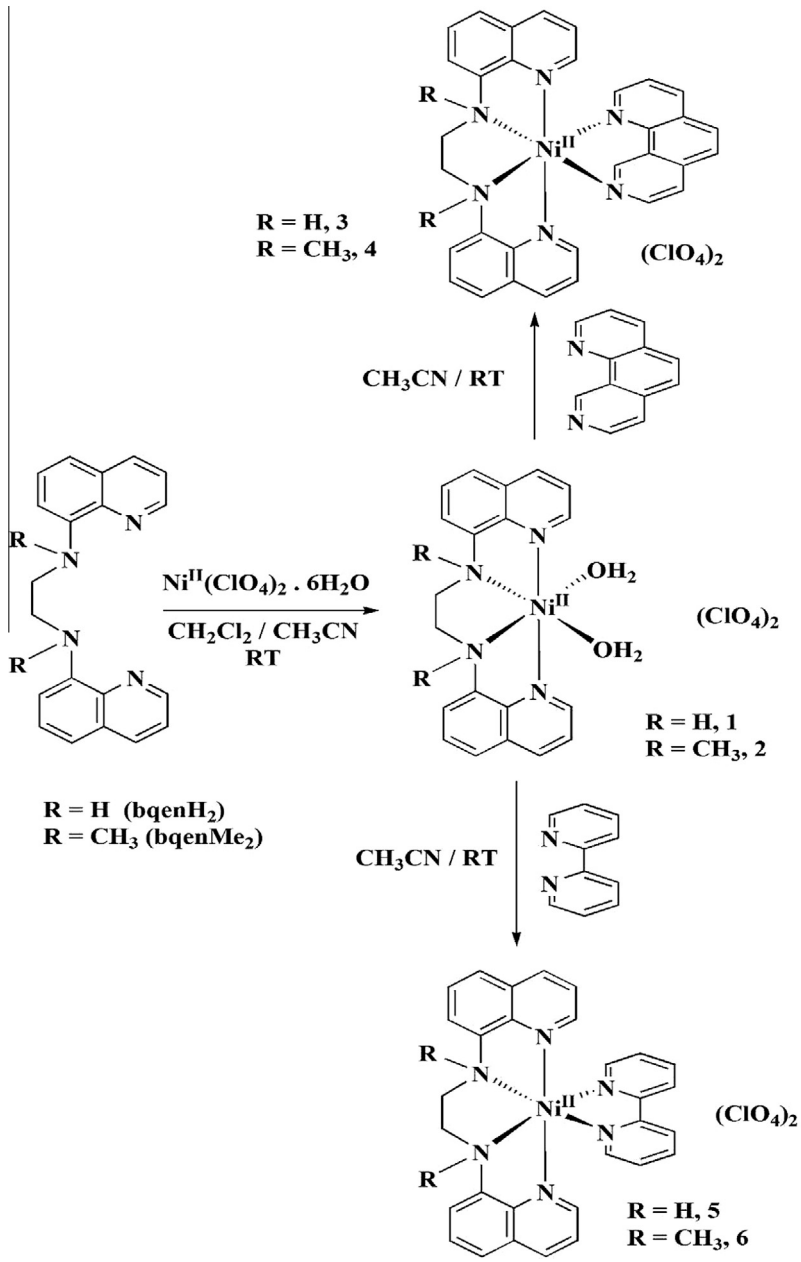

Scheme 3. Synthetic methodology used for the preparation of compounds **1**–**6**.

*2.2.4. Synthesis of [Ni(bqenMe$_2$)(H$_2$O)$_2$](ClO$_4$)$_2$ (**2**)*

The light pink colored compound was prepared by following the similar procedure as for compound **1** by taking bqenMe$_2$ (2.1 g, 6.0 mmol) instead of bqenH$_2$. Yield of **2** (3.1 g, 81.0%). *Anal.* Calc. for $C_{22}H_{26}N_4Cl_2O_{10}$ Ni: C, 41.54; H, 4.12; N, 8.81. Found: C, 41.16; H, 4.32; N, 8.65%. IR (KBr, cm^{-1}): 1518 ν(C=N); 1093, 621 ν(ClO$_4^{-1}$). λ_{max} (CH$_3$CN)/nm: 228, 302, 314, 528, 872 (ε/dm^3 mol^{-1} cm^{-1}): 57172, 11249, 9195, 9, 8.

*2.2.5. Synthesis of [Ni(bqenH$_2$)(phen)](ClO$_4$)$_2$ (**3**)*

Addition of CH$_3$CN (2 mL) solution of phen (0.20 g, 1.0 mmol) to the violet colored CH$_3$CN (3 mL) solution of **1** (0.61 g, 1.0 mmol) resulted in dark red colored solution. Slow diffusion of diethyl ether to this solution afforded red colored crystals after 4 days. Yield of **3** (0.6 g, 79.0%). *Anal.* Calc. for $C_{32}H_{26}N_6Cl_2O_8$Ni: C, 51.10; H, 3.48; N, 11.17. Found: C, 51.40; H, 3.71; N, 11.27%). IR (KBr, cm^{-1}): 3269 ν(NH); 1518 ν(C=N); 1093, 621 ν(ClO$_4^{-1}$). λ_{max} (CH$_3$CN)/nm: 227, 272, 294, 314, 589, 793 (ε/dm^3 mol^{-1} cm^{-1}) 65207, 30099, 15734, 7089, 21, 8.

*2.2.6. Synthesis of [Ni(bqenMe$_2$)(phen)](ClO$_4$)$_2$ CH$_3$CN (**4**)*

Similar procedure as mentioned for **3** was employed by reacting **2** (0.64 g, 1.0 mmol) in place of **1** to obtain violet colored crystals. Yield of **4** (0.62 g, 76.0%). *Anal.* Calc. for $C_{36}H_{33}N_7Cl_2O_8$Ni: C, 55.66; H, 4.05; N, 11.94. Found: C, 55.41; H, 4.17; N, 11.74%. IR (KBr, cm^{-1}): 1518 ν(C=N); 1093, 621 ν(ClO$_4^{-1}$). λ_{max} (CH$_3$CN)/nm: 225, 272, 296, 315, 501, 795 (ε/dm^3 mol^{-1} cm^{-1}) 67439, 23913, 31074, 6609, 11, 9.

*2.2.7. Synthesis of [Ni(bqenH$_2$)(bpy)](ClO$_4$)$_2$ (**5**)*

Reaction of bpy (0.16 g, 1.0 mmol) with compound **1** (0.61 g, 1.0 mmol) in CH$_3$CN resulted in dark reddish-brown colored solution. Slow diffusion of diethyl ether to this solution afforded dark reddish-brown colored crystalline compound. Yield of **5**

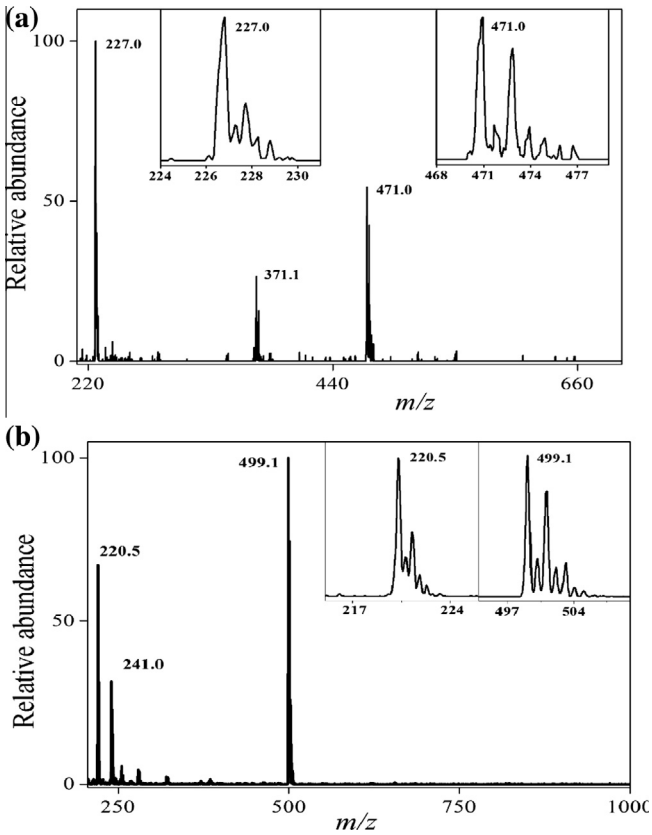

Fig. 2. ESI-MS spectrum of (a) **1** and (b) **2** measured in CH_3CN. Inset shows the isotope distribution patterns for the prominent peaks.

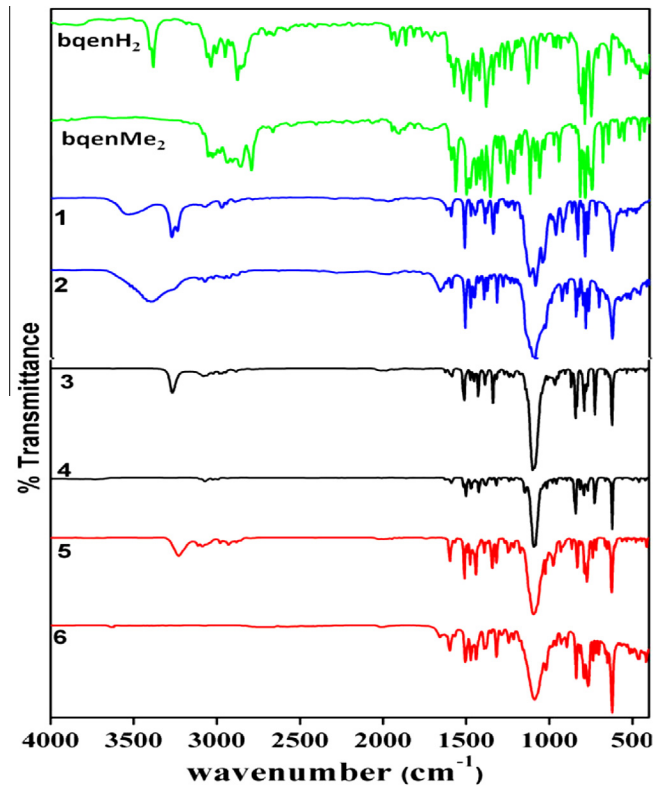

Fig. 3. Infrared spectra of ligands $bqenH_2$ and $bqenMe_2$ (green line), compounds **1**, **2** (blue line), **3**, **4** (black line) and **5**, **6** (red line). (For interpretation of the references to color in this figure legend, the reader is referred to the web version of this article.)

(0.7 g, 84.0%). *Anal.* Calc. for $C_{30}H_{26}N_6Cl_2O_8Ni$: C, 49.48; H, 3.60; N, 11.54. Found: C, 49.76; H, 3.35; N, 11.26%. IR (KBr, cm^{-1}): 3228 ν(NH); 1518 ν(C=N); 1093, 621 $\nu(ClO_4)^{-1}$. λ_{max} (CH_3CN)/nm: 230, 297, 308, 489, 793 ($\varepsilon/dm^3\ mol^{-1}\ cm^{-1}$) 57596, 24834, 22673, 29, 9.

*2.2.8. Synthesis of [Ni(bqenMe$_2$)(bpy)](ClO$_4$)$_2$ (**6**)*

Similar procedure as mentioned for **5** was used in the preparation of **6**. Here the reaction of bpy with **2** (0.64 g, 1.0 mmol) resulted in the formation of reddish crystalline solid. Yield of **6** (0.6 g, 82.0%). Calc. for $C_{32}H_{30}N_6Cl_2O_8Ni$: C, 50.83; H, 4.00; N, 11.11%. Found: C, 50.74; H, 4.14; N, 11.38%. IR (KBr, cm^{-1}): 1518 ν(C=N); 1093, 621 $\nu(ClO_4)^{-1}$. λ_{max} (CH_3CN)/nm: 229, 283, 315, 528, 872 ($\varepsilon/dm^3\ mol^{-1}\ cm^{-1}$) 56136, 19013, 7631, 10, 9.

3. Results and discussion

*3.1. Description for the synthesis of ligands, complexes 1,2 and cis-ligand exchange to form **3**–**6***

The first iron(II) complex namely [Fe(bqenMe$_2$)(CF_3SO_3)$_2$] of $bqenMe_2$ was reported by Britovsek et al. and shown to be an excellent catalyst for the oxidation of cyclohexane using H_2O_2 oxidant [33]. Nam and co-workers then demonstrated that $bqenMe_2$ complexes of manganese and iron such as [Mn($bqenMe_2$)(CF_3SO_3)$_2$] and [Fe($bqenMe_2$)(CF_3SO_3)$_2$] produce highly reactive intermediates that can oxidize alkanes and alcohols using peracetic acid [34,35]. The importance of $bqenMe_2$ ligand is thus clearly evidenced from these reports in biomimetic chemistry. For the ligand synthesis, the alkylation of R_2N–H is tedious and most challenging step which is normally carried out using an alkylating agent and strong base such as sodium hydride or *n*-butyllithium. However,

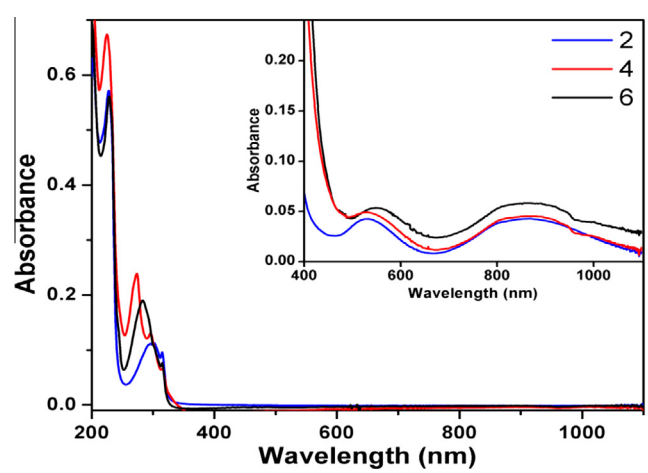

Fig. 4. Overlaid UV–Vis spectra of **2**, **4** and **6** (10^{-5} M) in CH_3CN. Inset show an expanded view of the region 400–1100 nm for *d*–*d* bands.

these reactions need special conditions such as dry solvents, inert atmospheres and low temperature (−78 °C). The synthesis of $bqenMe_2$ was earlier reported from the reaction of parent secondary amine $bqenH_2$, *n*-butyllithium and methyl iodide at −78 °C [33] (Scheme 2).

In this work, we have synthesized $bqenMe_2$ by a simple synthetic route that involves the reductive methylation of $bqenH_2$ using aqueous formaldehyde and sodium cyanoborohydride at room temperature (Scheme 2). The ligand $bqenH_2$ was prepared by following the reported procedure [33]. Both the ligands $bqenH_2$ and $bqenMe_2$ were characterized by ^1H and ^{13}C NMR spectroscopy

Table 1
UV–Vis data of compounds **1**–**6**.

Compound	$^3A_{2g} \rightarrow {}^3T_{1g}(F)$, nm ($\varepsilon$/dm^3 mol^{-1} cm^{-1})	$^3A_{2g} \rightarrow {}^3T_{2g}$, nm ($\varepsilon$/dm^3 mol^{-1} cm^{-1})
1	528 (8)	872 (9)
2	528 (9)	872 (8)
3	489 (21)	793 (8)
4	552 (11)	872 (9)
5	489 (29)	793 (9)
6	528 (10)	872 (12)

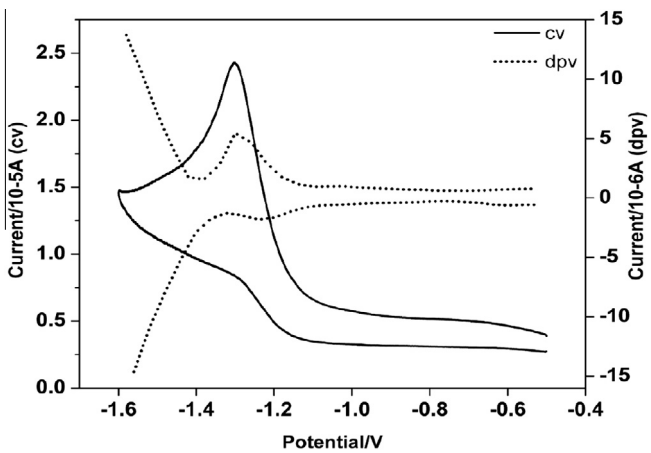

Fig. 5. CV (solid line) and DPV (dotted line) of **2** recorded at scan rate of 100 mV s^{-1} in DMSO containing 0.1 M of $TBAPF_6$ as supporting electrolyte.

(see Figs. S1–S4 in the supporting information). The reaction of $bqenH_2$ and $bqenMe_2$ with $Ni(ClO_4)_2{\cdot}6H_2O$ in CH_3CN afforded compounds **1** and **2** respectively in good yields. Our efforts to obtain the single crystals of compound **1** and **2** suitable for X-ray diffraction studies were not fruitful. Complex **1** was reacted with auxiliary bidentate N-donor ligands such as phen and bpy in CH_3CN resulting in the exchange of weakly coordinating solvent molecules (CH_3CN or H_2O) to obtain **3** and **5**. Under identical reaction conditions, the compounds **4** and **6** were prepared using **2** as a starting material. The single crystals of **3** and **4** were isolated on slow diffusion of diethyl ether into their solutions and directly used for X-ray data collection, however we were unable to grow the single crystals of **5** and **6**. The synthetic methodology adopted for the preparation of **1**–**6** is shown in Scheme 3.

3.2. ESI-Mass spectrometry

Compounds **1** and **2** were characterized by using ESI-Mass spectrometry in CH_3CN (see Fig. 2). The ESI-MS spectrum of **1**, shows prominent mass peaks at *m/z* 227.0 (calc. *m/z* 227.1) and 471.0 (calc. *m/z* 471.1) which are assigned to the $[Ni(bqenH_2)(CH_3CN)_2]^{2+}$ and $[Ni(bqenH_2)(ClO_4)]^+$ species respectively while the mass peak observed at *m/z* 371.1 (calc. *m/z* 371.0) is attributed to the $[Ni(bqenH)]^+$ species. On other hand, the ESI-MS spectrum of **2** exhibits prominent mass peaks at *m/z* 220.5 (calc. *m/z* 220.6), 241.0 (calc. *m/z* 241.1) and 499.1 (calc. *m/z* 499.1) which are assigned to the $[Ni(bqenMe_2)(CH_3CN)]^{2+}$, $[Ni(bqenMe_2)(CH_3CN)_2]^{2+}$ and $[Ni(bqenMe_2)(ClO_4)]^{2+}$ species respectively. Similarly, we have extended the ESI-MS spectrometry to the remaining complexes **3**–**6** (Fig. S5 in the supporting information).

The ESI-MS mass spectra of **3** and **4** show prominent mass peaks at m/z 276.0 (calc. *m/z* 276.1) and 290.0 (calc. *m/z* 290.1) which are assigned to the $[Ni(bqenH_2)(phen)]^{2+}$ and $[Ni(bqenMe_2)(phen)]^{2+}$ species respectively. For **5** and **6**, the mass peaks at 264.1 (calc. *m/z* 264.0) and 278.1 (calc. *m/z* 278.0) in the ESI-MS spectra are observed for $[Ni(bqenH_2)(bpy)]^{2+}$ and $[Ni(bqenMe_2)(bpy)]^{2+}$ species.

3.3. Infrared spectroscopy

The Infrared (IR) spectrum of $bqenMe_2$ shows absence of N-H vibration that is observed at ~3385 cm^{1-} for $bqenH_2$ (Fig. 3). This observation indicates that, the H atoms on two N atoms in $bqenH_2$ are replaced by the $-CH_3$ groups. The presence $-CH_3$ groups was further confirmed by the use of ^1H and ^{13}C NMR spectroscopy (Figs. S1–S4 in supplementary information). For compounds **1**, **3** and **5**, the N-H stretching vibrations occur at ~3265, 3269 and 3228 cm^{-1} respectively.

The N–H stretching vibrations in these three compounds are shifted to the lower frequencies as compared to that observed for the free ligand. This observation reveals that the ligand $bqenH_2$ is coordinated to the Ni(II) [36,37]. Further, no such bands were observed for compounds **2**, **4**, and **6** indicating the absence of N-H bonds in these compounds. Compounds **1** and **2** exhibit broad peaks at ~3547 cm^{-1} and ~3405 cm^{-1} respectively which are assigned to the O-H stretching vibrations of water. When **1** and **2** were dissolved in CH_3CN, the coordinated water molecules are exchanged with CH_3CN ligands [38]. The complete disappearance of -OH vibrations in **3**–**6** indicates the substitution of two H_2O molecules (which may be present as labile ligands) by bidentate phen and bpy in **3**–**6**. The presence of aromatic -C=N functionality is observed at ~1526 cm^{-1} for both the ligands while it is shifted to lower frequency of ~ 1518 cm^{-1} in all the compounds. This observation is not unusual as the two N donor atoms are coordinated to metal center [26,39,40]. The presence of perchlorate anions in **1**–**6** was revealed from the appearance of strong and medium absorption peaks at ~1093 and 621 cm^{-1} respectively [36,39].

3.4. UV–Vis spectroscopy

The electronic spectrum of nickel(II) ion in an octahedral environment is expected to show three *d–d* bands assignable for the $^3A_{2g} \rightarrow {}^3T_{2g}$, $^3A_{2g} \rightarrow {}^3T_{1g}(F)$ and $^3A_{2g} \rightarrow {}^3T_{1g}(P)$ transitions. The overlaid UV–Vis spectra of compounds **1**–**6** are shown in the Fig. 4 and Fig. S6 while the data for the intense *d–d* bands observed at different wavelengths in CH_3CN is summarized in the Table 1. The *d–d* band assigned to $^3A_{2g} \rightarrow {}^3T_{1g}(F)$ transition is observed in the region of 489–553 nm on the other hand the peak due to $^3A_{2g} \rightarrow {}^3T_{2g}$ transition is observed in the wavelength range 793–872 nm [41]. Both the bands are very weak in intensity and are observed only at higher concentrations of the compounds in CH_3CN. The tailing of a charge transfer band hinders the observation of third *d–d* band assigned to the $^3A_{2g} \rightarrow {}^3T_{1g}(P)$ transition in all six compounds [42].

The *d–d* absorption bands for **1** and **2** are similar in terms of their intensities and energies. Compounds **3** and **4** differ slightly in their absorption patterns from those of **5** and **6** which clearly suggests an influence of ligands (phen and bpy) on the crystal fields. The high-intensity bands observed in the UV region of 200–320 nm are assigned to the intra-ligand transitions. The band at ~272 nm in **3** and **4** is assigned to the π–π^* transition that arises from the coordination of the nickel to 1,10-phenanthroline [43]. The π–π^* transition due to bipyridine ligand is observed at 284 nm in compound 5 and at 296 nm in compound **6**. The bands in the region of 290–320 nm are assigned to the n–π^* transitions.

3.5. Cyclic and differential pulse voltammetry

Compounds **1**–**6** were characterized by using cyclic voltammetry (CV) and differential pulse voltammetry (DPV) to explore their

Table 2
Technical details of data acquisition and selected refinement results for **3** and **4**.

	Compound **3**	Compound **4**
Empirical formula	$C_{32}H_{26}Cl_2N_6$ NiO_8	C_{36} $H_{33}Cl_2N_7NiO_8$
Formula weight	752.2	821.3
Crystal color	red	violet
Crystal system	orthorhombic	monoclinic
Space group	$P2_12_12_1$	$P2_1/c$
T (K)	100(2)	100(2)
Unit cell dimensions		
a (Å)	11.304(2)	18.0780(4)
b (Å)	15.972(3)	11.3105(2)
c (Å)	17.680(3)	17.2253(3)
α (°)	90.00	90.00
β (°)	90.00	100.37
γ (°)	90.00	90.00
V (Å^3)	3192.3(10)	3464.58(12)
Z	4	4
Radiation type (Mo Kα) (Å)	0.71073	0.71073
Crystal size (mm)	0.30 × 0.20 × 0.10	0.20 × 0.20 × 0.10
Diffractometer	Bruker APEX-II CCD	Bruker APEX-II CCD
Absorption correction	None	None
Number of measured reflections	9790	9803
D_{calc} (g/cm^3)	1.565	1.575
Absorption coefficient (mm^{-1})	0.838	0.780
F(000)	1544	1696
θ range for data collection	2.14–28.37	2.40–28.31
Flack parameter	0.00	–
Limiting indices	$-15 \leqslant h \leqslant 15$, $-21 \leqslant k \leqslant 21$, $-23 \leqslant l \leqslant 23$	$-22 \leqslant h \leqslant 22$, $-13 \leqslant k \leqslant 13$, $-21 \leqslant l \leqslant 21$
Refinement method	SHELXS-97	SHELXS-97
Data/restraints/parameter	7919/0/442	6817/0/490
Final R indices[I > 2σ(I)]	R_1 = 0.0233, wR_2 = 0.0592	R_1 = 0.0299, wR_2 = 0.1182
R indices (all data)	R_1 = 0.0250, wR_2 = 0.0604	R_1 = 0.0341, wR_2 = 0.1239
Goodness of fit (GOF) on F^2	0.966	1.071

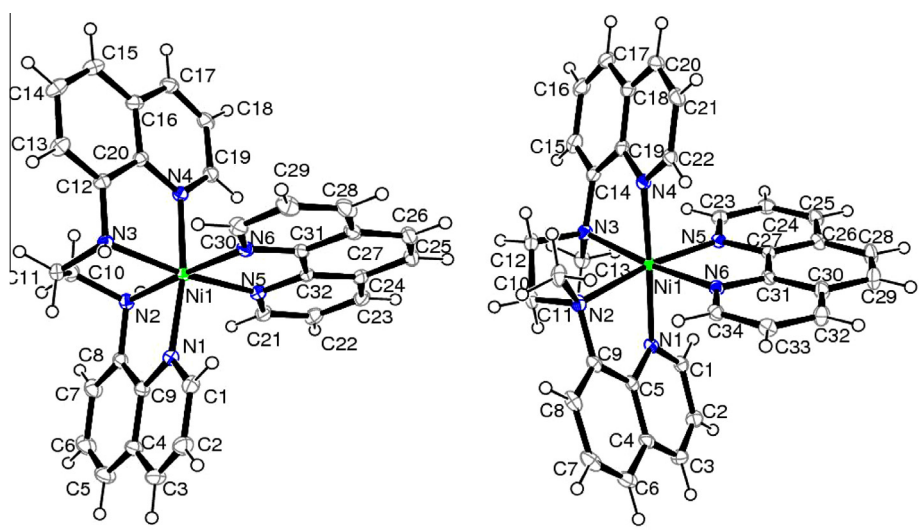

Fig. 6. The crystal structure of $[Ni(bqenH_2)]^{2+}$ cation in **3** (left) and $[Ni(bqenMe_2)]^{2+}$ cation in **4** (right) showing the atom labeling scheme. Displacement ellipsoids are drawn at 50% probability level except for the H atoms, which are shown as circles of arbitrary radius (top). The perchlorate anions are omitted for clarity.

electrochemical properties. The CV and DPV plots of compound **2** are depicted in Fig. 5. Compounds **1** and **2** exhibit a quasi-reversible cathodic and anodic waves which can be attributed for the reduction of Ni(II)/Ni(I) and N(I)/Ni(II) couples, for which the $E_{1/2}$ value is centered at ∼−1.3 volts (V) [44–48]. The anodic potential wave for compounds **1**–**6**, is poorly resolved in CV plots but same is distinctly visible in the DPV plots (see Fig. S7 in the supporting information). The CV and DPV plots of compounds **3** and **4** are similar to those of compounds **1** and **2** with $E_{1/2}$ value centered at ∼−1.45 V. Further, the $E_{1/2}$ value for Ni(II)/Ni(I) couple in compounds **5** and **6** is nearly the same as that observed in **1** and **2**. A poorly resolved anodic peak at ∼0.13 V (data not shown) for the oxidation of Ni(II) to Ni(III) species and the corresponding cathodic peak for the reduction of Ni(III) to Ni(II) species was also observed. The cyclic voltammograms recorded at different scan rates were identical and the peak currents increased proportionally with the increase in scan rates (see Fig. S8 for **1** in the supporting information). The CV and DPV plots of $bqenH_2$ as well as $bqenMe_2$ show no oxidation–reduction peaks in the measured potential range and thus suggest that the both ligands are electrochemically inactive under the experimental conditions (see Fig. S9 in the supporting information for CV and DPV of $bqenMe_2$). Hence, the observed peaks in the cyclic voltammograms of **1** and **2**

Table 3
Selected bond lengths (Å) and angles (°) for **3** and **4**.

Compound ***3***			
Bond length (Å)			
Ni1–N5	2.085(1)	Ni1–N4	2.097(1)
Ni1–N6	2.086(1)	Ni1–N2	2.104(1)
Ni1–N1	2.092(1)	Ni1–N3	2.126(1)
Bond angle (°)			
N5–Ni1–N6	80.10(5)	N1–Ni1–N2	80.69(5)
N5–Ni1–N1	93.50(5)	N4–Ni1–N2	90.41(5)
N6–Ni1–N1	97.34(5)	N5–Ni1–N3	172.67(5)
N5–Ni1–N4	97.34(5)	N6–Ni1–N3	98.30(5)
N6–Ni1–N4	91.76(5)	N1–Ni1–N3	93.80(5)
N1–Ni1–N4	169.89(5)	N4–Ni1–N3	80.48(5)
N5–Ni1–N2	97.41(5)	N2–Ni1–N3	84.43(5)
N6–Ni1–N2	176.76(5)		
Compound 4			
Bond length (Å)			
Ni1–N4	2.067(1)	Ni1–N5	2.116(2)
Ni1–N1	2.079(1)	Ni1–N3	2.162(2)
Ni1–N6	2.111(2)	Ni1–N2	2.182(2)
Bond angle (°)			
N4–Ni1–N1	177.84(6)	N6–Ni1–N3	173.76(6)
N4–Ni1–N6	94.98(6)	N5–Ni1–N3	99.22(6)
N1–Ni1–N6	86.41(6)	N4–Ni1–N2	100.11(6)
N4–Ni1–N5	88.14(6)	N1–Ni1–N2	78.06(6)
N1–Ni1–N5	93.74(6)	N6–Ni1–N2	97.54(6)
N6–Ni1–N5	79.42(6)	N5–Ni1–N2	171.47(6)
N4–Ni1–N3	78.85(6)	N3–Ni1–N2	84.63(6)
N1–Ni1–N3	99.78(6)		

Note: The values in the parentheses indicate estimated standard deviations.

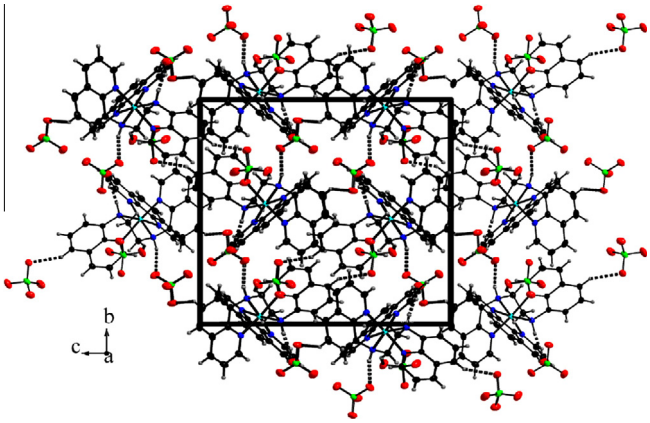

Fig. 7. A view of the packing diagram of **3** along the *a*-axis. N–H···O and C–H···O hydrogen bonds are shown as dashed lines. Color code: C, black; H, medium grey; N, blue; O, red; Cl, green and Ni, sky blue. (For interpretation of the references to color in this figure legend, the reader is referred to the web version of this article.)

are solely assigned to the quasi-reversible redox process of Ni(II)/Ni(I) couple.

3.6. Description for the crystal structures of compounds 3 and 4

All six compounds **1**–**6** were obtained as crystalline solids, however we were able to grow the single crystals of compounds **3** and **4** which were characterized by X-ray crystallography. Single crystals suitable for structure determination were obtained by slow diffusion of diethyl ether into the CH_3CN solutions of **3** and **4**. The technical details of data acquisition and selected refinement results for **3** and **4** are given in Table 2. Compound **3** crystallizes in the non-centrosymmetric orthorhombic space group $P2_12_12_1$, while **4** crystallizes in the centrosymmetric monoclinic space group $P2_1/c$. In both compounds all atoms are located in their general positions. The crystal structure of **3** and **4** contains a central nickel(II), a unique N4 ligand (bqenH_2 in **3** and bqenMe_2 in **4**), one phen ligand and two crystallographically independent perchlorate ions (Fig. 6). Interestingly, the compound **4** has an additional uncoordinated CH_3CN molecule in its crystal lattice (see Fig. S10) and this unique feature is absent in compound **3**.

The perchlorate ions behaves as charge balancing counter anions. The quinolyl nitrogen atoms N1 and N4 are *trans* to each other while the amine nitrogen atoms N2 and N3 occupy the adjacent positions. The two methyl groups, one on N2 and the other on N3 atoms of bqenMe_2 in **4** are located *anti* to each other unlike the *syn* H atoms on N2 and N3 atoms of bqenH_2 in **3**. The auxiliary ligand phen occupy the positions of two labile *cis*-ligands (CH_3CN or H_2O) through N5 and N6 atoms thereby completing the NiN6 octahedron (see Fig. S10). All the Ni–N bond distances and N–Ni–N bond angles are in normal range (Table 3) and are in good agreement with literature reports [31,42,49–53].

In both the complexes the N–Ni–N *trans* and *cis* angles deviates from 180° and 90° respectively suggesting the distortion of octahedral geometry. The *trans* angles in **3** ranges from 169.89(5)° to 176.76(5)° and in **4** it ranges from 171.47(6)° to 177.84(6)°. Whereas the *cis* angles vary between 80.10(5) to 98.30(5) in **3** and 79.42(6) to 100.11(6) in **4**. The Ni-N bond distances lies from 2.085(1) to 2.126(1) in complex **3** and 2.067(1) to 2.182(2) in complex **4**. Further, the electronegative atoms (N and O as well as C) in these compounds are involved in the intermolecular hydrogen bonding (N–H···O, C–H···O in **3** and only C–H···O in **4**) forming a supramolecular three-dimensional networks as shown in Fig. 7 and Fig. 8. The N–H···O and C–H···O hydrogen bonds are shorter than the sum of their Van der Waals radii revealing the strength of these H-bonds in stabilizing overall crystal structures of **3** and **4** (Table 4).

In the crystal structure of **4**, which lacks the N–H bonds, only C–H bonds of bqenMe_2 are involved in the C–H···O interactions with neighboring O atoms of perchlorate anions while structure of **3** is stabilized by the strong N–H···O and C–H···O interactions. Fig. S11 and S12 displays a symmetric organization of the octahedral units in **3** and **4** respectively.

3.7. Catalytic hydroxylation of alkanes by 1–6

Compounds **1**–**6** were tested for the efficacy of catalytic oxidations of hydrocarbons such as cumene, ethylbenzene, and cyclohexane using *m*-CPBA as an oxidant in CH_3CN at 25 °C under N_2 atmosphere. The hydroxylated products of alkanes were analyzed and quantified by gas chromatography (GC) using authentic samples and decane as an internal standard. Compounds **1**–**2** efficiently catalyzed the hydroxylation of C-H bonds in alkanes used in this study, however no organic products were obtained in the catalytic reactions when compounds **3**–**6** were used (Table 5, Scheme 4). There is no surprise in this observation as in the compounds **3**–**6**, the Ni(II) center is coordinatively saturated with the strongly bonded six donor N atoms (four of quinoline moiety and two each of phenanthroline or bipyridine) which has resulted in the poor oxidizing power of **3**–**6**. We propose a compounds **1** and **2** have an octahedral geometry with two H_2O molecules occupying the *cis*-positions. However, in the CH_3CN solution, the two H_2O molecules are exchanged rendering the two CH_3CN molecules at *cis* positions. The *cis*-ligands are thus labile and make nickel(II) center more susceptible for the oxidation by *m*-CPBA oxidant.

A comparative reactivity of **1** and **2**, reveals that compound **2** gives higher yield of hydroxylated products (Table 5). The high yield of alcohol and ketone using compound **2**, can be attributed to the differing nature of ligand in **1** and **2**. In compound **1**, the bqenH_2 has a secondary amine tail (R_2NH) on the other had in **2** the bqenMe_2 has all alkylated N atoms making it tertiary amine.

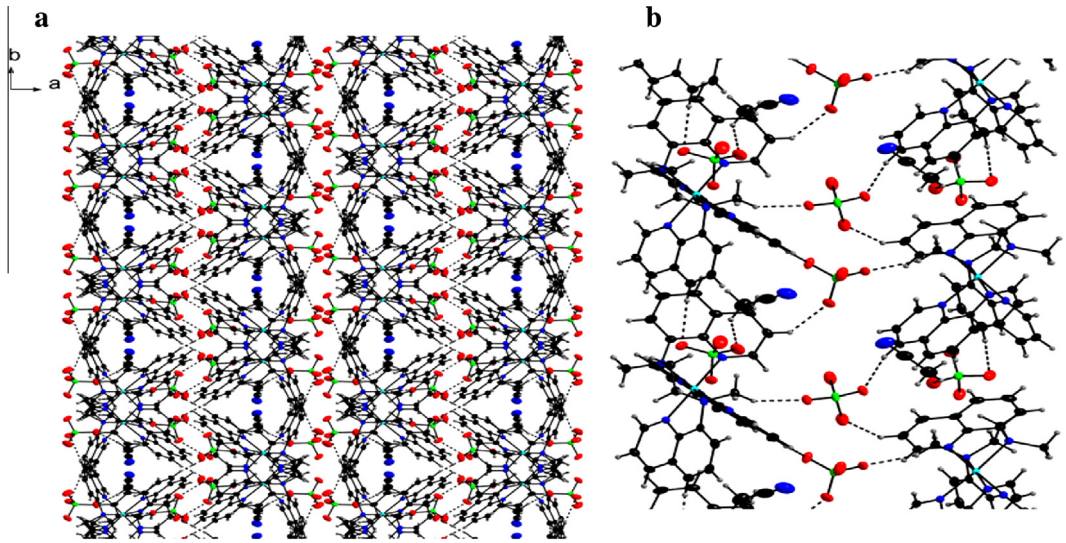

Fig. 8. (a) Helical style symmetric organization of $[Ni(bqen)(phen)]^{2+}$ cations and ClO_4^- anions with the pockets occupied by CH_3CN molecules in **4** along the *c*-axis. (b) Hydrogen bonding diagram showing C–H···O interactions between cation $[Ni(bqen)(phen)]^{2+}$ and ClO_4^- anion in **4**. Color code: C, black; H, medium grey; N, blue; O, red; Cl, green and Ni, sky blue. (For interpretation of the references to color in this figure legend, the reader is referred to the web version of this article.)

Table 4
Hydrogen bonding parameters (Å, °) for **3** and **4**.

D–H···A	D–H/Å	H···A/Å	D···A/Å	D–H···A/°
Compound ***3***				
C(15)–H(15)···O7[a]	0.95(2)	2.397(1)	3.203(2)	142.45(11)
C(6)–H(6)···O3[b]	0.951(2)	2.418(1)	3.255(2)	146.72(13)
C(10)–H(10A)···O6	0.99(2)	2.307(1)	3.197(2)	148.94(10)
N(2)–H(31)···O4	0.93(1)	2.087(1)	2.990(2)	163.57(9)
N(3)–H(32)···O1[c]	0.93(1)	2.201(1)	3.126(2)	172.90(9)
Compound ***4***				
C(10)–H(10C)···O8[a]	0.981(2)	2.418(2)	3.321(3)	152.97(12)
C(32)–H(32)···O5[b]	0.951(2)	2.422(2)	3.288(2)	151.39(12)
C(6)–H(6)···O3[c]	0.950(2)	2.486(2)	3.432(3)	173.99(13)
C(36)–H(36B)···O2	0.979(3)	2.439(2)	3.198(3)	134.08(16)
C21(3)–H(21)···O7[d]	0.950(2)	2.306(2)	3.082(3)	138.41(13)

[a] $-0.5 + x, 0.5 - y, 1 - z$, [b] $-0.5 + x, 0.5 - y, 2 - z$, [c] $1 - x, 0.5 + y, 1.5 - z$ for **3**
[a] $x, y, 1 + z$, [b] $-x, -0.5 + y, 0.5 - z$, [c] $x, 0.5 - y, 0.5 + z$ [d] $-x, 0.5 + y, 0.5 - z$ for **4**
Note: The values in the parentheses indicate estimated standard deviations.

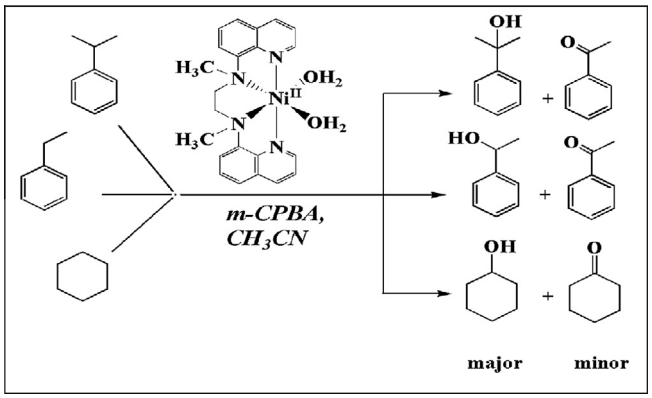

Scheme 4. Alkane hydroxylation by $[Ni(bqenMe_2)(H_2O)_2]^{2+}$ **2** in CH_3CN using *m*-CPBA oxidant.

In biomimetic non-heme oxidation chemistry, the $bqenMe_2$ complexes of iron(II) and manganese(II) have been used instead of $bqenH_2$ [33–35]. The oxidation of cyclam ligand which has four R_2NH groups, is reported in Ni(II)-cyclam complexes using H_2O_2 as oxidant [54]. It is likely that in **1**, the $bqenH_2$ which has secondary amine functionality can undergo partial oxidation thus reflecting on the observed low yields of organic products compared to **2** (Table 5). In the oxidation of cumene, 2-phenylpropan-2-ol was obtained in high yield while acetophenone and 2-methylstyrene were obtained as minor products. Use of ethylbenzene instead of cumene as a substrate, resulted in high yield of 1-phenylethanol along with minor products acetophenone and styrene.

Table 5
Organic product analysis using GC in the alkane hydroxylation by **1–6**[a].

Catalyst	Substrate	Alcohol[c]	(TON)[b] (A)	Ketone	(TON)[b] (K)	A/K
1	Cumene	2-Phenylpropan-2-ol	105	Acetophenone	23	4.6
	Ethylbenzene	1-Phenylethanol	121	Acetophenone	25	4.8
	Cyclohexane	Cyclohexanol	116	Cyclohexanone	23	5.0
2	Cumene	2-Phenylpropan-2-ol	361	Acetophenone	42	8.6
	Ethylbenzene	1-Phenylethanol	390	Acetophenone	38	10.3
	Cyclohexane	Cyclohexanol	410	Cyclohexanol	50	8.2
3–6	Cumene	2-Phenylpropan-2-ol	NIL	Acetophenone	NIL	NIL
	Ethylbenzene	1-Phenylethanol		Acetophenone		
	Cyclohexane	Cyclohexanol		Cyclohexanol		

Note:
[a] Reaction conditions: $[Ni^{2+}] = 0.5$ mM; [m-CPBA] = 0.5 M, [substrate] = 1 M in CH_3CN at 25 °C for 90 min under N_2.
[b] Turnover number [(moles of product)/(moles of catalyst)] determined by GC.
[c] Small amounts of desaturated products in the case of cumene and ethylbenzene while the small amount of ε-caprolactone in case of cyclohexanone were observed.

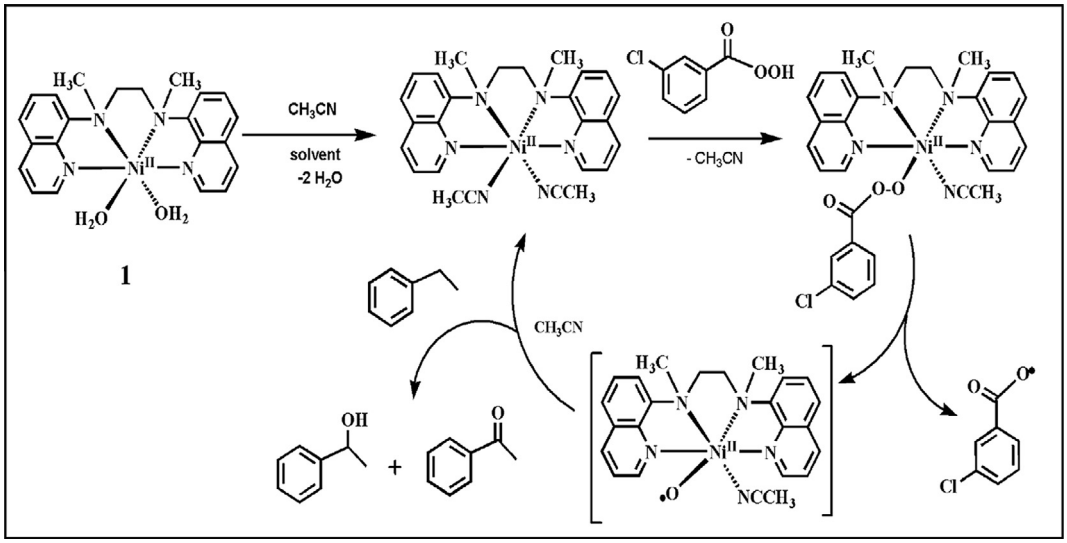

Scheme 5. Proposed mechanism for the alkane hydroxylation by $[Ni(bqenMe_2)(H_2O)_2]^{2+}$ using *m*-CPBA oxidant.

Cyclohexane was selectively oxidized to cyclohexanol with low yields of cyclohexanone and caprolactam. A mechanism for the C–H activation of alkanes to hydroxylated products is proposed under the similar lines as reported by others [17,21–25]. As shown in Scheme 5, the $[Ni(II)(bqen)(CH_3CN)(m\text{-CPBA})]^+$ adduct results in the generation of reactive intermediates $[Ni^{II}\text{-}O\cdot(bqen)(CH_3CN)]^+$ and *m*-chlorobenzoic acid radical via homolytic cleavage of O–O bond.

We propose that an intermediate $[Ni^{II}\text{-}O\cdot(bqen)(CH_3CN)]^+$ is responsible for the hydroxylation of alkanes giving us alcohols as the major products. Efforts are underway to investigate the alkane hydroxylation reactions using other transition metal compounds of tetradendate tripodal ligands.

4. Conclusions

In this paper, we have reported the synthesis and characterization of six new Ni(II) octahedral complexes **1**–**6** containing the tetradentate tripodal ligands $bqenH_2$ and $bqenMe_2$. Further, when **1** and **2** were reacted with the auxiliary ligands such as phen and bpy we obtained compounds **3**–**6** by a simple replacement of labile CH_3CN molecules. Compounds **3** and **4** were structurally characterized. CV and DPV experiments revealed the Ni(II)/Ni(III) and Ni(II)/Ni(I) quasi-reversible processes in compounds **1**–**6** against SCE in DMSO. All the compounds **1**–**6** were tested in the hydroxylation of alkanes using *m*-CPBA oxidant under catalytic conditions. Only **1** and **2** were found to be highly selective in hydroxylating the C-H bonds of alkanes giving alcohols as major products. Interestingly, compound **2** afforded us high TON (turn over number) of alcohol and ketone compared to **1**. The observation of high A/K (alkohol/ketone) ratio in the alkane hydroxylation by **1** and **2** thus make these compounds as highly efficient catalysts for alcohol production. The four compounds **3**–**6** are coordinatively saturated with six donor N atoms making them poor catalysts for alkane oxidation.

Acknowledgment

SND thank University Grant Commission (UGC), New Delhi (F.No.37-576/2009 (SR) and Department of Science and Technology (DST), New Delhi (SR/FT/CS-006/2010) for the financial support. DDN thank UGC for Junior Research Fellowship (UGC-BSR-JRF). The Department of Chemistry, Goa University, receives the grants from UGC-SAP and DST-FIST programs of UGC and DST, New Delhi. SND thank Prof. Wonwoo Nam, Ewha Womans University and Prof. Jaeheung Cho, Daegu Gyeongbuk Institute of Science & Technology, for their help in providing us crystal data. Authors thank Prof. B. R. Srinivasan, Goa University for helpful discussion.

Appendix A. Supplementary material

CCDC 948509 and 1019725 contains the supplementary crystallographic data for **3** and **4**. These data can be obtained free of charge from The Cambridge Crystallographic Data Centre via www.ccdc.cam.ac.uk/data_request/cif. Supplementary data associated with this article can be found, in the online version, at http://dx.doi.org/10.1016/j.ica.2015.01.009. These data include MOL files and InChiKeys of the most important compounds described in this article.

References

[1] M. Zhang, Z.-Y. Gu, M. Bosch, Z. Perry, H.-C. Zhou, Coord. Chem. Rev. (2015) (doi: 10.1016/j.ccr.2014.05.031) (in press).
[2] S.C. Sawant, X. Wu, J. Cho, K.-B. Cho, S.H. Kim, M.S. Seo, Y.-M. Lee, M. Kubo, T. Ogura, S. Shaik, W. Nam, Angew. Chem., Int. Ed. 49 (2010) 8190.
[3] N. Saravanan, M. Palaniandavar, Inorg. Chim. Acta 385 (2012) 100.
[4] S. Yu, C.-X. Miao, D. Wang, S. Wang, C. Xia, W. Sun, J. Mol. Catal. A 353–354 (2012) 185.
[5] X. Wu, M.S. Seo, K.M. Davis, Y.-M. Lee, J. Chen, K.-B. Cho, Y.N. Pushkar, W. Nam, J. Am. Chem. Soc. 133 (2011) 20088.
[6] J. Annaraj, S. Kim, M.S. Seo, Y.-M. Lee, Y. Kim, Inorg. Chim. Acta 362 (2009) 1031.
[7] G.J.P. Britovsek, J. England, A.J.P. White, Inorg. Chem. 44 (2005) 8125.
[8] Y. He, C.R. Goldsmith, Chem. Commun. 48 (2012) 10532.
[9] S.N. Dhuri, M.S. Seo, Y.-M. Lee, H. Hirao, Y. Wang, W. Nam, S. Shaik, Angew. Chem., Int. Ed. 47 (2008) 3356.
[10] Y.-M. Lee, S.N. Dhuri, S.C. Sawant, J. Cho, M. Kubo, T. Ogura, S. Fukuzumi, W. Nam, Angew. Chem., Int. Ed. 48 (2009) 1803.
[11] J. Kaizer, E.J. Klinker, N.Y. Oh, J.-U. Rohde, W.J. Song, A. Stubna, J. Kim, E. Munck, W. Nam, L. Que Jr., J. Am. Chem. Soc. 126 (2004) 472.
[12] D. Maiti, H.R. Lucas, A.A.N. Sarjeant, K.D. Karlin, J. Am. Chem. Soc. 129 (2007) 6998.
[13] D. Maiti, H.C. Fry, J.S. Woertink, M.A. Vance, E.I. Solomon, K.D. Karlin, J. Am. Chem. Soc. 129 (2007) 264.
[14] T. Tano, Y. Okubo, A. Kunishita, M. Kubo, H. Sugimoto, N. Fujieda, T. Ogura, Inorg. Chem. 52 (2013) 10431.
[15] J. Cho, R. Sarangi, H.Y. Kang, J.Y. Lee, M. Kubo, T. Ogura, E.I. Solomon, W. Nam, J. Am. Chem Soc. 132 (2010) 16977. and references cited therein.
[16] T. Nagataki, Y. Tachi, S. Itoh, Chem. Commun. (2006) 4016
[17] J. Cho, R. Sarangi, J. Annaraj, S.Y. Kim, M. Kubo, T. Ogura, E.I. Solomon, W. Nam, Nat. Chem. 1 (2009) 568.

[18] M.T. Kieber-Emmons, J. Annaraj, M.S. Seo, K.M. Van Heuvelen, T. Tosha, T. Kitagawa, T.C. Brunold, W. Nam, C.G. Riordan, J. Am. Chem. Soc. 128 (2006) 14230.
[19] J. Cho, H.Y. Kang, L.V. Liu, R. Sarangi, E.I. Solomon, W. Nam, Chem. Sci. 4 (2013) 1502.
[20] M. Balamurgan, R. Mayilmurugan, E. Suresh, M. Palaniandavar, Dalton Trans. 40 (2011) 9413.
[21] S. Hikichi, K. Hanaue, T. Fujimura, H. Okuda, J. Nakazawa, Y. Ohzu, C. Kobayashi, M. Akita, Dalton Trans. 42 (2013) 3346.
[22] S. Hikichi, H. Okuda, Y. Ohzu, M. Akita, Angew. Chem., Int. Ed. 48 (2009) 188.
[23] J. Nakazawa, S. Terada, M. Yamada, S. Hikichi, J. Am. Chem. Soc. 135 (2013) 6010.
[24] T. Nagataki, K. Ishii, Y. Tachi, S. Itoh, Dalton Trans. (2007) 1120
[25] E. Ramachandran, D.S. Raja, J.L. Mike, T.R. Wagner, M. Zeller, K. Natarajan, RSC Adv. 2 (2012) 8515.
[26] E.N. Nfor, S.N. Esemu, G.A. Ayimele, E.A. Eno, G.E. Iniama, O.E. Offiong, Bull. Chem. Soc. Ethiop. 25 (2011) 361.
[27] L.R. Gomes, J.N. Low, M.A.A. Rocha, L.M.N.B.F. Santos, B. Schröder, P. Brandão, C. Matos, J. Neves, J. Mol. Struct. 990 (2011) 86.
[28] L. Zhu, D.-M. Kong, X.-Z. Li, G.-Y. Wang, J. Wang, Y.-W. Jin, Polyhedron 29 (2010) 574.
[29] C.N. Sudhamani, H.S. Bhojya Naik, T.R. Ravikumar Naik, M.C. Prabhakara, Spectrochim. Acta, Part. A 72 (2009) 643.
[30] A.E.-M.M. Ramadan, J. Mol. Struct. 1015 (2012) 56.
[31] K.C. Skyrianou, V. Psycharis, C.P. Raptopoulou, D.P. Kessissoglou, G. Psomas, J. Inorg. Biochem. 105 (2011) 63.
[32] G.M. Sheldrick, SHELXTL/PC. Version 6.12 for Windows XP, Bruker AXS Inc., Madison, WI, USA (2001).
[33] J. England, G.J.P. Britosvek, N. Rabadla, A.J.P. White, Inorg. Chem. 46 (2007) 3752.
[34] K. Nehru, S.J. Kim, I.Y. Kim, M.S. Seo, Y. Kim, S.-J. Kim, J. Kim, W. Nam, Chem. Commun. (2007) 4623
[35] J. Yoon, S.A. Wilson, Y.K. Jang, M.S. Seo, K. Nehru, B. Hedman, K.O. Hodgson, E. Bill, E.I. Solomon, W. Nam, Angew. Chem., Int. Ed. 48 (2009) 1257.
[36] K. Nakamoto, Infrared and Raman Spectra of Inorganic and Coordination Compounds, sixth ed., John Wiley & Sons, 2008.
[37] B.V. Kumar, H.S. Bhojya Naik, D. Girija, N. Sharath, S.M. Pradeepa, H.J. Hoskeri, M.C. Prabhakara, Spectrochim. Acta, Part. A 94 (2012) 192.
[38] A.E. Wickenden, R.A. Krause, Inorg. Chem. 4 (1965) 404.
[39] P. Bhowmik, M.G.B. Drew, S. Chattopadhyay, Inorg. Chim. Acta 366 (2011) 62.
[40] R. Pastorek, Z. Trávníček, P. Štarha, Inorg. Chim. Acta 373 (2011) 286.
[41] R. Ivaniková, R. Boča, L. Dlháň, H. Fuess, A. Mašlejová, V. Mrázova, I. Svoboda, J. Titiš, Polyhedron 25 (2006) 3261.
[42] M.A. Ali, A.H. Mirza, F.H. Bujang, M.H.S.A. Hamid, P.V. Bernhardt, Polyhedron 25 (2006) 3245.
[43] A.I. El-Said, A.S.A. Zidan, M.S. El-Meligy, A.A.M. Aly, O.F. Mohammed, Trans. Met. Chem. 26 (2001) 13.
[44] K.-Y. Choi, S.N. Choi, I.-H. Suh, Polyhedron 17 (1998) 1415.
[45] H. Temel, S. İlhan, M. Aslanoğlu, A. Kılıçl, E. Tas, J. Chin. Chem. Soc. 53 (2006) 1027.
[46] S. Chandra, R. Kumar, Spectrochim. Acta, Part. A 62 (2005) 518.
[47] S. Manjunathan, C.N. Krishnan, Asian J. Chem. 19 (2007) 861.
[48] D.N. Huh, J.B. Gibbons, R.S. Haywood, C.E. Moore, A.L. Rheingold, M.J. Ferguson, C.J.A. Daley, Inorg. Chim. Acta 423 (2014) 290.
[49] B.A. Frenz, J.A. IBers, Inorg. Chem. 11 (1972) 1109.
[50] A.K. Sharma, S. Biswas, S.K. Barman, R. Mukherjee, Inorg. Chim. Acta 363 (2010) 2720.
[51] I. García-Santos, J. Sanmartín, A.M. García-Deibe, M. Fondo, E. Gómez, Inorg. Chim. Acta 363 (2010) 193.
[52] D. Sertphon, D.J. Harding, P. Harding, H. Adams, Polyhedron 30 (2011) 2740.
[53] F. Wagner, M.T. Mocella, M.J. D'Aniello Jr., A.H.J. Wang, E. Kent, J. Am. Chem. Soc. 96 (1974) 2625.
[54] A. McAuley, C. Xu, Inorg. Chem. 31 (1992) 5549.

Inorganica Chimica Acta 467 (2017) 405–414

Contents lists available at ScienceDirect

Inorganica Chimica Acta

journal homepage: www.elsevier.com/locate/ica

Research paper

Synthesis and characterization of N3Py2 ligand-based cobalt(II), nickel (II) and copper(II) catalysts for efficient conversion of hydrocarbons to alcohols

Dattaprasad D. Narulkar [a], Anant Kumar Srivastava [b], Raymond J. Butcher [c], Kanakappan M. Ansy [d], Sunder N. Dhuri [a,*]

[a] Department of Chemistry, Goa University, Taleigao Plateau, Goa, India
[b] Department of Chemistry, IISER, Pune 411008, India
[c] Department of Chemistry, Howard University, Washington, DC 20059, United States
[d] Department of Chemistry and Nanoscience, Ewha Womans University, 52, Ewhayeodae-gil, Seodaemun-gu, Seoul 03760, Republic of Korea

ARTICLE INFO

Article history:
Received 10 May 2017
Received in revised form 8 August 2017
Accepted 11 August 2017
Available online 18 August 2017

Keywords:
Cobalt
Nickel
Copper
X-ray crystallography
Cumene
Adamantane
Alcohol

ABSTRACT

Three new complexes $[Co(N3Py2)(H_2O)](ClO_4)_2$ **1**, $[Ni(N3Py2)(H_2O)](ClO_4)_2$ **2** and $[Cu(N3Py2)](ClO_4)_2$ **3** (N3Py2 is *N*,*N*′-dimethyl-*N*-(2-(methyl(pyridin-2-ylmethyl)amino)ethyl)-*N*′-(pyridin-2-ylmethyl) ethane-1,2-diamine) have been synthesized and characterized. Non-heme ligand N3Py2 have been prepared by Eschweiler-Clarke method and reported for the first time. Compounds **1** and **2** were characterized by single crystal X-ray structure analysis. The structure of **1** and **2** revealed that Co(II) cation in **1** and Ni(II) cation in **2** are bonded to the five nitrogen atoms of N3Py2 and a water molecule thus forming an octahedral motif $[M(N3Py2)(H_2O)]^{2+}$. For compound **3**, a square pyramidal geometry has been proposed based on the spectroscopic, elemental analysis and ESI-MS data. Compounds **1**–**3** were tested as catalysts in the oxidation of cumene and adamantane using *m*-CPBA. Comparative effect of counter anions on the product yields was observed when the perchlorates anions of **1**–**3** were replaced with tetraphenylborates to give compounds **1a**–**3a**. The turnover numbers of alcohol over ketone product increased in order of catalysts, **1**(**1a**) > **2**(**2a**) > **3**(**3a**).

1. Introduction

The transition metal complexes play key roles in bioinorganic chemistry as they are used as structural model complexes for metalloenzymes and as catalysts in oxidation reactions [1,2]. The design of novel transition metal complexes with nitrogen donor ligands is often a target of synthetic coordination chemists. So far a variety of metal complexes bearing amine and polypyridyl ligands exhibiting diverse structural features have been synthesised and their roles in oxygenation reactions are well understood [3–8]. The oxidation of cheaply available hydrocarbons in the natural feedstock to a commercially valued oxidized products under mild conditions is one of the imperative and quite difficult chemical process [9,10]. The late transition metal complexes of first-row are now known to be equally proficient catalysts for hydrocarbon oxidations. The selective oxidation of methane to methanol by dioxygen activation catalyzed by an enzyme, methane monooxygenase has been reported [11–14]. This has simultaneously led to the upsurge of research relevant to alkane oxidation by biomimetic model complexes with much attention on bio-inspired complexes of iron as potential catalysts [15–23]. In recent years, the cobalt(II) compounds have been widely used in biomimetic catalysis. The cobalt(II) substituted dioxygenase enzyme showed robust activity in vitro compared to that of the native enzyme [24]. A large number of cobalt(II) complexes in presence of alkylperoxides as oxidants proceed via formation of an alkylperoxo complex and perform the oxidation of hydrocarbons [25]. The high valent cobalt(IV)-oxo species unlike the iron(IV)-oxo or manganese(IV)-oxo species are very rare and only known in recent years. Nam and Ray group have reported the spectroscopic capture of a low spin Co(IV)-oxo intermediate in the presence of redox-inactive metal ions and investigated their reactivity in C–H activation and oxygen atom transfer reactions [26,27]. The spectroscopic characterization and reactivity study of Co(IV)-oxo species have been reported [28].

In addition to the cobalt(II) complexes in oxygenation reactions, the several nickel(II) compounds have been used as efficient cata-

* Corresponding author.
E-mail address: sndhuri@unigoa.ac.in (S.N. Dhuri).

http://dx.doi.org/10.1016/j.ica.2017.08.027
0020-1693/

lysts in alkane oxidations. In a recent study, it was observed that a $[Ni(TPA)]^{2+}$ (TPA is Tris(2-pyridylmethyl)amine) complex showed high TON (turnover numbers) of products over related TPA complexes of iron(II), manganese(II), and cobalt(II) in the presence of *m*-CPBA as an oxidant [29]. Later, the handful nickel(II) compounds were isolated and used as the catalysts in alkane hydroxylations [30–36]. It is noted that when such reactions are carried out in the presence of alkyl peroxide or acyl peroxide and the nickel(II) catalysts, they often proceed via the formation of a nickel(II)-alkylperoxy or nickel(II)-acylperoxo short lived intermediate species [30–34,37].

The copper(II) complexes in enzymatic, biomimetic and chemical oxidation reactions have also been investigated to a large extent. The copper(II)-dioxygen (Cu-O_2) species have been frequently invoked as the reactive intermediate in the C–H bond activation reactions catalyzed by copper(II) complexes [38–49]. In our recent study, we have shown the efficacy of nickel(II) complexes containing a quinoline based tetradentate non-heme ligand in alkanes hydroxylation [50]. In continuation to this work, herein we report the synthesis, characterization and catalytic hydroxylation of alkanes by three new compounds of cobalt(II), nickel(II) and copper(II) stabilized by a non-heme pentadentate ligand N3Py2.

2. Experimental

2.1. Materials and methods

All reagents were purchased from commercial sources and used without further purification. The solvents were distilled and dried under N_2 atmosphere prior to their use. ^{1}H and ^{13}C-NMR spectra were recorded on a Bruker Avance III, 400 MHz, NMR spectrometer using $CDCl_3$. The infrared (IR) spectra in the region of 4000–400 cm^{-1} were recorded on Shimadzu (IR-Prestige-21) FTIR spectrometer by diluting the compounds in KBr powder. The perchlorate salts of Co(II), Ni(II) and Cu(II) were synthesized carefully by reacting their carbonates with perchloric acid (70%, v/v) followed by slow crystallization [51]. The percentage of C, H and N were obtained using Elementar Variomicro Cube CHNS Analyser. The UV–Vis spectra were recorded on Agilent diode array 8453 UV–Vis spectrophotometer in the wavelength range of 200–1100 nm in CH_3CN. The electrospray ionization mass spectra (ESI-MS) of **1**–**3** in CH_3CN were recorded using Applied Biosystem Matrix-assisted Laser Desorption Ionization Time-of-flight (MALDI-TOF) spectrometer. The cyclic voltammograms (CV) and differential pulse voltammograms (DPV) were measured using Electrochemical Workstation-CH Instrument, Inc. CHI6107. A glass vessel containing the sample dissolved in CH_3CN was equipped with a platinum disc working electrode, a platinum wire as a counter electrode and a reference electrode, Ag/$AgNO_3$ (0.01 M). All the experiments were carried out using supporting electrolyte, tetrabutylammonium hexafluorophosphate ($TBAPF_6$) (0.1 M) and the solutions were purged with N_2 gas for around ~30 min prior to every measurement. The potentials (Vs Ag/Ag^+) were converted to the values *vs* the standard calomel electrode (SCE) by adding a value of 0.29 V [52]. The single crystals of **1** and **2** suitable for X-ray crystallography were picked up using the glycerol loop and mounted directly on the Bruker SMART APEX-II CCD diffractometer (Mo-K_α = 0.71073 Å). The CCD data were integrated and scaled using Bruker-SAINT software package while SHELXTL, v 6.12 was used for solving and refining the structures [53]. All non-hydrogen atoms were refined anisotropically, if not stated otherwise and the hydrogen atoms were located at the calculated positions. In the crystal structure of **1**, the disordered atom positions (in perchlorate anions) were freely refined isotropically over two positions using similar distances and U-restraints. The products formed in the reaction mixture were quantified using the Shimadzu GC 2014 equipped with HP capillary column (30 m × 0.25 mm × 2.5 μM) and a FID detector.

2.1.1. Synthesis of N,N′-dimethyl-N-(2-(methyl(pyridin-2-ylmethyl) amino)ethyl)-N′-(pyridin-2-ylmethyl)ethane-1,2-diamine)

N3Py2 was prepared by following three step procedures. *Step-I:* To the ethanolic solution of 2-pyridine-carboxaldehyde (3.0 g, 28.0 mmol) was added 1.52 mL of diethylenetriamine (1.44 g, 14.0 mmol). The mixture was refluxed for ~5 h, cooled to room temperature and the solvent was removed to give red semisolid product. Yield of product was 3.1 g (79%). IR data (KBr, cm^{-1}): 3295 ν(N–H), 3200–2700 ν(C–H), 1648 ν(C=N). *Step-II*: To the ice-cold methanolic solution of imine product (3.0 g, 10.7 mmol), the sodium borohydride (0.48 g, 12.8 mmol) was added slowly and the mixture stirred for it became brownish orange in colour (~6 h). The solvent was removed and water (20 mL) was added to the flask containing the crude product. The yellow viscous oil was then extracted using ethyl acetate (30 mL × 3). Yield of product was 2.8 g (92%). IR data (KBr, cm^{-1}): 3295 ν(N–H), 3200–2700 ν(C–H), 1670 ν(C=N). *Step-III*: The product (2.6 g, 9.1 mmol) of second step was taken in water (3.0 mL) and cooled in ice-bath. To this mixture, formaldehyde (37%, 22.0 mL) and formic acid (85%, 15.0 mL) were added and refluxed for ~24 h. The mixture was then cooled and basified (pH = 12) using 2 M NaOH solution. The crude reddish-brown oil obtained after extraction with chloroform (20 mL × 4) was dissolved in HCl solution (pH = ~1). The acidic mixture was then basified using NaOH solution (pH = 12) and the product was then extracted using diethyl ether (20 mL × 6). N3Py2 was formed as yellow oil with the yield 2.5 g (72%). IR data (KBr, cm^{-1}): 3200–2700 ν(C–H), 1670 ν(C=N). ^{1}H NMR ($CDCl_3$, ppm): δ 8.47 (d, 2H, *J* = 3.2 Hz, 2-PyH), δ 7.57 (t, 2H, *J* = 8.2 Hz, 4-PyH), δ 7.34 (d, 2H, *J* = 3.8 Hz, 5-PyH), δ 7.08 (t, 2H, *J* = 6.16 Hz, 3-PyH), δ 3.63 (s, 4H, Ar-CH_2), δ 2.57 (s, 8H, N-CH_2), δ 2.25 (s, 3H, NMe), δ 2.25 (s, 3H, NMe) δ 2.21 (s, 6H, NMe). ^{13}C NMR ($CDCl_3$, ppm): δ 159.1 (C6), 148.1 (C2), 136.2 (C4), 122.9(C5), 121.7(C3), 64.04 (Ar-CH_2), 55.3 (N-CH_2), 42.7 (N-CH_3).

2.1.2. Synthesis of $[Co(N3Py2)(H_2O)](ClO_4)_2$ **1**

N3Py2 (0.452 g, 1.37 mmol) was dissolved in CH_3CN (2 mL) and added to the stirring CH_3CN solution of $Co(ClO_4)_2{\cdot}6H_2O$ (0.5 g, 1.37 mmol) under the N_2 at room temperature. The mixture was stirred for ~12 h and filtered. To the resulting dark reddish-pink solution, the diethyl ether (10 mL) was added and the mixture was kept undisturbed for crystallization. The crystals formed after two days were isolated by filtration and dried in air. The yield of **1** was 0.7 g (80%). *Mol. Formula*, $C_{19}H_{31}N_5Cl_2O_9Co$: *calc.* C, 37.82; H, 5.18; N, 11.61%. *Found*, C, 37.78; H, 4.98; N, 11.62%. *IR-data* (KBr, cm^{-1}): 3420 ν(OH); 3137–2752 ν(CH); 1090, 621 ν(ClO_4^-). *UV–Vis data*, λ_{max}, CH_3CN/nm (ε/dm^3 mol^{-1} cm^{-1}): 262 (81642), 494 (42), 1028 (8). *ESI-MS*: *m*/*z* = 193.2 (*calc.* 193.2) for $[Co(N3Py2)]^{2+}$ and *m*/*z* = 485.9 (*calc.* 485.9) for $[Co(N3Py2)(ClO_4)]^+$.

2.1.3. Synthesis of $[Ni(N3Py2)(H_2O)](ClO_4)_2$ **2**

Compound **2** was prepared in a similar way as **1** by reacting N3Py2 (0.452 g, 1.37 mmol) and $Ni(ClO_4)_2.6H_2O$ (0.5 g, 1.37 mmol) in CH_3CN. Yield of **2** was 0.7 g (84%). *Mol. Formula*, $C_{19}H_{31}N_5Cl_2O_9Ni$: *calc.* C, 37.84; H, 5.18; N, 11.61%. *Found*, C, 37.78; H, 5.26; N, 11.90%. *IR-data* (KBr, cm^{-1}): 3420 ν(OH); 3137–2752 ν(CH); 1090, 621 ν (ClO_4). *UV–Vis data*, λ_{max}, CH_3CN/nm (ε/dm^3 mol^{-1} cm^{-1}): 262 (85439), 554(38), 920(27). *ESI-MS*: *m*/*z* = 193.1 (*calc.* 193.1) for $[Ni(N3Py2)]^{2+}$ and *m*/*z* = 485.5 (*calc.* 485.6) for $[Ni(N3Py2)(ClO_4)]^+$.

2.1.4. Synthesis of $[Cu(N3Py2)](ClO_4)_2$ 3

Compound **3** was prepared using similar methodology as in **1** and **2** wherein N3Py2 (0.452 g, 1.37 mmol) was reacted with Cu

$(ClO_4)_2.6H_2O$ (0.5 g, 1.349 mmol) in CH_3CN. The dark blue crystalline powder of **3** was obtained and the yield of **3** was 0.64 g (78%). *Mol. Formula*, $C_{19}H_{31}N_5Cl_2O_9Cu$: *calc.*, C, 38.68; H, 4.96; N, 11.87%. *Found*, C, 38.70; H, 5.06; N, 11.89%. *IR-data* (KBr, cm^{-1}): 3030–2825 ν(CH); 1093, 621 $\nu(ClO_4^{-1})$. *UV–Vis data*, λ_{max}, CH_3CN/nm ($\varepsilon/dm^3\ mol^{-1}\ cm^{-1}$): 256 (10804), 592 (216). *ESI-MS data*: *m*/*z* = 194.6 (*calc.* 194.6) for $[Cu(N3Py2)]^{2+}$ and *m*/*z* = 489.1 (*calc.* 489.1) for $[Cu(N3Py2)(ClO_4)]^+$.

*2.1.5. Synthesis of compounds **1a–3a***

Three other compounds, $[Co(N3Py2)(CH_3CN)](BPh_4)_2$ **1a**, $[Ni(N3Py2)(CH_3CN)](BPh_4)_2$ **2a** and $[Cu(N3Py2)](BPh_4)_2$ **3a** were prepared by the reaction of **1**, **2** and **3** with two equivalents of Na(BPh_4) (0.45 g, 1.3 mmol) in CH_3CN at room temperature. Analytical data for compounds **1a**, **2a** and **3a** is as follows. Yield of **1a** was 86%. *Mol. Formula*, $C_{69}H_{72}N_6B_2Co$: *calc.*, C, 77.57; H, 6.81; N, 7.88%. *Found*, C, 77.90; H, 6.72; N, 7.95%. *IR-data* (KBr, cm^{-1}): 3137–2752 ν(CH); 2280 $\nu(NCCH_3)$; 734, 705 (BPh_4). Yield of **2a** was 85%. *Mol. Formula*, $C_{69}H_{72}N_6B_2Ni$: *calc.*, C, 77.77; H, 6.81; N, 7.89%. *Found*, C, 77.60; H, 6.88; N, 7.61%. *IR-data* (KBr, cm^{-1}): 3137–2752 ν(CH); 2275 $\nu(NCCH_3)$; 734, 705 (BPh_4). Yield of **3a** was 83%. *Mol. Formula*, $C_{67}H_{69}N_5B_2Cu$: *calc.*, C, 78.17; H, 6.76; N, 6.80%. *Found*, C, 77.84; H, 6.90; N, 7.51%. *IR-data* (KBr, cm^{-1}): 3137–2752 ν(CH); 734, 705 (BPh_4).

2.2. Catalytic oxidations of cumene and adamantane

Compounds **1**–**3** were tested in the oxidation of alkyl hydrocarbons namely cumene and adamantane using *m*-CPBA as an oxidant in CH_2Cl_2:CH_3CN (3:1) mixture at room temperature under N_2 atmosphere. In a typical catalytic reaction, the complex was dissolved in CH_3CN (80 μL, 2.5 mM) was added to the stirring solution of cumene (350 mM) or adamantane (250 mM) in 3:1 CH_2Cl_2-CH_3CN (4 mL) in the presence of *m*-CPBA (50 mM). At every fixed interval of time, a fraction of the reaction mixture was quenched using triphenylphosphine and eluted over a silica column using diethyl ether. The eluted sample was then directly infused on GC column using *n*-decane internal standard.

3. Results and discussion

3.1. Synthesis and characterization of N3Py2

In heme and non-heme bioinspired chemistry, the ligands have been known to provide the environment to central metal ions such that the resulting structure behaves as a functional model for the enzymatic reactions. The transition metal complexes with different denticity ligands (amines and pyridyl based) are viable catalysts for organic oxidations which often proceed *via* formation of high-valent metal-oxygen intermediates [54]. The iron(IV)-oxo and manganese(IV)-oxo of non-heme ligands N4Py (*N*,*N*-bis(2-pyridylmethyl)-*N*-bis(2-pyridyl)-methylamine) and BnTPEN (*N*-benzyl-*N*,*N′*,*N′*-tris(2-pyridylmethyl)-1,2-diaminoethane) (Scheme 1) have been studied earlier in the C–H activation, epoxidation and oxygen transfer reactions [55–57]. It has been reported that the ligands with secondary –NH groups coordinated to metal ions tend to undergo fast degradation in the presence of oxidants such as *m*-CPBA, H_2O_2, etc., and thus decreases the efficiency of catalysts giving low yields of products. The complex of nickel(II), $[Ni(cyclam)]^{2+}$ has been reported to give low yields of products due to the degradation of cyclam [58]. In our earlier work, we also observed low yields of alcohol in the alkane oxidations catalyzed by $[Ni(bqenH_2)](ClO_4)_2$ ($bqenH_2$ is *N*,*N′*-bis(8-quinolyl)ethane-1,2-diamine) complex [50]. Thus, being inspired by the biomimetic applications of transition metal complexes having N-methylated ligands in the field of catalysis, herein we report synthesis of a new pentadentate N3Py2 ligand (Scheme 1) and its three new cobalt(II), nickel(II) and copper(II) complexes. N3Py2 was prepared in multi step method (Scheme 2). In the first step, the diethylenetriamine and pyridine-2-carboxaldehyde were condensed to give Schiff base imine, which was then reduced by sodium borohydride in step II [59–61]. In the final step, the amine was *N*-methylated following Eschweiler-Clarke reaction (Scheme 2). N3Py2 was characterized using IR, ^1H and ^{13}C NMR spectroscopic techniques (Fig. 1 and SI, Figs. S1–S3).

*3.2. Synthesis and characterization of **1–3***

The reaction of N3Py2 with metal salts, $Co(ClO_4)_2.6H_2O$ or $Ni(ClO_4)_2.6H_2O$ or $Cu(ClO_4)_2.6H_2O$ in CH_3CN in equal molar concentration afforded us three new compounds **1**, **2** and **3** (Scheme 3). The characteristic spectroscopic features of N3Py2 in all compounds were traced from their IR and UV–Vis spectra. The cyclic and differential pulse voltammetric techniques (CV/DPV) were used to obtain redox potentials of **1**–**3**. Based on the IR and UV–Vis spectroscopy, C,H,N analysis, ESI-MS and CV/DPV data, the compounds **1**–**3** were unambiguously formulated as $[Co(N3Py2)(H_2O)](ClO_4)_2$, $[Ni(N3Py2)(H_2O)](ClO_4)_2$ and $[Cu(N3Py2)](ClO_4)_2$. Compounds **1** and **2** were then characterized by single-crystal X-ray structure analysis. Compounds **1**–**3** were tested as catalysts in the oxidation of two alkyl hydrocarbons, cumene and adamantane using *m*-CPBA as an oxidant [35,55–57]. We also investigated the counter anion effect on the product yields formed in the oxidation of cumene and adamantane. The perchlorates of **1**–**3** were replaced by tetraphenylborates in acetonitrile to afford us compounds $[Co(N3Py2)(CH_3CN)](BPh_4)_2$ **1a**, $[Ni(N3Py2)(CH_3CN)](BPh_4)_2$ **2a** and $[Cu(N3Py2)](BPh_4)_2$ **3a**.

*3.2.1. Infrared spectra of N3Py2, **1–3** and **1a–3a***

Infrared spectroscopy is an affordable technique used by many inorganic chemists to extract the information on the ligation behaviour of ligands in the metal complexes. When ligand coordinates, the original bands due ligand often shift slightly to the lower wavenumbers [62]. We have used IR spectroscopy for the characterization of ligand and the complexes **1**–**3** and **1a**–**3a**. IR spectra of products obtained in step I-II showed stretching vibrations due to N–H bonds, while the IR spectrum of N3Py2 showed no N–H signals indicating N3Py2 has formed by methylation [SI, Fig. S1]. The

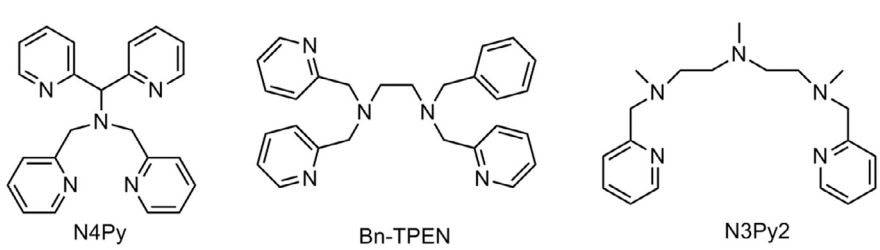

Scheme 1. Chemical structures of non-heme pentadentate nitrogen donor ligands.

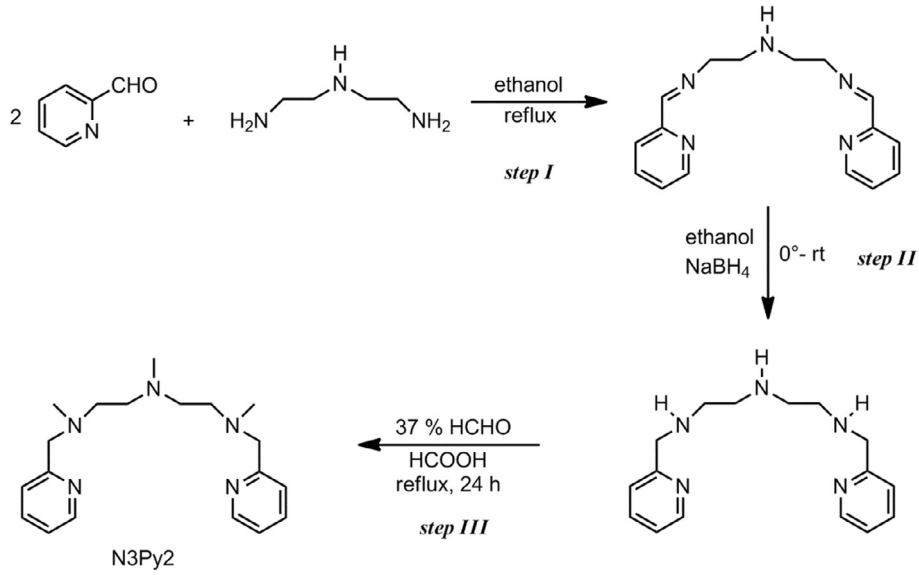

Scheme 2. Three step synthetic strategy used in the preparation of N3Py2.

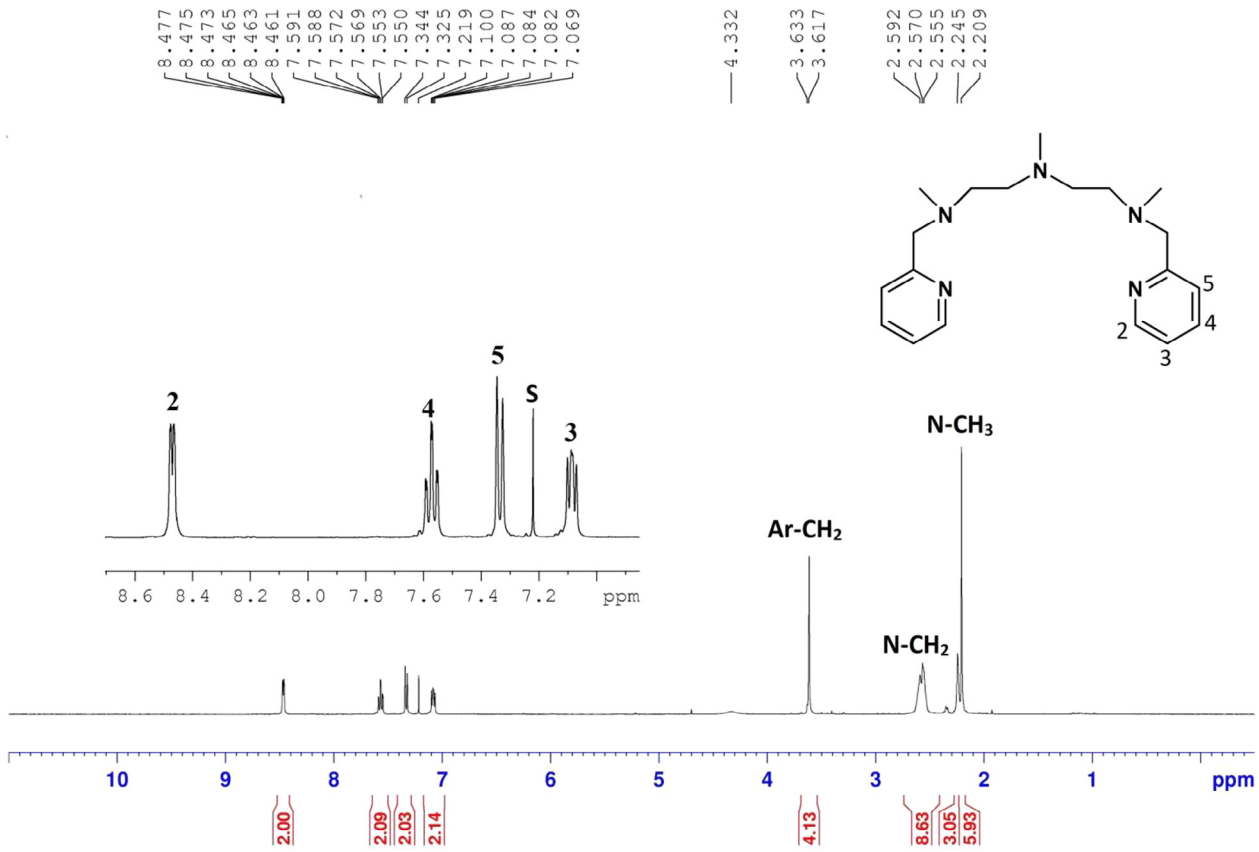

Fig. 1. ^{1}H NMR spectrum of N3Py2 recorded in $CDCl_3$.

overlaid IR spectra of N3Py2 and compounds **1**–**3** are shown in Fig. 2a. IR spectra of **1** and **2** shows a broad band centered at ~3420 cm^{-1} which has been assigned to the O–H vibration of water molecule. Interestingly, no O–H vibration was observed for compound **3** which suggest the absence of water molecule and thus square pyramidal geometry was proposed as in [Cu(bpmen)(ClO_4)]$^+$ (bpmen is tetradentateN,N′-dimethyl-N,N′-bis(2-pyridylmethyl)ethane-1,2-diamine) [63]. The lack of water or solvent molecule in nickel(II) and copper(II) complexes has been reported [63,64]. Further, the IR spectra of **1**–**3** shows strong absorption signals at ~1090 cm^{-1} and ~621 cm^{-1} due to uncoordinated perchlorates [62]. When we replaced two perchlorates by two tetraphenylborate anions in **1**–**3**, the IR spectra of resulting compounds **1a-3a** showed the bands at ~734 cm^{-1} and ~705 cm^{-1} corresponding to tetraphenylborates (SI, Fig. S4) [25]. In addition to tetraphenylborate bands, we also observed a new band at

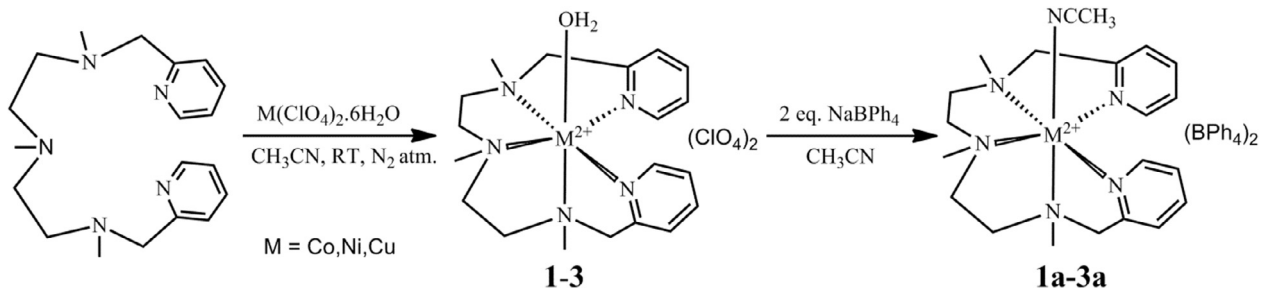

Scheme 3. Synthetic method for preparation of **1**–**3**.

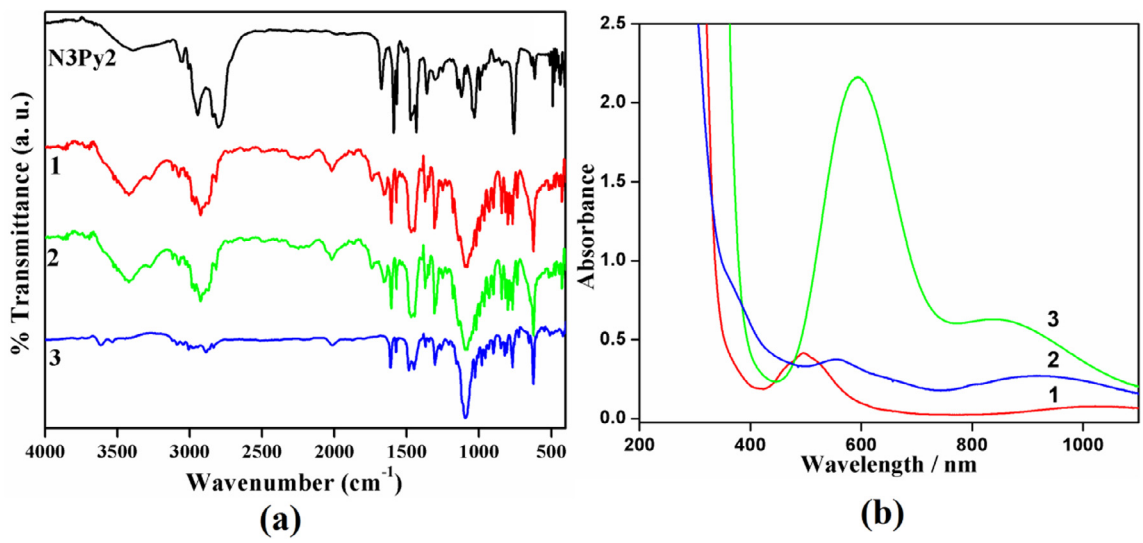

Fig. 2. (a) The overlaid IR spectra of N3Py2 and **1**–**3** (b) UV–Vis spectra of compounds **1**–**3** (10 mM) in CH_3CN.

2275 cm^{-1} for **1a** and 2280 cm^{-1} for **2a** due to incorporation of CH_3CN molecule [62,65]. Thus, from IR spectra, we infer that H_2O and CH_3CN molecules are essential components to stabilize the structures of **1**–**2** and **1a**-**2a** (*vide infra*). IR spectrum of **3a** showed no vibration attributed to CH_3CN indicating that complex **3a** adopts same geometry as in **3** [66,67].

3.2.2. Electronic spectra of *1–3*

UV–Vis spectra of compounds **1**–**3** were recorded in CH_3CN showed an intense band at ~262 nm in all compounds and this band has been assigned to the intra-ligand charge transfer transition. The weak bands due to spin allowed *d-d* transitions were observed in the visible region (Fig. 2b). In the UV–Vis spectrum of **1**, the bands at ~494 and ~1028 nm were assigned to $^4T_{1g}$(F)→$^4A_{2g}$(F) and $^4T_{1g}$(F)→$^4T_{2g}$(F) transitions respectively [68]. For compound **2** the bands at 554 and 920 nm were attributed to $^3A_{2g}$(F)→$^3T_{1g}$(F) and $^3A_{2g}$(F)→$^3T_{2g}$(F) transitions respectively [50,69,70]. The third band due to $^4T_{1g}$(F)→$^4T_{1g}$(P) in **1** and $^3A_{2g}$(F)→$^3T_{1g}$(P) in **2** were tailed in UV region due to overlapping with charge transfer band of N3Py2 and hence not seen [70,71]. Unlike low intensity

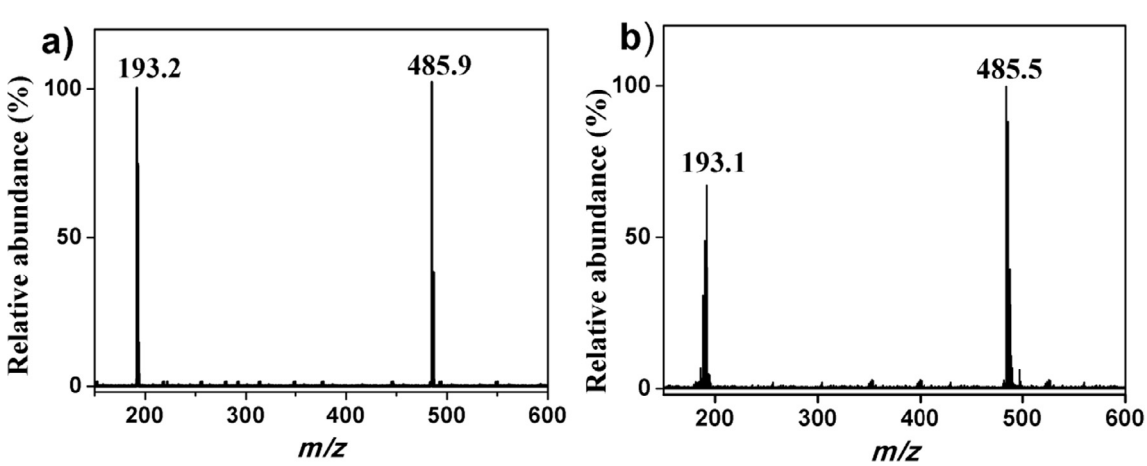

Fig. 3. ESI-MS spectra of 2 mM solution of (a) **1** (b) **2** recorded in CH_3CN.

bands in the UV–Vis spectra of **1** and **2**, the compound **3** exhibited a high intensity band at ~592 nm. Such bands are often seen in the spectrum when a molecule is non-centrosymmetric [72]. The high absorbance band was also observed in the UV–Vis spectrum of a square pyramidal non-centrosymmetric $[Cu^{II}DIEN\text{-}pyr)]^{2+}$ complex [66,67].

3.2.3. ESI-Mass spectrometry

The ESI-MS spectra of compounds **1** and **2** are shown in Fig. 3a and b. The ESI-MS spectrum of **1** in CH_3CN showed two prominent mass peaks at $m/z = 193.2$ and 485.9, which were assigned to $[Co(N3Py2)]^{2+}$ and $[Co(N3Py2)(ClO_4)]^{+}$ species respectively (Fig. 3a). Compound **2** showed two peaks at $m/z = 193.1$ and 485.5 corresponding to $[Ni(N3Py2)]^{2+}$ and $[Ni(N3Py2)(ClO_4)]^{+}$ species respectively (Fig. 3b). On measuring the ESI-MS spectrum of **3**, the two peaks at $m/z = 194.6$ and 489.1 corresponding to $[Cu(N3Py2)]^{2+}$ and $[Cu(N3Py2)(ClO_4)]^{+}$ ions respectively were observed (data not shown).

3.2.4. Crystal structures of 1 and 2

Single crystals of **1** and **2** suitable for X-ray crystallography were obtained by the slow diffusion of diethyl ether into their CH_3CN solutions. The technical details of data acquisition and selected refinement results for **1** and **2** are listed in Table 1. The selected bond lengths and bond angles for **1** and **2** are shown in Table 2. It has been reported that the metal complexes with the pentadentate N5 ligands can exist in four isomeric forms [73] (SI, Scheme S1). Based on this report and our X-ray structural charac-

Table 1
Technical details of data acquisition and selected refinement results for **1** and **2**.

	1	2
Empirical formula	$C_{19}H_{31}Cl_2N_5CoO_9$	$C_{19}H_{31}Cl_2N_5NiO_9$
Formula weight	603.32	603.08
Crystal description	Block	Block
Crystal colour	Brick red	Blue
Crystal system	Monoclinic	Monoclinic
Space group	$P2_1/c$(no. 14)	$P2_1/c$(no. 14)
Temperature (K)	100(2)	100(2)
Unit cell dimensions	$a = 8.967$ (3)Å $b = 32.954$ (12)Å $c = 8.662$ (3) Å $\alpha = 90°$ $\beta = 105.509$ (8)° $\gamma = 90°$	$a = 9.027$ (4)Å $b = 33.134$ (15)Å $c = 8.668$ (4) Å $\alpha = 90°$ $\beta = 105.805$ (6)° $\gamma = 90°$
Volume (Å^3)	2466.4(16)	2494.6(19)
Z	4	4
Radiation type (Mo-Kα)/Å	0.71073	0.71073
Crystal size (mm)	0.18 × 0.13 × 0.07	0.400 × 0.30 × 0.10
Diffractometer	Bruker Smart APEX-II Duo	Bruker Smart APEX-II Duo
Absorption correction	Semi-empirical from equivalents	multi scan
No. measured reflections	3363	6824
Calculated density (mg/m^3)	1.625	1.606
Absorption coefficient (mm^{-1})	0.972	1.051
F(0 0 0)	1252	1259.2
θ range for data collection	0.618–25.280	2.34–25.04
Limiting indices	$-10 \le h \le 8$ $-39 \le k \le 39$ $-10 \le l \le 10$	$-9 \le h \le 10$ $-37 \le k \le 39$ $-10 \le l \le 9$
Refinement method	Full-matrix least-squares on F^2	Full-matrix least-squares on F^2
Data/restraints/parameter	4455/23/352	4366/0/328
Final *R* Indices [I > 2σ(I)]	$R_1 = 0.0995$, $wR_2 = 0.2029$	$R_1 = 0.0572$, $wR_2 = 0.1100$
R indices (all data)	$R_1 = 0.1222$, $wR_2 = 0.2143$	$R_1 = 0.0718$, $wR_2 = 0.1160$
Goodness of fit on F^2	1.211	1.0720
Largest diff. peak and hole (e Å^{-3})	1.531 and −1.797 e.Å^{-3}	1.0110 and −0.8095 e.Å^{-3}
Reflections collected/unique	27156/4455 [R(int) = 0.1163]	14244/4366 [R(int) = 0.0444]

Table 2
Selected bond lengths (Å) and bond angles (°) for **1** and **2**.

$[Co(N3Py2)(H_2O)](ClO_4)_2$ (**1**)			
Bond lengths (Å)			
Co–N1	2.140(7)	Co–N4	2.219(7)
Co–N2	2.239(7)	Co–N5	2.149(6)
Co–N3	2.153(7)	Co–O1	2.132(6)
Bond angles (°)			
O1–Co–N1	85.93(2)	N5–Co–N4	77.49(1)
O1–Co–N5	98.06(1)	N3–Co–N4	80.76(1)
N1–Co–N5	98.30(1)	O1–Co–N2	160.31(2)
O1–Co–N3	94.71(2)	N1–Co–N2	76.30(2)
N1–Co–N3	104.41(2)	N5–Co–N2	92.90(2)
N5–Co–N3	154.63(2)	N3–Co–N2	81.80(2)
O1–Co–N4	89.68(1)	N4–Co–N2	108.71(3)
N1–Co–N4	173.45(2)		
$[Ni(N3Py2)(H_2O)](ClO_4)_2$ (**2**)			
Bond lengths (Å)			
Ni1–N1	2.103(8)	Ni1–N4	2.201(4)
Ni1–N5	2.120(5)	Ni1–N8	2.238(1)
Ni1–N2	2.166(5)	Ni1–O10	2.134(3)
Bond angles (°)			
N1–Ni1–O10	94.29(12)	N4–Ni1–N5	76.92(14)
N5–Ni1–O10	84.79(13)	N4–Ni1–N2	109.00(14)
N5–Ni1–N1	96.96(13)	N3–Ni1–O10	94.05(14)
N2–Ni1–O10	89.74(12)	N3–Ni1–N1	160.04(15)
N2–Ni1–N1	78.87(13)	N3–Ni1–N5	101.83(15)
N2–Ni1–N5	172.88(14)	N3–Ni1–N2	83.07(14)
N4–Ni1–O10	160.53(13)	N3–Ni1–N4	83.35(15)
N4–Ni1–N1	94.50(14)		

Note: The values in the parentheses indicate estimated standard deviations.

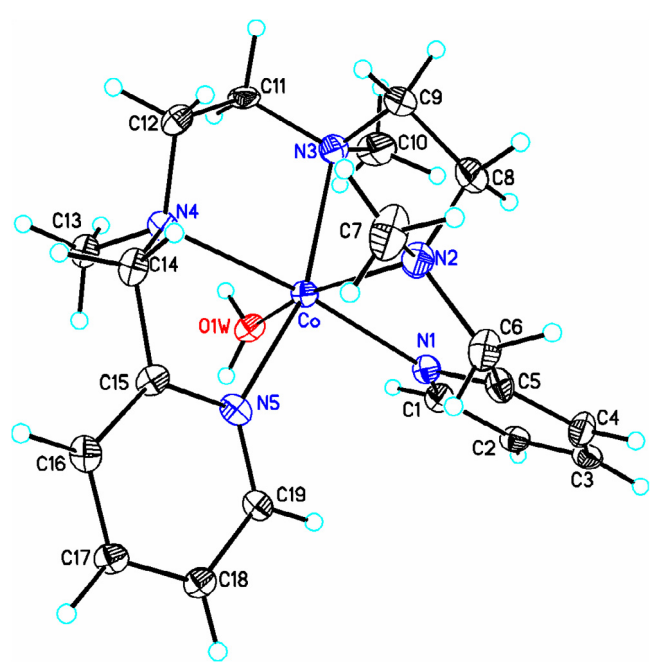

Fig. 4. Crystal structure of $[Co(N3Py2)(H_2O)](ClO_4)_2$ showing atom labelling scheme. Displacement ellipsoids are drawn at 50% probability except for H atoms which are shown as circles of arbitrary radius. The perchlorate anions are not shown for the clarity.

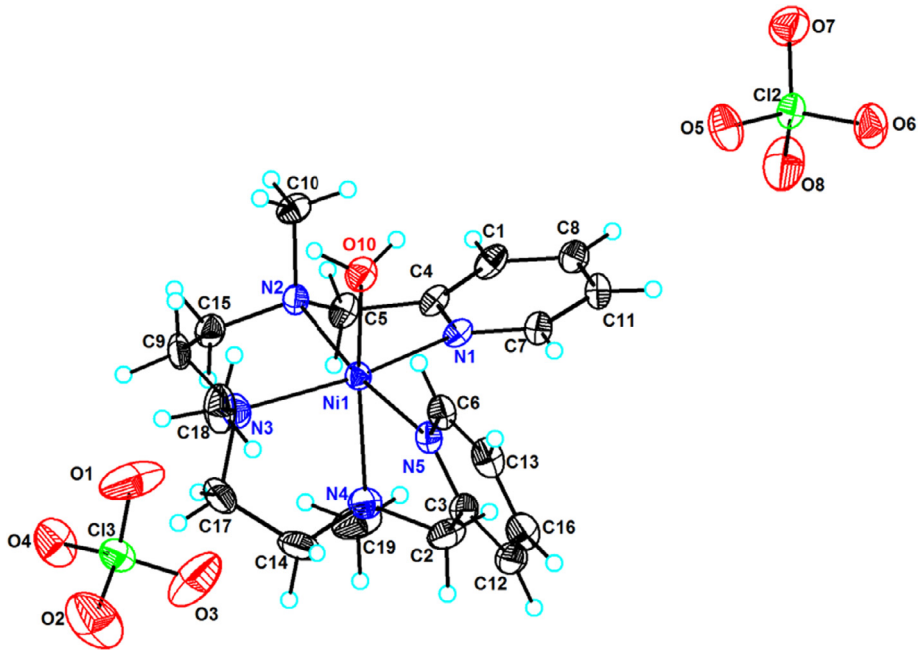

Fig. 5. Crystal structure of $[Ni(N3Py2)(H_2O)](ClO_4)_2$ showing atom labelling scheme. Displacement ellipsoids are drawn at 50% probability except for H atoms, which are shown as circles of arbitrary radius.

terization, we propose the isomeric structure II for compounds **1** and **2** (Fig. 4 and Fig. 5). Compounds **1** and **2** are isostructural and crystallize in a centrosymmetric space group $P2_1/c$. The crystal structures of both consist of a centrally located metal(II) ion (Co(II) in **1** and Ni(II) in **2**), a pentadentate N3Py2 and a H_2O molecule besides two crystallographically independent perchlorates (Fig. 4 and Fig. 5). The octahedral $[MN_5O]^{2+}$ unit (M = Co(II), Ni(II)) is slightly distorted due to the presence of two types of nitrogen-donor atoms (two of pyridyl part and three of tertiary amine backbone) and a water molecule. The octahedral distortion is clearly evident from the (N–Co–N and N–Ni–N) cis angles which range from 76.30(2)-108.71(3) Å in **1** and from 76.92(14)-109.00(14) Å in **2** and similarly from the *trans* angles which range between 154.63(2)-173.45(2) Å in **1** and 160.04(15)-172.88(14) in **2** (Table 3). In both the structures, the pyridyl nitrogen atoms are disposed *syn* to one another and the triamine part occupies the facial positions of the octahedron. The similar dispositions of donor atoms were also observed in compounds with pyrrole based pentadentate ligands [74]. The examples of triamine nitrogens occupying meridional positions of octahedron are also reported [75].

The perchlorates in **1** and **2** only behave as the counter anions for $[Co(N3Py2)]^{2+}$ and $[Ni(N3Py2)]^{2+}$ cations and do not participate in bonding with cobalt(II) or nickel(II) ions (Fig. 4 and Fig. 5). However, the perchlorate anions play important role in building the extended network through its oxygen atoms (O12 and O14 in **1** and O6 and O8 in **2**) which are involved in weak hydrogen bonding with a water molecule (Table 3). The resulting supramolecular three-dimensional metal organic framework structures formed by Cl–O···H contacts, $[MN_5O]^{2+}$ motifs, and perchlorates anions are shown in Fig. 6 and Fig. S5 in SI. The two O–Cl–O and two H–

Table 3
Hydrogen bonding parameters (Å, °) for **1** and **2**.

D–H···A	D–H/Å	H···A/Å	D···A/Å	D–H···A/°
Compound **1**				
O1w-H1W1···O12[c]	0.81(2)	2.02(4)	2.810(9)	162.00(9)
O1W-H1W2···O14	0.815(3)	1.988(7)	2.801(9)	174.50(4)
Compound **2**				
O10-H10b···O6[a]	0.847(19)	2.070(21)	2.840(5)	150.85(164)
O10-H10a···O8[b]	0.849(14)	2.037(21)	2.838(9)	156.99(157)

[a]1 − x, 1 − y, 1 − z [b]2 − x, −y, 2 − z, z [c]−1 + x, y.
Note: The values in the parentheses indicate estimated standard deviations.

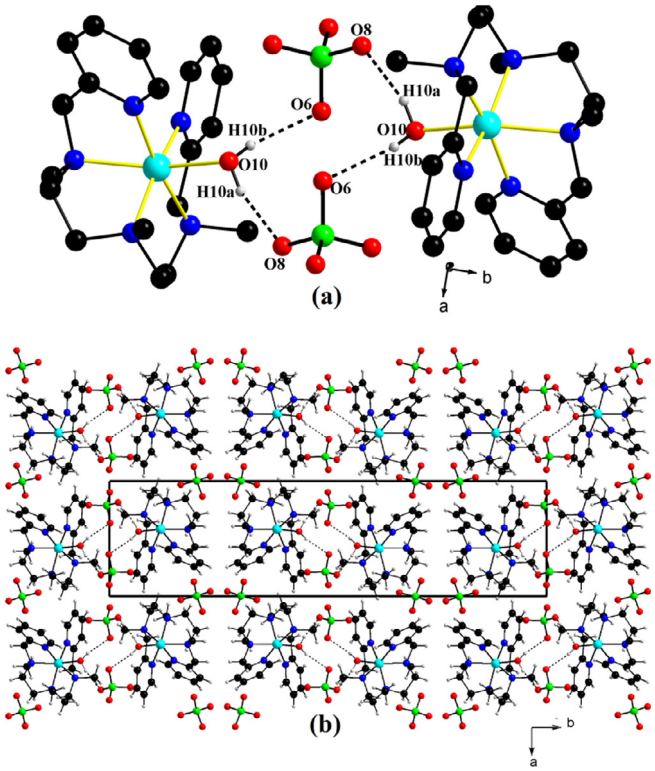

Fig. 6. (a) Cyclic structure formed due to hydrogen bonding interactions in **2** with atom labelling scheme of atoms involved hydrogen bonding. Hydrogen atoms attached to carbon are omitted for clarity (b) Enlarged view of a three dimensional network in **2** showing the symmetric organisation of $[Ni(N3Py2)(H_2O)]^{2+}$ cations and perchlorate anions in the crystallographic *ab* plane.

O–H linked through hydrogen bonds forms a twelve membered ring structure in **1** and **2** and these rings resemble like a chair form of cyclohexane when viewed along the '*ab*' plane (Fig. 6a, SI, Fig. S5a). The hydrogen bond distances in **1** and **2** are quite shorter than the sum of their Van der Waals radii of the atoms involved in the hydrogen bonding. The hydrogen bond distances range from 2.02 (4) to 1.988 (7) Å in **1** and from 2.037 (21) to 2.070 (21) Å in **2** (Table 3). Hydrogen bond distances in **1** are relatively shorter than in **2** with an average difference of 0.0495 Å. It is evident from the structural data that the hydrogen bonding basically originates due the presence of a water molecule and perchlorate ions in **1** and **2**. In spite of using acetonitrile as the solvent, the incorporation of water in the crystal structure of **1** and **2** could be justified based on the use of metal perchlorate hexahydrates in the synthesis. In other related nickel(II) compounds, the incorporation of water molecule was also observed although the reactions were carried out in methanol [29,30,32]. When the perchlorates ions were replaced by tetraphenyborates in acetonitrile, the new compounds **1a** and **2a** indeed showed the presence of acetonitrile. Our attempts to grow single crystals of $[Cu(N3Py2)](ClO_4)_2$ **3** were not fruitful and hence the compound **3** along with **1** and **2** were also characterized by powder X-ray diffraction (PXRD) technique. The PXRD patterns of **1** and **2** were identical and support the notion that they have same space groups as obtained from their single crystal X-ray structures [Fig. 7]. On the contrary, the PXRD pattern of **3**

Table 4
Products formed in the reaction of cumene and catalysts **1**–**3** and **1a**-**3a** in presence of *m*-CPBA.[a]

Catalyst	Cumene oxidation[b]			
	2-Phenyl-2-propanol (TON)	Acetophenone (TON)	Total TON[c]	A/K[d]
1	150	105	255	1.4
1a	293	210	503	1.4
2	142	101	243	1.4
2a	223	144	367	1.5
3	107	85	192	1.3
3a	152	108	260	1.4

[a] Yield based on the oxidant.
[b] Reaction conditions: catalyst (0.05 mmol dm^{-3}), cumene (350 mmol dm^{-3}), *m*-CPBA (50 mmol dm^{-3}) in CH_2Cl_2/CH_3CN solvent mixture (3:1 v/v, 4 mL); reaction time 12 h.
[c] Total TON = mmol of product/no. of mmol of catalyst.
[d] A/K = TON of 2-Phenyl-2-propanol (A)/TON of acetophenone (K).

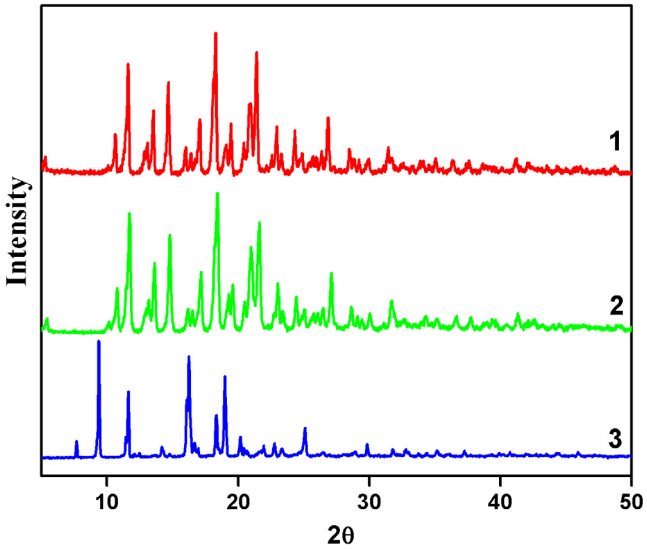

Fig. 7. Comparative PXRD patterns of $[Co(N3Py2)(H_2O)](ClO_4)_2$ **1** (red line), $[Ni(N3Py2)(H_2O)](ClO_4)_2$ **2** (green line) and $[Cu(N3Py2)](ClO_4)_2$ **3** (blue line). (For interpretation of the references to colour in this figure legend, the reader is referred to the web version of this article.)

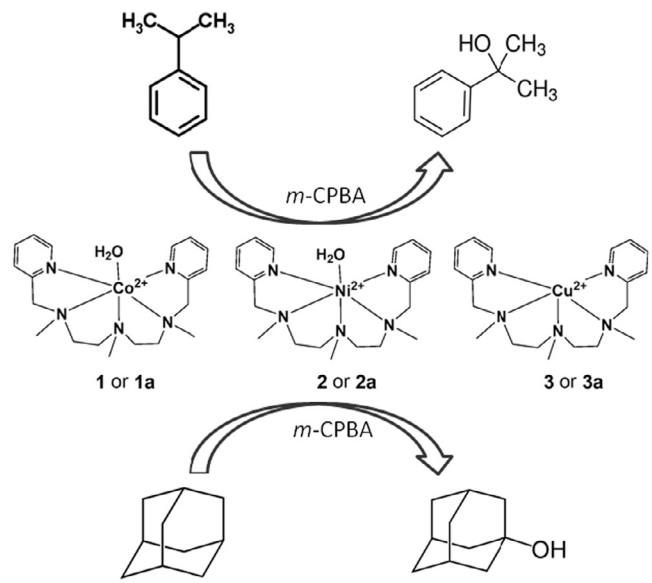

Scheme 4. The reaction scheme showing conversion of cumene and adamantane to 2-phenyl-2-propanol and 1-adamantanol respectively by catalysts **1**–**3** and **1a**–**3a**.

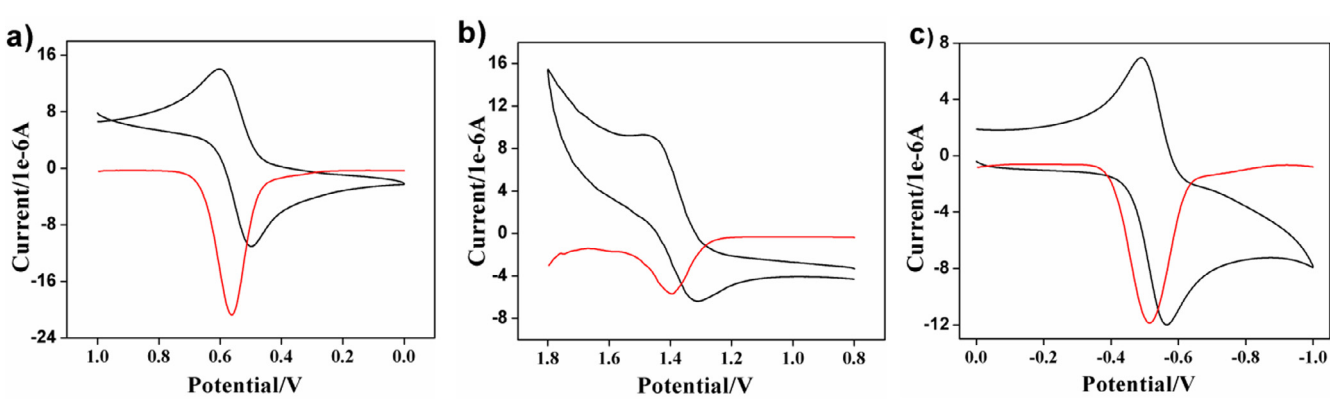

Fig. 8. CV (black line) and DPV (red line) of a) **1**, b) **2** and c) **3** recorded at scan rate of 100 mVs^{-1} in CH_3CN containing 0.1 M of $TBAPF_6$ as supporting electrolyte against $Ag/AgNO_3$ (0.01 M) reference electrode. (For interpretation of the references to colour in this figure legend, the reader is referred to the web version of this article.)

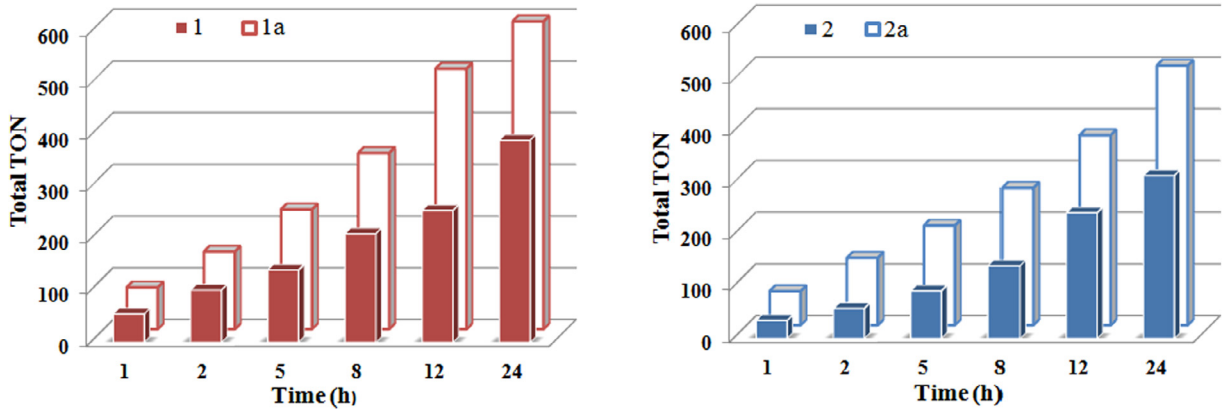

Fig. 9. Bar graphical diagram showing 2-phenyl-2-propanol formation with time in the reactions of cumene and A) $[Co(N3Py2)(H_2O)](ClO_4)_2$ **1** *vs* $[Co(N3Py2)(CH_3CN)](BPh_4)_2$ **1a** B) $[Ni(N3Py2)(H_2O)](ClO_4)_2$ **2** *vs* $[Ni(N3Py2)(CH_3CN)](BPh_4)_2$ **2a** in CH_2Cl_2/CH_3CN (3:1 v/v) mixture at room temperature.

was quite different and did not match with the powder patterns of **1** and **2** [Fig. 7]. The single crystal X-ray data and PXRD patterns thus confirm that **1** and **2** are isostructural while **3** crystallizes in a different space group.

*3.2.5. Electrochemical properties of **1–3***

Cyclic voltammetry (CV) and differential pulse voltammetry (DPV) techniques were applied to understand the redox behavior of the compounds **1–3**. CV of compound **1** in CH_3CN showed the anodic and cathodic waves corresponding to the Co(II)/Co(III) couple with a $E_{½}$ = 0.56 V v/s Ag/$AgNO_3$ (0.86 V v/s SCE) (Fig. 8a). The $E_{½}$ value was further confirmed from the DPV technique and was in good agreement with those of known cobalt(II) complexes with multidentate nitrogen donor ligands [76–78]. When we measured CV of **2** under identical conditions, we observed the peak attributed to Ni(II)/Ni(III) redox couple centered at quite higher potential of 1.39 V v/s Ag/$AgNO_3$ (1.68 V v/s SCE) (Fig. 8b) [35,70,79]. On contrary to the positive $E_{½}$ values of **1** and **2**, the complex **3** exhibited a reversible peak at $E_{½}$ = −0.52 V v/s Ag/$AgNO_3$ (−0.22 V v/s SCE) due to Cu(II)/Cu(I) redox couple (Fig. 8c) [47,80,81]. This large deviation of $E_{½}$ value for **3** compared to those of **1** and **2** suggest that the compound **3** have different structural properties. N3Py2 showed no peaks under the identical conditions indicating the redox peaks in the CV of **1–3** are solely due to the metal ions. The CV plots of **1** as well as **2** and **3** recorded at different scan rates were identical and showed a proportional increase in the peak currents (SI, Figs. S6–S8). ΔEp values at different scan rates suggest the quasi-reversible redox phenomenon occurring in **1** and **2** while the reversible behavior in **3** (SI, Table S1).

*3.3. Catalytic oxidations of cumene and adamantane by **1–3** and **1a–3a***

Since compounds **1–3** were stabilized by a non-heme ligand N3Py2 and differ from each other in terms of structural and electronic properties, we then decided to test their utility in the catalytic hydroxylation of alkyl hydrocarbons (cumene and adamantane) using *m*-CPBA as an oxidant. The catalytic oxidation of cumene by **1–3** gave 2-phenyl-2-propanol as the major product along with acetophenone (Table 4, Scheme 4). The oxidation of alkanes catalyzed by nickel(II) complexes in presence of *m*-CPBA with different counter anions such as acetate and nitrate have been previously reported [30]. It was observed that the yields of organic products were highly influenced by the type of counter anions present in the nickel(II) complexes. On similar lines, we investigated the catalytic reactions of three compounds **1a-3a** which were prepared by a simple metathesis reaction of **1–3** with two equivalents of sodium tetraphenylborate. Interestingly, the TONs of 2-phenyl-2-propanol and acetophenone increased considerably when compounds **1a-3a** were used as catalysts instead of **1–3** (Table 4). This observation suggests that the product yields could be fine-tuned by using different counter anions keeping the metal ions and N3Py2 unchanged. We also studied the time dependent oxidation of cumene in the presence of catalysts **1-1a** and **2-2a**. 2-phenyl-2-propanol increased with time and the yields were higher for **1** than those for **2** (Fig. 9). On reacting adamantane (250 mM) with **1–3** and **1a–3a** (5×10^{-5} M) in presence of *m*-CPBA (50 mM), we obtained 1-adamantanol in high yields and 2-admantanol with 2-adamantanone as the minor products (Table S2, Scheme 4). The yields of products for catalysts **1–3** and **1a–3a** in the hydroxylation of cumene and adamantane increased in the order **1**(**1a**) > 2 (**2a**) > **3**(**3 a**) and our results were comparable with the reported cases [82]. When the reactions were carried out only in presence of *m*-CPBA and substrates or in presence of **1–3** or **1a–3a** and substrates, no organic products were detected [83]. When H_2O_2 and *t*-BuOOH were used as oxidants instead of *m*-CPBA, only trace amounts of alcohol products were formed [32,35].

4. Conclusion

We have reported the synthesis and characterization of three new complexes, $[Co(N3Py2)(H_2O)](ClO_4)_2$ **1**, $[Ni(N3Py2)(H_2O)](ClO_4)_2$ **2** and $[Cu(N3Py2)](ClO_4)_2$ **3** stabilized by a non-heme ligand N3Py2. Compounds **1** and **2** were structurally characterized by single crystal X-ray diffractometry. Both are isostructural and crystallized in a centrosymmetric space group $P2_1/c$. The structures of **1** and **2** shows cobalt(II) and nickel(II) ions coordinating to N3Py2 and H_2O molecule forming slightly distorted octahedral geometry. PXRD patterns of **1–3** suggest that the compound **3** has different structure. Based on spectroscopic and elemental analysis, the square pyramidal geometry has been proposed for **3**. The catalytic activity of **1–3** was studied in the C–H activation of cumene and adamantane in presence of *m*-CPBA. The cumene gave 2-phenyl-2-propanol as well as acetophenone products in good yields while adamantane afforded 1-adamantanol as the major product. The counter anion effect on product yields by replacing perchlorates of **1–3** with tertraphenylborates was investigated.

Acknowledgement

SND acknowledges University Grants Commission (UGC) and Department of Science and Technology (DST), New Delhi, India for the support to Department of Chemistry, Goa University

through their SAP and FIST programs. DDN thanks UGC, New Delhi for SRF Fellowship (UGC-BSR). SND thanks Dr. M. Sankaralingam, Post-doctoral fellow at Centre for Biomimetic Systems, Ewha Womans University, Seoul, Korea for valuable discussions.

Appendix A. Supplementary data

CCDC 1532118 and 1532119 contains the supplementary crystallographic data for **1** and **2**. These data can be obtained free of charge from 'The Cambridge Crystallographic Data Centre' via www.ccdc.cam.ac.uk/data_request/cif. Supplementary data associated with this article can be found, in the online version, at http://dx.doi.org/10.1016/j.ica.2017.08.027. These data include MOL files and InChiKeys of the most important compounds described in this article.

References

[1] T. Joshi, B. Graham, L. Spiccia, Acc. Chem. Res. 48 (2015) 2366.
[2] B. Su, Z.-C. Cao, Z.-J. Shi, Acc. Chem. Res. 48 (2015) 886.
[3] S.N. Dhuri, K.-B. Cho, Y.-M. Lee, S.Y. Shin, J.H. Kim, D. Mandal, S. Shaik, W. Nam, J. Am. Chem. Soc. 137 (2015) 8623.
[4] S.N. Dhuri, Y.-M. Lee, M.S. Seo, J. Cho, D.D. Narulkar, S. Fukuzumi, W. Nam, Dalton Trans. 44 (2015) 7634.
[5] S.N. Dhuri, M.S. Seo, Y.-M. Lee, H. Hirao, Y. Wang, W. Nam, S. Shaik, Angew. Chem. Int. Ed. 47 (2008) 3356.
[6] T.A. Jackson, J.-U. Rohde, M.S. Seo, C.V. Sastri, R. DeHont, A. Stubna, T. Ohta, T. Kitagawa, E. Münck, W. Nam, L. Que Jr., J. Am. Chem. Soc. 130 (2008) 12394.
[7] Y.-M. Lee, S.N. Dhuri, S.C. Sawant, J. Cho, M. Kubo, T. Ogura, S. Fukuzumi, W. Nam, Angew. Chem. Int. Ed. 48 (2009) 1803.
[8] W. Nam, Acc. Chem. Res. 48 (2015) 2415.
[9] F.G.C. Reinhard, M.A. Sainna, P. Upadhyay, G.A. Balan, D. Kumar, S. Fornarini, M. E. Crestoni, S.P. de Visser, Chem. Eur. J. 22 (2016) 18608.
[10] A.E. Shilov, G.B. Shul'pin, Chem. Rev. 97 (1997) 2879.
[11] B.J. Wallar, J.D. Lipscomb, Chem. Rev. 96 (1996) 2625.
[12] A.L. Feig, S.J. Lippard, Chem. Rev. 94 (1994) 759.
[13] M. Costas, M.P. Mehn, M.P. Jensen, L. Que Jr., Chem. Rev. 104 (2004) 939.
[14] M.-H. Baik, M. Newcomb, R.A. Friesner, S.J. Lippard, Chem. Rev. 103 (2003) 2385.
[15] Y. Mekmouche, S. Ménage, C. Toia-Duboc, M. Fontecave, J.-B. Galey, C. Lebrun, J. Pécaut, Angew. Chem. Int. Ed. 40 (2001) 949.
[16] M. Kodera, H. Shimakoshi, K. Kano, Chem. Commun. (1996) 1737.
[17] N. Kitajima, H. Fukui, Y. Moro-oka, J. Chem. Soc., Chem. Commun. (1988) 485.
[18] N. Kitajima, M. Ito, H. Fukui, Y. Moro-oka, J. Chem. Soc., Chem. Commun. (1991) 102.
[19] K. Chen, L. Que Jr., J. Am. Chem. Soc. 123 (2001) 6327.
[20] K. Chen, L. Que Jr., Angew. Chem. Int. Ed. 38 (1999) 2227.
[21] K. Chen, L. Que Jr., Chem. Commun. (1999) 1375.
[22] K. Chen, M. Costas, L. Que Jr., J. Chem. Soc., Dalton Trans. (2002) 672.
[23] W. Nam, R. Ho, J.S. Valentine, J. Am. Chem. Soc. 113 (1991) 7052.
[24] A.J. Fielding, J.D. Lipscomb, L. Que Jr., J. Biol. Inorg. Chem. 19 (2014) 491.
[25] F.A. Chavez, P.K. Mascharak, Acc. Chem. Res. 33 (2000) 539.
[26] S. Hong, F.F. Pfaff, E. Kwon, Y. Wang, M.-S. Seo, E. Bill, K. Ray, W. Nam, Angew. Chem. Int. Ed. 53 (2014) 10403.
[27] F.F. Pfaff, S. Kundu, M. Risch, S. Pandian, F. Heims, I. Pryjomska-Ray, P. Haack, R. Metzinger, E. Bill, H. Dau, P. Comba, K. Ray, Angew. Chem. Int. Ed. 50 (2011) 1711.
[28] B. Wang, Y.-M. Lee, W.-Y. Tcho, S. Tussupbayev, S.-T. Kim, Yujeong Kim, M.S. Seo, K.-B. Cho, Y. Dede, B.C. Keegan, T. Ogura, S.H. Kim, T. Ohta, M.-H. Baik, K. Ray, J. Shearer, W. Nam, Nat. Commun. (2017). doi: 10.1038/ncomms14839.
[29] T. Nagataki, Y. Tachi, S. Itoh, Chem. Commun. (2006) 4016.
[30] T. Nagataki, K. Ishii, Y. Tachi, S. Itoh, Dalton Trans. (2007) 1120.
[31] S. Hikichi, H. Okuda, Y. Ohzu, M. Akita, Angew. Chem. Int. Ed. 48 (2009) 188.
[32] M. Balamurugan, R. Mayilmurugan, E. Suresh, M. Palaniandavar, Dalton Trans. 40 (2011) 9413.
[33] S. Hikichi, K. Hanaue, T. Fujimura, H. Okuda, J. Nakazawa, Y. Ohzu, C. Kobayashi, M. Akita, Dalton Trans. 42 (2013) 3346.
[34] J. Nakazawa, S. Terada, M. Yamada, S. Hikichi, J. Am. Chem. Soc. 135 (2013) 6010.
[35] M. Sankaralingam, M. Balamurugan, M. Palaniandavar, P. Vadivelu, C.H. Suresh, Chem. Eur. J. 20 (2014) 11346.
[36] M. Sankaralingam, P. Vadivelu, E. Suresh, M. Palaniandavar, Inorg. Chim. Acta 407 (2013) 98.
[37] F.F. Pfaff, F. Heims, S. Kundu, S. Mebs, K. Ray, Chem. Commun. 48 (2012) 3730.
[38] T. Tano, M.Z. Ertem, S. Yamaguchi, A. Kunishita, H. Sugimoto, N. Fujieda, T. Ogura, C.J. Cramer, S. Itoh, Dalton Trans. 40 (2011) 10326.
[39] P.P.-Y. Chen, P. Nagababu, S.S.-F. Yu, S.I. Chan, ChemCatChem 6 (2014) 429.
[40] M.R. Halvagar, P.V. Solntsev, H. Lim, B. Hedman, K.O. Hodgson, E.I. Solomon, C. J. Cramer, W.B. Tolman, J. Am. Chem. Soc. 136 (2014) 7269.
[41] R.A. Himes, K.D. Karlin, Curr. Opin. Chem. Biol. 13 (2009) 119.
[42] S. Itoh, Acc. Chem. Res. 48 (2015) 2066.
[43] W. Keown, J.B. Gary, T.D.P. Stack, J. Biol. Inorg. Chem. 22 (2017) 289.
[44] A.M. Kirillov, M.V. Kirillova, L.S. Shul'pina, P.J. Figiel, K.R. Gruenwald, M.F.C. Guedes da Silva, M. Kirillova, A.J.L. Pombeiro, G.B. Shul'pin, J. Mol. Catal. A: Chem. 350 (2011) 26.
[45] A. Kunishita, H. Ishimaru, S. Nakashima, T. Ogura, S. Itoh, J. Am. Chem. Soc. 130 (2008) 4244.
[46] M.A. Lockwood, T.J. Blubaugh, A.M. Collier, S. Lovell, J.M. Mayer, Angew. Chem. Int. Ed. 38 (1999) 225.
[47] L.R. Martins, E.T. Souza, T.L. Fernandez, B. de Souza, S. Rachinski, C.B. Pinheiro, R.B. Faria, A. Casellato, S.P. Machado, A.S. Mangrich, M. Scarpellini, J. Braz. Chem. Soc. 21 (2010) 1218.
[48] R.L. Peterson, R.A. Himes, H. Kotani, T. Suenobu, L. Tian, M.A. Siegler, E.I. Solomon, S. Fukuzumi, K.D. Karlin, J. Am. Chem. Soc. 133 (2011) 1702.
[49] H.V. Obias, Y. Lin, N.N. Murthy, E. Pidcock, E.I. Solomon, M. Ralle, N.J. Blackburn, Y.-M. Neuhold, A.D. Zuberbühler, K.D. Karlin, J. Am. Chem. Soc. 120 (1998) 12960.
[50] D.D. Narulkar, A.R. Patil, C.C. Naik, S.N. Dhuri, Inorg. Chim. Acta 427 (2015) 248.
[51] S.H. Rahaman, R. Ghosh, S.K. Sarkar, B.K. Ghosh, Indian J. Chem., Sect A 44A (2005) 2474.
[52] C.K. Mann, K.K. Barnes, Electrochemical Reactions in Non-aqueous Systems, Mercel Dekker, New York, 1971. 75, 958.
[53] G.M. Sheldrick, A short history of SHELX, Acta Crystallogr. Sect. A 64 (2008) 112.
[54] T. Corona, A. Draksharapu, S.K. Padamati, I. Gamba, V. Martin-Diaconescu, F. Acunña-Parés, W.R. Browne, A. Company, J. Am. Chem. Soc. 138 (2016) 12987.
[55] J. Kaizer, E.J. Klinker, N.Y. Oh, J.-U. Rohde, W.J. Song, A. Stubna, J. Kim, E. Münck, W. Nam, L. Que Jr., J. Am. Chem. Soc. 126 (2004) 472.
[56] D.F. Leto, R. Ingram, V.W. Day, T.A. Jackson, Chem. Commun. 49 (2013) 5378.
[57] X. Wu, M.S. Seo, K.M. Davis, Y.-M. Lee, J. Chen, K.-B. Cho, Y.N. Pushkar, W. Nam, J. Am. Chem. Soc. 133 (2011) 20088.
[58] A. McAuley, C. Xu, Inorg. Chem. 31 (1992) 5549.
[59] W.R. Harris, I. Murase, J.H. Timmons, A.E. Martell, Inorg. Chem. 17 (1978) 889.
[60] A. Sánchez-Sandoval, C. Álvarez-Toledano, R. Gutiérrez-Pérez, Y. Reyes-Ortega, Synth. Commun. 33 (2003) 481.
[61] S. Singha, K.M. Parida, Catal, Sci. Technol. 1 (2011) 1496.
[62] K. Nakamoto, Infrared and Raman Spectra of Inorganic and Coordination Compounds, Part B: Applications in Coordination, Organometallic, and Bioinorganic Chemistry, sixth ed., John Wiley, Hoboken, NJ, 2009.
[63] N. Singh, J. Niklas, O. Poluektov, K.M.V. Heuvelen, A. Mukherjee, Inorg. Chim. Acta 455 (2017) 221.
[64] M.S. Kryatova, O.V. Makhlynets, A.Y. Nazarenko, E.V. Rybak-Akimova, Inorg. Chim. Acta 387 (2012) 74.
[65] A.E. Wickenden, R.A. Krause, Inorg. Chem. 4 (1965) 404.
[66] J.R. Hartman, R.W. Vachet, W. Pearson, R.J. Wheat, J.H. Callahan, Inorg. Chim. Acta 343 (2003) 119.
[67] J.R. Hartman, A.L. Kammier, R.J. Spracklin, W.H. Pearson, M.Y. Combariza, R.W. Vachet, Inorg. Chim. Acta 357 (2004) 1141.
[68] I. García-Santos, J. Sanmartín, A.M. García-Deibe, M. Fondo, E. Gómez, Inorg. Chim. Acta 363 (2010) 193.
[69] R. Ivaniková, R. Boča, L. Dlhán, H. Fuess, A. Mašlejová, V. Mrázová, I. Svoboda, J. Titiš, Polyhedron 25 (2006) 3261.
[70] J.R. Hartman, R.W. Vachet, J.H. Callahan, Inorg. Chim. Acta 297 (2000) 79.
[71] M.A. Ali, A.H. Mirza, F.H. Bujang, M. Haniti, S.A. Hamid, P.V. Bernhardt, Polyhedron 25 (2006) 3245.
[72] J.E. Huheey, E.A. Keiter, R.L. Keiter, O.K. Medhi, Inorganic Chemistry, Principles of Structure and Reactivity, fourth ed., Pearson, 1993. 466.
[73] A. Panja, T.K. Mandal, Indian J. Chem., Sect A 55A (2016) 137.
[74] S. Meghdadi, M. Amirnasr, K. Mereiter, M.K. Abdolmaleki, Acta Crystallogr. Sect. E Struct. E 66 (2010) m332–m333.
[75] A. Panja, Dalton Trans. 43 (2014) 7760.
[76] Z. Wei, Y. Peng, D.L. Hughes, J. Zhao, L. Huang, X. Liu, Polyhedron 69 (2014) 181.
[77] T.F.S. Silva, L.M.D.R.S. Martins, M.F.C. Guedes da Silva, A.R. Fernandes, A. Silva, P.M. Borralho, S. Santos, C.M.P. Rodriguese, A.J.L. Pombeiro, Dalton Trans. 41 (2012) 12888.
[78] S. Nandi, D. Bannerjee, P. Datta, T.-H. Lu, A.M.Z. Slawin, C. Sinha, Polyhedron 28 (2009) 3519.
[79] J.C. Brodovitch, R.I. Haines, A. McAuley, Can. J. Chem. 59 (1981) 1610.
[80] S.M. de M. Romanowski, F. Tormena, V.A. dos Santos, M. de F. Hermann, A.S. Mangrich, J. Braz. Chem. Soc. 15 (2004) 897.
[81] A. Congreve, R. Kataky, M. Knell, D. Parker, H. Puschmann, K. Senanayake, L. Wylie, New J. Chem. 27 (2003) 98.
[82] E. Tordin, M. List, U. Monkowius, S. Schindler, G. Knör, Inorg. Chim. Acta 402 (2013) 90.
[83] A. Bravo, H.-R. Bjorsvik, F. Fontana, F. Minisci, A. Serri, J. Org. Chem. 61 (1996) 9409.

Dalton Transactions

PAPER

View Article Online
View Journal | View Issue

Cite this: *Dalton Trans.*, 2015, **44**, 7634

Mechanistic insights into the reactions of hydride transfer *versus* hydrogen atom transfer by a *trans*-dioxoruthenium(VI) complex†

Sunder N. Dhuri,[a,b] Yong-Min Lee,[a] Mi Sook Seo,[a] Jaeheung Cho,[a] Dattaprasad D. Narulkar,[b] Shunichi Fukuzumi*[a,c] and Wonwoo Nam*[a]

A mononuclear high-valent *trans*-dioxoruthenium(VI) complex, *trans*-$[Ru^{VI}(TMC)(O)_2]^{2+}$ (TMC = 1,4,8,11-tetramethyl-1,4,8,11-tetraazacyclotetradecane), was synthesized and characterized by various spectroscopic techniques and X-ray crystallography. The reactivity of the *trans*-$[Ru^{VI}(TMC)(O)_2]^{2+}$ complex was investigated in hydride transfer and hydrogen atom transfer reactions. The mechanism of hydride transfer from dihydronicotinamide adenine dinucleotide (NADH) analogues to *trans*-$[Ru^{VI}(TMC)(O)_2]^{2+}$, which proceeds *via* a proton-coupled electron transfer (PCET), followed by a rapid electron transfer (ET), has been proposed by the observation of a good linear correlation between the log rate constants of *trans*-$[Ru^{VI}(TMC)(O)_2]^{2+}$ and *p*-chloranil (Cl_4Q) and a large kinetic isotope effect (KIE) value of 13(1). In the case of the oxidation of alkyl hydrocarbons by the *trans*-$[Ru^{VI}(TMC)(O)_2]^{2+}$ complex, the second-order rate constants were dependent on the C–H bond dissociation energy (BDE) of the substrates, and a large KIE value of 26(2) was obtained in the oxidation of xanthene and deuterated xanthene-d_2 by the *trans*-$[Ru^{VI}(TMC)(O)_2]^{2+}$ complex, indicating that the C–H bond activation of alkyl hydrocarbons proceeds *via* an H-atom abstraction in the rate-determining step.

Received 25th February 2015,
Accepted 15th March 2015

DOI: 10.1039/c5dt00809c

www.rsc.org/dalton

Introduction

Mononuclear high-valent metal-oxo complexes of heme and non-heme ligands are active oxidants in a wide range of biological and chemical oxidation reactions.[1,2] The non-heme iron(IV)-oxo species exhibit reactivities in the activation of C–H bonds of substrates that usually occurs *via* a hydrogen atom abstraction as the rate-determining step (r.d.s.).[3] Analogous to iron(IV)-oxo complexes, high-valent ruthenium(IV)-oxo species are capable of oxidizing organic substrates with activated C–H bonds by an electron transfer (ET), proton-coupled electron transfer (PCET), hydrogen atom transfer (HAT), hydride transfer (HT) or oxygen atom transfer (OAT) in aqueous and non-aqueous media.[4]

The present scenario in ruthenium chemistry reveals that ruthenium complexes with different oxidation states play dynamic roles in water oxidation catalysis (WOC), wherein various mononuclear high-valent ruthenium-oxygen intermediates, such as $[Ru^{IV}(O)]^{2+}$, $[Ru^{V}(O)]^{3+}$, $[Ru^{III}(OOH)]^{2+}$, $[Ru^{IV}(O_2)]^{2+}$ and $[Ru^{V}(O_2)]^{3+}$, have been proposed to initiate the O–O formation.[5] Unfortunately, many of these intermediates have yet to be captured and characterized due to their instability in nature. Beyond the field of WOC, however, there has been much demand to develop ruthenium catalysts for the oxidation of biologically and industrially relevant organic substrates.[6]

While a large number of non-heme ruthenium(IV)-oxo complexes have been explored, the enhanced reactivity of the higher oxidation state of ruthenium such as dioxoruthenium(VI) has merited special attention.[7–9] In ruthenium-oxo chemistry, Groves and co-workers have reported the first example of a Ru-based biomimetic dioxygenase catalyst and reported a dioxo(tetramesitylporphyrinato)ruthenium(VI), which is an efficient catalyst in an aerobic epoxidation of olefins at ambient temperatures.[10] The reaction of Ru(II)-bleomycins with O_2, H_2O_2 or PhIO was subsequently reported by Garnier-Suillerot and coworkers.[11] While Che and co-workers were the pioneers in the chemistry of high-valent dioxoruthenium(VI) species, such as *trans*-$[Ru^{VI}L(O)_2]^{2+}$ where L is the tertiary

[a]*Department of Chemistry and Nano Science, Center for Biomimetic System, Ewha Womans University, Seoul 120-750, Korea. E-mail: wwnam@ewha.ac.kr*
[b]*Department of Chemistry, Goa University, Goa, 403 206, India*
[c]*Department of Material and Life Science, Graduate School of Engineering, ALCA, JST, Osaka University, Suita, Osaka 565-0871, Japan. E-mail: fukuzumi@chem.eng.osaka-u.ac.jp*

† Electronic supplementary information (ESI) available. CCDC 1049483. For ESI and crystallographic data in CIF or other electronic format see DOI: 10.1039/c5dt00809c

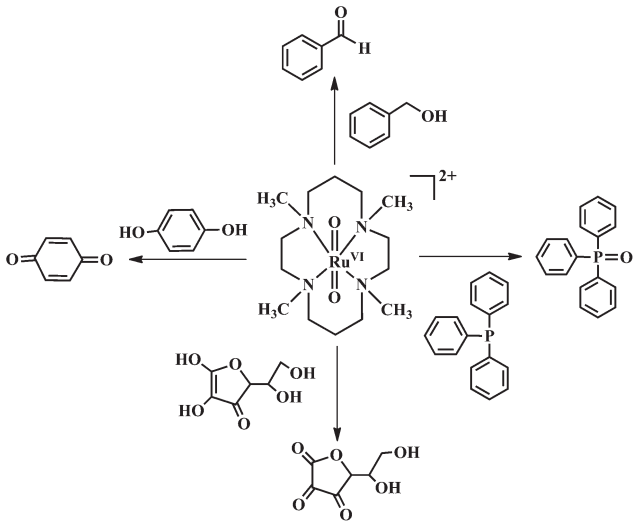

Scheme 1 Chemical structure of **1** and its reactivity in various oxidation reactions.

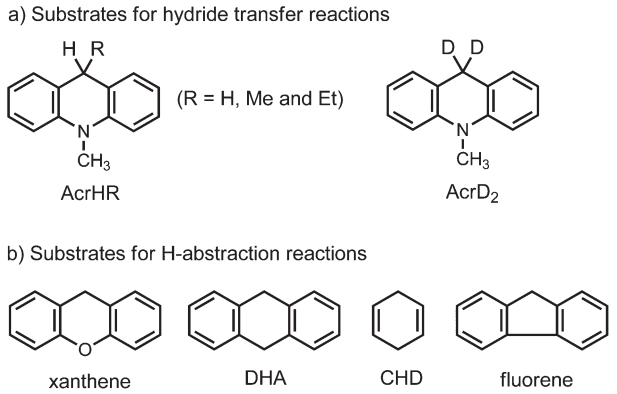

Scheme 2 Substrates used in the hydride transfer and hydrogen atom abstraction reactions.

macrocyclic amine (*e.g.*, 1,4,8,11-tetramethyl-1,4,8,11-tetraazacyclotetradecane (TMC), 1,4,8,12-tetramethyl-1,4,8,12-tetraazacyclopentadecane (15-TMC), 1,5,9,13-tetramethyl-1,5,9,13-tetraazacyclohexadecane (16-TMC) and 1,12-dimethyl-3,4:9,10-dibenzo-1,12-diaza-5,8-dioxacyclopentadecane (N_2O_2)),[9a,b,12] to the best of our knowledge, the reactivity of only two compounds, namely *trans*-$[Ru^{VI}(N_2O_2)(O)_2]^{2+}$ and *trans*-$[Ru^{VI}(TMC)(O)_2]^{2+}$ (**1**; see Scheme 1), has been explored to a large extent in the oxidative reactions of organic and inorganic substrates.[13,14] The oxidation reactions of organic compounds with **1** reported so far are summarized in Scheme 1.[13]

It is noteworthy that the dioxoruthenium(VI) complexes often react with substrates *via* different mechanisms unlike the monooxoruthenium(IV) species. For example, the oxidation of biologically relevant dihydronicotinamide adenine dinucleotide (NADH) analogues by the monooxoruthenium(IV) species, *cis*-$[Ru^{IV}(bpy)_2(py)(O)]^{2+}$, was proposed to follow hydrogen atom transfer (HAT) rather than hydride transfer (HT).[15] However, there has been no report on the reactivity of dioxoruthenium(VI) species with the NADH analogues, such as 10-methyl-9,10-dihydroacridine ($AcrH_2$) and its derivatives (see Scheme 2).[16] Although oxidation of NADH follows multiple pathways, it is usually converted to the corresponding cationic form, NAD^+, suggesting a preference the two-electron and one-proton transfer mechanism of HT.[17]

We report herein a detailed characterization of *trans*-$[Ru^{VI}(TMC)(O)_2]^{2+}$ (**1**) by various spectroscopic techniques together with X-ray crystallography and the first example of hydride transfer from NADH analogues to the high-valent dioxoruthenium(VI) complex **1** (see Schemes 1 and 2). In addition, C–H bond activation reactions of alkyl hydrocarbons by **1** were investigated to provide insights into the mechanism by which the C–H bond activation reaction proceeds *via* an H-atom abstraction as the rate-determining step.

Results and discussion

Synthesis and characterization of 1

The *trans*-$[Ru^{VI}(TMC)(O)_2](ClO_4)_2$ (**1**) complex was synthesized according to the literature procedure (see the Experimental section for the detailed synthetic method);[12] **1** is relatively stable in CH_3CN at 0 °C ($t_{1/2} \approx 6$ h). Although the UV-vis spectrum of **1** was reported previously,[12] no other spectroscopic and structural characterization of **1** has been reported yet. Thus, we have characterized this complex using various spectroscopic methods, such as ESI-MS, ^1H NMR and EPR, and X-ray crystallography. As shown in Fig. 1a, the UV-vis spectrum of **1** exhibits a vibronic band centred at 388 nm, which is characteristic of dioxo-metal complexes.[9a] ESI-MS of **1** exhibits prominent ion peaks at m/z = 195.1 and 489.0, whose mass and isotope distribution patterns correspond to $[Ru^{VI}(TMC)(O)_2]^{2+}$ (calc. m/z = 195.1) and $[Ru^{VI}(TMC)(O)_2(ClO_4)]^+$ (calc. m/z = 489.1) species, respectively (Fig. 1b). When *trans*-$[Ru^{VI}(TMC)(^{18}O)_2](ClO_4)_2$ (**1**-$^{18}O_2$) was generated using isotopically labelled $H_2{}^{18}O_2$, the mass peak at m/z = 489.0 shifts to 493.0, indicating that **1** contains two oxygen atoms. We then investigated an oxygen atom exchange reaction of **1** with isotope labelled water ($H_2{}^{18}O$). Addition of $H_2{}^{18}O$ into a solution of **1** resulted in the disappearance of the mass peak at 489.0 due to $[Ru^{VI}(TMC)(^{16}O)_2(ClO_4)]^+$ with the appearance of new mass peaks at m/z = 491 and 493, which correspond to $[Ru^{VI}(TMC)(^{16}O)(^{18}O)(ClO_4)]^+$ and $[Ru^{VI}(TMC)(^{18}O)_2(ClO_4)]^+$, respectively (Fig. 2). This result indicates that the two ^{16}O atoms bound to the ruthenium(VI) centre exchange with ^{18}O of $H_2{}^{18}O$ in a stepwise manner and the oxygen exchange takes place slowly.[18] The observations that **1** is EPR silent and the 2D ^1H–^1H COSY spectrum of **1** exhibits all peaks located in the diamagnetic region (Fig. 3) indicate that **1** is a diamagnetic low-spin (S = 0) d^2 Ru^{VI} species. Taken together, all the spectroscopic data demonstrate that **1** is a dioxoruthenium(VI) species.

In addition to the spectroscopic characterization described above, **1** was characterized structurally by X-ray crystallography. The greater thermal stability of **1** allowed the isolation of single crystals suitable for X-ray crystal structural analyses.

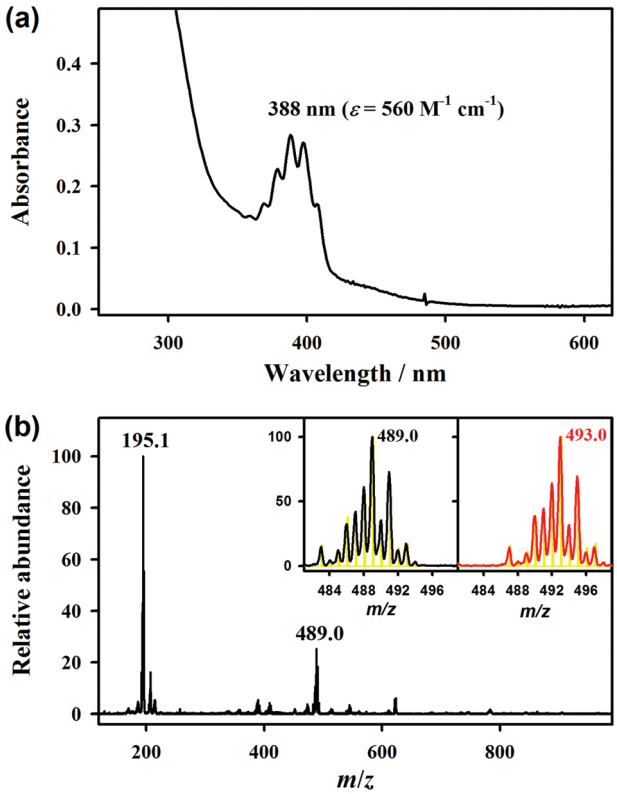

Fig. 1 (a) UV-vis spectrum of *trans*-$[Ru^{VI}(TMC)(O)_2]^{2+}$ (**1**) in CH_3CN at 0 °C. (b) ESI-MS spectrum of **1** in CH_3CN. Insets show the observed (black or red line) and calculated (yellow bar) isotope distribution patterns for **1**-$^{16}O_2$ (left panel) and **1**-$^{18}O_2$ (right panel).

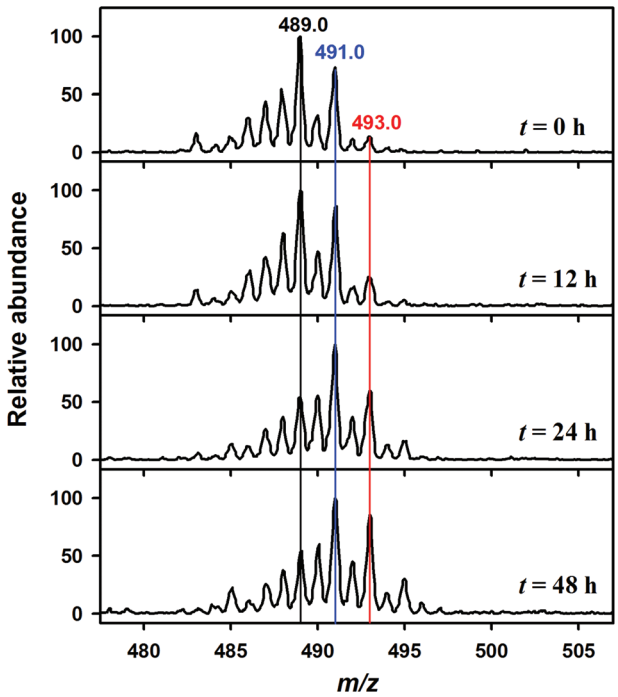

Fig. 2 ESI-MS spectra of the reaction solution obtained upon the addition of $H_2{}^{18}O$ (10 μL) to the solution of **1** (1.0 mM) at different time intervals (0 h, 12 h, 24 h and 48 h). The peaks at m/z = 489.0, 491.0 and 493.0 correspond to $[Ru^{VI}(TMC)(^{16}O)_2(ClO_4)]^{2+}$ (calc. m/z = 489.1), $[Ru^{VI}(TMC)(^{16}O)(^{18}O)(ClO_4)]^{2+}$ (calc. m/z = 491.1) and $[Ru^{VI}(TMC)(^{18}O)_2(ClO_4)]^{2+}$ (calc. m/z = 493.1), respectively.

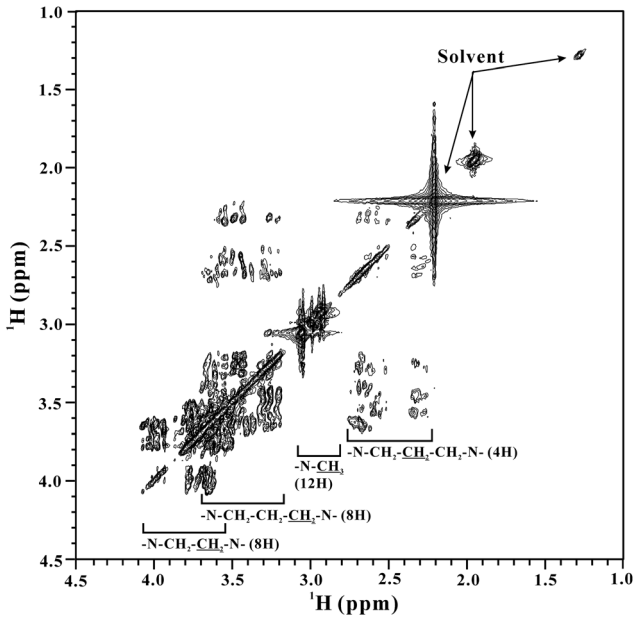

Fig. 3 2D ^1H–^1H-COSY spectrum of **1** in CD_3CN at 25 °C.

Although H atoms were not geometrically positioned due to the relatively high degree of disorders, the structure of **1** shows a perfect octahedral geometry with the space group $P2_1/c$ (Fig. S1 and Table S1, ESI†). In this structure, one oxo ligand is located *trans* to the other oxo ligand, and two *N*-methyl groups of the TMC ligand point toward one oxo ligand and the other two *N*-methyl groups of the TMC ligand point toward the other oxo ligand symmetrically. Both the *trans* Ru–O bond distances are 1.712(4) Å, which is quite similar to those reported in the dioxoruthenium(VI) complexes.[19]

Hydride transfer (HT) from NADH analogues to 1

The reactivity of **1** was investigated in HT reactions with NADH analogues, 10-methyl-9,10-dihydroacridine ($AcrH_2$) and its derivatives (see Scheme 2), in CH_3CN at 0 °C. Upon addition of $AcrH_2$ to a solution of **1** (5×10^{-5} M), $AcrH_2$ was converted to 10-methylacridinium ion ($AcrH^+$)[20] quantitatively as evidenced from the full formation of a band at 358 nm ($\varepsilon = 1.8 \times 10^4$ M^{-1} cm^{-1}) due to $AcrH^+$ (Fig. 4a) and the metal product was $[Ru^{IV}(TMC)(O)]^{2+}$ (Fig. S2, ESI† for ESI-MS).[21] First-order rate constants (k_{obs}), determined by pseudo-first order fitting of the kinetic data for the formation of $AcrH^+$ monitored at 358 nm, increased linearly with an increase in the concentration of $AcrH_2$, leading us to determine the second-order rate constant (k_{HT}) of 63(4) M^{-1} s^{-1} (Fig. 4b; see also Fig. S3a, ESI†). By using the dideuterated substrate, $AcrD_2$, a large kinetic isotope effect (KIE) value of 13(1) was determined in the reactions of

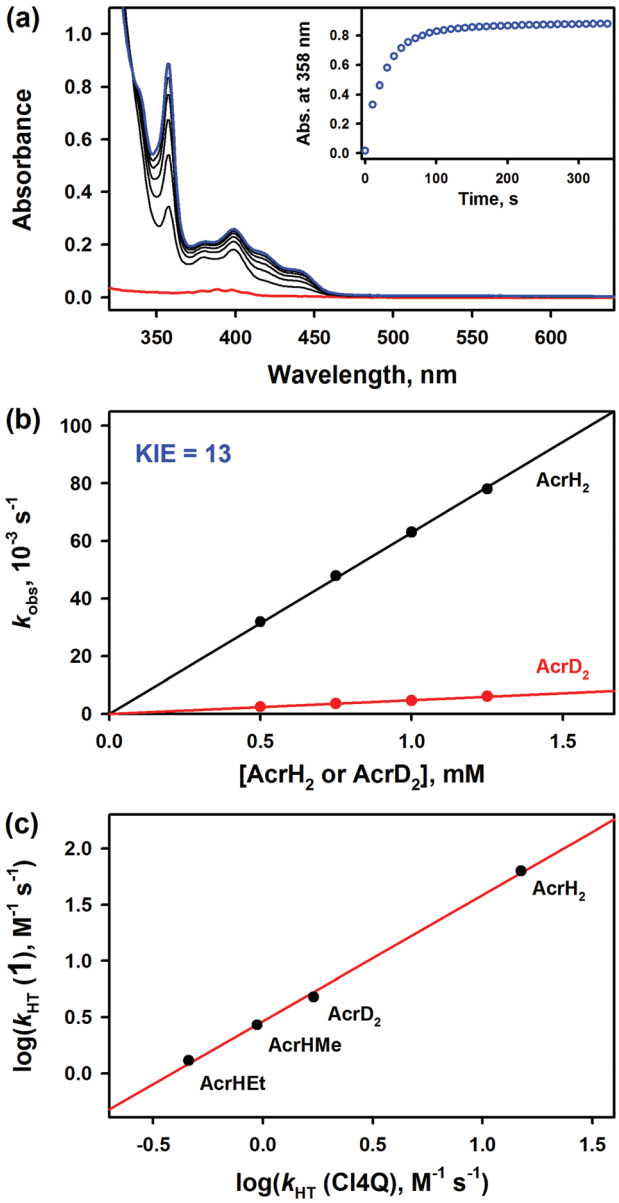

Fig. 4 (a) UV-vis spectral changes of **1** observed in the reaction of **1** (0.050 mM) and $AcrH_2$ (1.0 mM) in CH_3CN at 0 °C. Inset shows the time course monitored at 358 nm due to the formation of $AcrH^+$. (b) Plots of k_{obs} against the concentrations of $AcrH_2$ and $AcrD_2$. (c) Plot of log k_{HT} for hydride transfer from NADH analogues to **1** in CH_3CN at 0 °C *versus* log k_{HT} for hydride transfer from the same series of NADH analogues to Cl_4Q[22] in CH_3CN at 25 °C.

$AcrH_2$ *versus* $AcrD_2$ (Fig. 4b), indicating that the C–H bond cleavage of NADH analogues is involved in the rate-determining step in the HT reactions by **1**. The HT reactions were also investigated with other $AcrH_2$ derivatives bearing a substituent R at the C-9 position (*i.e.*, AcrHR), such as AcrHMe and AcrHEt. The reaction rates (k_{HT}), which were determined to be 2.7(2) M^{-1} s^{-1} for AcrHMe and 1.3(1) M^{-1} s^{-1} for AcrHEt (Fig. S3, ESI†), were significantly affected by the substituent R in the AcrHR. The observation that reactivity of AcrHR bearing an electron-donating R group is lower than that of $AcrH_2$ suggests that the HT reaction occurs *via* a sequential electron and proton transfer, followed by a rapid ET, rather than a one-step HT mechanism.[22,23] The decrease in the second-order rate constants with the increasing electron-donating ability of R (methyl or ethyl) at the C-9 position rather indicates that the reactivity is determined by the process in which a positive charge is released.[20,22] It should be noted that the reaction of $[Ru^{IV}(TMC)(O)]^{2+}$ with $AcrH_2$, which was performed as a control experiment, does not occur under identical conditions.

As reported previously, HT from NADH analogues to hydride acceptors, such as *p*-chloranil (Cl_4Q) and 2,3-dichloro-5,6-dicyano-*p*-benzoquinone, occurs *via* a proton-coupled electron transfer (PCET), followed by a rapid ET.[24,25] Further, the reactivity comparison between high-valent metal-oxo complexes and Cl_4Q was used as indirect evidence for proposing the PCET mechanism in HT reactions.[25] Thus, the rate constants of HT (k_{HT}) from NADH analogues to **1** were compared with those of HT from the same NADH analogues to Cl_4Q.[20,25,26] As shown in Fig. 4c, there is a good linear correlation between the k_{HT} values of **1** and the corresponding values of Cl_4Q with the slope of ~1, implying that HT from NADH analogues to **1** follows the same HT mechanism of Cl_4Q, which is the PCET, followed by rapid ET.[24] In addition, the k_{HT} values of HT from NADH analogues to **1** are also well correlated with the rate constants of deprotonation (k_d) of NADH radical cations (*i.e.*, one-electron oxidized product of AcrHR, $AcrHR^{\bullet+}$) as shown in Fig. S4, ESI.† As reported previously, the decay of $AcrHR^{\bullet+}$ obeys first-order kinetics and the decay rate constant of $AcrHR^{\bullet+}$ (k_d) corresponds to the rate constant of deprotonation from $AcrHR^{\bullet+}$ to produce $AcrR^{\bullet}$.[20,22] The k_d value becomes smaller by changing R from H to Me and Et because of an increase in the deprotonation barrier to form the planar $AcrR^{\bullet}$ caused by the increase in the magnitude of nonplanarity of the acridine ring upon introduction of a substituent R at the C-9 position in $AcrH_2$.[20,22] Therefore, such a linear correlation between the k_{HT} values of HT from NADH analogues to **1** and the k_d values of deprotonation of $AcrHR^{\bullet+}$ (Fig. S4, ESI†) indicates that the proton transfer (PT) from $AcrHR^{\bullet+}$ to $[Ru^{V}(TMC)(O)_2]^+$, which is the one-electron reduced species of **1**, is involved as the rate-determining step.[20,22] Based on the results of the mechanistic studies discussed above, we propose the following mechanism in the HT reactions by **1** (see Scheme 3): the HT from NADH analogues, AcrHR, to **1** occurs *via* an uphill ET from AcrHR to **1**, followed by the rate-limiting PT from $AcrHR^{\bullet+}$ to $[Ru^{V}(TMC)(O)_2]^+$ in competition with the back electron transfer, and then a rapid ET from $AcrR^{\bullet}$ to the $[Ru^{V}(TMC)(O)(OH)]^{2+}$ species to produce $AcrR^+$, which is an NAD^+ analogue, and the $[Ru^{IV}(TMC)(O)]^{2+}$ complex.

C–H bond activation of alkyl hydrocarbons by 1

The reactivity of **1** in the oxidation of alkyl hydrocarbons was also investigated. The reactions of **1** with alkyl hydrocarbons having weak C–H bond dissociation energies (BDE),[27] such as xanthene (75.5 kcal mol^{-1}), dihydroanthracene (DHA; 77.0 kcal

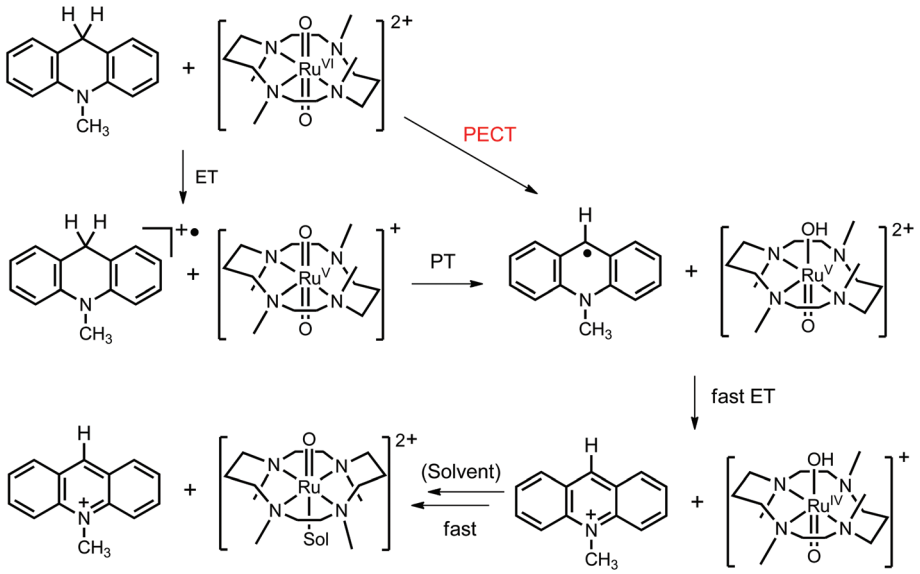

Scheme 3 Proposed mechanism for HT from NADH analogues, AcrHR, to **1**.

mol^{-1}), 1,4-cyclohexadiene (CHD; 78.0 kcal mol^{-1}) and fluorene (80.0 kcal mol^{-1}) (see Scheme 2), were carried out in CH_3CN at 35 °C. As shown in Fig. 5a, addition of xanthene to the acetonitrile solution of **1** (0.50 mM) afforded the disappearance of a vibronic structural absorption peak at 388 nm due to **1**, accompanied by a new absorption band formation at 420 nm, which corresponds to $[Ru^{IV}(TMC)(O)(CH_3CN)]^{2+}$,[21] with clean isosbestic points at 345 and 415 nm (Fig. 5a). The formation of $[Ru^{IV}(TMC)(O)(CH_3CN)]^{2+}$ was confirmed by ESI-MS spectroscopy (Fig. 5b); the ESI-MS spectrum of the reaction solution exhibits prominent ion peaks at m/z = 207.5 and 473.0, whose mass and isotope distribution patterns correspond to $[Ru^{IV}(TMC)(O)(CH_3CN)]^{2+}$ (calc. m/z = 207.6) and $[Ru^{IV}(TMC)(O)(ClO_4)]^{+}$ (calc. m/z = 473.1), respectively. This was also confirmed by cyclic voltammetry for the reaction of **1** with DHA (Fig. S5, ESI†). The first-order rate constants (k_{obs}) determined by pseudo-first-order fitting of the kinetic data for the decay of **1** at 388 nm increased proportionally with the increase of xanthene concentration, leading us to determine the second-order rate constant (k_{HAT}) of 5.7(4) × 10^{-2} M^{-1} s^{-1} at 35 °C (Fig. 5c; see also Fig. S6a, ESI†). It should be noted that, although the reaction product, $[Ru^{IV}(TMC)(O)(CH_3CN)]^{2+}$, reacts further with xanthene,[21] the rate of xanthene oxidation by **1** is 20-fold faster than that of the $[Ru^{IV}(TMC)(O)(CH_3CN)]^{2+}$ reaction with xanthene at the same temperature. In order to determine the KIE value, xanthene-d_2 was used as a substrate and the second-order rate constant of 2.2(2) × 10^{-3} M^{-1} s^{-1} was obtained (Fig. 5c), resulting in a large KIE value of 26(2) for the reactions of xanthene *versus* xanthene-d_2 (Fig. 5d). This result indicates that the H-atom abstraction of alkyl hydrocarbons by **1** is involved in the rate-determining step. It should be noted that such a large KIE value in HAT reactions as well as in HT reactions is probably attributable to the tunnelling effects.[4d,f,h,7b,9e,15]

The C–H bond activation reactions were also investigated with other alkyl hydrocarbons, such as DHA, CHD and fluorene. The second-order rate constants (k_{HAT}) of 3.6(4) × 10^{-2} and 1.5(2) × 10^{-2} M^{-1} s^{-1} were determined in the reactions of **1** with DHA and CHD, respectively (Fig. S6, ESI†). However, **1** did not show a reactivity with fluorene, which has a relatively strong C–H BDE value (80.0 kcal mol^{-1}) compared to other alkyl hydrocarbons used in this study. As expected, the rate constants (k_{HAT}) decreased with an increase in the C–H BDE of alkyl hydrocarbons. Fig. 5d shows a linear correlation between the log k'_2 values and the C–H BDE values of the substrates (the k_{HAT} values are divided by the number of equivalent target C–H bonds of substrates to obtain the k'_2 values).[28,29] The final reaction solutions obtained in the oxidation of alkyl hydrocarbons by **1** were analyzed by gas chromatography (GC). Xanthone (87 ± 4%), anthracene (90 ± 4%) and benzene (88 ± 5%) were formed as the major organic products in the oxidation of xanthene, DHA and CHD by **1**, respectively.

The results of the large KIE values, the good correlation between the log k_{HAT} and C–H BDE of alkyl hydrocarbons and organic/inorganic product analyses allowed us to propose that the C–H bond activation of alkyl hydrocarbons by **1** occurs *via* an H-atom abstraction mechanism as shown in Scheme 4.

Conclusions

In summary, we have synthesized and characterized the mononuclear high-valent *trans*-dioxoruthenium(VI) complex bearing a macrocyclic supporting ligand, *trans*-$[Ru^{VI}(TMC)(O)_2]^{2+}$ (**1**). Reactivities of **1** in HT reactions with NADH analogues and HAT reactions with alkyl hydrocarbons were investigated. On the basis of the reactivity studies, the mechanisms of HT from the NADH analogues to **1** and the HAT of alkyl hydrocarbons

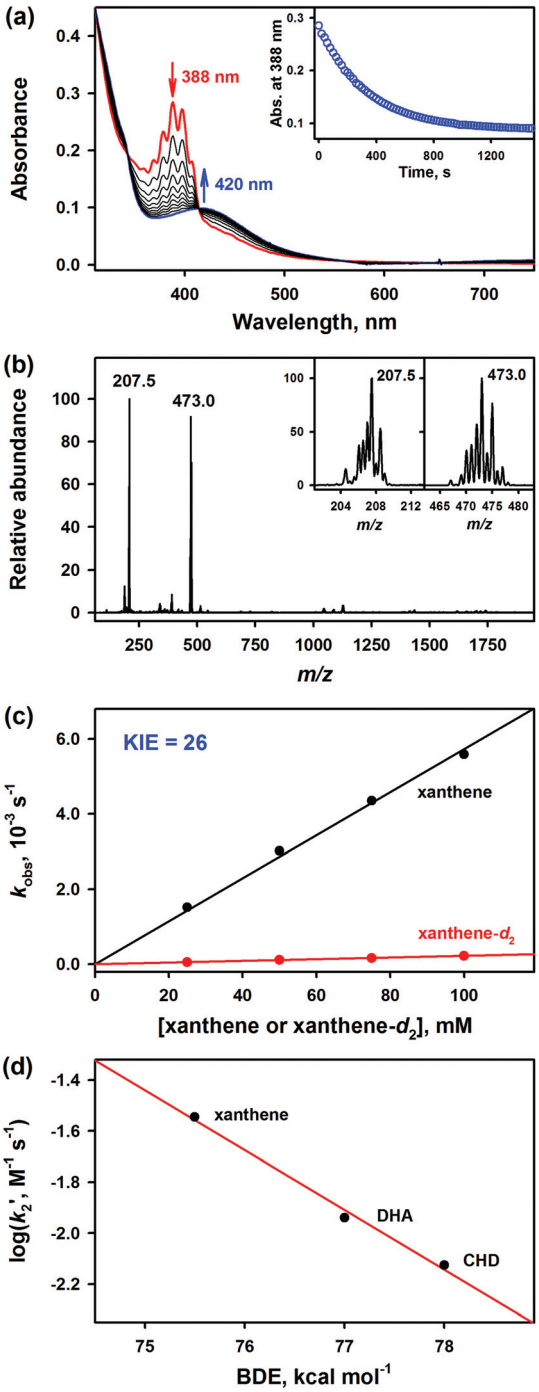

Fig. 5 (a) UV-vis spectral changes of **1** (0.50 mM) upon the addition of xanthene (50 mM) at 35 °C. Inset shows the time course of the decay of **1** monitored at 388 nm. (b) ESI-MS spectrum of the reaction solution obtained in the reaction of **1** (1.0 mM) with xanthene (50 mM) in CH_3CN at 35 °C. The peaks at m/z = 207.5 and 473.0 correspond to $[Ru^{IV}(TMC)(O)(CH_3CN)]^{2+}$ (calc. m/z = 207.6) and $[Ru^{IV}(TMC)(O)(ClO_4)]^{+}$ (calc. m/z = 473.1), respectively. Insets show the isotopic distribution patterns of the peaks at m/z = 207.5 and 473.0. (c) Plots of k_{obs} against the concentrations of xanthene and xanthene-d_2 to determine the KIE value of 26(2). (d) Plot of log k'_2 of **1** against C–H BDE of the substrates. Second-order rate constants (k_{HAT}) were determined at 35 °C and then adjusted for the reaction stoichiometry to yield k'_2 based on the number of equivalent target C–H bonds of the substrates (*e.g.*, 2 for xanthene and 4 for DHA and CHD).

by **1** have been proposed; the HT from NADH analogues, AcrHR, to **1** occurs *via* an uphill ET from AcrHR to **1**, followed by the rate-limiting PT from $AcrHR^{\bullet+}$ to $[Ru^{V}(TMC)(O)_2]^{+}$ species, and then a rapid ET from $AcrR^{\bullet}$ to the $[Ru^{V}(TMC)(O)(OH)]^{2+}$ species. In the case of the HAT reaction by **1**, the C–H bond activation of alkyl hydrocarbons by **1** occurs *via* an H-atom abstraction mechanism. The mechanistic distinction between NADH analogues and alkyl hydrocarbons may result from the significantly lower one-electron oxidation potentials of NADH analogues than those of alkyl hydrocarbons, which enables the ET pathway.[22–24] Thus, the present work provides valuable insights into the mechanism of the HT and HAT reactions by high-valent dioxoruthenium(VI) species.

Experimental

Materials

Commercially available chemicals were used without further purification unless otherwise indicated. The solvents were distilled under N_2 prior to use according to the published procedures.[30] Potassium aquapentachlororuthenate(III) ($K_2[Ru(H_2O)(Cl)_5]$), TMC, xanthene, 9,10-dihydroanthracene, 1,4-cyclohexadiene, $HClO_4$, H_2O_2 (30%) and $NaClO_4$ were purchased from Aldrich Chemical Co. The isotope labelled $H_2{}^{18}O$ (95% ^{18}O-atom enriched) and $H_2{}^{18}O_2$ (90% ^{18}O-enriched, 2% $H_2{}^{18}O_2$ in $H_2{}^{18}O$) were obtained from ICON Services Inc. (Summit, NJ, USA). The NADH analogues, 10-methyl-9,10-dihydroacridine ($AcrH_2$), 10-methyl-9,10-dideuteroacridine ($AcrD_2$) and 9-alkyl-10-methyl-9,10-dihydroacridine (AcrHR; R = Me and Et), were prepared by the literature methods.[22] The dideuterated substrate xanthene-d_2, was also prepared by a literature method.[31] Xanthene (0.50 g, 2.7 mmol) was reacted with NaH (0.20 g, 8.1 mmol) in DMSO-d_6 (3.0 mL) under an inert atmosphere. The deep red solution was stirred at room temperature for 8 h and then quenched with D_2O (5.0 mL). The crude product was filtered and washed with copious amounts of D_2O. ^1H NMR confirmed >99% deuteration. Ruthenium complexes, *trans*-$[Ru^{III}(TMC)Cl_2]Cl$ and $[Ru^{IV}(TMC)(O)(CH_3CN)](ClO_4)_2$ were prepared by the literature method.[9a,32]

Instrumentation

UV-vis spectra and kinetic data were collected using a Hewlett Packard Agilent 8453 UV-visible spectrophotometer equipped with an UNISOKU Scientific Instruments or with a circulating water bath. Electrospray ionization mass (ESI-MS) spectra were collected using a Thermo Finnigan (San Jose, CA, USA) LCQ™ Advantage MAX quadrupole ion trap instrument, by infusing samples directly into the source at 20 μL min^{-1} using a syringe pump. The spray voltage was set at 4.7 kV while the capillary temperature was maintained at 80 °C. The electron paramagnetic resonance (EPR) spectra were recorded using an X-band Bruker EMX-plus spectrometer equipped with a dual mode cavity (ER 4116DM). Low temperatures were achieved by using an Oxford Instruments ESR900 liquid He quartz cryostat with

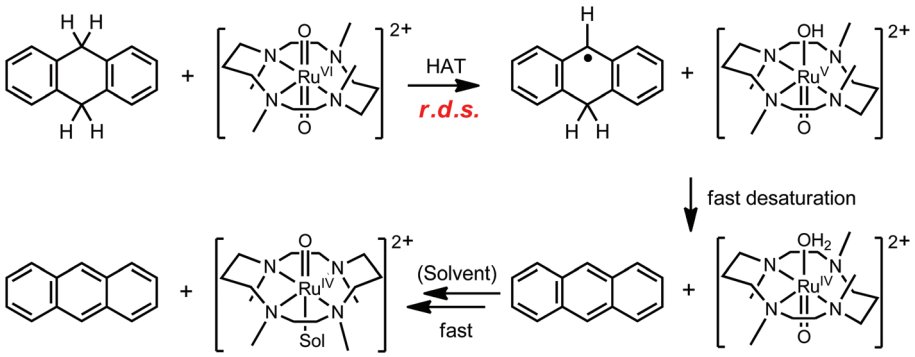

Scheme 4 Proposed mechanism for HAT reactions of DHA by **1**.

an Oxford Instruments ITC503 temperature and gas flow controller. The experimental parameters for EPR spectra were as follows: microwave frequency = 9.648 GHz, microwave power = 1.0 mW, modulation amplitude = 10 G, gain = 1×10^4, modulation frequency 100 kHz, time constant = 40.96 ms, conversion time = 85.00 ms and measuring temperature = 5 K. ^{1}H NMR spectra were recorded using a Bruker model digital AVANCE III 400 FT-NMR spectrometer. Electrochemical measurements (*i.e.*, cyclic voltammetry) were performed using a CH Instrument (CHI630B) electrochemical analyzer in deaerated CH_3CN in the presence of 0.10 M tetra-*n*-butylammonium hexafluorophosphate (Bu_4NPF_6) as a supporting electrolyte. A conventional three-electrode cell was used with a platinum working electrode (surface area of 0.3 mm^2) and a platinum wire as a counter electrode. The platinum working electrodes (BAS) were routinely polished with a BAS polishing alumina suspension and rinsed with CH_3CN before use. The measured potentials were recorded as a function of the Ag/$AgNO_3$ (0.01 M) reference electrode. All potentials (*vs.* Ag/Ag$^+$) were converted to values *vs.* SCE by adding 0.29 V.[33] An organic product analysis was carried out using an Agilent Technologies 6890N gas chromatograph (GC) and a Thermo Finnigan (Austin, Texas, USA) FOCUS DSQ (dual stage quadrupole) mass spectrometer interfaced with a Finnigan FOCUS gas chromatograph (GC-MS).

Preparation of *trans*-[Ru^{VI}(TMC)(O)$_2$]$^{2+}$ (1)

Trans-[Ru^{VI}(TMC)(O)$_2$]$^{2+}$ (**1**) was prepared by a literature procedure.[12] Silver *p*-toluenesulfonate (0.54 g, 1.9 mmol) was added to the aqueous solution of *trans*-[Ru^{III}(TMC)Cl$_2$]Cl (0.30 g, 0.58 mmol) and the mixture was warmed on a water bath for 30 min. The white precipitates of AgCl formed were filtered and H_2O_2 (30%, 3.0 mL) was added to the filtrate. The solution was then heated on a water bath until the full formation of a peak at 388 nm in the UV-vis spectrum for **1** was observed. The saturated solution (5.0 mL) of $NaClO_4$ was then added to the mixture and kept for cooling in a refrigerator. After 2 days, a yellow solid complex with a yield of 55% was formed.

Kinetic measurements and reactivity study

All the reactions were run in a 1 cm quartz cuvette and followed by monitoring the UV-vis spectral changes of the reaction solutions. The rate constants were determined under pseudo-first-order conditions (*e.g.*, [substrate]/[**1**] > 10), by fitting the changes in absorbance for the formation of a 358 nm peak due to AcrH$^+$ ions in the reaction of **1** with NADH analogues at 0 °C. In the oxidation of alkyl hydrocarbons by **1**, the reactions were monitored by UV-vis spectral changes of the absorption band at 388 nm due to the decay of **1**. First order rate constants were obtained by fitting of the kinetic data at 388 nm. The hydrocarbons with C–H bond dissociation energies (BDE) ranging between 75–80 kcal mol^{-1} were chosen for the reactivity studies. The reactions were run at least in triplicate, and the data reported here represent the average of these reactions.

Product analysis

The organic product AcrH$^+$ formed in the reaction of **1** and AcrH$_2$ was quantitatively detected by the absorption band at 358 nm due to AcrH$^+$ ions by UV-vis spectroscopy. The AcrH$^+$ was also detected by an ESI-MS spectrum, which showed a peak at m/z = 194.1 for AcrH$^+$ ions (Fig. S2, ESI†). In the oxidation of xanthene, DHA and CHD by **1**, the complete reaction solutions were analyzed by GC. Product yields were determined by comparing the peak areas with the standard curves obtained using authentic samples and decane as an internal standard. The reaction products for xanthene, DHA and CHD were determined to be xanthone (87 ± 4%), anthracene (90 ± 4%) and benzene (88 ± 5%) as the major organic products, respectively. The ruthenium products formed in the reaction of **1** with AcrH$_2$ as well as alkyl hydrocarbons were analyzed by EPR and ESI-MS techniques. In both reactions, [Ru^{IV}(TMC)(O)]$^{2+}$ species was formed as a final product.[9a,21]

Acknowledgements

The authors gratefully acknowledge research support of this work by the NRF of Korea through CRI (NRF-2012R1A3A2048842

to W.N.) and GRL (NRF-2010-00353 to W.N.), and by an ALCA project from JST, Japan (to S.F). S.N.D. acknowledges research support from the Department of Science and Technology (DST), New Delhi, India through the SR/FT/CS-006/2010 project.

Notes and references

1 (*a*) R. A. Sheldon and J. K. Kochi, *Metal-Catalyzed Oxidations of Organic Compounds*, Academic Press, New York, 1981; (*b*) B. Meunier, *Biomimetic Oxidations Catalyzed by Transition Metal Complexes*, Imperial College Press, London, 1998; (*c*) P. R. Ortiz de Montellano, *Cytochrome P450: Structure, Mechanism, and Biochemistry*, Kluwer Academic/Plenum Publishers, New York, 3rd edn, 2005.

2 (*a*) C. Krebs, D. G. Fujimori, C. T. Walsh and J. M. Bollinger, Jr., *Acc. Chem. Res.*, 2007, **40**, 484–492; (*b*) J. Hohenberger, K. Ray and K. Meyer, *Nat. Commun.*, 2012, **3**, DOI: 10.1038/ncomms1718; (*c*) C.-M. Che, V. K.-Y. Lo, C.-Y. Zhou and J.-S. Huang, *Chem. Soc. Rev.*, 2011, **40**, 1950–1975; (*d*) T. Punniyamurthy, S. Velusamy and J. Iqbal, *Chem. Rev.*, 2005, **105**, 2329–2363; (*e*) A. S. Borovik, *Chem. Soc. Rev.*, 2011, **40**, 1870–1874; (*f*) H. Kotani, S. Kaida, T. Ishizuka, M. Sakaguchi, T. Ogura, Y. Shiota, K. Yoshizawa and T. Kojima, *Chem. Sci.*, 2015, **6**, 945–955.

3 (*a*) W. Nam, Y.-M. Lee and S. Fukuzumi, *Acc. Chem. Res.*, 2014, **47**, 1146–1154; (*b*) W. Nam, *Acc. Chem. Res.*, 2007, **40**, 522–531; (*c*) S. P. de Visser, J.-U. Rohde, Y.-M. Lee, J. Cho and W. Nam, *Coord. Chem. Rev.*, 2013, **257**, 381–393; (*d*) S. Shaik, H. Hirao and D. Kumar, *Acc. Chem. Res.*, 2007, **40**, 532–542; (*e*) M. T. Green, *Curr. Opin. Chem. Biol.*, 2009, **13**, 84–88; (*f*) J. Kaizer, E. J. Klinker, N. Y. Oh, J.-U. Rohde, W. J. Song, A. Stubna, J. Kim, E. Münck, W. Nam and L. Que, Jr., *J. Am. Chem. Soc.*, 2004, **126**, 472–473; (*g*) A. Gunay and K. H. Theopold, *Chem. Rev.*, 2010, **110**, 1060–1081; (*h*) K. Ray, F. F. Pfaff, B. Wang and W. Nam, *J. Am. Chem. Soc.*, 2014, **136**, 13942–13958.

4 (*a*) S. A. Trammell, J. C. Wimbish, F. Odobel, L. A. Gallagher, P. M. Narula and T. J. Meyer, *J. Am. Chem. Soc.*, 1998, **120**, 13248–13249; (*b*) L. K. Stultz, M. H. V. Huynh, R. A. Binstead, M. Curry and T. J. Meyer, *J. Am. Chem. Soc.*, 2000, **122**, 5984–5996; (*c*) W. K. Seok and T. J. Meyer, *J. Am. Chem. Soc.*, 1988, **110**, 7358–7367; (*d*) L. Roecker and T. J. Meyer, *J. Am. Chem. Soc.*, 1987, **109**, 746–754; (*e*) M. S. Thompson and T. J. Meyer, *J. Am. Chem. Soc.*, 1982, **104**, 5070–5076; (*f*) M. S. Thompson and T. J. Meyer, *J. Am. Chem. Soc.*, 1982, **104**, 4106–4115; (*g*) W. K. Seok and T. J. Meyer, *Inorg. Chem.*, 2004, **43**, 5205–5215; (*h*) J. R. Bryant and J. M. Mayer, *J. Am. Chem. Soc.*, 2003, **125**, 10351–10361.

5 (*a*) I. López, M. Z. Ertem, S. Maji, J. Benet-Buchholz, A. Keidel, U. Kuhlmann, P. Hildebrandt, C. J. Cramer, V. S. Batista and A. Llobet, *Angew. Chem., Int. Ed.*, 2014, **53**, 205–209; (*b*) J. J. Concepcion, J. W. Jurss, J. L. Templeton and T. J. Meyer, *J. Am. Chem. Soc.*, 2008, **130**, 16462–16463; (*c*) Z. Chen, J. J. Concepcion, H. Luo, J. F. Hull, A. Paul and T. J. Meyer, *J. Am. Chem. Soc.*, 2010, **132**, 17670–17673; (*d*) X. Liu and F. Wang, *Coord. Chem. Rev.*, 2012, **256**, 1115–1136; (*e*) C.-M. Che, V. W.-W. Yam and T. C. W. Mak, *J. Am. Chem. Soc.*, 1990, **112**, 2284–2291; (*f*) X. Guan, S. L.-F. Chan and C.-M. Che, *Chem. – Asian J.*, 2013, **8**, 2046–2056.

6 (*a*) A. K. Vannucci, J. F. Hull, Z. Chen, R. A. Binstead, J. J. Concepcion and T. J. Meyer, *J. Am. Chem. Soc.*, 2012, **134**, 3972–3975; (*b*) T. Naota, H. Takaya and S.-I. Murahashi, *Chem. Rev.*, 1998, **98**, 2599–2660; (*c*) M. Pagliaro, S. Campestrini and R. Ciriminna, *Chem. Soc. Rev.*, 2005, **34**, 837–845; (*d*) P. B. Arockiam, C. Bruneau and P. H. Dixneuf, *Chem. Rev.*, 2012, **112**, 5879–5918; (*e*) T. Ishizuka, S. Ohzu and T. Kojima, *Synlett*, 2014, **25**, 1667–1679; (*f*) T. Ishizuka, S. Ohzu, H. Kotani, Y. Shiota, K. Yoshizawa and T. Kojima, *Chem. Sci.*, 2014, **5**, 1429–1436; (*g*) S. Ohzu, T. Ishizuka, Y. Hirai, H. Jiang, M. Sakaguchi, T. Ogura, S. Fukuzumi and T. Kojima, *Chem. Sci.*, 2012, **3**, 3421–3431.

7 (*a*) S. L.-F. Chan, Y.-H. Kan, K.-L. Yip, J.-S. Huang and C.-M. Che, *Coord. Chem. Rev.*, 2011, **255**, 899–919; (*b*) W. W. Y. Lam, S.-M. Yiu, D. T. Y. Yieu, T.-C. Lau, W.-P. Yip and C.-M. Che, *Inorg. Chem.*, 2003, **42**, 8011–8018; (*c*) T. Kojima, Y. Hirai, T. Ishizuka, Y. Shiota, K. Yoshizawa, K. Ikemura, T. Ogura and S. Fukuzumi, *Angew. Chem., Int. Ed.*, 2010, **49**, 8449–8453; (*d*) M. Rodríguez, I. Romeroa, C. Sens and A. Llobet, *J. Mol. Catal. A: Chem.*, 2006, **282**, 215–220.

8 (*a*) Y.-N. Wang, K.-C. Lau, W. W. Y. Lam, W.-L. Man, C.-F. Leung and T.-C. Lau, *Inorg. Chem.*, 2009, **48**, 400–406; (*b*) Y. Huang, E. Vanover and R. Zhang, *Chem. Commun.*, 2010, **46**, 3776–3778.

9 (*a*) C.-M. Che, T.-F. Lai and K.-Y. Wong, *Inorg. Chem.*, 1987, **26**, 2289–2299; (*b*) C.-M. Che, W.-T. Tang, W.-T. Wong and T.-F. Lai, *J. Am. Chem. Soc.*, 1989, **111**, 9048–9056; (*c*) C. Abebrese, Y. Huang, A. Pan, Z. Yuan and R. Zhang, *J. Inorg. Biochem.*, 2011, **105**, 1555–1561; (*d*) C.-M. Che, W.-T. Tang, W.-O. Lee, K.-Y. Wong and T.-C. Lau, *J. Chem. Soc., Dalton Trans.*, 1992, 1551–1556; (*e*) E. L. Lebeau and T. J. Meyer, *Inorg. Chem.*, 1999, **38**, 2174–2181.

10 J. T. Groves and R. Quinn, *J. Am. Chem. Soc.*, 1985, **107**, 5790–5792.

11 B. Mouzopoulou, H. Kozlowski, N. Katsaros and A. Garnier-Suillerot, *Inorg. Chem.*, 2001, **40**, 6923–6929.

12 C.-M. Che, K.-Y. Wong and C.-K. Poon, *Inorg. Chem.*, 1985, **24**, 1797–1800.

13 W. W. Y. Lam, W.-L. Man and T.-C. Lau, *Coord. Chem. Rev.*, 2007, **251**, 2238–2252.

14 (*a*) W.-C. Cheng, W.-Y. Yu, C.-K. Li and C.-M. Che, *J. Org. Chem.*, 1995, **60**, 6840–6846; (*b*) W. W. Y. Lam, W.-L. Man, Y.-N. Wang and T.-C. Lau, *Inorg. Chem.*, 2008, **47**, 6771–6778; (*c*) W. W. Y. Lam, M. F. W. Lee and T.-C. Lau, *Inorg. Chem.*, 2006, **45**, 315–321; (*d*) W.-L. Man, W. W. Y. Lam, W.-Y. Wong and T.-C. Lau, *J. Am. Chem. Soc.*, 2006, **128**, 14669–14675; (*e*) C.-M. Che and K.-Y. Wong, *J. Chem. Soc., Dalton Trans.*, 1989, 2065–2067; (*f*) W.-L. Man,

W. W. Y. Lam, S.-M. Ng, W. Y. K. Tsang and T.-C. Lau, *Chem. – Eur. J.*, 2012, **18**, 138–144; (*g*) D. T. Y. Yiu, M. F. W. Lee, W. W. Y. Lam and T.-C. Lau, *Inorg. Chem.*, 2003, **42**, 1225–1232.

15 T. Matsuo and J. M. Mayer, *Inorg. Chem.*, 2005, **44**, 2150–2158.

16 (*a*) D. Mauzerall and F. H. Westheimer, *J. Am. Chem. Soc.*, 1955, **77**, 2261–2264; (*b*) L. Stryer, *Biochemistry*, Freeman, New York, 3rd edn, 1988, ch. 17.

17 N. Song, M.-T. Zhang, R. A. Binstead, Z. Fang and T. J. Meyer, *Inorg. Chem.*, 2014, **53**, 4100–4105.

18 M. S. Seo, J.-H. In, S. O. Kim, N. Y. Oh, J. Hong, J. Kim, L. Que, Jr. and W. Nam, *Angew. Chem., Int. Ed.*, 2004, **43**, 2417–2420.

19 (*a*) T. C. W. Mak, C.-M. Che and K.-Y. Wong, *J. Chem. Soc., Chem. Commun.*, 1985, 986–988; (*b*) C.-M. Che, J.-L. Zhang, R. Zhang, J.-S. Huang, T.-S. Lai, W.-M. Tsui, X.-G. Zhou, Z.-Y. Zhou, N. Zhu and C. M. Chang, *Chem. – Eur. J.*, 2005, **11**, 7040–7053; (*c*) T.-S. Lai, R. Zhang, K.-K. Cheung, H.-L. Kwong and C.-M. Che, *Chem. Commun.*, 1998, 1583–1584; (*d*) T. J. Meyer and M. H. V. Huynh, *Inorg. Chem.*, 2003, **42**, 8140–8160.

20 S. Fukuzumi, H. Kotani, Y.-M. Lee and W. Nam, *J. Am. Chem. Soc.*, 2008, **130**, 15134–15142.

21 S. N. Dhuri, M. S. Seo, Y.-M. Lee, H. Hirao, Y. Wang, W. Nam and S. Shaik, *Angew. Chem., Int. Ed.*, 2008, **47**, 3356–3359.

22 S. Fukuzumi, Y. Tokuda, T. Kitano, T. Okamoto and J. Otera, *J. Am. Chem. Soc.*, 1993, **115**, 8960–8968.

23 H. Yoon, Y.-M. Lee, W. Nam and S. Fukuzumi, *Chem. Commun.*, 2014, **50**, 12944–12946.

24 (*a*) S. Fukuzumi, S. Koumitsu, K. Hironaka and T. Tanaka, *J. Am. Chem. Soc.*, 1987, **109**, 305–316; (*b*) S. Fukuzumi, K. Ohkubo, Y. Tokuda and T. Suenobu, *J. Am. Chem. Soc.*, 2000, **122**, 4286–4294.

25 Y. J. Jeong, Y. Kang, A.-R. Han, Y.-M. Lee, H. Kotani, S. Fukuzumi and W. Nam, *Angew. Chem., Int. Ed.*, 2008, **47**, 7321–7324.

26 (*a*) J. Y. Lee, Y.-M. Lee, H. Kotani, W. Nam and S. Fukuzumi, *Chem. Commun.*, 2009, 704–706; (*b*) S. Fukuzumi, N. Fujioka, H. Kotani, K. Ohkubo, Y.-M. Lee and W. Nam, *J. Am. Chem. Soc.*, 2009, **131**, 17127–17134; (*c*) Y. Han, Y.-M. Lee, M. Mariappan, S. Fukuzumi and W. Nam, *Chem. Commun.*, 2010, **46**, 8160–8162; (*d*) S. Fukuzumi, H. Kotani, K. A. Prokop and D. P. Goldberg, *J. Am. Chem. Soc.*, 2011, **133**, 1859–1869.

27 Y.-R. Luo, *Handbook of Bond Dissociation Energies in Organic Compounds*, CRC Press, New York, 2003.

28 (*a*) J. M. Mayer, *Acc. Chem. Res.*, 1998, **31**, 441–450; (*b*) A. S. Borovik, *Acc. Chem. Res.*, 2005, **38**, 54–61; (*c*) C. R. Goldsmith, A. P. Cole and T. D. P. Stack, *J. Am. Chem. Soc.*, 2005, **127**, 9904–9912.

29 (*a*) T. Kojima, K. Nakayama, K. Ikemura, T. Ogura and S. Fukuzumi, *J. Am. Chem. Soc.*, 2011, **133**, 11692–11700; (*b*) K.-B. Cho, X. Wu, Y.-M. Lee, Y. H. Kwon, S. Shaik and W. Nam, *J. Am. Chem. Soc.*, 2012, **134**, 20222–20225.

30 W. L. F. Armarego and C. L. L. Chai, *Purification of Laboratory Chemicals*, Pergamon Press, Oxford, UK, 6th edn, 2009.

31 C. V. Sastri, J. Lee, K. Oh, Y. J. Lee, J. Lee, T. A. Jackson, K. Ray, H. Hirao, W. Shin, J. A. Halfen, J. Kim, L. Que, Jr., S. Shaik and W. Nam, *Proc. Natl. Acad. Sci. USA*, 2007, **104**, 19181–19186.

32 C.-M. Che, S.-S. Kwong and C.-K. Poon, *Inorg. Chem.*, 1985, **24**, 1601–1602.

33 C. K. Mann and K. K. Barnes, *Electrochemical Reactions in Non-aqueous Systems*, Marcel Dekker, New York, 1970.

ЖУРНАЛ СТРУКТУРНОЙ ХИМИИ

2018. Том 59, № 5 *Июнь – июль* *С. 1207 – 1214*

CRYSTAL STRUCTURE OF THE MONONUCLEAR NON-HEME Ni(II) OCTAHEDRAL COMPLEX: $[Ni(II)(bqenH_2)(bpy)](ClO_4)_2$

D.D. Narulkar[1], A.K. Srivastava[2], R.J. Butcher[3], S.N. Dhuri[1]

[1]*Department of Chemistry, Goa University, Panaji, Goa, India*
E-mail: sndhuri@unigoa.ac.in
[2]*Department of Chemistry, Indian Institute of Science Education and Research (IISER) Pune, Pune, India*
[3]*Department of Chemistry, Howard University, Washington DC 20059*

Received February, 7, 2016 *Revised March, 6, 2017*

The crystal structure of a mononuclear Ni(II) complex $[Ni(bqenH_2)(bpy)](ClO_4)_2$ **1** (where $bqenH_2$ is *N*,*N*′-bis(8-quinolyl)ethane-1,2-diamine, bpy = 2,2-bipyridine) is reported here. The crystallographic data for **1** are as follows: monoclinic crystal system, $P2_1/n$ space group, $a = 17.3255(11)$, $b = 10.6110(7)$, $c = 34.328(2)$ Å, $\alpha = 90°$, $\beta = 93.9480(13)°$, $\gamma = 90°$, $V = 6295.8(7)$ Å^3, $Z = 4$, $d_x = 1.541$ mg/m^3. The nickel(II) ion coordinates four N atoms of the tetradentate ligand $bqenH_2$ and two N atoms of the auxiliary bidentate 2,2′-bipyridine ligand, resulting in a slightly distorted NiN6 octahedron with two perchlorates serving as charge balancing counter anions. The overall structure of **1** is stabilized by the presence of water of crystallization in the crystal lattice. The crystal structure shows two symmetrically identical octahedral NiN6 units in its asymmetric unit. The extensive hydrogen bonding network resulting in a supramolecular architecture is observed due to the N—H···O, O—H···O, O—H···Cl, and N—H···Cl interactions.

DOI: 10.26902/JSC20180520

Keywords: nickel(II), single crystal X-ray crystallography, $bqenH_2$, 2,2′-bipyridine, hydrogen bonding, centrosymmetric, monoclinic.

INTRODUCTION

The properties of transition metal complexes such as variable coordination environments, structural diversity are responsible for their wide use in several disciplines of science. In biomimetic chemistry, the high valent metal complexes (such as Fe(IV), Ru(IV), Ru(VI), Mn(V), Fe(III), etc.) have been extensively exploited in organic oxidations such as C—H activation, oxygen transfer reactions, alcohol oxidation, deformylation reactions [1—7]. Apart from this work, in bioinorganic chemistry nickel(II) complexes have been explored as model complexes of several metalloenzymes [8—10]. The Ni(II) complexes are gaining importance since they exhibit antimicrobial [11—13] and DNA binding and cleaving activities [14—21]. In addition, the nickel(II) complexes are also known to catalyze a wide range of organic reactions [22—28]. Therefore, the understanding of the structural features of the nickel(II) complexes has become of a prime importance, especially to coordination chemists. In this article we report the crystal structure of $[Ni(bqenH_2)(bpy)](ClO_4)_2$ **1** where $bqenH_2$ is *N*,*N*′-bis(8-quinolyl)ethane-1,2-diamine, bpy = 2,2′-bipyridine. In recent studies, metal (Fe, Mn, Ni) complexes of $bqenH_2$ and $bqenMe_2$ ligands have been used as catalysts in several biomimetic oxidations [28—34]. We have previously reported the synthesis, C,H,N analysis, spectroscopic and electrochemical characterization of $[Ni(bqenH_2)(H_2O)_2](ClO_4)_2$ **1a** [34]. However, our attempts to characterize **1a** by X-ray crystallography were not fruitful. Compound $[Ni(bqenH_2)(H_2O)_2](ClO_4)_2$ **1a** was re-

acted with auxiliary ligands such as 2,2′-bipyridine, 1,10-phenanthroline, and ethylenediamine to give compounds **1**, **2**, and **3** respectively. Again we reported the crystal structures of $[Ni(bqenH_2)(phen)](ClO_4)_2$ **2** and $[Ni(bqenH_2)(en)](ClO_4)_2$ **3**, but at the same time we could not isolate single crystals of **1** [34, 36]. The formula of **1** was proposed as $[Ni(bqenH_2)(bpy)](ClO_4)_2$ with the help of C,H,N spectroscopic data and ESI-MS [34]. After several attempts, we isolated single crystals of $[Ni(bqenH_2)(bpy)](ClO_4)_2$ **1** whose structure is now solved by X-ray crystallography and is reported in this paper. Based on our earlier results [34], compound **1a** with two coordinated water molecules can be proposed to exist in one of the isomeric forms similar to those reported for iron(II) complexes containing $bqenMe_2$ (*N*,*N*′-dimethyl-*N*,*N*′-bis(8-quinolyl)ethane-1,2-diamine) and bqcn (*N*,*N*′-dimethyl-*N*,*N*′-bis(8-quinolyl)cyclohexanediamine) ligands [31, 32] (Scheme 1).

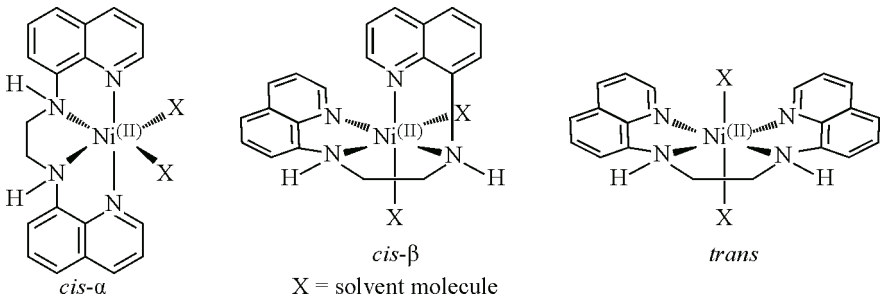

Scheme 1. Proposed isomeric forms of **1a**

EXPERIMENTAL

Materials and methods. All chemicals were purchased from the commercial sources and used without further purification. The starting Ni(II) salt $Ni(ClO_4)_2 \cdot 6H_2O$ was prepared by the slow addition of conc. $HClO_4$ to the aqueous suspension of $NiCO_3$ followed by recrystallization in water. The *N*,*N*′-bis(8-quinolyl)ethane-1,2-diamine ($bqenH_2$) ligand was prepared according to the literature procedure [31] and compounds **1a** and **1** were prepared using our earlier synthetic protocol [34].

Crystal structure determination. Intensity data for **1** were collected on a Bruker Smart Apex Duo diffractometer using graphite monochromated MoK_α radiation (λ = 0.71073 Å) at 100 K. The structural refinement was carried out by full-matrix least-squares against F^2 using all data (SHELX) [35]. The non-hydrogen atoms were refined with the anisotropic displacement parameters while the hydrogen atoms were located at the calculated positions. The CIF file containing complete information on the structure of **1** have been deposited at the Cambridge Crystallographic Data Centre (CCDC) with CCDC number 1517007 and is available free of cost upon request (www.ccdc.cam.ac.uk/data_request/cif).

RESULTS AND DISCUSSION

Compound $[Ni(bqenH_2)(bpy)](ClO_4)_2$ **1** was synthesized from its parent compound $[Ni(bqenH_2)(H_2O)_2](ClO_4)_2$ **1a** according to our reported procedure where a simple displacement of two water molecules was achieved by a 2,2′-bipyridine ligand in the acetonitrile solvent (Scheme 2) [34]. The slow diffusion of diethylether into the CH_3CN solution of **1** afforded single crystals of **1** suitable for the structure determination by X-ray crystallography. The crystal structure of **1** is shown in Fig. 1.

Technical details of data acquisition and selected refinement results for compound **1** are as follows: empirical formula $C_{60}H_{52}Cl_4N_{12}Ni_2O_{16} \cdot 0.25H_2O$; formula weight 1460.86; block crystal; dark red crystal; monoclinic crystal system; $P2_1/n$ space group; temperature, K 100(2); unit cell dimensions a = 17.3255(11), b = 10.6110(7), c = 34.328(2) Å, $\alpha = \gamma = 90°$, β = 93.9480(13)°; volume, Å^3 6295.8(7); Z = 4; radiation type (MoK_α) = 0.71073 Å; crystal size, mm 0.15×0.13×0.07; Bruker Smart APEX-II Duo diffractometer; semi-empirical absorption correction from equivalents; number of

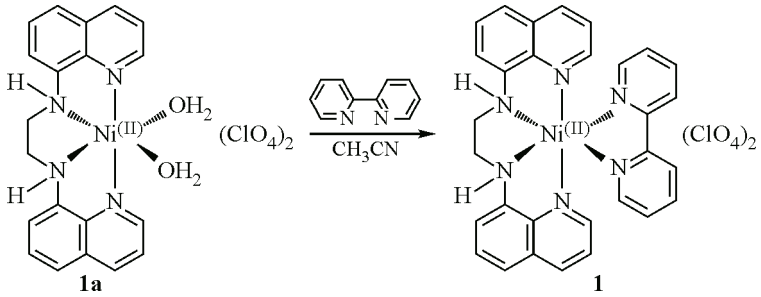

Scheme 2. Synthetic route to obtain **1** from **1a**

measured reflections 9787; calculated density, mg/m^3 1.541; absorption coefficient, mm^{-1} 0.847; F(000) 3002; θ range for data collection from 2.009 to 28.308°; limiting indices $-23 \le h \le 20$, $-10 \le k \le 14$, $-45 \le l \le 45$; refinement method, full-matrix least-squares on F^2; data / restraints / parameter 15530 / 1545 / 983; final R Indices [$I > 2\sigma(I)$] $R1 = 0.0402$, $wR2 = 0.0868$, R indices (all data), $R1 = 0.0635$, $wR2 = 0.0966$; goodness-of-fit on F^2 1.013; largest diff. peak and hole, e/Å^3 0.830 and –0.410 e/Å^3; reflections collected (unique) 49149 / 15530 [R(int) = 0.0543].

Compound **1** crystallizes in the centrosymmetric monoclinic space group $P2_1/n$ with all the atoms located in general positions. The crystal structure of **1** consists of two symmetry related independent NiN6 octahedral units of the tetradentate bqenH_2 ligand, bidentate 2,2′-bipyridine, perchlorate counter anions, and water of crystallization. The tetradentate bqenH_2 ligand surrounds the Ni(II) ion in such a way that the two quinoline nitrogen atoms are disposed *trans* to each other, and the amine nitrogen atoms of the bqenH_2 ligand occupy the adjacent positions (Fig. 1). This arrangement is similar to those of the other recently reported Ni(II) complexes containing bqenH_2 and bqenMe_2 ligands [34, 36]. The remaining two *cis* sites are occupied by the auxiliary 2,2′-bipyridine ligand, resulting in a slightly distorted NiN6 octahedron.

The extent of distortion in the Ni octahedron can be precisely measured from the deviation of the *trans* angle from normal 180°. The *trans* and *cis* angles in **1** range within 169.48(9)—176.03(8) and 78.78(8)—100.59(8)° respectively. All the N—Ni—N bond angles and the Ni—N bond distances (Table 1) are in good agreement with other similar Ni(II) compounds known in the literature [37—40]. Being weakly coordinating, perchlorate ions do not take part in the coordination with Ni(II), and thus simply serve as charge balancing counter anions. However, the two perchlorate ions are exten-

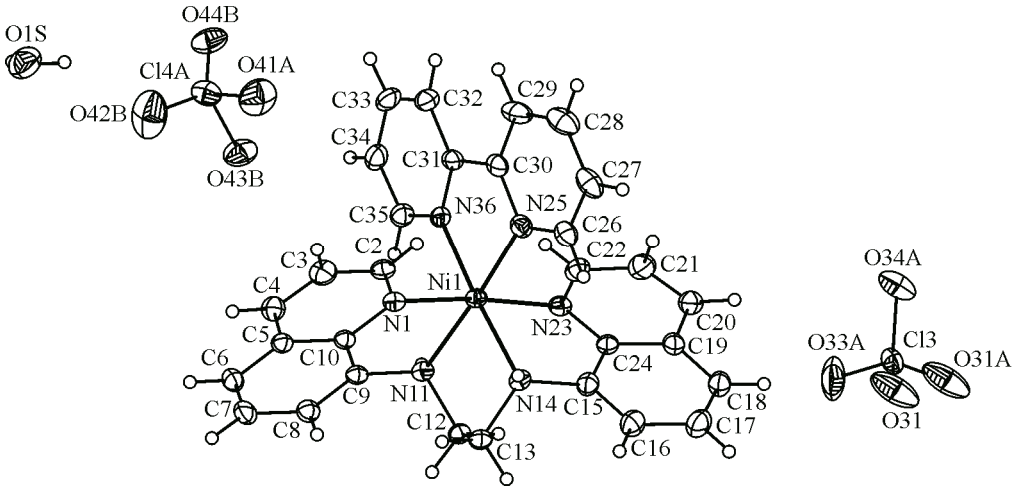

Fig. 1. Crystal structure of [Ni(bqenH_2)(bpy)](ClO_4)$_2$ **1** with the atom labeling scheme. Displacement ellipsoids are drawn at a 50 % probability, except for the H atoms shown as circles of an arbitrary radius. The distortion in perchlorate molecules is not shown for clarity

Table 1

Selected bond lengths (Å) *and angles* (deg.) *for* **1**

Compound **2**					
Bond length		Bond angle			
Ni1—N36	2.072(2)	N36—Ni1—N23	96.40(9)	N61—Ni2—N72	78.78(8)
Ni1—N23	2.074(3)	N36—Ni1—N1	89.74(9)	N61—Ni2—N37	97.11(8)
Ni1—N1	2.075(3)	N23—Ni1—N1	173.67(9)	N72—Ni2—N37	96.99(9)
Ni1—N25	2.078(2)	N36—Ni1—N25	79.11(8)	N61—Ni2—N59	88.56(8)
Ni1—N11	2.115(2)	N23—Ni1—N25	89.11(9)	N72—Ni2—N59	92.80(8)
Ni1—N14	2.119(2)	N1—Ni1—N25	93.56(9)	N37—Ni2—N59	169.48(9)
Ni2—N61	2.073(2)	N36—Ni1—N11	99.34(8)	N61—Ni2—N47	174.83(9)
Ni2—N72	2.077(2)	N23—Ni1—N11	96.24(9)	N72—Ni2—N47	96.65(9)
Ni2—N37	2.086(3)	N1—Ni1—N11	81.21(9)	N37—Ni2—N47	80.96(9)
Ni2—N59	2.099(3)	N25—Ni1—N11	174.58(9)	N59—Ni2—N47	94.11(9)
Ni2—N47	2.116(2)	N36—Ni1—N14	176.03(8)	N61—Ni2—N50	100.59(8)
Ni2—N50	2.130(3)	N23—Ni1—N14	80.70(8)	N72—Ni2—N50	172.93(9)
		N1—Ni1—N14	93.24(8)	N37—Ni2—N50	90.07(9)
		N25—Ni1—N14	98.06(8)	N59—Ni2—N50	80.14(9)
		N11—Ni1—N14	83.73(8)	N47—Ni2—N50	84.25(9)

N o t e: The values in the parentheses indicate estimated standard deviations.

sively involved in the hydrogen bonding with hydrogen atoms of water molecule and those H atoms on nitrogen atoms of the ligand bqenH_2, resulting in a supramolecular 3D structure (Fig. 2, Table 2). All such interactions have resulted in a symmetrically organized three-dimensional extended structure (Fig. 3*a*). All the $NiN6^{2+}$ octahedra, ClO_4^{-1} tetrahedra, and uncoordinated H_2O molecules are symmetrically stacked one above each other (Fig. 3*b*). The unit cell of **1** consists of ten $NiN6^{2+}$ octahedra and twenty ClO_4^{-1} tetrahedral motifs (Fig. 3*c*), maintaining the 1 cation:2 anion (Ni(II):2 ClO_4^{-1}) ratio. Out of the ten octahedra, four NiN6 are present inside the unit cell and six are sharing the neighboring unit

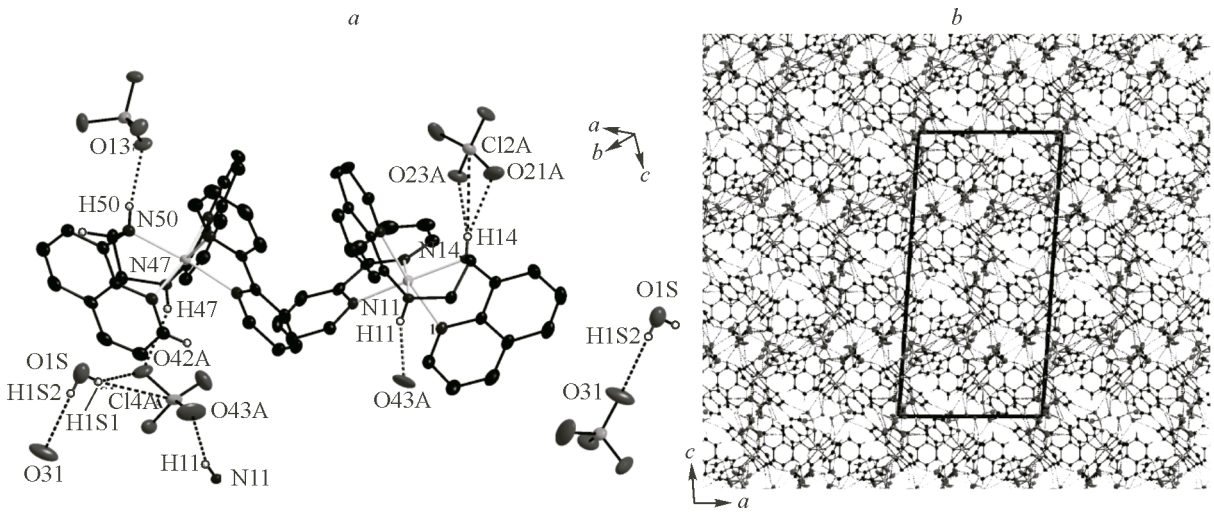

Fig. 2. Hydrogen bonding interactions in **1** with the atom labeling scheme of atoms involved in the hydrogen bonding (*a*). Hydrogen atoms not involved in the hydrogen bonding are omitted for clarity; enlarged view of the hydrogen bonding network (*b*) in **1** showing the symmetric organization of $[Ni(bqenH_2)(bpy)]^{2+}$ cations and $[ClO_4]^{-1}$ anions in the crystallographic *ac* plane

Table 2

Hydrogen bonding parameters (Å, deg.) *for* **1**

D—H…A	D—H, Å	H…A, Å	D…A, Å	D—H…A, deg.
O(1S)—H(1S2)…O(31)[a]	0.818(0)	2.651(0)	3.170()	122.86(1)
O(1S)—H(1S1)…O(42A)	0.826(0)	1.890(1)	2.634(0)	149.42(1)
N(50)—H(50)…O(13)	0.821(0)	2.127(0)	2.939(0)	169.47(1)
N(14)—H(14)…O(21B)	0.789(0)	2.301(0)	3.040(1)	156.15(1)
N(14)—H(14)…O(23A)	0.789(0)	2.188(1)	2.962(1)	166.62(1)
N(11)—H(11)…O(43A)[b]	0.844(0)	2.097(0)	2.889(1)	156.04(1)
N(47)—H(47)…O(42A)	0.827(0)	2.254(0)	3.003(0)	150.82(1)
N(14)—H(14)…Cl(2A)	0.789(0)	2.948(0)	3.688(0)	157.15(1)
O(1S)—H(1S1)…Cl(4A)	0.826(0)	2.958(1)	3.763(1)	165.53(1)

[a] $+x, 1+y, z$; [b] $0.5-x, -0.5+y, 0.5-z$.

N o t e: The values in parentheses indicate the estimated standard deviations.

cell. Similarly, out of the twenty ClO_4^{-1} tetrahedral motifs, the eight NiN6 units occupy the space inside the unit cell while the remaining twelve share the neighboring unit cells. In addition, four water molecules are present in the unit cell.

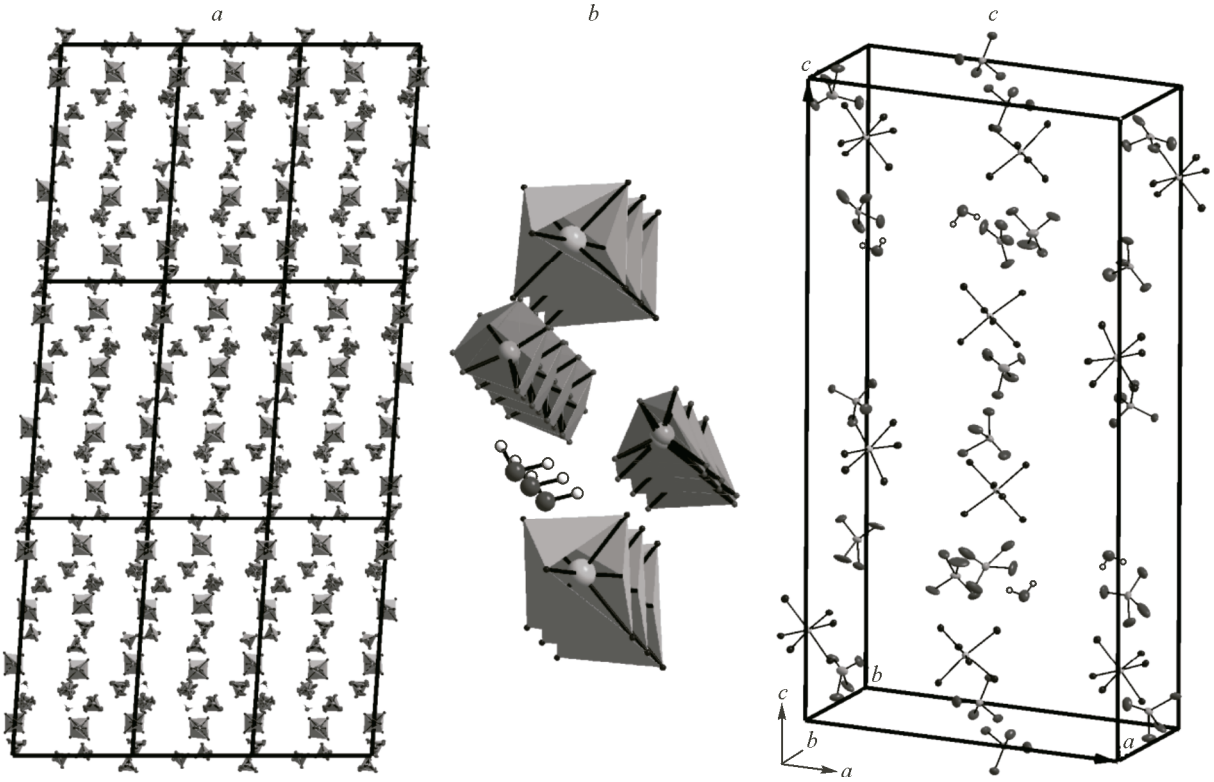

Fig. 3. Symmetric organization of {NiN} octahedra and {ClO4} tetrahedra in the crystallographic *ac* plane (*a*); enlarged view showing the stacking pattern of the octahedra and the tetrahedra one above another (*b*); unit cell showing the arrangement of the octahedra and the tetrahedral (*c*)

Table 3

Crystal system and space group of compounds obtained from $bqenH_2$ *and related ligands*

Compounds	Crystal system /space group	Ref.
$[Ni(bqenH_2)(bpy)](ClO_4)_2 \cdot 0.125H_2O$ **1**	Monoclinic / $P2_1/n$	[This work]
$[Ni(bqenH_2)(phen)](ClO_4)_2 \cdot$ **2**	Orthorhombic / $P2_12_12_1$	[34]
$[Ni(bqenH_2)(en)] \cdot CH_3CN$ **3**	Triclinic / $P\bar{1}$	[36]
$[Ni(bqenMe_2)(phen)] \cdot CH_3CN$	Monoclinic / $P2_1/c$	[34]
$[Fe(bqenMe_2)(CF_3SO_3)_2]$	Orthorhombic / $P2_12_12_1$	[31]
$[Fe(bqpn)(CF_3SO_3)_2]$	Triclinic / $P\bar{1}$	[31]
$[Fe(bqmen)((CF_3SO_3)_2]$	Monoclinic / $P2_1/c$	[31]
$[Fe(bqcn)(CH_3CN)_2](ClO_4)_2$	Orthorhombic / $Pna2_1$	[32]
$[Fe(bqcn)(CH_3CN)_2](CF_3SO_3)_2$	Orthorhombic / $Pbca$	[32]
$[Fe(bqcn)](CF_3SO_3)_2] \cdot (CH_3CN)$	Monoclinic / $P2_1/c$	[32]
$[Mn(bqenMe_2)(CF_3SO_3)_2]$	Orthorhombic / $P2_12_12_1$	[29]
$[Mn(bqcn)(CF_3SO_3)_2]$	Monoclinic / $C2/c$	[33]

The crystal structures of Fe(II), Ni(II), and Mn(II) compounds stabilized by the ligands such as $bqenMe_2$ (*N*,*N′*-dimethyl-N,*N′*-bis(8-quinolyl)ethane-1,2-diamine), bqpn (*N*,*N′*-dimethyl-N,*N′*-bis(8-quinolyl)propane-1,2-diamine), bqmen (*N*,*N′*-dimethyl-*N*,*N′*-bis(8-quinolylmethyl)ethane-1,2-diamine), bqcn (*N*,*N′*-dimethyl-*N*,*N′*-bis(8-quinolyl)cyclohexane-diamine), which are identical to the denticity of $bqenH_2$, are reported (Table 3).

It is evident from Table 3 that all three compounds **1**—**3** (Fig. 4) crystallize in different crystal systems. The careful analysis of the structural data of compounds **1**—**3** also shows that the crystal structure of only compound **1** has disordered perchlorate anions: the feature lacking in compounds **2** and **3** [34, 36]. Although the synthetic methodology adopted in the preparation of compounds **1**—**3** is similar to that involving the use of the CH_3CN solvent, the structure of compound **1** has H_2O in its crystal lattice, the structure of **3** has CH_3CN in its crystal lattice, while no solvent of crystallization is required for the crystal stability of compound **2.** Additionally, another significant difference in the crystal structure of **1** when compared with the crystal structures of **2** and **3** is that the asymmetric unit of **1** has two symmetry-related NiN6 units, four perchlorate anions, and water of crystallization

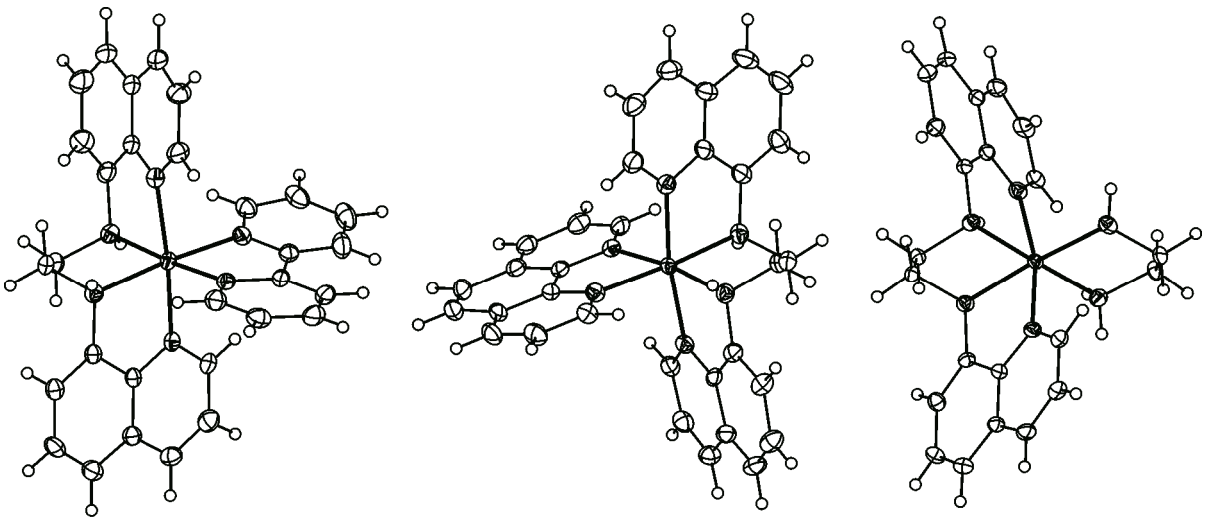

$[Ni(bqenH_2)(bpy)]^{2+}$ **1** $[Ni(bqenH_2)(phe)]^{2+}$ **2** $[Ni(bqenH_2)(en)]^{2+}$ **3**

Fig. 4. Structures of cationic moieties in compounds **1**, **2**, and **3**

(Fig. 1) while the asymmetric units of **2** and **3** have a single NiN6 unit [34, 36]. These structural observations clearly suggest the influence of auxiliary bpy, phen, and en ligands in deciding the preference for the specific crystal system in the structures of **1**, **2**, and **3** (Fig. 4). Since structurally characterized compounds **1**—**3** are obtained from parent compound **1a**, further it is rationalized that compound **1a** can exist in two isomeric topologies (*cis*-α or *cis*-β) in which the two H_2O molecules must occupy the *cis* positions.

CONCLUSIONS

Here we have reported the single crystal X-ray structure of mononuclear Ni(II) complex $[Ni(bqenH_2)(bpy)](ClO_4)_2$ **1**. Compound **1** crystallizes in the monoclinic $P2_1/n$ centrosymmetric space group and exhibits a supramolecular 3D H-bonding network through O—H⋯O, N—H⋯O, O—H⋯Cl, N—H⋯Cl interactions. Compound **1** also has an uncoordinated water molecule in the crystal lattice, which further participates in the H-bonding. Based on the orientation positions of four N atoms of the $bqenH_2$ ligand and two N atoms of bpy in compound **1**, parent complex $[Ni(bqenH_2)(H_2O)_2](ClO_4)_2$ **1a** is speculated to have the *cis*-α coordination mode.

The authors acknowledge DST-FIST, UGC-SAP for their support of the Department of Chemistry, Goa University. D.D. Narulkar thanks UGC for UGC-BSR fellowship.

REFERENCES

1. W. Nam. *Acc. Chem. Res.*, **2015**, *8*, 2415.
2. P. Barman, P. Upadhyay, A.S. Faponle, J. Kumar, S.S. Nag, D. Kumar, C.V. Sastri, S.P. de Visser. *Angew. Chem. Int. Ed.*, **2016**, *55*, 11091.
3. T.A. Jackson, J.-U. Rohde, M.S. Seo, C.V. Sastri, R. DeHont, A. Stubna, T. Ohta, T. Kitagawa, E. Munck, W. Nam, Jr. L. Que. *J. Am. Chem. Soc.*, **2008**, *130*, 12394.
4. S.N. Dhuri, K.-B. Cho, Y.M. Lee, S.Y. Shin, J.H. Kim, D. Mandal, S. Shaik, W. Nam. *J. Am. Chem. Soc.*, **2015**, *137*, 8623.
5. Y.-M. Lee, S.N. Dhuri, S.C. Sawant, J. Cho, M. Kubo, T. Ogura, S. Fukuzumi, W. Nam. *Angew. Chem. Int. Ed.*, **2009**, *48*, 1803.
6. S.N. Dhuri, M.S. Seo, Y.-M. Lee, H. Hirao, Y. Wang, W. Nam, S. Shaik. *Angew. Chem. Int. Ed.*, **2008**, *47*, 3356.
7. S.N. Dhuri, Y.-M. Lee, M.S. Seo, J. Cho, D.D. Narulkar, S. Fukuzumi, W. Nam. *Dalton Trans.*, **2015**, *44*, 7634.
8. M.T. Kieber-Emmons, J. Annaraj, M.S. Seo, K.M. Van Heuvelen, T. Tosha, T. Kitagawa, T.C. Brunold, W. Nam, C.G. Riordan. *J. Am. Chem. Soc.*, **2011**, *128*, 14230.
9. J. Cho, H.Y. Kang, L.V. Liu, R. Sarangi. *Chem. Sci.*, **2013**, *4*, 1502.
10. J. Cho, R. Sarangi, J. Annaraj, S.Y. Kim, M. Kubo, T. Ogura, E.I. Solomon, W. Nam. *Nature Chem.*, **2009**, *1*, 568.
11. K.C. Skyrianou, F. Perdih, I. Turel, D.P. Kessissoglou, G. Psomas. *J. Inorg. Biochem.*, **2010**, *104*, 740.
12. L.R. Gomes, J.N. Low, M.A.A. Rocha, L.M.n.B.F. Santos, B. Schröder, P. Brandão, C. Matos, J. Neves. *J. Mol. Struct.*, **2011**, *990*, 86.
13. S. Anitha, J. Karthikeyan, A.N. Shetty. *Indian J. Chem.*, **2013**, *42A*, 45.
14. E. Ramachandran, D.S. Raja, J.L. Mike, T.R. Wagner, M. Zeller, K. Natarajan. *RSC Advances*, **2012**, *2*, 8515.
15. L.-N. Zhu, D.-M. Kong, X.-Z. Li, G.-Y. Wang, J. Wang, Y.-W. Jin. *Polyhedron*, **2010**, *29*, 574.
16. C.N. Sudhamani, H.S.B. Naik, T.R.R. Naik, M.C. Prabhakara. *Spectrochim. Acta. Part A*, **2009**, *72*, 643.
17. A.E.-M.M. Ramadan. *J. Mol. Struct.*, **2012**, *1015*, 56.
18. K.C. Skyrianou, V. Psycharis, C.P. Raptopoulou, D.P. Kessissoglou, G. Psomas. *J. Inorg. Biochem.*, **2011**, *105*, 63.
19. M.S.S. Babu, P.G. Krishna, K.S. Reddy, G.H. Philip. *Indian J. Chem.*, **2008**, *47A*, 1668.
20. R.P. Reddy, N. Raju, K. Rao, A. Shilpa. *Indian J. Chem.*, **2009**, *48A*, 761.
21. M. Pragathi, K.H. Reddy. *Indian J Chem*, **2013**, *52A*, 845.
22. P.K. Suganthy, R.N. Prabhu, V.S. Sridevi. *Inorg. Chim. Acta*, **2016**, *449*, 127.
23. M. Zhang, M.-T. Zhang, C. Hou, Z.-H. Ke, T.-B. Lu. *Angew. Chem. Int. Ed.*, **2014**, *53*, 13042.
24. M. Sankaralingam, P. Vadivelu, E. Suresh, M. Palaniandavar. *Inorg. Chim. Acta*, **2013**, *407*, 98.

25. T. Nagataki, K. Ishii, Y. Tachi, S. Itoh. *Dalton Trans*., **2007**, 1120.
26. M. Balamurugan, R. Mayilmurugan, E. Suresh, M. Palaniandavar. *Dalton Trans*., **2011**, *40*, 9413.
27. S. Hikichi, K. Hanaue, T. Fujimura, H. Okuda, J. Nakazawa, Y. Ohzu, C. Kobayashi, M. Akita. *Dalton Trans*., **2013**, *42*, 3346.
28. J. Nakazawa, S. Terada, M. Yamada, S. Hikichi. *J. Am. Chem. Soc.*, **2013**, *135*, 6010.
29. K. Nehru, S.J. Kim, I.Y. Kim, M.S. Seo, Y. Kim, S.-J. Kim, J. Kim, W. Nam. *Chem. Commun.*, **2007**, *1*, 4623.
30. J. Yoon, S.A. Wilson, Y.K. Jang, M.S. Seo, K. Nehru, B. Hedman, K.O. Hodgson, E. Bill, E.I. Solomon, W. Nam. *Angew. Che. Int. Ed.*, **2009**, *48*, 1257.
31. J. England, G.J.P. Britovsek, N. Rabadia, A.J.P. White. *Inorg. Chem*., **2007**, *46*, 672.
32. S.S. Hong, Y.-M. Lee, K.-B. Cho, K. Sundaravel, J. Cho, M.J. Kim, W. Shin, W. Nam. *J. Am. Chem. Soc.*, **2011**, *133*, 11876.
33. S.C. Sawant, X. Wu, J. Cho, K.-B. Cho, S.H. Kim, M.S. Seo, Y.-M. Lee, M. Kubo, T. Ogura, S. Shaik, W. Nam. *Angew. Chem., Int. Ed*., **2010**, *49*, 8190.
34. D.D. Narulkar, A.R. Patil, C.C. Naik, S.N. Dhuri. *Inorg. Chim. Acta*, **2015**, *427*, 248.
35. G.M. Sheldrick. *A short history of SHELX. Acta Crystallogr., Sect. A*: *Found. Crystallogr*., **2008**, *64*, 112.
36. D.D. Narulkar, A.K. Srivastava, S.N. Dhuri. *Indian J. Chem*. (under revision).
37. I. García-Santos, J. Sanmartín, A.M. García-Deibe, M. Fondo, E. Gómez. *Inorg. Chim. Acta*, **2010**, *363*, 193.
38. D. Sertphon, D.J. Harding, P. Harding, H. Adams. *Polyhedron*, **2011**, *30*, 2740.
39. Q. Zhang, X.Q. Zhang, Z.X. Wang. *Dalton Trans*., **2012**, *41*, 10453.
40. A. McAuley, C. Xu. *Inorg. Chem.*, **1992**, *31*, 5549.

Inorganica Chimica Acta 486 (2019) 425–434

Contents lists available at ScienceDirect

Inorganica Chimica Acta

journal homepage: www.elsevier.com/locate/ica

Research paper

Dual-site aqua mononuclear nickel(II) complexes of non-heme tetradentate ligands: Synthesis, characterization and reactivity

Sarvesh S. Harmalkar[a], Dattaprasad D. Narulkar[a], Raymond J. Butcher[b], Mahesh S. Deshmukh[c], Anant Kumar Srivastava[c], Mariappan Mariappan[d], Prem Lama[a], Sunder N. Dhuri[a,*]

[a] Department of Chemistry, Goa University, 403206 Goa, India
[b] Department of Chemistry, Howard University, Washington, DC 20059, United States
[c] Department of Chemistry, IISER, Dr. Homi Bhabha Road Pune, 411008, India
[d] Department of Chemistry, SRM IST, Chennai 603203, India

ARTICLE INFO

Dedicated to Prof. Dr. Wolfgang Bensch on the occasion of his 65th birthday.

InChIKeys:
KOTWKWYVOFHUIW-UHFFFAOYSA-L
LDBMZSOKMZNZQN-UHFFFAOYSA-L
RYFIGDSKHPDOKH-UHFFFAOYSA-N
FTDMRTYJJUJLEW-UHFFFAOYSA-N
DTYZLLZISXAQMW-UHFFFAOYSA-N
WZTCSZVURLYVSC-UHFFFAOYSA-N
VQXFYFRBGNKBLE-UHFFFAOYSA-N
MFPQZNWMMWSMAD-UHFFFAOYSA-N

Keywords:
Nickel(II) compounds
Non-heme ligands
Spectroscopy
Crystal structure
Hydroxylation

ABSTRACT

Mononuclear compounds $[Ni(BQCNMe_2)(H_2O)_2](ClO_4)_2$ **1** and $[Ni(BQCNH_2)(H_2O)_2](ClO_4)_2$ **2** of *N,N′*-dimethyl-*N,N′*-di(quinolin-8-yl)cyclohexane-1,2-diamine ($BQCNMe_2$) and *N,N′*-di(quinolin-8-yl)cyclohexane-1,2-diamine ($BQCNH_2$) were synthesised and characterized by elemental analysis, IR/UV-Vis spectroscopy, cyclic voltammetry (CV)/differential pulse voltammetry (DPV) and X-ray powder pattern. $[Ni(BQCNMe_2)(en)](ClO_4)_2$ **3** and $[Ni(BQCNMe_2)(phen)](ClO_4)_2$ **4** were prepared by reacting **1** with ethylenediamine (en) and 1,10-phenanthroline (phen) respectively while $[Ni(BQCNH_2)(en)](ClO_4)_2$ **5** and $[Ni(BQCNH_2)(phen)](ClO_4)_2$ **6** were obtained from the reaction of **2**. Compounds $[Ni(BQENMe_2)(en)](ClO_4)_2$ **7** and $[Ni(BQENH_2)(en)](ClO_4)_2.CH_3CN$ **8** ($BQENMe_2$ is *N,N′*-dimethyl-*N,N′*-bis(8-quinolyl)ethane-1,2-diamine) and $BQENH_2$ is *N,N′*-bis(8-quinolyl) ethane-1,2-diamine) were synthesised similarly. Compounds **6** and **8** were characterized by single crystal X-ray diffractometry and their structural features are presented. The reactivity of **2** with H_2O_2/base was investigated. A new peak at 570 nm in the UV-Vis spectrum corresponding to **2a** was obtained which on addition of 2-phenylpropionaldehyde (2-PPA) decays giving pseudo-first order rate constant of $9.2 \times 10^{-3} s^{-1}$ and acetophenone as a major product. The catalytic hydroxylation of cumene and ethylbenzene by **1** and **2** in the presence of *meta*-chloroperbenzoic acid (*m*-CPBA) was investigated.

1. Introduction

The chemistry of first row transition metal compounds containing non-heme *N*-donor ligands is an area of research with growing attention [1]. In metalloenzymes, a metal active site plays a vital role in biochemical reactions [2]. The elements of the first transition metal series are abundant and available for specific functions as they exhibit a variety of coordination numbers and the flexible geometries over *sp*, sp^2 and sp^3 hybridisations of carbon [3]. The late transition metals viz. cobalt and nickel have been less investigated in biomimetic studies due to their limited scope in biology. In recent years, a large amount of work has been carried on understanding the roles of high valent cobalt and nickel-oxygen intermediates in a variety of biomimetic oxidations [4–13]. The roles of nickel(II) compounds in hydrogen gas generation and oxygen gas evolution is also documented [14–18]. The nickel(II) compounds have been also used as the models for several metalloenzymes [19–21]. They display DNA binding-cleavage activities [22–29] and antimicrobial properties [30–32] in biological systems and have been used in various reactions like cross-coupling reaction [33], electrolytic water oxidation [34] and alkane oxidation [35–39] as catalysts.

In our recent work, we have reported hydroxylation of alkanes by nickel(II) compounds of non-heme *N,N′*-bis(8-quinolyl)ethane-1,2-diamine ($BQENH_2$) and *N,N′*-dimethyl-*N,N′*-bis(8-quinolyl)ethane-1,2-diamine ($BQENMe_2$) ligands [40]. Nam *et al.* have reported iron(II) and manganese(II) compounds of $BQENMe_2$ as the models in biomimetic reactions [41,42]. The same group also reported $[Mn(BQCNMe_2)]^{2+}$ compound in water oxidation catalysis and various organic oxidations [43,44]. In recent years, the structural and spectroscopic elucidation of nickel(II)-superoxide and nickel(III)-peroxide of tetramethylated cyclams has attracted the attention of bioinorganic chemists in the modelling chemistry [20,21]. Although a large amount research on

* Corresponding author.
E-mail address: sndhuri@unigoa.ac.in (S.N. Dhuri).

https://doi.org/10.1016/j.ica.2018.10.069
Received 21 May 2018; Received in revised form 6 October 2018; Accepted 31 October 2018
Available online 03 November 2018

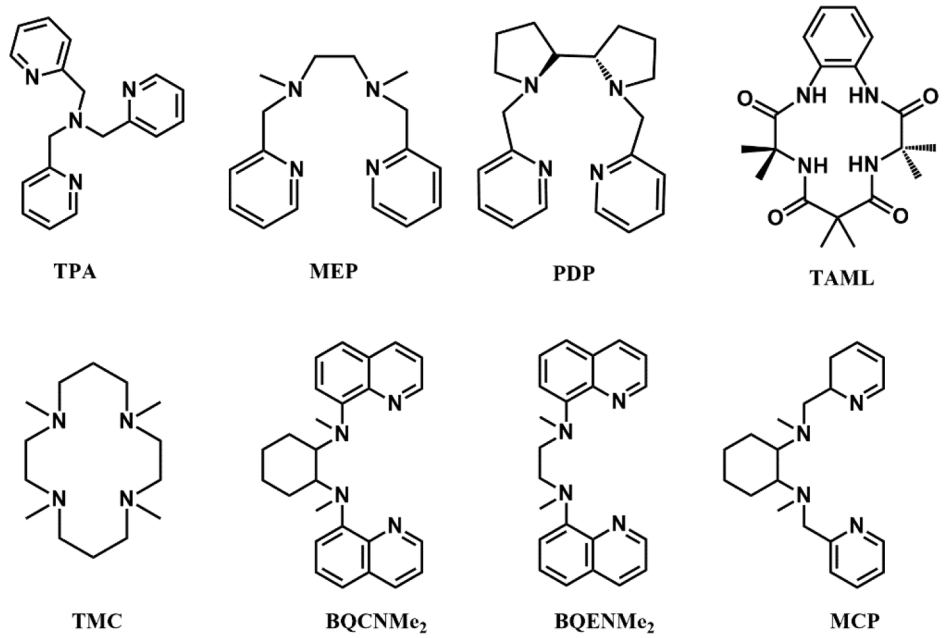

Scheme 1. Structures of known non-heme tetradentate *N*-donor ligands.

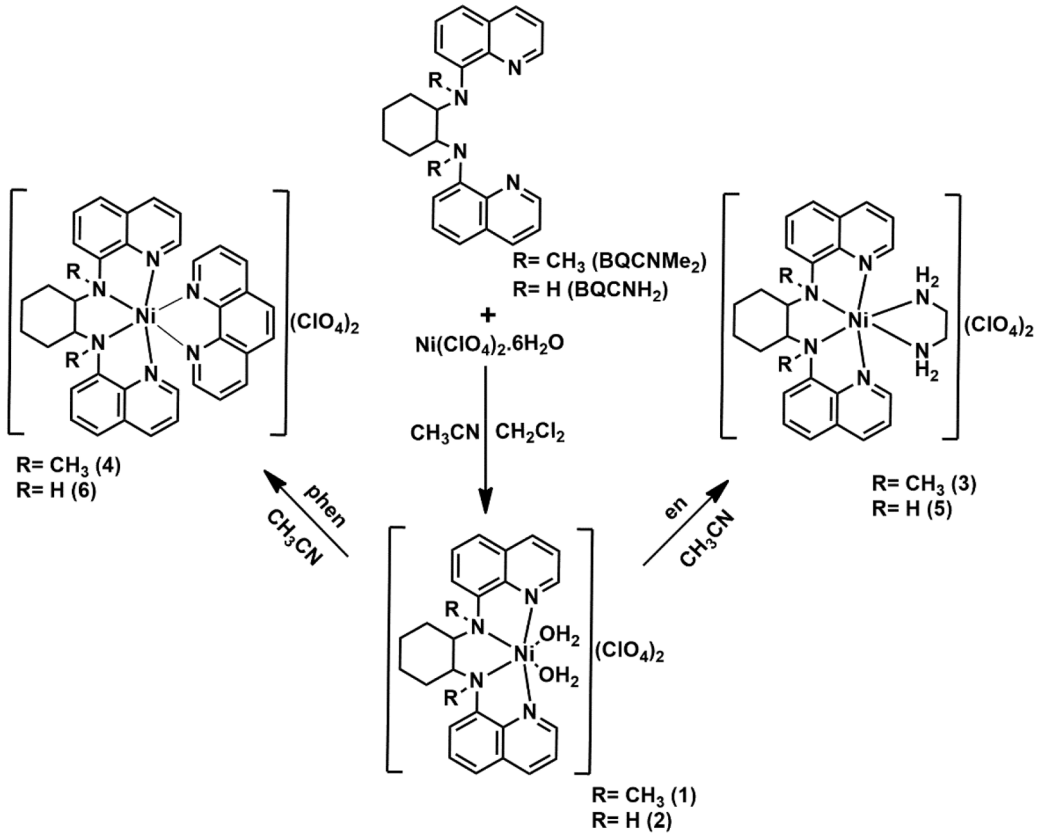

Scheme 2. Synthetic methods used to obtain the compounds **1**–**6**.

non-heme nickel(II) compounds has been carried out, our understanding in this area suggests that there is scope in designing the new topological ligands which stabilize nickel(II) ion. In the present work, we report synthesis, characterization and reactivity of two dual site aqua mononuclear nickel(II) compounds stabilized by *N*,*N*′-dimethyl-*N*,*N*′-di(quinolin-8-yl)cyclohexane-1,2-diamine ($BQCNMe_2$) and *N*,*N*′-di(quinolin-8-yl)cyclohexane-1,2-diamine ($BQCNH_2$). The two water molecules in 1 and 2 are replaced by auxiliary bidentate ethylenediamine (en) and 1, 10-phenanthroline (phen) affording four nickel(II) compounds (**3**–**6**). The two other compounds, **7** and **8** containing $BQENMe_2$ and $BQENH_2$ have been also investigated.

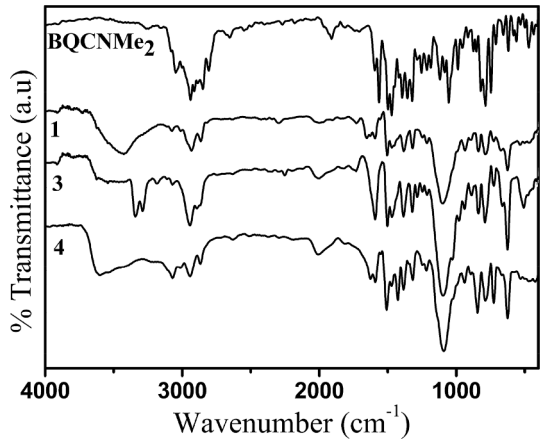

Fig. 1. IR spectra of $BQCNMe_2$ ligand, **1**, **3** and **4**.

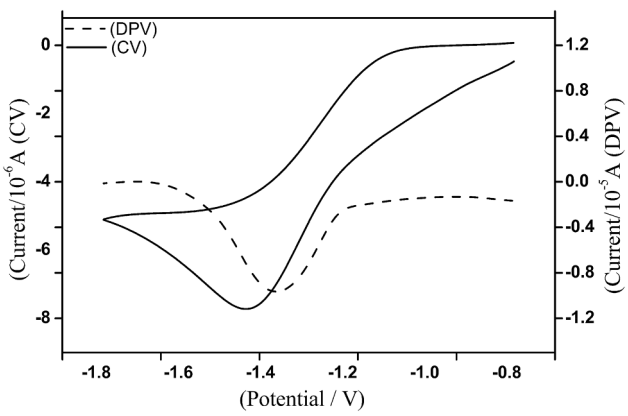

Fig. 2. CV (solid line) and DPV (dotted line) of **1** recorded in CH_3CN containing 0.1 M of $TBAPF_6$ as supporting electrolyte against 0.01 M Ag/Ag^+ reference electrode.

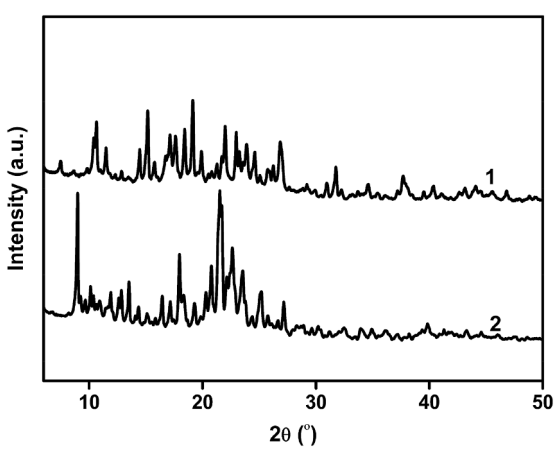

Fig. 3. X-ray powder patterns of **1** and **2**.

2. Experimental details

2.1. Materials and methods

All the chemicals were used as obtained without further purification. $BQCNH_2$, $BQENH_2$, $BQENMe_2$, $[Ni(BQENH_2)(H_2O)_2](ClO_4)_2]$ and $[Ni(BQENMe_2)(H_2O)_2](ClO_4)_2$ were prepared using reported procedure [40,45]. The ligands were characterized by IR, ^1H and ^{13}C NMR spectroscopy (Fig. S1-S4). IR spectra in the region 4000–400 cm^{-1} were recorded on a Shimadzu (IR Prestige-21) FT-IR spectrometer. The NMR spectra were recorded on a Bruker Avance III 400 MHz NMR spectrometer. UV-Vis spectra were recorded on an Agilent UV-Vis spectrophotometer 8453. Elemental analysis (C,H,N) was performed using Elementar Variomicro Cube CHNS Analyser. The redox potentials were obtained from cyclic voltammograms (CV) and differential pulse voltammograms (DPV) on Electrochemical Workstation-CH Instrument, Inc. CHI6107. In CV/DPV measurements, a glass vessel containing sample solution was equipped with a Pt disc (working electrode), Pt wire (counter electrode), reference electrode, $Ag/AgNO_3$ (0.01 M) and tetrabutylammonium hexafluorophosphate ($TBAPF_6$) (0.1 M) as supporting electrolyte. The sample solutions were purged with N_2 gas for ~30 min before each measurement. The powder X-ray Diffraction patterns were obtained using a Panalytical Xpert3 Powder X-ray Diffractometer using Cu Kα radiation. Crystal structures of 6 and 8 were obtained using Bruker Smart Apex Duo diffractometer at 100 K. The structural refinement was done by full-matrix least-squares against F^2 using all data (SHELXL) [46]. The non-hydrogen atoms were refined with the anisotropic displacement parameters while the hydrogen atoms were located at the calculated positions. Even though the structure was collected at 100 K, the quinoline moiety was found to be disordered over two positions in 6. The site occupancy of the disordered atoms was refined first using a variable command to get an approximate contribution from each fraction and then fixed at that value to get the best model. The first part contains ¾ occupancy whereas the second

Table 1
Technical details of crystal data and structural refinement parameters of **6** and **8**.

Parameters	**6**	**8**
Empirical formula	$C_{36}H_{32}Cl_2N_6NiO_8$	$C_{24}H_{29}Cl_2N_7NiO_8$
Formula weight	806.28	673.15
Crystal description	Prismatic	Block
Crystal colour	pale green-purple	dark red
Crystal system	Triclinic	Triclinic
Space group	$P\bar{1}$	$P\bar{1}$
Temperature (K)	100(2)	100(2)
Unit cell dimensions	a = 8.6908(9) Å b = 11.9334(12)Å c = 18.6099(19)Å α = 100.900(2) ° β = 101.104(2)° γ = 107.0900(10)°	a = 10.9192(11) Å b = 12.3327(12)Å c = 12.6497(13)Å α = 60.9370(10) ° β = 70.0320(2)° γ = 75.4400(2)°
volume (Å^3)	1747.1(3)	1391.9(2)
Z	2	2
Radiation type (Mo-Kα)/Å	0.71073	0.71073
Crystal size (mm)	0.32 × 0.22 × 0.16	0.16 × 0.12 × 0.09
X-ray Diffractometer	Bruker Smart APEX-II Duo	Bruker Smart APEX-II Duo
Absorption correction	Multi scan	Multi scan
No. measured reflections	26,448	20,590
Calculated density (mg/m^3)	1.533	1.606
Absorption coefficient (mm^{-1})	0.771	0.951
F(0 0 0)	832	696
θ range for data collection	1.850–25.000	1.899–25.000
Limiting indices	$-10 \le h \le 10$ $-14 \le k \le 14$ $-22 \le l \le 22$	$-12 \le h \le 11$ $-14 \le k \le 14$ $-15 \le l \le 15$
Refinement method	Full-matrix least-squares on F^2	Full-matrix least-squares on F^2
Data/restraints/parameter	6149/217/579	4876/0/388
Final R Indices[I > 2σ(I)]	R_1 = 0.0535, wR_2 = 0.1369	R_1 = 0.0238, wR_2 = 0.0629
R indices (all data)	R_1 = 0.0586, wR_2 = 0.1402	R_1 = 0.0254, wR_2 = 0.0638
Goodness of fit on F^2	1.060	1.063
Largest diff. peak and hole (eÅ^{-3})	1.134 and −0.890	0.460 and −0.410
Reflections collected/ unique	26,448/6146 [R(int) = 0.0558]	20,590/4876 [R(int) = 0.0236]

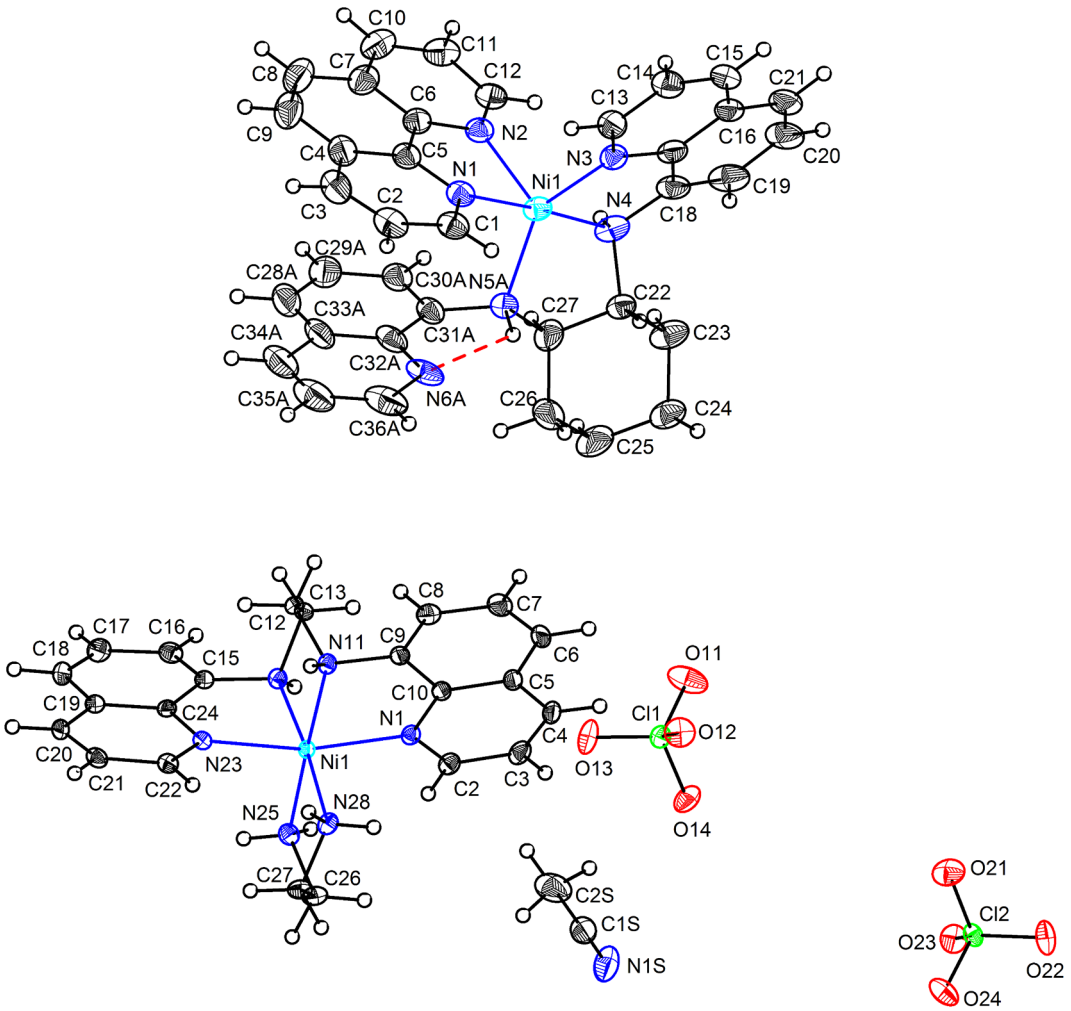

Fig. 4. The crystal structure of compound (**6**) showing the atom labelling scheme and the penta coordination sphere of Ni(II) **(top)**, intramolecular H-bonding is shown in broken line. The crystal structure of compound (**8**) showing the atom labelling scheme and the hexa coordination sphere of Ni(II) **(bottom)**. Displacement ellipsoids are drawn at the 50% probability level excepting for the H atoms, which are shown as circles of arbitrary radius. For clarity the disordered atoms and the anions in **6** (See Fig. S11) are not shown.

Table 2
Selected bond lengths (Å) and angles (°) for **6** and **8**.

Compound **6**			
Ni1-N1	2.001(3)	Ni1-N2	2.156(3)
Ni1-N3	2.012(3)	Ni1-N4	2.022(3)
Ni1-N5A	2.041(4)	Ni1-N5B	2.154(12)
N1-Ni-N2	80.42(11)	N1-Ni-N3	99.08(11)
N1-Ni-N4	176.48(12)	N1-Ni-N5A	93.43(14)
N1-Ni-N5B	88.1(3)	N2-Ni-N3	105.30(11)
N2-Ni-N4	99.94(12)	N2-Ni-N5A	111.05(15)
N2-Ni-N5B	127.5(4)	N3-Ni-N4	84.23(12)
N3-Ni-N5A	143.03(16)	N3-Ni-N5B	127.1(4)
N4-Ni-N5A	83.16(14)	N4-Ni-N5B	89.0(3)
Compound **8**			
Ni1-N1	2.1191(13)	Ni1-N11	2.1105(14)
Ni1-N14	2.1032(14)	Ni1-N23	2.1094(13)
Ni1-N25	2.0977(14)	Ni1-N28	2.0918(14)
N1-Ni1-N11	80.17(5)	N1-Ni1-N14	91.49(5)
N1-Ni1-N23	167.47(5)	N1-Ni1-N25	98.35(5)
N1-Ni1-N28	92.65(5)	N11-Ni1-N14	85.79(6)
N11-Ni1-N23	89.57(5)	N11-Ni1-N25	178.51(5)
N11-Ni1-N28	97.18(5)	N14-Ni1-N23	80.51(5)
N14-Ni1-N25	94.44(5)	N14-Ni1-N28	175.27(5)
N23-Ni1-N25	91.92(5)	N23-Ni1-N28	95.79(5)
N25-Ni1-N28	82.69(5)		

Note: The values in the parentheses indicate estimated standard deviations.

part contains ¼ of quinoline unit. Apart from that, the nitrogen atom bonded to the quinoline group is also disordered over two positions (N5A = 3/4 occupancy and N5B = 1/4 occupancy). AFIX 116 command was used to get the idealized quinoline group and in addition, SIMU and ISOR command were also applied to get the best model for the disordered fraction. In catalytic oxidation reactions, the organic products were analysed using the Shimadzu GC 2014 equipped with HP capillary column (30 m × 0.25 mm × 2.5 μM) and an FID detector. The retention time and peak areas of the products were compared with authentic samples using decane as an internal standard.

2.2. Synthesis of $BQCNMe_2$

$BQCNMe_2$ was prepared by modification of a reported procedure [45]. To a stirred THF solution (40 mL) of $BQCNH_2$ (4.0 g, 10.86 mmol), 21.0 mL of aqueous formaldehyde (37%) (6.48 g, 217 mmol) was added. The solution slowly turned dark red after ~5 min. To this red mixture, the sodium cyanoborohydride (1.38 g, 22.0 mmol) was added slowly till an yellow colour solution is obtained. The solution was stirred for ~24 h and THF was removed which afforded yellow crude powder. This crude product on recrystallization in hot ethanol resulted in a crystalline solid. Yield was 3.0 g. Anal. Calc. for $C_{26}H_{28}N_4$ (%): C, 78.75; H 7.12; N 14.13; Found: C, 78.35; H, 7.12; N, 14.06. Selected IR bands (KBr, cm^{-1}): 1562 ν(C=N); 3134–2746 ν(CH). ^1H NMR

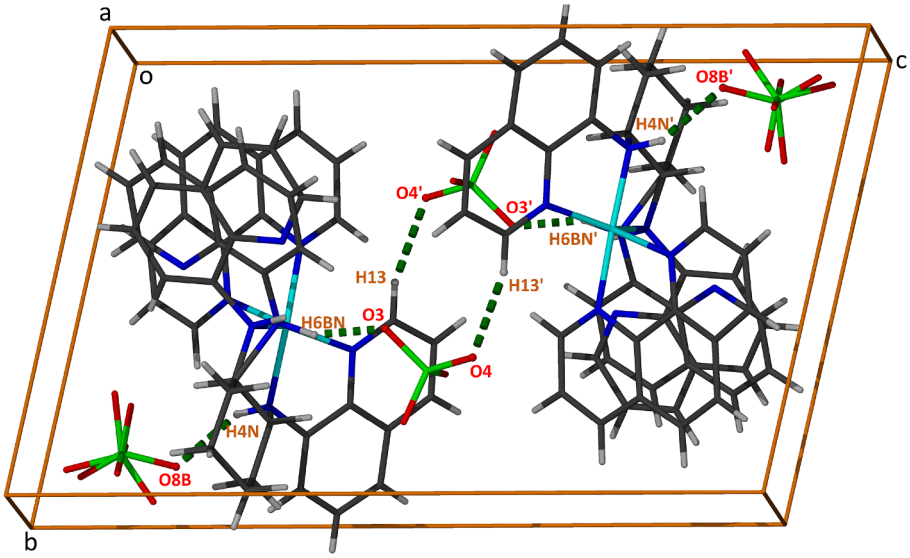

Fig. 5. Hydrogen bonding interactions in **6** with atom labelling scheme of atoms involved hydrogen bonding along *bc* plane. O3′, O4′, O8B′, H13′, H4N′ and H6BN′ are symmetry generated atoms. The symmetry code for all symmetry generated atoms are 1 − x, 1 − y, 1 − z.

Table 3
Hydrogen bonding Parameters (Å, °) for **6** and **8**.

Compound **6**				
D-H···A	D-H/Å	H···A/Å	D···A/Å	D-H···A/°
N5A-H5AN···N(6A)	1.00	2.12	2.7302	117
N5A-H4N···O(3)[a]	1.00	2.50	3.2878	135
N4-H4N···O(5B)	0.84	2.56	3.3389	155
N(4)-H4)N···O(8B)	0.84	2.15	2.9352	155
a = 1 − x, 1 − y, 1 − z				
Compound **8**				
D-H···A	D-H/Å	H···A/Å	D···A/Å	D-H···A/°
N(11)-H(11)···O(11)[a]	0.83	2.18	2.9942	169
N(14)-H(14) ···O(21)[b]	0.85	2.17	3.0158	176
N(25)-H(25A) ···O(24)[c]	0.91	2.21	3.1038	166
N(25)-H(25B) ···O(24)[b]	0.91	2.11	2.9974	164
N(28)-H(28A) ···N(14)[d]	0.91	2.29	3.1478	158
N(28)-H(28B) ···O(13) [a]	0.91	2.17	3.0649	168

a = x, −1 + y, z; b = 1 − x, 1 − y, −z; c = −1 +x, y, z; d = −x, 1 − y, 1 − z.

(400 MHz, $CDCl_3$): δ (ppm) 8.73 (d, 2H, J = 1.2 Hz, 2-QnH), 7.99 (d, 2H, J = 8 Hz, 4-QnH), 7.26 (m, 4H, 3-QnH & d 5-QnH), 7.14 (d, 2H, J = 7.6 Hz, 6-QnH), 6.60 (d, 2H, J = 7.2 Hz, 7-QnH), 4.70 (d, 2H, J = 8 Hz, NCH), 2.43 (s, 6H, NMe), 2.29 (d, 2H, J = 12.4 Hz, CH), 1.75 (d, 2H, J = 7.2 Hz, CH), 1.60 (d, 2H, J = 8 Hz, CH), 1.28 (m, 2H, CH). ^{13}C NMR ($CDCl_3$): δ (ppm) 149.4, 146.4, 142.3, 136.2, 129.7, 126.7, 120.5, 117.7, 115.5, 63.2 (NCH), 33.6 (NMe), 30.3 ($NCHCH_2$), 26.0 ($NCHCH_2CH_2$).

2.3. Synthesis of compounds 1–2

$Ni(ClO_4)_2{\cdot}6H_2O$ (2.2 g, 6.0 mmol) was dissolved in CH_3CN (5 mL) and treated with $BQCNMe_2$ (2.38 g, 6.0 mmol) in CH_2Cl_2 (5 mL) resulting in red coloured solution. The solution was filtered after 2 h and violet colour crystalline powder was obtained by slow diffusion of diethylether. Yield of **1** was 3.2 g. Anal. Calc. for **1** $C_{26}H_{32}N_4Cl_2O_{10}Ni$ (%): C, 45.25; H, 4.67; N, 8.12. Found: C, 44.91; H, 4.56; N, 8.01. Selected IR bands (KBr, cm^{-1}): 3433 ν(OH); 3020–2814 ν(CH); 1101

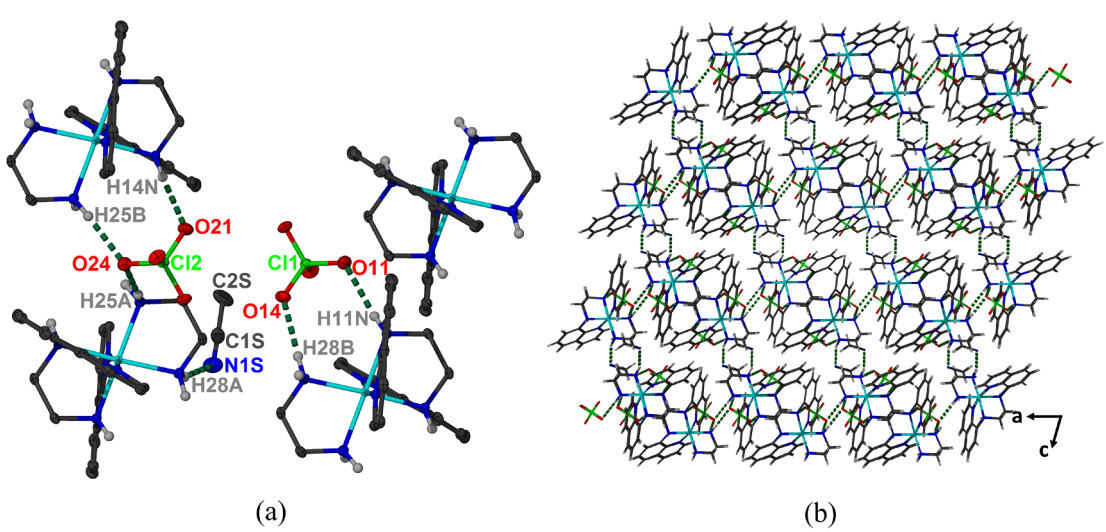

Fig. 6. a) H-bonding situation around the unique anions. Hydrogen atoms which are not involved in hydrogen bonding are omitted for clarity b) Enlarged view of network of hydrogen bonding in **8** showing symmetric organization of cations $[Ni(BQENH_2)(en)]^{2+}$ and anions $[ClO_4]^-$ in a crystallographic *ac* plane.

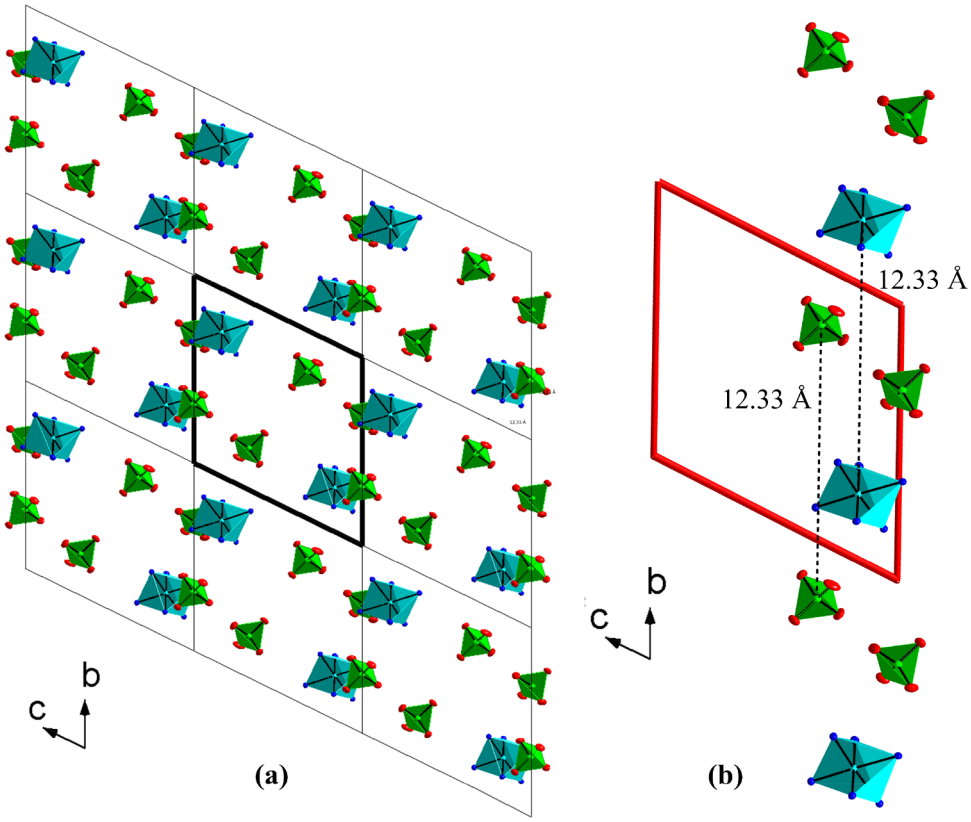

Fig. 7. a) A view along *a* showing the crystallographic packing of $\{NiN_6\}^{2+}$ cations (blue) and perchlorate anions in polyhedral representation. b) alignment of $\{NiN_6\}^{+2}$ octahedra and perchlorate anions along a axis showing separation between the two geometric units.

(ν_3), 624 (ν_4) (ClO_4^{-1}). λ(nm/dm^{3}mol^{-1}cm^{-1}): 228 (12092), 293 (2498), 542 (9), 890 (10).

Compound **2** was prepared using $BQCNH_2$ (2.2 g, 6.0 mmol) by employing a similar method as above. Yield of **2** was 2.9 g. Anal. Calc. for **2** $C_{24}H_{28}N_4Cl_2O_{10}Ni$ (%): C, 43.54; H, 4.26; N, 8.86. Found: C, 43.42; H, 4.26; N, 8.63. Selected IR bands (KBr, cm^{-1}): 3435 ν(OH); 3246 ν(NH); 3030–2825 ν(CH); 1087 (ν_3), 624 (ν_4) (ClO_4^{-1}). λ(nm/dm^{3}mol^{-1}cm^{-1}): 230 (17796), 302 (3923), 526 (12), 905 (12).

2.4. Reactivity of 1 and 2 with en and phen to obtain compounds 3–6

The ethylenediamine, en (0.09 g, 1.5 mmol) was added to the violet coloured CH_3CN solution of **1** (0.1 g, 1.5 mmol). After ~1 h the solution was filtered in a glass vial (10 mL) and left open in a dessicator containing diethylether for slow diffusion. A pale-red crystalline compound was obtained. Yield of **3** was 0.12 g. Anal. Calc. for **3** $C_{28}H_{36}N_6Cl_2O_8Ni$ (%): C, 47.09; H, 5.08; N 11.77. Found: C, 47.48; H, 5.28; N, 11.64. Selected IR bands (KBr, cm^{-1}): 3296 ν(NH); 3024–2816 ν(CH); 1109 (ν_3), 624 (ν_4) (ClO_4^{-1}). λ(nm/dm^{3}mol^{-1}cm^{-1}): 230 (15657), 291 (3569), 525 (13), 866 (11).

Compound **4** was prepared by taking phen instead of en. Yield of **4** was 0.13 g. Anal. Calc. for **4** $C_{38}H_{36}N_6Cl_2O_8Ni$ (%): C, 54.70; H, 4.35; N, 10.07. Found: C, 54.64; H, 4.30; N, 9.33. Selected IR bands (KBr, cm^{-1}): 3028–2814 ν(CH); 1095 (ν_3), 623 (ν_4) (ClO_4^{-1}). λ(nm/dm^{3}mol^{-1}cm^{-1}): 226 (32632), 268 (16113), 525 (15), 866 (13).

Compounds **5** and **6** were prepared by reaction of en and phen with $[Ni(BQCNH_2)(H_2O)_2](ClO_4)_2$ (**2**) in CH_3CN. The single crystals of **6** were grown by slow diffusion of diethylether into its CH_3CN solution. Anal. Calc. for **5** $C_{26}H_{32}N_6Cl_2O_8Ni$ (%): C, 45.51; H, 4.70; N, 12.25. Found: C, 45.43; H, 4.51; N, 12.15. Selected IR bands (KBr, cm^{-1}): 3346 ν(NH); 3020–2827 ν(CH); 1089 ν_3, 624 ν_4 ν(ClO_4^{-1}). λ (nm/dm^{3}mol^{-1}cm^{-1}): 230 (20666), 303 (3986), 535 (13), 886 (8). Anal. Calc. for **6** $C_{36}H_{32}N_6Cl_2O_8Ni$ (%): C, 53.63; H, 4.00; N, 10.42. Found: C, 53.68; H, 3.95; N, 10.24. Selected IR bands (KBr, cm^{-1}): 3255 ν(NH); 2983–2808 ν(CH); 1093 (ν_3), 623 (ν_4) (ClO_4^{-1}). λ(nm/dm^{3}mol^{-1}cm^{-1}): 225 (25559), 270 (12184), 526 (15), 875 (10).

2.5. Synthesis of compounds 7 and 8

Compounds **7** and **8** were synthesized by reacting $[Ni(BQENMe_2)(H_2O)_2](ClO_4)_2$ and $[Ni(BQENH_2)(H_2O)_2](ClO_4)_2$ with en as above. The single crystals of **8** were obtained by slow diffusion of diethylether. Yields of **7** and **8** were 0.12 and 0.13 g respectively. Anal. Calc. for **7** $C_{24}H_{30}N_6Cl_2O_8Ni$ (%): C, 43.67; H, 4.58; N, 12.73. Found: C, 43.39; H, 4.36; N, 12.86. Selected IR bands (KBr, cm^{-1}): 3275 ν(NH); 3030–2825 ν(CH); 1093 ν_3, 621 ν_4 (ClO_4^{-1}). λ(nm/dm^{3}mol^{-1}cm^{-1}): 230 (15657), 291 (3569), 538 (13), 894 (11). Anal. Calc. for **8** $C_{22}H_{26}N_6Cl_2O_8Ni$ (%): C, 41.80; H, 4.15; N, 13.30. Found: C, 41.31; H. 3.87; N, 12.96. Selected IR bands (KBr, cm^{-1}): 3300 ν(NH); 3030-2825 ν(CH); 1093 (ν_3), 621(ν_4) (ClO_4^{-1}). λ(nm/dm^{3}mol^{-1}cm^{-1}): 227 (57263), 297 (11759), 315 (10169), 530 (12), 862 (9).

2.6. Reactivity of 1 and 2 with H_2O_2 in presence of TBAH

On addition of 10 eq. of H_2O_2 (30%) and 5 eq. tetrabutylammonium hydroxide (TBAH) to the CH_3CN solution of **2** (0.25 mM in 2 mL) gave an intense band at 570 nm in the UV-Vis spectrum. This species (**2a**) formed was kinetically quite stable. To the intermediate solution, 40 eq. of 2-PPA was added which resulted in the decay of the peak at 570 nm. The solution after the end of the reaction was analysed by GC and the products formed were quantified based on the catalyst used. Acetophenone was obtained as the major product in the reaction with 2-PPA (*vide infra*). Interestingly under identical reaction conditions, **1** showed no reactivity with H_2O_2 and TBAH.

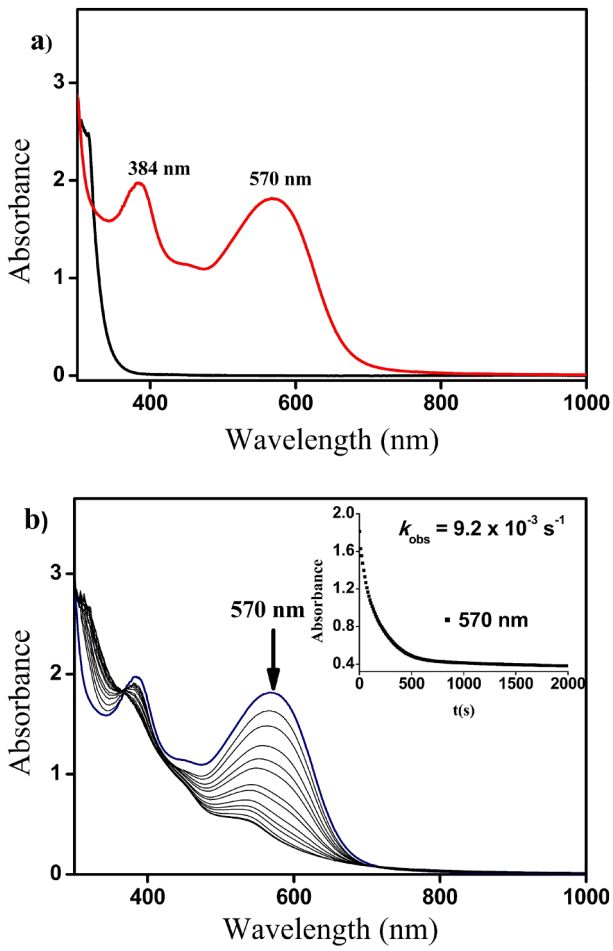

Fig. 8. a) UV-Vis spectra of 2 (black line) and new peaks formed at 570 and 384 nm (red line) in CH_3CN at 25 °C on addition of H_2O_2/TBAH due to species 2a; b) UV-Vis spectral changes occurring at 570 nm on addition of 2-PPA (10 mM). Inset shows the pseudo first order time trace for the decay of peak 570 nm on addition of 2-PPA.

2.7. Catalytic reactions by 1–8

The efficacy of compounds **1–8** as a catalyst was tested in the catalytic oxidation of hydrocarbons such as cumene and ethylbenzene in presence of *meta*-chloroperbenzoic acid (*m*-CPBA) oxidant in CH_2Cl_2/CH_3CN (3:1) under N_2 atmosphere at room temperature. The products formed in the reaction were analysed and quantified by GC using internal standard *n*-decane.

3. Results and discussion

3.1. Synthesis of BQCNMe$_2$ and 1 and 2

Several non-heme metal compounds which carry out selective oxidation of C—H and C=C bonds are known in natural systems [47,48]. The topology of ligands has very a high influence on the stability and reactivity patterns of high valent metal-oxygen intermediates [45]. The chemical structures of few non-heme *N*-donor ligands which have been extensively employed to stabilize high valent iron(IV/V) and manganese(IV/V)-oxo species are shown in Scheme 1. The reactivity of these metal-oxo species in biomimetic oxidations (O-transfer, C—H activation, aromatic hydroxylation and epoxidation) has been well understood [49]. The non-heme metal compounds containing ligands with N—H groups when used in organic substrate oxidations often results in degradation of ligand itself in presence of oxidants like *m*-CPBA and thus result in low yields of organic products [50]. The lower yields of hydroxylated products were also obtained by us when we used the nickel(II) compounds containing BQENH$_2$ which has two –NH groups [40]. In the present investigation, we have chosen a tetradentate *N*-methylated ligand BQCNMe$_2$ for stabilizing nickel(II) compounds (Scheme 2). The BQCNMe$_2$ was earlier prepared by alkylating BQCNH$_2$ with a strong base *n*-BuLi and CH_3I. One of the issue with the method is that it works only at a very low temperature (−78 °C) and under inert atmosphere due to the pyrophoric nature of *n*-BuLi. To overcome this cumbersome procedure, we adopted a simple methodology for the synthesis of BQCNMe$_2$ wherein we have carried out the reductive methylation of BQCNH$_2$ using aqueous formaldehyde and sodium cyanoborohydride at room temperature [40].

The first compound containing BQCNMe$_2$, [Fe^{II}(BQCNMe$_2$)(CF$_3$SO$_3$)$_2$] was reported by Britovsek et al. which showed high reactivity in the oxidation of cyclohexane [45]. Nam et al. then prepared [Mn^{II}(BQCNMe$_2$)(CF$_3$SO$_3$)$_2$] which worked out to be an excellent catalyst in water oxidation [43,44]. In the present work, we have prepared and characterized two new compounds [Ni(BQCNMe$_2$)(H$_2$O)$_2$](ClO$_4$)$_2$ (**1**) and [Ni(BQCNH$_2$)(H$_2$O)$_2$](ClO$_4$)$_2$ (**2**) (Scheme 2).

3.2. Substitution of cis-waters by en or phen in 1 and 2

The dual site *cis*-water compounds **1** and **2** were reacted with symmetrical bidentate auxiliary ligands en and phen in a 1:1 stoichiometric ratio to afford four new compounds viz. [Ni(BQCNMe$_2$)(en)](ClO$_4$)$_2$ **3**, [Ni(BQCNMe$_2$)(phen)](ClO$_4$)$_2$ **4**, [Ni(BQCNH$_2$)(en)](ClO$_4$)$_2$ **5** and [Ni(BQCNH$_2$)(phen)](ClO$_4$)$_2$ **6** in nearly quantitative yields (Scheme 2). We have earlier investigated the substitution of two *cis*-H$_2$O molecules of [Ni(BQENH$_2$)(H$_2$O)$_2$]$^{2+}$ and [Ni(BQENMe$_2$)(H$_2$O)$_2$]$^{2+}$ by bpy and phen [40]. In addition to **3-6**, we also report synthesis and characterization of [Ni(BQENMe$_2$)(en)](ClO$_4$)$_2$] **7** and [Ni(BQENH$_2$)(en)](ClO$_4$)$_2$ **8**.

3.3. Infrared spectra of ligands and compounds 1–8

Infrared spectra of ligands and solid samples of **1–8** were recorded in the region of 4000–400 cm^{-1} by diluting samples with KBr powder. IR spectra of BQCNMe$_2$, **1**, **3** and **4** are shown in Fig. 1 while the IR spectra of BQCNH$_2$, **2**, **5** and **6** are depicted in Fig. S5 (SI). The IR spectra of **1** and **2** exhibited broad bands at ~3547 and ~3405 cm^{-1} respectively corresponding to O—H vibrations of water. IR spectrum of **3** exhibits N—H stretching vibrations due to the incorporation of en while similar peaks were not seen in **1** and **4** as amines are methylated.

Table 4
The yields of oxidised products formed in the catalytic oxidation of cumene and ethylbenzene by **1** and **2** in presence of *m*-CPBA[a] analysed by GC.

	substrate	alcohol (A)	(TON)[b] (A)	ketone (K)	(TON)[b] (B)	A/K
1	cumene	2-phenylpropane-2-ol	460	acetophenone	60	7.6
	ethylbenzene	1-phenylethanol	165	acetophenone	42	4.0
2	cumene	2-phenylpropane-2-ol	420	acetophenone	55	7.7
	ethylbenzene	1-phenylethanol	130	acetophenone	32	3.9

[a] Reaction conditions: [Ni^{2+}] = 0.5 mM; [*m*-CPBA] = 0.5 M, [substrate] = 1 M in CH_3CN at 25 °C for 90 min under N_2.
[b] Turnover number [(moles of product)/(moles of catalyst)] determined by GC.

On the other hand, **2**, **5** and **6** showed peaks corresponding to the N—H vibrations in the region 3350–3430 cm^{-1}. The bands due O—H vibrations are absent in the IR spectra of **3–6** indicating that the two waters are replaced by en and phen. IR spectra of **7** and **8** also suggested replacement of waters by en (Fig. S6 in SI). The additional band due to C—N vibration was observed in the IR spectrum of **8** due to CH_3CN. All complexes have incorporated perchlorate anions as evidenced from well resolved absorption bands at 1093 (s) and 621 (m) cm^{-1} [51,52].

3.4. UV-Vis spectra of 1–8

UV-Visible spectra of **1–8** in CH_3CN were recorded to obtain the information on electronic transitions of nickel(II) ion and the ligands. UV-Vis spectra of **1**, **3** and **4** and those of **2**, **5** and **6** are depicted in Fig. S7 (SI). The weak *d-d* bands are observed for all the compounds in the visible region. Out of expected three *d-d* bands ($^3A_{2g} \rightarrow {}^3T_{2g}(F)$, $^3A_{2g} \rightarrow {}^3T_{1g}(F)$, $^3A_{2g} \rightarrow {}^3T_{1g}(P)$) for complexed nickel(II) ion, only two bands are seen in the UV-Vis spectrum. The two *d-d* bands in **1** and **3** occur nearly at the same wavelengths (540 and 894 nm), while the bands in **4** shifted to slightly lower wavelengths (526 and 852 nm). This observation reveals that phen has incorporated in **4**. The *d–d* band assigned to $^3A_{2g} \rightarrow {}^3T_{2g}$ transition is centered at 850–900 nm while the second peak due to $^3A_{2g} \rightarrow {}^3T_{1g}(F)$ transition is centered at 450–550 nm [53]. The third high energy transition $^3A_{2g} \rightarrow {}^3T_{1g}(P)$ transition is not observed as it is tailing towards high energy CT region [54]. The bands in the higher energy region are assigned to intra-ligand charge transfer transitions the n-π^* (270–320 nm) and π-π^* (220–230 nm). The UV-Vis spectra of compounds **7** and **8** can be explained on similar lines (Fig. S8 in SI).

3.5. Electrochemical properties of 1–8

Compounds **1–8** were investigated using cyclic voltammetry (CV) and differential pulse voltammetry (DPV) to understand their electrochemical behavior that correlates with structural and reactivity properties. The quasi-reversible voltammograms corresponding to the Ni(II)/Ni(I) and Ni(I)/Ni(II) couples were observed in all the cases. CV/DPV plots of **1** are shown in Fig. 2. The $E_{1/2}$ value of these compounds lies between −1.19 and −1.38 V (Fig S9 in SI). $BQCNH_2$ and $BQCNMe_2$ ligands showed no redox signals under identical conditions. The CV/DPV plots of **7** and **8** are shown in Fig S10 in SI.

3.6. Crystal structure description of 6 and 8 and PXRD description of 1–8

The single crystals of **6** and **8** were obtained by slow diffusion of diethylether into their CH_3CN solutions. The remaining compounds did not give crystals suitable for single crystal analysis under identical conditions after several attempts, hence they were studied by Powder X-ray pattern. Compounds **1** and **2** exhibit the sharp Bragg lines suggesting that both compounds are highly crystalline. However, the powder patterns of **1** and **2** do not match on overlaying on one another indicating that they have different structures (Fig. 3). This is obvious because **1** contains $BQCNMe_2$ while **2** contain $BQCNH_2$.

The technical details of data collection and selected refinement parameters of **6** and **8** are given in Table 1. Both **6** and **8** crystallize in the centrosymmetric triclinic space group *P*$\bar{1}$ with all the atoms located in general positions. The crystal structure of **6** contains a unique Ni(II) cation, one bidentate ligand phen, $BQCNH_2$ functioning as a tridentate ligand and two unique perchlorate anions (Fig. 4). In contrast the crystal structure of **8** contain an unique Ni(II) cation, one bidentate en, tetradentate $BQENH_2$, two perchlorate anions and an acetonitrile solvate (Fig. 4). In both compounds the two crystallographically independent perchlorate anions lie outside the coordination sphere and act as counter anions. One more additional feature in the structure of **8** is that it has crystal lattice CH_3CN molecule which contributes to the stability of the structure. In compound **6**, the Ni(II) ion is coordinated by five N atoms. A notable fact being one of the quinoline rings has a two-fold disorder (Fig S11 in SI). The distances of Ni from the phen nitrogens N1 and N2 are 2.001(3) and 2.156(3) Å respectively while amine nitrogens N4, N5A and N5B are 2.022(3), 2.041(4) and 2.154(12) Å respectively. The Ni(II) ion is 2.012(3) Å away from quinoline nitrogen N3 (Table 2). The axial positions of trigonal bipyramidal (tbp) geometry are occupied by N4 of amine part and N1 of phenanthroline part, on the other hand, the equatorial positions are occupied by N5A of amine, N2 of phen and N3 of quinoline moiety. The bond angles N2-Ni-N3; 105.30°(11), N2-Ni-N5A; 111.05°(15) and N3-Ni-N5A; 143.03°(16) sum to 359.38°, the value which is very close to the expected 360° of tbp geometry. The bond angle, N1-Ni-N4; 176.48°(12) deviates from 180° indicating that the structure of **6** is slightly distorted. The chlorine atoms of perchlorate anions are all involved in the hydrogen bonding with the N's of $BQCNH_2$ ligand as well as phen ligand moieties (Fig. 5, Table 3). In the crystal structure of **6**, the Ni(II) ion adopts trigonal bipyramidal geometry despite the ligand $BQCNH_2$ being tetradentate which is quite rare. It is often seen that the tridentate ligands along with auxiliary bidentate ligands adopt trigonal bipyramidal geometry with metal ions [55–58].

In the crystal structure of **8** the two amine nitrogen atoms N11 and N14 occupy the adjacent positions, while the quinolyl nitrogen atoms, N1 and N23 are located *trans* to each other (Fig. 4). The remaining two *cis* sides of the octahedron are occupied by the two nitrogen atoms of the en ligand. The Ni-N bond distances range from 2.0918(14) to 2.1191(13) Å (Table 2). All the Ni-N bond distances and *N*-Ni-N bond angles are in good agreement with literature values [59–62]. There is a small deviation from the normal bond angle of octahedron (90° for *cis* and 180° for *trans*) indicates a distorted octahedral geometry. The *cis* angle varies from 80.17(5) to 98.35(5) and the *trans* angle varies from 167.47(5) to 178.51(5). The oxygen atoms and chlorine atom of perchlorate anions and the nitrogen atom of CH_3CN molecule are all involved in the hydrogen bonding with the N's of $BQENH_2$ as well as en ligand moieties (Fig. 6, Table 3). The two perchlorate anions associated with each $\{NiN_6\}^{2+}$ octahedron are connected to three other octahedra by O···H—N hydrogen bonding interactions (Fig. 6a). These interactions further extend connecting other $\{NiN_6\}^{2+}$ octahedra and $[ClO_4]^-$ tetrahedra resulting in a three dimensional network structure (Fig. 6b). All $\{NiN_6\}^{2+}$ octahedra and $[ClO_4]^-$ tetrahedra are organized symmetrically when viewed through all the three crystallographic planes (*bc*, *ab*, *ac*) (Fig. 7, Fig. S12 in SI). In the crystal structure of **8**, all the octaheda are aligned and far apart at a distance of 12.33 Å (Fig. 7b).

3.7. Reactivity of 1 and 2 with H_2O_2 in presence of TBAH

On adding 10 eq. of H_2O_2 to a CH_3CN solution of **2** (0.25 mM in 2 mL) in the presence of 5 eq. TBAH at room temperature resulted in the formation a new species (**2a**) as evidenced by the appearance of a peak at 570 nm in the UV-Vis spectrum of **2** with a colour change from light green to purple (Fig. 8a). Similar observations were earlier reported for the Ni(III)-oxygen species by others [63,64]. Assuming that the intermediate (**2a**) formed in the solution could be Ni(III)-oxygen species, we then treated this solution with 40 eq. of 2-phenylpropionaldehyde (2-PPA) at 25 °C. The spectral changes for the decay of 570 nm peak with time were monitored (Fig. 8b). The isobestic points were observed at 365 nm and 727 nm. The peak at 570 nm slowly decayed following pseudo-first order kinetics affording us a pseudo-first order rate constant, k_{obs} of $9.2 \times 10^{-3}\,s^{-1}$ (Fig. 8b inset). The k_{obs} values increased with increase in the concentration of 2-PPA and thus afforded us a second order rate constant, $k_2 = 9.05 \times 10^{-4}\,M^{-1}\,s^{-1}$ (Fig. S13 in SI). On subjecting final reaction solution to GC analysis, the acetophenone was obtained as the major product, these results suggest that the intermediate formed at 570 nm has nucleophilic character [65–68]. Efforts are underway to elucidate the structure and formula of this intermediate. In the case of **1**, no clear formation of new species was observed in the reaction **1** and H_2O_2/TBAH (Fig. S14 in SI).

3.8. Catalytic hydroxylation of alkanes by 1 and 2

The oxidation of cumene and ethylbenzene gave 2-phenylpropane-2-ol and 1-phenylethanol respectively as the major products and acetophenone as the minor product (Table 4). On comparing the oxidising ability of **1** and **2** it is observed that **1** showed slightly higher yields of hydroxylated products over **2**. In compounds **1** and **2** the two solvent molecules coordinated to Ni(II) ion are labile thus making the geometry flexible for oxidation of Ni(II) to Ni(III) as compared to compounds **3–8** where Ni(II) ion is coordinately saturated. The Ni(III) species proposed here in the catalytic oxidation of cumene and ethylbenzene by **1** and **2** was further traced using CV/DPV which showed anodic peak potentials for Ni(II)/Ni(III) couple at centred 0.689 in **1** and 0.637 V in **2** (Fig. S15 in SI). Based on the yields of hydroxylated products obtained in the catalytic reactions and the appearance of Ni(II)/N(III) anodic peaks in the CV/DPV we suggest that the catalytic cycle may involve H-atom abstraction of alkanes by Ni(III)-oxygen intermediate [69]. Compounds **3–8** were also tested in the catalytic oxidations of alkanes however no products were obtained in these cases [40].

4. Conclusion

We have reported synthesis and characterization of two new dual-site aqua nickel(II) compounds **1** and **2** stabilized by non-heme $BQCNMe_2$ and $BQCNH_2$. $BQCNMe_2$ was prepared by a modified procedure. Compounds **3–6** were prepared by simple substitution of labile solvent molecules of **1** and **2** by relatively stronger bases en and phen. Compounds **7** and **8** with the other two ligands $BQENMe_2$ and $BQENH_2$ have been also reported. All compounds were characterized by C, H, N analysis, IR, UV-Vis and CV/DPV techniques to obtain their correct formulas. We attempted to obtain single crystals of **1–8** and we were successful in getting crystals of only **6** and **8**, hence their structures are reported. Both **6** and **8** crystallizes in a centrosymmetric triclinic *P*$\bar{1}$ space group and isostructural with **5**. Compound **6** shows five coordinated geometry while **8** has a slightly distorted octahedral structure with additional crystal lattice acetonitrile. The reaction of **2** with H_2O_2/TBAH forms a reactive species as evidenced from the UV-Vis spectrum which undergoes deformylation of 2-PPA to acetophenone. Finally, we reported catalytic hydroxylation of cumene and ethylbenzene by **1** and **2** using *m*-CPBA.

Acknowledgment

SND thank UGC, New Delhi (F.No.37-576/2009 (SR) and CSIR, New Delhi (No. 01(2923)/18/EMR-II) for financial support. SH thank Goa University for the research studentship. DDN acknowledge support from UGC, New Delhi (Basic Scientific Research).

Appendix A. Supplementary data

Supplementary data to this article can be found online at https://doi.org/10.1016/j.ica.2018.10.069. These data include MOL files and InChiKeys of the most important compounds described in this article.

References

[1] (a) S. Fukuzumi, Y.-M. Lee, W. Nam, ChemCatChem. 10 (2018) 9;
(b) S. Hong, Y.-M. Lee, K. Ray, W. Nam, Coord. Chem. Rev. 334 (2017) 25;
(c) K. Ray, F.F. Pfaff, B. Wang, W. Nam, J. Am. Chem. Soc. 136 (2014) 13942;
(d) S. Chandra, K. Ruchi, S. Qanungo, K. Sharma, Spectrochim. Acta, Part A 79 (2011) 1326.
[2] (a) K. Ray, F. Heims, M. Schwalbe, W. Nam, Curr. Opin. Chem. Biol. 25 (2015) 159;
(b) F. Schwizer, Y. Okamoto, T. Heinisch, Y. Gu, M.M. Pellizzoni, V. Lebrun, R. Reuter, V. Köhler, J.C. Lewis, T.R. Ward, Chem. Rev. 118 (2018) 142;
(c) S.A. Cook, E.A. Hill, A.S. Borovik, Biochemistry 54 (2015) 4167.
[3] E. Meggers, Curr. Opin. Chem. Biol. 11 (2007) 287.
[4] J.G. McAlpin, Y. Surendranath, M. Dincă, T.A. Stich, S.A. Stoian, W.H. Casey, D.G. Nocera, R. David Britt, J. Am. Chem. Soc. 132 (2010) 6882.
[5] B. Wang, Y.-M. Lee, W.-Y. Tcho, S. Tussupbayev, S.-T. Kim, Y. Kim, M.S. Seo, K.-B. Cho, Y. Dede, B.C. Keegan, T. Ogura, S.H. Kim, T. Ohta, M.-H. Baik, K. Ray, J. Shearer, W. Nam, Nat. Commun. 8 (2017) 14839.
[6] C.N. Brodsky, R.G. Hadt, D. Hayes, B.J. Reinhart, N. Li, L.X. Chen, D.G. Nocera, Proc. Natl. Acad. Sci. U.S.A. 14 (2017) 3855.
[7] S. Hong, F.F. Pfaff, E. Kwon, Y. Wang, M.-S. Seo, E. Bill, K. Ray, W. Nam, Angew. Chem. Intl. 53 (2014) 10403.
[8] F.F. Pfaff, S. Kundu, M. Risch, S. Pandian, F. Heims, I. Pryjomska-Ray, P. Haack, R. Metzinger, E. Bill, H. Dau, P. Comba, K. Ray, Angew. Chem. Intl. 50 (2011) 1711.
[9] G.E. Martinez, C. Ocampo, Y.J. Park, A.R. Fout, J. Am. Chem. Soc. 138 (2016) 4290.
[10] M.B. Watson, N.P. Rath, L.M. Mirica, J. Am. Chem. Soc. 139 (2017) 35.
[11] J.W. Schultz, K. Fuchigami, B. Zheng, N.P. Rath, L.M. Mirica, J. Am. Chem. Soc. 138 (2016) 12928.
[12] S.K. Padamati, D. Angelone, A. Draksharapu, G. Primi, D.J. Martin, M. Tromp, M. Swart, W.R. Browne, J. Am. Chem. Soc. 139 (2017) 8718.
[13] K.H. Bok, M.M. Lee, G.R. You, H.M. Ahn, K.Y. Ryu, S.-J. Kim, Y. Kim, C. Kim, Chem. Euro. J. 23 (2017) 3117.
[14] A.L. García-Lario, M. Azna, G.S. Grasa, T. García, R. Murillo, J. Power Sour. 242 (2013) 371.
[15] G. Busca, U. Costantino, T. Montanar, G. Ramis, C. Resini, M. Sisani, Int. J. Hydrogen Energy 35 (2010) 5356.
[16] M.P. Stewart, M.-H. Ho, S. Wiese, M.L. Lindstrom, C.E. Thogerson, S. Raugei, R.M. Bullock, M.L. Helm, J. Am. Chem. Soc. 135 (2013) 6033.
[17] H.J.S. Brown, S. Wiese, J.A.S. Roberts, R.M. Bullock, M.L. Helm, ACS Catal. 5 (2015) 2116.
[18] A. Das, Z. Han, W.W. Brennessel, P.L. Holland, R. Eisenberg, ACS Catal. 5 (2015) 1397.
[19] M.T. Kieber-Emmons, J. Annaraj, M.S. Seo, K.M.V. Heuvelen, T. Tosha, T. Kitagawa, T.C. Brunold, W. Nam, C.G. Riordan, J. Am. Chem. Soc. 128 (2006) 14230.
[20] J. Cho, H.Y. Kang, L.V. Liu, R. Sarangi, Chem. Sci. 4 (2013) 1502.
[21] J. Cho, R. Sarangi, J. Annaraj, S.Y. Kim, M. Kubo, T. Ogura, E.I. Solomon, W. Nam, Nat. Chem. 1 (2009) 568.
[22] E. Ramachandran, D.S. Raja, J.L. Mike, T.R. Wagner, M. Zeller, K. Natarajan, RSC Adv. 2 (2012) 8515.
[23] L.-N. Zhu, D.-M. Kong, X.-Z. Li, G.-Y. Wang, J. Wang, Y.-W. Jin, Polyhedron 29 (2010) 574.
[24] C.N. Sudhamani, H.S.B. Naik, T.R.R. Naik, M.C. Prabhakara, Spectrochim. Acta. Part A 72 (2009) 643.
[25] A.E.-M.M. Ramadan, J. Mol. Struct. 1015 (2012) 56.
[26] K.C. Skyrianou, V. Psycharis, C.P. Raptopoulou, D.P. Kessissoglou, G. Psomas, J. Inorg. Biochem. 105 (2011) 63.
[27] M.S.S. Babu, P.G. Krishna, K.S. Reddy, G.H. Philip, Indian J. Chem. 47A (2008) 1668.
[28] R.P. Reddy, N. Raju, K. Rao, A. Shilpa, Indian J. Chem. 48A (2009) 761.
[29] M. Pragathi, K.H. Reddy, Indian J. Chem. 52A (2013) 845.
[30] K.C. Skyrianou, F. Perdih, I. Turel, D.P. Kessissoglou, G. Psomas, J. Inorg. Biochem. 104 (2010) 740.
[31] L.R. Gomes, J.N. Low, M.A.A. Rocha, L.M.N.B.F. Santos, B. Schröder, P. Brandão, C. Matos, J. Neves, J. Mol. Struct. 990 (2011) 86.
[32] S. Anitha, J. Karthikeyan, A.N. Shetty, Indian J. Chem. 42A (2013) 45.
[33] P.K. Suganthy, R.N. Prabhu, V.S. Sridevi, Inorg. Chim. Acta 449 (2016) 127.
[34] M. Zhang, M.-T. Zhang, C. Hou, Z.-H. Ke, T.-B. Lu, Angew. Chem. Int. Ed. 43 (2014) 13042.
[35] M. Sankaralingam, P. Vadivelu, E. Suresh, M. Palaniandavar, Inorg. Chim. Acta 407 (2013) 98.
[36] T. Nagataki, K. Ishii, Y. Tachi, S. Itoh, Dalton Trans. (2007) 1120.
[37] M. Balamurugan, R. Mayilmurugan, E. Suredh, M. Palaniandavar, Dalton Trans. 40 (2011) 9413.
[38] S. Hikichi, K. Hanaue, T. Fujimura, H. Okuda, J. Nakazawa, Y. Ohzu, C. Kobayashi, M. Akita, Dalton Trans. 42 (2013) 3346.
[39] J. Nakazawa, S. Terada, M. Yamada, S. Hikichi, J. Am. Chem. Soc. 135 (2013) 6010.
[40] D.D. Narulkar, A.R. Patil, C.C. Naik, S.N. Dhuri, Inorg. Chim. Acta 427 (2015) 248.
[41] K. Nehru, S.J. Kim, I.Y. Kim, M.S. Seo, Y. Kim, S.-J. Kim, J. Kim, W. Nam, Chem. Commun. 1 (2007) 4623.
[42] J. Yoon, S.A. Wilson, Y.K. Jang, M.S. Seo, K. Nehru, B. Hedman, K.O. Hodgson, E. Bill, E.I. Solomon, W. Nam, Angew. Chem. Int. Ed. 48 (2009) 1257.
[43] S.C. Sawant, X. Wu, J. Cho, K.-B. Cho, S.H. Kim, M.S. Seo, Y.-M. Lee, M. Kubo, K. Ogura, S. Shaik, W. Nam, Angew. Chem. Int. Ed. 49 (2010) 8190.
[44] D. Hong, S. Mandal, Y. Yamada, Y.-M. Lee, W. Nam, A. Llobet, S. Fukuzumi, Inorg. Chem. 52 (2013) 9522.
[45] J. England, G.J.P. Britovsek, N. Rabadia, A.J.P. White, Inorg. Chem. 46 (2007) 672.
[46] G.M. Sheldrick, Acta Cryst. 71 (2015) 3.
[47] L. Que Jr., R.Y.N. Ho, Chem. Rev. 96 (1996) 2607.
[48] E.I. Solomon, T.C. Brunold, M.I. Davis, J.N. Kemsley, S.-K. Lee, N. Lehnert, F. Neese, A.J. Skulan, Y.-S. Yang, J. Zhou, Chem. Rev. 100 (2000) 235.
[49] (a) R.E. Norman, S. Yan, L. Que Jr., G. Backes, J. Ling, J. Sandersloehr, J.H. Zhang, C.J. O'Connor, J. Am. Chem. Soc. 112 (1990) 1554;
(b) C. Kim, K. Chen, J. Kim, L. Que Jr., J. Am. Chem. Soc. 119 (1997) 5964;
(c) T. Okuno, S. Ito, S. Ohba, Y. Nishida, J. Chem. Soc., Dalton Trans. (1997) 3547;
(d) K. Chen, L. Que Jr., Chem. Commun. (1999) 1375;
(e) M.S. Chen, M.C. White, Science 318 (2007) 783;
(f) M.C. White, A.G. Doyle, E.N. Jacobsen, J. Am. Chem. Soc. 123 (2001) 7194.
[50] A. McAuley, C. Xu, Inorg. Chem. 31 (1992) 5549.
[51] K. Nakamoto, Infrared Spectra and Raman Spectra of Inorganic and Coordination Compound Part B: Application in Coordination, Organometallic and Bioinorganic Chemistry, 6th Ed., John Wiley, Hoboken, NJ, 2009, p. 88.

[52] P. Bhowmik, M.G.B. Drew, S. Chattopadhyay, Inorg. Chim. Acta 366 (2011) 62.
[53] R. Boc, I. Svoboda, J. Titis, Polyhedron 25 (2006) 3261.
[54] M.A. Ali, A.H. Mirza, F.H. Bujang, M.H.S.A. Hamid, P.V. Bernhardt, Polyhedron 25 (2006) 3245.
[55] K. Gudasi, R. Vadavi, R. Shenoy, M. Patil, S.A. Patil, M. Nethaji, Inorg. Chim. Acta 358 (2005) 3799.
[56] A.W. Addison, T.N. Rao, J. Reedijk, J. van Rijn, G.C. Verschoor, J. Chem. Soc. Dalton Trans. (1984) 1349.
[57] C. Mantel, C. Baffert, I. Romero, A. Deronzier, J. Pécaut, M.N. Collomb, C. Duboc, Inorg. Chem. 43 (2004) 6455.
[58] M. Broring, S. Prikhodovski, C.D. Brandt, Inorg. Chim. Acta. 357 (2004) 1733.
[59] I. García-Santos, J. Sanmartín, A.M. García-Deibe, M. Fondo, E. Gómez, Inorg. Chim. Acta 363 (2010) 193.
[60] D. Sertphon, D.J. Harding, P. Harding, H. Adams, Polyhedron 30 (2011) 2740.
[61] Q. Zhang, X.-Q. Zhang, Z.X. Wang, Dalton. Trans. 41 (2012) 10453.
[62] R.L. Ellis, H.H. Jaffe, C.A. Masmanidis, J. Am. Chem. Soc. 96 (1975) 2623.
[63] N.T. Kieber-Emmons, J. Annaraj, M.S. Seo, K.M. Van Heuvelen, T. Tosha, T. Kitagawa, T.C. Brunold, W. Nam, C.G. Riordan, J. Am. Chem. Soc. 128 (2006) 14230.
[64] R. Sarangi, J. Cho, W. Nam, E.I. Solomon, Inorg. Chem. 50 (2011) 614.
[65] D.L. Wertz, J.S. Valentine, Struct. Bonding 97 (2000) 37.
[66] M.S. Seo, J.Y. Kim, J. Annaraj, Y. Kim, Y.-M. Lee, S.-J. Kim, J. Kim, W. Nam, Angew. Chem. Int. Ed. 46 (2007) 377.
[67] J. Annaraj, J. Cho, Y.-M. Lee, S.Y. Kim, R. Latifi, S.P. de Visser, W. Nam, Angew. Chem. Int. Ed. 48 (2009) 4150.
[68] J. Cho, R. Sarangi, H.Y. Kang, J.Y. Lee, M. Kubo, T. Ogura, E.I. Solomon, W. Nam, J. Am. Chem. Soc. 132 (2010) 16977.
[69] F.F. Pfaff, F. Heims, S. Kundu, S. Mebs, K. Ray, Chem. Commun. 48 (2012) 3730.